Molecular Composition and Isotope Mapping of Natural Gas in the British Columbia Natural Gas Atlas

By:

Curtis Evans

B.Sc., University of Calgary, 1989

A Thesis Submitted in Partial Fulfillment of the Requirements for the Degree of

MASTER OF SCIENCE

In the School of Earth and Ocean Sciences

University of Victoria

Supervisory Committee

Molecular Composition and Isotope Mapping of Natural Gas in the British Columbia Natural Gas Atlas

By:

Curtis Evans

B.Sc., University of Calgary, 1989

Supervisory Committee

Dr. Michael J. Whiticar, (School of Earth and Ocean Sciences)

Supervisor

Dr. Vera Pospelova, (School of Earth and Ocean Sciences)

Departmental member

Mr. F. Michael Dawson, (School of Earth and Ocean Sciences)

Departmental member

ABSTRACT

This thesis provides a geochemical interpretation of natural gas resources in north eastern British Columbia (NEBC), Canada. The work is part of the three-year project, British Columbia Natural Gas Atlas (BC-NGA) to collect samples and compile data on molecular (C_1 to C_5) and stable isotope ratio ($\delta^{13}C$ and $\delta^{2}H$) compositions of natural gases in NEBC. The primary objective of the BC-NGA project is to produce a comprehensive, public, web database with maps of the gas geochemical data from a variety of gas tests including mudgas collected during drilling, downhole flow tests, production gas, and gas collected from surface emissions. The area of study in NEBC is a large portion of the Western Canadian Sedimentary Basin (WCSB) with Paleozoic, Mesozoic, and Cenozoic strata of thousands of meters thickness. Within this stratigraphic package there are numerous depositional hiatus and regional aquitards complicating the generation of regional maps and profiles. This M.Sc. thesis utilizes the geochemical gas parameters to characterize the range of gases in the BC-NGA database. The thesis found that the petroleum sources and active generation processes are not uniform in the NEBC. In some cases, the original gas signatures have been overprinted by localized processes in specific strata. The results of this new data plus compilation of existing data in the BC-NGA dataset indicate that many classical interpretive diagrams, e.g., Bernard Diagram ($C_1/[C_2+C_3]$ vs. $\delta^{13}C_1$) and CD Diagram ($\delta^{13}C_1$ vs. $\delta^{2}H$-C_1), confirm the microbial/ thermogenic nature of the gases, but lack the resolution for detailed stratigraphic interpretation of gas sources and migration. A particularly interesting finding is that $\delta^{13}C_{kerogen}$ (-33 ‰) estimated from $\delta^{13}C_1$ observed for most strata in NEBC is ^{13}C depleted compared with conventional kerogens and the data supports new calibration of the methane isotopes. This $\delta^{13}C_{kerogen}$ value is an unlikely value and therefore the offset observed compared with conventional natural gases requires a different explanation, including commingling of ^{13}C depleted methane from microbial sources. Enhanced characterization is obtained by combinations of the gas parameter ratios: $\delta^{13}C_1$, $\delta^{13}C_2$, $\delta^{13}C_3$, C_2/C_3, C_2/iC_4, (e.g., 'Berner-Faber Diagram', 'Prinzhofer Diagram', 'Lorant Diagram'). In addition, a new plot of $\delta^{13}C_2$-$\delta^{13}C_1$ versus iC_4/nC_4 ratio was developed in this thesis.

Table of Contents

List of Tables:

List of Figures:

Acknowledgements:

The author must express deep thanks to his supervisor, Dr. Michael Whiticar, for much more than the guidance and understanding during the BC-NGA project, but also the opportunity to experience far more in terms of chemical oceanography, organic geochemistry, deep carbon cycles, and the myriad of other topics between those 3 points. The learning has been astounding during my mid-career transition from one form of geoscience to another. My committee consists of 2 very good friends and important academic staff with a rich history of geoscience and industry between them – thank you for all the vibrant discussions. Extra editorial effort from Michael Dawson is deeply appreciated. The faculty members and staff of SEOS at UVic have become accepting of my "just one question today" almost every day. Of course, the entire BC-NGA project would not have started its existence without the foresight, initiative, and funding from the staff at Geoscience BC – the entirety of the project depended on the impetus from the volunteer Project Advisory Committee, the Technical Advisory Committee behind them, and Carlos Salas as the committee chair. The Oil and Gas Commission and their data services have been key in supporting the data along with sample submissions. Many of the publications referenced here were written by previous classmates and colleagues that I have known for years and they have my gratitude for their choice of career path in geochemistry has made this work much easier – thanks for being productive during my digression in the coal mines. However, most of all, a great debt is owed to my wife Sonja for tolerance during long nights of writing, bad moods, and missed vacation periods – I hope to resume having her editorial assistance after this.

1 Scientific Question

The scientific question at the core of this thesis is “Which natural gas geochemical parameters can be applied successfully to best identify and differentiate natural gases from different plays in North Eastern British Columbia (NEBC), Canada?”

2 Introduction

Natural gas is a valuable commodity as a combustible fossil fuel (EnergyBC 2012). Natural gas is composed mainly of methane (CH_4 labeled C_1) with smaller amounts of ethane (C_2H_6 labeled C_2), propane (C_3H_8 labeled C_3), butane (C_4H_{10} labeled nC_4), iso-butane (C_4H_{10} branching and labeled iC_4), and occasionally sour gas (hydrogen sulphide or H_2S) (e.g., Tissot and Welte 1984, Hunt 1996, Berkowitz 1997). These definitions are listed in Table 1. Compositionally, data exists for many other gases present in small quantities, including noble gases, in the British Columbia Natural Gas Atlas (BC-NGA) project database, but they are not discussed in the context of this thesis. Natural gas is also a source for chemical derivatives, such as, feedstock to the plastics industry (Hunt 1996). It can also be a large component of natural and artificial greenhouse gas emissions (Whiticar 1990, 1993, Khalil 2000, Prentice et al. 2001, Archer 2009, 2010, Etiope 2009, Kirschke et al. 2013). Natural gases in the rock formations (Figure 2) of NEBC have been a large part of economic growth and responsible resource development for the province (Adams et al. 2016). The petroleum geochemistry of the depositional system and reservoir conditions is key to understanding the generation of, exploration for, and production of natural gas (Hunt 1996).

The worldwide scale of natural gas supply and demand has grown in recent years (EIA 2016, BP 2017, Alam et al. 2017) and has resulted in growth of potential new export markets for the province (BC Govt 2012a, 2012b, 2012c, 2013, 2016, 2018) via liquified natural gas technology (Raj et al. 2016). Natural gas is one of the largest energy sources in British Columbia along with coal, hydropower, and oil (EnergyBC 2012). Recently, commercial natural gas production has transitioned to unconventional reservoirs (Soeder 2018) as seen in Figure 1 (Hayes 2018). Primary unconventional gas production in British Columbia is from the Montney Formation (Hayes 2018, OGC 2018) and a large part of production growth (MEM 2013) includes the extension of the Montney Formation from NEBC into Alberta (AER 2018, Davies et al. 2018). The geochemistry processes that determine gas sources are applicable to all formations in NEBC, but the combination of recent data requirements and new drilling/production activity has resulted in most of the new data being from the Montney Formation. Coalbed Methane (CBM), as an unconventional play, is fairly limited in NEBC (Hayes 2018) despite aerially extensive coal seams present in the strata. Other large unconventional natural gas plays are currently distant from gas infrastructure (Hayes 2018, Adams et al. 2016), including the Horn River sub-basin (MEM 2011), Cordova Embayment (MEM 2015), and Liard sub-basins (Ferri et al. 2017).

Table 1. Abbreviations used in thesis.

C_1 = methane CH_4
C_2 = ethane C_2H_6
C_3 = propane C_3H_8
nC_4 = butane C_4H_{10}
iC_4 = iso-butane C_4H_{10}
C_5 = all forms of pentane C_5H_{12}
C_6 = all forms of hexane C_6H_{14}
H_2S = sour gas or Hydrogen Sulphide
NEBC = North Eastern British Columbia
BC-NGA = British Columbia Natural Gas Atlas
BF-SEOS = Biogeochemistry Facility at the School of Earth and Ocean Sciences, University of Victoria
MEM = British Columbia Ministry of Energy and Mines (occ. "and Petroleum Resources")
OGC = British Columbia Oil and Gas Commission
MC = molecular composition of natural gas
ISO = stable carbon and hydrogen isotope ratios of natural gas
COTS = Commercial Off The Shelf software
WA# = OGC designated well approval number
VT = vertical well profiles
HZ = horizontal well profiles
SCVF = Surface Casing Vent Flow
ppm = parts per million
$\delta^{13}C$ = stable isotope ratio of carbon
$\delta^{2}H$ = stable isotope ratio of hydrogen
$\delta^{2}H$-C_1 = stable isotope ratio of hydrogen only in methane
‰ = per mille
BR = Bernard Ratio = $C_1/(C_2+C_3)$
Dryness = ratio of $C_1/(C_1+C_2+C_3+nC_4+ iC_4+C_5)$
WCSB = Western Canadian Sedimentary Basin
KIE = Kinetic Isotope Effect
CBM = Coalbed Methane
LNG = Liquified Natural Gas
Biogenic = products formed from organic matter
Microbial = gas created by microbial processes from organic matter
Thermogenic = gas created by temperature and pressure from organic matter

Environmental impacts of resource development are briefly included in Section 3.4 below.

This thesis interprets geochemistry data and creates profiles from the BC-NGA that will be available on the open-source Geoscience BC's Earth Science Viewer, a publicly accessible database hosted at http://www.geosciencebc.com/. The website itself does not provide any interpretation of the data. The interpretation of the data in this thesis forms the foundation to assist the decision-making process for resource development and identification of potential impacts of natural gas development on the environment in NEBC. In recent years, concerns have been raised regarding suitability and impact of the exploration and production of natural gas in NEBC. Geochemistry has the potential to assist scientific assessment of these and other concerns of methane in groundwater, and emissions to the atmosphere.

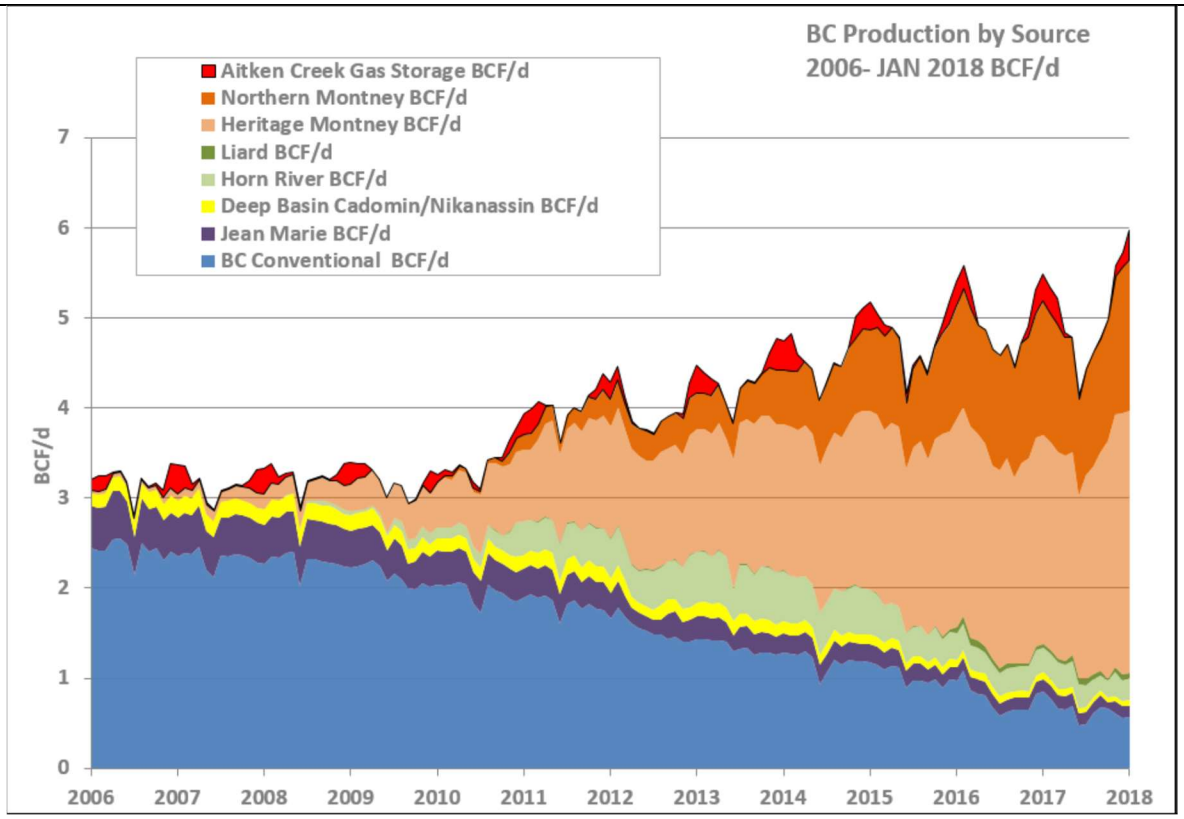

Figure 1. Trends in British Columbia gas production from 2006 to 2018 (Hayes 2018).

The BC-NGA project is sponsored by Geoscience BC and conducted through the Biogeochemistry Facility at the School of Earth and Ocean Sciences, University of Victoria (BF-SEOS) (Evans and Whiticar 2017). The BC-NGA project created the geochemistry database of natural gas occurrences in NEBC (Evans and Whiticar 2016a, Evans and Whiticar 2017, Evans and Hayes 2018, Evans in press) that is used as the basis for the characterization in this thesis. This thesis placed these geochemical data in the geologic framework already published in the British Columbia Ministry of Energy and Mines (MEM) Publication 2006-01 *Conventional Natural Gas Play Atlas* (MEM 2006a, b, c). To complete this component of the

study, extensive data validation and stratigraphic correlation was required (Evans and Hayes 2018). The thesis attempts broad geochemical interpretations of the distributions and character (Evans and Whiticar 2016b) of the various natural gases in NEBC to identify gases by play or type of emission (Evans 2018). Data from detailed vertical and horizontal geochemistry profiles from individual wells are shown here with additional analysis that are not mappable in the regional dataset. These profiles are considered to be a crucial part of the data for other users such as OGC and MEM.

The use of basic software is intentional. Using standard *Commercial Off the Shelf* software (COTS) on a personal laptop is an example for data access by everyday users. Readers should be aware that the geographic well identifier used by industry is not used in this study. The only well reference for the maps and database is the OGC designated well approval number (WA#) and there is no geographic information inherent to those well numbers. To ensure completely unbiased data analysis, not only in terms of operating company or geographic location, the WA# is the only data reference system, along with the UTM location, used here and further data description that is referenced to tables maintained by the OGC at https://www.bcogc.ca/online-services/elibrary . Further work may be needed to relate recently released geological cross-sections (e.g., Davies et al. 2018) to the BC-NGA database.

3 Background and Context

The geochemical character of natural gas is dependent on the geologic situation and history, including: composition of the source rock, reservoir rock types, burial histories, maturation, primary and secondary migration, as well as trapping mechanism in a reservoir. Although several factors ultimately determine the composition of natural gas, the organic matter type and amount in the source sediments are the most critical factors. Structural complications, including the selective removal of overburden, depressurization, and recent gas generation can also influence the ultimate natural gas composition.

Previous work on natural gas isotope geochemistry of NEBC is limited to: Norville 2014, Tilley et al. 2001, Tilley and Muehlenbachs 2006, Tilley and Muehlenbachs 2007, Tilley et al. 2011, Tilley and Muehlenbachs 2012, Tilley and Muehlenbachs 2013. These studies have graphical representation of geochemistry data from NEBC that are not captured in the BC-NGA project as there is no source data archived at OGC. Rather, in general, they show area-limited gas geochemistry with a focus on interpreting gas maturity, but the authors did not have the opportunity to relate their unpublished data to regional gas identification.

Interpretation of the initial geochemical dataset suggests that the question of geochemistry characterization based on compositional variability should be examined from two different perspectives:

1. Analytically based on different data sources (e.g., vertical profiles (VT) vs horizontal profiles (HZ), both in Appendix A; each summarized to a single point to be included in the formation by formation mapping);
2. Stratigraphically as formation by formation – this was from the creation of the BC-NGA database used for mapping (listed as MEM 2006 plays in Appendix B).

These perspectives are reflected in the data structure where Appendix A presents the profile data (both vertical and horizontal) that were not able to be transferred to the maps, and Appendix B is the map data that cannot be shown on profiles as the data is a single point in specific strata with broader geographic coverage.

The geochemical data from profiles are usually generated from mudgas samples as part of the regulatory requirements of the OGC (OGC 2015a, b, 2016). These geochemistry profiles usually reflect a vertical profile through the stratigraphic horizons penetrated during drilling. Horizontal (HZ) profiles along multi-lateral HZ legs of unconventional gas wells are also submitted as an additional profile orientation. Future work using these new HZ profiles may provide further insights into the geochemistry of the lateral character of unconventional reservoirs.

The complete dataset, as described in Evans and Whiticar (2016a), will be useful to:

- Provide baseline mapping of the geochemical conditions of NEBC's ongoing/future regions of petroleum exploration and production;
- Contribute to understanding the geologic framework of natural gas deposits in NEBC at a variety of scales from field levels to basin levels;
- Assist petroleum system models to de-risk plays by understanding and predicting generation occurrences, histories and potential productivity of natural gas in BC;

- Provide a robust baseline of gas signatures to identify and track fugitive emissions of natural gas (in groundwaters and atmosphere), e.g., to distinguish microbial vs thermogenic gases;
- Offer a geochemical catalogue for different gas sources for provenance analysis in production, well completions, processing and transport.

Beyond the characterizations presented in this thesis, future interest in the data set and website may come from increased public awareness of potential contamination issues, fugitive emissions, and supply/demand issues, such as the need for gas pipelines and Liquified Natural Gas terminals.

3.1 NEBC geology

This section briefly summarizes the geological framework and stratigraphy (Figure 2) that was presented in the first natural gas atlas *Conventional Natural Gas Play Atlas Northeast British Columbia* (MEM 2006a, b, c). NEBC is underlain by a portion of the Western Canadian Sedimentary Basin (WCSB) that stretches from Montana to the North West Territories (Mossop and Shetsen 1994). Before the Late Jurassic (Price 1994), the sediments in the WCSB were deposited in a series of rift basins, back arc basins, accretionary settings, uplifting and subsiding arches, and a passive continental margin (miogeocline of Price 1994). After the Late Jurassic (Price 1994), the sediments in the WCSB formed a series of stacked "sedimentary wedges" (Stott 1975, Jerzykiewicz 1997) tapering from thicker in the west to thinner in the east and filling a foreland basin with a mountain belt bounding it to the west. The orogenic uplift of the mountains in the west were the source of much of the younger sediments that filled the basin (Dawson et al. 1994, Jerzykiewicz 1997). These depositional cycles and changing environments are documented in various summaries (e.g., Nelson 1970, Caldwell 1975) and illustrated for NEBC in the previously mentioned atlas (MEM 2006a, b, c).

The MEM (2006a, b, c) atlas consists of a compiled summary of stratigraphic, structural, pooling, and resource descriptions for 33 natural gas plays, but there is limited geochemistry data included in the 2006 atlas. An early review of the OGC data, as part of the BC-NGA project, resulted in a recognition that a number of those plays have no data, or geochemistry analysis, or only a few points that could not support regional mapping. No public data compilations of geochemistry for NEBC, other than the BC-NGA project, are known at this time. As published, the MEM (2006a, b, c) atlas did not have more recently defined unconventional resource plays that have been added as auxiliary plays in this thesis.

It should be noted that most of the mapping in both the 2006 atlas and this thesis is on a 'play' basis, but some of the geological and stratigraphic descriptions below are based upon defined formations. This may lead to some confusion, but hopefully the annotated differences between 'play' and 'formation' make that clear. The geological settings for most formations are best summarized in the MEM (2006a, b, c) atlas, but there is no description in the atlas for the Triassic age Montney play, or for the plays in the Liard and Horn River sub-basins. An amendment (OGC 2012) to the atlas was made to describe the Montney Formation which has the majority of NEBC gas production. More recent publications (e.g., Euzen et al. 2018) have expanded the descriptions and a geochemistry volume was recently prepared for the Montney play (e.g., Moslow et al. 2018).

The Triassic age Montney Formation has a large petroleum potential (OGC 2012) in NEBC. The sediments were deposited in a complex series of incision events and stratigraphic cycles that centered around the Peace River Embayment that was created by a collapsed geological arch (Gibson 1993, Edwards et al. 1994, Wright et al. 1994). Recent geological studies including detailed biostratigraphy (Golding et al. 2015), sequence stratigraphy (Chalmers and Bustin 2012, Crombez et al. 2016, Crombez et al. 2017a), diagenesis modelling (Chalmers et al. 2012, Chalmers and Bustin 2015) and depositional modelling for organic materials (Crombez et al. 2014, Crombez et al. 2017b) have been published. More recent stratigraphic subdivisions have been proposed (Figure 3, Davies et al. 2018, Zonneveld and Moslow 2018) and may create a framework for more detailed mapping of geochemistry on a regional basis.

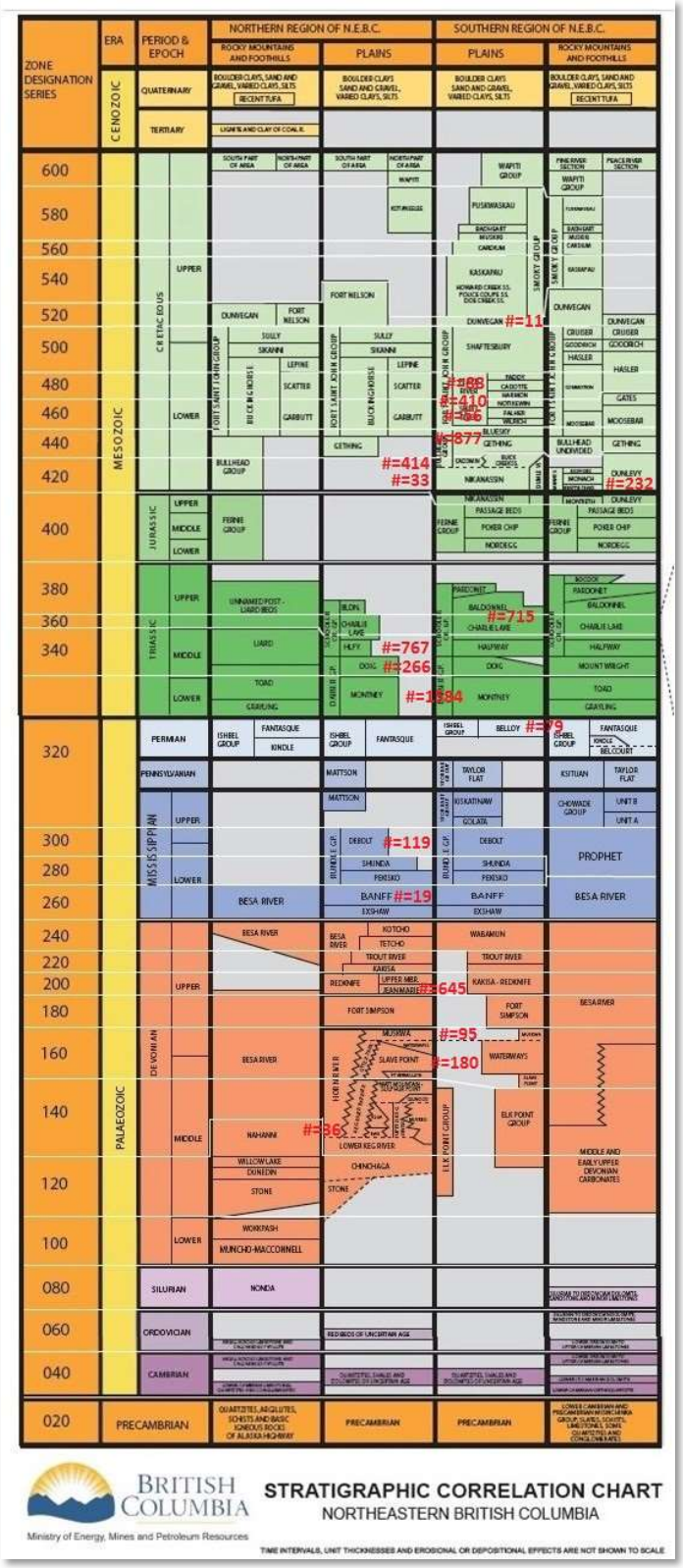

Figure 2. Revised stratigraphic chart for NEBC including sample counts (Evans and Whiticar 2016a after MEM).

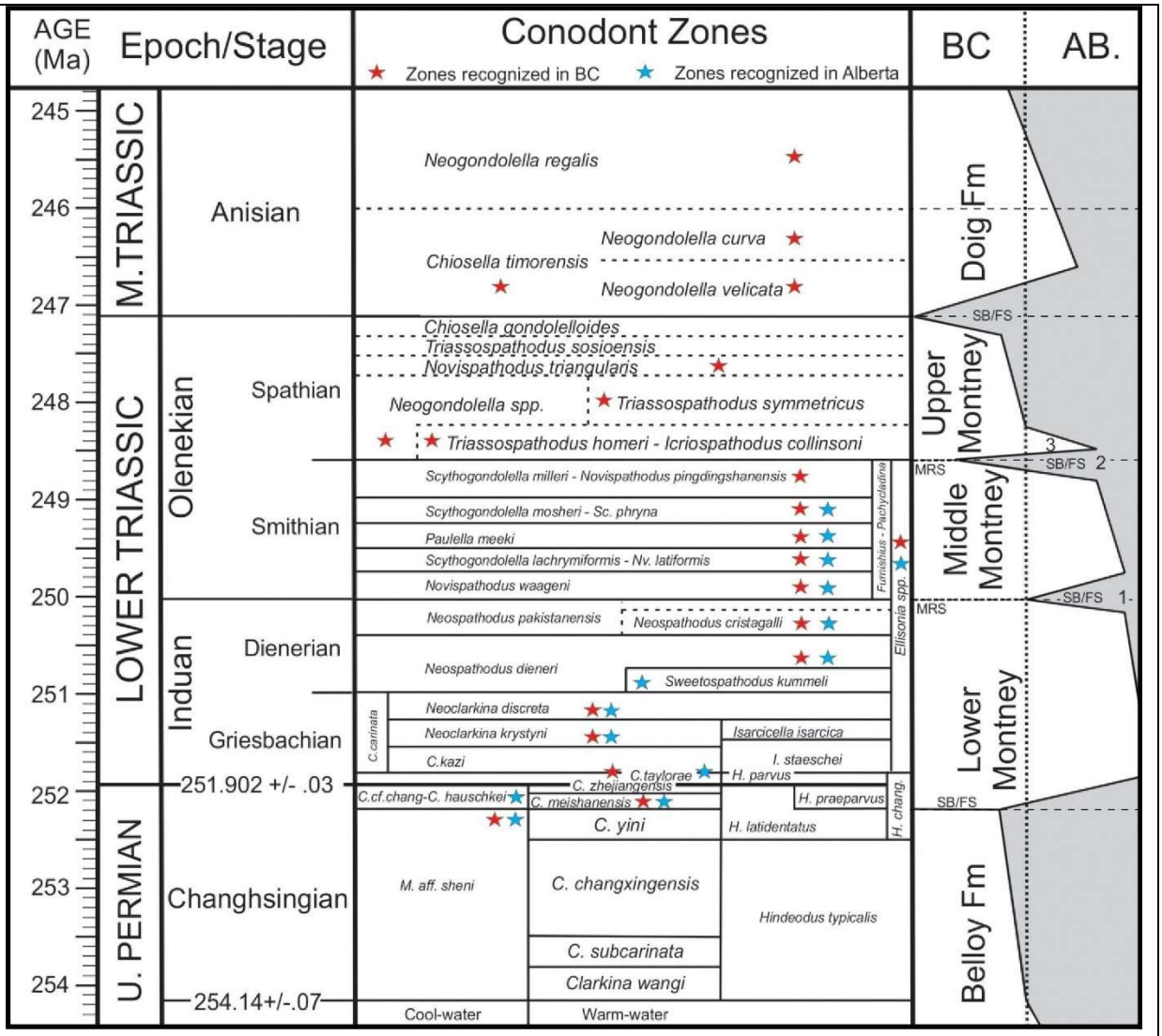

Figure 3. Montney detailed stratigraphy (after Euzen et al. 2018a).

All Triassic age formations are truncated unconformably by the Jurassic age Fernie Group, except where the younger sub-Cretaceous unconformity has downcut through the Jurassic and into the Triassic (Edwards et al. 1994). Current research is focussing on the geology and geochemistry of the Doig Formation (Silva and Bustin 2018) along with determination of new kerogen types and preliminary regional geological maximum temperature maps (Silva and Bustin 2018 figures 5 and 11 therein). Other Triassic formations are known for their oil reservoirs (e.g., Baldonnel and Halfway formations, Gibson 1993) and sour gas (H_2S, e.g., some members of the Charlie Lake Formation, Edwards et al. 1994). The other formations are referred to in the MEM (2006a, b, c) atlas.

The formations in the Horn River (OGC 2014) and Liard sub-basins are not clearly listed in the MEM (2006a, b, c) atlas and are briefly described here for completeness. Detailed subsurface mapping has identified a Paleozoic stratigraphic interval along the Devonian age shelf edge (Edwards et al. 1994). Previous work on the hydrocarbon potential of these sub-basins has been limited (Moore 1993). More recent publications on the Horn River sub-basin (MEM 2011), Cordova Embayment (MEM 2015), and Liard sub-basins (Ferri et al. 2017) have addressed the 'shale' gas potential that had little mention in previous MEM publications (MEM 2011, MEM 2015, Adams et al. 2016). The unconventional gas target formations of the Liard and Horn River sub-basins are the Devonian age Evie, Otter Park, and Muskwa (Figure 4, Oldale and Munday 1994) as deposited in the "Northern Starved Basin" (Moore 1993). The Muskwa Formation was probably the source for the Jean Marie gas reservoirs (Ferri and Griffiths 2014). These Devonian shales outcrop in the foothills disturbed belt (Rocheleau et al. 2014, Grasby et al. 2016b, NEB 2016), further to the west, but there is even less geochemical data in the foothills than in the Liard sub-basin.

As a result of exploratory drilling, more detailed formation descriptions have been published (OGC 2014, Norville 2014, Dong 2016, Dong et al. 2015, Dong et al. 2017, Ayranci et al. 2018). Detailed core analysis for geochemistry (Dong et al. 2016) focussed on the mineralogy and geomechanics (Dong 2016), but did not have molecular composition or isotope data.

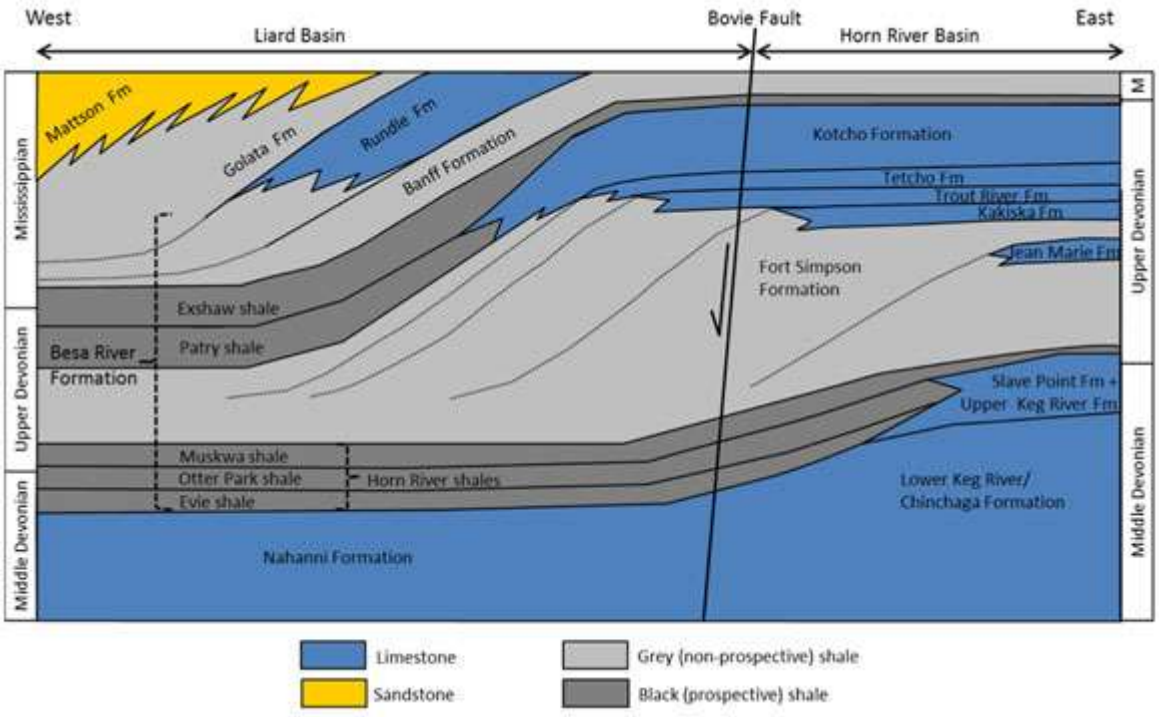

Figure 4. Generalized stratigraphy of the Horn River and Liard sub-basins (NEB 2016).

The regional geological setting for the Horn River and Liard sub-basins is that of a transgressive depositional environment followed by high temperature burial and later normal faulting (Wilson and Bustin 2018). The Bovie fault dropped the western portion into the Liard sub-basin, which extends

northwest into Yukon and Northwest Territories a short distance (NEB 2016, Ferri et al. 2017, Fiess et al. 2013, Rocheleau et al. 2014). Drilling data (Currie et al. 2014 figure 1 therein) is far less available than in the Horn River (Wilson and Bustin 2018). Preliminary geochemistry studies suggest that there is equivalent maturity in both the Liard and Horn River sub-basins (Wilson and Bustin 2018) shown by preliminary maps of vitrinite reflectance and gas chemistry (Wilson and Bustin 2018 figures 7 and 12 therein). The Liard sub-basin has additional potential hydrocarbon resources in younger Cretaceous strata (Ferri et al. 2017, Ardakani et al. 2017).

3.2 Geochemistry: Molecular and Isotope Composition

The characterization of natural gas composition falls within the larger category of petroleum systems analysis that incorporates all hydrocarbons and associated fluids into a holistic geologic framework. Hydrocarbon geochemistry has a long history of interpretation (e.g., Van Krevelen 1961, Stahl 1977, Tissot and Welte 1984, Rashid 1985, Hunt 1996, Killops and Killops 2005) of various aspects, from oil migration to methane generation, (reviewed in Galimov 2006, Vinson et al, 2017). Most of these studies are based on the assumption that the generated petroleum is compositionally correlated to its source despite interference through geologic time and interacting processes.

All strata in NEBC contain organic material that is the source for most, if not all, of the natural gases present. In this thesis, these gases are termed 'biogenic', as they are ultimately sourced from organic matter, regardless of whether the gas formation involves microbial or thermogenic mechanisms. This is in contrast to 'abiotic' gases that do not involve organic matter transformation processes (Etiope and Sherwood Lollar 2013). Abiotic gases are assumed to be of low importance in this sedimentary basin (e.g., Jenden et al. 1993) and not discussed further. Traditionally, the term 'biogenic' in the petroleum industry has been used to refer only to gas produced by microbial activity (bacteria or methanogens). This thesis follows the more recent and accurate designation of this microbial type of biogenic gas as 'microbial' gas. 'Thermogenic' gas is also a sub-category of biogenic gas, separate from the microbial sub-category, and is formed by the thermocatalytic transformation of organic matter at elevated temperatures (>70 °C) over time (>10^7 yr).

The dominant components of natural gas are the normal and branched alkanes: methane, ethane, propane, normal butane and isobutene (abbreviated as C_1, C_2, C_3, nC_4, iC_4, defined in Section 2). Other gases, such as pentanes (C_5), carbon dioxide (CO_2), hydrogen sulfide (H_2S), hydrogen (H_2), unsaturated hydrocarbons (alkenes) and noble gases (He, Ar, etc.) can comprise variable, but generally minor amounts in natural gases (data is included in the BC-NGA project database, but not discussed here). The molecular composition (MC) of the natural gas is often reported as various ratios of the hydrocarbons, either as molar ratios or a relative percentage or parts per million (ppm) by volume. The chosen unit for this thesis is ppm and volume is implicit by gas molar fraction.

In addition to the molecular composition, natural gases can also be characterized by their stable carbon ($^{13}C/^{12}C$) and hydrogen ($^{2}H/^{1}H$) isotope ratios of the hydrocarbon in concert with those of water and/or CO_2. The isotope data are reported using the conventional stable isotope delta notation, (McKinney et al., 1950), i.e., $\delta^{13}C$, $\delta^{2}H$:

$$\delta X\ (‰) = (R_{sample}/R_{standard} - 1) \bullet 1000 \qquad \text{(Eq. 1)}$$

where $\delta X = \delta^{13}C$ or $\delta^{2}H$ and $R = {}^{13}C/{}^{12}C$ or ${}^{2}H/{}^{1}H$, respectively, and are reported relative to the Vienna PeeDee Belemnite (VPDB for $\delta^{13}C$) and Vienna Standard Mean Ocean Water (VSMOW for $\delta^{2}H$) scales.

In this thesis, the stable carbon isotope ratios and, less frequently, the hydrogen isotope ratios, of the hydrocarbons are collectively referred to as the 'ISO' data.

This thesis will focus on the concept of natural gas characterization by geochemistry analysis (e.g., Craig 1953, Sackett et al. 1965, Sackett 1968, Stahl 1973, Barnes and Goldberg 1976, Fuex 1977, Stahl 1977, Eadie et al. 1978, Redding 1978, Sackett 1978, Wong and Sackett 1978, Chung and Sackett 1979, Stahl 1979, Redding et al. 1980, Schoell 1980, Barker and Fritz 1981, Rice and Claypool 1981, Holmes et al. 1981, Schoell 1983, Faber and Stahl 1984, Schoell 1984, Berner and Faber 1988, Galimov 1988, Schoell 1988, Clayton 1991, Jenden et al. 1993, Whiticar 1994, 1996, 1999, Berner and Faber 1996, Sackett and Conkright 1997, Prinzhofer and Battani 2003, Galimov 2006, Etiope et al. 2009, Prinzhofer et al. 2009, Cheung et al. 2010, Prinzhofer et al. 2010, Strąpoć et al. 2011, Golding et al. 2013, Prinzhofer and Deville 2013, Hamilton et al. 2014, Kotarba et al. 2014, Curiale and Curtis 2016, Humez et al. 2016b).

There are a number of secondary processes that impact the molecular composition (MC) and isotope ratios (ISO) of thermogenic natural gases, which, in turn, can complicate the geochemical classification. A major secondary process is the admixture of microbial gas to thermogenic gas, which can dramatically change the geochemical composition of the former (Whiticar 1996, 1999, Kempin 2012, Curiale and Curtis 2016, Niemann and Whiticar 2017). Microbial gas is formed under strict anaerobic conditions via 3 possible methanogenic pathways, i.e., acetoclastic/acetotrophic, hydrogenotrophic, and/or methylotrophic methanogenesis (e.g., Whiticar 1999, Strąpoć et al. 2011, Vinson et al, 2017). Methanogenesis is associated with large kinetic isotopic effects that result in ^{13}C-depletions relative to the precursor substrates and $\delta^{13}C_1$ of ca. -50 ‰ to -112 ‰ (Whiticar 1999). This contrast with the more ^{13}C-rich methane in thermogenic gas, i.e., $\delta^{13}C_1$ of ca. -45 to -35 ‰. Based on this, data from NEBC has been quickly assessed in error to be all thermogenic.

The industrial production of CBM usually results in early production MC being almost pure methane due to the desorption effects of releasing methane preferentially before other gas molecules, especially CO_2 (Clarkson and Bustin 2000). Isotopic composition shifts with time for CBM (Niemann and Whiticar 2017). The other isotope effects are described in other summaries (Strąpoć et al. 2011, Golding et al. 2013, Vinson et al. 2017). The timing of gas generation is complicated due to the shift from microbial methane early in the burial of the depositional system, to thermogenic gas generation associated with maximum burial and temperature, and later microbial gas generation from meteoric input of nutrients and/or biodegradation. The concept of continental glaciation affecting stratigraphy in Canada has been extrapolated to the hydrological conditions (Grasby 2013) and thus another factor unique to Canadian shale plays needs to be considered in ISO characterization.

In order to further understand the geochemistry of the natural gases, the review of various ratios comparing molecular composition and isotope data using interpretive plots is common. The concept of multivariate analysis has attained some level of complexity (e.g., Skuce et al. 2014), but 3 axes displays of multiple components (e.g., Whiticar 1994) have not really been widely used. As a result, for this thesis the types of diagrams used as templates for the characterization of the geochemistry data are a series of 2D plots previously published (e.g., Whiticar 1999). The first plot, the Bernard Diagram (Figure 5), specifically is a combination of $\delta^{13}C_1$ and the Bernard Ratio:

$$\text{Bernard Ratio (vol.)} = C_1 / (C_2 + C_3) \qquad \text{(Eq. 2)}$$

and the second plot, the CD Diagram (Figure 6), is a combination of $\delta^{13}C_1$ and $\delta^{2}H\text{-}C_1$ (e.g., Whiticar 1994). These plots are used to characterize the various types of methane in context of the theoretical thermal maturity pathways from different source kerogens initially having longer chain hydrocarbons and being altered through: 1) either microbial or thermogenic pathways to the gas composition in the

reservoir (Whiticar 1999), 2) interpret a combination of both those pathways plus the secondary effects such as oxidization or fractionation (Whiticar 1994). Other interpretive ratios and plots are mentioned in the discussion, but the only other MC plots extensively used involve the ratio between the 2 forms of butanes (iC_4/nC_4):

$$iC_4/nC_4 \text{ Ratio (vol.)} = iC_4 / nC_4 \quad \text{(Eq. 3)}$$

and gas 'dryness':

$$\text{'dryness'} = C_1 / (C_1 + C_2 + C_3 + iC_4 + nC_4 + \text{total } C_5) \quad \text{(Eq. 4)}$$

These 2 ratios have been used to express how microbial processes: a) consume the different forms of C_4 at different rates (Hunt 1996), b) increase the relative proportion of higher hydrocarbons (Whiticar 1994), c) have minimal C_2 and C_3 generation (Whiticar 1999). Other minor gases in natural gas are often in trace amounts, and their isotopic data are rarely captured. The samples are described in Section 4.

The sources of microbial gas admixed to the thermogenic natural gas in NEBC can be either 'relic' microbial methane formed in the low temperature soils or sediments, or post-depositional at later stages. The latter can be generated from either lacustrine or marine depositional environments (e.g., Davies et al. 2018) of Type I or II kerogens as organic material that has been preserved in the rock record (Rashid 1985), or terrestrial organic material of Type III kerogens of coals and coaly material (e.g., Strąpoć et al. 2011, Golding et al. 2013, Niemann and Whiticar 2017, Vinson et al. 2017) in coalbeds (Dawson et al. 2000) associated with many of the hydrocarbon bearing strata in NEBC. The mechanisms of generating natural gas from the organic compounds in those environments is well documented (e.g., Tissot and Welte 1984, Rashid 1985, Killops and Killops 2005). The theoretical and modelling systematics are also well documented (e.g., Berner and Faber 1988, 1996, Whiticar 1994, 1996, 1999, Galimov 2006) and provide the basis of the characterization strategy used in this thesis for the thermogenic natural gas accumulations in the NEBC study area.

3.3 Geochemistry: Interpretive Approaches

To answer the question in Section 1, geochemical approaches are used by many authors to identify natural gases, plus the association with other reservoir fluids such as petroleum and reservoir water within the geological framework. Only gas data are available from the BC-NGA project. The first concern is if the samples collected are representative of the natural gas in the play. Some samples are not primary, i.e., they have undergone secondary alteration after sampling. For example, the gases maybe from a contaminated gas stream or have effects from storage (i.e., heating, oxidation, or microbial activities). Discussion in Section 7.1.1 illustrates some basic plots to assist in identifying gas samples that may have been secondarily altered.

Geochemical interpretation is based upon the commonly-used Bernard Diagram (Figure 5, based on ratios described in Section 3.2) and CD Diagram (Figure 6, Whiticar 1990, 1994, 1999). These diagrams focus on natural gas source typing with distinction between microbial and thermogenic gases.

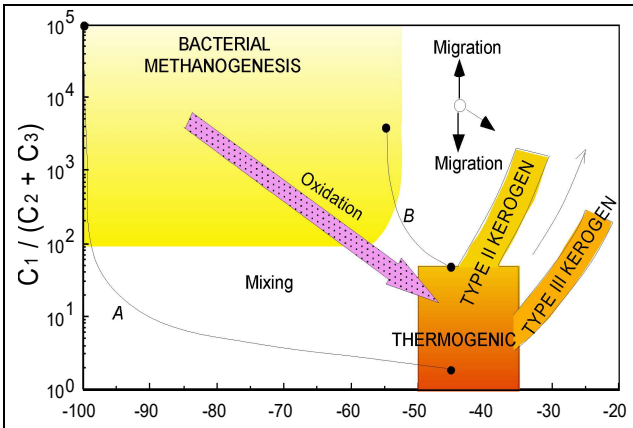

Figure 5. Template for Bernard Diagram (Whiticar, 2018 pers. comm., after Whiticar 1999).

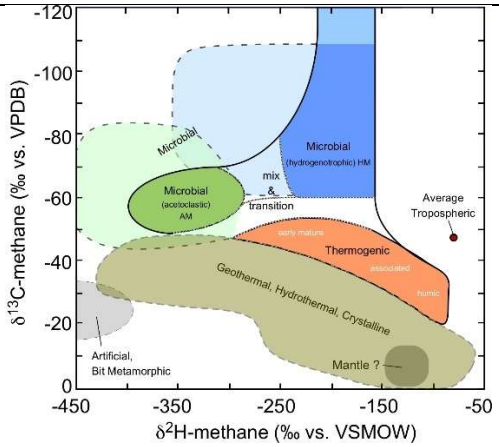

Figure 6. Template for CD Diagram (Whiticar, 2018 pers. comm., after Whiticar 1999).

In addition, I added the Berner-Faber Diagrams of $\delta^{13}C_1$ vs $\delta^{13}C_2$ (Figure 7) and $\delta^{13}C_2$ vs $\delta^{13}C_3$ (Figure 8, Whiticar 1990, 1994, 1999) and included Type II and III kerogen lines (after Berner and Faber 1988, 1999) plus the thermal maturation of the kerogen. The Berner-Faber Diagrams serve as a better characterization plot as shown in Section 7.6 and relate the gas to the kerogen type.

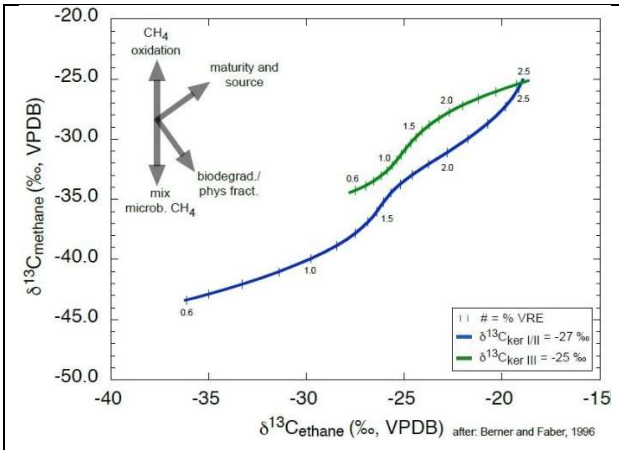

Figure 7. Template for $\delta^{13}C_1$ vs $\delta^{13}C_2$ diagram (Whiticar, 2018 pers. comm., after Berner and Faber 1996).

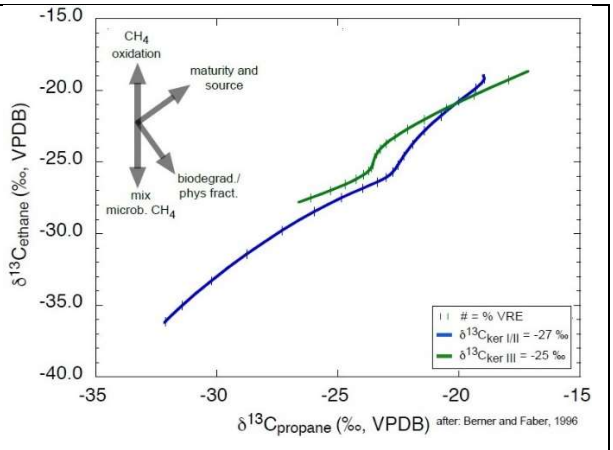

Figure 8. Template for $\delta^{13}C_2$ vs $\delta^{13}C_3$ diagram (Whiticar, 2018 pers. comm., after Berner and Faber 1996).

The inclusion of the plot $\delta^{13}C_2$-$\delta^{13}C_3$ versus molecular ratio of C_2/C_3 ('Lorant Diagram', Figure 10, Prinzhofer and Battani 2003) enhanced the interpretation of petroleum system processes along with a plot of molecular ratios C_2/C_3 versus C_2/iC_4 ('Prinzhofer Diagram', Figure 9, Prinzhofer and Battani 2003) as an approach to further distinguish between microbial and thermogenic gases.

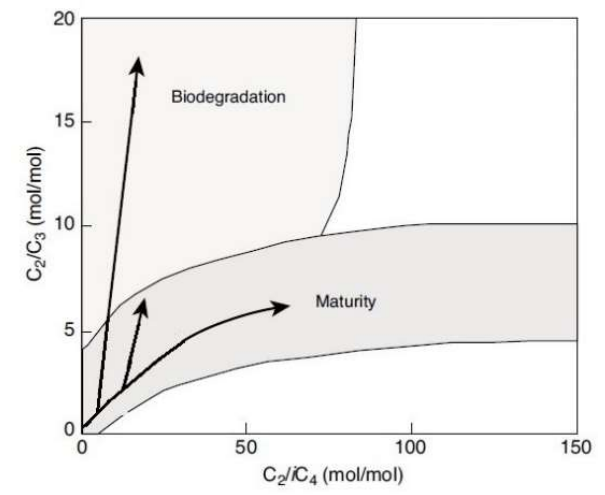

Figure 9. Template for Prinzhofer Diagram (Prinzhofer and Battani 2003).

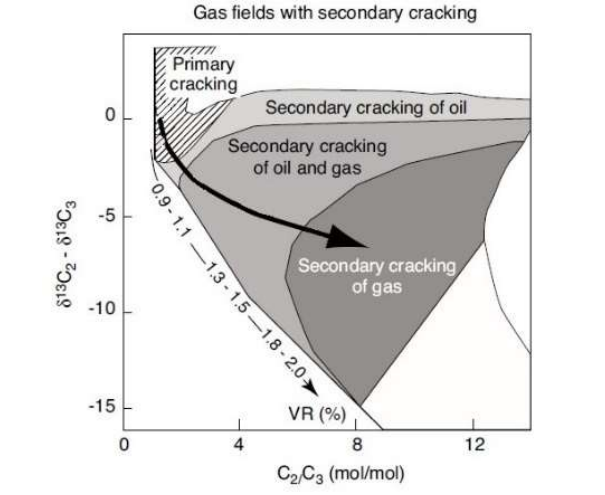

Figure 10. Template for Lorant Diagram (Prinzhofer and Battani 2003).

Although the use of carbon isotope data on carbon dioxide can be useful in some instances to characterize natural gases (Whiticar 1999), data exists for only one well profile (WA#32990, Figure 49). The CO_2 plot is very instructive in determining the types of microbial processes preserved in the few samples with that analysis.

Mudgas samples for geochemistry (Whiticar 1994, Ing 2015, Tilley and Muehlenbachs 2006, 2007, 2012, 2013, Tilley et al. 2001, Tilley et al. 2011) have been described as baseline data for determining sources of fugitive emissions (Rowe and Muehlenbachs 1999), but mudgas geochemistry data can also be applied to a number of other purposes described in Section 2. Mudgases are collected from the drilling mud while the well is being drilled and can serve as a proxy for the natural gas chemistry of the formation being drilled at the time. The characterization of isotope data from mudgases is the primary basis for the OGC regulations mentioned earlier. Mudgas sampling is generally contaminated by the circulation of air and drilling fluids down the wellbore. This contamination during sampling will dilute the true 'in-place' gas in the well, thereby strongly influencing the actual mole fraction of the hydrocarbons based on the total gas present. In some cases, this can be resolved by using comparative ratios (i.e., using normalized abundances to account for the contamination) rather than absolute ratios of composition by ppm. Further discussion on data selection in this category is in Section 4.1.1.

Noble gases, mixing models, clumped isotopes, and radiogenic isotopes can also augment natural gas interpretations (e.g., Hunt 1996 p.53, Etiope and Sherwood Lollar 2013, Stolper et al. 2014a, b, 2015, Douglas et al. 2016, Douglas et al. 2017, Shuai et al. 2018, Webb et al. 2017, Young et al. 2017). Unfortunately, these data are not collected routinely in NEBC.

3.4 Environmental gas geochemistry applications

It has been suggested that drilling activity by the natural gas industry leads to environmental groundwater concerns (Cheung et al. 2009, Cheung et al. 2010, Hakala 2014, Vengosh et al. 2014, Rice et al. 2018, Soeder 2018), including NEBC (Nowamooz et al. 2015). In addition, it has been demonstrated that the production of natural gas contributes to greenhouse gas budgets (Merritt et al. 1995, Etiope et al. 2008, Schwietzke et al. 2017, Townsend-Small et al. 2016) including methane leakages (e.g., Rivard et al. 2014, Hakala 2014, Ing et al. 2014, Skuce et al. 2014, Ing 2015, Humez et al. 2016a). These contributions are commonly in the form of well-site emissions, but also include pipeline emissions (e.g., Karion et al. 2015, Lamb et al. 2015, Marchese et al. 2015, Lavoie et al. 2017, von Fischer et al. 2017). Well-site emissions can include from a vent required by regulations on the surface casing of the well, (listed as Surface Casing Vent Flow, SCVF), or fugitive emissions from outside the wellhead, commonly referred to as bubbling or "gas migration" (Bachu 2017) and "bubble gas" in the lab reports. These well and pipeline emissions have previously been claimed to be much worse than predicted (Atherton et al. 2017, Johnson et al. 2017) and current research is ongoing to better determine emissions by aerial sensing (Whiticar et al. 2018).

World-wide concerns relating to the emission of gases during exploration and production have focussed on three primary areas: 1) fracturing/stimulation operations (e.g., Botner et al. 2018, Barth-Naftilan et al. 2018), 2) casing failure (Davies et al. 2014), or 3) lack of remediation of wells that have been abandoned (e.g., Kang et al. 2014, 2016, Boothroyd et al. 2016, Townsend-Small et al. 2016). There are many previous studies on SCVF from various areas of petroleum production in Canada (Kempin 2012, Rivard et al. 2014, Bachu 2017 [updating Watson and Bachu 2009]). Studies in Alberta show gas migration has occurred from immature shallow Colorado Group shales (Rowe and Muehlenbachs 1999), glacial till (Hendry et al. 2017a, b), and shallower coals (Humez et al. 2016b). These sources are not related to natural gas production activities, but rather from microbial sources. The geochemistry of the sources of shallow methane, however, is complex (Hakala 2014) and enhanced characterization of provenance could benefit from: 1) noble gas analyses such as Neon / Xenon (Darrah et al. 2014, Darrah et al. 2015), 2) radiocarbon (^{14}C) studies (Botner et al. 2018), or 3) clumped isotopic ratios (Stolper et al. 2014a, b, 2015, Douglas et al. 2016, Douglas et al. 2017, Shuai et al. 2018, Webb et al. 2017, Young et al. 2017). The latter analyses have data requirements (Ono et al. 2014) that are not currently included in BC-NGA data, but could be informative in further studies.

Resolving the uncertainty between water well testing for "lighter" isotopes (Taylor et al. 2000) and oil and gas well isotopes (Humez et al. 2016a) relies on a geographically widely distributed sample set. It is the concerns about atmospheric emissions and also possible contamination of local groundwater in western Canada (Cheung et al. 2009, Cheung et al. 2010) that have led to the use of a "natural gas fingerprint" (Rowe and Muehlenbachs 1999, Tilley et al. 2001) to identify gas sources and correlations. Research in NEBC to characterize fugitive gas emissions and the groundwater isotopes is currently under study (Cahill et al. 2018).

4 Samples, Methods, and Data

Gas samples from the petroleum industry were collected by different operating companies (mudgas on three wells and production gas from twenty wells) and sent to BF-SEOS for MC plus ISO analysis and is described in Section 4.3. The data collected as new data specific to the BC-NGA project are listed in Table 2 of Section 5. Other data were obtained directly from the OGC web site but have not been reported as a consolidated database prior to this thesis. Data previously released as individual reports are added to Sections 6.1 and 6.2. The study included the evaluation for mapping of more than 14,000 OGC records for previous MC analysis on production gas (see Section 4.1).

4.1 Open Source (Public) Data

The BC Oil and Gas Commission (OGC) is the primary source of the natural gas data summarized by the BC-NGA project and used in this thesis. All the data submissions are archived on the OGC web-site https://files.bcogc.ca/thinclient/Login.aspx. All data generated by the BC-NGA project, as described in Section 5, are public data available through the OGC. In order to access the data, users must know the WA# (well application number defined in Section 2). A map view of the data elements is available online from the OGC at:
https://data-bcogc.opendata.arcgis.com/datasets/9149cb556e694617970a5774621af8be_0/data and details of further data access are posted on the main OGC web-site. Public usefulness of the data is facilitated by providing the basic characterization plots provided in this thesis. Another part of the need for open source use of the data is the direct visualization of the raw data by those with access to COTS software, e.g., a spreadsheet program with graphing capabilities. All of the figures created for this thesis as profiles and interpretive plots were made with Microsoft Excel™. All of the data can be downloaded from the OGC file library and visualized directly using a COTS laptop computer.

The OGC https://www.bcogc.ca/ is a public regulatory commission, with data collection and dissemination as part of its mandate. Manual sorting of the data was required because, although industry data since the 19th century is available, usable geochemistry data has only recently been available from NEBC since the use of GC-CF-IRMS starting before 1988 (Tilley 1988). The other constraint is that very recent data are still held confidential by the OGC for a time period prescribed by regulations ranging from weeks to years. The OGC also retains samples of rock (core and chips) collected during drilling, and additional data of rock properties, such as kerogen and/or pyrobitumen stable isotopes, could be generated from analysis of those samples.

4.1.1 Data validation process

Mudgas sampling is generally contaminated by the circulation of air and drilling fluids down the wellbore. This contamination during sampling will dilute the true 'in-place' gas in the well, thereby strongly influencing the actual mole fraction of the hydrocarbons based on the total gas present. In some cases, this can be resolved by using relative rather than absolute ratios, i.e., using normalized abundances to account for the contamination. These relative compositional ratios of hydrocarbons can be more representative of the in-situ composition. However, they cannot be used when the drilling mud has additives, which can introduce contaminating hydrocarbons (e.g., 'invert mud' that can contain propane, butane, pentane, etc.). Similarly, a sample that is collected from a well after a well stimulation that includes hydrocarbons (e.g., 'propane frac') typically has highly contaminated hydrocarbon compositional ratios, deeming them unsuitable as a representative sample. Mixing of production gas can also present a serious issue, especially where gas flow from different wellbores and formations are commingled before the sampling point (e.g., the 'metering station').

Microbial activity can sometimes occur in samples where natural or introduced microbes activate or reactivate with changing geochemical conditions (e.g., changes in water, nutrients, or redox conditions). Some samples could be affected by microbial activity during storage. This can be seen in core samples or chip collection where the material is stored in desorption canisters for extended periods of time at reservoir temperatures.

Biodegradation can affect natural gas during sample storage and cautions are mentioned (e.g., Hendry et al. 2017b) to ensure that oxidation of methane, if it occurred in the sample containers, is accounted for. Figure 11 shows the plot of C_1 (methane) ppm vs C_2 (ethane) ppm for all profile datapoints in the BC-NGA project.

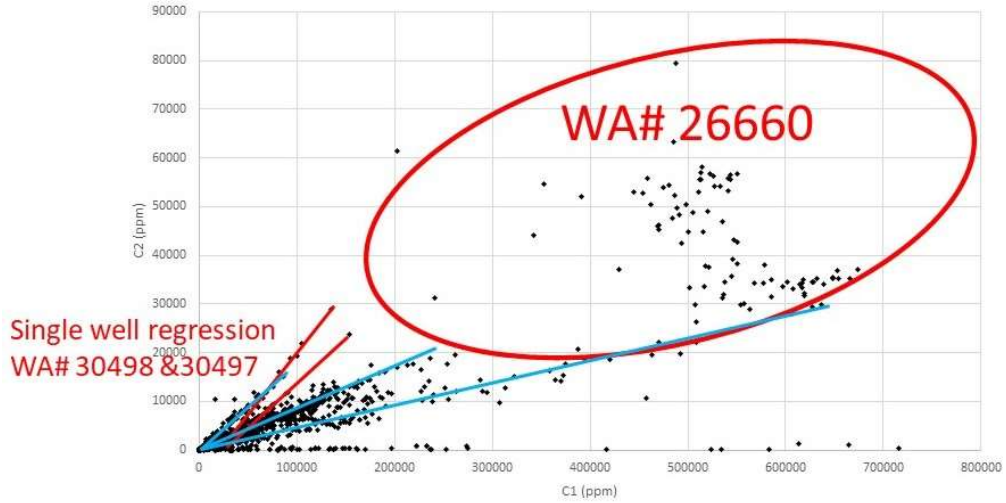

Figure 11. Plot of C_2 (ppm) vs C_1 (ppm) for all profile data (OGC+BF-SEOS) with highlighting for anomalies.

A reasonably constant ratio for C_1 (ppm) vs C_2 (ppm) that fit to 3 main trend (blue) lines indicates that there is no unusual gas contamination. Exceptions to these trends are 2 other linear trends for WA#30498 and its twin WA#30497 that were deemed to be internally consistent and retained as valid data. WA#26660 was the other exception with a non-linear scatter indicating contamination. This well had no isotope data and was excluded from this study.

Using the data from the BC-NGA project has some data legacy as filtering multiple data reducing to one location was required for mapping. Some of the filtering was to create a time series that is not discussed here, but other filtering is the selection of the most representative data for each location. This process will be re-evaluated as the BC-NGA project continues, but it skews the MC dataset used in this thesis. After BC-NGA project determined that the sample is representative by having consistent internal trends in gas contents seen on plots, other plots are used to determine if the gas source is microbial or thermogenic with a confirmation that it is not abiotic as mentioned in Section 3.2. The most common diagnostic tool (e.g., Etiope and Sherwood-Lollar 2013) for this determination is the CD Diagram (Figure 6, modified after Schoell 1983). Changes from kerogen to gas with different conditions of microbial or thermogenic activity (e.g., Tissot and Welte 1984, Rashid 1985, Hunt 1996) are also often expressed by the Bernard Diagram (Figure 5, Evans and Whiticar 2016a). As can be seen in Sections 7.3 and 7.4, the Bernard and CD Diagrams were initially confusing until other plots such as the $\delta^{13}C_1$ vs $\delta^{13}C_2$ plots (after Berner and Faber 1988, 1996) were added to the interpretation.

4.2 Well Configuration and Data Structure

An important question in the thesis is how best to represent the new data type sourced from directional drilling. One limitation to COTS software is that it does not necessarily handle sophisticated data concepts – a data *point* is a single 3D X/Y/Z location plus a time stamp (becoming 4D that will be summarized in future publications and is not included here). The configuration of the analytical reports archived by the OGC for unconventional production in the oil and gas industry involves data *segments*. Most common of the data types is a segment of a stimulated (e.g., 'frac-ed') horizontal (HZ) well bore as an 'open tunnel of data collection' drilled sideways through the reservoir, often in multiple directions from a 'motherbore'. For production gas testing the whole interval of the HZ completion is treated as a single sample. The vertical (VT) borehole or 'motherbore' is most commonly viewed as the well profile as it intersects columns of other strata before turning to a HZ configuration, but it almost never has gas production assigned to the VT section. Radial HZ multi-lateral wells (imagine an upside-down umbrella with the fabric removed) are becoming rare, being replaced by recent completions by industry are with long HZ legs running parallel to each other like the tines of a fork bent perpendicular to the vertical fork handle, which represents the 'motherbore'. Figure 12 depicts this form of data representation. Presenting that 3D configuration on a map means that some vertical aspects are hidden and a flat 2D profile can be either a horizontal graph or a vertical graph that will not show the well curvature and other deviations. Unless the user has access to petroleum industry software, which can be both expensive and complicated, the results of data display will be necessarily be simplified.

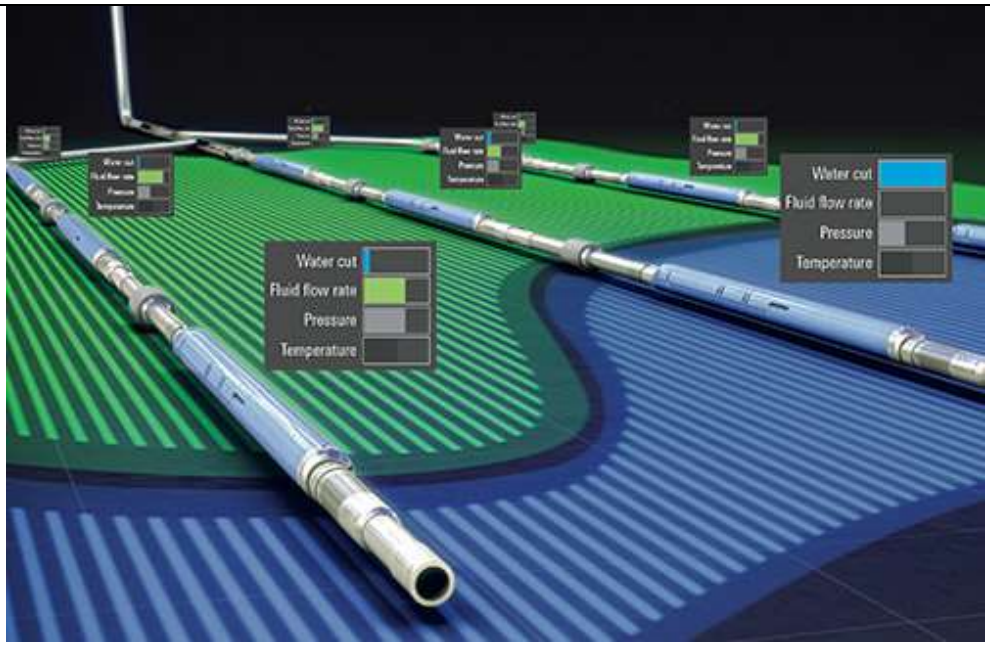

Figure 12. Schematic representation of data collection in a HZ multi-lateral well – from slb.com.

These data constraints result in each map data point in this thesis represents a number of subsurface data segments called HZ laterals, each with its own WA# and often stretching kilometers from the surface location that is the map point. The data are collected vertically through many layers of strata along a VT column, then turning through a radius to a HZ row of data suspended in a portion of a rock layer below the VT segments.

The regional database is constructed around a well location that is the surface hole X/Y coordinates plus the Z as the measured depth (MD on the profiles) down the wellbore path irrespective of deviations to the top of the testing segment. This is not the true geospatial location as that needs to be calculated from the well elevation and deviation survey. In addition, the thickness of the test interval and/or bottom depth/location needs to be factored in to determine the location centroid. More detailed queries to locate specific data at sub-kilometer specific locations, should be referred to the well survey reports held by the OGC. The samples collected as mudgas, which is the gas exsolved from the circulation fluids during the drilling activities, is usually assumed to have a small thickness where the bottom depth is very close to the top depth. The data category is the only one that usually cannot have a time series of multiple tests at the same location. Other types of data can test multiple intervals of different thicknesses multiple times over a span of days or years.

4.3 Gas Sample Submission processes and Analytical Methods

For gas samples submitted to BF-SEOS, only sweet gas intervals were sampled by the operating companies and issues with shipping the toxic gas H_2S to BF-SEOS were avoided. As the category of wells requiring sampling by the regulations for ISO analysis was limited in number over the past three years, the project scope was expanded to include natural gas from commercial production activities (usually called 'production gas'). Only a few of these samples had minor H_2S composition. The usual HAZMAT shipping procedures were adhered to and the samples were stored in a secure safety facility for hazardous gases.

The analytical procedures to generate the MC and ISO data are described in the reports submitted by BF-SEOS. The analytical procedure for the stable isotope ratio measurements, known as Compound Specific Isotope Analyses (CSIA, Hayes et al. 1989, Brand et al. 1994, Jochmann et al. 2006) or Gas Chromatography Combustion Isotope Ratio-Mass Spectrometry (GC-C-IRMS; Merritt et al. 1995, Whiticar and Eek 2001). (Figure 13) illustrates the basic analytical procedure for $^{13}C/^{12}C$ measurements by Continuous Flow Isotope Ratio-Mass Spectrometry (CF-IRMS).

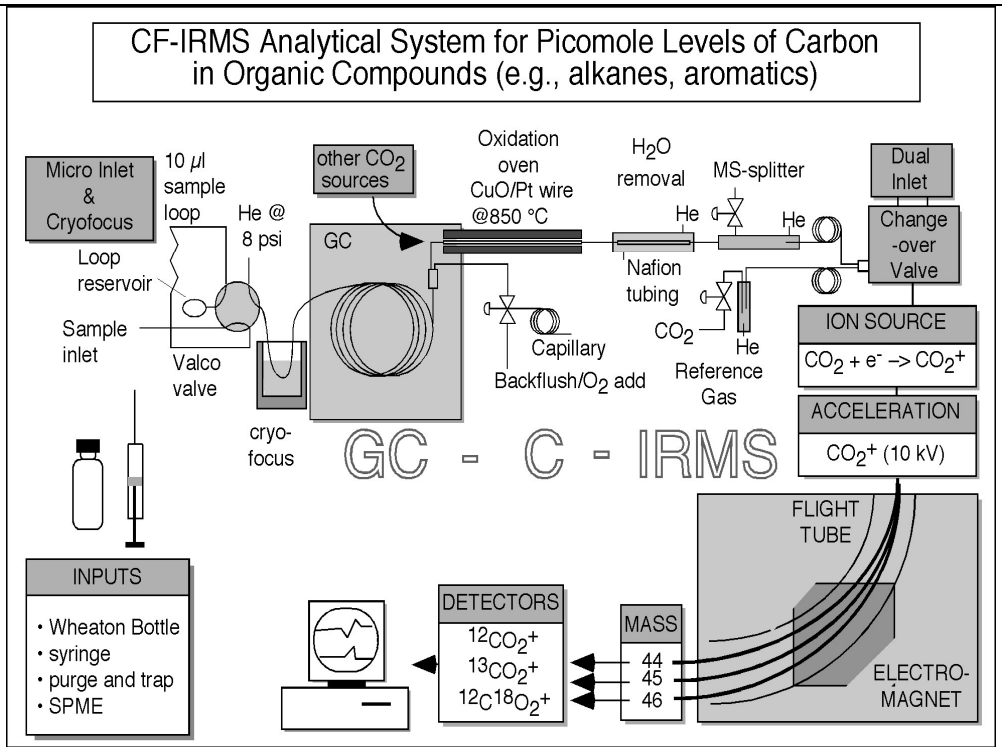

Figure 13. Schematic diagram for $^{13}C/^{12}C$ measurements by Continuous Flow Isotope Ratio-Mass Spectrometry (CF-IRMS) from Standard Operating Procedure, BF-SEOS reports (Whiticar and Eek 2001).

The samples are analyzed for light hydrocarbon molecular composition 'MC' by injection into a Gas Chromatograph with Flame Ionization Detection to obtain C_1, C_2, C_3, nC_4, iC_4 abundances (relative mole fractions as ppm C_1-C_4 hydrocarbons). The stable isotope ratio measurements are made by CF-IRMS where the gas mixture in the sample is carried by helium through a gas chromatograph column to partition the compounds. This is followed by combustion in an oxidation oven with combination of copper oxide / platinum wires at 870 °C. This combustion quantitatively oxidizes the hydrocarbon gases to the products carbon dioxide and combustion water for each gas species eluting sequentially from the gas chromatograph column. The combustion water is removed by a Nafion™ trap and the combustion carbon dioxide is inlet on-line to the IRMS where the isotopologues (molecular masses of 44, 45, and 46) from each hydrocarbon species are separated and individually quantified (e.g., Whiticar and Eek 2001).

After completion of sample analysis, the results were compiled (e.g., Figure 14) and reported to the operating company who submitted it to the OGC. Additional samples were analyzed by other labs (e.g., AGAT, Maxxam, Weatherford, Isotech, GChem) with similar reports sent to OGC and held under the usual confidentiality period for the wells. All the reports were downloaded by BC-NGA and merged into the data compilation.

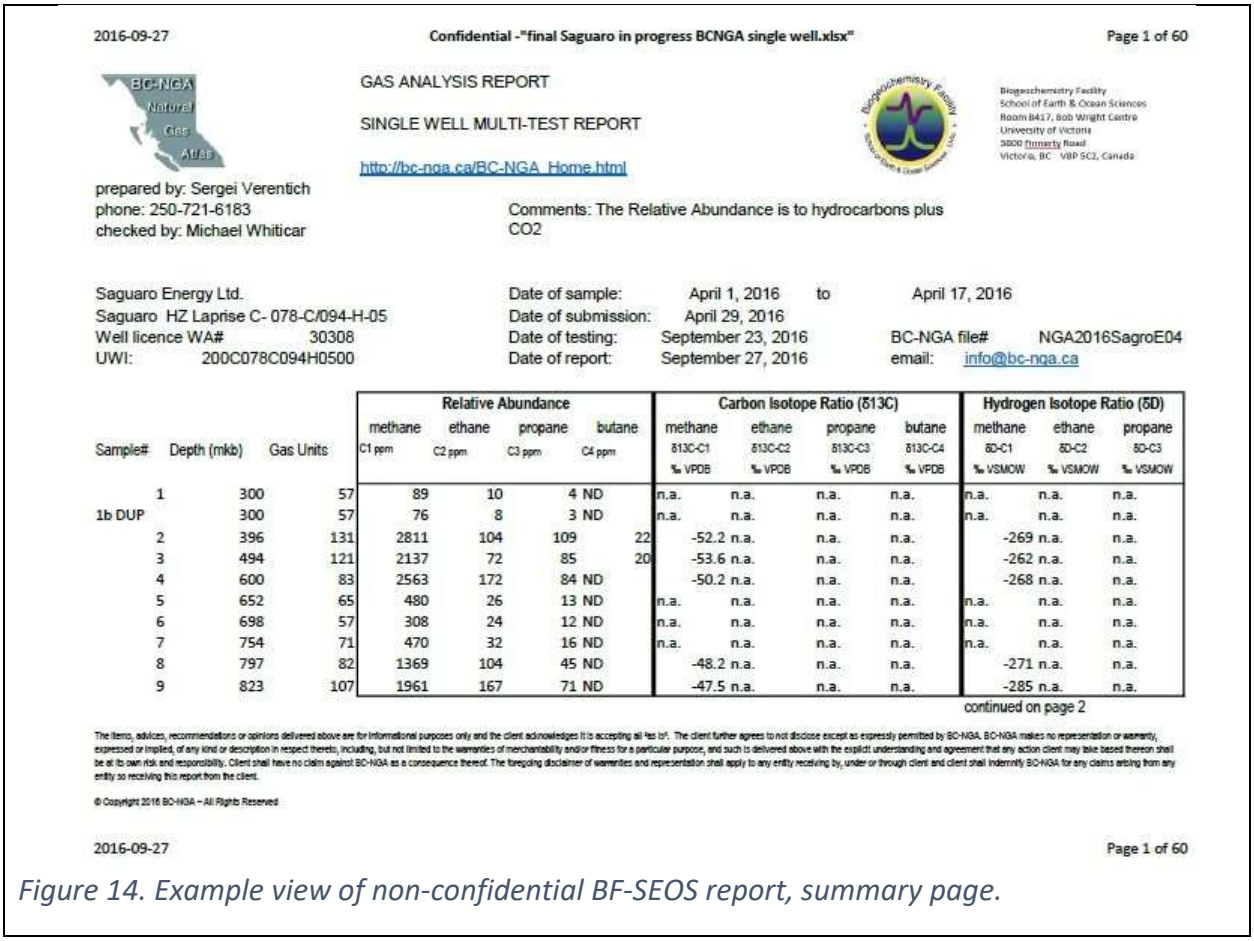

2016-09-27 Confidential -"final Saguaro in progress BCNGA single well.xlsx" Page 1 of 60

BC-NGA Natural Gas Atlas

GAS ANALYSIS REPORT

SINGLE WELL MULTI-TEST REPORT

http://bc-nga.ca/BC-NGA_Home.html

Biogeochemistry Facility
School of Earth & Ocean Sciences
Room B417, Bob Wright Centre
University of Victoria
3800 Finnerty Road
Victoria, BC V8P 5C2, Canada

prepared by: Sergei Verentich
phone: 250-721-6183
checked by: Michael Whiticar

Comments: The Relative Abundance is to hydrocarbons plus CO2

Saguaro Energy Ltd.
Saguaro HZ Laprise C- 078-C/094-H-05
Well licence WA# 30308
UWI: 200C078C094H0500

Date of sample: April 1, 2016 to April 17, 2016
Date of submission: April 29, 2016
Date of testing: September 23, 2016
Date of report: September 27, 2016

BC-NGA file# NGA2016SagroE04
email: info@bc-nga.ca

			Relative Abundance				Carbon Isotope Ratio (δ13C)				Hydrogen Isotope Ratio (δD)		
			methane	ethane	propane	butane	methane	ethane	propane	butane	methane	ethane	propane
Sample#	Depth (mkb)	Gas Units	C1 ppm	C2 ppm	C3 ppm	C4 ppm	δ13C-C1 ‰ VPDB	δ13C-C2 ‰ VPDB	δ13C-C3 ‰ VPDB	δ13C-C4 ‰ VPDB	δD-C1 ‰ VSMOW	δD-C2 ‰ VSMOW	δD-C3 ‰ VSMOW
1	300	57	89	10	4	ND	n.a.	n.a.	n.a.	n.a.	n.a.	n.a.	n.a.
1b DUP	300	57	76	8	3	ND	n.a.	n.a.	n.a.	n.a.	n.a.	n.a.	n.a.
2	396	131	2811	104	109	22	-52.2	n.a.	n.a.	n.a.	-269	n.a.	n.a.
3	494	121	2137	72	85	20	-53.6	n.a.	n.a.	n.a.	-262	n.a.	n.a.
4	600	83	2563	172	84	ND	-50.2	n.a.	n.a.	n.a.	-268	n.a.	n.a.
5	652	65	480	26	13	ND	n.a.	n.a.	n.a.	n.a.	n.a.	n.a.	n.a.
6	698	57	308	24	12	ND	n.a.	n.a.	n.a.	n.a.	n.a.	n.a.	n.a.
7	754	71	470	32	16	ND	n.a.	n.a.	n.a.	n.a.	n.a.	n.a.	n.a.
8	797	82	1369	104	45	ND	-48.2	n.a.	n.a.	n.a.	-271	n.a.	n.a.
9	823	107	1961	167	71	ND	-47.5	n.a.	n.a.	n.a.	-285	n.a.	n.a.

continued on page 2

2016-09-27 Page 1 of 60

Figure 14. Example view of non-confidential BF-SEOS report, summary page.

4.4 Open Source Data Examples and Structure

As stated in Section 4.1, the OGC has a large archive of publicly available gas well data reports. To create a database for this thesis, the data were extracted and formatted into one large compilation. Prior to the creation of this new database, every user wanting to access the data had to selectively retrieve and extract thousands of individual reports. In addition, the OGC dataset required editing, for example to correct entry errors or remove duplicate entries. An example of the database view is provided as Figure 15 and the metadata for the new database design is provided as Appendix C.

Data were downloaded as a gas analysis table in CSV format plus individual gas analysis reports as PDF, JPG, or CSV files with multiple types of layout for data addition or confirmation. Data loading masks were employed to select and load data fields and manual confirmation of almost every data load was completed. The resulting database is the first public compilation of gas geochemistry data for NEBC.

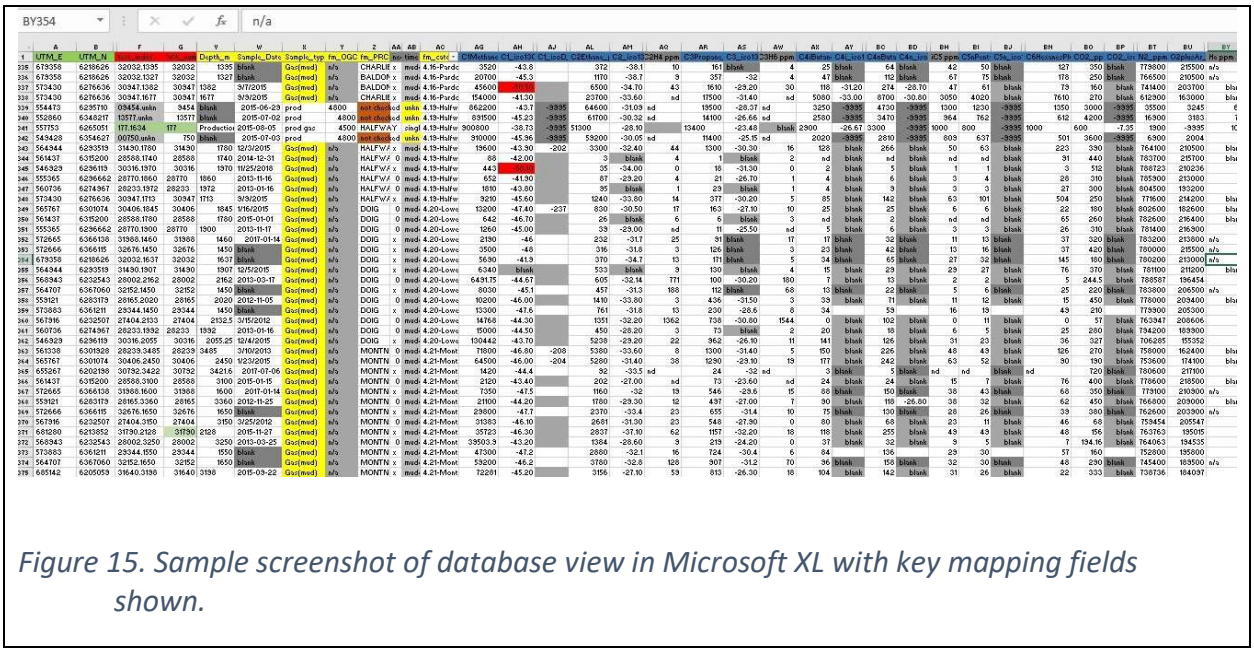

Figure 15. Sample screenshot of database view in Microsoft XL with key mapping fields shown.

Over 14,000 records (i.e., sample entries) of gas composition (MC) data were downloaded from the OGC gas analysis database. I subsequently edited the dataset to 9,275 records of mappable location and stratigraphy combinations for the plays in NEBC. Each well location can have multiple test depths and thus a 3D picture of the geochemistry is preserved by data indexed to WA# in combination with the test depth and its associated stratigraphic formation. The database, as seen in Figure 15, has each data record as a WA# and depth (but possibly multiple dates) and is represented by one record in the database. The 9,275 records were validated for correlation with the stratigraphy by a third-party contract (Evans and Hayes 2018). There are over 600 records of natural gas stable isotope ratio data (ISO) held by the OGC. I merged these ISO data with the main MC database.

Dataset editing was done manually, and the details of that filtering depended on the decision described in Section 4.2 to complete the regional scale mapping based on the surface well location only. This reduced the deviated well bottom hole locations to a single pad location and thus the statistical weighting of hundreds of horizontal well bores having multiple test results from a single pad and/or motherbore, was reduced in the database to a few for each map location. The data filtering focussed on age and style of data collection (e.g., recent drillstem testing and metering station production gas was preferred to older 'casing gas' or 'unknown'). Obvious errors in the data (e.g., $\delta^{13}C_1$ for any type of reservoir gas having a positive isotope value) were communicated back to OGC for an update from the lab.

5 Results: BF-SEOS data summary

BF-SEOS had received slightly over 200 natural gas samples from wells in NEBC by October 2018. As only final reported samples are listed in Table 2, there are only 186 samples listed in this thesis as released. An example of the data report is shown as Figure 14, but more detail is available in the reports available for download from OGC using the WA# as the reference on the web-site. BF-SEOS completed 7 reports for the hydrocarbon isotopic analysis by GC-IRMS processes (3 mudgas profiles, 3 sets of production gas and 1 set of samples for SCVF) described in Section 4.3 and summarized in Table 2.

Table 2. List of gas samples submitted to BF-SEOS with new analysis completed for ISO.

operator	#wells prodgas	#wells mudgas	# of samples	WA# listed	date rec'd (BF-SEOS lab)
'Yoho'		1	32	32990 single	4-Oct-2017
'Suncor'	2		2	SCVF surface only	8-Nov-2016
'Crew'	2		3	30876 and 31960	28-Oct-2016
'Shell'	2		4	29926, 29921	19-Jul-2016
'Crew'	14		29	for list see results	7-Jun-2016
'Saguaro'		1	61	30308 single	29-Apr-2016
'Chevron'		1	55	29747/29727double	22-Apr-2016

Three vertical well profiles (WA#32990, WA#30308 and WA#29747/29727) listed in Table 2 are extracted from the main display of profiles in Appendix A and shown in graphical form (Figure 16, Figure 17, Figure 18). Characterization plots for these profiles are part of Section 6.1. Other maps and profiles are included in the appendices, but as they are not from the BF-SEOS analysis, and as such, only described as part of Section 6.2.

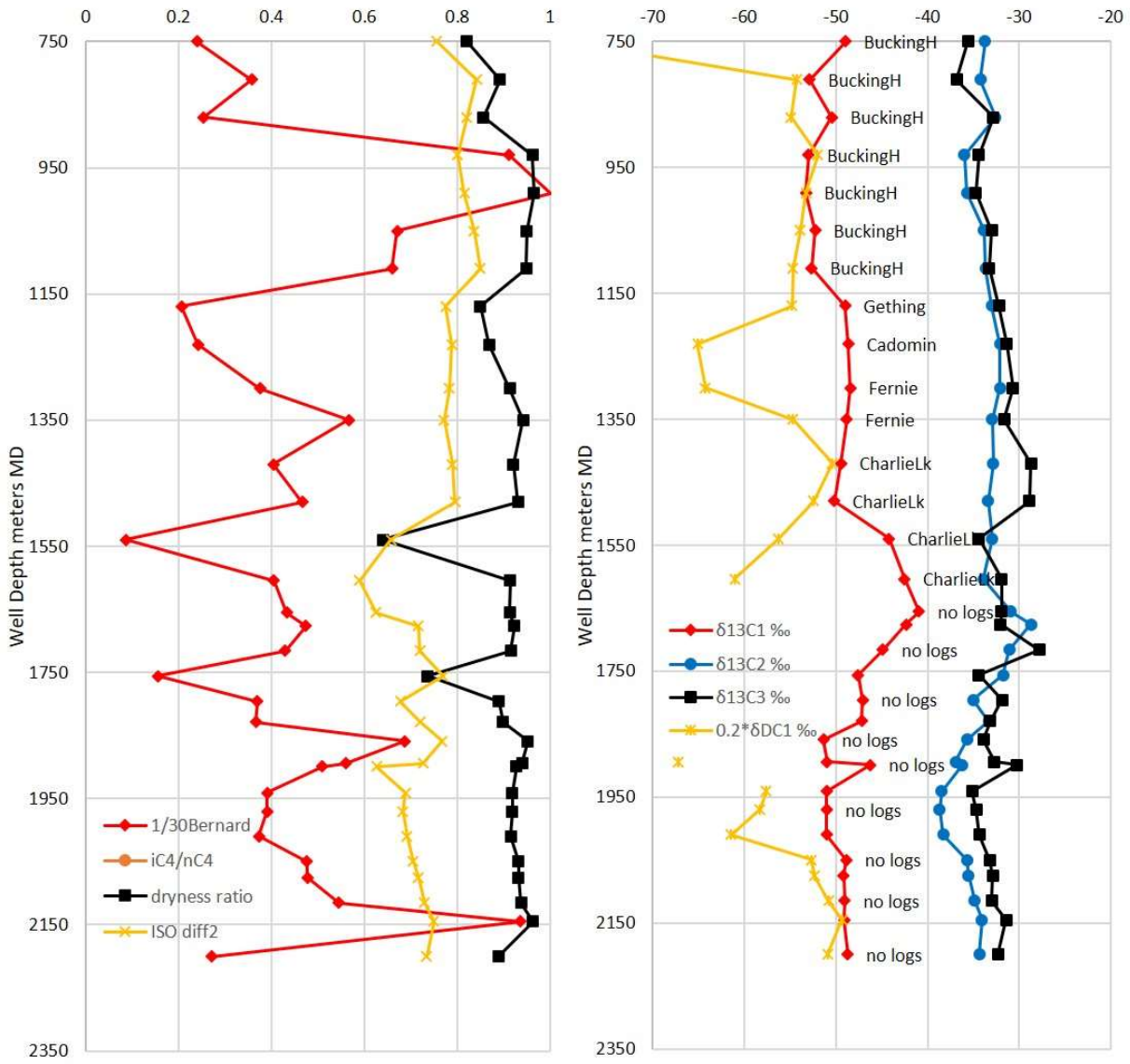

Figure 16. Well profile, MC ratios and ISO data for WA#32990 (Appendix A, Upper Cretaceous to Triassic VT well [no geophysical well logs for deeper horizons, but total depth was just below the Montney]).

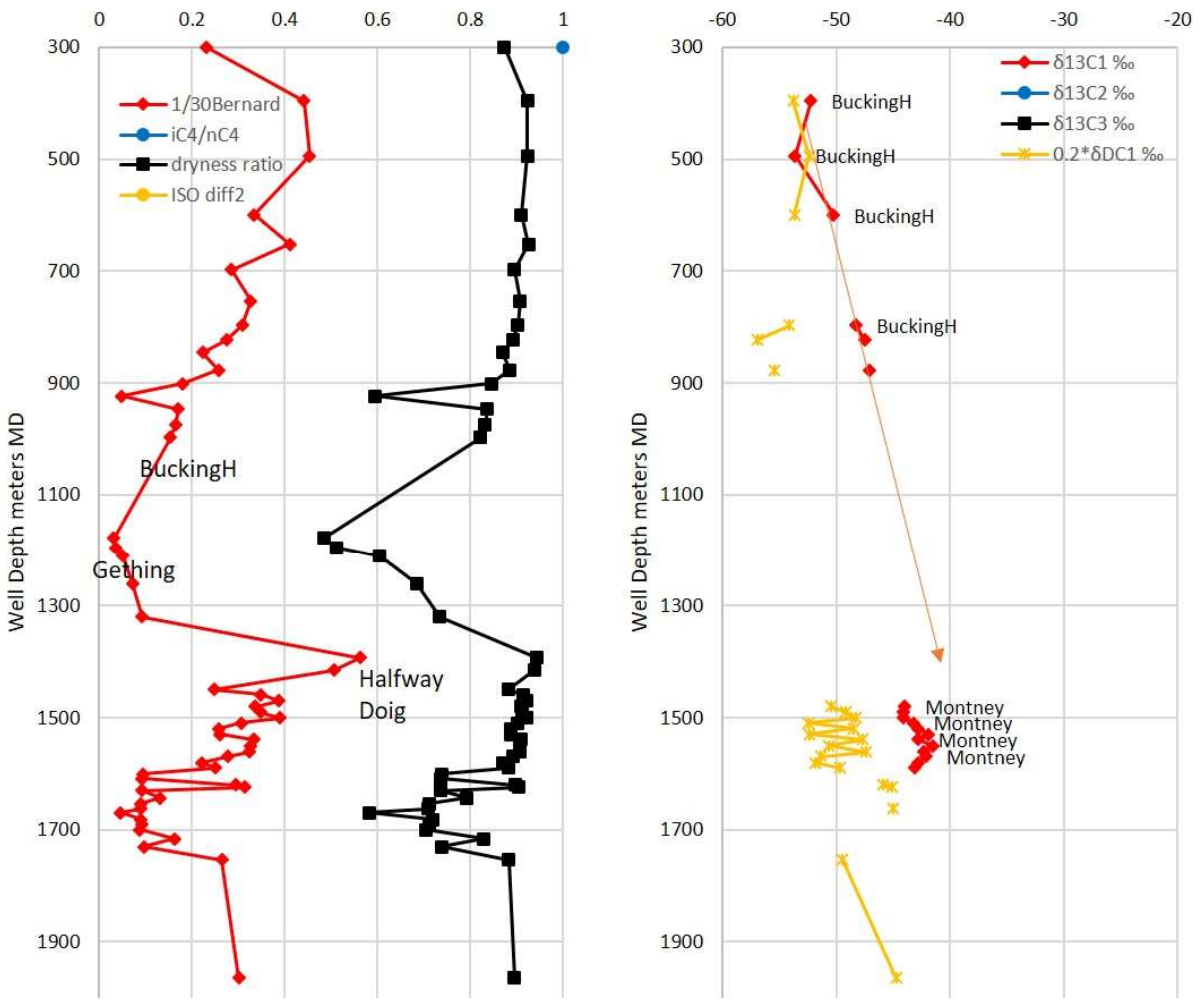

Figure 17. Well profile, MC ratios and ISO data for WA#30308 (Appendix A, Upper Cretaceous to Triassic VT well. Detailed sampling was completed as seen on the right, but the isotopic analysis and iC_4/nC_4 was limited to relative concentrations greater than 1000 ppm = a few $\delta^{13}C_1$ and $\delta^{2}H\text{-}C_1$ have values, but not $\delta^{13}C_2$ or $\delta^{13}C_3$, constraining the plots.).

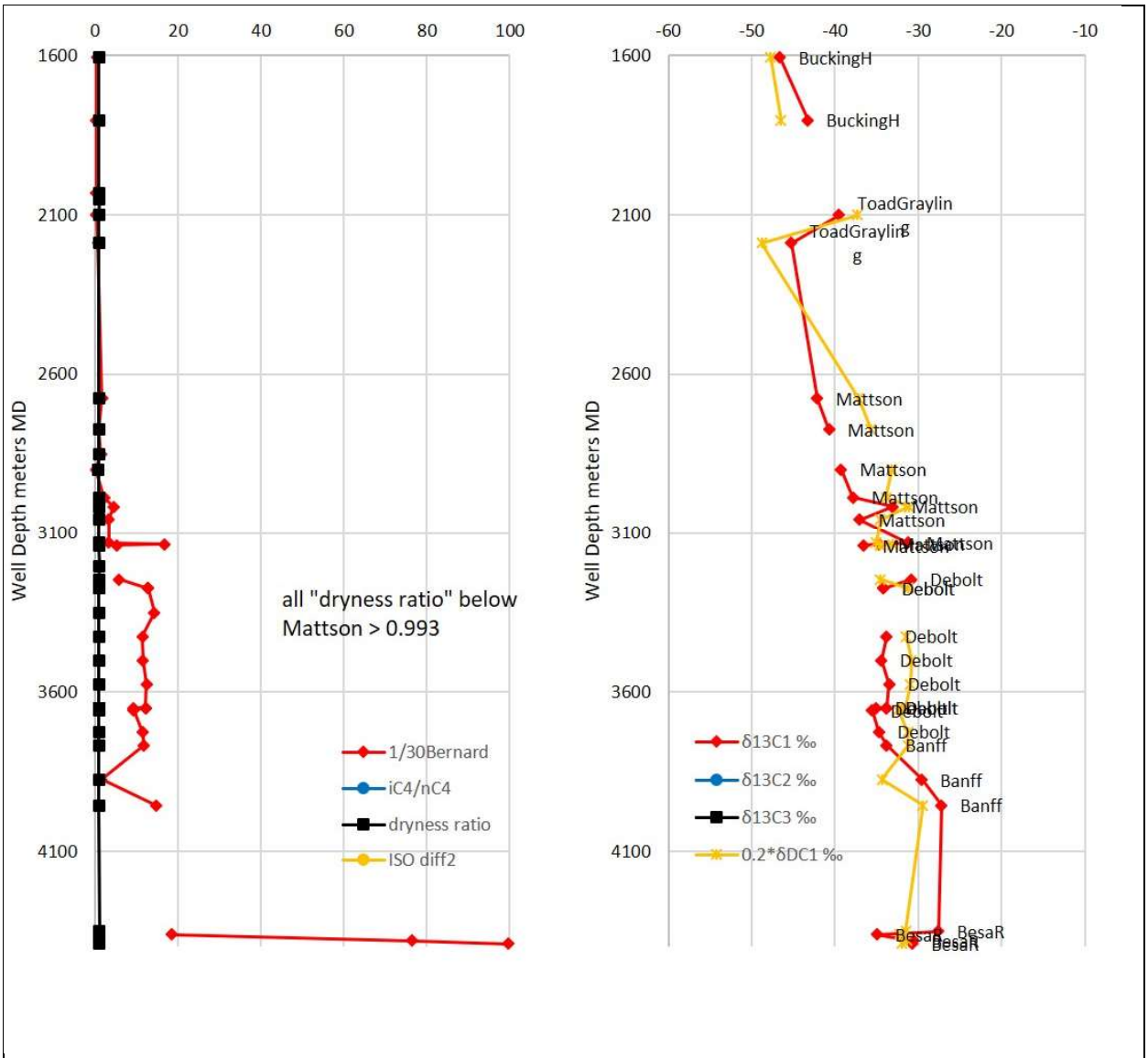

Figure 18. Well profile, ISO data for WA#29727 (Appendix A, Liard Devonian well with some uphole samples. ISO data is only for methane as longer chain hydrocarbons had ppm less than 1000. The 1/30 Bernard ratio is off scale and the dryness ratio is between 1.0 and 0.993).

6 Data, database, and data presentation

This thesis is based on data stored in a set of sub-categories of 'profiles' and 'maps', described in Sections 6.1 and 6.2 with an additional map type described in Section 8.

6.1 Profile preparation and presentations

Data from BF-SEOS are incorporated into the well profiles in Appendix A of this thesis. The separate dataset for the profiles generated from OGC archives (separated from the mapping dataset) initially had 2000 lines of data, but there were 335 duplicate records from repeat reports that were removed by filtering. This resulted in 1639 usable records of gas isotope (ISO) data. Most of the records had associated molecular composition (MC) data, H_2S is 'TSTM' (too small to measure), and useable Bernard ratios and iC_4/nC_4 ratios. The data from previous authors in Section 7.8 were not included. Thus, profiles include 1192 $\delta^{13}C_1$ values, 1059 $\delta^{13}C_2$ values, 967 $\delta^{13}C_3$ values, and 313 $\delta^{2}H$ values for C_1. Other data categories (e.g., $\delta^{2}H$ for C_2 and $\delta^{13}CO_2$ for only WA#32990) were only shown once (Figure 49) as they were rarely reported.

The total number of profiles available for review in this Section (listed in Table 3) is 57 wells comprised of 14 vertical only data (VT) for multiple formations, 32 horizontal only data (HZ) for the Montney formation, and 7 profiles where samples were taken down the vertical portion and continued along the horizontal portion and labelled 'both'. The 'both' wells were split into their respective VT and HZ portions. Of the HZ portions from 'both' wells, 2 were in the Besa River formation and analyzed only as continuation to the vertical leg, and the other 5 were Montney wells and grouped with the HZ wells. Subsequent to that, 8 profiles (indicated by '<10' or 'no data' in Table 3) were removed as 5 wells had zero isotope data (3 HZ and 2 VT) and another 3 wells being HZ with fewer than 10 datapoints. These were flagged to OGC for confirmation to collect the ISO data. No further analysis was completed on these wells. The totals are 20 VT profiles and 31 HZ profiles.

The remaining 20 VT, 29 HZ Montney, and 2 HZ Besa River profiles were reviewed in the following fashion: the 29 HZ for the Montney completions were grouped as being generally representing the target middle member of the formation. The profile for WA# 28770 is one exception being mapped separately due to different behaviour (this profile has sawtooth analysis for different sample types, see below). The 20 VT (Table 3) profiles were all unique and plotted in Appendix A, but in order from north to south by location.

The profiles include ratios defined in Section 3.2 with the Bernard ratio reduced by a factor of 30 to be viewable on the same plots. There is also an additional ratio of "ISO diff2" that is an internal data check to confirm plotting of the ISO data on the adjacent profile.

The profile locations are mapped in Figure 20 modified from Appendix A.

Table 3. List of wells with profiles and data quality – ordered from South to North.

OGC WA#	same pad *a	VT data	HZ data	both data	VT profile	HZ profile *b	$\delta^{13}C$ data	$\delta^{2}H$ data	CD Diagram *c
total>	15	21	39	7	20	32	48	16	6
30200			●			●	●		
31521			●			●	●		
31522	y31521		●			●	●		
31101			●			●	●		
31102	y31101		●			●	●		
31103	y31101		●			●	●		
30792			●			●	●		
30791	y30792		●			●	●		
29568			●			●	●		
31699			●			●	●		
31640			●			●	●		
31790			●			<10	●		
32032		●			●		●		
31977			●			●	●		
26657		●			●		●		
27404			●			●	●		
28002			●			●	●		
25587	y26949		●				no data		
26949		●			●		●		
26918		●			●		●		
26660			●				no data		
32990		●			●		●	●	●
28233		●	●	●	●	●	●		
33348			●			<10	●		
30947			●			●	●	●	M
30948	y30947		●			●	●	●	M
30949	y30947		●			●	●	●	M
28165		●	●	●	●	●	●		
28167	y28165		●			●	●		
31226			●			●	●	●	M
31228	y31226		●			●	●	●	M
31490		●	●	●	●	●	●	●	●
31491	y31490		●			●	●	●	M
31492	y31490		●			●	●	●	M
30316		●	●	●	●	●	●		
28770		●	●	●	●	●	●		
30406			●			●	●	●	M
30407	y30406		●			●	●	●	M
30408	y30406		●				no data		
28239			●			●	●	●	M
28588		●	●	●	●	●	●	●	●
32739			●			<10	●		
31987			●				no data		
30308		●			●		●	●	●
29344		●			●		●		
32676		●			●		●		
31988		●			●		●		
32152		●			●		●		
32153	y32152	●			●		●		
30415		●					no data		
29747		●			●		●	●	●
29727	y29747	●	●	●	●	●	●	●	●
29046		●			●		●		

*a = y means see other entry for preferred profile;

*b = "<10" means a few datapoints and profile not created, only map data;

*c = "M" means only plotted with Montney all profiles.

6.2 Map sourced data

Most map data were sourced from public data archived at the OGC with the vast majority being MC-only data (Figure 19). Initial review maps have already been released as part of the BC-NGA project (Evans and Whiticar 2016b). All geological formations were considered initially for geochemical mapping in NEBC, but some formations do not have sufficient hydrocarbon data, other formations are too shallow for regional data collection, and other formations are very deep with limited borehole intersections. Most formations with a history of petroleum production have had extensive geological summaries that are briefly noted in the 2006 atlas where they are listed as 'plays' (MEM 2006a, b, c). The map data for each play are listed in Table 4 and also along with the metadata in Appendix C.

A new play was introduced above the stratigraphic sequence of the 2006 atlas (MEM 2006a, b, c), for surface emissions captured as a data horizon above the land surface and is described in Section 8.

All plays above the Dunvegan (Tertiary, Belly River, Chinook, Cardium, Doe Creek) and a few in the middle of the stratigraphic section (Sikanni, Scatter) have very limited data and aerial extent and thus are not included in Table 4. All plays stratigraphically below the Slave Point 4.30 and some above (e.g., Wabamun, Kakisa, Leduc) were deemed to have insufficient or complex data. In addition to the new 4.29a-Muskwa play (plotted with Jean Marie 4.28) and 4.32a-Evie play (Slave Point 4.30), there is also the play 4.15a-Fernie Group (including the Nordegg Formation) as extracted from the vertical profiles described in Section 6.1.

The well profiles from Section 6.1 did not add data to certain formations if those formations were thick (e.g., Bucking Horse Formation) and had a wide range of values for a single play. I marked as mappable only formations with a minimum number of data points, but the minimum depended on the geographic distribution and data quality. For example, if a play had data of only a few points in each formation but collated into some reasonable spread of geographic distribution and recent analysis, that play would be supported as mappable data, despite having fewer points than an oil horizon where the data were decades old and concentrated in one location. Geochemical and gas production evaluation indicated merging some plays (e.g., Gething with Bluesky, Cadotte with Paddy, Charlie Lake upper and lower). This reduced the map data set down to 20 horizons that have been listed in Table 4. Most formations correspond to the list of plays in the 2006 atlas (MEM 2006a, b, c), but only the plays with mappable number of datapoints are listed below.

The transfer of data from the profiles (Appendix A) to the map data (Appendix B) was done by manual selection of the profile intervals (if there was more than one for a formation) that appeared to match the trend of the well. This matching process was filtered to identify anomalies, as seen in the profiles. There was a risk that the potential mis-match of data would shift trends identified in the mapping, but this was back-corrected with an annotation in the profiles data. Thick shallow formations (e.g., Buckinghorse and Spirit River formations) and formations with complicated member level stratigraphy (e.g., Charlie Lake Formation) or variable profiles (e.g., Halfway Formation) were not transferred to the maps as the profiles are currently impossible to reconcile to one data point. In these cases, further work is needed to determine subsets of the formations that can be mapped as a unit based on stratigraphic correlation of members within these large packages. Where a complicated formation had only one data point, mapping created anomalies by data availability. There were hundreds of samples not transferred

from the Montney HZ profiles as only one data point was selected for each pad. The selection was done by visual check for fit to trend.

Table 4. List of formations/plays in the 2006 Atlas annotated with data for mapping and which ones were included in Appendix B (shaded portions of table indicate insufficient data for mapping).

play#	merged	MC no ISO	MC w ISO	$\delta^{13}C$ data	$\delta^{2}H$ data	ISO plots	maps
4.00-surface data		0	**137**	**252**	**21**	•	triangle'
4.06-Dunvegan Formation		**23**	0	0	0		MC only
4.09-Paddy /Cadotte Mmbr	incl Peace R	**204**	1	1	0		MC only
4.11-Spirit River Formation		**641**	1	1	0		MC only
4.12-Bluesky Formation	+Gething4.13	**1810**	**31**	**31**	1	•	MC + ISO
4.14-Cadomin / Chinkeh Fm		**462**	**4**	**4**	0	•	MC + ISO
4.15a-Fernie / Nordegg add		0	**6**	**6**	3	•	MC + ISO
4.15-Nikanassin Formation / Buick Creek Sandstone		**509**	**7**	**7**	1	•	MC + ISO
4.16-Pardonet / Baldonnel / Upper Charlie Lake	incl all CharlieL	**1766**	**26**	**26**	3	•	MC + ISO + H_2S
4.19-Halfway Formation		**1419**	**10**	**10**	1	•	MC + ISO
4.20-Lower Halfway / Doig Formations		**419**	**23**	**24**	1	•	MC + ISO + H_2S
4.21-Montney Formation		**970**	**172**	**176**	**66**	•	MC + ISO
4.22-Belloy / Taylor Flat / Fantasque Formations		**272**	1	1	0		MC only
4.23-Mattson / Kiskatinaw Formations		**82**	0	only profile	0		MC only
4.24-Debolt Formation		**299**	**8**	**8**	2	•	MC + ISO
4.25 Banff / Exshaw / Besa R		**39**	2	2	0		MC only
4.28-Jean Marie Formation	plot with 4.29a	**857**	2	2	0	**merged**	MC only
4.29a-Muskwa (add to atlas)		**44**	**16**	**16**	0	•	MC + ISO
4.30-Slave Point Formation	limited areal extent	**493**	**6**	**6**	4	•	MC + ISO
4.32a Evie (add to atlas)	plot with 4.30	**36**	2	2	0	**merged**	MC only

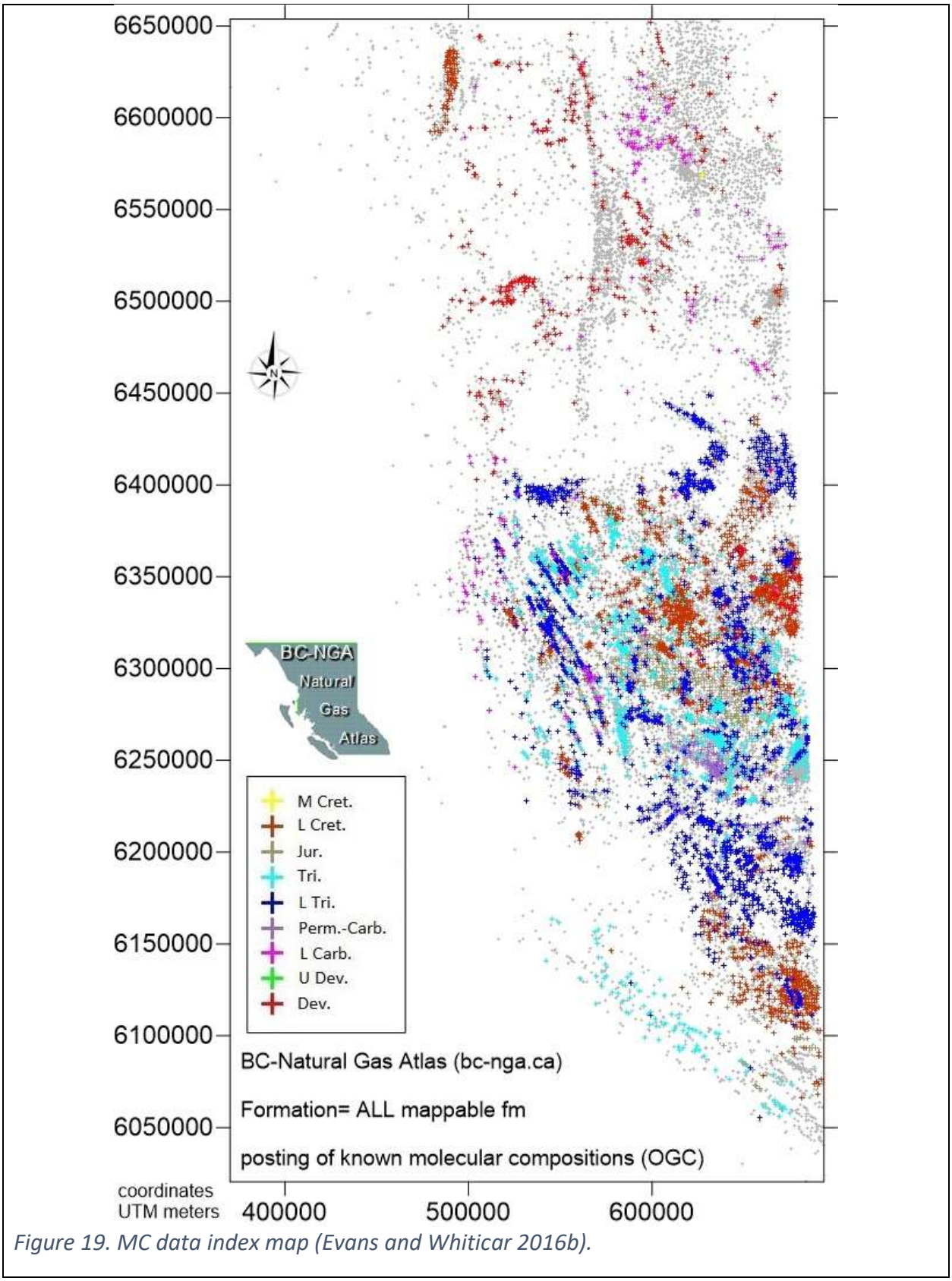

Figure 19. MC data index map (Evans and Whiticar 2016b).

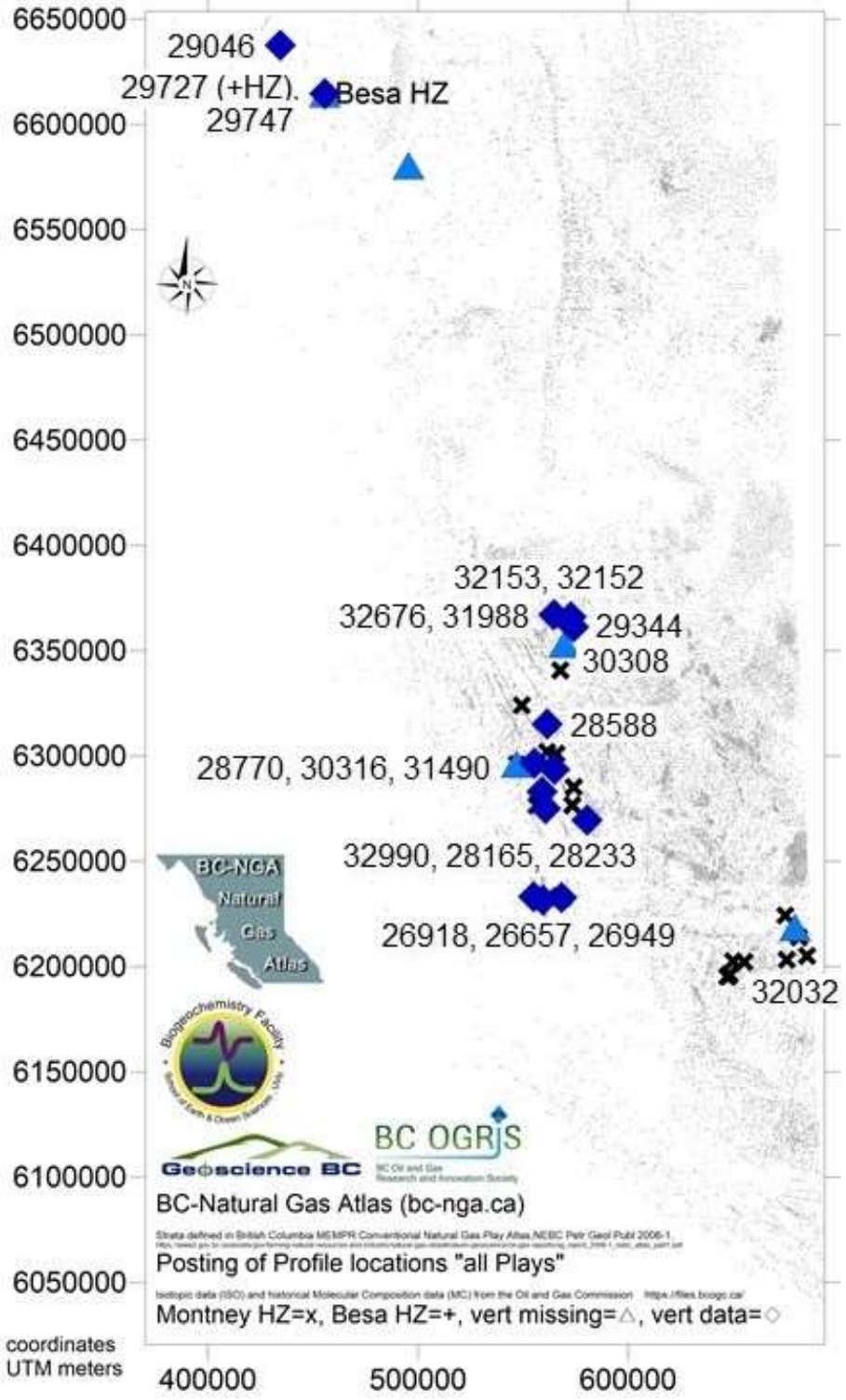

Figure 20. Location map of profiles with vertical profiles labelled (modified from Appendix A).

7 Data interpretation and discussion

The BC-NGA project intended to use the "natural gas fingerprint" (Rowe and Muehlenbachs 1999, Tilley et al. 2001) to identify gas sources and correlate to geologic settings (Evans and Whiticar 2016a). Graphical methods are an essential approach for the characterization of natural gases. These can include both the MC and ISO parameters, often as ratios or plots, which are the current interpretation tools for complex multivariate characterization.

From the BC-NGA data, I calculate various ratios based on the MC data and the mathematical difference in isotope ratios between different species ('isotope difference plots' e.g., $\delta^{13}C_2$-$\delta^{13}C_3$) from the ISO data. In these plots, stable carbon and hydrogen isotope ratios are combined with every gas species (6 used here as C_1, C_2, C_3, iC_4, nC_4, CO_2) to create 11 variables, plus the molecular composition for 6 variables, as well as a number of calculated ratios and differentials (e.g., $\delta^{13}C_2$-$\delta^{13}C_3$, iC_4/nC_4 ratio, Bernard ratio, etc.) for over 20 variables. At least 10 more variables would be needed if time series were included in this thesis.

The process of interpretation of the two datasets was to use plots and proceed from basic hydrocarbon molecular composition ratios, through Bernard and CD Diagrams for methane only data, into Prinzhofer and Lorant Diagrams on the higher hydrocarbons, to Berner-Faber Diagrams of $\delta^{13}C_1$, $\delta^{13}C_2$, $\delta^{13}C_3$ and the final proposed characterization plot of $\delta^{13}C_3$ vs iC_4/nC_4 ratio.

Most geochemical characterizations use the classical 'Bernard' (Figure 5) and 'CD' (Figure 6) Diagrams as plots for interpretation (e.g., Schoell 1983, Berner and Faber 1988, 1996, Schoell 1988, Jenden et al. 1993, Whiticar 1994, 1996, 1999, Etiope et al. 2009, Cheung et al. 2010, Kotarba et al. 2014, etc.). These diagrams form the foundation, where possible, for the well profiles in Appendix A and most maps in Appendix B. However, these diagrams can sometimes lead to ambiguous classifications due to overlaps in gas-source data fields and secondary processes, such as mixing and alteration (e.g., Whiticar 1994, 1996, Etiope et al. 2009). The interpretations can be improved by including less common, interpretative diagrams (e.g., Prinzhofer and Battani 2003, Prinzhofer et al. 2009, Prinzhofer et al. 2010, Prinzhofer and Deville 2013). I have found the 'Prinzhofer Diagram' (the MC ratios C_2/C_3 vs C_2/iC_4) and the 'Lorant Diagram' (the ISO ratio $\delta^{13}C_2$- $\delta^{13}C_3$ vs the MC ratio C_2/C_3) more useful in distinguishing between surface emissions and reservoir gas. These can augment or supplant the Bernard and CD Diagrams especially considering that δ^2H-C_1 data are not often available for the CD Diagram. The preferred diagrams for characterization are the Berner-Faber Diagrams of $\delta^{13}C_1$, $\delta^{13}C_2$, $\delta^{13}C_3$ and the final proposed characterization plot of $\delta^{13}C_3$ vs iC_4/nC_4 ratio which are presented in sequence.

The data is sourced from 2 parts of the database: well profiles (Section 6.1) and map data (Section 6.2) but is discussed in a combined manner in the following sections. The dataset for well profiles includes the three BF-SEOS profiles shown in Section 5 (Figure 16, Figure 17, Figure 18) and other profiles used by the BC-NGA project in Appendix A. The map data have interpretive diagrams for plays with data in Appendix B, but selected diagrams are presented here. Detailed maps for each of the parameters in Appendix B are shown at http://bc-nga.ca/

Horizontal profiles are included here despite being very different in the analysis: when the profile is in the target reservoir, there is not very much deviation from a mean value and thus the data can be used

as a single point in the map data. One exception to this is WA#28770 in Appendix A has data that leads to a new plot proposed in this thesis (Section 7.7) for gas characterization.

7.1.1 Data limitations or constraints

Molecular composition data has thousands of results. Isotopic analysis has hundreds of results and interpretation is noticeably limited in geographic occurrence of the data. Another issue is that $\delta^2H\text{-}C_1$ is commonly not analyzed, so only a small fraction of ISO data have $\delta^{13}C_1$ / $\delta^2H\text{-}C_1$ isotope pairs from which I could generate CD Diagrams. Many samples do not have isotope analysis for hydrocarbons larger than methane ($\delta^{13}C_1$). Only one well (WA#32990, Figure 49) and one play (4.21 Montney) has carbon dioxide isotope data ($\delta^{13}CO_2$). Additional concerns arise from lack of correlation of the gas signature obtained from mudgas analyses compared to the reservoir gas and there may be a shift due to well production from the true reservoir gas to production gas compositions. The data most frequently reported appear to be: 1) molecular composition (MC) values for production gas, 2) MC ratios for mudgas diluted by atmospheric circulation, and 3) ISO data of $\delta^{13}C_1$, $\delta^{13}C_2$, and $\delta^{13}C_3$ for both mudgas and production gas.

The results from mudgas sampling (most of the profiles in Appendix A) do show contaminant mixing of the gases with atmospheric circulation from the drilling process. Although undesirable, it is the standard for testing intermediate strata at this time. Correlating the mudgas results to reservoir gas testing from production gas samples is also problematic as production gas has similar data constraints with possible contamination from well stimulations, commingling, service injections, and swabbing as only a few examples. A working theory for future work is that mudgas isotopes will be different than desorption canister isotopes and production gas isotopes will shift over the life of the reservoir and a time-series will need to be further evaluated.

In looking for example for shallow biodegradation, the BC-NGA data must be assessed for the shallowest samples. All but four of the profiles in Appendix A have ISO data at a minimum depth of greater than 700m and only two of those four have $\delta^{13}C_2$ data. This contrasts with other studies that have a shallower maximum depth (e.g., Rowe and Muehlenbachs 1999: from surface to a maximum depth of 650m) and have data of $^{13}C_1$ depleted to $\delta^{13}C_1$ less than -55 ‰ plus $^{13}C_2$ depleted to $\delta^{13}C_2$ less than -45 ‰ (further depleted towards the surface). The four exceptions to the BC-NGA shallowest depth (WA# 29344, 30308, 32032, 32152) have data where $^{13}C_1$ is depleted to $\delta^{13}C_1$ between -50 and -60 ‰ and $^{13}C_2$ is depleted to $\delta^{13}C_2$ between -43 and -37 ‰. However, those depletions continue to depth on the profiles with 11 samples at depths greater than 390 mKB for $\delta^{13}C_1$ and 4 samples for $\delta^{13}C_2$. There are only 2 BC-NGA profiles with data deeper than 700 mKB where $^{13}C_1$ is depleted to $\delta^{13}C_1$ less than -55 ‰ (WA#29344 and 32676), but the shallowest points in some profiles still have $^{13}C_2$ trending enriched from $\delta^{13}C_2$ approximately -29 ‰ and are assumed to be biodegraded during updip migration (e.g., Rowe and Muehlenbachs 1999). There are still 53 other samples deeper than 700 mKB with ^{13}C depleted to $\delta^{13}C_1$ more than -50 ‰. The deepest of those is at 3720 mKB well depth. The $\delta^{13}C_2$ data appear to be more suitable for interpreting ‘shallow’ versus ‘deep’ gas, but it is also less frequently analysed.

7.2 Natural Gas Characterization from Molecular Composition diagrams

Following the example of Figure 11 in Section 4.1.1, MC data plots composed of all data are presented here (e.g., all map data in Figure 23). Well profiles from Appendix A do not support general plots of MC data as the mudgas sampling skews plotting of results that have atmospheric contamination. The exception to this is the horizontal profiles in the Montney as previous described to be homogeneous and used in many interpretive diagrams in this thesis.

Further confirmation of the 3 main trendlines in Figure 11 is better expressed as an example from a single well profile WA#26657 in the plot Figure 21a. In this single well profile, a 'V' pattern of 2 populations is shown that reflect two of the trendlines from Figure 11. The $\delta^{13}C_1$ vs $\delta^{13}C_2$ diagram for the same well (WA#26657, Figure 21b) shows a shift from the kerogen line to depleted $^{13}C_1$ with depth, then a second trend for deeper samples. The bimodal geochemistry is either constrained by the stratigraphy or by the sampling having very low levels of hydrocarbons and thus lower accuracy. A different example of a reasonable MC plot is the well profile for WA#28588 (Figure 22a, where the composition is on trend versus depth) and the $\delta^{13}C_1$ vs $\delta^{13}C_2$ diagram (Figure 22b, where a multi-depth deviation from the kerogen line is not related to composition). The lower trendline to higher maturity on Figure 11 is from the Liard/Horn River strata and is not present in the Montney areas. There is clear stratigraphic separation between trends, but further work is needed to better express that as the depth or stratigraphy where the trends switch apparently is not consistent from well to well. The interpretation of the Berner-Faber Diagrams is discussed in Section 7.6.

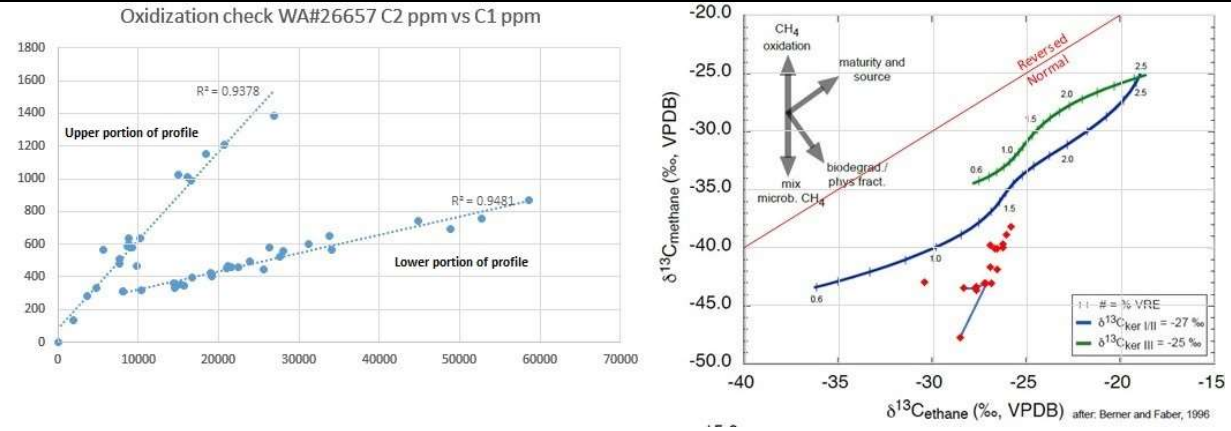

Figure 21a and b. Plot of C_2 (ppm) vs C_1 (ppm) for WA#26657 plus Appendix A $\delta^{13}C_1$ versus $\delta^{13}C_2$ plot for WA#26657 (Whiticar, 2018 pers. comm., after Berner and Faber 1996).

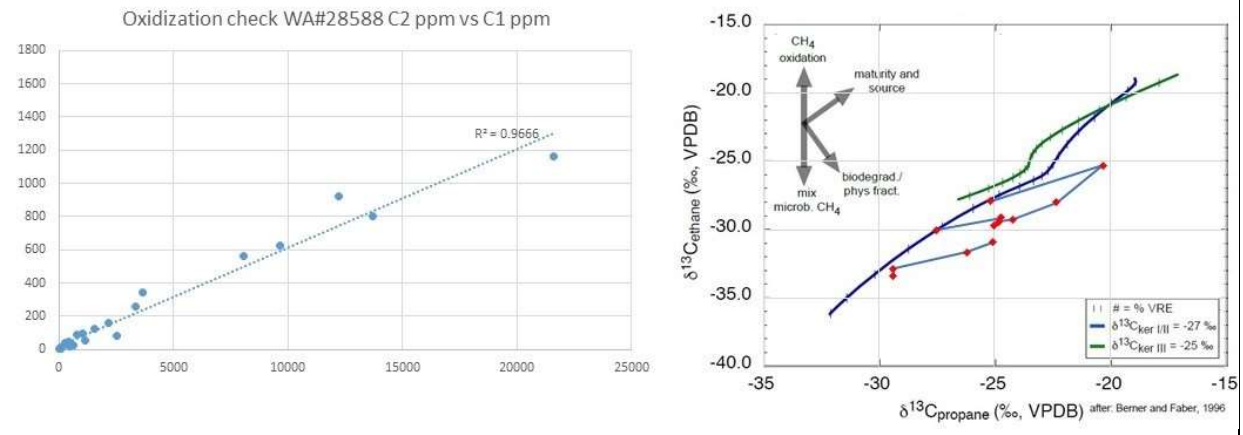

Figure 22a and b. Plot of C_2 (ppm) vs C_1 (ppm) for WA#28588 plus Appendix A $\delta^{13}C_1$ versus $\delta^{13}C_2$ plot for WA#28588 (Whiticar, 2018 pers. comm., after Berner and Faber 1996).

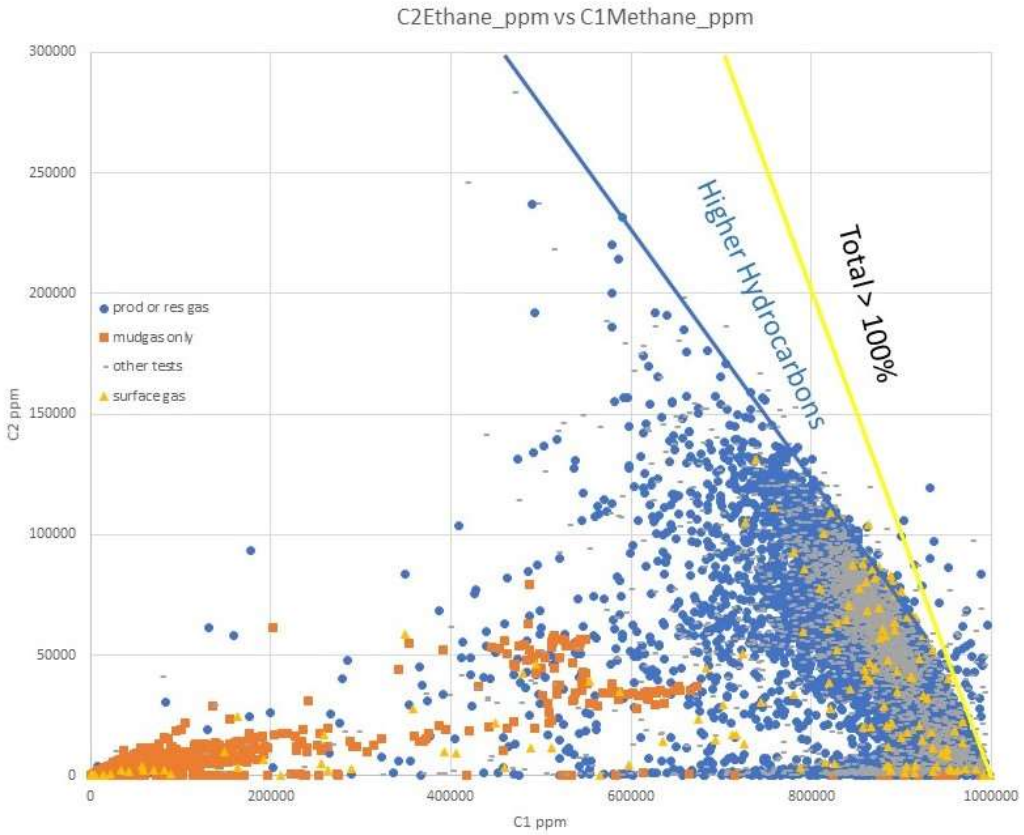

Figure 23. Plot of C_2 (ppm) vs C_1 (ppm) for all map data (OGC+BF-SEOS) for all plays with 4 categories of sample types [note shift from saturated reservoir gas and high hydrocarbon surface gas to diluted surface gas and mudgas].

There are distinct data errors, some of which plot off the graph limits and are flagged to the data source for correction, and others that are on the graph and still an error (e.g., totalling more than 100 %). However, there appears to be contamination due to dilution of gas samples from surface or mudgas collection. Figure 23 shows the mathematical limit where data totals more than 100 % and where higher hydrocarbons than methane and ethane are present in the sample. When a normalization function of dividing the value by the total hydrocarbons reported is applied, the analyses tend to group together along with production gas (Figure 24). This suggests that some mudgas samples are representative of reservoir gas, but the mudgas data scatter is too large to be certain of gas characterization. Surface gas is not easily identified using this geochemical approach.

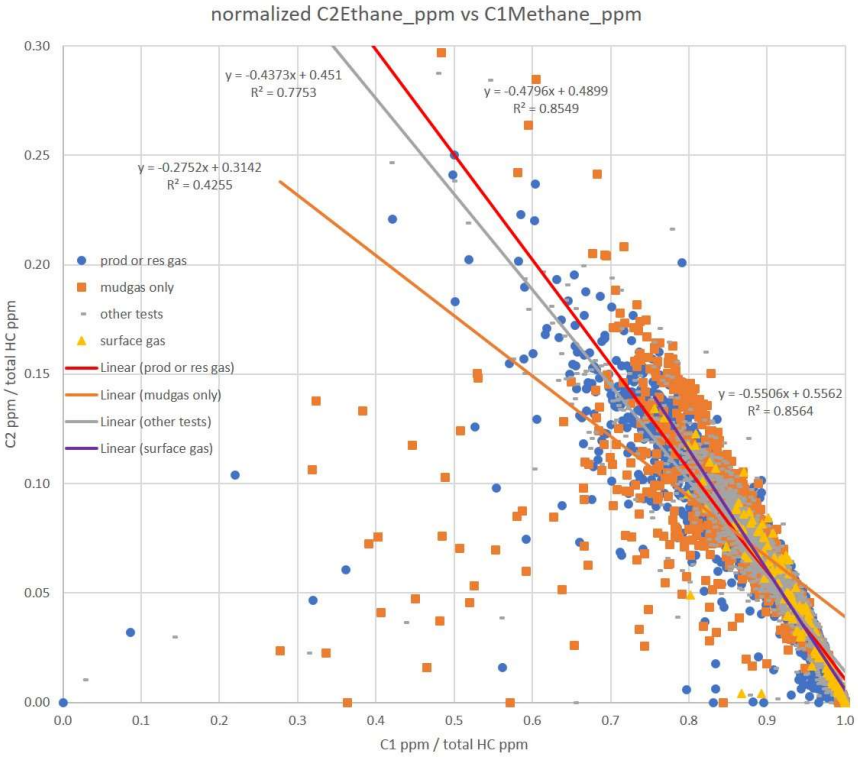

Figure 24. Plot of C_2 (ppm) vs C_1 (ppm) normalized to total hydrocarbons for all map data (OGC+BF-SEOS) for all plays with 4 categories of sample types that generally are close to the regression line for production gas.

The process of shifting from the raw MC data (Figure 23) to the normalized MC data (Figure 24) is not needed on plots for the ISO data (e.g., Figure 30 and Figure 33) as the ISO ratios stay constant even with dilution by atmospheric gases.

As the C_2 (ppm) versus C_1 (ppm) plot shows no clear separation between surface gas and production (or reservoir gas), but also mudgas samples are not diagnostic, so other gas species are plotted to C_1 (ppm)

normalized to all hydrocarbons (Figure 25, Figure 26a and b). The C_3 (ppm) vs C_1 (ppm) plot (Figure 25) shows a tighter trend, but still little separation between gases other than mudgas is not very reliable.

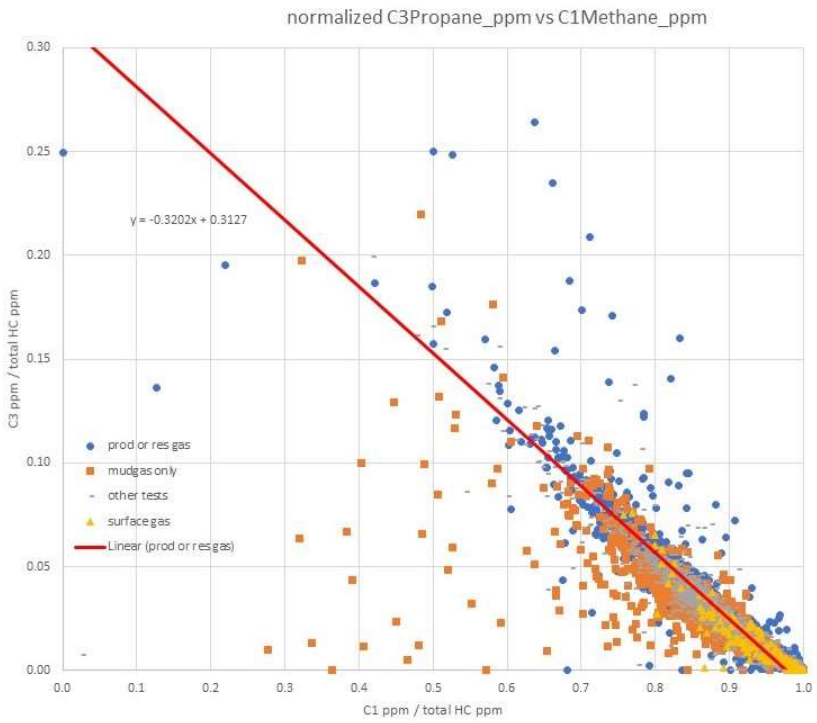

Figure 25. Plot of C_3 (ppm) vs C_1 (ppm) normalized to total hydrocarbons for all map data (OGC+BF-SEOS) for all plays with 4 categories of sample types that generally are close to the regression line for reservoir gas.

When the plot changes to another hydrocarbon species, the regression line for production gas changes gradient. When the regression line for C_2 ppm (Figure 24) is compared with C_3 ppm (Figure 25) there is a difference in slope. This difference is used as the X axis in the Lorant Diagram (Figure 10) for interpretation of sources. The ratio of C_3 ppm vs C_2 ppm does not show separation of gas in NEBC as well as the difference between $\delta^{13}C_2$ and $\delta^{13}C_3$ isotopes.

As butane is differentially reduced by biodegration, the last plots showing iC_4 ppm vs C_1 ppm and nC_4 ppm vs C_1 ppm are a little more instructive (Figure 26a and b). These show the basis for normalized butane plots being informative for gas sources due to different patterns between iC_4 and nC_4 with some separation between surface gas samples and production gas samples. Figure 26a and b are normalized versions of the butane plots and are used as the basis for Figure 27.

The iC_4/nC_4 data set has more samples with higher concentrations than the iC_5/nC_5 data and pentanes often condense out of the samples at surface pressures and temperatures. This usually means that that iC_4/nC_4 data is commonly used and iC_5/nC_5 can have sampling bias.

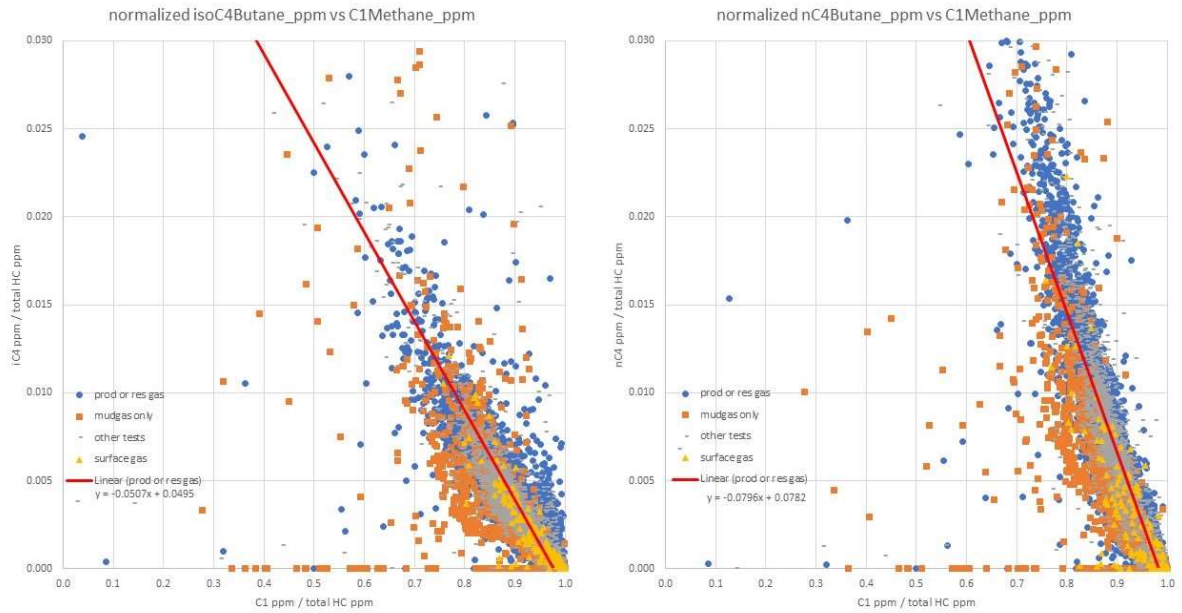

Figure 26a and b. Plots of iC_4 (ppm) vs C_1 (ppm) and nC_4 (ppm) vs C_1 (ppm) normalized for all map data (OGC+BF-SEOS) for all plays with 4 categories of sample types that generally are close to the regression line for reservoir gas.

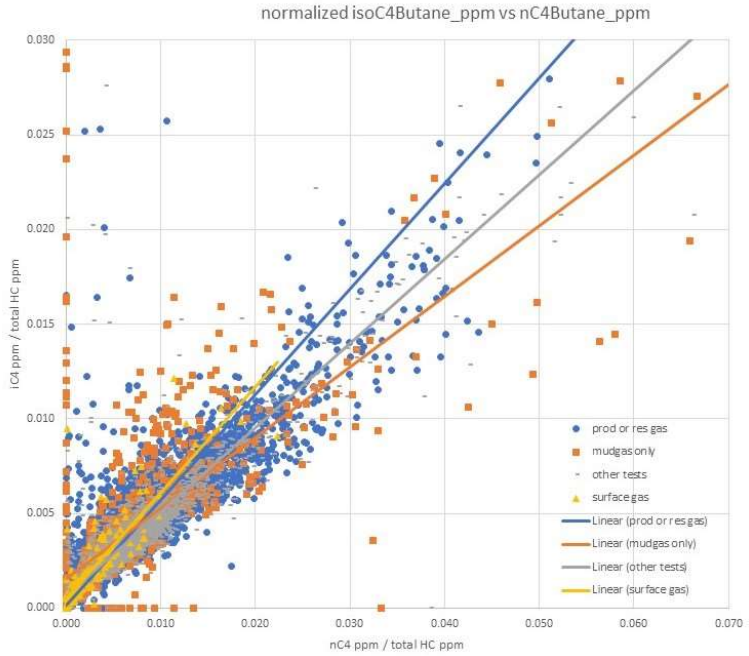

Figure 27. Plot of iC_4 (ppm) vs nC_4 (ppm) normalized to total hydrocarbons for all map data (OGC+BF-SEOS) for all plays with 4 categories of sample types that generally are close to the regression line for reservoir gas.

Individual formation level subdivisions of the C_3 ppm vs C_2 ppm plots are reproduced from Appendix B here as further examples. Most formations within the plays fit general trends that overlap as shown in the example for the Halfway, Doig, and Montney formations as plays 4.19, 4.20, 4.21 (Figure 28a). The distinction between the formations is visible for this one case in when H_2S is plotted against dryness (Figure 28b). The other example of a shallower play with a few formations included (Figure 29a and b) shows that the grouping of these formations to a single play crosses a geochemical boundary. This different in composition may be due to the shift from more terrigenous sources to marine sources. Unfortunately, the only ISO data that is present for the strata in this last example is a few samples in the well profiles that cannot be used for interpretation.

Figure 28a and b. Plot of C_3 (ppm) vs C_2 (ppm) and H_2S (ppm) vs dryness ratio for plays 4.19, 4.20, 4.21 as specific map data separated by formation (total map data).

The data scatter on $C_{dryness}$ vs iC_4/nC_4 plots of older 'MC only' data from the OGC archive indicate sample contamination and assessment for representative sampling was completed by confirming deviations to either side of the thermal maturity trend. In cases where the deviation indicates agreement with previous work on oil migration as a source for gas generation (Wood and Sanei 2016), that is an indication of sample being representative of reservoir gases. These gases might include mixing from sources that do not produce any butanes (C_4), such as Coalbed Methane and gas generation from biodegradation that preferentially use one type of butane. Deviations to higher iC_4/nC_4 ratios compared to the presumed thermal trend need to be investigated further, including one ISO outlier data point. The ratio of iC_4/nC_4 is used further in gas characterization is Section 7.7.

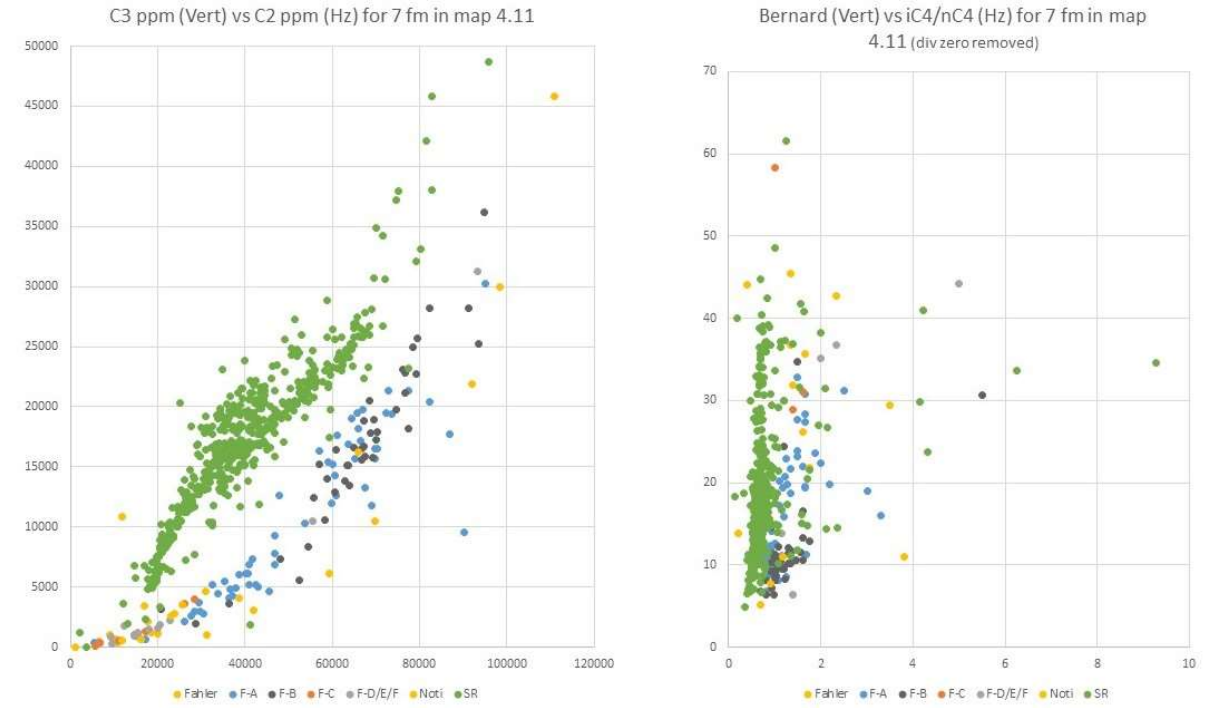

Figure 29a and b. Plots of C_3 (ppm) vs C_2 (ppm) and Bernard ratio vs iC_4/nC_4 ratio for play 4.11 as specific map data separated by formation ('SR' in green is Spirit River – archived data only from OGC – no ISO data present).

7.3 Natural Gas Characterization from Bernard Diagrams

The map data for a representative series of plays in the middle of the stratigraphy can be plotted (including the Montney profile data coloured uniquely) using the Bernard ratio without a template (Figure 30). This allows for the detailed separation between plays to be noted: there is apparently one central cluster of datapoints for Triassic to Cretaceous plays and an exception as the Devonian Jean Marie / Muskwa combination play is higher maturity. The Montney profile data (mainly mudgas in red) shows a clear separation from the Montney map data (mainly production gas in green), and thus intraformational data separation by sampling type is assumed to affect the Bernard ratio for mudgas analysis. The same Bernard Diagram using the template illustrates a pervasive thermogenic component to the data (Figure 31). This results in a tight cluster of all plays with little separation for characterization.

The corresponding Bernard Diagram for the 3 BF-SEOS profiles (Figure 32) illustrates a progression in geographic location from the Montney areas for WA#30308 and WA#32990 to the Liard area for the profile combination WA#29747-29727. There is a corresponding increase in thermal maturity. On Figure 32, the shallowest samples of the well profile plot outside the thermogenic zone, but only by a small amount and are still outside the common field for microbial gas ('Bacterial Methanogenesis'). A better expression of the well profile data is seen in the next sections.

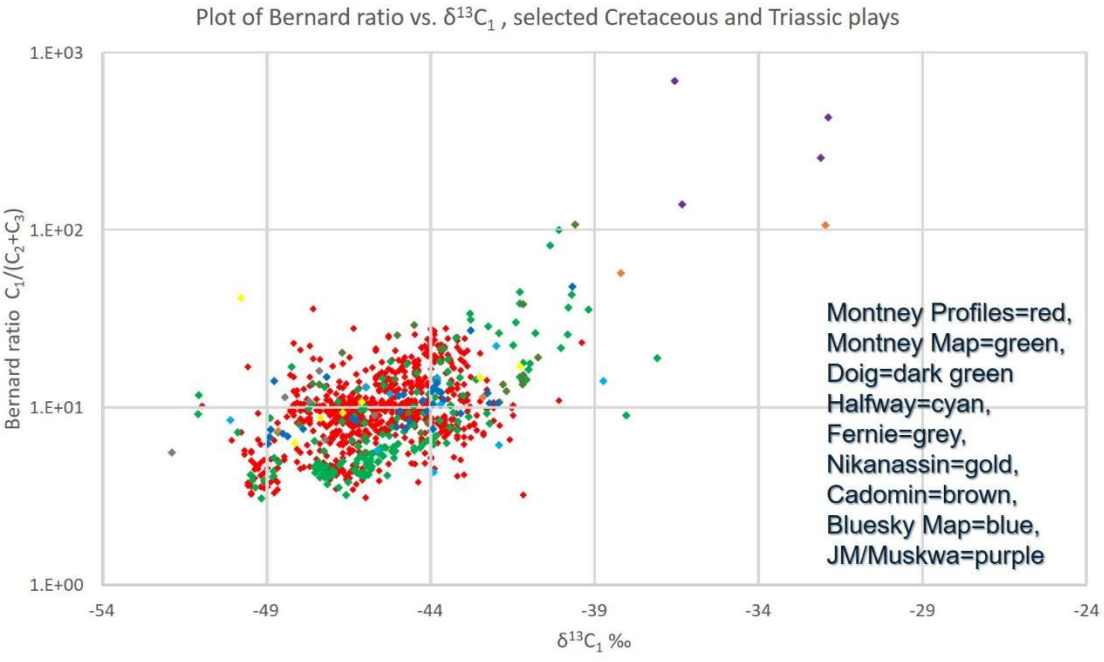

Figure 30. Plot of Bernard ratio vs. $\delta^{13}C_1$ of selected Triassic and Cretaceous plays (maps and profiles data) without interpretive template.

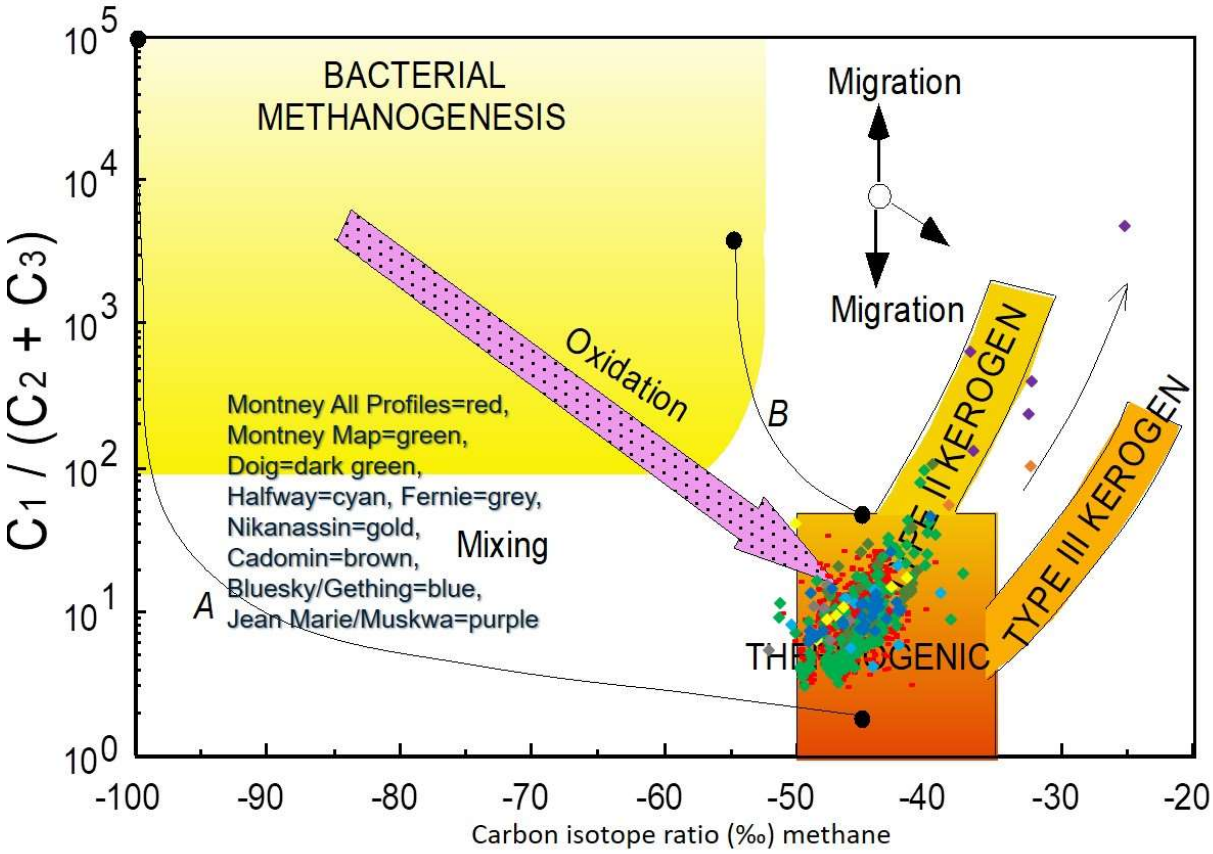

Figure 31. Interpretive Bernard Diagram for selected plays from Triassic to Cretaceous ages and one Devonian age (Whiticar, 2018 pers. comm., after Whiticar 1999).

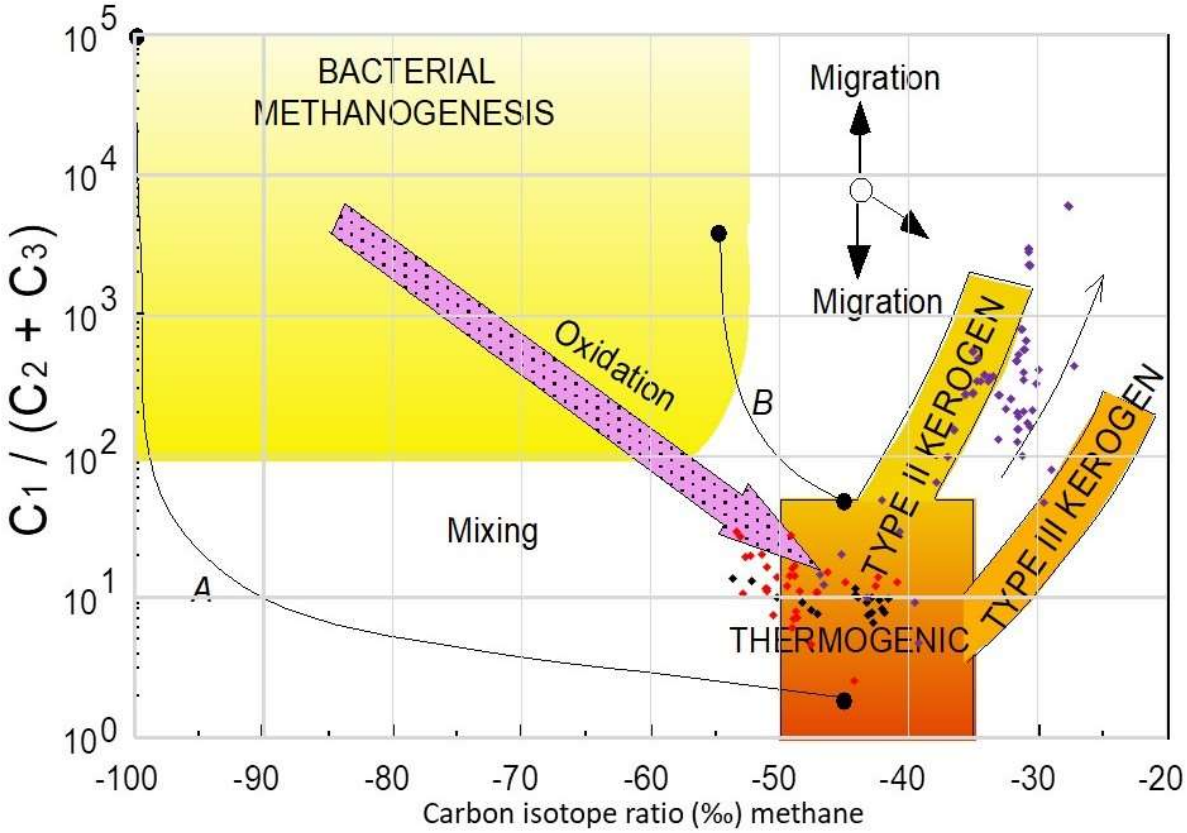

Figure 32. Interpretive Bernard Diagram, 4 BF-SEOS profiles, WA#32990 (red), 30308 (black), 29747 (green), 29727 (purple). (Whiticar, 2018 pers. comm., after Whiticar 1999)

7.4 Natural Gas Characterization from CD Diagrams

The Montney profiles and map data can also be shown on a CD Diagram (Figure 33) as many data points have both $\delta^{13}C_1$ and $\delta^2H\text{-}C_1$. When the CD template is used (Figure 34) the result is a spread of data through the thermogenic window, but no clear characterization is noted. Only a Bernard Diagram is relevant for the Bluesky/ Gething data, as that play has only a single suspect data point with both $\delta^{13}C_1$ and $\delta^2H\text{-}C_1$. All of the other plays discussed here as examples have either no data or a single data point with both $\delta^{13}C_1$ and $\delta^2H\text{-}C_1$. As the Bernard Diagram (Figure 31) demonstrates, the two populations of Montney data types completely overlap, in agreement with the CD Diagram, but there is an extension into the hydrothermal field. Some samples plot in the geothermal field due to isotope shifts, which is consistent with other work (Niemann and Whiticar 2017).

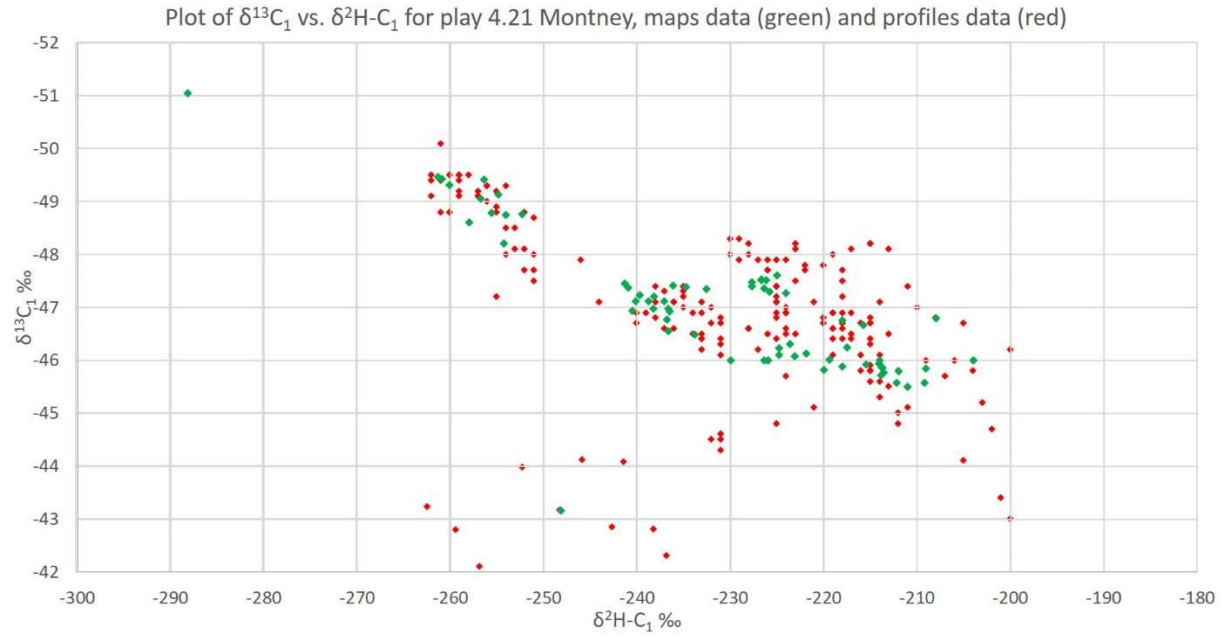

Figure 33. Plot of $\delta^{13}C_1$ vs. $\delta^2H\text{-}C_1$ for Montney (maps and profiles data).

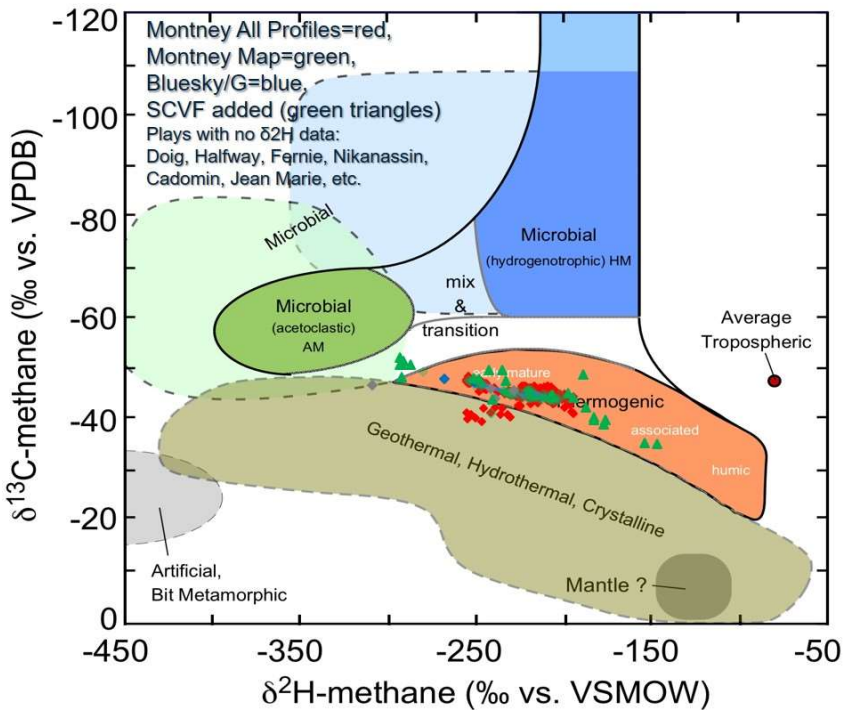

Figure 34. Isotope CD Diagram for Montney profile data (red) and Montney play map data (green) with a single Bluesky/Gething sample (blue) and surface gas (green triangles).

The corresponding CD Diagram for the 3 BF-SEOS profiles (Figure 35) shows the same progression in geographic location from the Montney areas for WA#30308 and WA#32990 to the Liard area for the profile combination WA#29747-29727 can be seen by a corresponding increase in thermal maturity. These three profiles are revisited in Section 7.6.

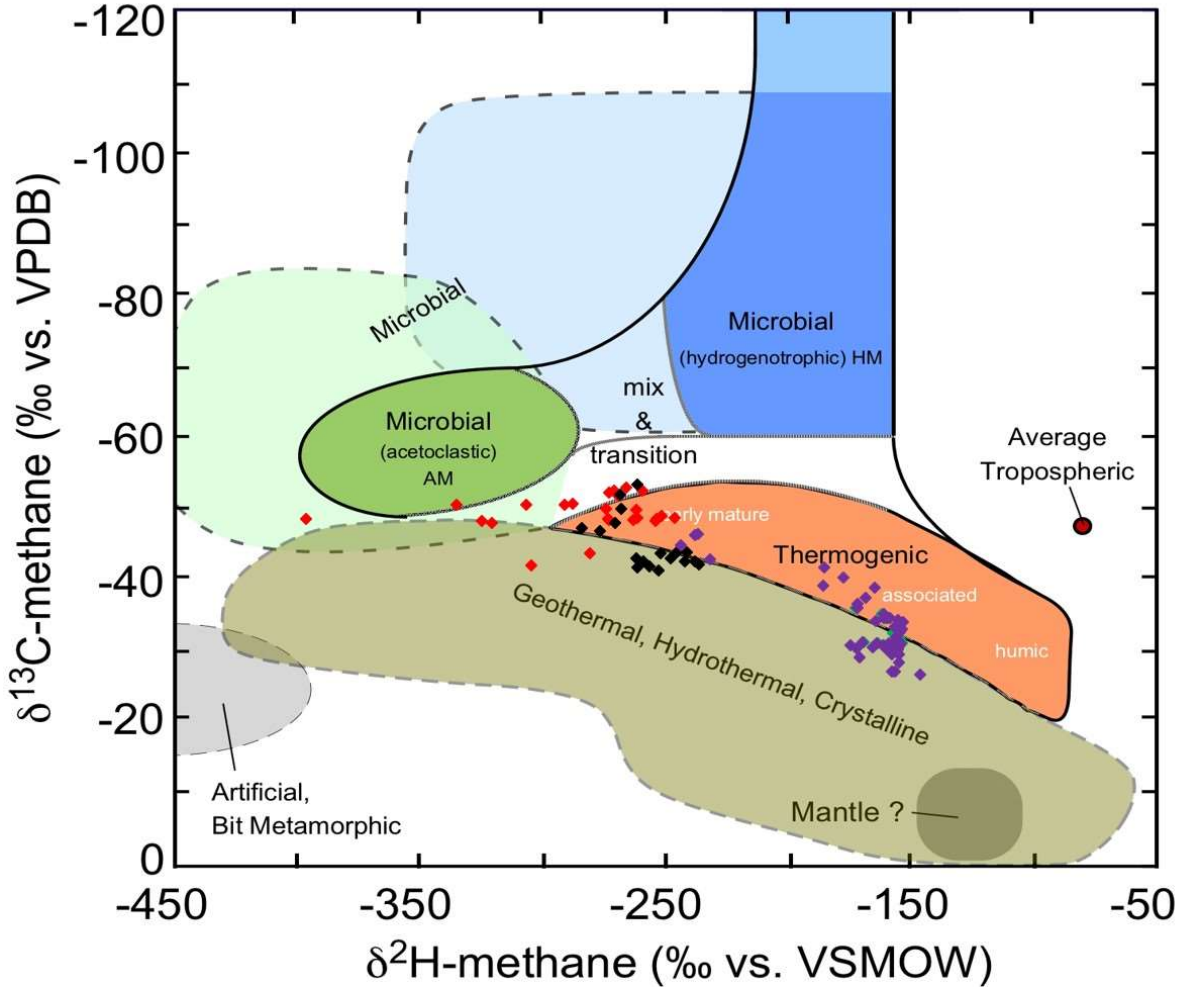

Figure 35. Isotope CD Diagram for 3 BF-SEOS profiles, WA#32990 (red), 30308 (black), 29747 / 29727 (purple). (Whiticar, 2018 pers. comm., after Whiticar 1999).

7.5 Natural Gas Characterization with Prinzhofer and Lorant Diagrams

Two diagrams are grouped together in this Section. The 'Prinzhofer diagram', which is strictly molecular composition (has MC ratios for axis) is complemented by the carbon isotope-based 'Lorant diagram'. The 'Prinzhofer diagram' uses only MC data, so it opens up the entire gas geochemistry database (blue triangles on plots of map data in Appendix B. The samples from NEBC have a consistent $\delta^{13}C_2$-$\delta^{13}C_3$ differential, and the Berner-Faber Diagrams of Section 7.6 have more functionality for gas characterization than relying on $\delta^{13}C_2$-$\delta^{13}C_3$. The petroleum system analysis for gas sources appears to have a consistent result based on the Prinzhofer and Lorant Diagrams (Appendix B).

The plot of Montney map data on Prinzhofer (Figure 36) and Lorant Diagrams (Figure 37) show secondary cracking in numerous stages of thermal maturity depending on the geographic location, but also extend to gases of higher maturity and biodegradation than in the Prinzhofer (Figure 38) and Lorant (Figure 39) Diagrams for the Bluesky/Gething play. These plots, and others in Appendix B show the trend is common for the Cretaceous rocks and the Triassic Montney play. The maturity effect may be amplified by the proximity of coal seams as additional sources for the methane.

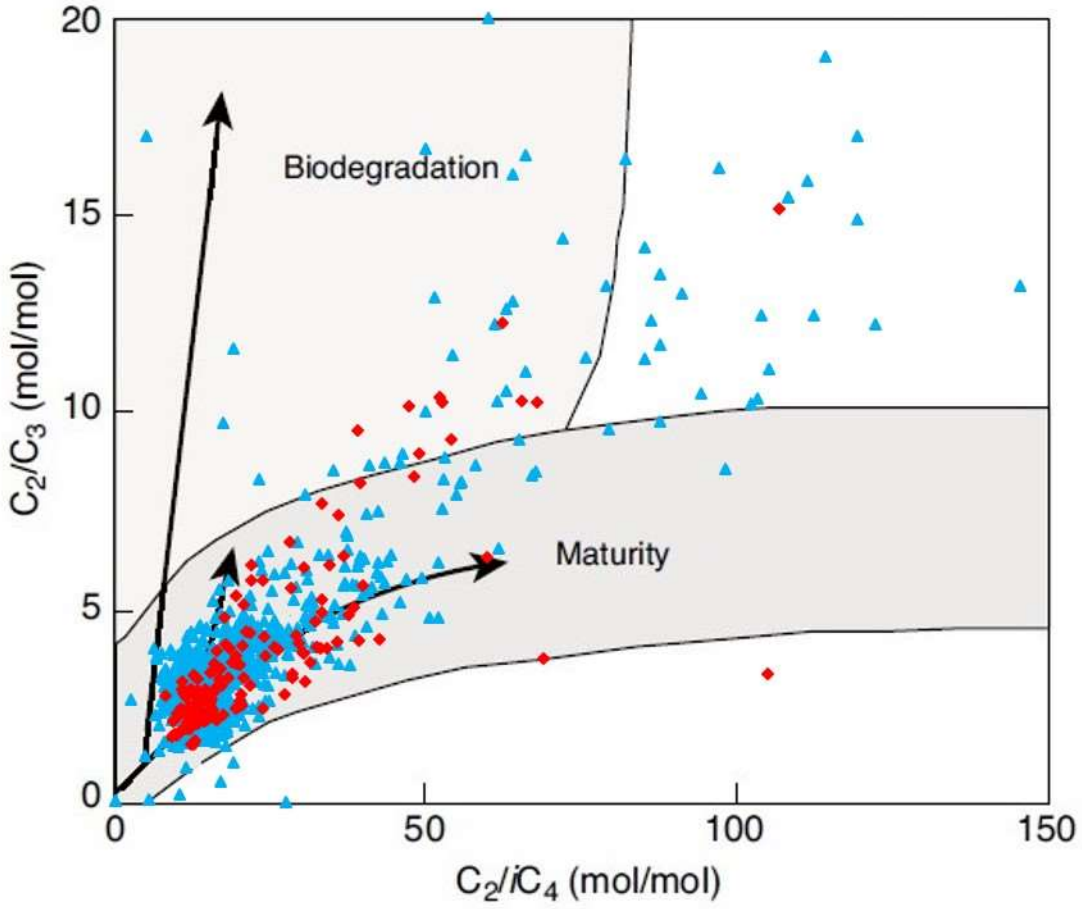

Figure 36. Molecular ratio C_2/C_3 vs. C_2/iC_4 'Prinzhofer Diagram' for the Montney map data (Almost all Montney gas is interpreted to be intermediate between thermogenic and biodegradation).

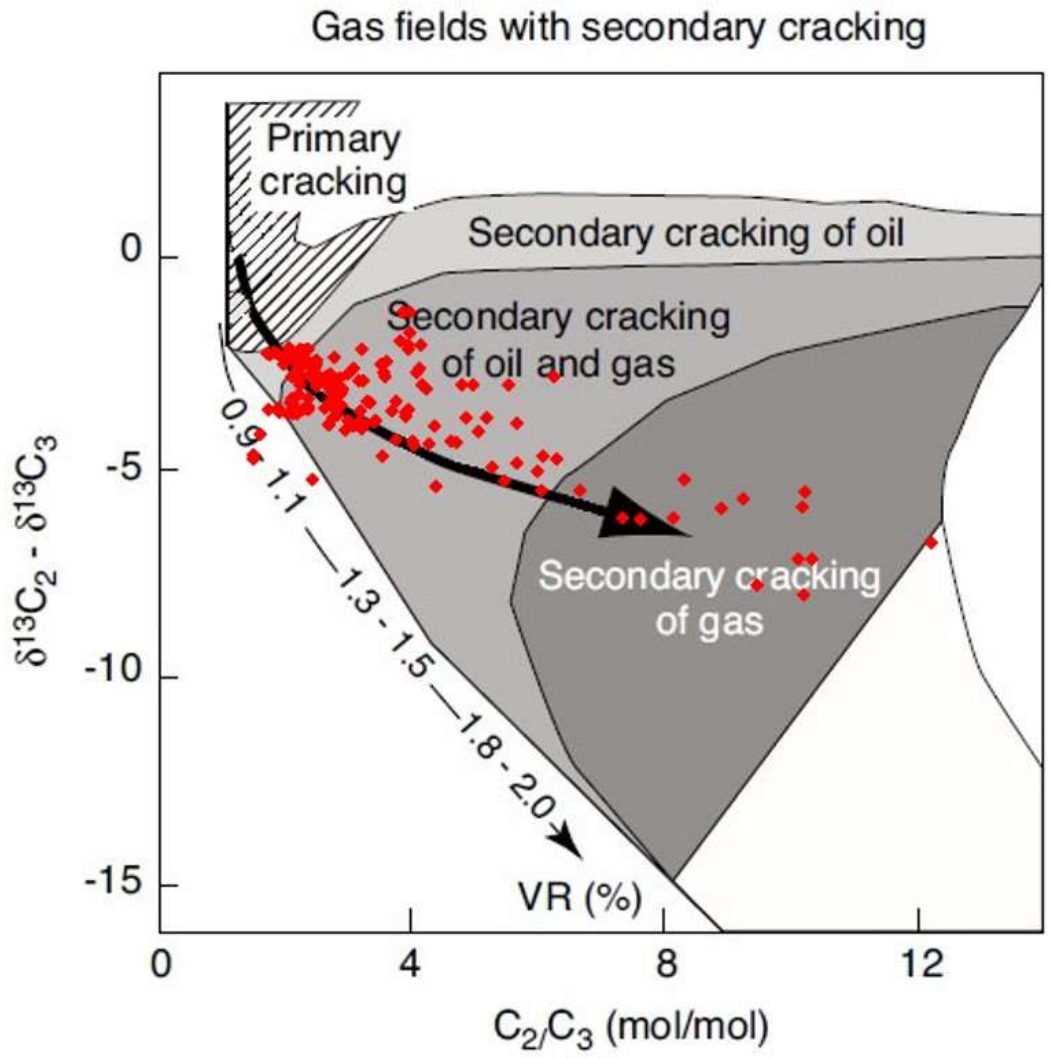

Figure 37. Plot of $\delta^{13}C_2$-$\delta^{13}C_3$ vs. C_2/C_3 'Lorant Diagram' for the Montney map data (Almost all Montney gas is secondary cracking of oil and gas, with strong indication of secondary cracking of gas).

Generally, these diagrams are a good indication of gas generation processes, but are less useful for gas characterization.

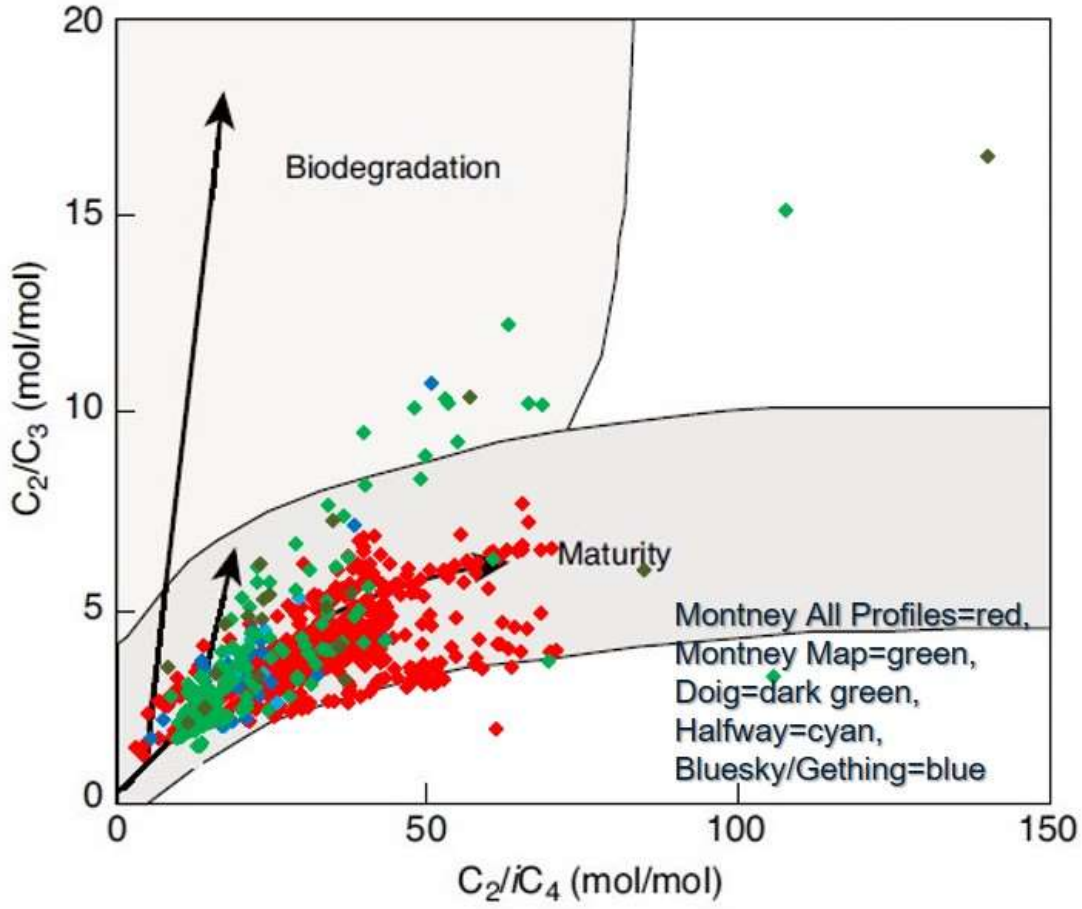

Figure 38. Molecular ratio C_2/C_3 vs. C_2/iC_4 'Prinzhofer Diagram' for the Bluesky to Montney plays from map data (Much Bluesky gas is similar to the lower maturity portion of the Montney play, but Gething might be CBM and Montney map data is different than Montney profile data).

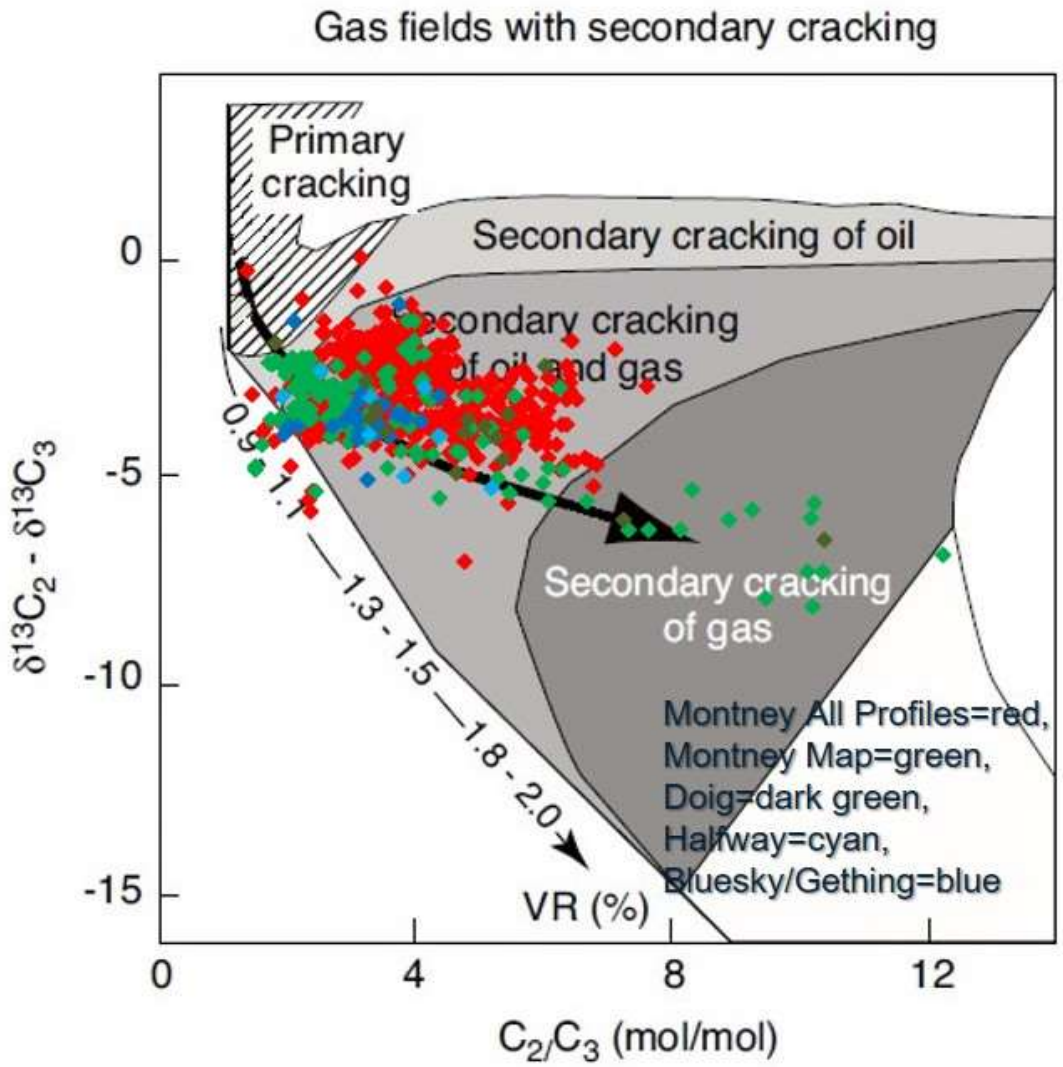

Figure 39. Plot of $\delta^{13}C_2$-$\delta^{13}C_3$ vs. C_2/C_3 'Lorant Diagram' for the Bluesky to Montney plays from map data (Much Bluesky gas is possibly secondary cracking of oil and gas, similar to the lower maturity portion of the Montney play, but Gething might be CBM).

7.6 Natural Gas Characterization from Berner-Faber Diagrams

Isotope plots of $\delta^{13}C_1$ vs $\delta^{13}C_2$ and $\delta^{13}C_2$ vs $\delta^{13}C_3$ were applied by Stahl 1973, 1977, 1979, Redding et al. 1980, Schoell 1980, Rice and Claypool 1981, Holmes et al. 1981, Schoell 1983, 1984, Faber and Stahl 1984, Berner and Faber 1988, 1996 to assess the thermal maturity of natural gas (see Section 7.8). Their plots were based on pyrolysis experiments, so need to be 'calibrated' for different source types and basins. A reminder is necessary that there are two forms of data presented here: mudgas data from the well profiles, and other sample sources marked as map data.

The Montney map data (Figure 40 and Figure 41) when presented on $\delta^{13}C_1$ vs $\delta^{13}C_2$ and $\delta^{13}C_2$ vs $\delta^{13}C_3$ plots are similar to Bluesky/Gething (Figure 42 and Figure 43), but also similar to the Montney profile data (Figure 44 and Figure 45). The separate map data confirm the profile data quite well and shows the same shift on the plot to ^{13}C depleted $\delta^{13}C_1$ than the modeled kerogen line. The Bluesky/Gething map data (not extracted from the well profile data) demonstrate a similar trend to the Montney data with approximately the same shift to ^{13}C depleted $\delta^{13}C_1$. Continuing from Figure 44 and Figure 45 with only the trendlines from the Montney and Bluesky plots, many other plays within NEBC have a similar shift despite some very low data counts (Figure 46 and Figure 47). A possible interpretation is that the methane is possibly a mixed gas, which can complicate its use for source typing.

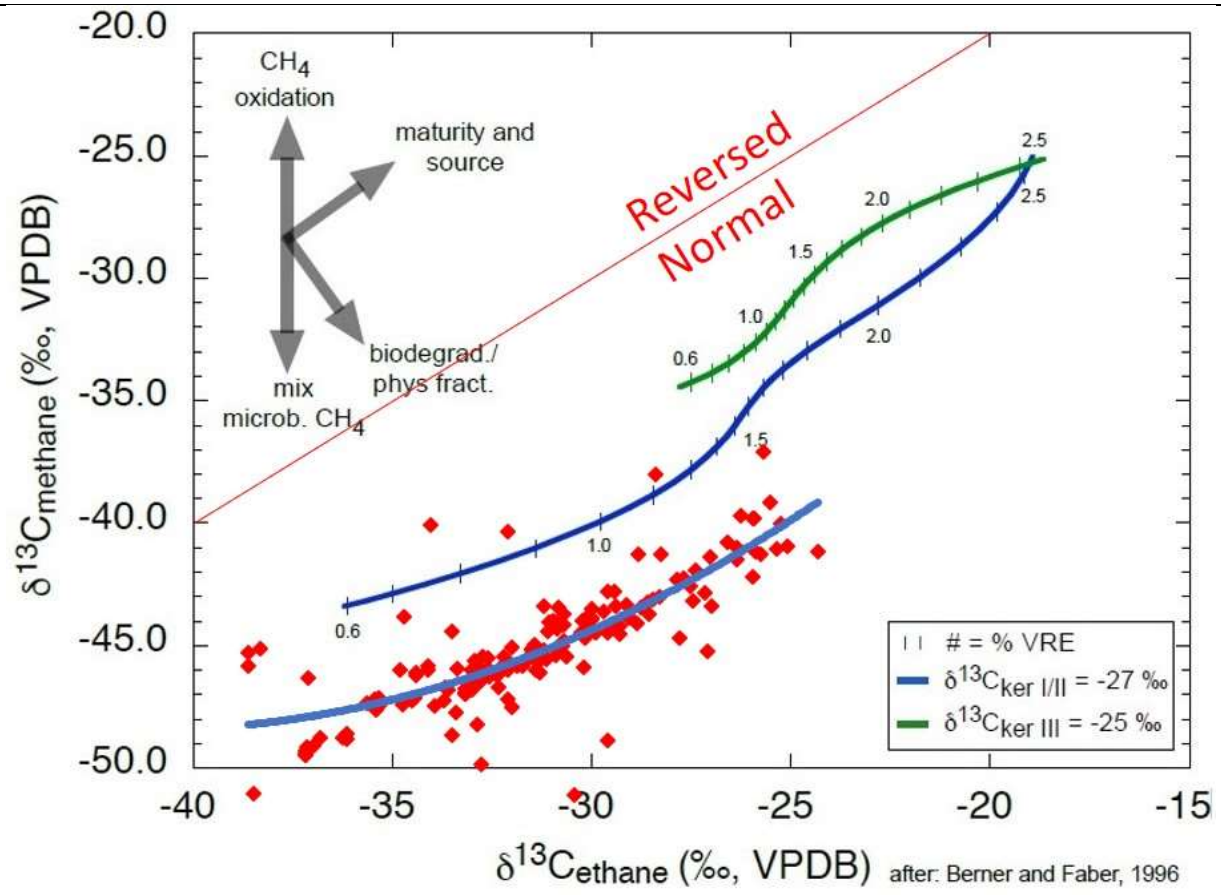

Figure 40. Interpretive diagram $\delta^{13}C_1$ vs $\delta^{13}C_2$ plot for Montney maps in Appendix B (Figure B 83) with additional trendline to represent data on composite diagrams (Whiticar, 2018 pers. comm., after Berner and Faber 1996).

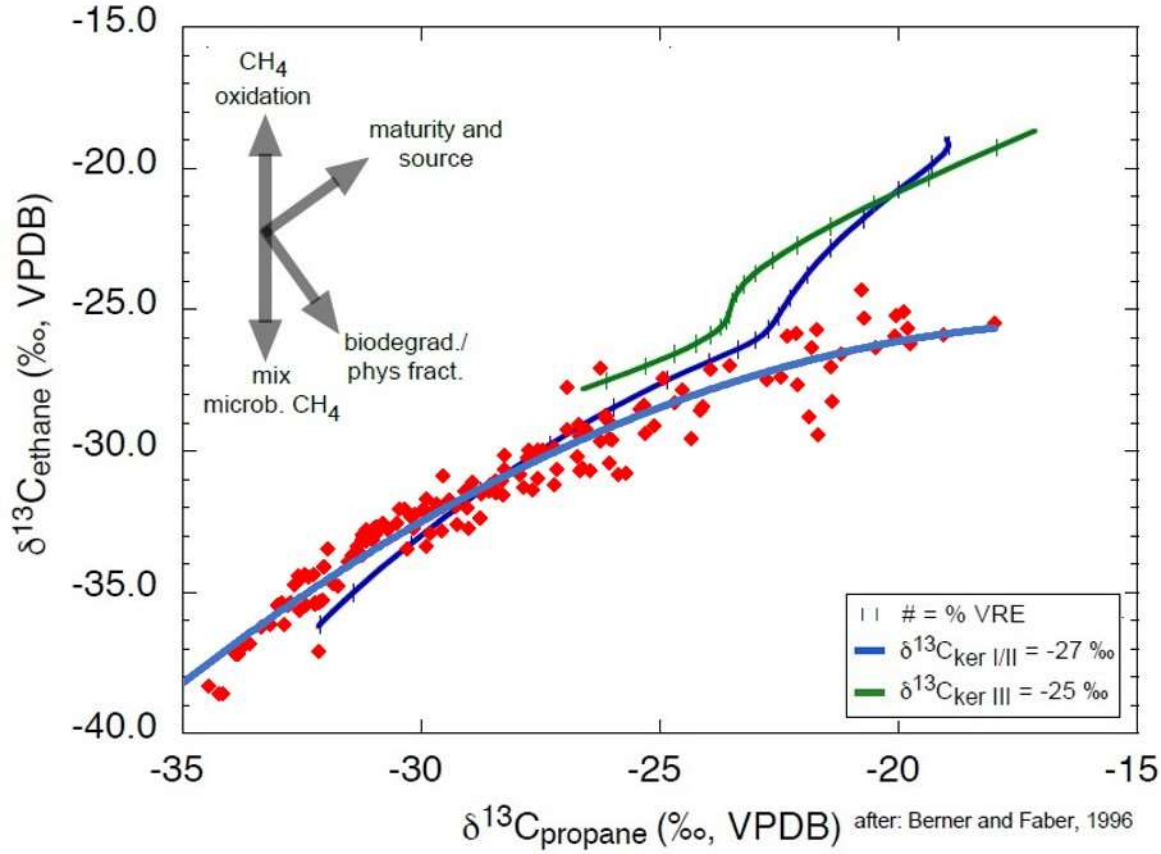

Figure 41. Interpretive diagram $\delta^{13}C_2$ vs $\delta^{13}C_3$ plot for Montney maps in Appendix B with additional trendline to represent data on composite diagrams (Whiticar, 2018 pers. comm., after Berner and Faber 1996).

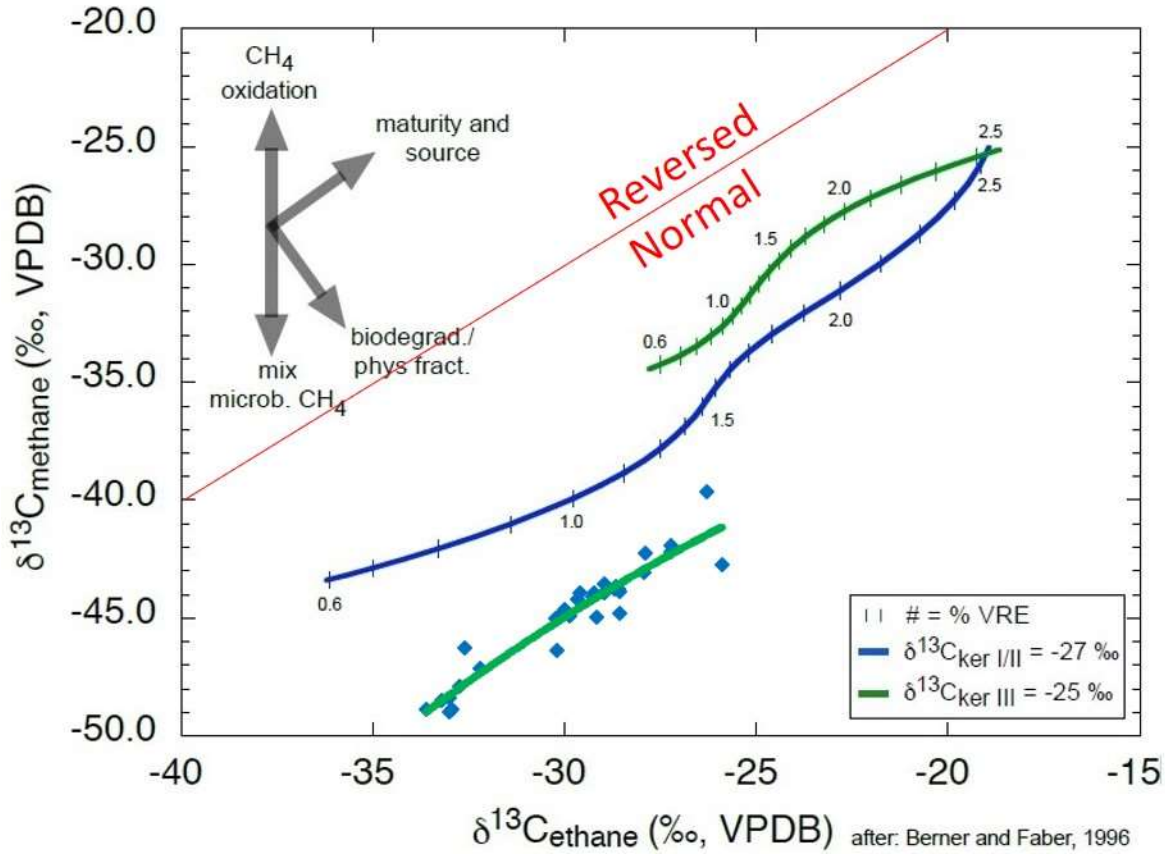

Figure 42. Interpretive diagram $\delta^{13}C_1$ vs $\delta^{13}C_2$ plot for Bluesky/Gething maps in Appendix B with additional trendline to represent data on composite diagrams (Whiticar, 2018 pers. comm., after Berner and Faber 1996).

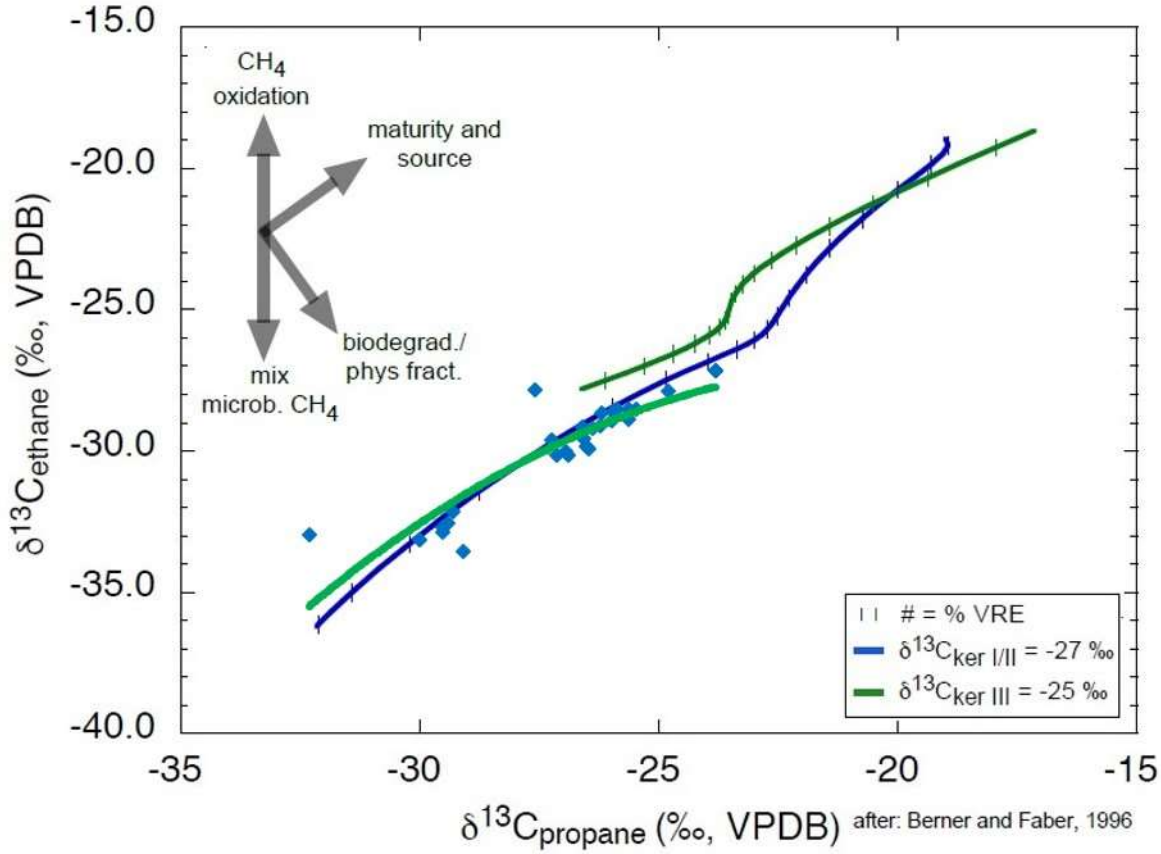

Figure 43. Interpretive diagram $\delta^{13}C_2$ vs $\delta^{13}C_3$ plot for Bluesky/Gething maps in Appendix B with additional trendline to represent data on composite diagrams (Whiticar, 2018 pers. comm., after Berner and Faber 1996).

Appendix A presents profiles across the whole of NEBC, but there is a skew of the data in the Montney Heritage area (Hayes 2018) to only data from horizontal profiles (Montney HZ) which are included with all Montney data in the next $\delta^{13}C_1$ vs $\delta^{13}C_2$ and $\delta^{13}C_2$ vs $\delta^{13}C_3$ plots.

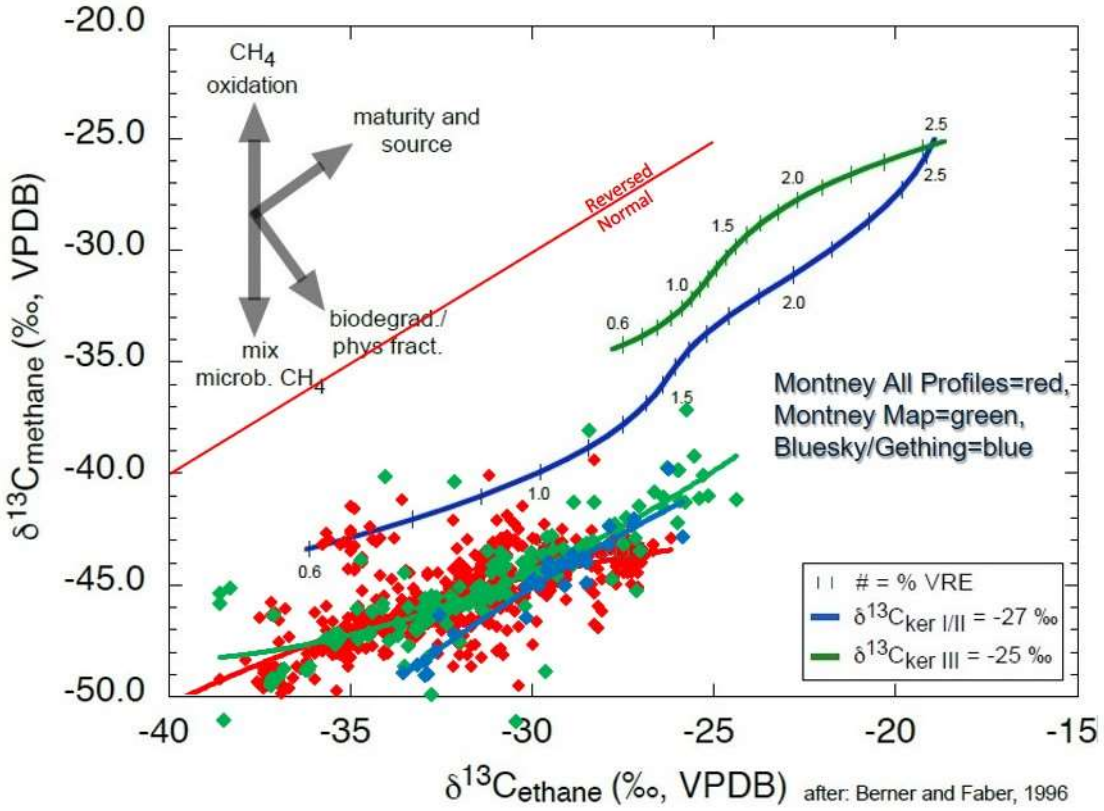

Figure 44. Interpretive diagram $\delta^{13}C_1$ vs $\delta^{13}C_2$ plot for Montney profiles (VT and HZ), Montney map data, Bluesky/Gething map data in Appendix B with additional trendlines to represent data on composite diagrams (Whiticar, 2018 pers. comm., after Berner and Faber 1996).

The corresponding Berner-Faber Diagrams for the three BF-SEOS profiles is reduced to a single well profile, WA#32990, that has $\delta^{13}C_2$ and $\delta^{13}C_3$ data to support the $\delta^{13}C_1$ vs $\delta^{13}C_2$ and $\delta^{13}C_2$ vs $\delta^{13}C_3$ diagrams (Figure 48a and b). The other two well profiles from BF-SEOS data had low hydrocarbon gas contents and do not plot on Berner-Faber Diagrams. The primary question that arises from analysis of these plots is the shift from the previously used kerogen lines in the $\delta^{13}C_1$ vs $\delta^{13}C_2$ and $\delta^{13}C_2$ vs $\delta^{13}C_3$ plots for WA#32990. This may be explained by examining a plot of $\delta^{13}CO_2$ vs $\delta^{13}C_1$ (Figure 49) that indicates a possible different source for the methane (Whiticar at al 1986) that corresponds with the CD Diagrams (Figure 34 and Figure 35) having no data in the hydrogenotrophic field and shallower data is only trending to the acetoclastic field. This aspect is discussed further in conjunction with the other plots including OGC archived data to determine overall trend and how the methane may be from other sources.

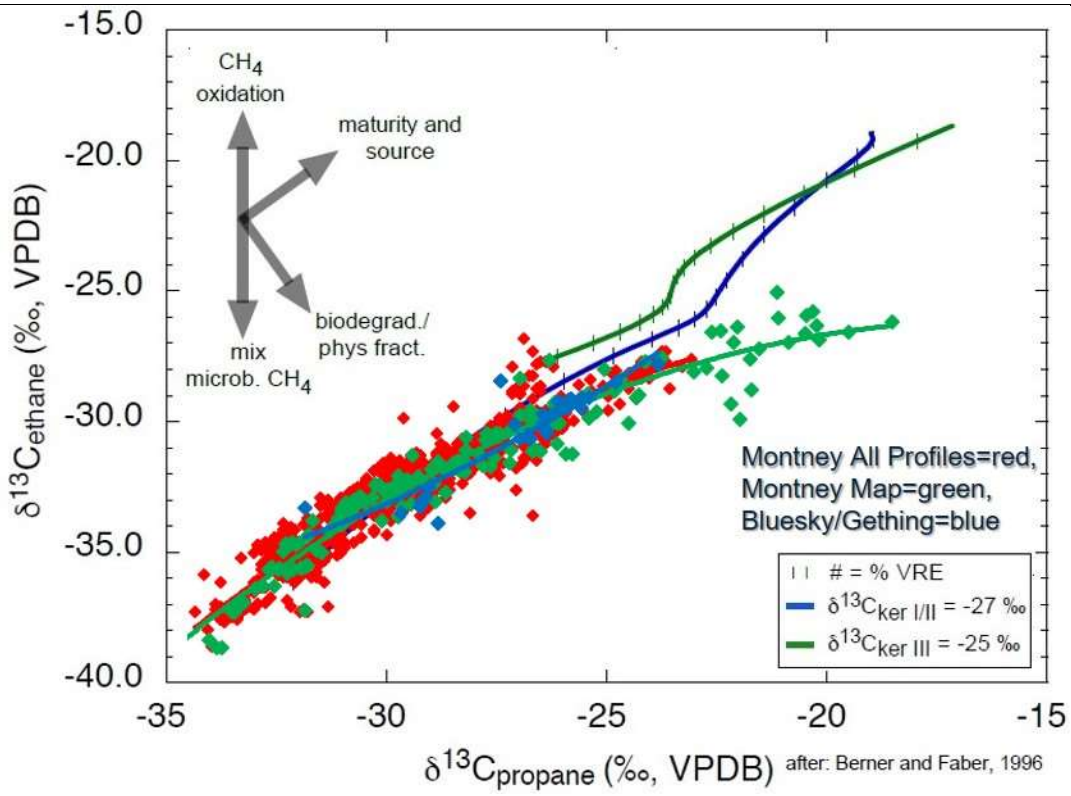

Figure 45. Interpretive diagram $\delta^{13}C_2$ vs $\delta^{13}C_3$ plot for Montney profiles (VT and HZ), Montney map data, Bluesky/Gething map data in Appendix B with additional trendlines to represent data on composite diagrams (Whiticar, 2018 pers. comm., after Berner and Faber 1996).

The issue with the $\delta^{13}C_1$ vs $\delta^{13}C_2$ plot for WA#32990 (Figure 48a) and the Montney plus Bluesky/ Gething plot (Figure 44) depends on the apparently uniform $\delta^{13}C_1$ depletion. On the $\delta^{13}C_2$ vs $\delta^{13}C_3$ plot (Figure 45, Figure 48b) data plots near or along the kerogen line, but the $\delta^{13}C_1$ vs $\delta^{13}C_2$ plot (Figure 44, Figure 48a) has most of the data shifted down to depleted $^{13}C_1$. The points that plot near the $\delta^{13}C_1$ vs $\delta^{13}C_2$ kerogen line are the furthest south locations (WA#32032 and WA#26918 in Appendix A). These well locations are closer to the Alberta region of the Montney play. If the kerogen line is shifted for $\delta^{13}C_1$ in these plots, do all the plots that depend on $\delta^{13}C_1$, such as the Bernard and CD Diagrams, need to also be shifted? This question cannot be answered at this time, but it creates doubt on the use of methane only plots for gas characterization.

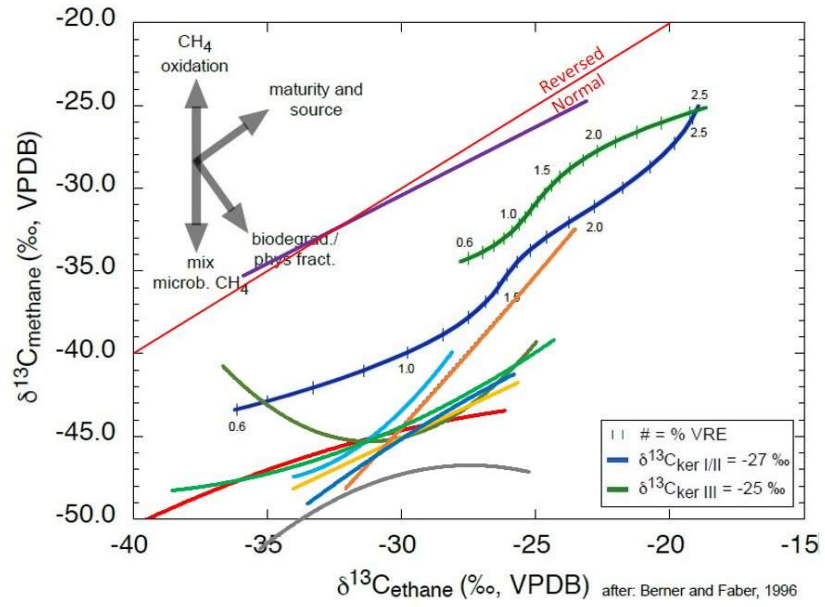

Montney All Profiles=red,
Montney Map=green,
Doig=dark green,
Halfway=cyan,
Fernie=grey,
Nikanassin=gold,
Cadomin=brown,
Bluesky/G=blue,
Jean Marie/Muskwa=purple

SCVF=green triangles

Figure 46. Interpretive diagram $\delta^{13}C_1$ vs $\delta^{13}C_2$ plot for only trendlines from example Triassic to Cretaceous maps in Appendix B and Montney profiles.

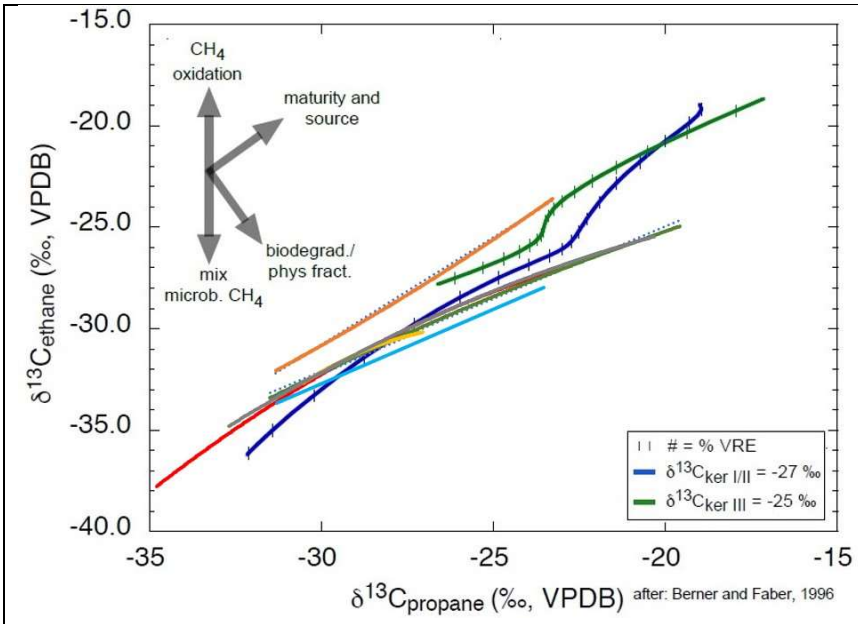

Montney All Profiles=red,
Montney Map=green,
Doig=dark green,
Halfway=cyan,
Fernie=grey,

Nikanassin=gold,
Cadomin=brown,
Bluesky/G=blue,
Jean Marie/Muskwa=purple

SCVF=green triangles

Figure 47. Interpretive diagram $\delta^{13}C_2$ vs $\delta^{13}C_3$ plot for only trendlines from example Triassic to Cretaceous maps in Appendix B and Montney profiles.

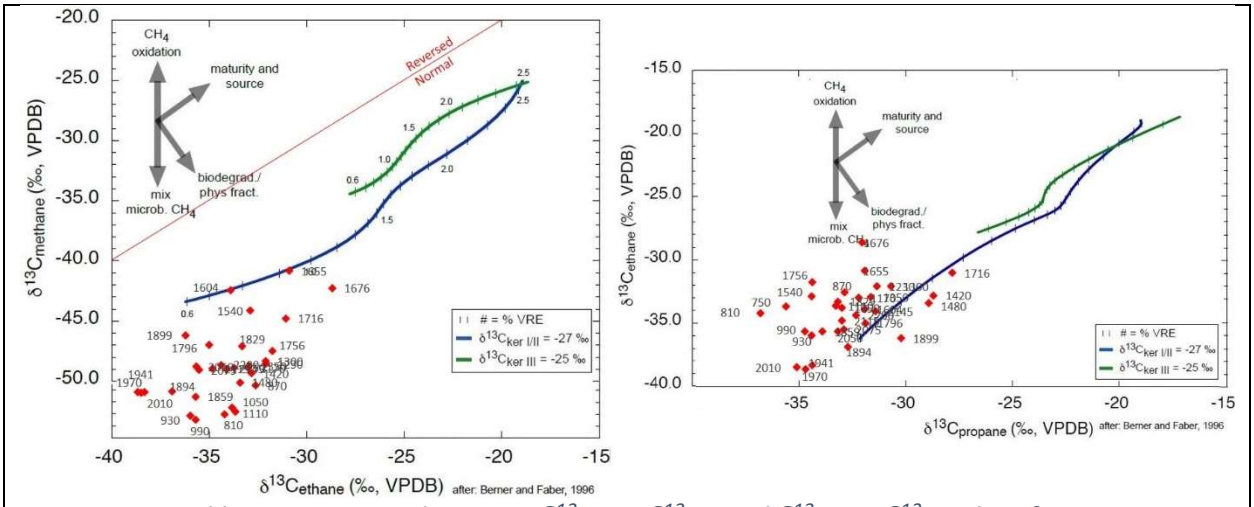

Figure 48a and b. Interpretive diagrams $\delta^{13}C_1$ vs $\delta^{13}C_2$ and $\delta^{13}C_2$ vs $\delta^{13}C_3$ plots for WA#32990 with profile depths (mkb).

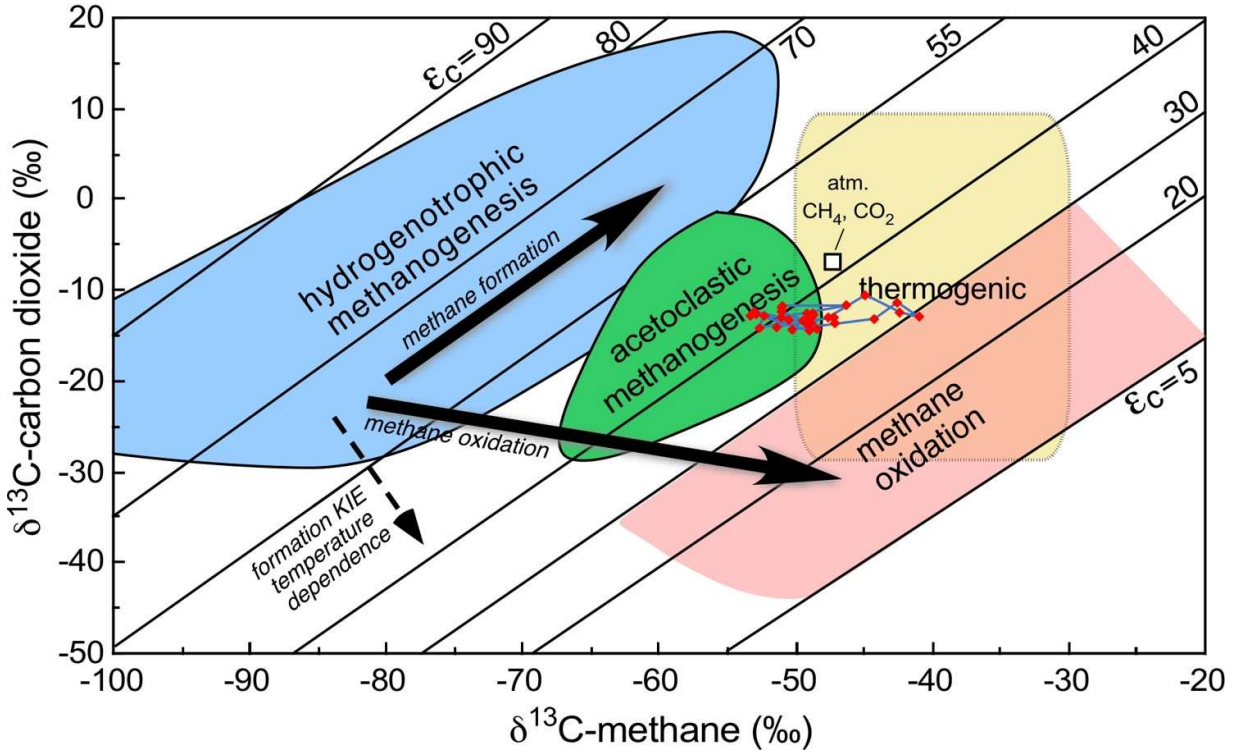

Figure 49. Plot $\delta^{13}CO_2$ vs $\delta^{13}C_1$ from Appendix A for WA#32990 showing a trend outside of the marine depositional environment assumed for most of the strata.

To get $\delta^{13}C_1$ depletion to plot below the $\delta^{13}C_1$ vs $\delta^{13}C_2$ kerogen curve modelled from other petroleum systems, other alternatives of depletion such as biodegradation, mixing, or migration from sources like CBM are possible. Both $\delta^{13}C_2$ and $\delta^{13}C_3$ usually do plot close to the kerogen curve. This is seen in

Appendix A and B having the $\delta^{13}C_1$ vs $\delta^{13}C_2$ plot shifted consistently for most Lower Cretaceous to Triassic strata (in the profiles and maps) as ^{13}C depleted by about 4 ‰ from the kerogen line defined in Figure 7. Could the altered $\delta^{13}C_1$ be due to a shift related to a change in $\delta^{13}C_{kerogen}$? Probably not, as basin wide depleted kerogen is unlikely and biodegradation is most likely to cause uniform depletion. The other possible methane source, pyrobitumen (Wood et al. 2015, Wood and Sanei 2016), may have depleted ^{13}C, but there is no $\delta^{13}C$ analysis despite many samples possible from core at the OGC. Having a source kerogen depleted to a $^{13}C_{kerogen}$ of approximately -34 ‰ would be an extraordinary depositional environment. While the early Triassic was just recovering from the largest extinction event, but a kerogen shift would have also shifted both $\delta^{13}C_2$ and $\delta^{13}C_3$. This suggests that the source of the ethane and propane is derived from the local kerogens while the methane may be from a different process. Some of the NEBC gases plot as being sourced from higher temperature sources such as geothermal portions of the CD Diagram (Whiticar 1996), but none of the plot trends fit on a normal generation curve (e.g., Jenden et al. 1993). The northern sub-basins cannot have the same plots as the data is limited for hydrocarbons higher than C_1 and samples with CO_2 were not tested for CO_2 isotopes. Note that the deepest sample in WA#32990 now shows a sudden change to biodegradation not seen in other plots in Section 6.1.

Another topic that is worth discussing is the Triassic sour gas plays. It should be noted that the examples in Section 6.2 did not include the Charlie Lake/ Baldonnel play. Some profiles here show that there is intra-formational complexity beyond the H_2S that I cannot explain. Example profiles WA#31490 (see Appendix A, Figure A58) and WA#28558 (see Appendix A, Figure A81) have a single Charlie Lake datapoint being a high maturity kerogen Type III, which goes against the reservoir gas assumptions The trends of $\delta^{13}C_1$ depletion seen in the strata surrounding the Charlie Lake play by upto a thousand meters is abruptly reverted to non-depleted for some of the Charlie Lake members. Further work is needed to categorize subdivisions of the Charlie Lake play beyond the scope of this thesis.

The composition of the gas depends on the composition of the source kerogen. Recent geological studies have data that kerogens plot in the ambiguous low index area of a pseudo van Krevelen diagram (Chalmers and Bustin 2012) and thus are not diagnostic of the source rock, but other data plot more on the middle maturity of Type III kerogen with planktonic marine sources (Crombez et al. 2017a) or as standard Type II kerogen (Romero-Sarmiento et al. 2016), but no isotope data is reported. The levels of anoxia (Crombez et al. 2017b) are still under review by other authors. The geochemistry has been affected by the end-Permian extinction event (Zonneveld and Moslow 2018) changing the organic material and thus the complex geochemistry needs to be taken into account for that event and during a similar event that occurred during the deposition of the Montney (e.g., Grasby et al. 2016a). Cretaceous strata in the Liard sub-basin has an immature to overmature trend of Type II kerogens from north to south, but no isotope data is reported (Ardakani et al. 2017).

7.7 Natural Gas Characterization with new plot format

The variables $\delta^{13}C_2$ and $\delta^{13}C_3$ or iC_4/nC_4 could be diagnostic parameters, but the $\delta^{13}C_3$-$\delta^{13}C_2$ differential did not show variation as the profiles are sub-parallel across most strata and hiatus. The Lorant Diagram mentioned in Section 3.2 (Figure 10) is not diagnostic. A new format of interpretive diagram is proposed as a direct plot of $\delta^{13}C_2$-$\delta^{13}C_1$ versus iC_4/nC_4 ratio. This plot appears to be effective in differentiating the variability created by the wellbore sidetracks (see WA#28770). Plots utilizing methane data only do not appear to be diagnostic in detail of this example and the Bernard and CD Diagrams do not distinguish data variability. To test the effectiveness of this new plot style, an 'all Montney profiles' plot of $\delta^{13}C_2$-$\delta^{13}C_1$ vs iC_4/nC_4 was created for possible consideration as a diagnostic plot for NEBC. If it is expanded to include the Montney maps data (play 4.21) and the 'surface gas' data (play 4.00), the resulting diagram (Figure 50, Figure 51) must have an expanded scale. A variation (Figure 52) of the proposed characterization diagram has a log10 scale for the iC_4/nC_4 ratio on the X-axis to show better separation between the plays with lower values for that ratio. The surface gas also has a shift in $\delta^{13}C_3$ as seen on the Berner-Faber Diagram in the next Section.

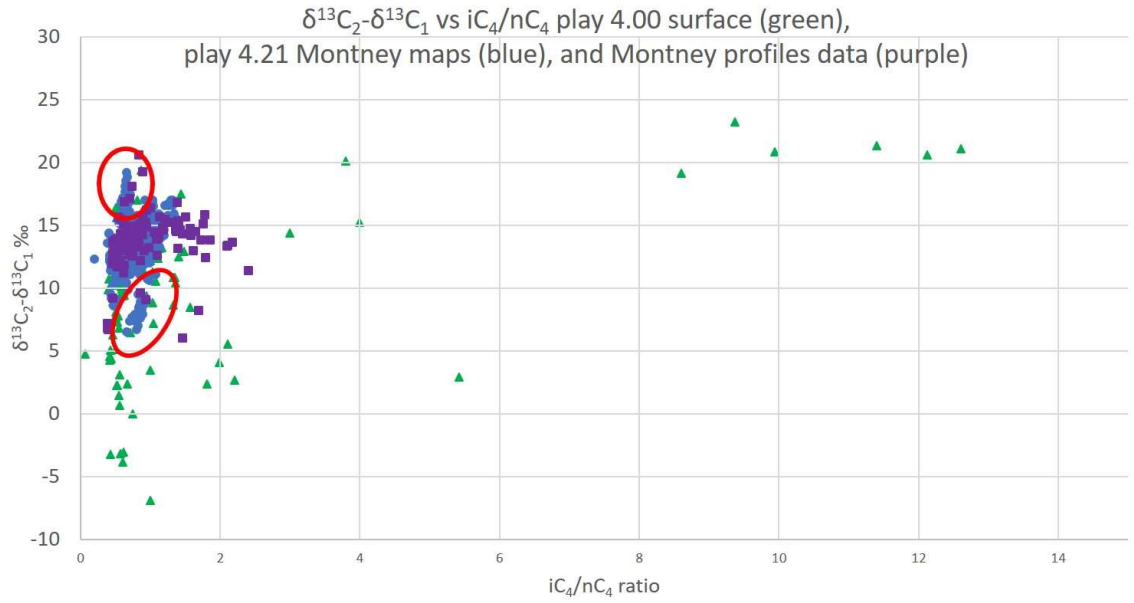

Figure 50. New format plot of $\delta^{13}C_2$-$\delta^{13}C_1$ vs iC_4/nC_4 for Montney all profiles data, Montney map data, and surface play 4.00 map data with general trend and excursions, linear axis.

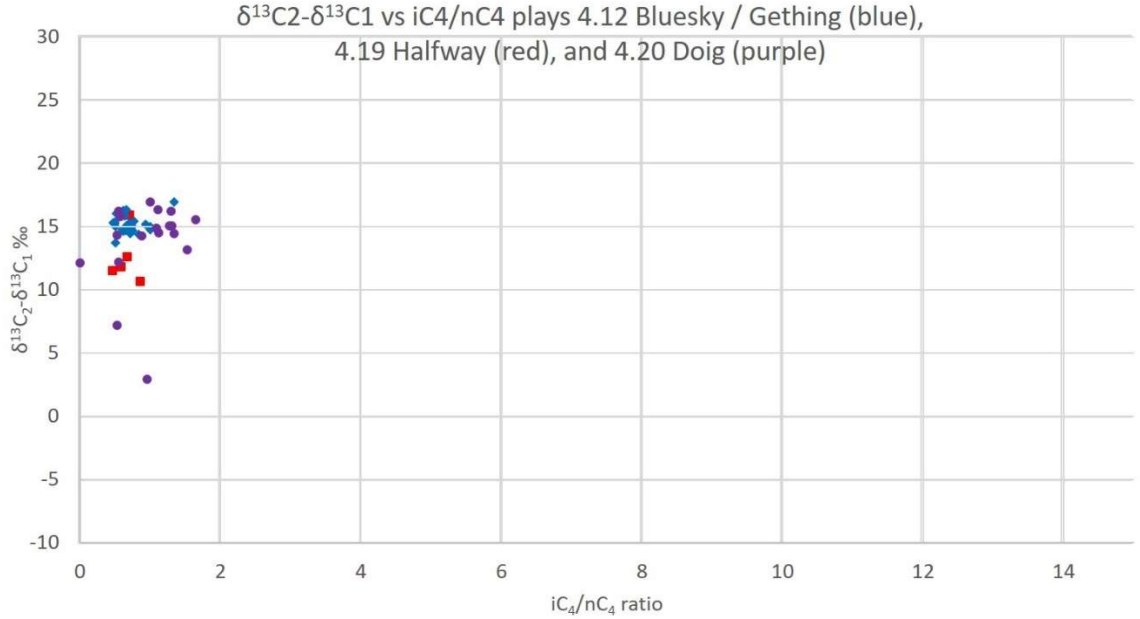

Figure 51. New format plot of $\delta^{13}C_2$-$\delta^{13}C_1$ vs iC_4/nC_4 for plays data for Bluesky/Gething 4.12, Halfway 4.19, Doig and Lower Halfway 4.20 at scale of surface data linear axis.

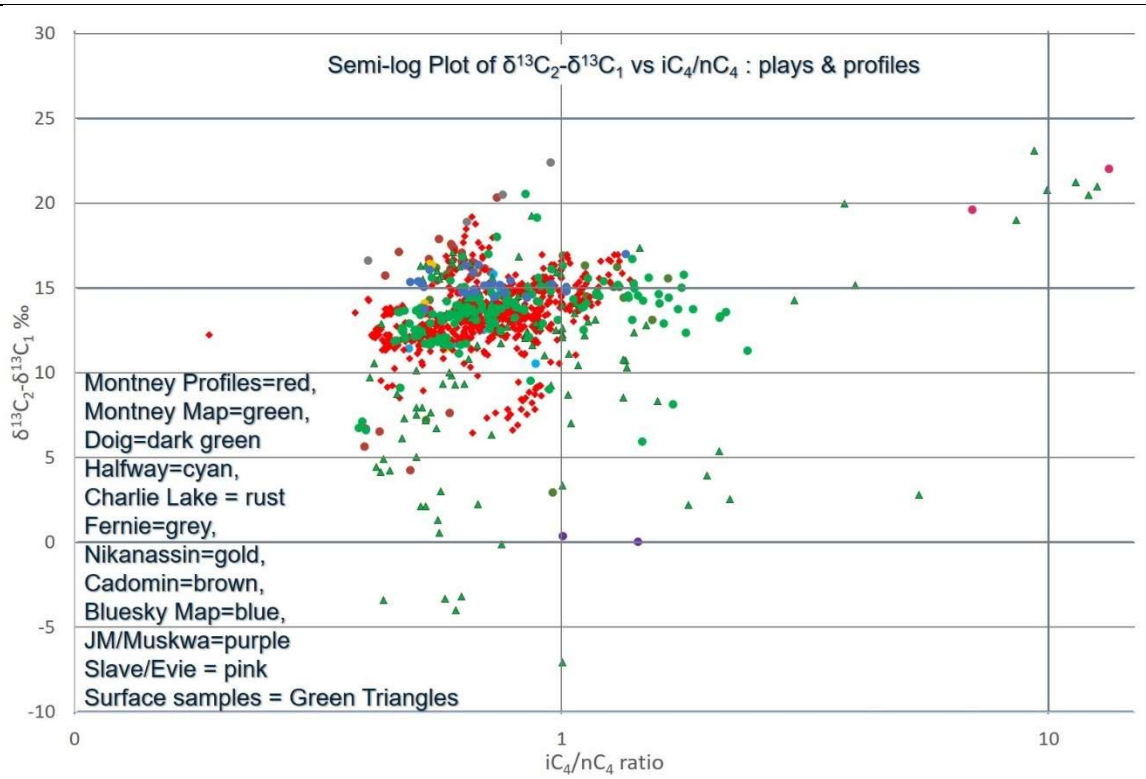

Figure 52. New format plot of $\delta^{13}C_2$-$\delta^{13}C_1$ vs iC_4/nC_4 for major plays data and Montney profiles data at scale of surface data, logarithmic axis (base 10).

7.8 Thermal maturity calculation and basin calibration of Berner-Faber relationships

The first indication of high maturity, isotope reversals, occur in NEBC specifically in the Liard and Horn River sub-basins and in the deepest strata of the WCSB. Reversals are different than isotopic 'rollover' (e.g., Zumberge et al. 2012) observed by other studies in NEBC (Figure 56 after Tilley and Muehlenbachs 2013) and have to be interpreted from seeing a progression in the whole well profile including C_2 and C_3 composition and isotopes (Xia et al 2013, Curiale and Curtis 2016). Isotopic reversals are where the values for higher hydrocarbons are more depleted for ^{13}C than lower hydrocarbons (e.g., $\delta^{13}C_2$ is a more negative number than $\delta^{13}C_1$, or $\delta^{13}C_3$ is a more negative number than $\delta^{13}C_2$). The isotopic reversals for methane seen in the BC-NGA data is a small percentage of the samples in Appendix A as $\delta^{13}C_2$-$\delta^{13}C_1$ results in only 16 samples with large reversal of 1 ‰ to 8 ‰ and only 28 more samples with a small reversal of 1 ‰ or less. All of these samples are from the Besa River and Otter Park formations. The remainder of 878 samples have a non-reversed $\delta^{13}C_2$-$\delta^{13}C_1$ value and cover the rest of the strata in NEBC. Of the 943 data points where $\delta^{13}C_3$-$\delta^{13}C_2$ can be calculated, only 17 with large reversal of 1 ‰ to 8 ‰ and another 13 have a small reversal of 1 ‰ or less. The propane/ethane reversals are scattered more widely including Montney, BuckingHorse, and Charlie Lake formations in addition to the certain Besa River and Otter Park formations. Ethane isotope 'reversals' within a single well demonstrate overpressure/effective seals (Curiale and Curtis 2016) and these may be isolated occurrences.

Other basins show $\delta^{13}C_1$ values well above $\delta^{13}C_2$ and $\delta^{13}C_3$ (e.g., Kotarba et al. 2014) with general agreement to lab results (Gao et al. 2014). This is an opposite effect to what is seen on the profiles from the Montney areas. There is multiple iteration oil migration with later gas generation known in the area, with specific examples for the Montney (Wood and Sanei 2016). However, it is highly likely that combinations of extreme gas generation and mixing are responsible for the isotope signatures observed.

Differences between previously published $\delta^{13}C_2$ vs $\delta^{13}C_1$ and $\delta^{13}C_3$ vs $\delta^{13}C_2$ kerogen lines (Berner and Faber 1988) shown previously (Figure 7 and Figure 8) and the data from this study (Figure 46, Figure 47) have prompted a comparison of thermal maturity. The relations used by Berner and Faber (1988, Tables 1 and 2 therein) are listed as:

$$\delta^{13}C_1\,(‰) = 15.4*\log(R_o\,\%) - 41.3 \quad \text{(Eq. 5a)}$$

$$\delta^{13}C_2\,(‰) = 22.6*\log(R_o\,\%) - 32.2 \quad \text{(Eq. 5b)}$$

$$\delta^{13}C_3\,(‰) = 20.9*\log(R_o\,\%) - 29.7 \quad \text{(Eq. 5c)}$$

$$C_1\,\%(MC) = 9.1*\ln(R_o\,\%) + 93.1 \quad \text{(Eq. 5d)}$$

$$C_2\,\%(MC) = -6.3*\ln(R_o\,\%) + 4.8 \quad \text{(Eq. 5e)}$$

$$C_3\,\%(MC) = -2.9*\ln(R_o\,\%) + 1.9 \quad \text{(Eq. 5f)}$$

These are inverted to solve for thermal maturity as a function of vitrinite reflectance (R_o) as:

$$R_o\,(\%_{C1}) = 10^{((\delta 13C1\ ‰ + 41.3)*.0649)} \quad \text{(Eq. 6a)}$$

$$R_o\,(\%_{C2}) = 10^{((\delta 13C2\ ‰ + 32.2)*.0442)} \quad \text{(Eq. 6b)}$$

$$R_o\,(\%_{C3}) = 10^{((\delta 13C3\ ‰ + 29.7)*.0478)} \quad \text{(Eq. 6c)}$$

$$R_o\,(\%) = e^{((C1\% - 93.1)*.1099)} \quad \text{(Eq. 6d)}$$

$$R_o\,(\%) = e^{((C2\% - 04.8)*-.1587)} \quad \text{(Eq. 6e)}$$

$$R_o\,(\%) = e^{((C3\% - 01.9)*-.3448)} \quad \text{(Eq. 6f)}$$

The resulting values from equations 6a, 6b, 6c were plotted for the Montney profiles (individually as Figure 53, Figure 54, Figure 55). More recent comprehensive versions of the equations (Berner and Faber 1996) will be revised in new publications (Whiticar 2018 pers. comm.,). The equations 6d, 6e, 6f are based only on composition and could not be applied to mudgas samples in the profiles dataset as the equations rely on unaltered reservoir gas which is essentially impossible to obtain during mudgas collection.

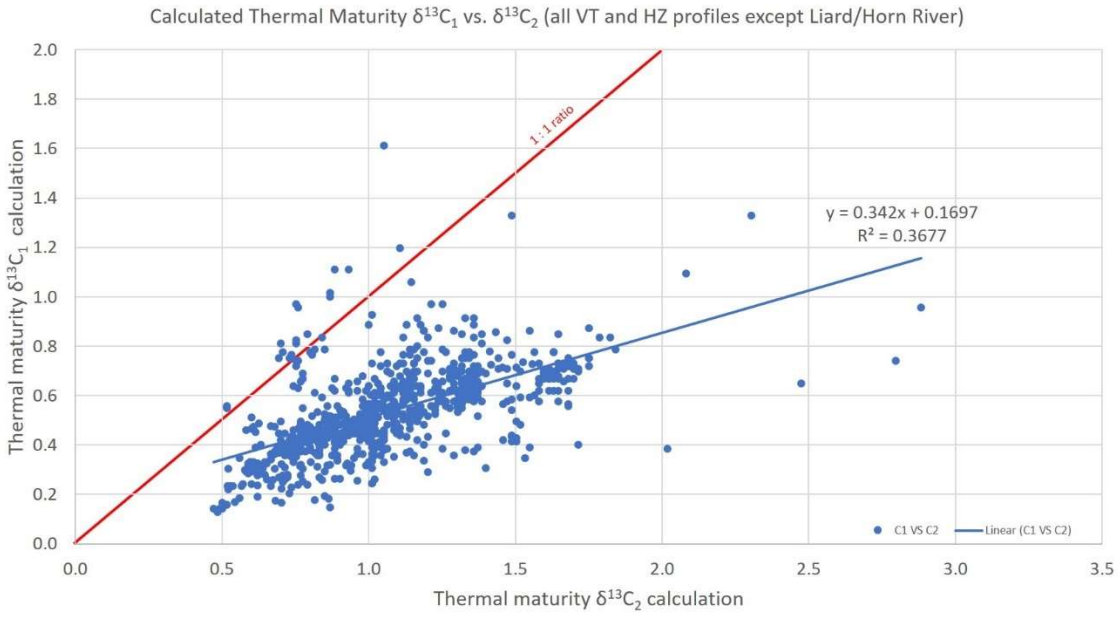

Figure 53. Plot of calculated thermal maturity from $\delta^{13}C_1$ versus $\delta^{13}C_2$ (Berner and Faber 1988) and compared between the three populations for consistency. The red trendline is a slope of 1 for best correspondence and only a few samples fit.

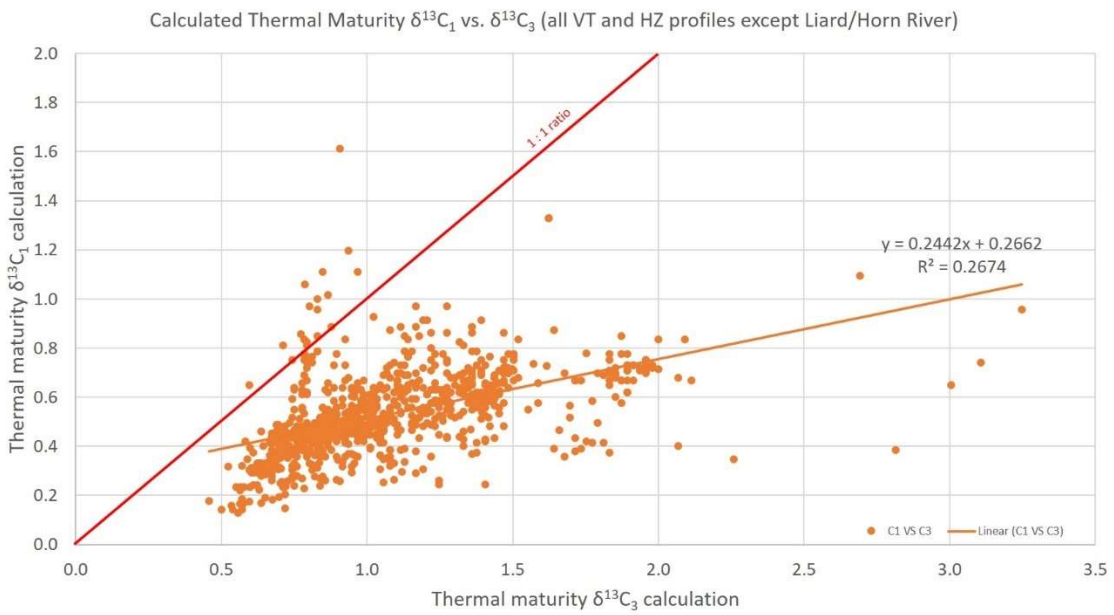

Figure 54. Plot of calculated thermal maturity from $\delta^{13}C_1$ versus $\delta^{13}C_3$ (Berner and Faber 1988) and compared between the three populations for consistency. The red trendline is a slope of 1 for best correspondence and only a few samples fit.

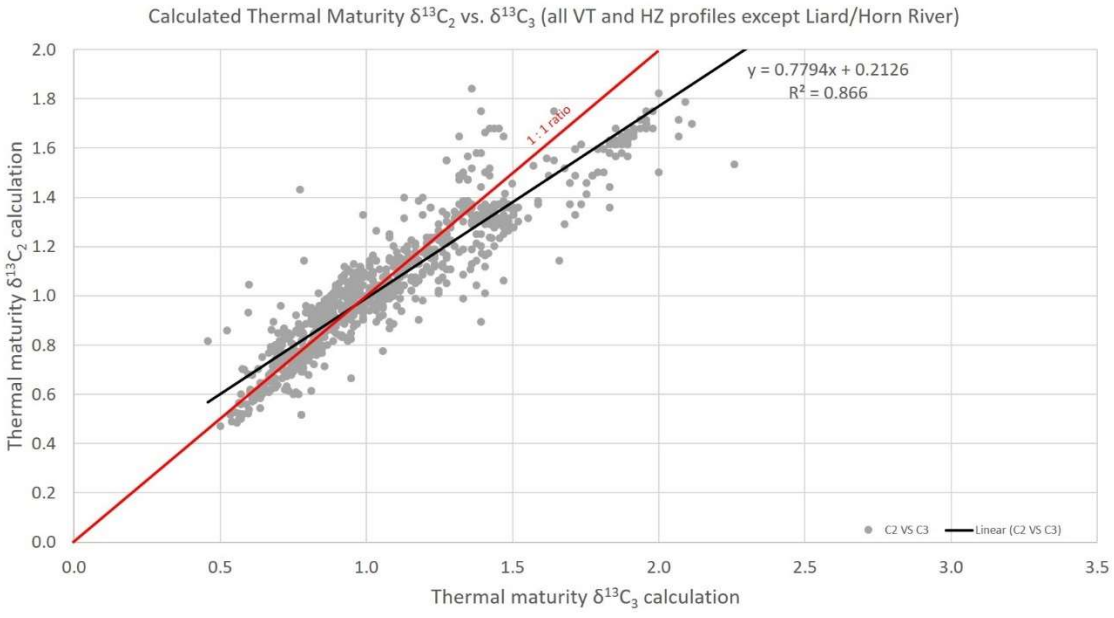

Figure 55. Plot of calculated thermal maturity from $\delta^{13}C_2$ versus $\delta^{13}C_3$ (Berner and Faber 1988) and compared between the three populations for consistency. The red trendline is a slope of 1 for best correspondence and many low maturity samples fit.

It is obvious that the thermal maturity estimate from $\delta^{13}C_1$ fall on a trend with a slope below 0.4, while the slope from $\delta^{13}C_2$ or $\delta^{13}C_3$ is almost 0.8, but even $\delta^{13}C_2$ does not completely agree with $\delta^{13}C_3$, especially at higher maturity. The Liard and Horn River samples are not plotted on these graphs as there was only a few datapoints with $\delta^{13}C_1$,C_2,C_3 values. Also, for Liard and Horn River, the $\delta^{13}C_1$ values calculated from the Berner-Faber equations to nonsensical values between 60 and 120 Ro% (e.g., WA#29046 has $\delta^{13}C_1$ between -9.6 and -25.7 ‰; WA#29727,29747 have $\delta^{13}C_1$ between -27.2 and -36.5 ‰) indicating that $\delta^{13}C_1$ interpretation for the Liard and Horn River sub-basins needs separate calibration of thermal maturity. The well profile WA#29046 is from core that has thermal maturity data where R_o for the Besa River formation is between 2.5 and 3.0%. As shown in the preliminary work by Wilson and Bustin (2018), the thermal maturities of the Horn River and Liard Basins are high (2.6-3.1%R_o and 1.75-3.2%R_o respectively). They are surprisingly similar to each other despite the Bovie fault (Wilson and Bustin 2018), suggesting that much of the thermal maturation occurred prior to fault movement.

One paper established the path of gas maturation relative to other well-known 'shale gas' plays (Tilley and Muehlenbachs 2013) on the $\delta^{13}C_2$ vs $\delta^{13}C_1$ and $\delta^{13}C_3$ vs $\delta^{13}C_2$ plots (Figure 56, note the reversal of the plot axis only used in Tilley and Muehlenbachs 2013).

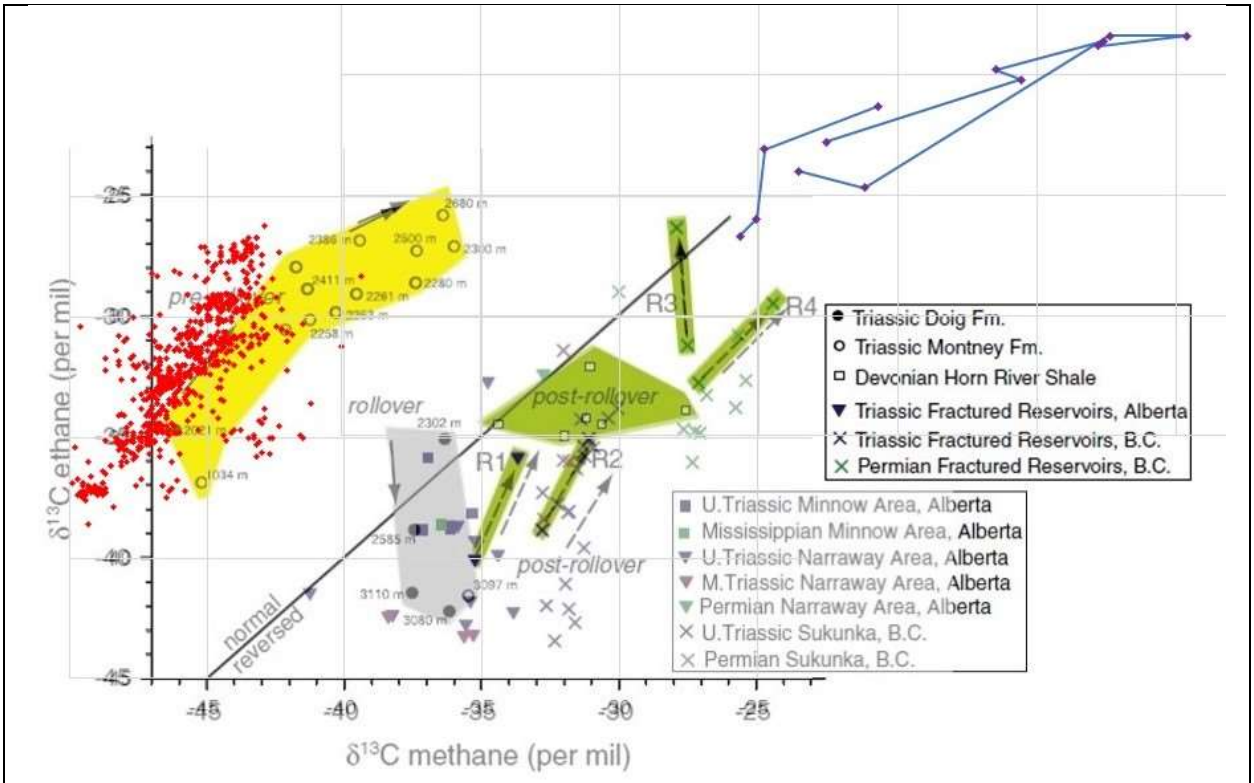

Figure 56. Plot of $\delta^{13}C_2$ vs $\delta^{13}C_1$ after Tilley and Muehlenbachs 2013 Figure 6a and Figure 7a therein with overlays from Montney data in red and Liard (WA#29046) in purple from this thesis.

This $\delta^{13}C_2$ vs $\delta^{13}C_1$ plot is replicated here with additional data from this thesis for wells WA#29747-29727 in purple and a new overlay of Montney all profiles dataset in red. Obviously, the higher maturity samples for the Triassic in the BC-NGA database is under-represented in this thesis for a number of locations. The merging of Montney and Liard data with data from the structurally complicated foothills area of Tilley and Muehlenbachs (2013) might be crossing geological boundaries of structural complications, but it indicates that there is further work needed to identify the isotopic rollover between the geographic locations of the Montney play and the Triassic equivalent strata in the Liard sub-basin. Also, the shift between the thermogenic Jean Marie and possibly roll-over Muskwa strata should be identified. The location where rollover occurs in NEBC has not been located and is not discussed further here.

8 Surface Gas Samples - Characterization

A new play (4.00) was introduced above the stratigraphic sequence of the 2006 atlas (MEM 2006a, b, c), to reflect surface emissions captured as a data horizon above the land surface. 'Play 4.00' included SCVF and other samples of fugitive emissions above the shallowest play in the 2006 atlas. As a special category of data, 'play 4.00' has special triangular symbols, due to SCVF and bubble gas having data that is indeterminate in geospatial relationships as the gas sources are not obvious and are possibly highly variable. There is no profile data in Appendix A for surface gases, but there could be revisiting sampling to some locations to generate a time series. Other datasets in Appendix B have other data quality issues discussed previously.

A problem with surface collected gases is that the Bernard and CD Diagrams (Figure 57 and Figure 58) show that the surface gases plot in the region of thermogenic reservoir gases. This goes against assumptions as some gases sourced from recent surficial environments, such as bubble gas from wetlands, should plot in the microbial sections of the diagrams, but only one sample shows that gas character. Some reports of surface gas geochemistry have ISO data for C_2 and C_3 hydrocarbons despite having very low ppm of gas composition.

The Bernard Diagram (Figure 57) and the CD Diagram (Figure 58) do not clearly classify the surface gases as being in a separate microbial sector different from the reservoir gases. Further work is needed to confirm if NEBC surface gas is all thermogenic.

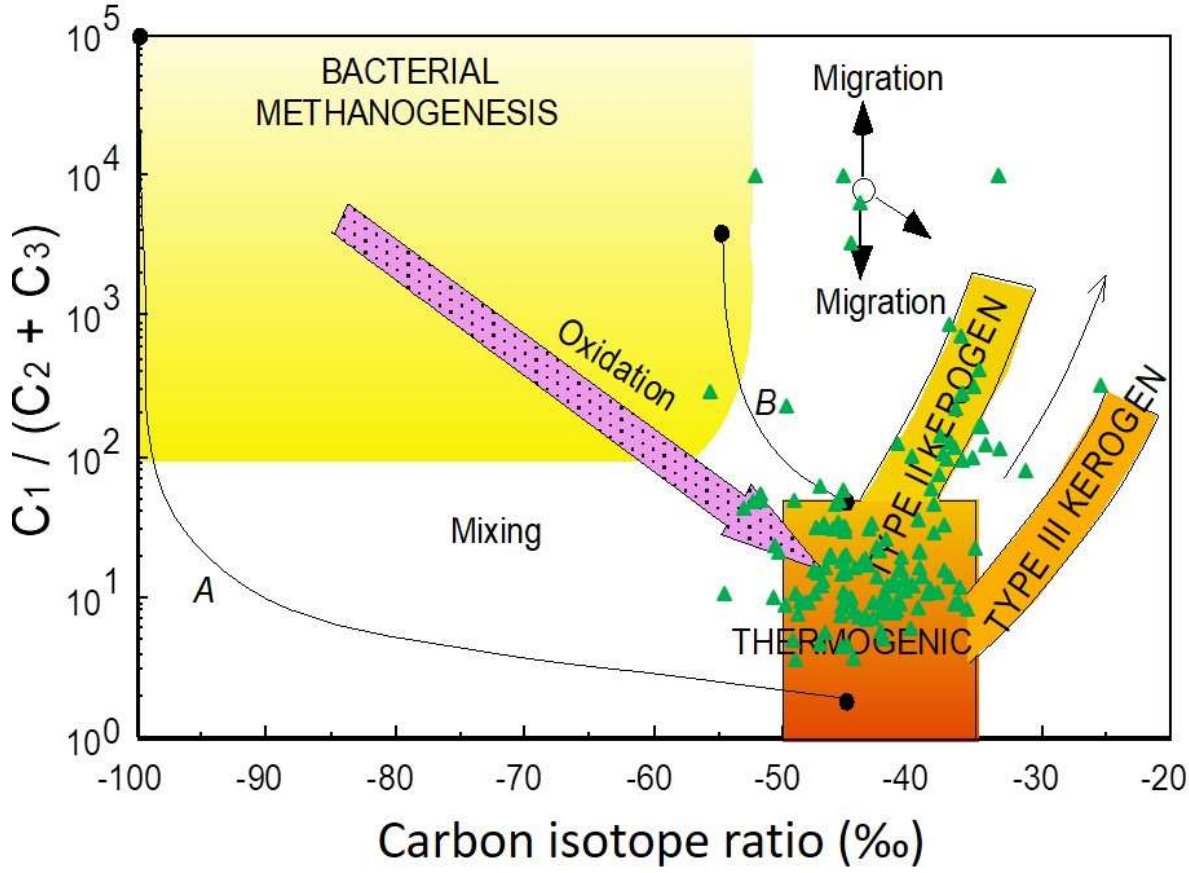

Figure 57. Bernard Diagram for only 'surface play 4.00' (including SCVF and bubble gas map data in Appendix B, Whiticar, 2018 pers. comm., after Whiticar 1999).

In fact, most surface gases plot in the thermogenic area where the other plays plot with a few exceptions to higher thermal maturity, which is counter intuitive. It is more likely that these samples are sourced from completely microbial activity with a mix of different gases from very shallow but extreme processes that should include oxidation and biodegradation. Similarly, surface gases are in the same data envelope as reservoir gases for MC only plots and are not identified by those interpretive tools.

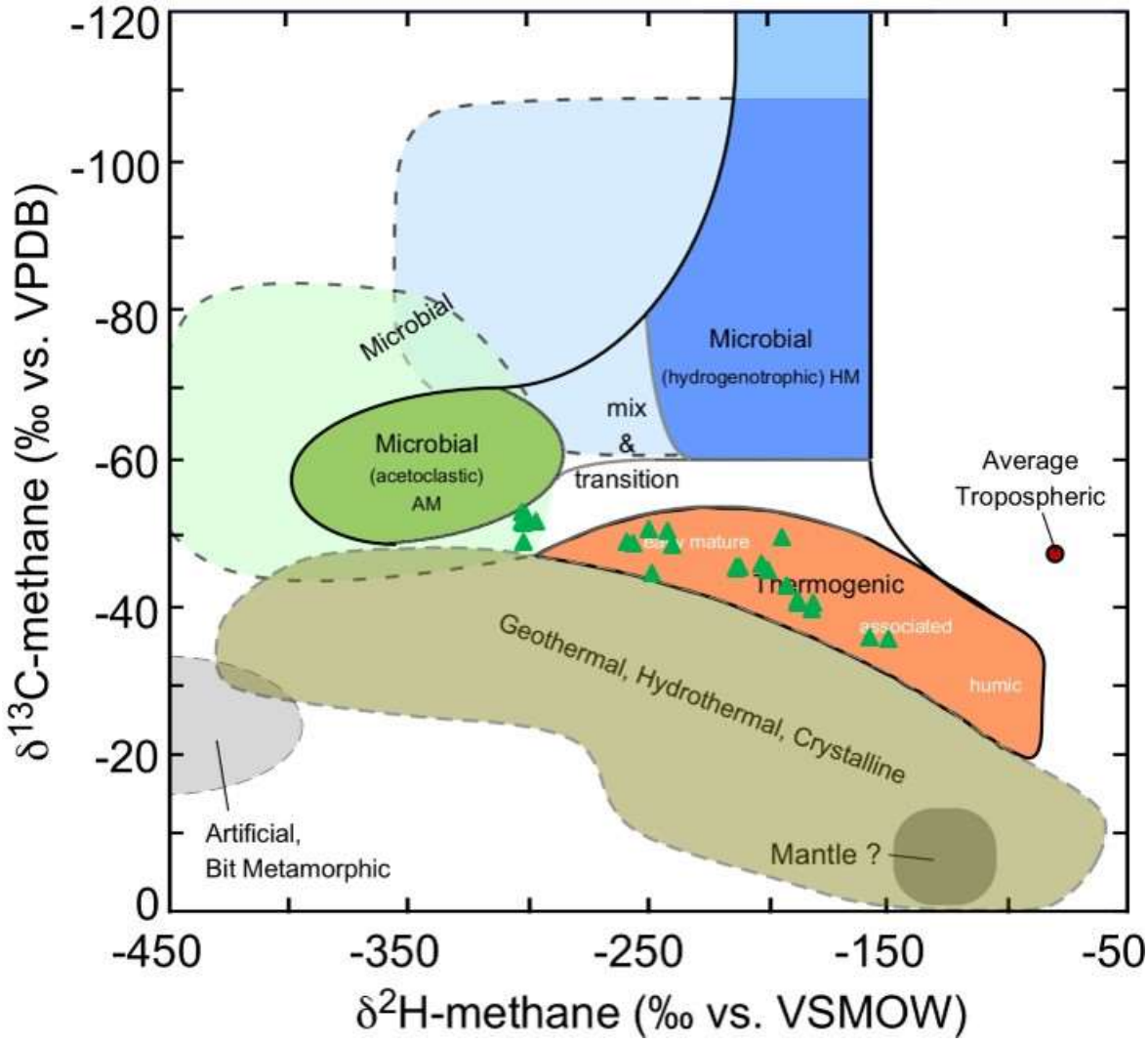

Figure 58. CD Diagram for only 'surface play 4.00' (including SCVF and bubble gas map data in Appendix B, Whiticar, 2018 pers. comm., after Whiticar 1999)).

The Berner-Faber Diagrams (Figure 59 and Figure 60) are more functional even though the data cannot have a trendline on the $\delta^{13}C_1$ vs $\delta^{13}C_2$ plot as the data distribution are scattered by the nature of unknown mixed sources. The $\delta^{13}C_2$ vs $\delta^{13}C_3$ does have potential for a trendline, but it is $\delta^{13}C_2$ enriched compared to the reservoir gas trendlines (except for the Cadomin samples) and both enriched and depleted for $^{13}C_3$. In fact, some surface gas sources could be assumed from recent sources outside the petroleum system. The $\delta^{13}C_1$ vs $\delta^{13}C_2$ and $\delta^{13}C_2$ vs $\delta^{13}C_3$ plots are highly scattered with a few possible trends but very little matching the cluster of trendlines from what is probably representing reservoir gases (Figure 46, Figure 47).

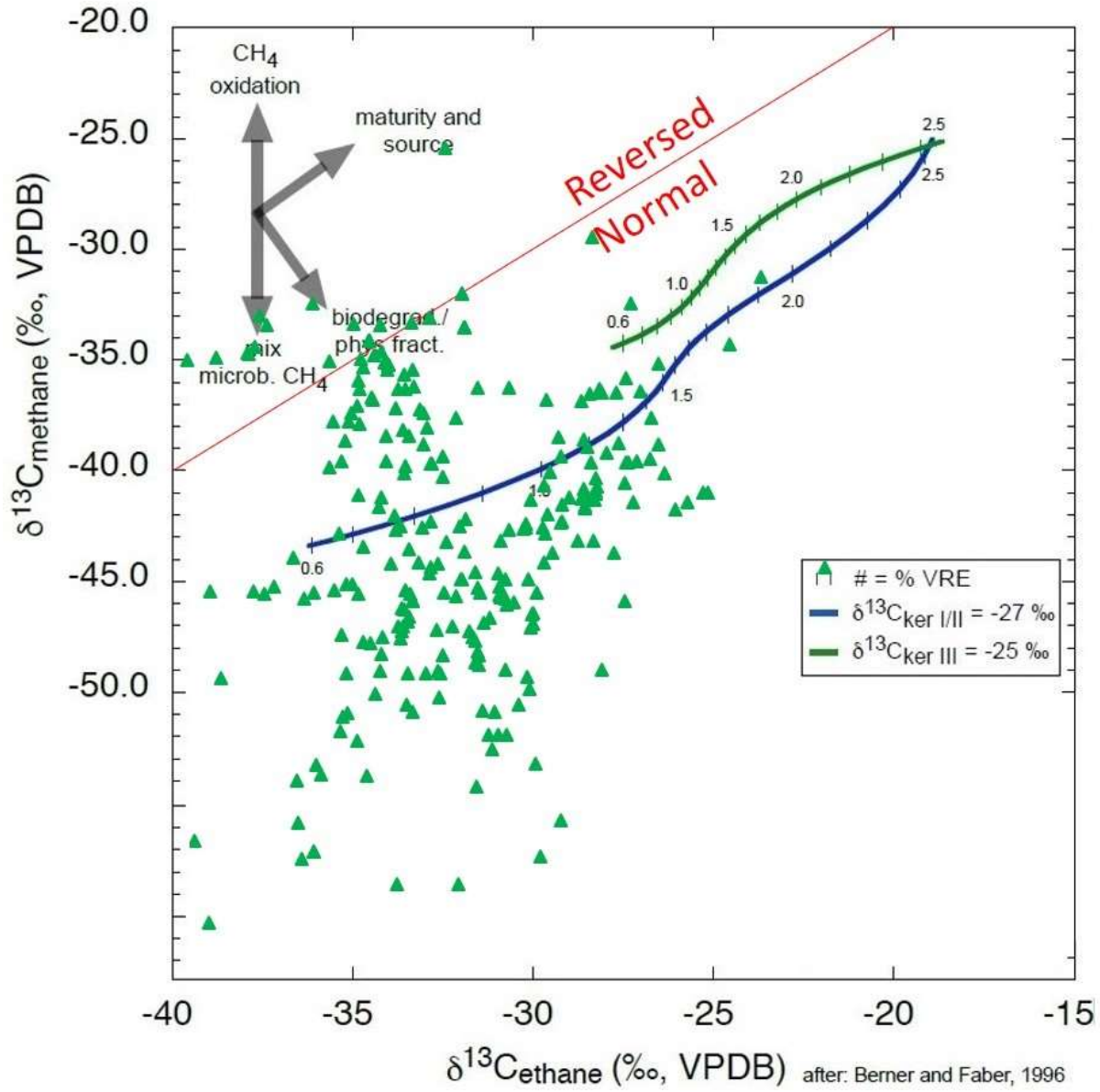

Figure 59. Interpretive diagram $\delta^{13}C_1$ vs $\delta^{13}C_2$ plot for only 'play 4.00' (including SCVF and bubble gas map data in Appendix B, Whiticar, 2018 pers comm., after Berner and Faber 1996, no trendlines).

A new interpretive diagram is proposed (Figure 61) with play 4.00 data plotted and it should be compared against Figure 50 and Figure 51.

The $\delta^{13}C_1$ vs $\delta^{13}C_2$ and $\delta^{13}C_2$ vs $\delta^{13}C_3$ plots are probably more indicative to show the range of isotope data and that many of the gases are not from the petroleum system.

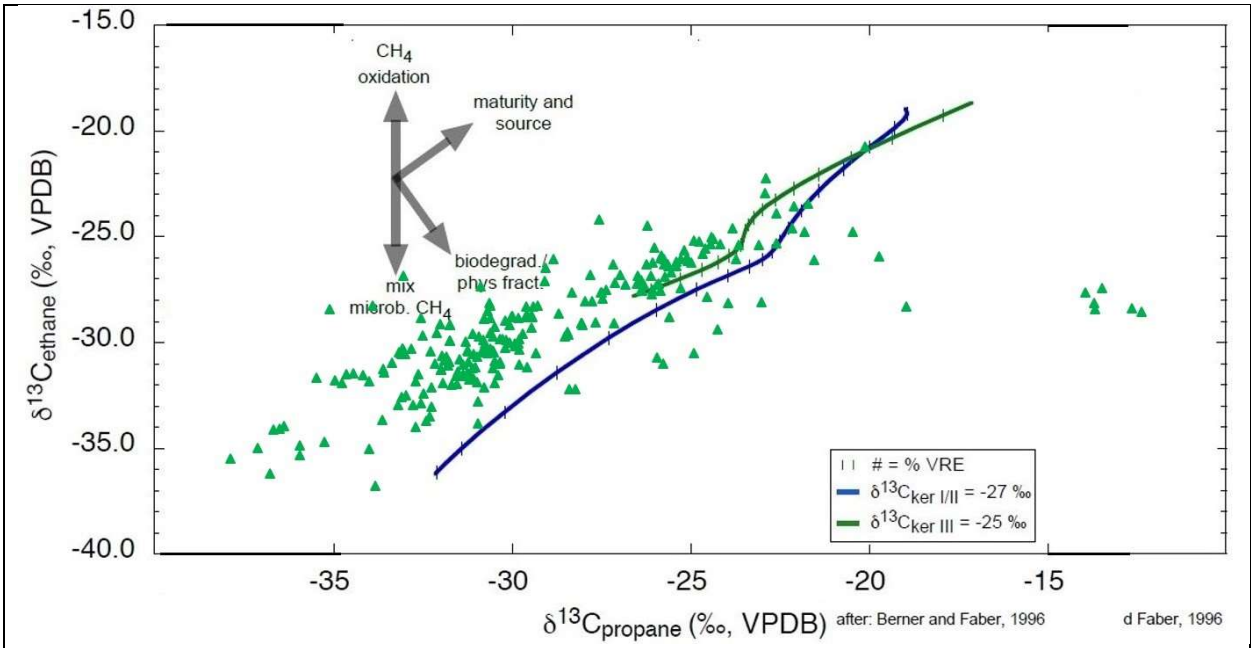

Figure 60. Interpretive diagram $\delta^{13}C_2$ vs $\delta^{13}C_3$ plot for only 'play 4.00' (including SCVF and bubble gas map data in Appendix B, Whiticar, 2018 pers comm., after Berner and Faber 1996, no trendlines).

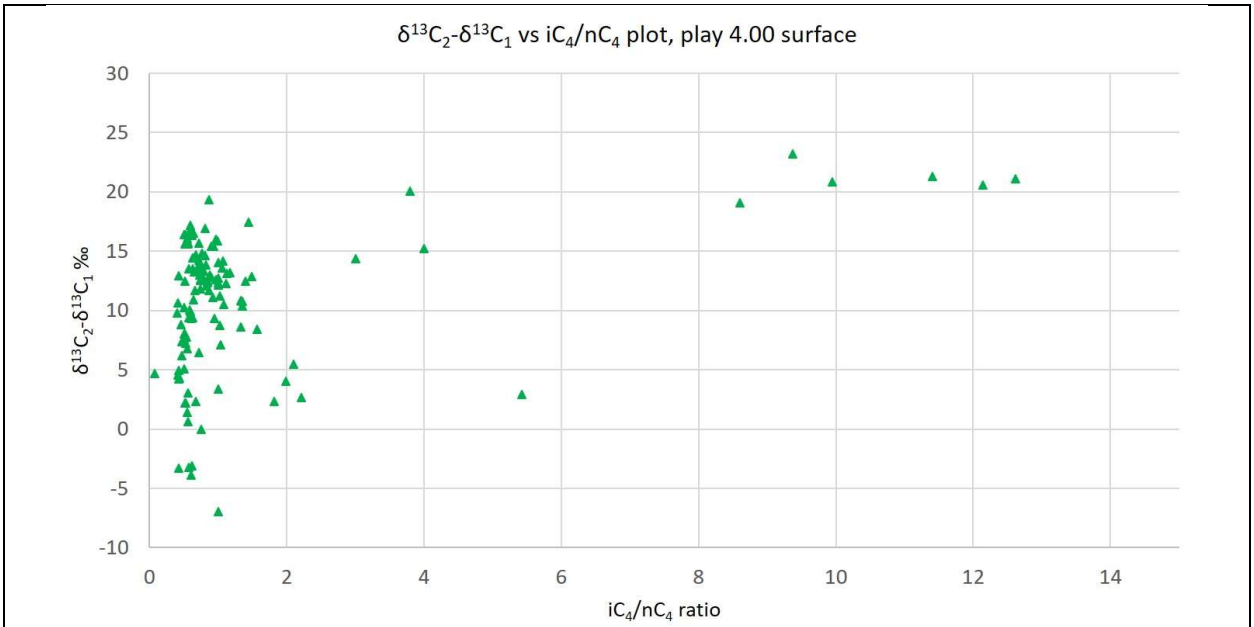

Figure 61. New format plot of $\delta^{13}C_2$-$\delta^{13}C_1$ vs iC_4/nC_4 for surface map data (play 4.00) [compared in Figure 52]

A final diagram for the Surface gas samples is from the $\delta^{13}CO_2$ isotopes (Figure 62).

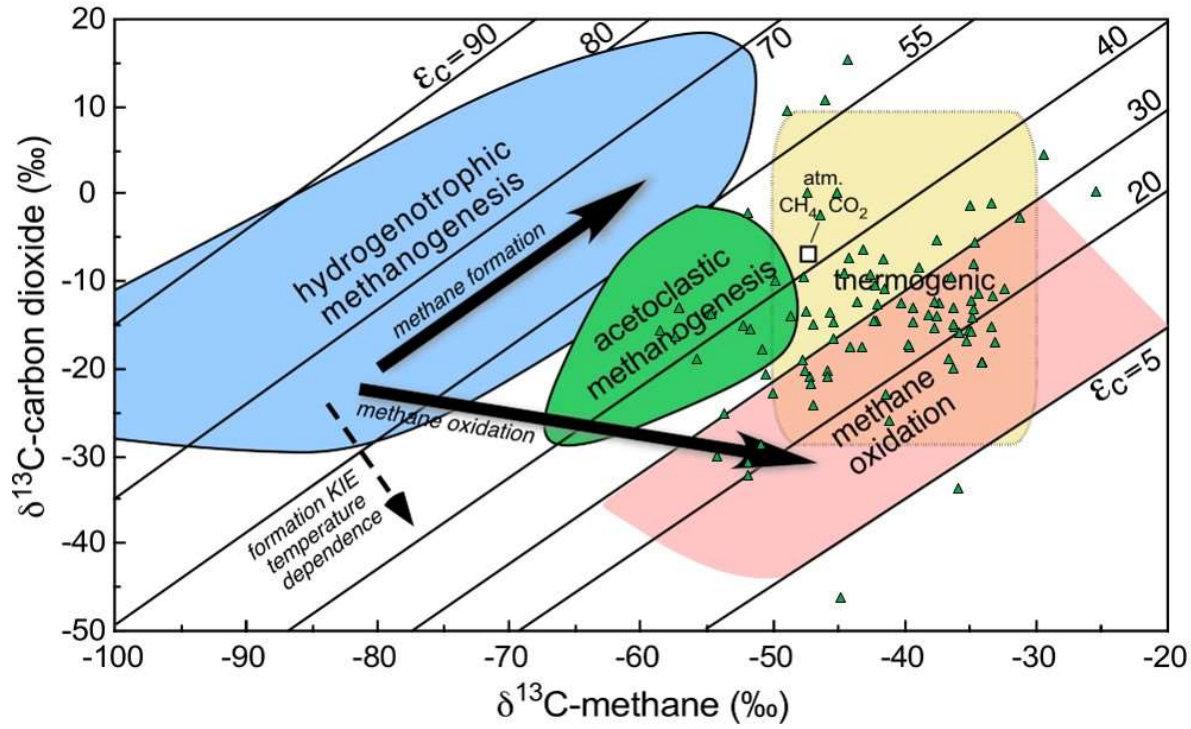

Figure 62. Plot $\delta^{13}CO_2$ vs $\delta^{13}C_1$ from Appendix B for 'play 4.00' showing an ambiguous trend.

9 Conclusions

A fundamental question was: Which natural gas geochemical parameters can be applied successfully to best identify and differentiate natural gases from different plays? This analysis used 3 new well profiles to total just over 1700 ISO profile data entries and over 570 ISO map data entries, some of which are extracted from the profiles.

The use of only molecular composition plots was insufficient for gas identification due to sampling artifacts. As a result of the limited value of molecular composition plots, the focus of the thesis' analytical approach shifted to characterization and differentiation using isotopic data. Conventional Bernard Diagrams, Lorant Diagrams, and CD Diagrams to characterize the petroleum system specifically for NEBC, did not produce significant results to differentiate gases at specific formation and play levels within the hydrocarbon bearing stratigraphic column. Most of the plots ended up with a cluster of data points from multiple formations or plays with no clear separation of isotopic composition. Surface collected natural gas from a few different sources was even more scattered making the "natural gas fingerprint" question about source of natural gas surface emissions problematic.

The analysis of the data shows that relying mainly on the isotope data for C_1 (methane) was inadequate to unambiguously characterize the natural gases. There is too much data scatter for unique identification. The reliance on methane (C_1) in insufficient to differentiate NEBC reservoir gases. In contrast, the isotopic data for ethane and propane provides better resolution of the thermogenic gas, as used in the plots of $\delta^{13}C_1$ vs $\delta^{13}C_2$ and $\delta^{13}C_2$-$\delta^{13}C_1$ vs iC_4/nC_4. This latter plot is particularly diagnostic to illustrate gas specific characterization at the level of sidetracks on a horizontal well and may be useful for sub-play level characterization of natural gas in the future. This is due to a secondary cracking shift in $\delta^{13}C_1$ for the reservoir gas requiring a depleted $^{13}C_{kerogen}$ line shifted by approximately -4 ‰ for only $\delta^{13}C_1$, which is highly unlikely (and contradicted by often a zero shift needed for $\delta^{13}C_2$), or a different model of mixing specifically for methane. Unfortunately, the $\delta^{13}C_1$ shift is seen in most strata of NEBC and might also indicate mixing or migration between strata.

The plots of $\delta^{13}C_1$ versus $\delta^{13}C_2$ and $\delta^{13}C_2$ versus $\delta^{13}C_3$ ('Berner-Faber Diagrams') have shown some plays to have a unique signature. Surface emission gases (primarily from Surface Casing Vent Flow) can often be identified as non-formation gases (sourced from a shallower unknown gas source) despite appearing thermogenic on other characterization plots.

As part of this thesis, significant analyses of the isotopic data for C_1, C_2, and C_3 were undertaken. Results from this aspect of the study have generated a number of questions relating to the possible depletion of $\delta^{13}C_1$ as seen on the Berner-Faber Diagrams. These diagrams show that methane is $^{13}C_1$ depleted uniformly from a modelled kerogen line for almost all plays in NEBC while $^{13}C_3$ and $^{13}C_2$ are not depleted and usually plot on the modelled kerogen line with the exception of surface gases. The possible explanation for this "shift" towards depletion for C_1 is that the source of methane within the reservoirs is unrelated to the sources of the ethane and propane components of the natural gas. While data are very limited (one vertical profile and one play), a plot of $\delta^{13}CO_2$ versus $\delta^{13}C_1$ produced the most

information for the $\delta^{13}C_1$ depletion that is seen on the Berner-Faber Diagrams. The possible causes for the $\delta^{13}C_1$ depletion are under further review.

Gas geochemistry characterization requires an assumption that the composition of the source kerogen controls the composition of the derived gases (Hunt 1996) and if there is any public kerogen ISO analysis from the stratigraphy in NEBC, it would be included in the dataset. The $\delta^{13}C_{kerogen}$ and $\delta^{13}C$ of any bitumen should be analyzed from existing core to characterize the original material that sourced the lighter hydrocarbon gases.

From my work, it appears that for NEBC a subset suite of parameters and their respective interpretive diagrams are best positioned to describe and delineate the different gas sources and types. Methane in NEBC appears to depart from expected relationships to higher hydrocarbons when determined by different views of the data as plots of $\delta^{13}C_1$ vs $\delta^{13}C_2$ and the unique $\delta^{13}C_2$-$\delta^{13}C_1$ vs iC_4/nC_4 diagram. One possibility is that there are multiple sources for only the methane. The methane compositions do not compare with other basins, such as North Sea (Berner and Faber 1988) or Arkoma/Fort Worth (Zumberge et al. 2012). The ISO differences between $\delta^{13}C_1$ and $\delta^{13}C_2$ as compared with the value of $\delta^{13}C_3$ plus the MC ratio of iC_4/nC_4 should be the primary tool for characterization. NEBC has a regional scale feature for most strata as uniformly ^{13}C depleted methane versus un-depleted ethane and propane. This is unlikely caused by microbial activity as it is too consistent and widespread, but may be from other kerogen or pyrobitumen processes outside the standard petroleum system model.

10 References

Adams, C., Janicki, E., Balogun A. 2016 Summary of Shale Gas Activity in Northeast British Columbia 2014. British Columbia Ministry of Energy and Mines Oil and Gas Report 2016-1 URL < https://www2.gov.bc.ca/assets/gov/farming-natural-resources-and-industry/natural-gas-oil/petroleum-geoscience/oil-gas-reports/oil_and_gas_report_2016-1.pdf >

AER 2018 ST98: Alberta's Energy Reserves and Supply/Demand Outlook (Commodity Forecast and Analysis, Natural Gas). Alberta Energy Regulator URL < http://www.aer.ca/providing-information/data-and-reports/statistical-reports/st98 > [June 2018].

Alam, M.S., Paramati, S.R., Shahbaz, M., Bhattacharya, M. 2017 Natural gas, trade and sustainable growth: empirical evidence from the top gas consumers of the developing world, Applied Economics, 49:7, 635-649, http://dx.doi.org/10.1080/00036846.2016.1203064

Archer, D. 2009 The Long Thaw: How humans are changing the next 100,000 years of Earth's Climate. (Princeton University Press) ISBN 978-0-691-13654-7

Archer, D. 2010 The Global Carbon Cycle. (Princeton Primers in Climate) ISBN 978-0-691-14414-6

Ardakani, H., Sanei, H., Ghanizadeh, A., McMechan, M., Ferri, F., Clarkson, C.R. 2017 Hydrocarbon potential and reservoir characteristics of Lower Cretaceous Garbutt Formation, Liard Basin Canada. Fuel 209 : 274-289 https://doi.org/10.1016/j.fuel.2017.07.106

Atherton, E., Risk, D., Fougère, C., Lavoie, M., Marshall, A., Werring, J., Williams, J. P., and Minions, C. 2017 Mobile measurement of methane emissions from natural gas developments in northeastern British Columbia, Canada. Atmospheric Chemistry and Physics Discussions 17 : 12405-12420 http://dx.doi.org/10.5194/acp-2017-109

Ayranci, K., Harris, N.B., Dong, T. 2018 High resolution sequence stratigraphic reconstruction of mud-dominated systems below storm wave base; A case study from the Middle to Upper Devonian Horn River Group, British Columbia, Canada. Sedimentary Geology 373 : Pages 239-253 https://doi.org/10.1016/j.sedgeo.2018.06.009

Bachu, S. 2017 Analysis of gas leakage occurrence along wells in Alberta, Canada, from a GHG perspective – Gas migration outside well casing. International Journal of Greenhouse Gas Control 61 : 146-154 https://doi.org/10.1016/j.ijggc.2017.04.003

Barker, J.F. and Fritz, P. 1981 Carbon isotope fractionation during microbial methane oxidation. Nature 293 : 5830 : 289-291 http://dx.doi.org/10.1038/293289a0

Barnes, R. 0. and Goldberg, E. D. 1976 Methane production and consumption in anoxic marine sediments. Geology 4 : 5 : 297-300 http://dx.doi.org/10.1130/0091-7613(1976)4<297:MPACIA>2.0.CO;2

Barth-Naftilan, E., Sohng, J., Saiers, J.E. 2018 Methane in groundwater before, during, and after hydraulic fracturing of the Marcellus Shale. PNAS 115 : 27 : 6970-6975 https://doi.org/10.1073/pnas.1720898115

BC Govt 2012a British Columbia's Natural Gas Strategy: Fuelling B.C.' Economy for the Next Decade and Beyond. http://www.gov.bc.ca/ener/popt/down/natural_gas_strategy.pdf Feb 3 2012

BC Govt 2012b 2012 LNG: Liquified Natural Gas A Strategy for B.C.'s Newest Industry. http://www.gov.bc.ca/ener/popt/down/liquefied_natural_gas_strategy.pdf

BC Govt 2012c LNG 101: A Guide to British Columbia’s Liquefied Natural Gas Sector. http://www.gov.bc.ca/mngd/doc/LNG101.pdf

BC Govt 2013 LNG British Columbia' Liquified Natural Gas Strategy: One Year Update. https://news.gov.bc.ca/stories/major-progress-job-creation-evident-in-lng-update or http://lnginbc.gov.bc.ca/

BC Govt 2016 Clean BC [Climate Leadership Plan]. https://www2.gov.bc.ca/assets/gov/environment/climate-change/action/cleanbc/cleanbc_2018-bc-climate-strategy.pdf August 2018. [October 2017].

BC govt 2018 New framework for natural gas development puts focus on economic and climate targets. British Columbia Government news 2018PREM0012-000480 March 22, 2018 URL < https://news.gov.bc.ca/16681 > or <https://archive.news.gov.bc.ca/releases/news_releases_2017-2021/2018PREM0012-000480.htm > [April 2018]

Berkowitz, N. 1997 Fossil Hydrocarbons: Chemistry and Technology. Academic Press, San Diego ISBN 0-12-091090-X TP343.B47

Berner, U. and Faber, E. 1988 Maturity related mixing model for methane, ethane and propane, based on carbon isotopes. Organic Geochemistry 13 : 1-3 : 67-72 http://dx.doi.org/10.1016/0146-6380(88)90026-5

Berner, U. and Faber, E. 1996 Empirical carbon isotope/maturity relationships for gases from algal kerogens and terrigenous organic matter, based on dry, open-system pyrolysis; Organic Geochemistry 24 : 947–955 https://doi.org/10.1016/S0146-6380(96)00090-3

Boothroyd, I.M., Almond, S., Qassim, S.M., Worrall, F., Davies, R.J., 2016 Fugitive emissions of methane from abandoned, decommissioned oil and gas wells. Science of The Total Environment 547 : 461-469 https://doi.org/10.1016/j.scitotenv.2015.12.096

Botner, E.C., Townsend-Small, A., Nash, D.B., Xu, X.M., Schimmelmann, A., Miller, J.H. 2018 Monitoring concentration and isotopic composition of methane in groundwater in the Utica Shale hydraulic fracturing region of Ohio. Environmental Monitoring and Assessment 190 : 6 #322 https://doi.org/10.1007/s10661-018-6696-1

BP (British Petroleum) 2017 Statistical Review of World Energy http://www.bp.com/en/global/corporate/energy-economics/statistical-review-of-world-energy/downloads.html or http://www.bp.com/content/dam/bp/pdf/energy-economics/statistical-review-2016/bp-statistical-review-of-world-energy-2016-full-report.pdf

Brand, W.A., Tegtmeyer, A.R., Hilkert, A. 1994 Compound-specific isotope analysis: extending toward 15N/14N and 18O/16O. Organic Geochemistry, 21 : 6-7 : 585-594 http://dx.doi.org/10.1016/0146-6380(94)90004-3

Cahill, A.G., Chao, J., Ford, O., Ladd, B., Prystupa, E., Mayer, K.U., Tannant, D., Black, A., Crowe, S., Hallam, S., Mayer, B., van Geloven, C., Welch, L.A., Levson, V. and Beckie, R.D. 2018 Establishment of field stations for the multidisciplinary study of fugitive gas, northeastern British Columbia in Geoscience BC Summary of Activities 2017: Energy, Geoscience BC, Report 2018-4, p. 65–76 http://cdn.geosciencebc.com/pdf/SummaryofActivities2017/Energy/SoA2017_E_Cahill.pdf

Caldwell, W.G.E. 1975 The Cretaceous System in the Western Interior of North America. Geological Association of Canada Special Paper 13.

Chalmers, G.R., Ross, D.J., Bustin, R.M. 2012 Geological controls on matrix permeability of Devonian Gas Shales in the Horn River and Liard basins, northeastern British Columbia, Canada. International Journal of Coal Geology 103 : 120-131 http://dx.doi.org/10.1016/j.coal.2012.05.006

Chalmers, G.R.L. and Bustin, R.M. 2012 Geological evaluation of Halfway-Doig-Montney hybrid gas shale-tight gas reservoir, northeastern British Columbia. Marine and Petroleum Geology 38 : 1 : 53-72 https://doi.org/10.1016/j.marpetgeo.2012.08.004

Chalmers, G.R.L. and Bustin, R.M. 2015 Porosity and pore size distribution of deeply-buried fine-grained rocks: Influence of diagenetic and metamorphic processes on shale reservoir quality and exploration. Journal of Unconventional Oil and Gas Resources 12 : 134-142 https://doi.org/10.1016/j.juogr.2015.09.005

Cheung, K., Klassen, P., Mayer, B., Goodarzi, F., Aravena, R. 2010 Major ion and isotope geochemistry of fluids and gases from coalbed methane and shallow groundwater wells in Alberta, Canada. Applied Geochemistry 25 : 9 : 1307-1329 http://dx.doi.org/10.1016/j.apgeochem.2010.06.002

Cheung, K., Sanei, H., Klassen, P., Mayer, B., Goodarzi, F. 2009 Produced fluids and shallow groundwater in coalbed methane (CBM) producing regions of Alberta, Canada: Trace element and rare earth element geochemistry. IJCG 77 : 3-4 : 338-349 : SI http://dx.doi.org/10.1016/j.coal.2008.07.012

Chung, H.M. and Sackett, W.M. 1979 Use of stable isotope compositions of pyrolytically derived methane as a maturity indices for carbonaceous materials. Geochimica et Cosmochimica Acta 43 : 12 : 1979-1988 http://dx.doi.org/10.1016/0016-7037(79)90010-3

Clarkson, C.R. and Bustin, R.M. 2000 Binary gas adsorption/desorption isotherms: effect of moisture and coal composition upon carbon dioxide selectivity over methane. IJCG 42 : 4 : 241-271 http://dx.doi.org/10.1016/S0166-5162(99)00032-4

Clayton, C. 1991 Carbon isotope fractionation during natural gas generation from kerogen. Marine and Petroleum Geology, 8 : 2 : 232-240 http://dx.doi.org/10.1016/0264-8172(91)90010-X

Craig, H. 1953 The geochemistry of the stable carbon isotopes. Geochimica et Cosmochimica Acta 3 : 2-3 : 53-92 http://dx.doi.org/10.1016/0016-7037(53)90001-5

Crombez, V., Baudin, F., Rohais, S., Riquier, L., Euzen, T., Pauthier, S., Ducros, M., Caron, B., Vaisblat, N. 2017a Basin scale distribution of organic matter in marine fine-grained sedimentary rocks: Insight from sequence stratigraphy and multi-

proxies analysis in the Montney and Doig Formations. Marine and Petroleum Geology 83 : 382-401 https://doi.org/10.1016/j.marpetgeo.2016.10.013

Crombez, V., Rohais, S., Baudin, F., Chauveau, B., Euzen, T., Granjeon, D. 2017b Controlling factors on source rock development: implications from 3D stratigraphic modeling of Triassic deposits in the Western Canada Sedimentary Basin. Bulletin de la Societe Geologique de France 188 : 5 https://doi.org/10.1051/bsgf/2017188

Crombez, V., Rohais, S., Baudin, F., Euzen, T. 2014 Organic content variations and links to sequence stratigraphy in the Montney and Doig Formations (Alberta / British columbia). Geoconvention 2014 abstracts

Crombez, V., Rohais, S., Baudin, F., Euzen, T. 2016 Facies, well-log patterns, geometries and sequence stratigraphy of a wave-dominated margin: insight from the Montney Formation (Alberta, British Columbia, Canada). Bulletin of Canadian Petroleum Geology 64 : 4 : 516-537

Curiale, J.A. and Curtis, J.B. 2016 Organic geochemical applications to the exploration for source-rock reservoirs - A review. Journal of Unconventional Oil and Gas Resources 13 : 1-31 https://doi.org/10.1016/j.juogr.2015.10.001

Currie, L.D., McMechan, M.E., Ferri, F., O'Sullivan, P.B. 2014 Thermal Modelling of Apatite Fission Track Analyses from the Liard Basin, Northeast British Columbia. Geoconvention 2014 abstract http://www.geoconvention.com/archives/2014/275_CGC2014_Thermal_Modelling_of_Apatite_Fission_Track_Analyses.pdf

Darrah, T.H., Jackson, R.B., Vengosh, A., Warner, N.R., Whyte, C.J., Walsh, T.B., Kondash, A.J., Poreda, R.J. 2015 The evolution of Devonian hydrocarbon gases in shallow aquifers of the northern Appalachian Basin: Insights from integrating noble gas and hydrocarbon geochemistry. Geochimica et CosmoChimica Acta 170 : 321-355 https://doi.org/10.1016/j.gca.2015.09.006

Darrah, T.H., Vengosh, A., Jackson, R.B., Warner, N.R., Poreda, R.J. 2014 Noble gases identify the mechanisms of fugitive gas contamination in drinking-water wells overlying the Marcellus and Barnett Shales. PNAS 111 : 39 : 14076-14081 published ahead of print https://doi.org/10.1073/pnas.1322107111

Davies, G.R., Watson, N., Moslow, T.F., MacEachern, J.A. 2018 Regional subdivisions, sequences, correlations and facies relationships of the Lower Triassic Montney Formation, west-central Alberta to northeastern British Columbia, Canada — with emphasis on role of paleostructure. Bulletin of Canadian Petroleum Geology 66 : 1 : 23–92. URL temp <http://www.cspg.org/CSPG/IMIS20/Publications/Bulletin/Current_Issue/CSPGIMIS20/Publications/Bulletin.aspx> https://pubs.geoscienceworld.org/cspg/bcpg/article-abstract/66/1/23/538508/regional-subdivisions-sequences-correlations-and

Davies, R.J., Almond, S., Ward, R.S., Jackson, R.B., Adams, C., Worrall, F., Herringshaw, L.G., Gluyas, J.G., Whiteheade, M.A. 2014 Oil and gas wells and their integrity: Implications for shale and unconventional resource exploitation. Marine and Petroleum Geology 56 : 239-254 https://doi.org/10.1016/j.marpetgeo.2014.03.001

Dawson, F.M., Marsh, R., Richardson, R.J., Evans, C.E. 1994 Uppermost Cretaceous and Tertiary. in Mossop, G. and Shetsen, I. (compilers)(1994) Geological Atlas of the Western Canada Sedimentary Basin. Cdn. Soc. Petrol Geol. and Alberta Research Council, Calgary, Alberta, 510pp. ISBN-13: 978-0920230534 URL <http://www.cspg.org/CSPG/IMIS20/Publications/Geological_Atlas/CSPGIMIS20/Publications/Geological_Atlas.aspx > [July 2018]

Dawson, F.M., Marchioni, D.L., Anderson, T.C., McDougall, W.J. 2000 An Assessment of Coalbed Methane Exploration Projects in Canada. GSC Bull. 549 ISBN: 978-0-660-17871-0.

Dong, T. 2016 Geochemical, petrophysical and geochemical properties of stratigraphic sequences in Horn River shale, Middle and Upper Devonian, northeastern British Columbia, Canada. Ph.D. thesis, University of Alberta 258 p https://doi.org/10.7939/R3CZ32G43 https://era.library.ualberta.ca/items/ea54fbcf-34f5-439c-86c7-ff74b0714be7 PDF at https://era.library.ualberta.ca/items/ea54fbcf-34f5-439c-86c7-ff74b0714be7/download/60b23769-37e0-4eab-9bd0-b89f1d3a9e20

Dong, T., Harris, N.B., Ayranci, K. 2017 Relative sea-level cycles and organic matter accumulation in shales of the Middle and Upper Devonian Horn River Group, northeastern British Columbia, Canada: Insights into sediment flux, redox conditions, and bioproductivity. GSA Bulletin 130 : 5-6 : 859-880 https://doi.org/10.1130/B31851.1

Dong, T., Harris, N.B., Ayranci, K., Twemlow, C.E., Nassichuk, B.R. 2015 Porosity characteristics of the Devonian Horn River shale, Canada: Insights from lithofacies classification and shale composition. International Journal of Coal Geology 141 : 74-90 https://doi.org/10.1016/j.coal.2015.03.001

Douglas, P.M.J., Stolper, D.A., Eiler, J.M., Sessions, A.L., Lawson, M., Shuai, Y.H., Bishop, A., Podlaha, O.G., Ferreira, A.A., Neto, E.V.S., Niemann, M., Steen, A.S., Huang, L., Chimiak, L., Valentine, D.L., Fiebig, J., Luhmann, A.J., Seyfried, W.E., Etiope, G., Schoell, M., Inskeep, W.P., Moran, J.J., Kitchen, N. 2017 Methane clumped isotopes: progress and potential for a new isotopic tracer. Organic Geochemistry 113 : 262-282 http://dx.doi.org/10.1016/j.orggeochem.2017.07.016

Douglas, P.M.J., Stolper, D.A., Smith, D.A., Anthony, K.M.W., Paull, C.K., Dallimore, S., Wik, M., Crill, P.M., Winterdahl, M., Eiler, J.M., Sessions, A.L. 2016 Diverse origins of Arctic and Subarctic methane point source emissions identified with multiply-substituted isotopologues. Geochimica et Cosmochimica Acta 188 : 163-188 http://dx.doi.org/10.1016/j.gca.2016.05.031

Eadie, B.J., Jeffrey, L.M. and Sackett, W.M. 1978 Some observations on the stable carbon isotope composition of dissolved and particulate organic carbon in the marine environment. Geochimica et Cosmochimica Acta 42 : 8 : 1265-1269 http://dx.doi.org/10.1016/0016-7037(78)90120-5

Edwards, D.E., Barclay, J.E., Gibson, D.W., Kvill, G.E., Halton, E. 1994 Triassic Strata of the Western Canada Sedimentary Basin. in Mossop, G. and Shetsen, I. (compilers)(1994) Geological Atlas of the Western Canada Sedimentary Basin. Cdn. Soc. Petrol Geol. and Alberta Research Council, Calgary, Alberta, 510pp. ISBN-13: 978-0920230534 URL <http://www.cspg.org/CSPG/IMIS20/Publications/Geological_Atlas/CSPGIMIS20/Publications/Geological_Atlas.aspx > [July 2018]

EIA (US Energy Information Administration) 2016 International Energy Outlook. IEO2016 https://www.eia.gov/outlooks/ieo/ https://www.eia.gov/outlooks/ieo/pdf/0484(2016).pdf

EnergyBC 2012 Natural Gas. < http://www.energybc.ca/naturalgas.html >

Etiope, G. 2009 Natural emissions of methane from geological seepage in Europe. Atmospheric Environment 43 : 1430-1443 http://dx.doi.org/10.1016/j.atmosenv.2008.03.014

Etiope, G. and Sherwood Lollar, B. 2013 Abiotic Methane on Earth. Rev.Geophys. 51 276-299 http://dx.doi.org/10.1002/rog.20011

Etiope, G., Feyzullayev, A., Baciu, C.L. 2009 Terrestrial methane seeps and mud volcanoes: A global perspective of gas origin. Marine and Petroleum Geology 26 333-344 http://dx.doi.org/10.1016/j.marpetgeo.2008.03.001

Etiope, G., Lassey, K.R., Klusman, R.W., Boschi, E. 2008 Reappraisal of the fossil methane budget and related emission from geologic sources. GRL 35 : 9 : L09307 http://dx.doi.org/10.1029/2008GL033623

Euzen, T., Moslow, T.F., Caplan, M. 2018 The Montney Play of Western Canada: Deposition to Development. Bulletin of Canadian Petroleum Geology 66 : 1 : 1-6. URL temp <http://www.cspg.org/CSPG/IMIS20/Publications/Bulletin/Current_Issue/CSPGIMIS20/Publications/Bulletin.aspx >

Evans, C. 2018 BC Natural Gas Atlas: Preliminary insights into Geochemistry from Profiles. Presentation at 11th Unconventional Gas Technical Forum, April 24th, 2018, Victoria, British Columbia. URL < https://www.bcogc.ca/11th-bc-unconventional-gas-technical-forum-agenda > [June 2018].

Evans, C. in press Molecular composition and isotope mapping of natural gas in the British Columbia Natural Gas Atlas; in Geoscience BC Summary of Activities 2018, Geoscience BC, Report 2019-1, p. 77–84.

Evans, C. and Hayes, B.J. 2018 BC Natural Gas Atlas: Recorrelation Changes the Picture. in Geoscience BC Summary of Activities 2017, Geoscience BC, Report 2018-1, p. 11-14 URL <http://cdn.geosciencebc.com/pdf/SummaryofActivities2017/Energy/SoA2017_E_Evans.pdf > [May 2018]

Evans, C. and Whiticar, M.J. 2016a BC Natural Gas Atlas: geochemical characterization of our energy resources. Poster at Unconventional Gas Technical Forum, April 4th, 2016, Victoria, British Columbia. URL < https://www.bcogc.ca/10th-bc-unconventional-gas-technical-forum > [October 2016].

Evans, C. and Whiticar, M.J. 2016b BC Natural Gas Atlas: initial results of gas geochemical mapping. Poster at Unconventional Gas Technical Forum, April 4th, 2016, Victoria, British Columbia. URL < https://www.bcogc.ca/10th-bc-unconventional-gas-technical-forum > [October 2016].

Evans, C. and Whiticar, M.J. 2017 British Columbia Natural Gas Atlas project: 2016 project update; in Geoscience BC Summary of Activities 2016, Geoscience BC, Report 2017-1, p. 75–78, URL <http://www.geosciencebc.com/i/pdf/SummaryofActivities2007/SoA2016 SoA2016_Evans.pdf > [October 2017].

Faber, E. and Stahl, W. 1984 Geochemical surface exploration for hydrocarbons in the North Sea. Bull. Am. Assoc. Petrol. Geol., 68 : 3 : 363-386 http://archives.datapages.com/data/bulletns/1984-85/data/pg/0068/0003/0350/0363.htm

Ferri, F. and Griffiths, M. 2014 Thermal maturity and regional distribution of the Muskwa Formation, northeastern British Columbia. Geoscience Reports 2014, BC Ministry of Natural Gas Development, p. 37–45 https://www2.gov.bc.ca/assets/gov/farming-natural-resources-and-industry/natural-gas-oil/petroleum-geoscience/geoscience-reports/2014/ferri_and_griffiths.pdf

Ferri, F., McMechan, M., Ardakani, O.H., Sanei, H. 2017 The Garbutt Formation of Liard Basin, British Columbia: a potential liquids-rich play. Bulletin of Canadian Petroleum Geology 65 : 2 : 279-306 https://doi.org/10.2113/gscpgbull.65.2.279

Fiess, K.M., Ferri, F., Fraser, T.L., Pyle, L.J., Rocheleau, J. 2013 Liard Basin Hydrocarbon Project: Shale Gas Potential of Devonian-Carboniferous Strata in the Northwest Territories, Yukon and Northeastern British Columbia. Geoconvention 2013 abstract https://www.geoconvention.com/archives/2013/263_GC2013_Liard_Basin_Hydrocarbon_Project.pdf

Fuex, A.N. 1977 Use of Stable Carbon Isotopes in Hydrocarbon Exploration. Journal of Geochemical Exploration, 7 : 2 : 155-188 http://dx.doi.org/10.1016/0375-6742(77)90080-2

Galimov, E.M. 1988 Sources and mechanisms of formation of gaseous hydrocarbons in sedimentary rocks. Chemical Geology 71 : 1-3 : 77-95 http://dx.doi.org/10.1016/0009-2541(88)90107-6

Galimov, E.M. 2006 Isotope organic geochemistry. Organic Geochemistry 37 : 1200–1262 http://dx.doi.org/10.1016/j.orggeochem.2006.04.009

Gao, L., Schimmelmann, A., Tang, Y.C., Mastalerz, M. 2014 Isotope rollover in shale gas observed in laboratory pyrolysis experiments: Insight to the role of water in thermogenesis of mature gas. Organic Geochemistry 68 : 95-106 https://doi.org/10.1016/j.orggeochem.2014.01.010

Gibson, D.W. 1993 Triassic. In Stott, D.F. and Aitken, J.D. eds. Sedimentary Cover of the Craton in Canada. Geology Society of America Decade of North American Geology volume D-1, pp. 294-320. ISBN 0-660-13133-1.

Golding, M.L., Orchard, M.J., Zonneveld, J.P., Wilson, N.S.F. 2015 Determining the age and depositional model of the Doig Phosphate Zone in northeastern British Columbia using conodont biostratigraphy. Bulletin of Canadian Petroleum Geology 63 : 2 : 143-170 https://doi.org/10.2113/gscpgbull.63.2.143

Golding, S.D., Boreham, C.J., Esterle, J.S. 2013 Stable isotope geochemistry of coal bed and shale gas and related production waters: A review. International Journal of Coal Geology 120 : 24-40 http://dx.doi.org/10.1016/j.coal.2013.09.001

Grasby, S.E. 2013 Pickled Shale Gas Play – How Continental Glaciation Drives Biogenic Gas Formation. Geoconvention Abstract 2013 https://www.geoconvention.com/archives/2013/195_GC2013_Pickled_Shale_Gas_Play.pdf

Grasby, S.E., Beauchamp, B., Bond, D.P.G., Wignall, P., Sanei, H. 2016a Mercury anomalies associated with three extinction events (Capitanian Crisis, Latest Permian Extinction and the Smithian/Spathian Extinction) in NW Pangea. Geol. Mag. 153 (2) 285-297 https://doi.org/10.1017/S0016756815000436

Grasby, S.E., Ferguson, G., Brady, A., Sharp, C., Dunfield, P., McMechan, M. 2016b Deep groundwater circulation and associated methane leakage in the northern Canadian Rocky Mountains. Applied Geochemistry 68 : 10-18 https://doi.org/10.1016/j.apgeochem.2016.03.004

Hakala, J.A. 2014 Use of stable isotopes to identify sources of methane in Appalachian Basin shallow groundwaters: a review. Environmental Science - Processes and Impacts 16 : 9 : 2080-2086 https://doi.org/10.1039/c4em00140k

Hamilton, S.K., Golding, S.D., Baublys, K.A., Esterle, J.S. 2014 Stable isotopic and molecular composition of desorbed coal seam gases from the Walloon Subgroup, eastern Surat Basin, Australia. IJCG 122 : 21-36 http://dx.doi.org/10.1016/j.coal.2013.12.003

Hayes, J.M., Freeman, K.H., Popp, B.N. and Hoham, C.H. 1989 Compound-specific isotopic analyses: A novel tool for reconstruction of ancient biogeochemical processes. Organic Geochemistry, 16 : 4-6 : 1115-1128 http://dx.doi.org/10.1016/0146-6380(90)90147-R

Hayes, M. 2018 BC Natural Gas Production: An Overview 2017. Presentation at 11th Unconventional Gas Technical Forum, April 24th, 2018, Victoria, British Columbia. URL < https://www.bcogc.ca/11th-bc-unconventional-gas-technical-forum-agenda> [June 2018].

Hendry, M.J., Barbour, S.L., Schmeling, E.E., Mundle, S.O.C. 2017b Measuring Concentrations of Dissolved Methane and Ethane and the C-13 of Methane in Shale and Till. Groundwater 55 : 1 : 119-128 http://dx.doi.org/10.1111/gwat.12445

Hendry, M.J., Schmeling, E.E., Barbour, S.L., Huang, M., Mundle, S.O.C. 2017a Fate and Transport of Shale-derived, Biogenic Methane. Scientific Reports 7 : 4881 http://dx.doi.org/10.1038/s41598-017-05103-8

Humez, P., Mayer, B., Nightingale, M., Becker, V., Kingston, A., Taylor, S., Bayegnak, G., Millot, R., Kloppmann, W. 2016b Redox controls on methane formation, migration and fate in shallow aquifers. Hydrology and Earth System Sciences 20 : 7 : 2759-2777 http://dx.doi.org/10.5194/hess-20-2759-2016

Humez, P., Mayer, B., Nightingale, M., Ing, J., Becker, V., Jones, D., Lam, V. 2016a An 8-year record of gas geochemistry and isotopic composition of methane during baseline sampling at a groundwater observation well in Alberta (Canada). Hydrogeology Journal 24 : 1 : 109-122 https://doi.org/10.1007/s10040-015-1319-1

Hunt, J.M. 1996 Petroleum Geochemistry and Geology, 2nd Edition. W.H. Freeman and Company, New York ISBN 0-7167-2441-3 TN870.5 H86

Ing, J. 2015 Occurrence and Origin of Methane in Shallow Groundwater in Alberta, Canada. University of Calgary Thesis URL <https://prism.ucalgary.ca/handle/11023/2617 > [July 2018]

Ing, J., Nightingale, M., Humez, P., Mayer. B. 2014 Assessment of Methane Occurences and Sources in Groundwater in Alberta: A Progress Report. Geoconvention 2014 Abstract https://www.geoconvention.com/archives/2014/228_GC2014_Assessment_of_Methane_Occurences_and_Sources_in_Groundwater_in_AB.pdf

Jenden, P.D., Drazan, D.J., Kaplan, I.R. 1993 Mixing of Thermogenic Natural Gases in Northern Appalachian Basin. AAPG Bulletin 77 : 6 : 980-998 http://archives.datapages.com/data/bulletns/1992-93/data/pg/0077/0006/0950/0980.htm

Jerzykiewicz, T. 1997 Stratigraphic framework of the uppermost Cretaceous to Paleocene strata of the Alberta Basin. Geological Survey of Canada, Bulletin 510, 121 pages https://doi.org/10.4095/208902

Jochmann, M.A., Blessing, M., Haderlein, S.B., Schmidt, T.C. 2006 A new approach to determine method detection limits for compound-specific isotope analysis of volatile organic compounds. Rapid Communications in Mass Spectrometry 20 : 24 : 3639-3648 http://dx.doi.org/10.1002/rcm.2784

Johnson, M.R., Tyner, D.R., Conley, S., Schwietzke, S., Zavala-Araiza, D. 2017 Comparisons of Airborne Measurements and Inventory Estimates of Methane Emissions in the Alberta Upstream Oil and Gas Sector. Environmental Science & Technology 51 : 21 : 13008-13017 http://dx.doi.org/10.1021/acs.est.7b03525

Kang, M., Christian, S., Celia, M.A., Mauzerall, D.L., Bill, M., Miller, A.R., Chen, Y., Conrad, M.E., Darrah, T.H., Jackson, R.B. 2016 Identification and characterization of high methane-emitting abandoned oil and gas wells. PNAS 113 : 48 : 13636-13641 https://doi.org/10.1073/pnas.1605913113

Kang, M., Kanno, C.M., Reid, M.C., Zhang, X., Mauzerall, D.L., Celia, M.A., Chen, Y.H., Onstott, T.C. 2014 Direct measurements of methane emissions from abandoned oil and gas wells in Pennsylvania. PNAS 111 : 51 : 18173-18177 https://doi.org/10.1073/pnas.1408315111

Karion, A., Sweeney, C., Kort, E.A., Shepson, P.B., Brewer, A., Cambaliza, M., Conley, S.A., Davis, K., Deng, A.J., Hardesty, M., Herndon, S.C., Lauvaux, T., Lavoie, T., Lyon, D., Newberger, T., Petron, G., Rella, C., Smith, M., Wolter, S., Yacovitch, T.I., Tans, P. 2015 Aircraft-Based Estimate of Total Methane Emissions from the Barnett Shale Region. Environmental Science & Technology 49 8124-8131 http://dx.doi.org/ 10.1021/acs.est.5b00217

Kempin, E. 2012 H_2S Source(s) in Surface Casing Vent Flows for In Situ Thermal Wells in the Athabasca and Cold Lake Oil Sands Areas. Univeristy of Calgary Masters Thesis.

Khalil, M.A.K. 2000 Atmospheric Methane: An Introduction. In: Khalil M.A.K. (eds) Atmospheric Methane. Springer, Berlin, Heidelberg https://doi.org/10.1007/978-3-662-04145-1_1 ISBN 978-3-642-08451-5

Killops, S. and Killops, V. 2005 Introduction to Organic Geochemistry, 2nd Ed. ISBN 0-632-06504-4

Kirschke, S., Bousquet, P., Ciais, P., Saunois, M., Canadell, J.G., Dlugokencky, E.J., Bergamaschi, P., Bergmann, D., Blake, D.R., Bruhwiler, L., Cameron-Smith, P., Castaldi, S., Chevallier, F., Feng, L., Fraser, A., Heimann, M., Hodson, E.L., Houweling, S., Josse, B., Fraser, P.J., Krummel, P.B., Lamarque, J.F., Langenfelds, R.L., Le Quere, C., Naik, V., O'Doherty, S., Palmer, P.I., Pison, I., Plummer, D., Poulter, B., Prinn, R.G., Rigby, M., Ringeval, B., Santini, M., Schmidt, M., Shindell, D.T., Simpson, I.J., Spahni, R., Steele, L.P., Strode, S.A., Sudo, K., Szopa, S., van der Werf, G.R., Voulgarakis, A., van Weele, M., Weiss, R.F., Williams, J.E., Zeng, G. 2013 Three decades of global methane sources and sinks. Nature Geoscience 6 813-822 http://dx.doi.org/0.1038/NGEO1955

Kotarba, M.J., Nagao, K., Karnkowski, P.H. 2014 Origin of gaseous hydrocarbons, noble gases, carbon dioxide and nitrogen in Carboniferous and Permian strata of the distal part of the Polish Basin: Geological and isotopic approach. Chemical Geology 383 : 164-179 https://doi.org/10.1016/j.chemgeo.2014.06.012

Lamb, B.K., Edburg, S.L., Ferrara, T.W., Howard, T., Harrison, M.R., Kolb, C.E., Townsend-Small, A., Dyck, W., Possolo, A., Whetstone, J.R. 2015 Direct Measurements Show Decreasing Methane Emissions from Natural Gas Local Distribution Systems in the United States. Environmental Science & Technology 49 5161-5169 http://dx.doi.org/10.1021/es505116p

Lavoie, T.N., Shepson, P.B., Gore, C.A., Stirm, B.H., Kaeser, R., Wulle, B., Lyon, D., Rudek, J. 2017 Assessing the Methane Emissions from Natural Gas-Fired Power Plants and Oil Refineries. Environ. Sci. Technol. 51 (6) 3373-3381 http://dx.doi.org/10.1021/acs.est.6b05531

Marchese, A.J., Vaughn, T.L., Zimmerle, D.J., Martinez, D.M., Williams, L.L., Robinson, A.L., Mitchell, A.L., Subramanian, R., Tkacik, D.S., Roscioli, J.R., Herndon, S.C. 2015 Methane Emissions from United States Natural Gas Gathering and Processing. Environmental Science & Technology 49 10718-10727 http://dx.doi.org/10.1021/acs.est.5b02275

McKinney, C.R., McCrea, J.M., Epstein, S., Allen, H.A., Urey, H.C. 1950 Improvements in mass spectrometers for the measurement of small differences in isotope abundance ratios. Rev. Sci. Instrum. 21 : 8 : 724–730 http://dx.doi.org/10.1063/1.1745698

MEM 2006a Conventional natural gas play atlas, part 1. BC Ministry of Energy and Mines Petroleum Geology Publication 2006-01, Oil & Gas Division, Resource Development & Geoscience Branch, URL < http://www2.gov.bc.ca/assets/gov/farming-natural-resources-and-industry/natural-gas-oil/petroleum-geoscience/oil-gas-reports/og_report_2006-1_nebc_atlas_part1.pdf > [October 2016].

MEM 2006b Conventional natural gas play atlas. BC Ministry of Energy and Mines Petroleum Geology Publication 2006-01, Oil & Gas Division, Resource Development & Geoscience Branch, URL < http://www2.gov.bc.ca/assets/gov/farming-natural-resources-and-industry/natural-gas-oil/petroleum-geoscience/oil-gas-reports/og_report_2006-1_nebc_atlas-2_part2.pdf > [October 2016].

MEM 2006c Conventional natural gas play atlas. BC Ministry of Energy and Mines Petroleum Geology Publication 2006-01, Oil & Gas Division, Resource Development & Geoscience Branch, URL < http://www2.gov.bc.ca/assets/gov/farming-natural-resources-and-industry/natural-gas-oil/petroleum-geoscience/oil-gas-reports/og_report_2006-1_nebc_atlas_part3.pdf > [October 2016].

MEM 2011 The Ultimate Potential for Unconventional Natural Gas in Northeastern British Columbia's Horn River Basin. National Energy Board and Ministry of Energy and Mines 2011-1. URL < https://www2.gov.bc.ca/assets/gov/farming-natural-resources-and-industry/natural-gas-oil/petroleum-geoscience/oil-gas-reports/og_report2011-1.pdf > [October 2016]

MEM 2013 The Ultimate Potential for Unconventional Petroleum from the Montney Formation of British Columbia and Alberta. National Energy Board, BC Oil & Gas Commission, Alberta Energy Regulator, Ministry of Natural Gas Development 2013-3. URL < https://www2.gov.bc.ca/assets/gov/farming-natural-resources-and-industry/natural-gas-oil/petroleum-geoscience/oil-gas-reports/og_report_2013-1_montney_assessment.pdf > [October 2016]

MEM 2015 Unconventional Natural Gas Assessment for the Cordova Embayment in Northeastern British Columbia. Ministry of Natural Gas Development and BC Oil & Gas Commission 2015-1. URL < https://www2.gov.bc.ca/assets/gov/farming-natural-resources-and-industry/natural-gas-oil/petroleum-geoscience/oil-gas-reports/og_report_2015-1.pdf > [October 2016]

Merritt, D.A., Hayes, J.M., Des Marais, D.J. 1995 Carbon isotopic analysis of atmospheric methane by isotope-ratio-monitoring gas chromatography-mass spectrometry. Journal of Geophysical Research 100 : D1 : 1317-1326 http://dx.doi.org/10.1029/94JD02689

Moore, P.F. 1993 Devonian. In Stott, D.F. and Aitken, J.D. eds. Sedimentary Cover of the Craton in Canada. Geology Society of America Decade of North American Geology volume D-1, pp. 150-201. ISBN 0-660-13133-1.

Moslow, T.F., Euzen, T., Caplan, M. 2018 The Montney Play of Western Canada: Deposition to Development. Bulletin of Canadian Petroleum Geology 66 : 2 : 359-362. URL temp < http://www.cspg.org/CSPG/IMIS20/Publications/Bulletin/Current_Issue/CSPGIMIS20/Publications/Bulletin.aspx >

Mossop, G. and Shetsen, I. (compilers)(1994) Geological Atlas of the Western Canada Sedimentary Basin. Cdn. Soc. Petrol Geol. and Alberta Research Council, Calgary, Alberta, 510pp. ISBN-13: 978-0920230534 URL <http://www.cspg.org/CSPG/IMIS20/Publications/Geological_Atlas/CSPGIMIS20/Publications/Geological_Atlas.aspx > [July 2018]

NEB 2016 The Unconventional Gas Resources of Mississippian-Devonian Shales in the Liard Basin of British Columbia, the Northwest Territories, and Yukon - Energy Briefing Note. National Energy Board, Canada. ISBN 978-0-660-04668-6 https://www.neb-one.gc.ca/nrg/sttstc/ntrlgs/rprt/ltmtptntlbcnwtkn2016/index-eng.html

Nelson, S.J. 1970 The Face of Time: the geological history of Western Canada. Canadian Society of Petroleum Geologists.

Niemann, M. and Whiticar, M.J. 2017 Stable Isotope Systematics of Coalbed Gas during Desorption and Production. Geosciences 7 : 43 : 1-21 http://dx.doi.org/10.3390/geosciences7020043

Norville, G. 2014 Isotope Geochemistry of Natural Gas from the Horn River Basin: Understanding Gas Origin, Storage and Transport in an Unconventional Shale Play. Univeristy of Alberta Ph.D. Thesis URL < https://era.library.ualberta.ca/items/e3c79a1f-5d5b-48da-8764-0ea5ab32c5d0 > PDF at https://era.library.ualberta.ca/items/e3c79a1f-5d5b-48da-8764-0ea5ab32c5d0/view/8a257210-4f00-4d66-b76a-47ebd8c77d00/Norville_Giselle_A_201406_PhD.pdf [January 2016]

Nowamooz, A., Lemieux, J.M., Molson, J., Therrien, R. 2015 Numerical investigation of methane and formation fluid leakage along the casing of a decommissioned shale gas well. Water Resources Research 51 : 6 : 4592-4622 https://doi.org/10.1002/2014WR016146

OGC 2012 Montney Formation Play Atlas NEBC. British Columbia Oil and Gas Commission URL <https://www.bcogc.ca/montney-formation-play-atlas-neb c> [July 2018]

OGC 2014 Horn River Basin Unconventional Shale Gas Play Atlas. British Columbia Oil and Gas Commission URL <https://www.bcogc.ca/horn-river-basin-play-atlas > [July 2018]

OGC 2015a Isotopic analysis and submission guideline, BC Oil and Gas Commission URL < https://www.bcogc.ca/isotopic-analysis-and-submission-guideline > [October 2016].

OGC 2015b Section 34: tests, analyses, surveys and logs; in Oil and Gas Activities Act: BC Oil and Gas Commission Drilling and Production Regulation, B.C. Reg. 165/2015, URL <http://www.bclaws.ca/civix/document/id/loo97/loo97/282_2010#section34 > [November 2016]

OGC 2016 INDB 2016-07 submission of isotopic gas analyses, BC Oil and Gas Commission URL < https://www.bcogc.ca/indb-2016-07-submission-isotopic-gas-analyses > [October 2016].

OGC 2018 BC Oil and Gas Commission 2016/17 Annual Service Plan Report. BC Oil and Gas Commission URL <https://www.bcogc.ca/node/14394/download > [July 2018]

Oldale, H. and Munday, R. 1994 Devonian Beaverhill Lake Group of the Western Canada Sedimentary Basin. in Mossop, G. and Shetsen, I. (compilers)(1994) Geological Atlas of the Western Canada Sedimentary Basin. Cdn. Soc. Petrol Geol. and Alberta Research Council, Calgary, Alberta, p. 149-164. ISBN-13: 978-0920230534 URL <http://www.cspg.org/CSPG/IMIS20/Publications/Geological_Atlas/CSPGIMIS20/Publications/Geological_Atlas.aspx > [July 2018]

Ono, S., Wang, D.T., Gruen, D.S., Sherwood-Lollar, B., Zahniser, M., McManus, B.J., Nelson, D.D. 2014 Measurement of a doubly-substituted methane isotopologue, 13CH3D, by tunable infrared laser direct absorption spectroscopy. Analytical Chemistry 86 : 6487– 6494 http://dx.doi.org/10.1021/ac5010579

Prentice, I.C., G.D. Farquhar, M.J.R. Fasham, M.L. Goulden, M. Heimann, V.J. Jaramillo, H.S. Kheshgi, C. Le Quéré, R.J. Scholes, D.W.R. Wallace, D. Archer, M.R. Ashmore, O. Aumont, D. Baker, M. Battle, M. Bender, L.P. Bopp, P. Bousquet, K. Caldeira, P. Ciais, P.M. Cox, W. Cramer, F. Dentener, I.G. Enting, C.B. Field, P. Friedlingstein, E.A. Holland, R.A. Houghton, J.I. House, A. Ishida, A.K. Jain, I.A. Janssens, F. Joos, T. Kaminski, C.D. Keeling, R.F. Keeling, D.W. Kicklighter, K.E. Kohfeld, W. Knorr, R. Law, T. Lenton, K. Lindsay, E. Maier-Reimer, A.C. Manning, R.J. Matear, A.D. McGuire, J.M. Melillo, R. Meyer, M. Mund, J.C. Orr, S. Piper, K. Plattner, P.J. Rayner, S. Sitch, R. Slater, S. Taguchi, P.P. Tans, H.Q. Tian, M.F. Weirig, T. Whorf, A. Yool, L. Pitelka, A. Ramirez Rojas 2001 The Carbon Cycle and Atmospheric Carbon Dioxide [chapter 3] in IPCC, 2001: Climate Change 2001: The Scientific Basis. Contribution of Working Group I to the Third Assessment Report of the Intergovernmental Panel on Climate Change [Houghton, J.T., Y. Ding, D.J. Griggs, M. Noguer, P.J. van der Linden, X. Dai, K. Maskell, and C.A. Johnson (eds.)]. ISBN 0521-01495-6 http://www.grida.no/publications/other/ipcc_tar/

Price, R.A. 1994 Cordilleran Tectonics and the Evolution of the Western Canada Sedimentary Basin. in Mossop, G. and Shetsen, I. (compilers)(1994) Geological Atlas of the Western Canada Sedimentary Basin. Cdn. Soc. Petrol Geol. and Alberta Research Council, Calgary, Alberta, 510pp. ISBN-13: 978-0920230534 URL <http://www.cspg.org/CSPG/IMIS20/Publications/Geological_Atlas/CSPGIMIS20/Publications/Geological_Atlas.aspx > [July 2018]

Prinzhofer, A. and Battani, A. 2003 Gas isotopes tracing: an important tool for hydrocarbons exploration. Oil & Gas Science and Technology-Revue 58 : 2 : 299-311 http://dx.doi.org/10.2516/ogst:2003018

Prinzhofer, A. and Deville, E. 2013 Origins of hydrocarbon gas seeping out from offshore mud volcanoes in the Nile delta. Tectonophysics 591 : 52-61 : SI http://dx.doi.org/10.1016/j.tecto.2011.06.028

Prinzhofer, A., Girard, J.P., Buschaert, S., Huiban, Y., Noirez, S. 2009 Chemical and isotopic characterization of hydrocarbon gas traces in porewater of very low permeability rocks: The example of the Callovo-Oxfordian argillites of the eastern part of the Paris Basin. Chemical Geology 260 : 3-4 : 269-277 http://dx.doi.org/10.1016/j.chemgeo.2008.12.021

Prinzhofer, A., Neto, E.V.D., Battani, A. 2010 Coupled use of carbon isotopes and noble gas isotopes in the Potiguar basin (Brazil): Fluids migration and mantle influence. Marine and Petroleum Geology 27 : 6 : 1273-1284 http://dx.doi.org/10.1016/j.marpetgeo.2010.03.004

Raj, R., Suman, R., Ghandehariun, S., Kumar, A., Tiwari, M.K. 2016 A techno-economic assessment of the liquefied natural gas (LNG) production facilities in Western Canada. Sustainable Energy Technologies and Assessments 18 : 140–152 http://dx.doi.org/10.1016/j.seta.2016.10.005

Rashid, M.A. 1985 Geochemistry of Marine Humic Compounds. ISBN 0-387-96135-6

Redding, C. 1978 Hydrogen and carbon isotopes in coals and kerogens. In: R.E. Zartman (Editor), 4th Int. Conf. Geochronology, Cosmochronology, Isotope Geology. US Geol. Surv. Open File Rep., 78-701, 348 PP.

Redding, C.E., Schoell, M., Monin, J.C., Durand, B. 1980 Hydrogen and carbon isotopic composition of coals and kerogens. Physics and Chemistry of the Earth 12 : 711-723 https://doi.org/10.1016/0079-1946(79)90152-6

Rice, D.D. and Claypool, G.E. 1981 Generation, accumulation and resource potential of biogenic gas. Bull AAPG 65 : 1 : 5-25 http://archives.datapages.com/data/bulletns/1980-81/data/pg/0065/0001/0000/0005.htm

Rice, A.K., Lackey, G., Proctor, J., Singha, K. 2018 Groundwater-quality hazards of methane leakage from hydrocarbon wells: A review of observational and numerical studies and four testable hypotheses. https://doi.org/10.1002/wat2.1283

Rivard, C., Lavoie, D., Lefebvre, R., Sejourne, S., Lamontagne, C., Duchesne, M. 2014 An overview of Canadian shale gas production and environmental concerns. International Journal of Coal Geology 126 : 64-76 https://doi.org/10.1016/j.coal.2013.12.004

Rocheleau, J.,Fiess, K.M., Pyle, L.J., Ferri, F., Fraser, T.A. 2014 Source Rock Characterization of the Carboniferous Golata Formation and Devonian Besa River Formation Outcrops, Liard Basin, Northwest Territories. Geoconvention 2014 abstract https://www.geoconvention.com/archives/2014/301_GC2014_Source_Rock_Characterization_of_Carboniferous_Golata_Fm.pdf

Romero-Sarmiento, M.F., Euzen, T., Rohais, S., Jiang, C.Q., Littke, R. 2016 Artificial thermal maturation of source rocks at different thermal maturity levels: Application to the Triassic Montney and Doig formations in the Western Canada Sedimentary Basin. Organic Geochemistry 97 : 148-162 https://doi.org/10.1016/j.orggeochem.2016.05.002

Rowe, D. and Muehlenbachs, K. 1999 Isotopic fingerprints of shallow gases in the Western Canadian sedimentary basin: Tools for remediation of leaking heavy oil wells. Organic Geochemistry 30 : 8 A : 861-871 https://doi.org/10.1016/S0146-6380(99)00068-6

Sackett, W.M. 1968 Carbon isotope composition of natural methane occurrences. Am. Assoc. Petrol. Geol. Bull., 52 : 5 : 853-857 http://archives.datapages.com/data/bulletns/1968-70/data/pg/0052/0005/0850/0853.htm

Sackett, W.M. 1978 Carbon and hydrogen carbon effects during the thermocatalytic production of hydrocarbons in laboratory simulation experiments. Geochimica et Cosmochimica Acta 42 : 6 : 571-580 https://doi.org/10.1016/0016-7037(78)90002-9

Sackett, W.M. and Conkright, M.E. 1997 Summary and re-evaluation of the high-temperature isotope geochemistry of methane. Geochimica et Cosmochimica Acta 61 : 9 : 1941-1952 https://doi.org/10.1016/S0016-7037(97)00039-2

Schoell, M. 1980 The hydrogen and carbon isotopic composition of methane from natural gases of various origins. Geochimica et Cosmochimica Acta 44 : 5 : 649-661 https://doi.org/10.1016/0016-7037(80)90155-6

Schoell, M. 1984 Stable Isotopes in Petroleum Research. in Brooks, J. and Welte, D. eds. Advances in Petroleum Geochemistry, Volume 1 pp 215-246.

Schoell, M. 1983 Genetic characterization of natural gases. AAPG Bulletin 67 : 12 : 2225-2238 http://archives.datapages.com/data/bulletns/1982-83/data/pg/0067/0012/2200/2225.htm

Schoell, M. 1988 Multiple origins of methane in the Earth. Chemical Geology 71 : 1-3 : 1-10 https://doi.org/10.1016/0009-2541(88)90101-5

Schwietzke, S., Sherwood, O.A., Bruhwiler, L.M.P., Miller, J.B., Etiope, G., Dlugokencky, E.J., Michel, S.E., Arling, V.A., Vaughn, B.H., White, J.W.C., Tans, P.P. 2017 Upward revision of global fossil fuel methane emissions based on isotope database. Nature 543 : 7645 452-452 http://dx.doi.org/10.1038/nature21422

Shuai, Y.H., Douglas, P.M.J., Zhang, S.C., Stolper, D.A., Ellis, G.S., Lawson, M., Lewan, M.D., Formolo, M., Mi, J.K., He, K., Hu, G.Y., Eiler, J.M. 2018 Equilibrium and non-equilibrium controls on the abundances of clumped isotopologues of methane during thermogenic formation in laboratory experiments: Implications for the chemistry of pyrolysis and the origins of natural gases. Geochimica et Cosmochimica Acta 223 : 159-174 http://dx.doi.org/10.1016/j.gca.2017.11.024

Silva, P.L. and Bustin, R.M. 2018 Preliminary liquid hydrocarbon potential assessment of the Doig Formation, northeastern British Columbia and west-central Alberta, based on thickness, organic richness and maturity; in Geoscience BC Summary of Activities 2017: Energy, Geoscience BC, Report 2018-4, p. 39–50 http://cdn.geosciencebc.com/pdf/SummaryofActivities2017/Energy/SoA2017_E_Silva.pdf

Skuce, M., Longstaffe, F.J., Potter, J., Carter, T.R. 2014 Development of a geochemical tool for sourcing leaking well fluids in southwestern Ontario. Geoconvention 2014 Abstract https://www.geoconvention.com/archives/2014/178_GC2014_Development_of_a_geochemical_tool.pdf

Soeder, D.J. 2018 The successful development of gas and oil resources from shales in North America. Journal of Petroleum Science and Engineering 163 : 399-420 https://doi.org/10.1016/j.petrol.2017.12.084

Stahl, W., 1973. Carbon isotope ratios of German natural gases in comparison with isotopic data of gaseous hydrocarbons from other parts of the World. in Tissot, B. and Bienner, F. eds. Advances in Organic Geochemistry. Pergamon, Oxford, pp. 453-462.

Stahl. W.. 1977. Carbon and nitrogen isotopes in hydrocarbon research and exploration. Chemical Geology 20 : 2 : 121-149 http://dx.doi.org/10.1016/0009-2541(77)90041-9

Stahl. W., 1979. Carbon isotopes in petroleum geochemistry. in Jager, F. and Hunziker, J.C. eds. Lectures in Isotope Geology. Springer, New York, pp. 274-283.

Stolper, D.A., Lawson, M., Davis, C.L., Ferreira, A.A., Neto, E.V.S., Ellis, G.S., Lewan, M.D., Martini, A.M., Tang, Y., Schoell, M., Sessions, A.L., Eiler, J.M. 2014a Formation temperatures of thermogenic and biogenic methane. Science 344 : 6191 : 1500-1503 http://dx.doi.org/10.1126/science.1254509

Stolper, D.A., Martini, A.M., Clog, M., Douglas, P.M., Shusta, S.S., Valentine, D.L., Sessions, A.L., Eiler, J.M. 2015 Distinguishing and understanding thermogenic and biogenic sources of methane using multiply substituted isotopologues. Geochimica et Cosmochimica Acta 161 : 219-247 http://dx.doi.org/10.1016/j.gca.2015.04.015

Stolper, D.A., Sessions, A.L., Ferreira, A.A., Neto, E.V.S., Schimmelmann, A., Shusta, S.S., Valentine, D.L., Eiler, J.M. 2014b Combined 13C-D and D-D clumping in methane: methods and preliminary results. Geochimica et Cosmochimica Acta 126 : 169-191 http://dx.doi.org/10.1016/j.gca.2013.10.045

Stott, D.F. 1975 The Cretaceous System in Northeastern British Columbia. In Caldwell, W.G.E. ed. The Cretaceous System in the Western Interior of North America. Geological Association of Canada Special Paper 13. pp. 441-467.

Strąpoć, D., Mastalerz, M., Dawson, K., Macalady, J., Callaghan, A.V., Wawrik, B., Turich, C., Ashby, M. 2011 Biogeochemistry of Microbial Coal-Bed Methane. Annual Review of Earth and Planetary Sciences 39 : 617–656 http://dx.doi.org/10.1146/annurev-earth-040610-133343

Taylor, S.W., Sherwood-Lollar, B., Wassenaar, L.I. 2000 Bacteriogenic ethane in near-surface aquifers: Implications for leaking hydrocarbon well bores. Environmental Science and Technology 34 : 22 : 4727-4732 http://dx.doi.org/10.1021/es001066x

Tilley, B. 1988 Diagenesis and Porewater Evolution in Cretaceous Sedimentary Rocks of the Alberta Deep Basin. University of Alberta Ph.D. thesis https://doi.org/10.7939/R38P5VJ8H < https://era.library.ualberta.ca/items/3a146bc4-ee09-493e-9b1a-77420f83e4e2 > [October 2016]

Tilley, B. and Muehlenbachs, K. 2006 Gas maturity and alteration systematics across the Western Canada Sedimentary Basin from four mud gas isotope depth profiles. Organic Geochemistry, vol. 37, no. 12, p. 1857-1868. https://doi.org/10.1016/j.orggeochem.2006.08.010

Tilley, B. and Muehlenbachs, K. 2007, Isotopically Determined Mannville Group Gas Families. CSPG/CSEG 2007 Convention, Abstracts Volume, p.67-69. http://www.cspg.org/CSPG/Conferences/Archives/2007/Conferences/Geoconvention/2007_Abstract_Archives.aspx <http://geoconvention.org/archives/2007abstracts/021S0122.pdf > [Jan 2016]

Tilley, B. and Muehlenbachs, K. 2012, Isotope Systematics of High Maturity Shale Gases in the WCSB Compared to Other North Amercan Shale Gases. CSPG convention Abstracts http://www.cspg.org/CSPG/Conferences/Archives/2012/Conferences/Geoconvention/2012_Abstract_Archives.aspx <http://www.cspg.org/documents/Conventions/Archives/Annual/2012/026_GC2012_Isotope_Systematics_of_High_Maturity_Shale_Gases.pdf > [Jan 2016]

Tilley, B. and Muehlenbachs, K. 2013, Isotope reversals and universal stages and trends of gas maturation in sealed, self-contained petroleum systems, Chemical Geology, vol. 339, p. 194-204. https://doi.org/0.1016/j.chemgeo.2012.08.002

Tilley, B.J., Muehlenbachs, K. and Szatkowski, B. J. 2001 Compartmentalization of Gas Reservoirs: Insights From Carbon Isotope Ratios. CSPG Annual convention 2001 http://www.cspg.org/CSPG/Conferences/Archives/2001/Conferences/Geoconvention/2001_Abstract_Archives.aspx <http://www.cspg.org/documents/Conventions/Archives/Annual/2001/14-102.pdf > [March 2017]

Tilley, B., McLellan, S., Hiebert, S., Quartero, B., Veilleux, B., Muehlenbachs, K. 2011 Gas isotope reversals in fractured gas reservoirs of the western Canadian foothills: mature shale gases in disguise. AAPG Bull. 95 : 1399–1422 http://archives.datapages.com/data/bulletns/2011/08aug/BLTN10103/BLTN10103.HTM https://doi.org/10.1306/01031110103

Tissot, B. P. and Welte, D. H. 1984. Petroleum formation and occurrence, 2nd ed. Springer-Verlag, Berlin ISBN: 0-387-13281-3

Townsend-Small, A., Ferrara, T.W., Lyon, D.R., Fries, A.E., Lamb, B.K. 2016 Emissions of coalbed and natural gas methane from abandoned oil and gas wells in the United States. Geophysical Research Letters 43 : 5 : 2283-2290 https://doi.org/10.1002/2015GL067623

Van Krevelen, D.W. 1961 Coal : Typology – Physics – Chemistry – Constitution. Elsevier ISBN: 978-0444406002.

Vengosh, A., Jackson, R.B., Warner, N., Darrah, T.H., Kondash, A. 2014 A Critical Review of the Risks to Water Resources from Unconventional Shale Gas Development and Hydraulic Fracturing in the United States. Environmental Science & Technology 48 : 15 : 8334-8348 : SI http://dx.doi.org/10.1021/es405118y

Vinson, D.S., Blair, N.E., Martini, A.M., Larter, S., Orem, W.H., McIntosh, J.C. 2017 Microbial methane from in situ biodegradation of coal and shale: A review and reevaluation of hydrogen and carbon isotope signatures. Chem. Geol. 453 : 128-145 http://dx.doi.org/10.1016/j.chemgeo.2017.01.027

von Fischer, J.C., Cooley, D., Chamberlain, S., Gaylord, A., Griebenow, C.J., Hamburg, S.P., Salo, J., Schumacher, R., Theobald, D., Ham, J. 2017 Rapid, Vehicle-Based Identification of Location and Magnitude of Urban Natural Gas Pipeline Leaks. Environmental Science & Technology 51 : 7 : 4091-4099 http://dx.doi.org/10.1021/acs.est.6b06095

Watson, T.L. and Bachu, S. 2009 Evaluation of the potential for gas and CO2 leakage along wellbores. SPE Paper 106817 SPE Drill. Complet. 24 : 1 : 115–126 https://doi.org/10.2118/106817-PA

Webb, M.A., Wang, Y.M., Braams, B.J., Bowman, J.M., Miller, T.F. 2017 Equilibrium clumped-isotope effects in doubly substituted isotopologues of ethane. Geochimica et Cosmochimica Acta 197 : 14-26 http://dx.doi.org/10.1016/j.gca.2016.10.001

Whiticar, M.J. 1990 A Geochemical Perspective of Natural-Gas and Atmospheric Methane. Organic Geochemistry 16 : 1-3 : 531-547 http://dx.doi.org/10.1016/0146-6380(90)90068-B

Whiticar, M.J. 1993 Stable Isotopes and Global Budgets. In: Khalil MAK (ed) Atmospheric Methane: Sources, Sinks, and Role in Global Change. NATO ASI Series (Series I: Global Environmental Change), vol 13. Springer, Berlin, Heidelberg ISBN:978-3-642-84607-6 https://doi.org/10.1007/978-3-642-84605-2_8

Whiticar, M.J. 1994 Correlation of Natural Gases with Their Sources. In: Magoon, L.B. and Dow, W.G. eds The Petroleum System – from source to trap. AAPG Memoir 60. https://www.aapg.org/publications/special-publications/cds/details/articleid/3938/m60-cd-the-petroleum-system-from-source-to-trap

Whiticar, M.J. 1996 Stable isotope geochemistry of coals, humic kerogens and related natural gases. Int. J. Coal Geol. 32 : 1-4 : 191-215 http://dx.doi.org/10.1016/S0166-5162(96)00042-0

Whiticar, M.J. 1999 Carbon and hydrogen isotope systematics of bacterial formation and oxidation of methane. Chem. Geol. 161 : 1-3 : 291-314 http://dx.doi.org/10.1016/S0009-2541(99)00092-3

Whiticar, M.J. and Eek, M.K. 2001 Challenges of 13C/12C measurements by CF-IRMS of biogeochemical samples at sub-nanomolar levels in IAEA eds. New approaches for stable isotope ratio measurements. IAEA TECDOC-1247 pp.75-95 ISSN 1011–4289 https://www-pub.iaea.org/MTCD/Publications/PDF/te_1247_prn.pdf https://www-pub.iaea.org/books/IAEABooks/6293/New-Approaches-for-Stable-Isotope-Ratio-Measurements

Whiticar, M.J., Faber, E., Schoell, M. 1986 Biogenic methane formation in marine and freshwater environments: CO2 reduction vs. acetate fermentation-Isotope evidence. Geochemica et Cosmochimica Acta 50 : 693-709 http://dx.doi.org/10.1016/0016-7037(86)90346-7

Whiticar, M.J., Christensen, L.E., Salas, C.J. and Reece, P. 2018 GHGMap: novel approach for aerial measurements of greenhouse gas emissions, British Columbia; in Geoscience BC Summary of Activities 2017: Energy, Geoscience BC, Report 2018-4, p. 1–10. http://cdn.geosciencebc.com/pdf/SummaryofActivities2017/Energy/SoA2017_E_Whiticar.pdf

Wilson, T.K. and Bustin, R.M. 2018 Regional variability of reservoir properties of the Devonian shales of northeastern British Columbia in Geoscience BC Summary of Activities 2017: Energy, Geoscience BC, Report 2018-4, p. 51–64 http://cdn.geosciencebc.com/pdf/SummaryofActivities2017/Energy/SoA2017_E_Wilson.pdf

Wong, W.W. and Sackett, W.M. 1978 Fractionation of Stable Carbon isotopes by Marine Phytoplankton. Geochimica et Cosmochimica Acta 42 : 12 : 1809-1815 http://dx.doi.org/10.1016/0016-7037(78)90236-3

Wood, J.M. and Sanei, H. 2016 Secondary migration and leakage of methane from a major tight-gas system; Nature Communications, v. 7, art. 13614, http://dx.doi.org/10.1038/ncomms13614

Wood, J.M., Sanei, H., Curtis, M.E., Clarkson, C.R. 2015 Solid bitumen as a determinant of reservoir quality in an unconventional tight gas siltstone play. International Journal of Coal Geology 150 : 287-295 https://doi.org/10.1016/j.coal.2015.03.015

Wright, G.N., McMechan, M.E., Potter, D.E.G. 1994 Structure and Architecture of the Western Canada Sedimentary Basin. in Mossop, G. and Shetsen, I. (compilers)(1994) Geological Atlas of the Western Canada Sedimentary Basin. Cdn. Soc. Petrol Geol. and Alberta Research Council, Calgary, Alberta, p. 149-164. ISBN-13: 978-0920230534 URL <http://www.cspg.org/CSPG/IMIS20/Publications/Geological_Atlas/CSPGIMIS20/Publications/Geological_Atlas.aspx > [July 2018]

Xia, X.Y., Chen, J., Braun, R., Tang, Y.C. 2013 Isotopic reversals with respect to maturity trends due to mixing of primary and secondary products in source rocks. Chemical Geology 339 : 205-212 : SI http://dx.doi.org/10.1016/j.chemgeo.2012.07.025

Young, E.D., Kohl, I.E., Sherwood-Lollar, B., Etiope, G., Rumble, D., Li, S., Haghnegahdar, M.A., Schauble, E.A., McCain, K.A., Foustoukos, D.I., Sutclife, C., Warr, O., Ballentine, C.J., Onstott, T.C., Hosgormez, H., Neubeck, A., Marques, J.M., Perez-Rodriguez, I., Rowe, A.R., LaRowe, D.E., Magnabosco, C., Yeung, L.Y., Ash, J.L., Bryndzia, L.T. 2017 The relative abundances of resolved (CH2D2)-C-12 and (CH3D)-C-13 and mechanisms controlling isotopic bond ordering in abiotic and biotic methane gases. Geochimica Et Cosmochimica Acta 203 : 235-264 https://doi.org/10.1016/j.gca.2016.12.041

Zonneveld, J.P. and Moslow, T.F. 2018 Palaeogeographic setting, lithostratigraphy, and sedimentary framework of the Lower Triassic Montney Formation of western Alberta and northeastern British Columbia. Bulletin of Canadian Petroleum Geology 66 : 1 : 93-127. URL temp <http://www.cspg.org/CSPG/IMIS20/Publications/Bulletin/Current_Issue/CSPGIMIS20/Publications/Bulletin.aspx >

Zumberge, J., Ferworn, K., Brown, S., 2012 Isotopic reversal ('rollover') in shale gases produced from the Mississippian Barnett and Fayetteville formations. Marine and Petroleum Geology 31 : 1 : 43–52. http://dx.doi.org/10.1016/j.marpetgeo.2011.06.009

Appendix A: BC-NGA Isotopic Profiles and interpretation from public data

(http://bc-nga.ca/BC-NGA_Home.html).

This section of the thesis contains the supporting ISO data presented in graphical form with interpretive diagrams to support discussion in the main text of the thesis.

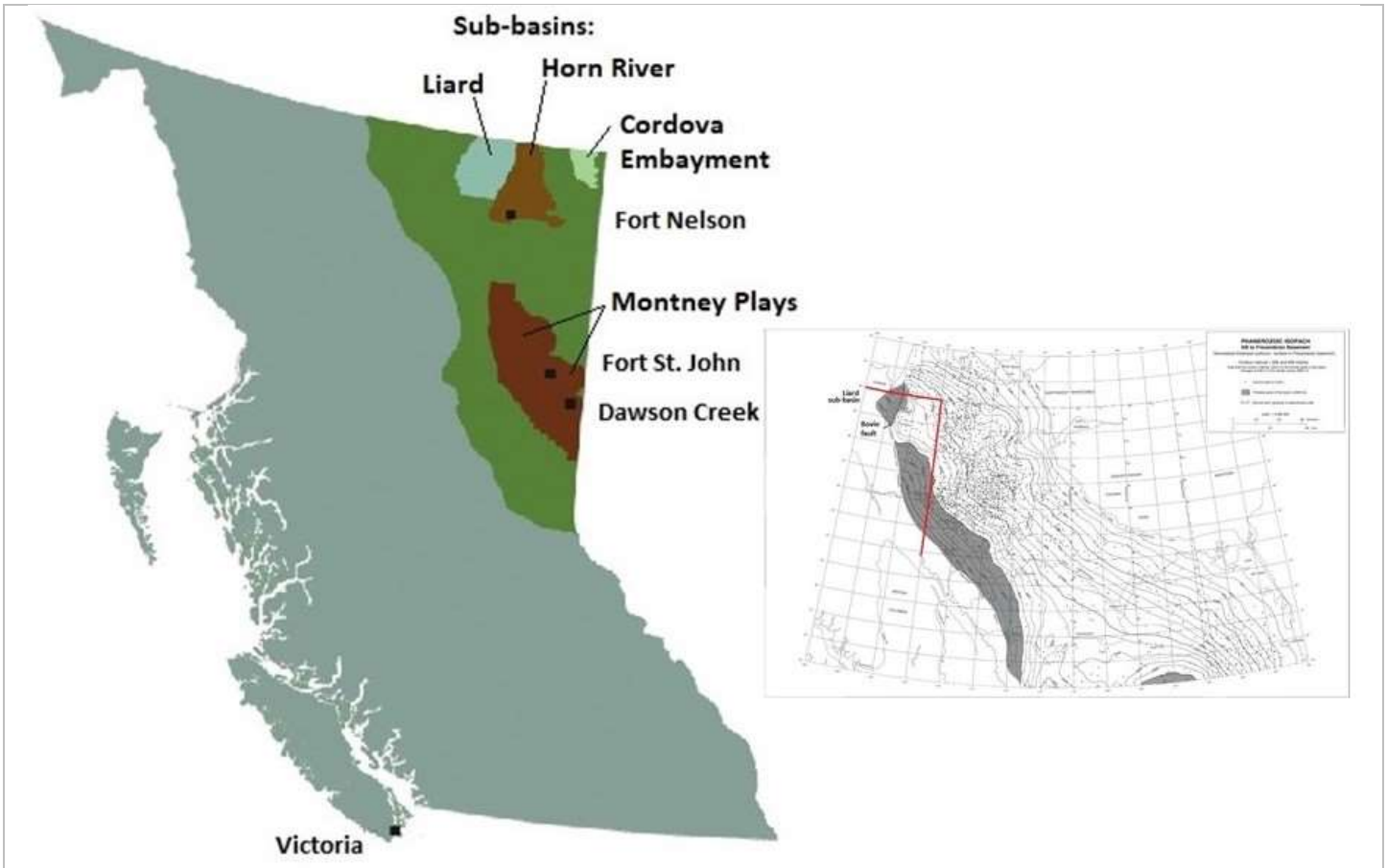

Figure A 1a and b. Area of study (area of WCSB in green and including plays and sub-basins. Other gas bearing basins in B.C. are not shown); right = WCSB extent and thickness with NEBC outline added in red and Liard basin and bounding fault labelled (after Wright et al 1994).

The types of plots included hear are (see the main text for definitions):

1. Gas Content (MC) ratio profiles as: Bernard Ratio (BR modified by 1/30 to fit same scale as others to have graphical comparison), iC_4/nC_4 Ratio, dryness Ratio, isotope difference ratio (1/40 of 15 plus $\delta^{13}C_2$ minus $\delta^{13}C_1$);
2. Raw Gas Isotope data as: $\delta^{13}C_1$, $\delta^{13}C_2$, $\delta^{13}C_3$, and $\delta^{2}H\text{-}C_1$ (modified by *0.2 to fit same scale as others to have graphical comparison);
3. Bernard diagram (each vertical profile plus a single HZ diagram as composite of all Montney HZ – all profiles except 8);
4. CD diagram (where both $\delta^{13}C_1$ and both $\delta^{2}H\text{-}C_1$ have data);
5. Berner-Faber Diagram $\delta^{13}C_1$ vs. $\delta^{13}C_2$ (where both $\delta^{13}C_1$ and $\delta^{13}C_2$ have data);
6. Berner-Faber Diagram $\delta^{13}C_2$ vs. $\delta^{13}C_3$ (where both $\delta^{13}C_2$ and $\delta^{13}C_3$ have data);
7. Plot $\delta^{13}C_1$ vs. $\delta^{13}CO_2$ diagram (where both $\delta^{13}C1$ and $\delta^{13}CO2$ have data).
8. Plot of $\delta^{13}C_2\text{-}\delta^{13}C_1$ ‰ versus $\delta^{13}C_3\text{-}\delta^{13}C_2$ ‰

The well profiles of ISO data are presented approximately in geographic order from South to North.

OGC WA#	same pad *a	VT data	HZ data	both data	VT profile	HZ profile *b	$\delta^{13}C$ data	$\delta^{2}H$ data	CD Diagram *c
total>	15	21	39	7	20	32	48	16	6
30200			●			●	●		
31521			●			●	●		
31522	y31521		●			●	●		
31101			●			●	●		
31102	y31101		●			●	●		
31103	y31101		●			●	●		
30792			●			●	●		
30791	y30792		●			●	●		
29568			●			●	●		
31699			●			●	●		
31640			●			●	●		
31790			●			<10	●		
32032		●			●		●		
31977			●			●	●		
26657		●			●		●		
27404			●			●	●		
28002			●			●	●		
25587	y26949		●				no data		
26949		●			●		●		
26918		●			●		●		
26660			●				no data		
32990		●			●		●	●	●
28233		●	●	●	●	●	●		
33348			●			<10	●		
30947			●			●	●	●	M
30948	y30947		●			●	●	●	M
30949	y30947		●			●	●	●	M
28165		●	●	●	●	●	●		
28167	y28165		●			●	●		
31226			●			●	●	●	M
31228	y31226		●			●	●	●	M
31490		●	●	●	●	●	●	●	●
31491	y31490		●			●	●	●	M
31492	y31490		●			●	●	●	M
30316		●	●	●	●	●	●		
28770		●	●	●	●	●	●		
30406			●			●	●	●	M
30407	y30406		●			●	●	●	M
30408	y30406		●				no data		
28239			●			●	●	●	M
28588		●	●	●	●	●	●	●	●
32739			●			<10	●		
31987			●				no data		
30308		●			●		●	●	●
29344		●			●		●		
32676		●			●		●		
31988		●			●		●		
32152		●			●		●		
32153	y32152	●			●		●		
30415		●					no data		
29747		●			●		●	●	●
29727	y29747	●	●	●	●	●	●	●	●
29046		●			●		●		

*a = y means see other entry for preferred profile;
*b = "<10" means a few datapoints and profile not created, only map data;
*c = "M" means only plotted with Montney all profiles.

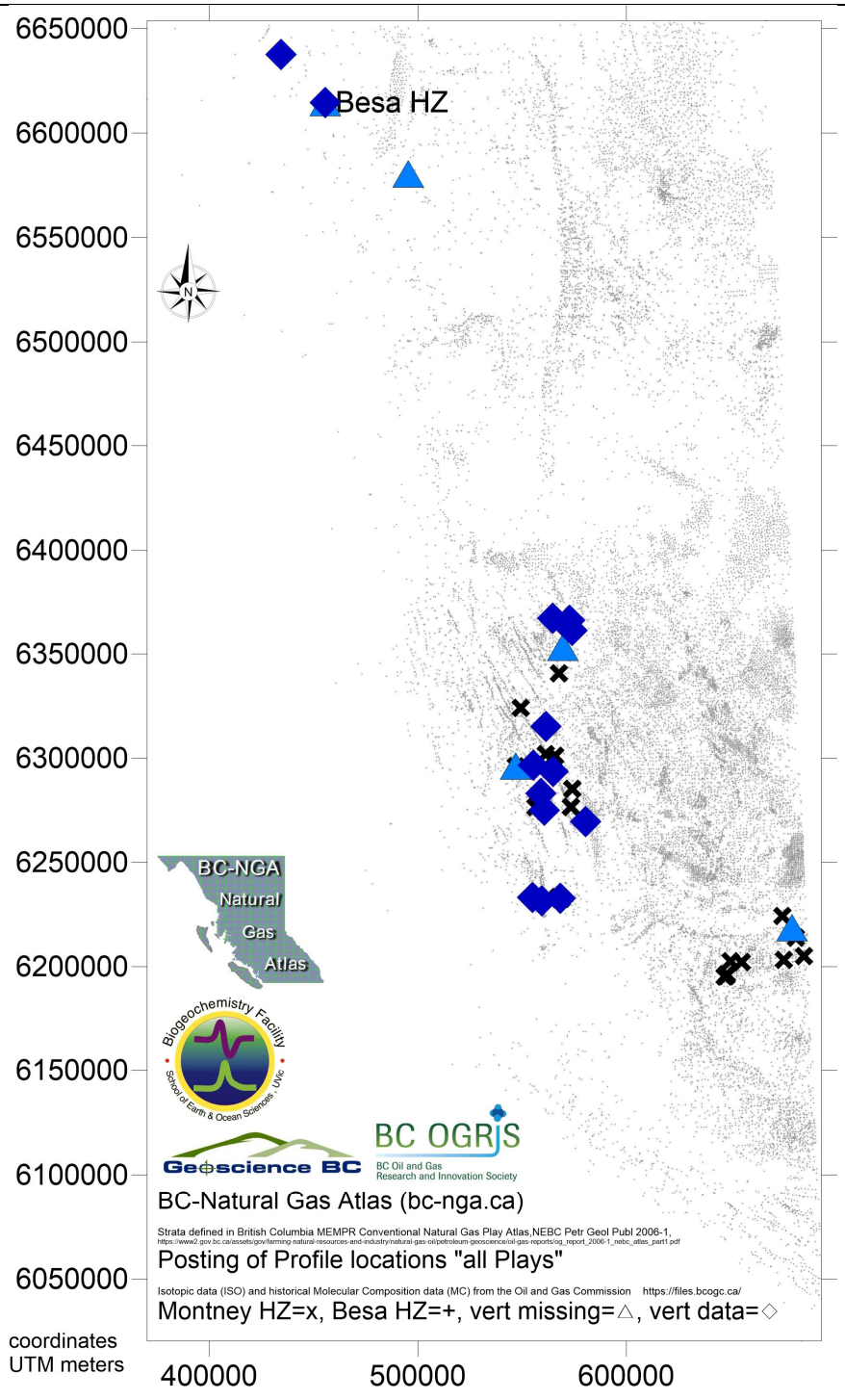

Figure A 2. Profile Location map – All profiles: Posting map of all profiles marked by blue for vertical profiles, Grey for Besa River horizontal profiles (obscured by vertical locations) and Black for Montney Horizontal well profiles. All profiles are listed in Table A01. The well profiles of ISO data are presented approximately in geographic order from South to North.

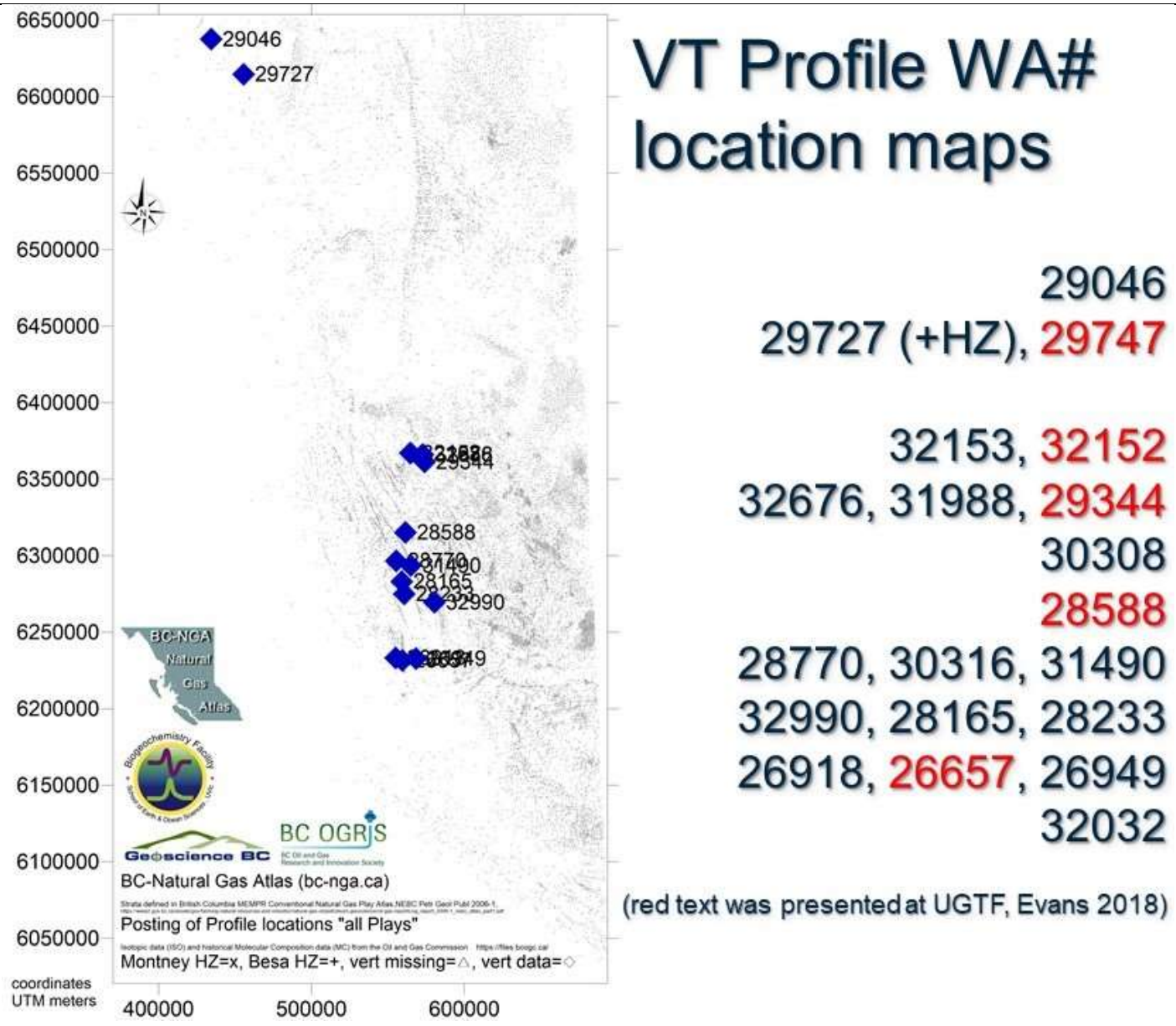

Figure A 3. Profile Location map – Reduced to the vertical profiles only with red highlights of the example profiles used in previous publications (eg. Evans 2018).

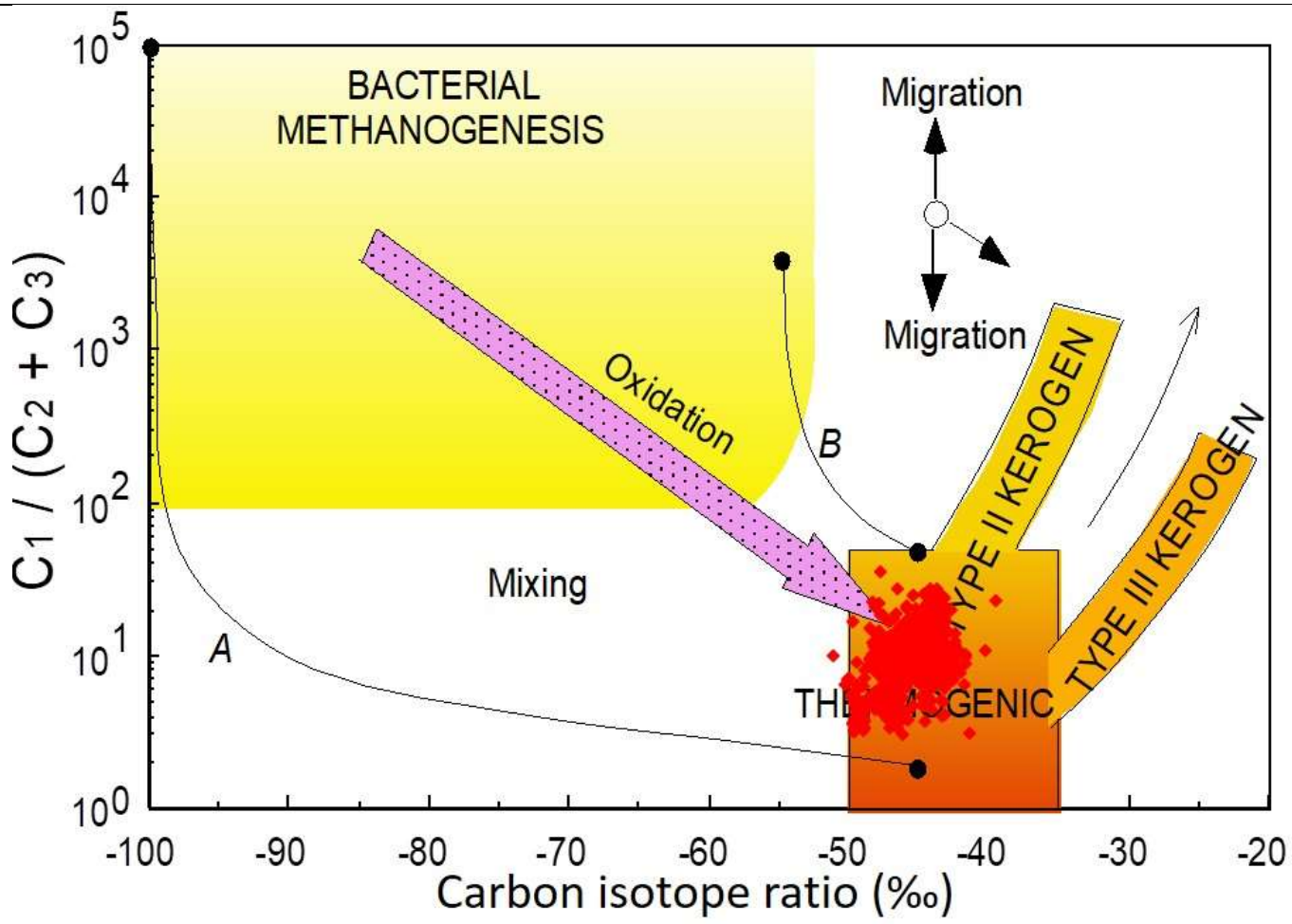

Figure A 4. ISO profile data – Interpretive Bernard Diagram for all Montney samples (HZ and VT wells) that are presented later in this appendix – summary diagram only (Whiticar, 2018 pers. comm., after Whiticar 1999). Note that despite many locations, the thermal maturity is the same.

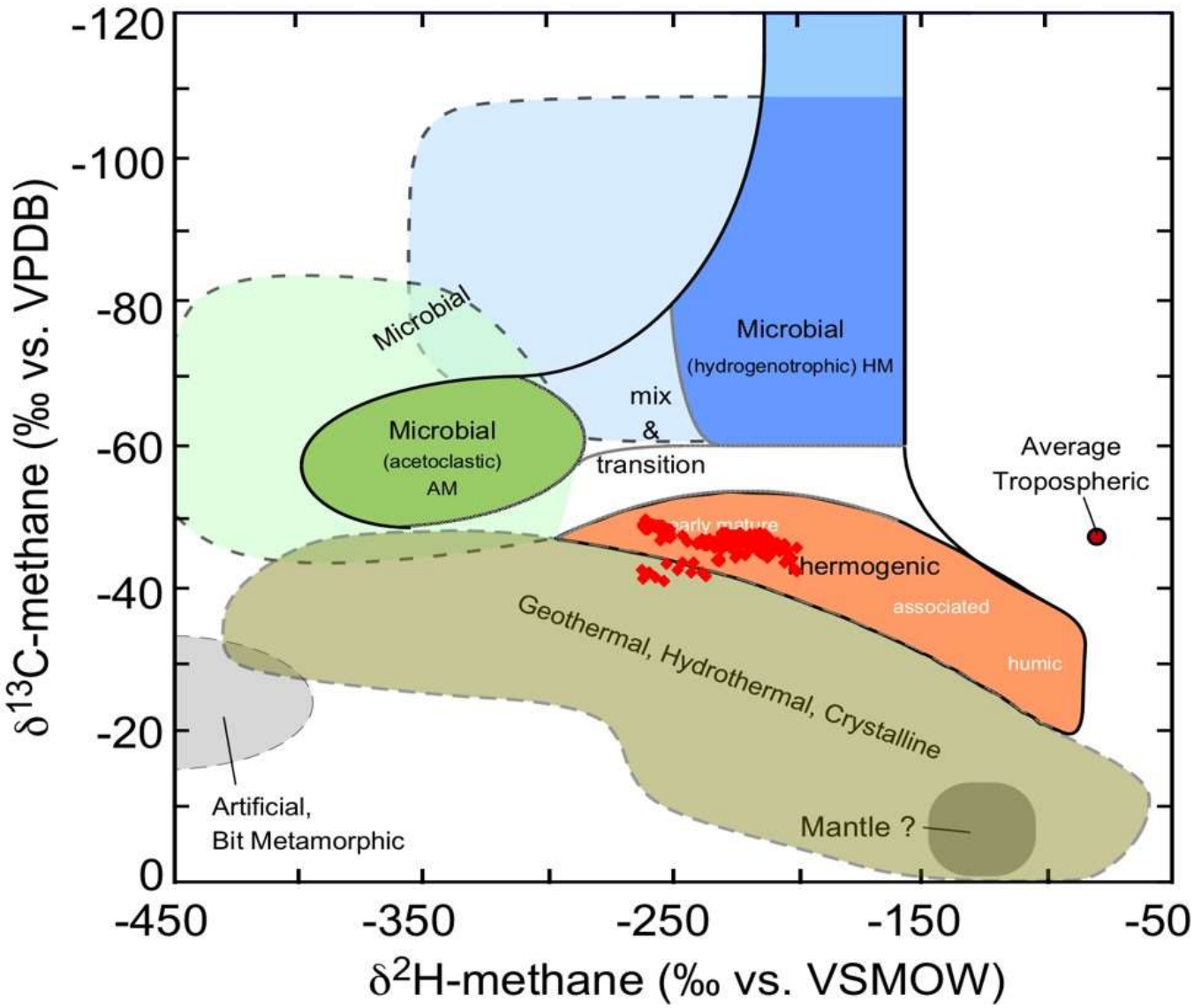

Figure A 5. ISO profile data – Interpretive CD Diagram for all Montney samples (HZ and VT wells) that are presented later in this appendix – summary diagram only (Whiticar, 2018 pers. comm., after Whiticar 1999). Note that despite many locations, the thermal maturity is the same except for one cluster of samples.

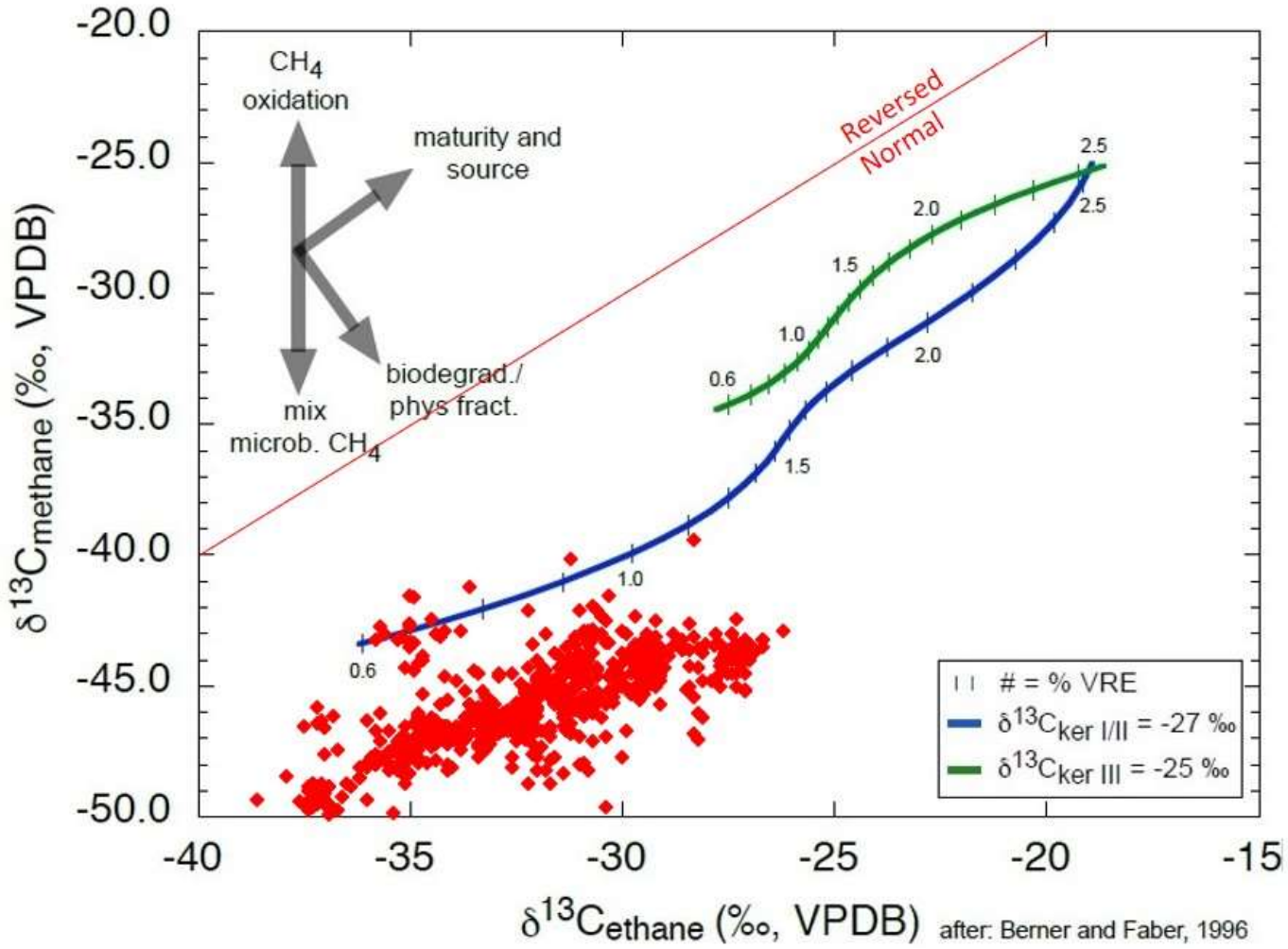

Figure A 6. ISO profile data – Interpretive ISO $\delta^{13}C_1$ versus $\delta^{13}C_2$ plot for all Montney samples (HZ and VT wells) that are presented later in this appendix – summary diagram only (Whiticar, 2018 pers. comm., after Berner and Faber 1996, no trendlines). Note most samples are $\delta^{13}C_1$ depleted except for a few samples located far to the east.

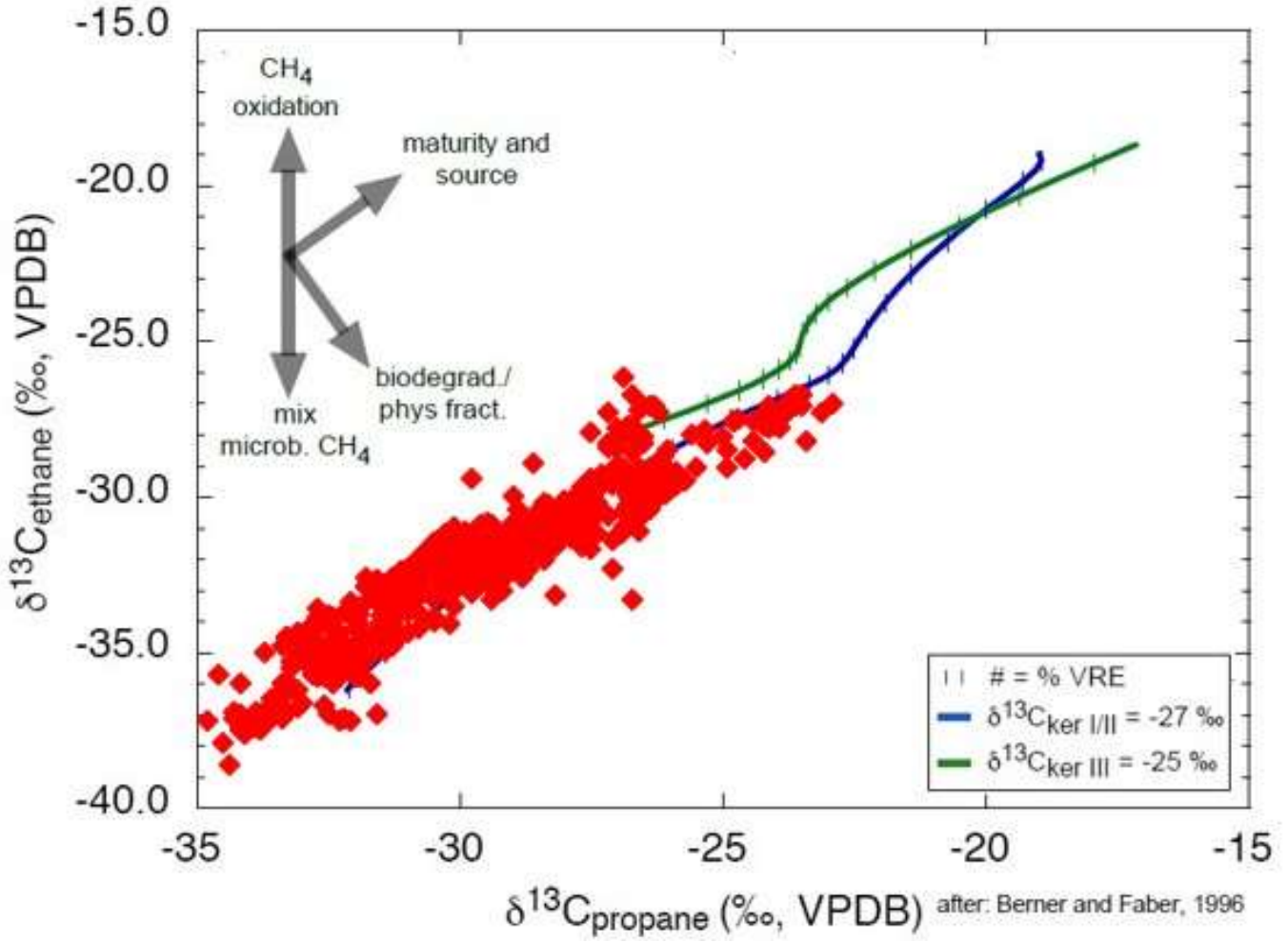

Figure A 7. ISO profile data – Interpretive ISO $\delta^{13}C_2$ versus $\delta^{13}C_3$ plot for all Montney samples (HZ and VT wells) that are presented later in this appendix – summary diagram only (Whiticar, 2018 pers. comm., after Berner and Faber 1996, no trendlines). Note that despite C_2 and C_3 plotting along the Type II kerogen curve, the methane in the previous diagram appears to be unrelated and skewed to "biodegraded" – the samples noted as undepleted previously (few samples located far to the east) are on the Type III line and may be depleted also.

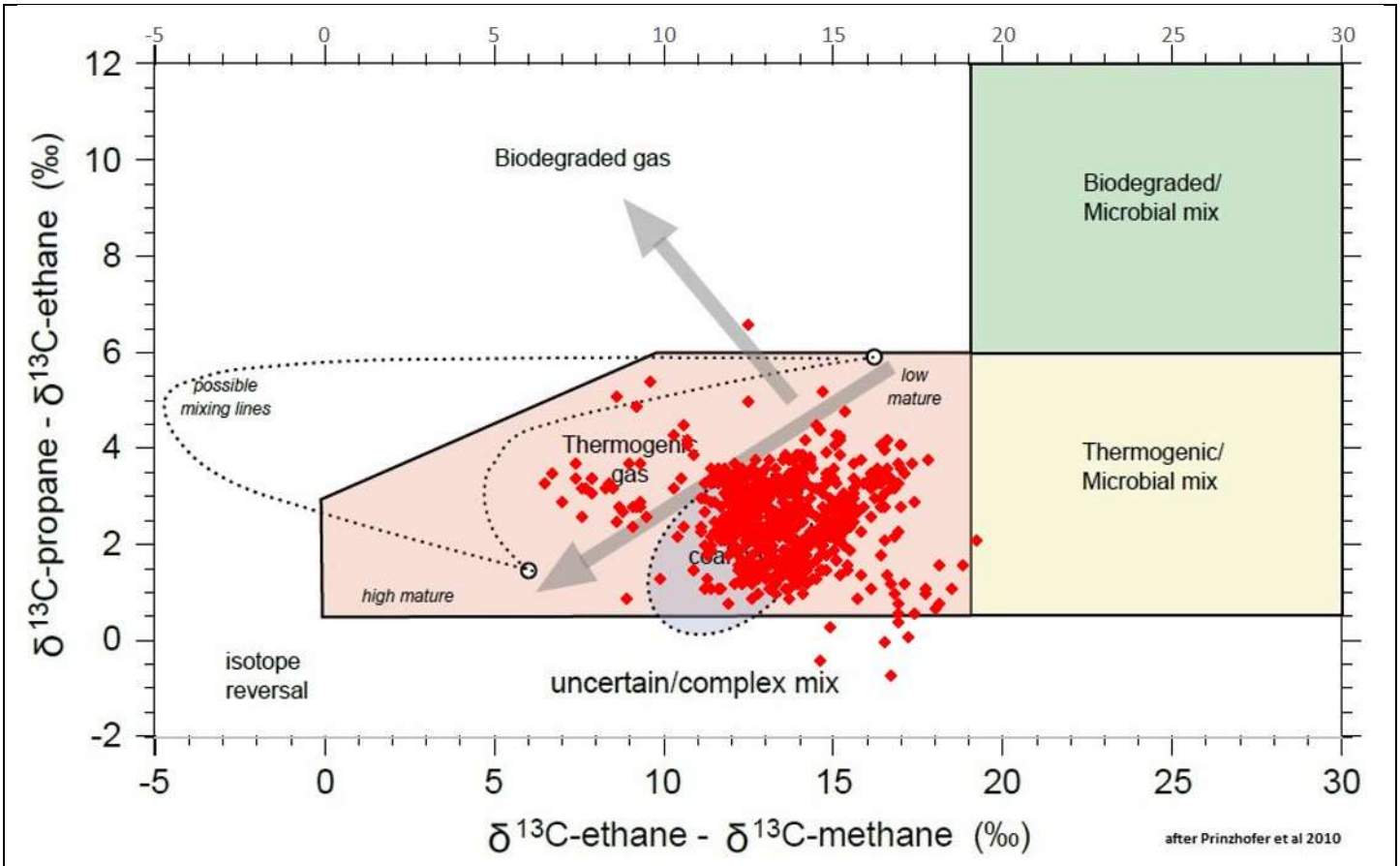

Figure A 8. ISO profile data – Interpretive $\delta^{13}C_2$- $\delta^{13}C_1$ versus $\delta^{13}C_3$- $\delta^{13}C_2$ plot for all Montney samples (HZ and VT wells) that are presented later in this appendix – summary diagram only (no trendlines). Note this infers that the majority is "coal gas" with very little along known mixing curves.

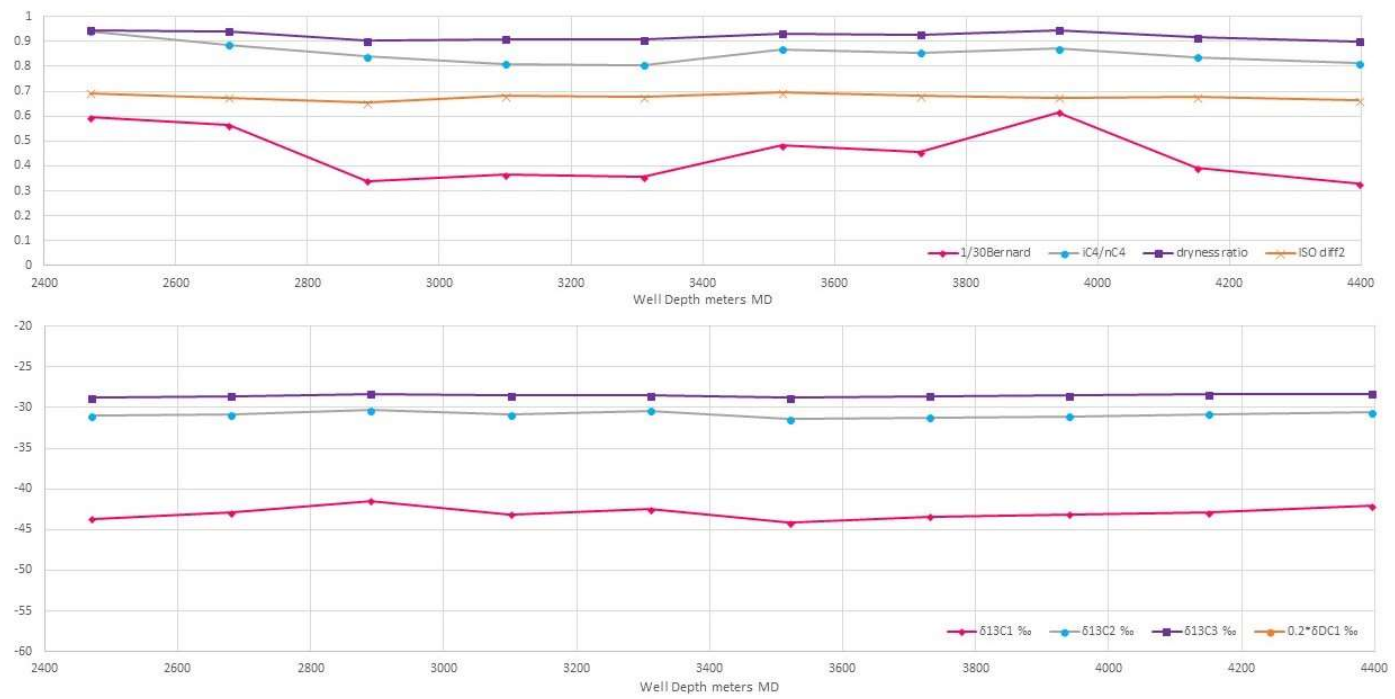

Figure A 9. Well profile, MC ratios and ISO data for WA#30200 (Montney HZ leg).

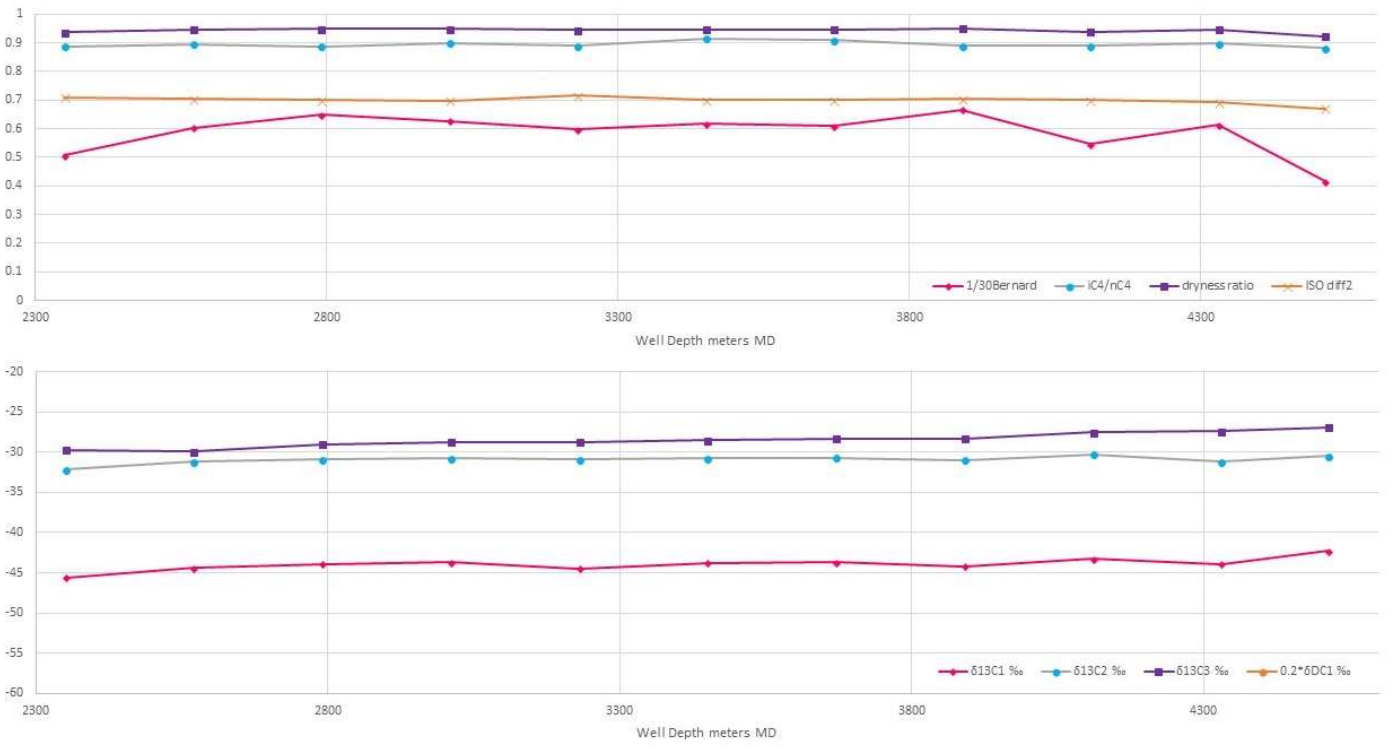

Figure A 10. Well profile, MC ratios and ISO data for WA#32521 (Montney HZ leg).

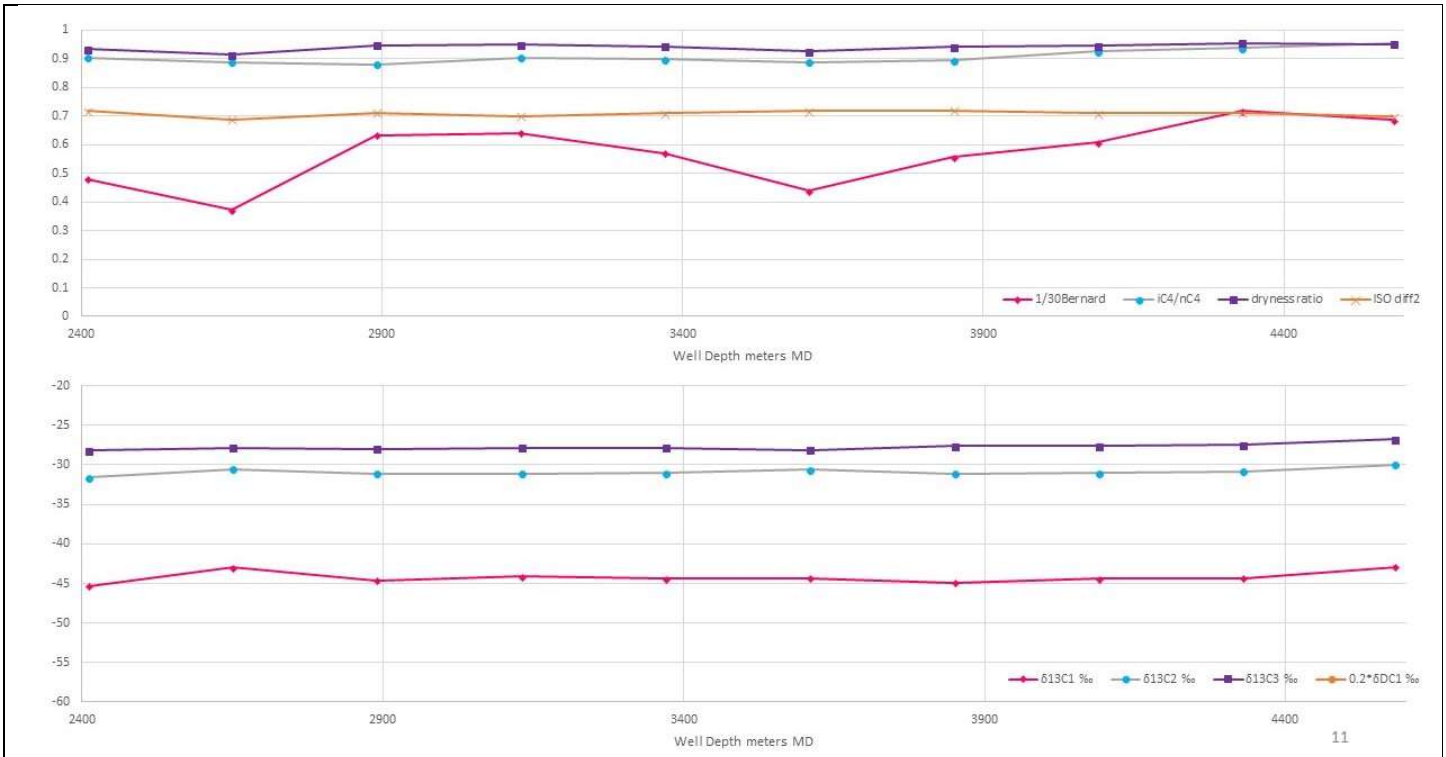

Figure A 11. Well profile, MC ratios and ISO data for WA#31522 (Montney HZ leg).

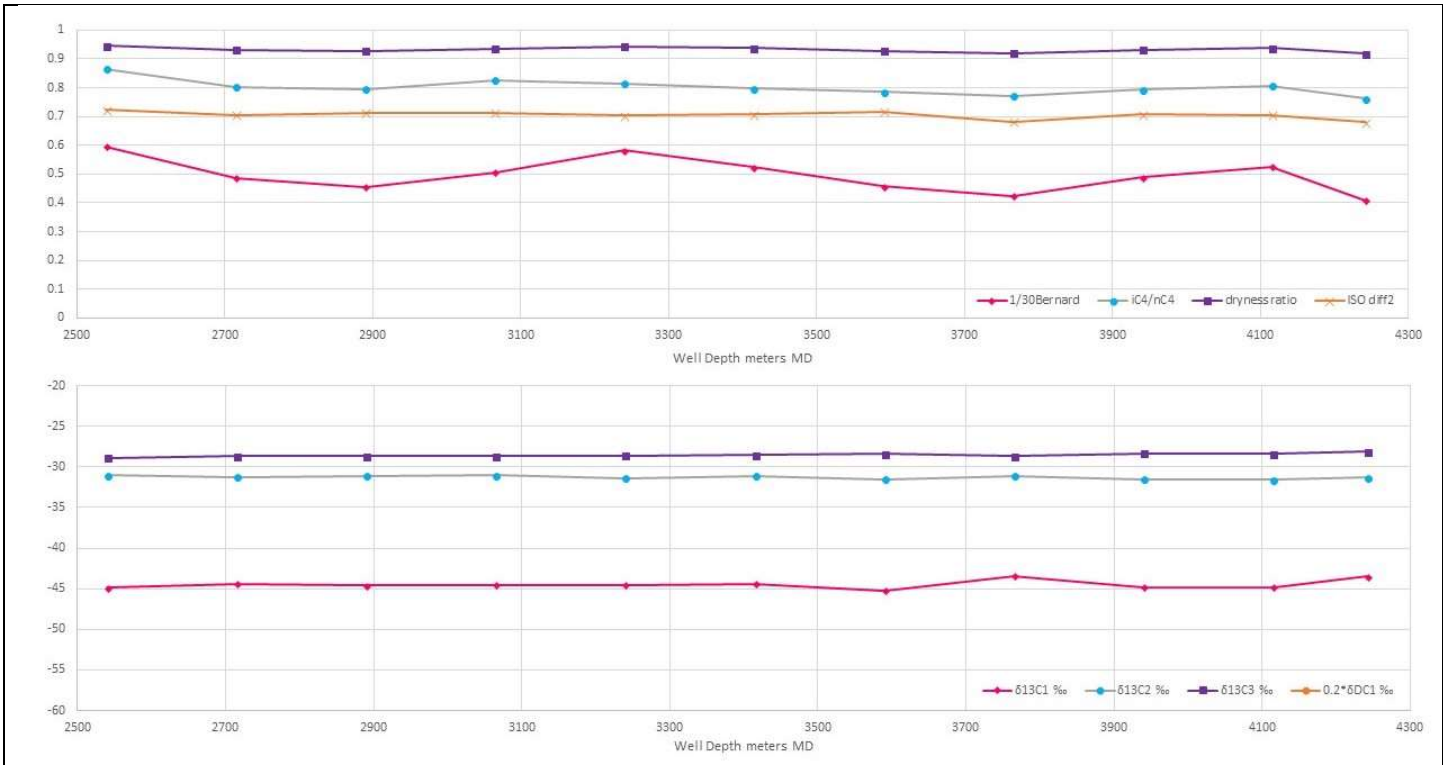

Figure A 12. Well profile, MC ratios and ISO data for WA#31101 (Montney HZ leg).

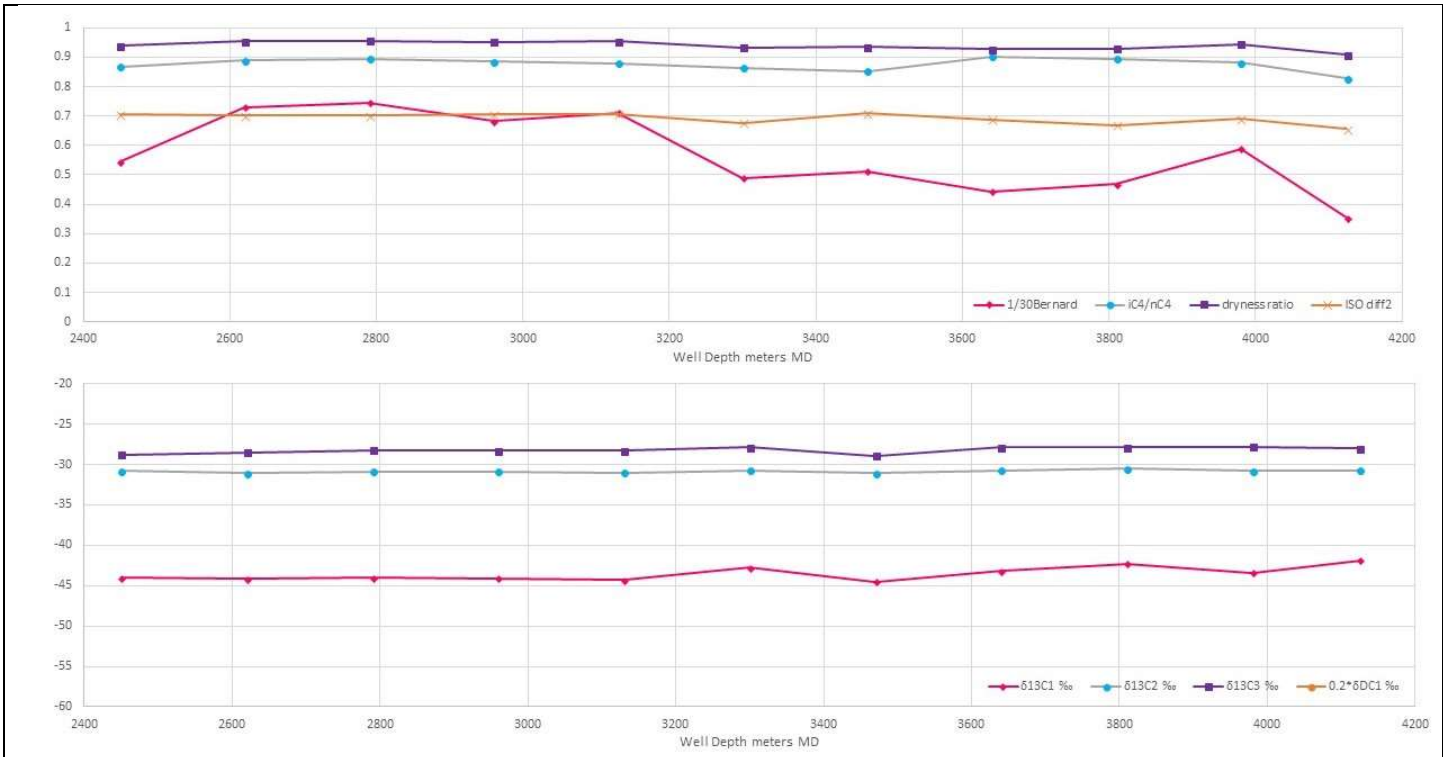

Figure A 13. Well profile, MC ratios and ISO data for WA#31102 (Montney HZ leg).

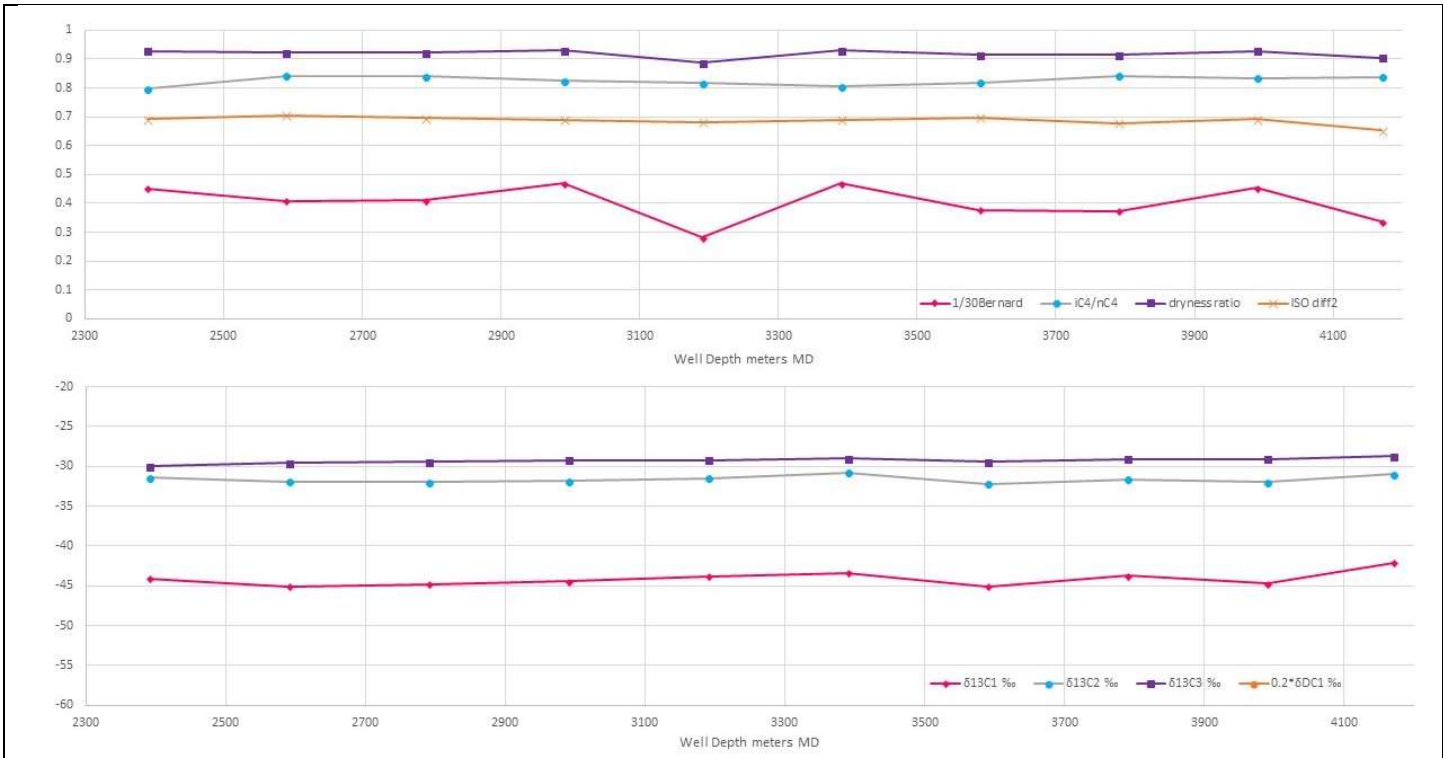

Figure A 14. Well profile, MC ratios and ISO data for WA#31103 (Montney HZ leg).

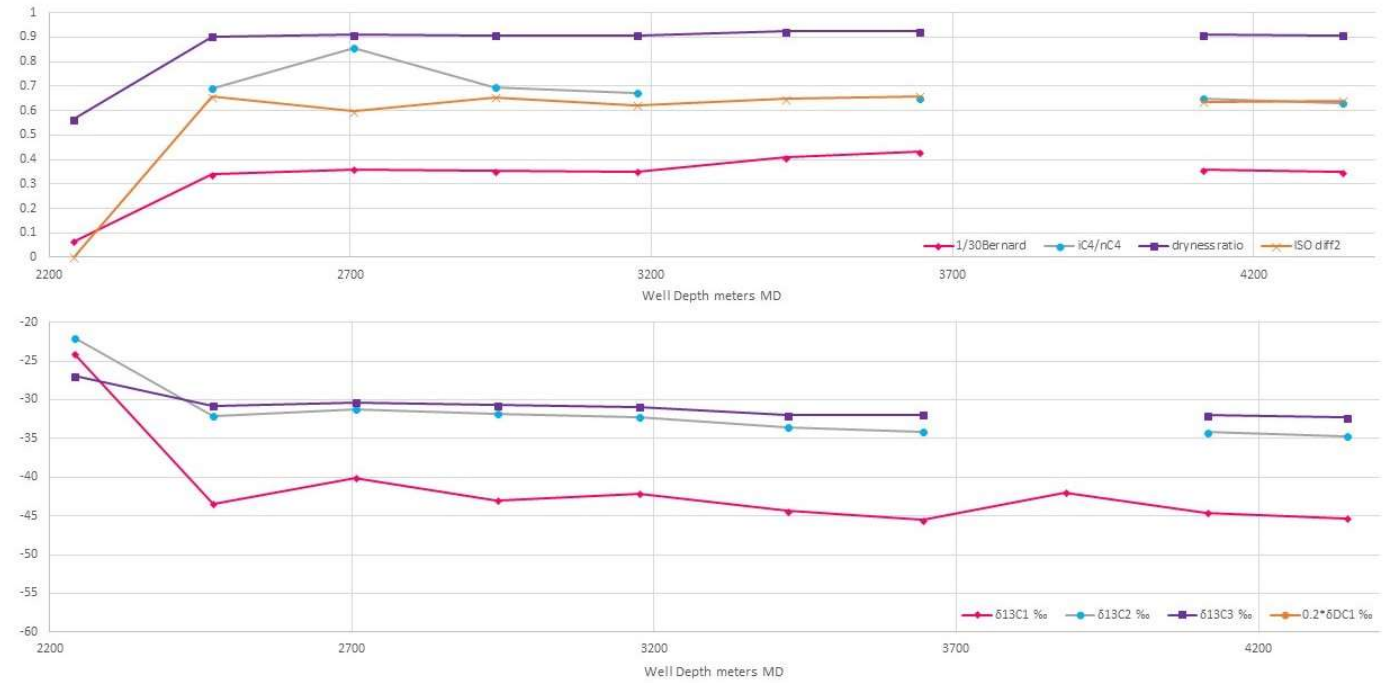

Figure A 15. Well profile, MC ratios and ISO data for WA#30792 (Montney HZ leg with uphole completion included in another formation that is difficult to determine. This upper sample is showing "isotope reversal").

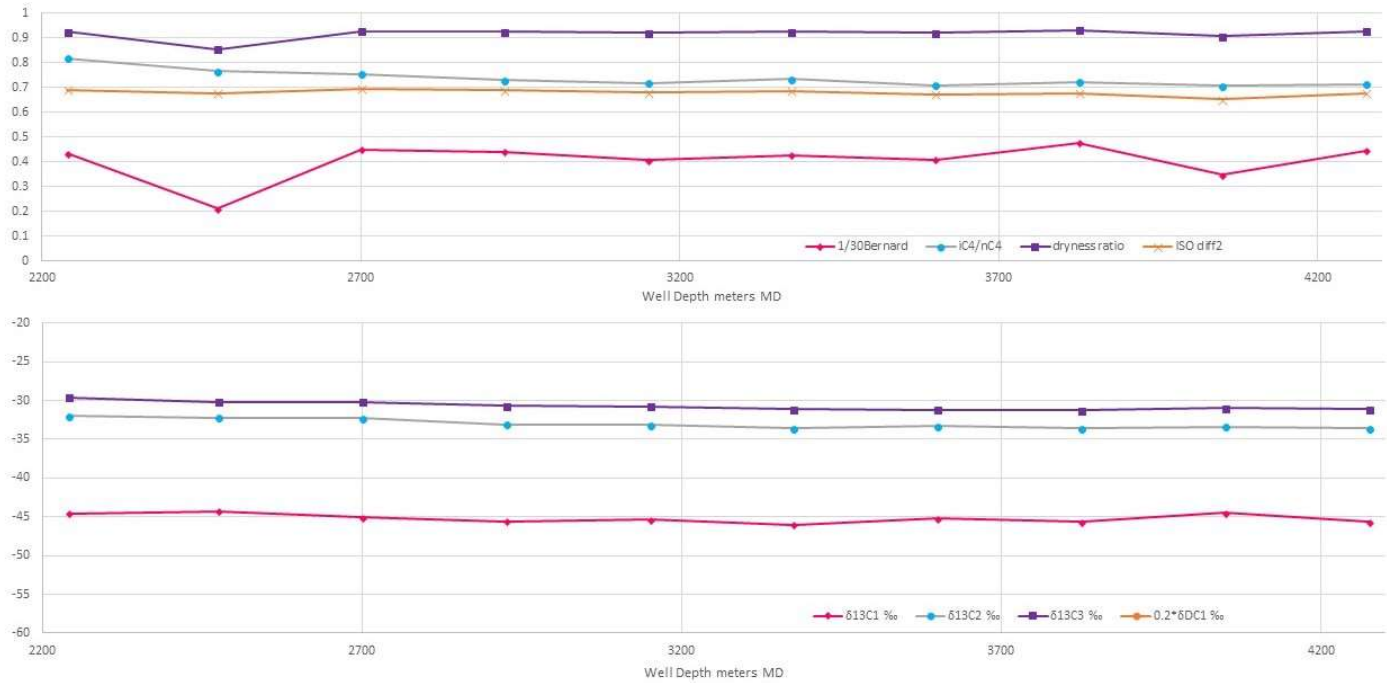

Figure A 16. Well profile, MC ratios and ISO data for WA#30791 (Montney HZ leg).

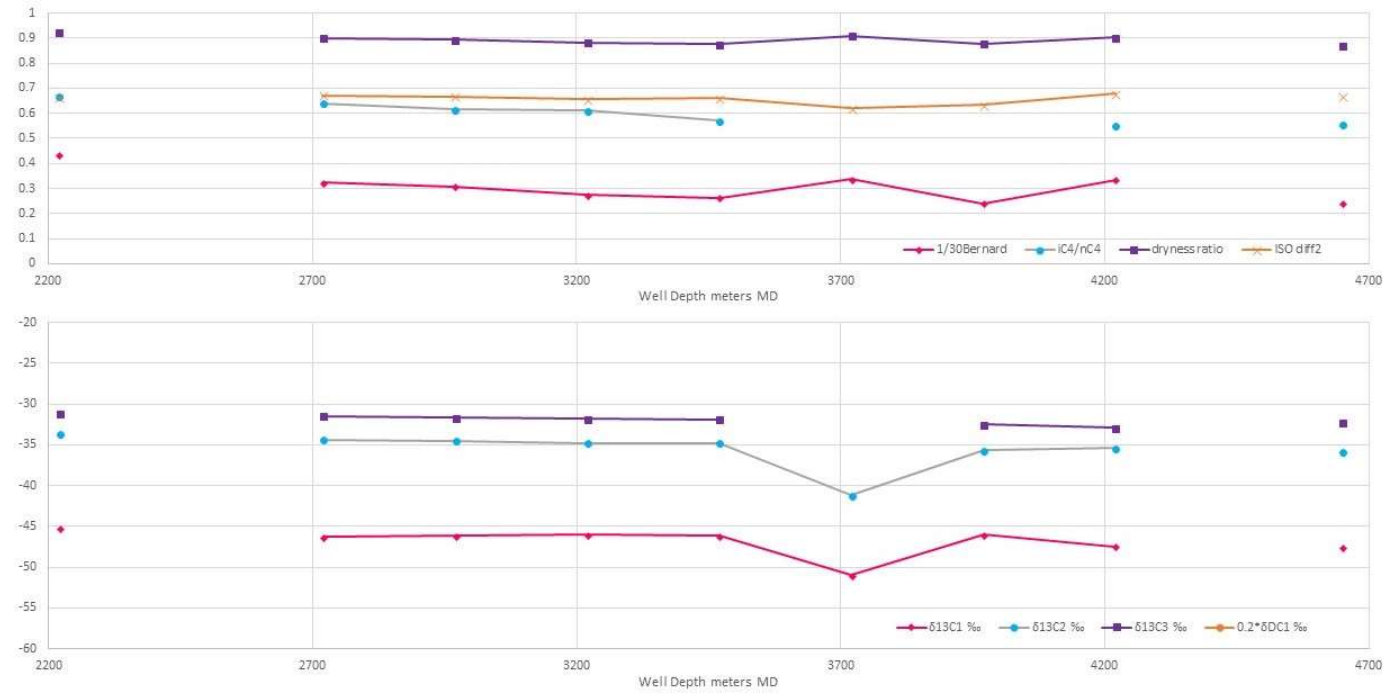

Figure A 17. Well profile, MC ratios and ISO data for WA#29568 (Montney HZ leg).

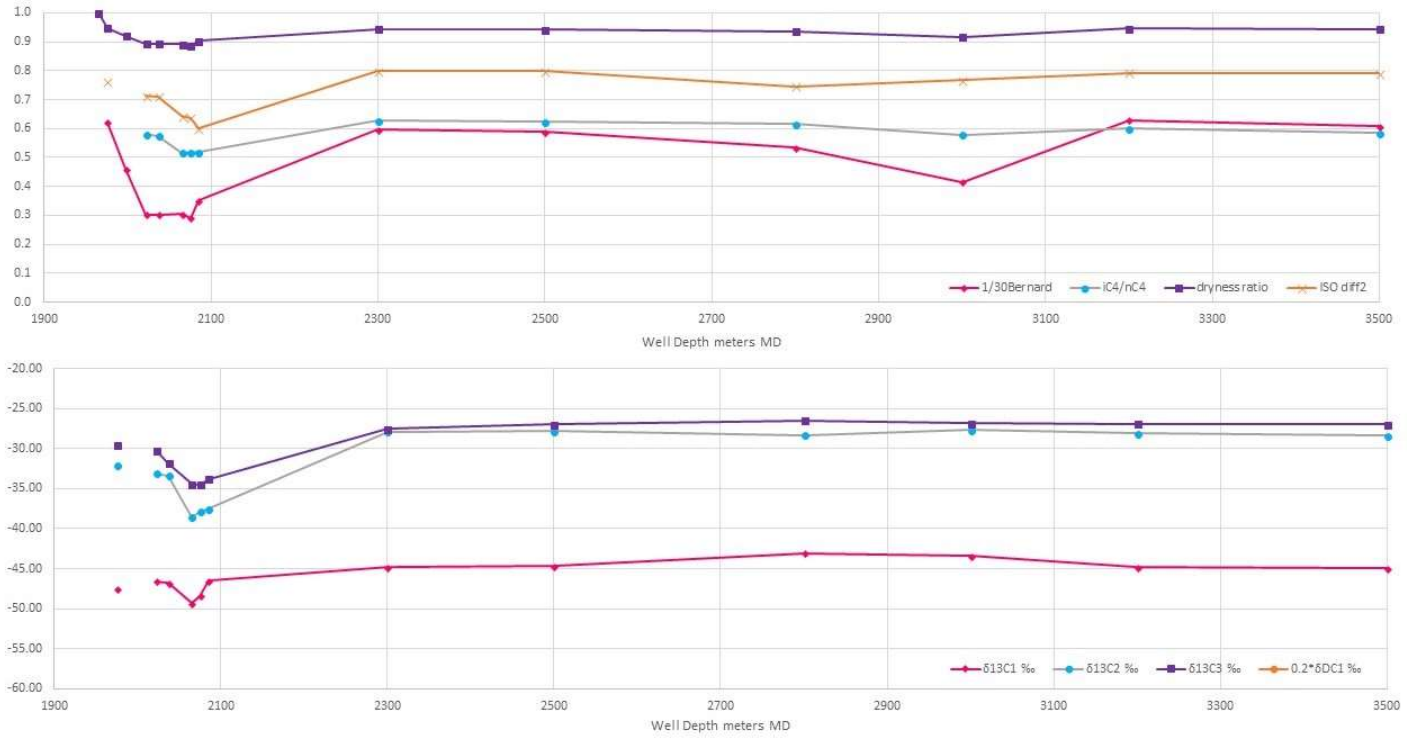

Figure A 18. Well profile, MC ratios and ISO data for WA#31699 (Montney HZ leg with uphole completion included as confirmed Doig for the first sample and the next few being Upper Montney and not the target Middle Montney).

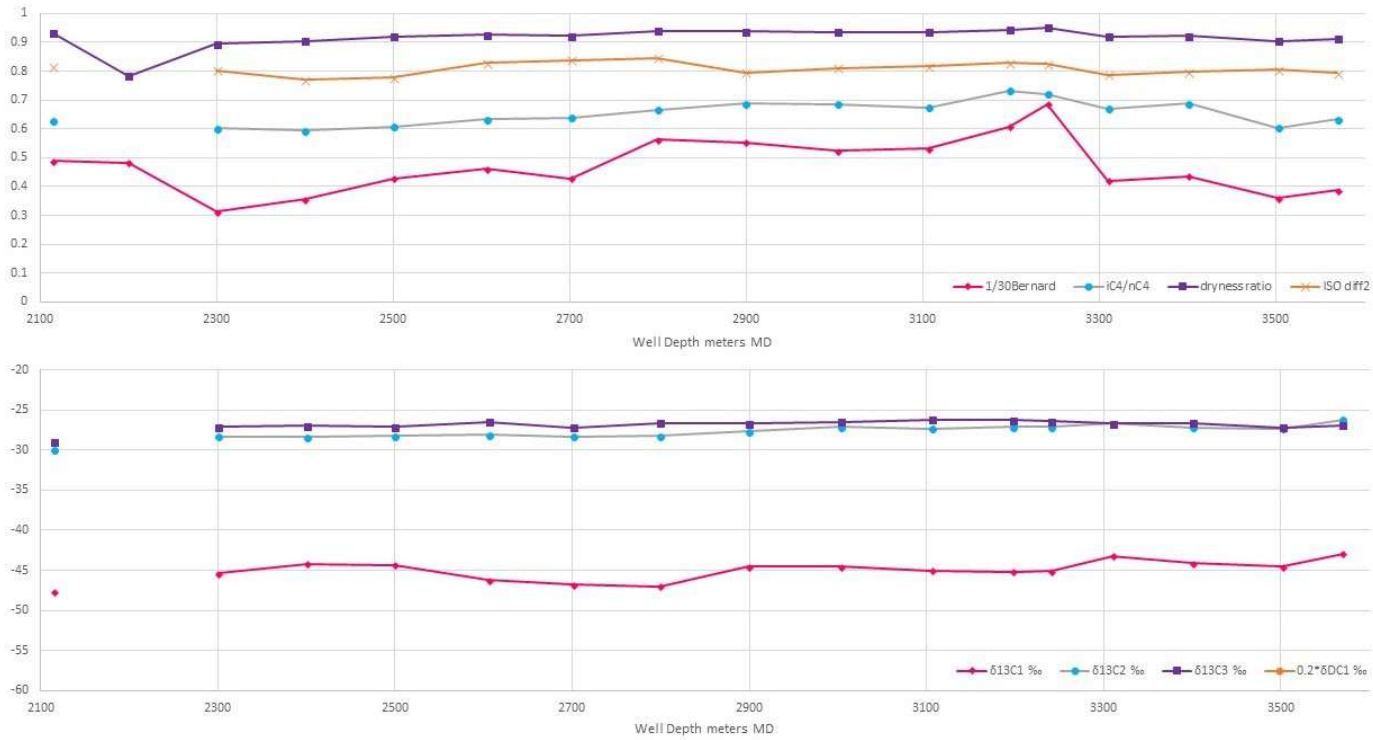

Figure A 19. Well profile, MC ratios and ISO data for WA#31640 (Montney HZ leg).

No DATA

Figure A 20. Well profile, MC ratios not shown with HZ<10 ISO data WA#31790.

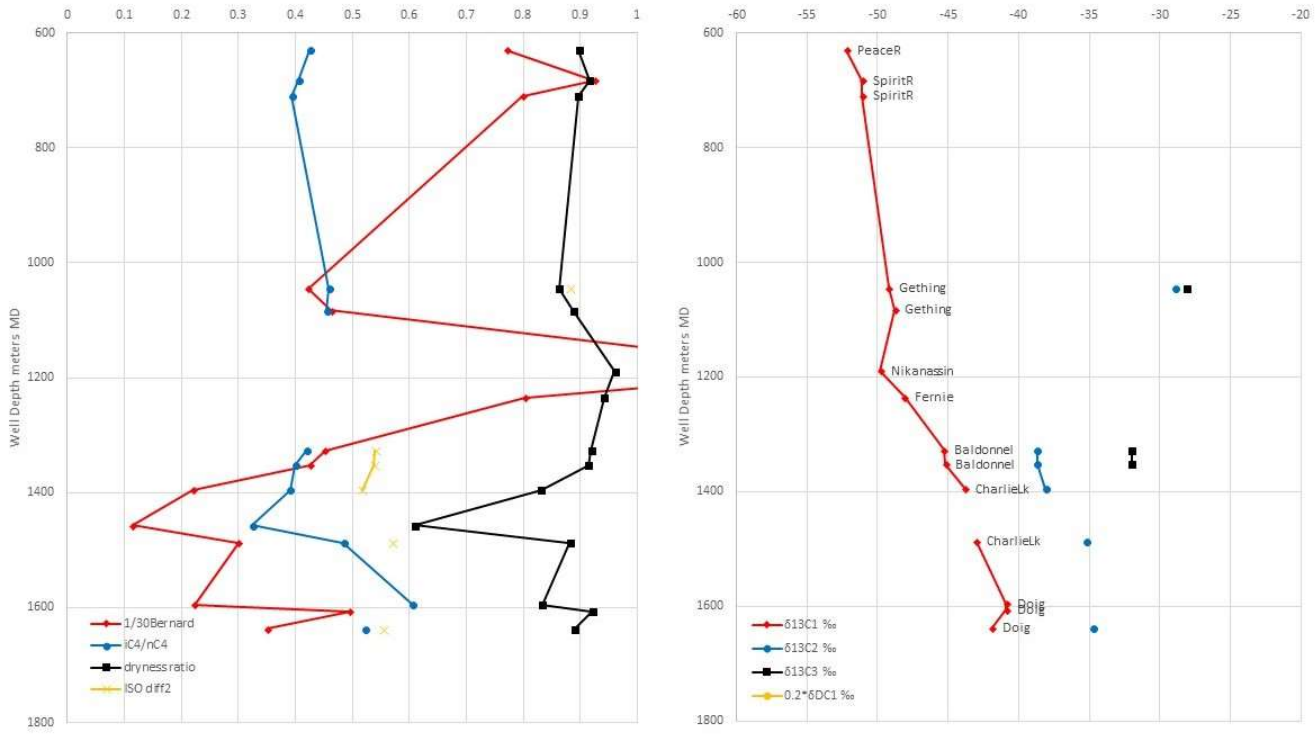

Figure A 21. Well profile, MC ratios and ISO data for WA#32032 (Upper Cretaceous to Triassic VT well. Nikanassin sample has Bernard ratio of 40 while the Fernie sample below it has Bernard ratio of 24).

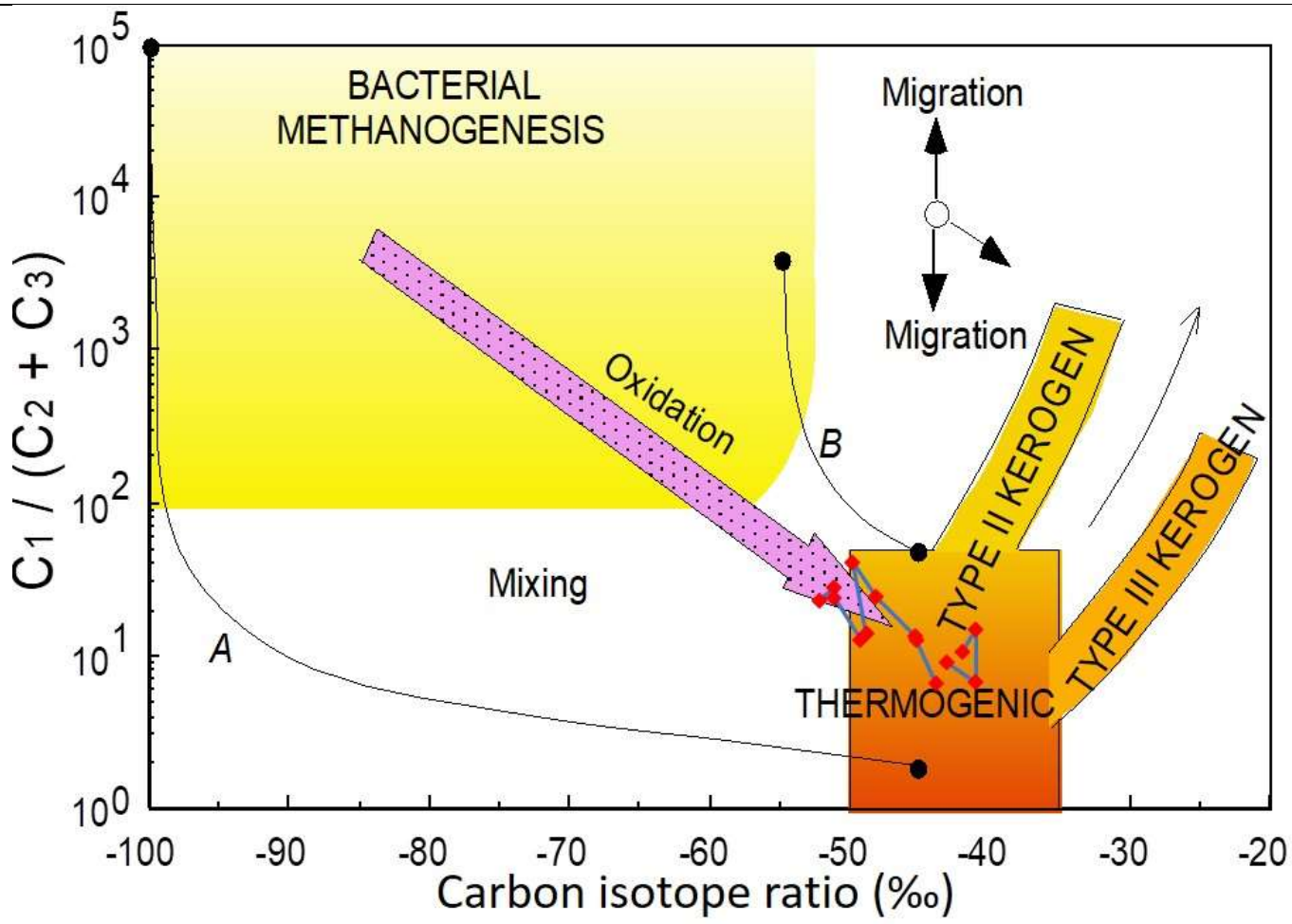

Figure A 22. ISO profile data – Interpretive Bernard Diagram for WA#32032 (Upper Cretaceous to Triassic VT well. Good potential with samples in some under-represented formations, but the ISO data is irregular, Whiticar, 2018 pers. comm., after Whiticar 1999).

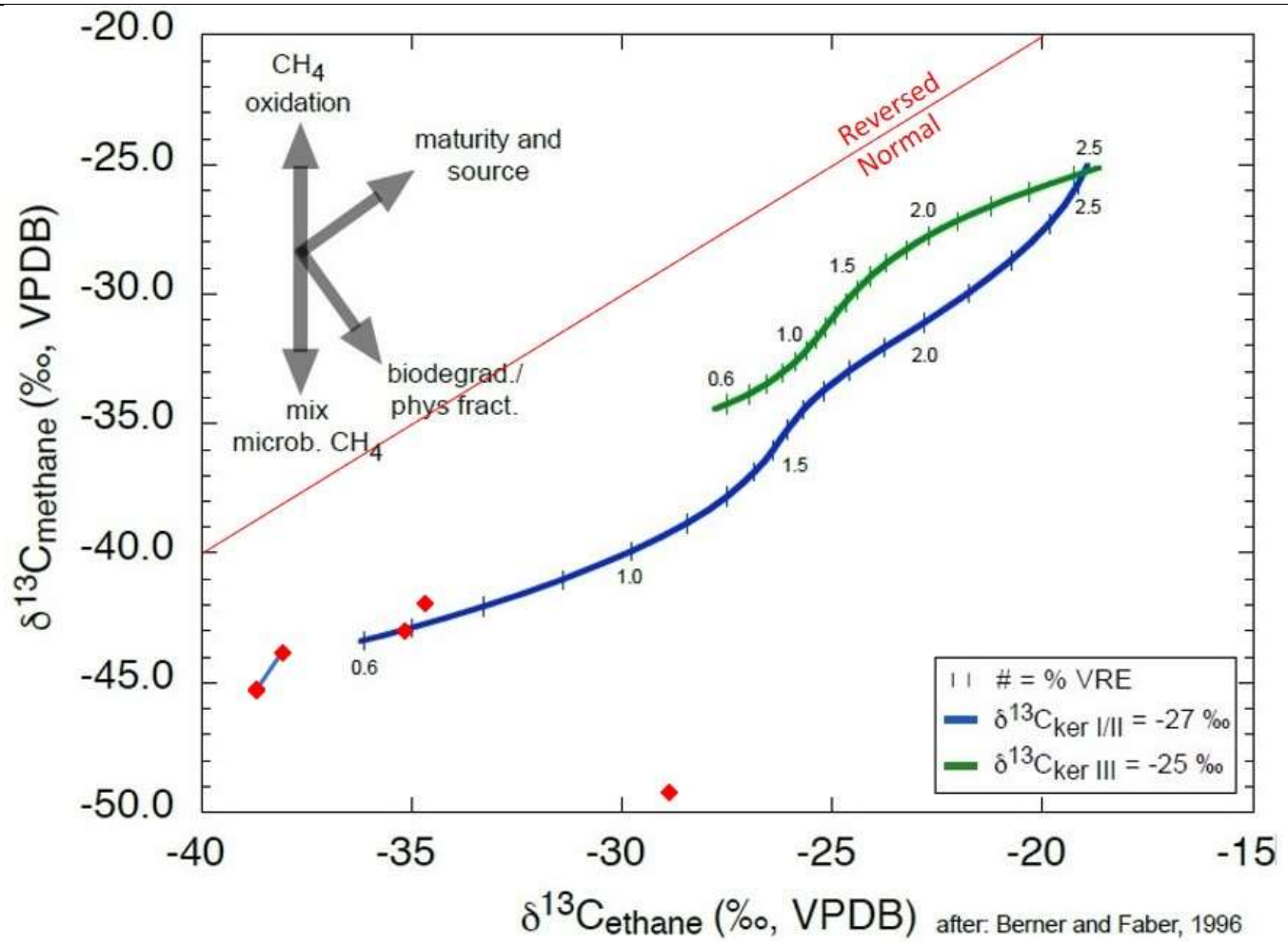

Figure A 23. ISO profile data – Interpretive ISO $\delta^{13}C_1$ versus $\delta^{13}C_2$ plot for WA#32032 (Upper Cretaceous to Triassic VT well. Baldonnel and Charlie Lake Formations are to the left and Gething Formation is near the bottom. This is one of two profiles with most methane responses along the Type II curve as other wells are $\delta^{13}C1$ depleted, Whiticar, 2018 pers. comm., after Berner and Faber 1996, limited data for C3, no trendlines).

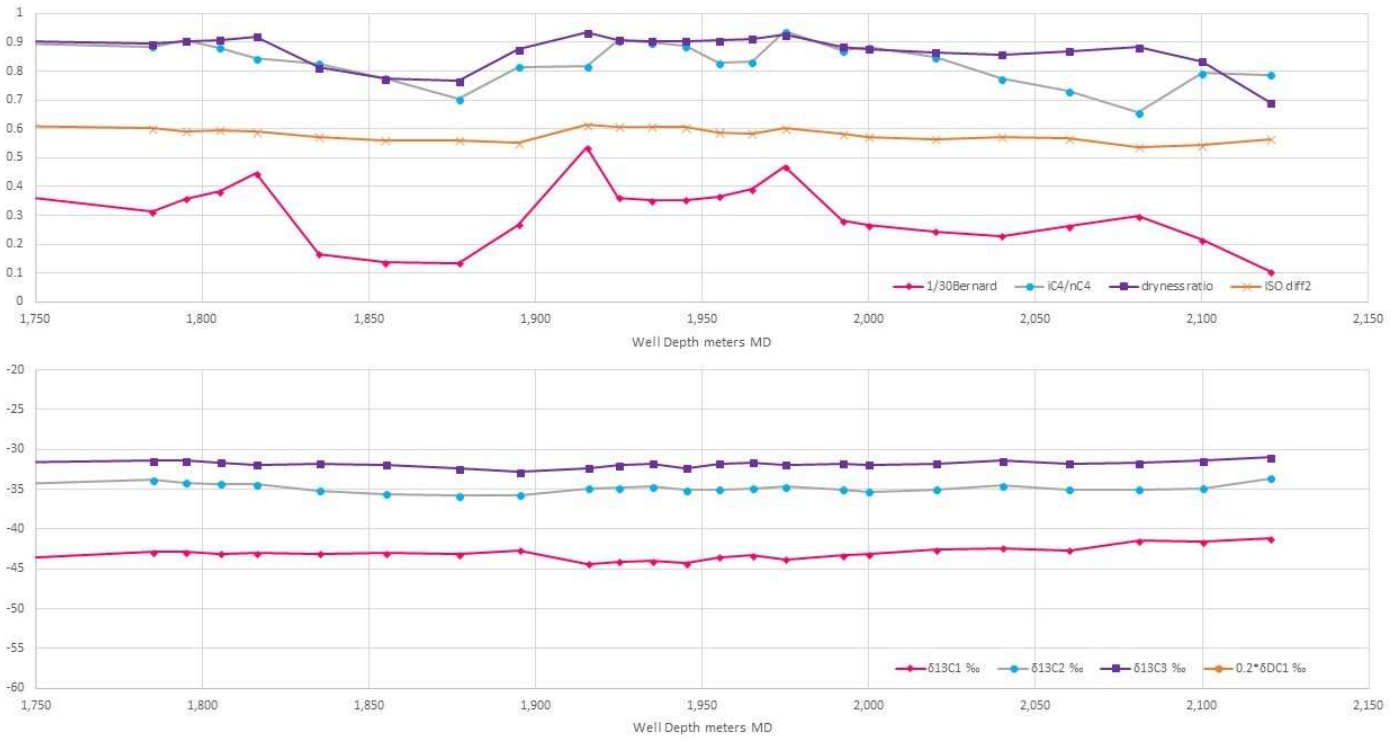

Figure A 24. Well profile, MC ratios and ISO data for WA#31977 (Montney HZ leg).

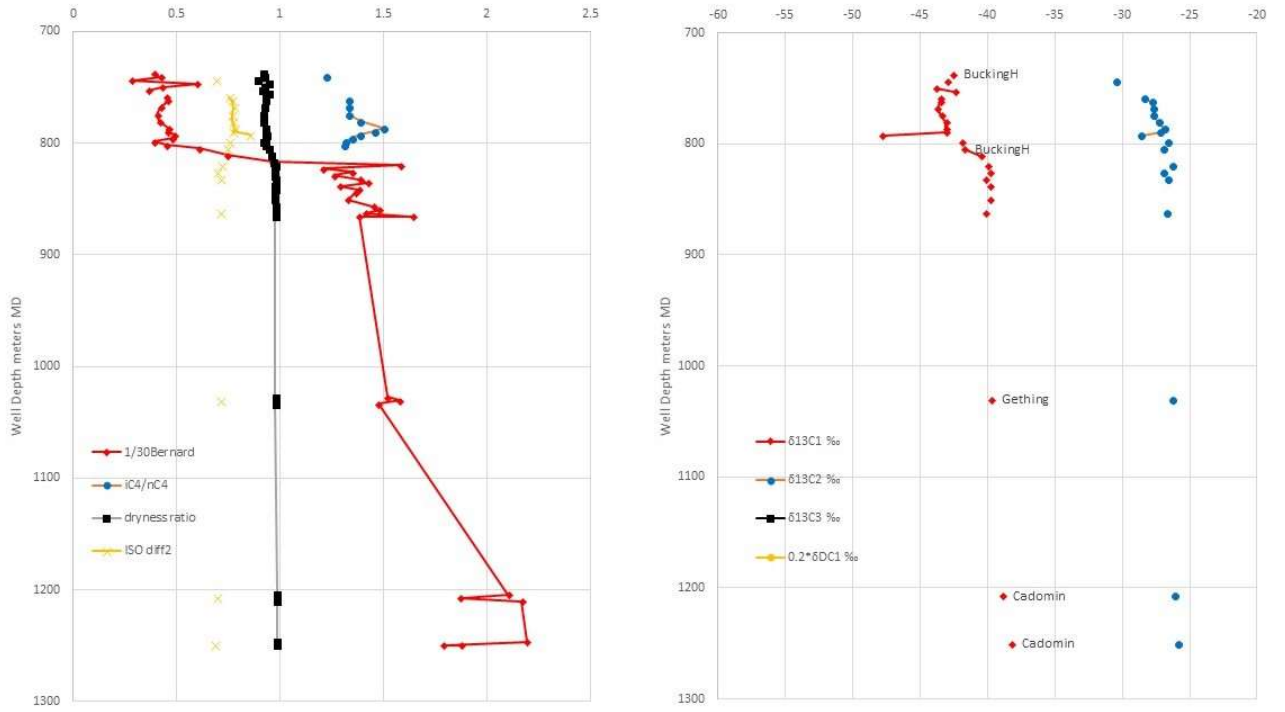

Figure A 25. Well profile, MC ratios and ISO data for WA#26657 (Upper Cretaceous to Triassic VT well. Sampling in detail from upper Buckinghorse Formation then skipped to single Gething and 2 Cadomin samples, but no analysis for $\delta^{13}C$ was completed. Note a different scale for the display of the Bernard ratio and deep gas is too dry to have iC4/nC4 ratios. Note $\delta^{13}C1$ extra low value at 792.48 depth).

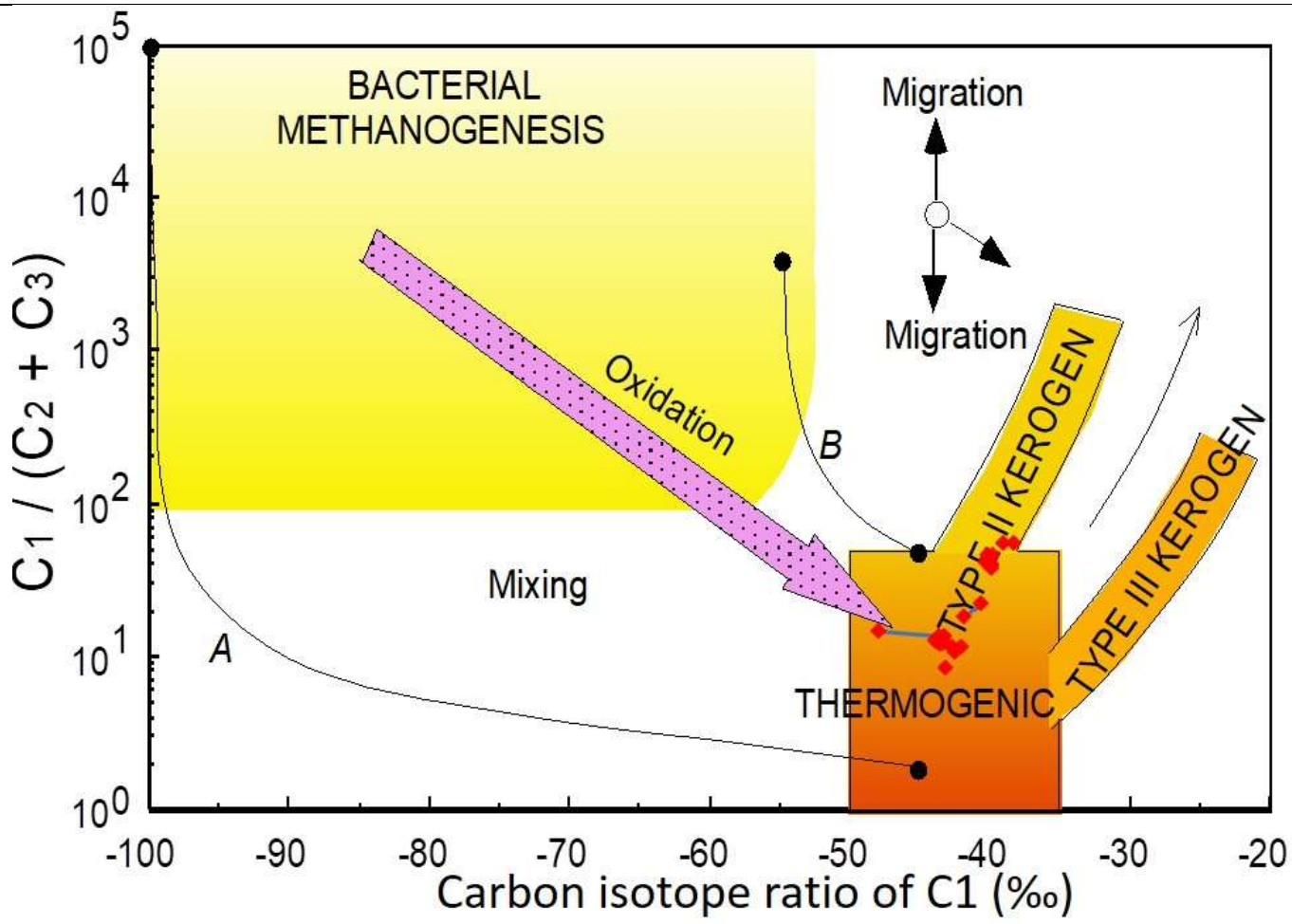

Figure A 26. ISO profile data – Interpretive Bernard Diagram for WA#26657 (Upper Cretaceous to Triassic VT well. Note a strong indication of thermogenic even at shallow depths, Whiticar, 2018 pers. comm., after Whiticar 1999).

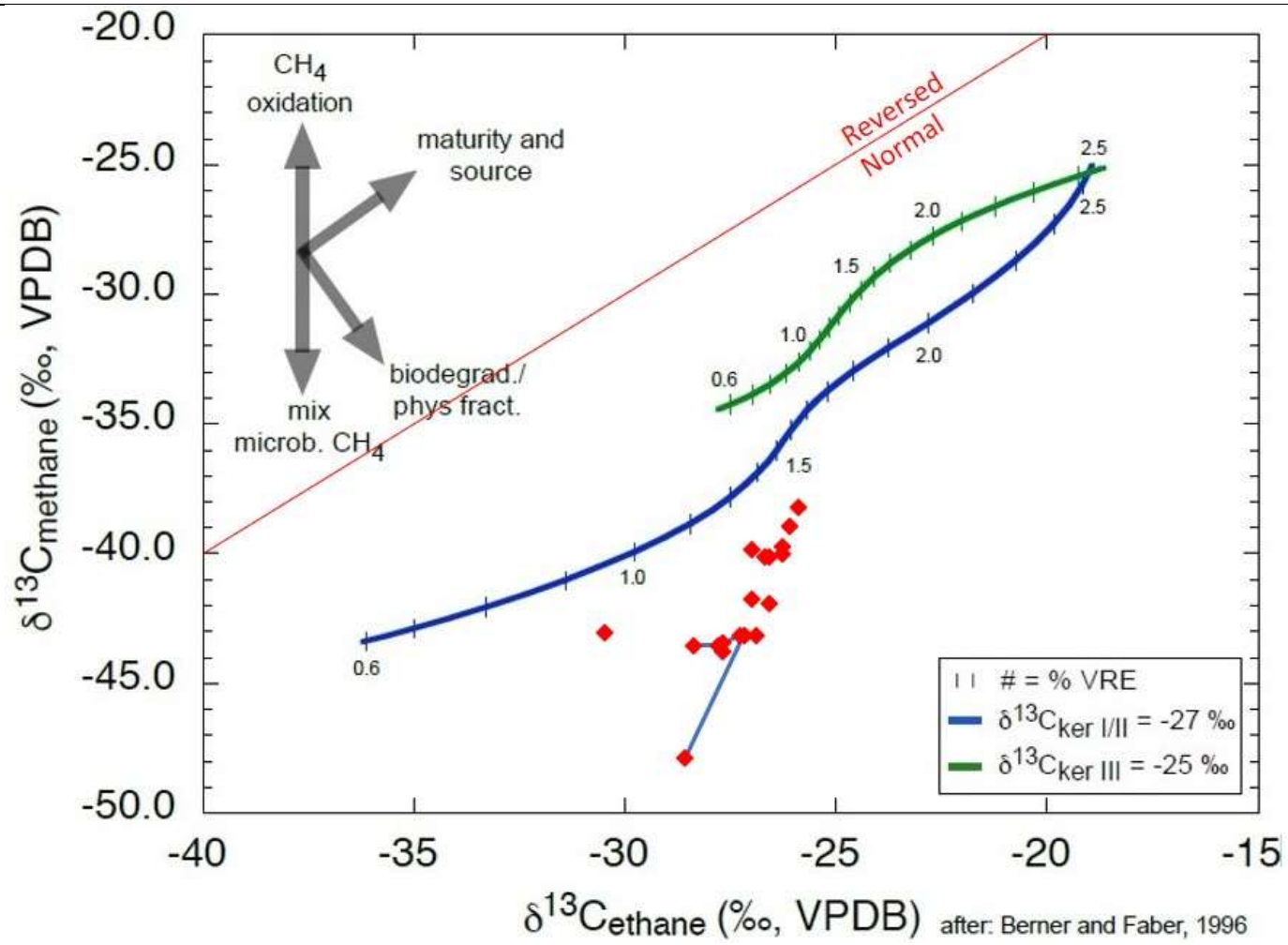

Figure A 27. ISO profile data – Interpretive ISO $\delta^{13}C_1$ versus $\delta^{13}C_2$ plot for WA#26657 (Upper Cretaceous to Triassic VT well. Note a strong indication of biodegradation with the sample at 800 m is at a steep angle to the Type II curve for methane. Is this a migration boundary at this depth inside the shallow shale formation? Whiticar, 2018 pers. comm., after Berner and Faber 1996, limited data for C3, no trendlines).

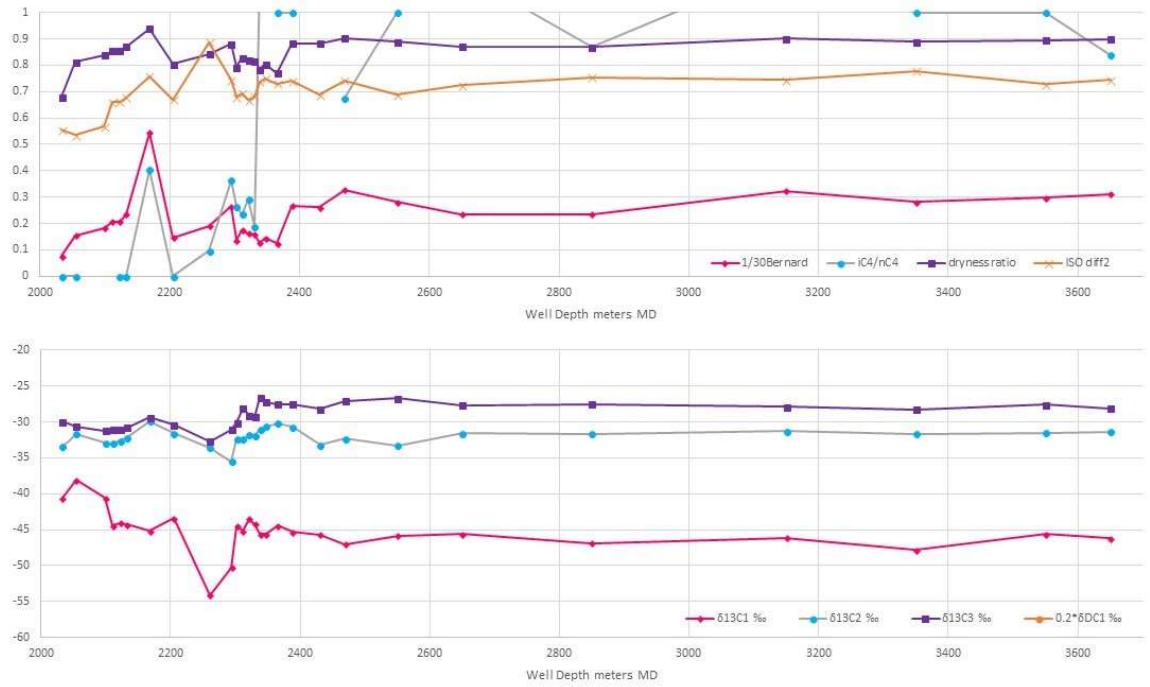

Figure A 28. Well profile, MC ratios and ISO data for WA#27404 (Montney HZ leg with uphole completion included for Charlie Lake, Halfway, Doig, Doig Phosphate, Upper Montney to approximately 2400 m).

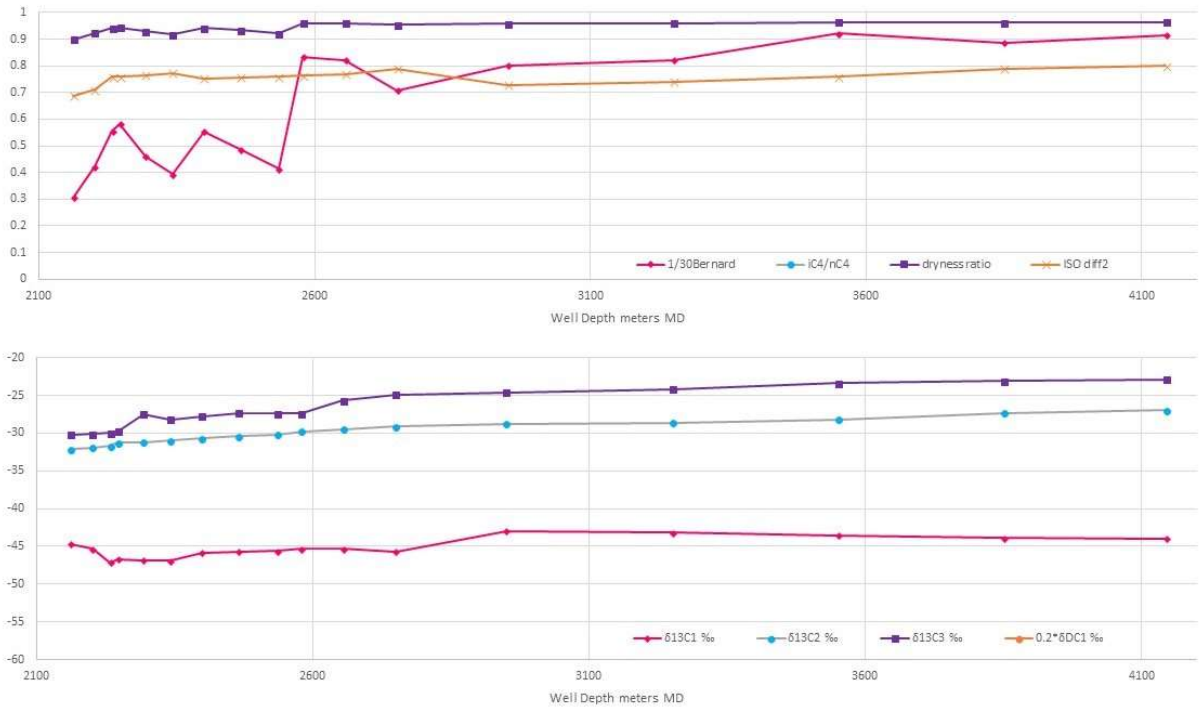

Figure A 29. Well profile, MC ratios and ISO data for WA#28002 (Montney HZ leg with uphole completion included for Charlie Lake, Halfway, Doig, Doig Phosphate, Upper Montney to approximately 2500 m).

No DATA

Figure A 30. Well profile, MC ratios not shown with null ISO data WA#25587.

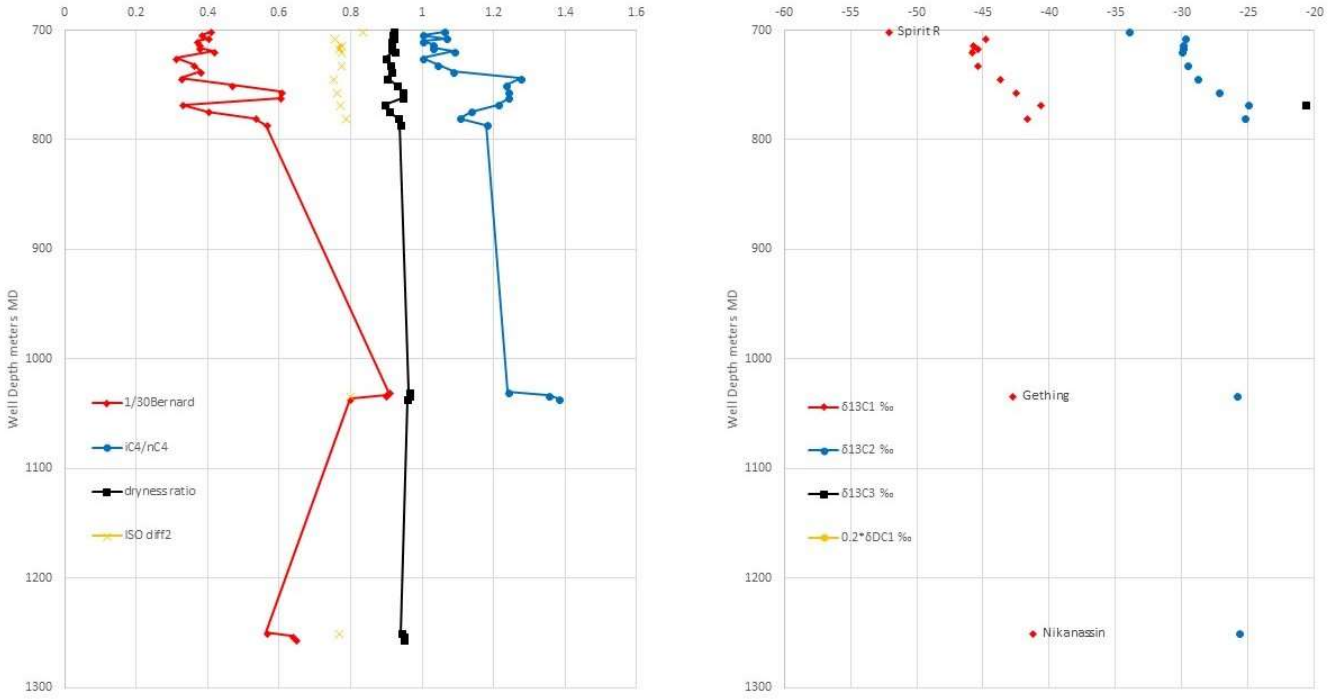

Figure A 31. Well profile, MC ratios and ISO data for WA#26949 (Upper Cretaceous to Triassic VT well. Another well with detailed sampling in the shallower section followed by a skip to one Gething sample and one Nikanassin sample. Note a different scale for the display of the iC4/nC4 is a bit unusual and shift to $\delta^{13}C1$ low value at 701.04 depth.).

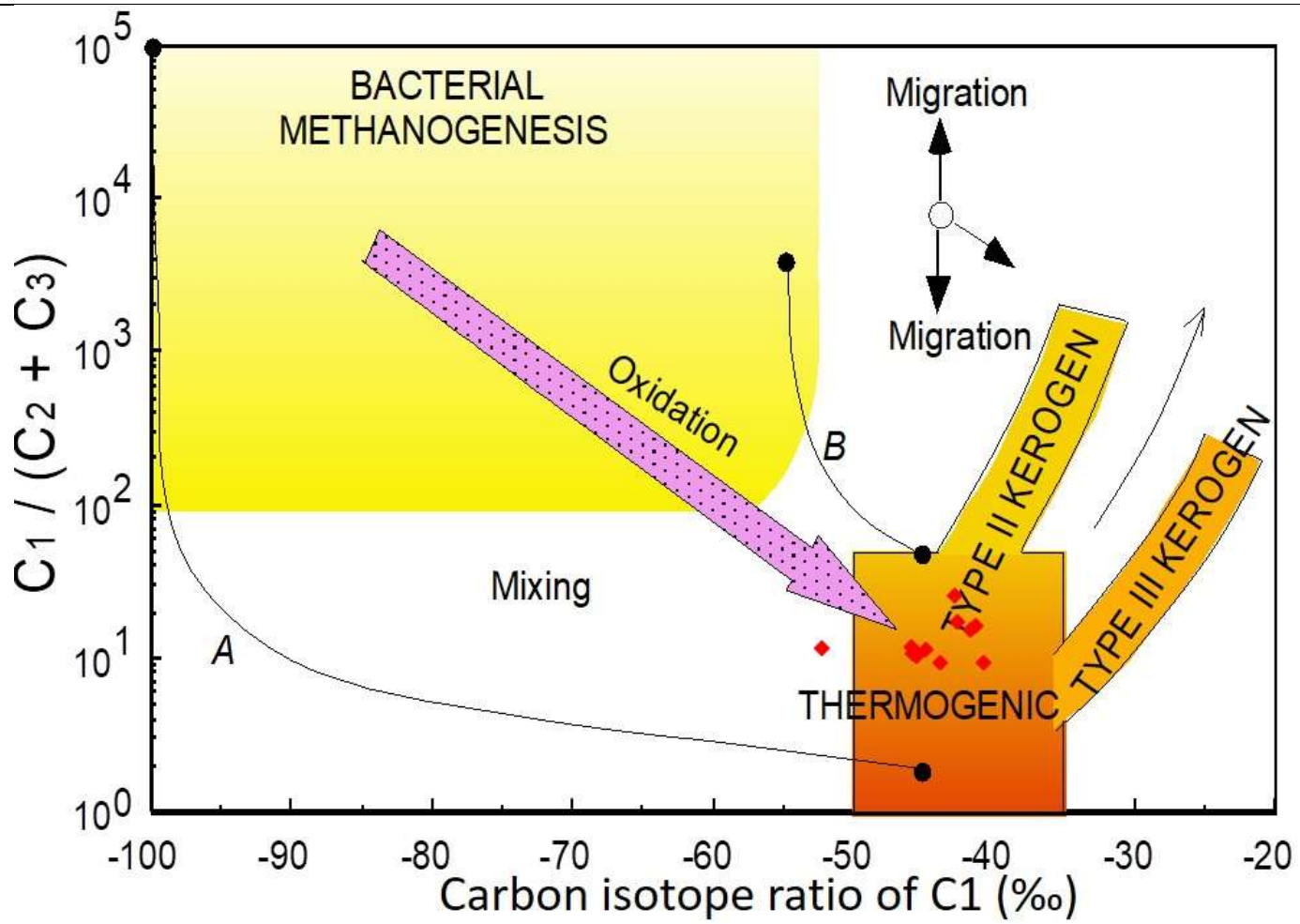

Figure A 32. ISO profile data – Interpretive Bernard Diagram for WA#26949 (Upper Cretaceous to Triassic VT well. Note a strong thermogenic indication even at shallow depths, Whiticar, 2018 pers. comm., after Whiticar 1999).

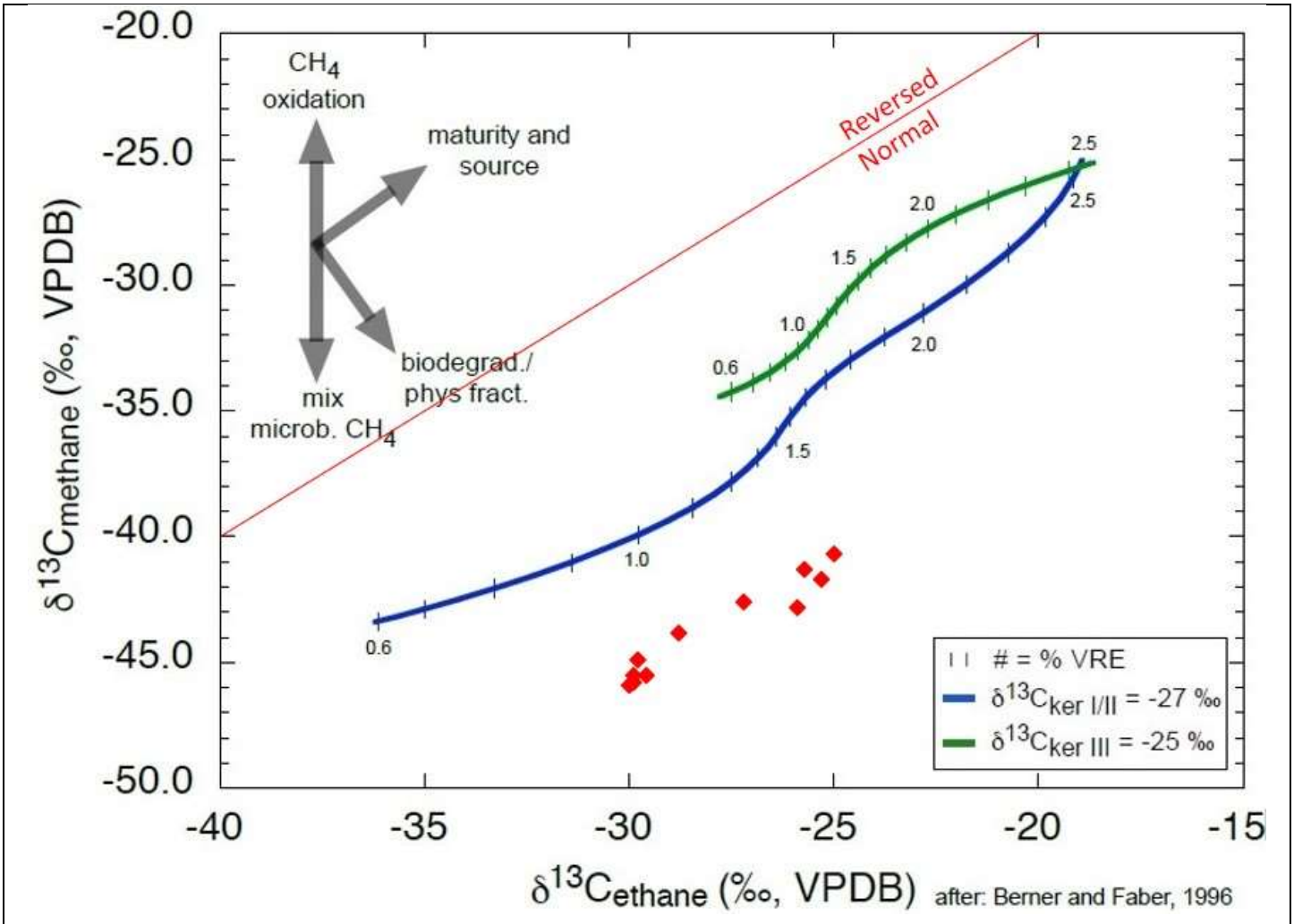

Figure A 33. ISO profile data – Interpretive ISO $\delta^{13}C_1$ versus $\delta^{13}C_2$ plot for WA#26949 (Upper Cretaceous to Triassic VT well. Note a strong indication of biodegradation, but at a parallel angle to the Type II curve for methane, Whiticar, 2018 pers. comm., after Berner and Faber 1996, no trendlines).

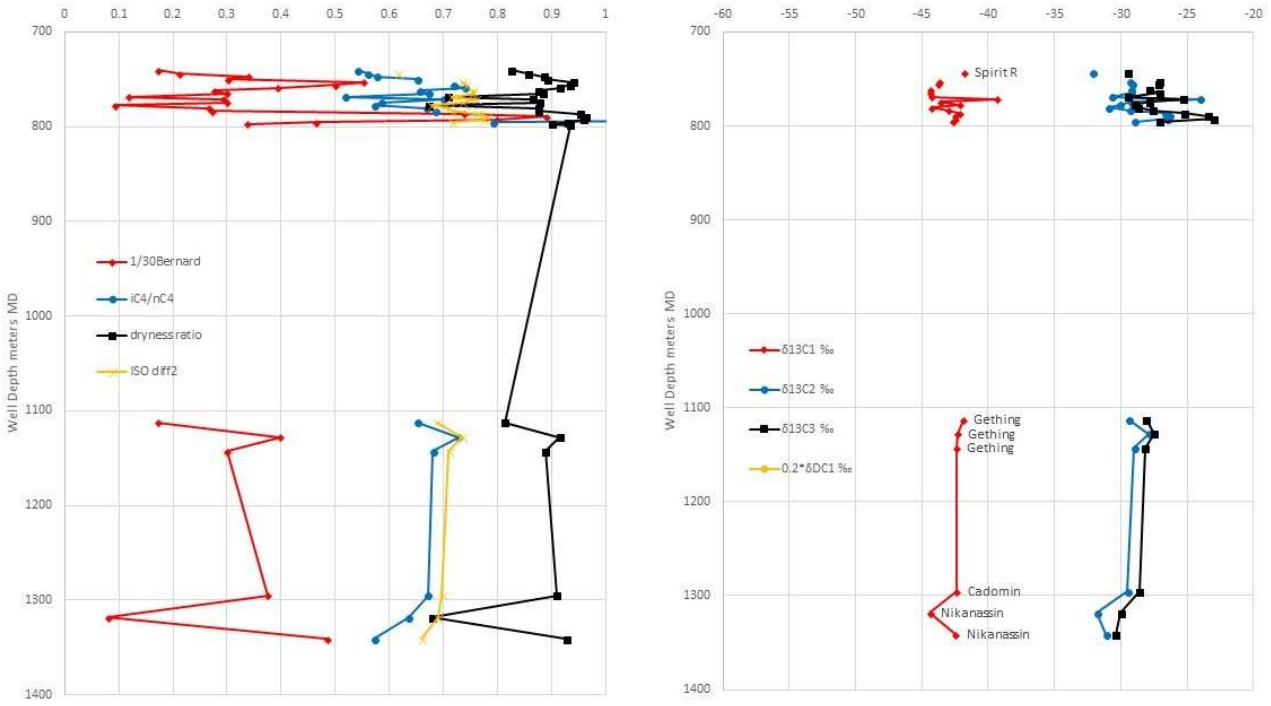

Figure A 34. Well profile, MC ratios and ISO data for WA#26918 (Upper Cretaceous to Triassic VT well. Another well with detailed sampling in the shallower section followed by a skip to a few Gething / Cadomin / Nikanassin samples. Note a different scale for the display is not needed and shift to $\delta^{13}C1$ high value is at 771m depth).

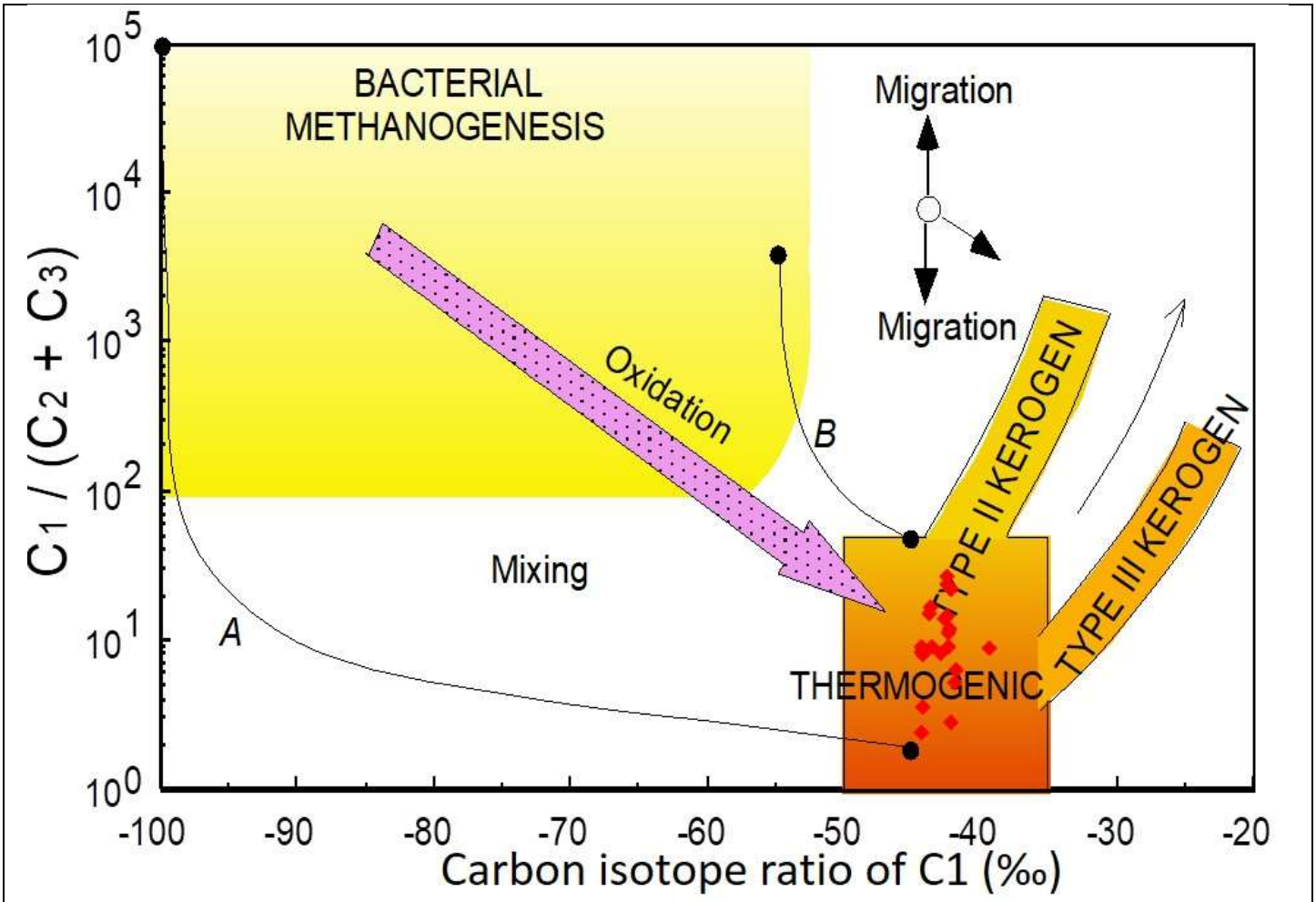

Figure A 35. ISO profile data – Interpretive Bernard Diagram for WA#26918 (Upper Cretaceous to Triassic VT well. Note more thermogenic indication even at shallow depths, Whiticar, 2018 pers. comm., after Whiticar 1999).

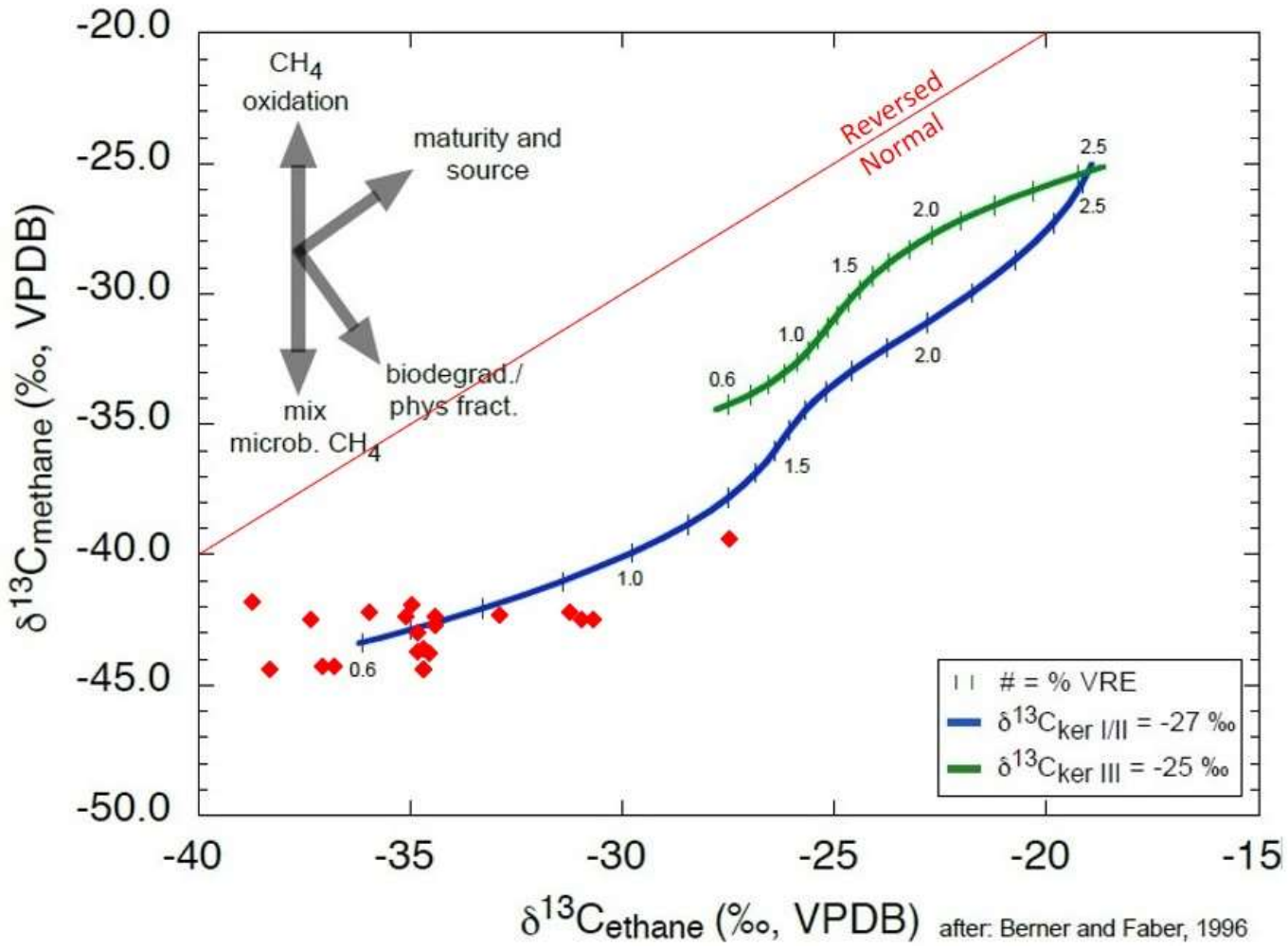

Figure A 36. ISO profile data – Interpretive ISO $\delta^{13}C_1$ versus $\delta^{13}C_2$ plot for WA#26918 (Upper Cretaceous to Triassic VT well. The data is on the Type II curve for methane, but not in depth order as 771 m depth is higher maturity than the others, Whiticar, 2018 pers. comm., after Berner and Faber 1996, no trendlines, no trendlines).

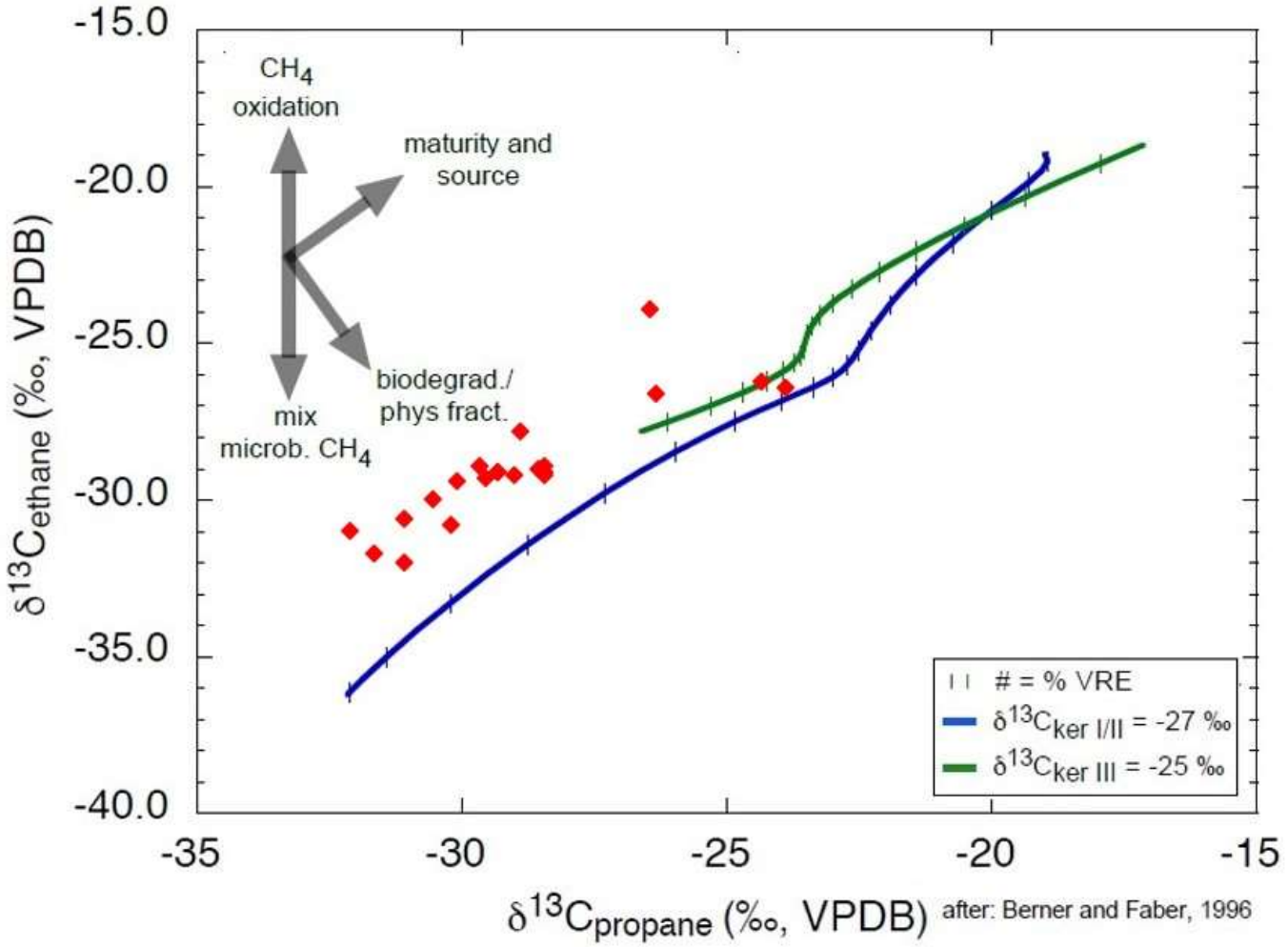

Figure A 37. ISO profile data – Interpretive ISO $\delta^{13}C_2$ versus $\delta^{13}C_3$ plot for WA#26918 (Upper Cretaceous to Triassic VT well. This is the first well from the south that has $\delta^{13}C_{2/3}$ data and it fits to Type II kerogen but apparently at a different maturity, Whiticar, 2018 pers. comm., after Berner and Faber 1996, no trendlines, no trendlines).

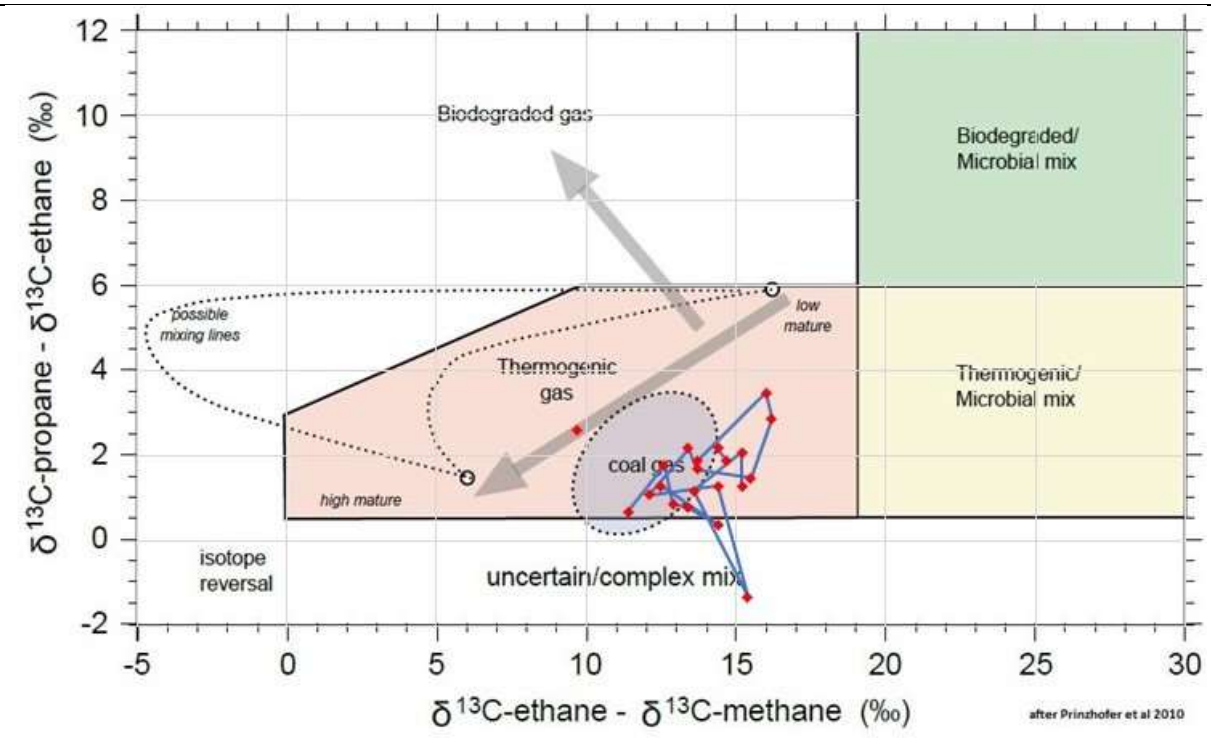

Figure A 38. Interpretive $\delta^{13}C_2$- $\delta^{13}C_1$ versus $\delta^{13}C_3$- $\delta^{13}C_2$ plot for WA#26918 (Upper Cretaceous to Triassic VT well. All depths except one at 768m depth fit on the biogenic side of "coal gas" with the shallow high methane value showing inversion between propane and ethane).

No DATA

Figure A 39. Well profile, MC ratios not shown with null ISO data WA#26660.

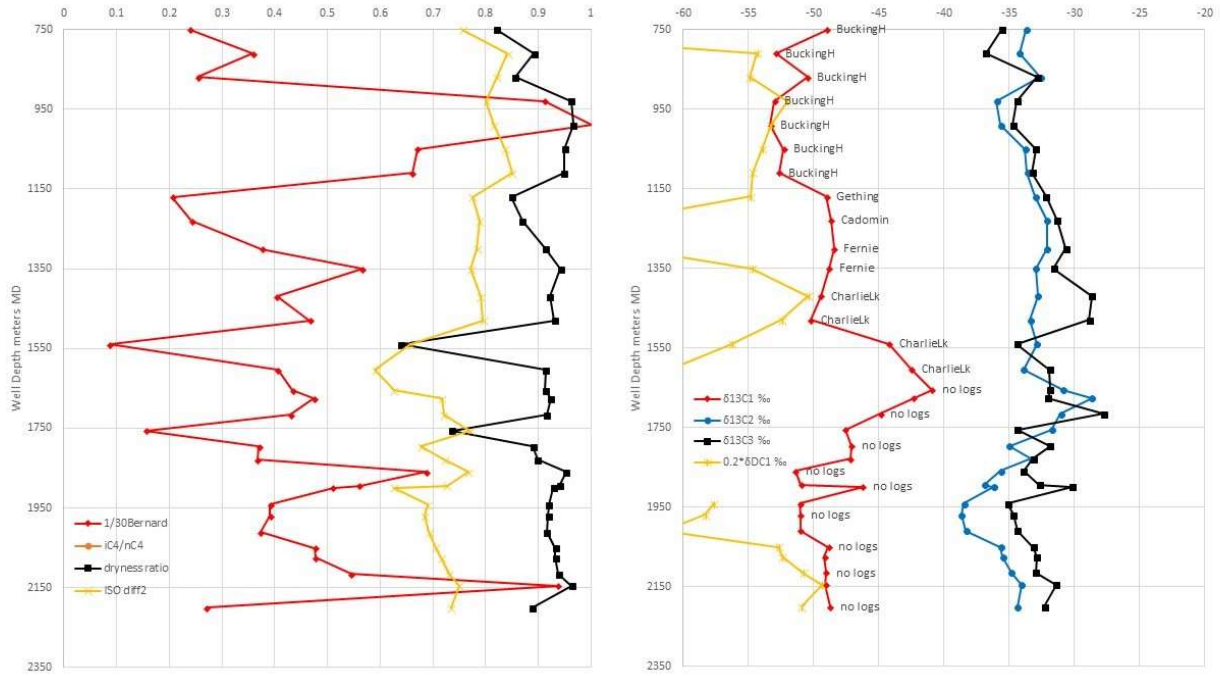

Figure A 40. Well profile, MC ratios and ISO data for WA#32990 (Upper Cretaceous to Triassic VT well. iC_4/nC_4 plots off the chart with ranges from $34x10^6$ to $840x10^6$ [there were no geophysical well logs available for the stratigraphy at deeper horizons, but total depth was just below the Montney]).

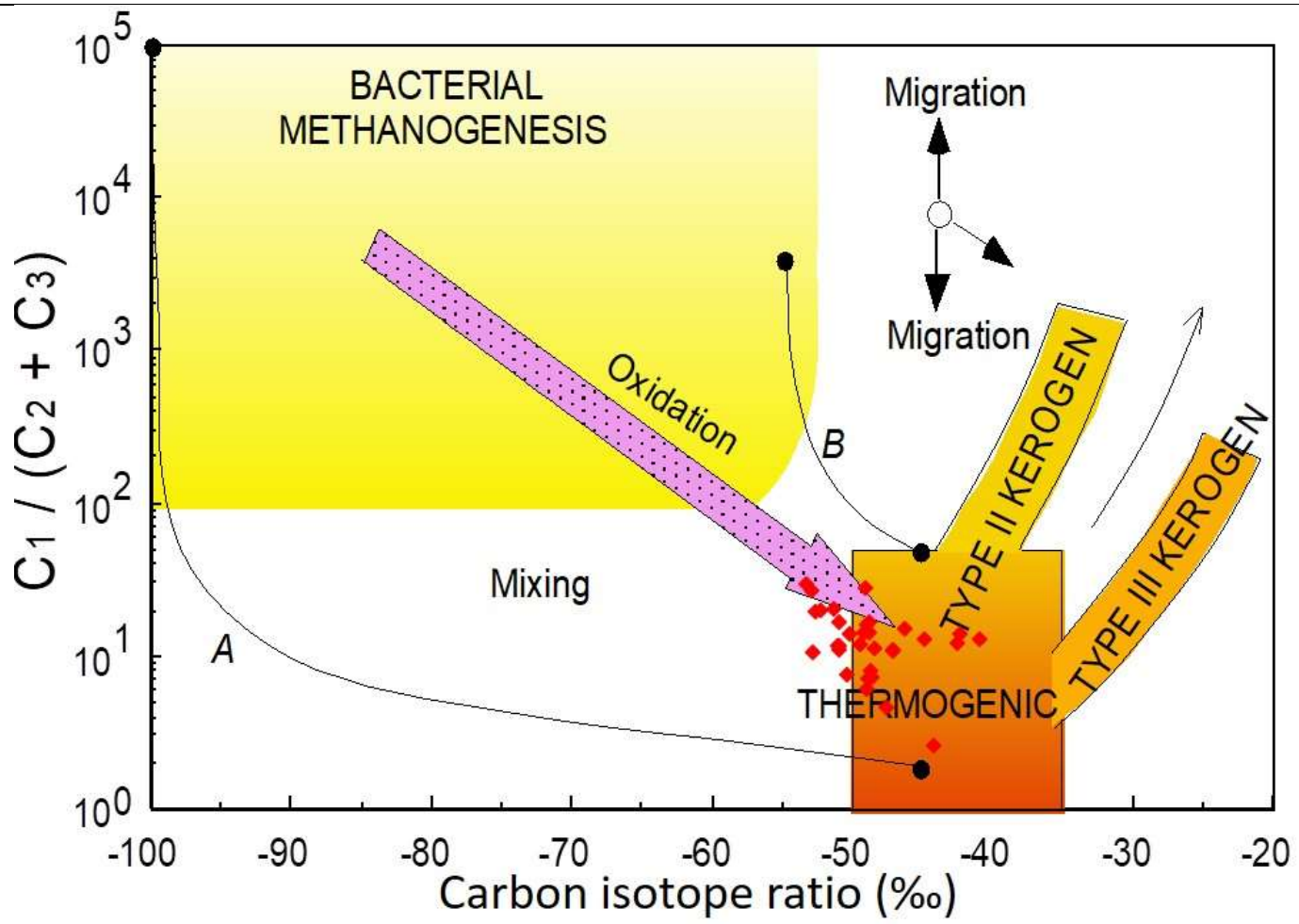

Figure A 41. ISO profile data – Interpretive Bernard Diagram for WA#32990 (Upper Cretaceous to Triassic VT well. This is the most recent mudgas samples in the BC-NGA program and showing consistent depth intervals. There is a clear transition from the shallowest sample being more microbial to more thermogenic but confused at depth, Whiticar, 2018 pers. comm., after Whiticar 1999).

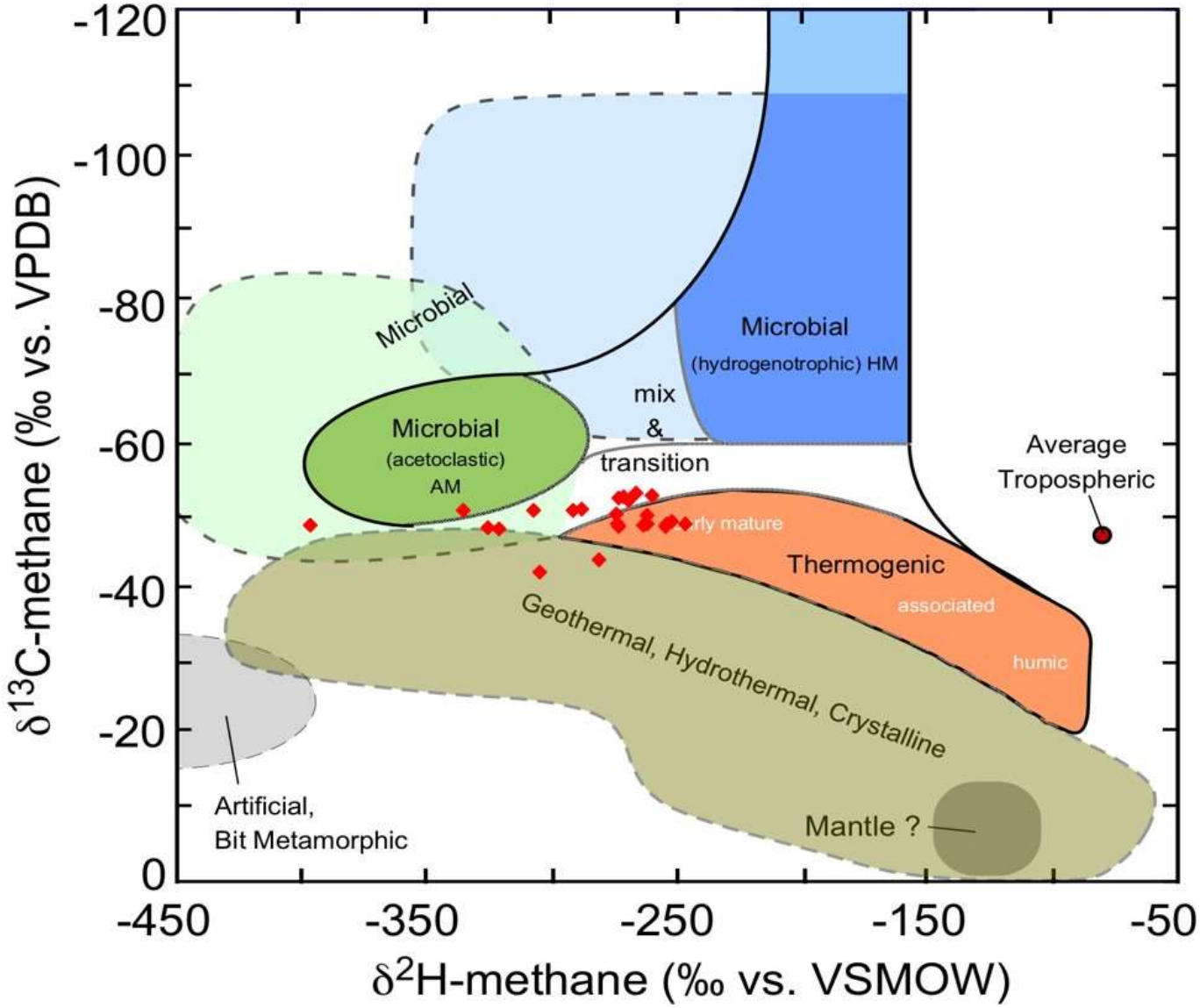

Figure A 42. ISO profile data – Interpretive CD Diagram for WA#32990 (Upper Cretaceous to Triassic VT well, Whiticar, 2018 pers. comm., after Whiticar 1999).

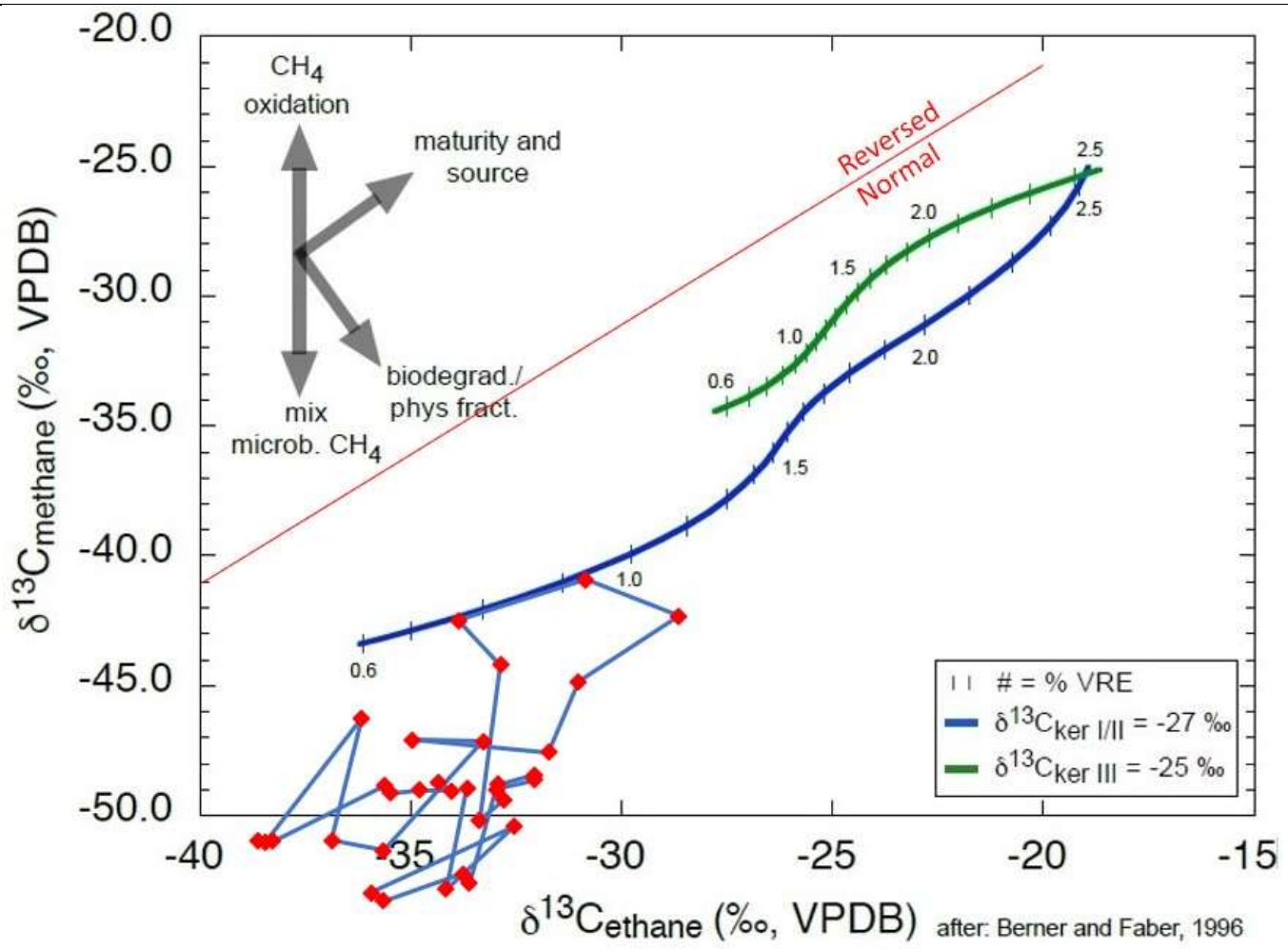

Figure A 43. ISO profile data – Interpretive ISO $\delta^{13}C_1$ versus $\delta^{13}C_2$ plot for WA#32990 (Upper Cretaceous to Triassic VT well. These plots express the depth related confusion clearly with intervals jumping from one set of four levels of conditions to another and only middle intervals on the kerogen Type II curve, but methane appears inconsistent with ethane and propane, Whiticar, 2018 pers. comm., after Berner and Faber 1996, no trendlines).

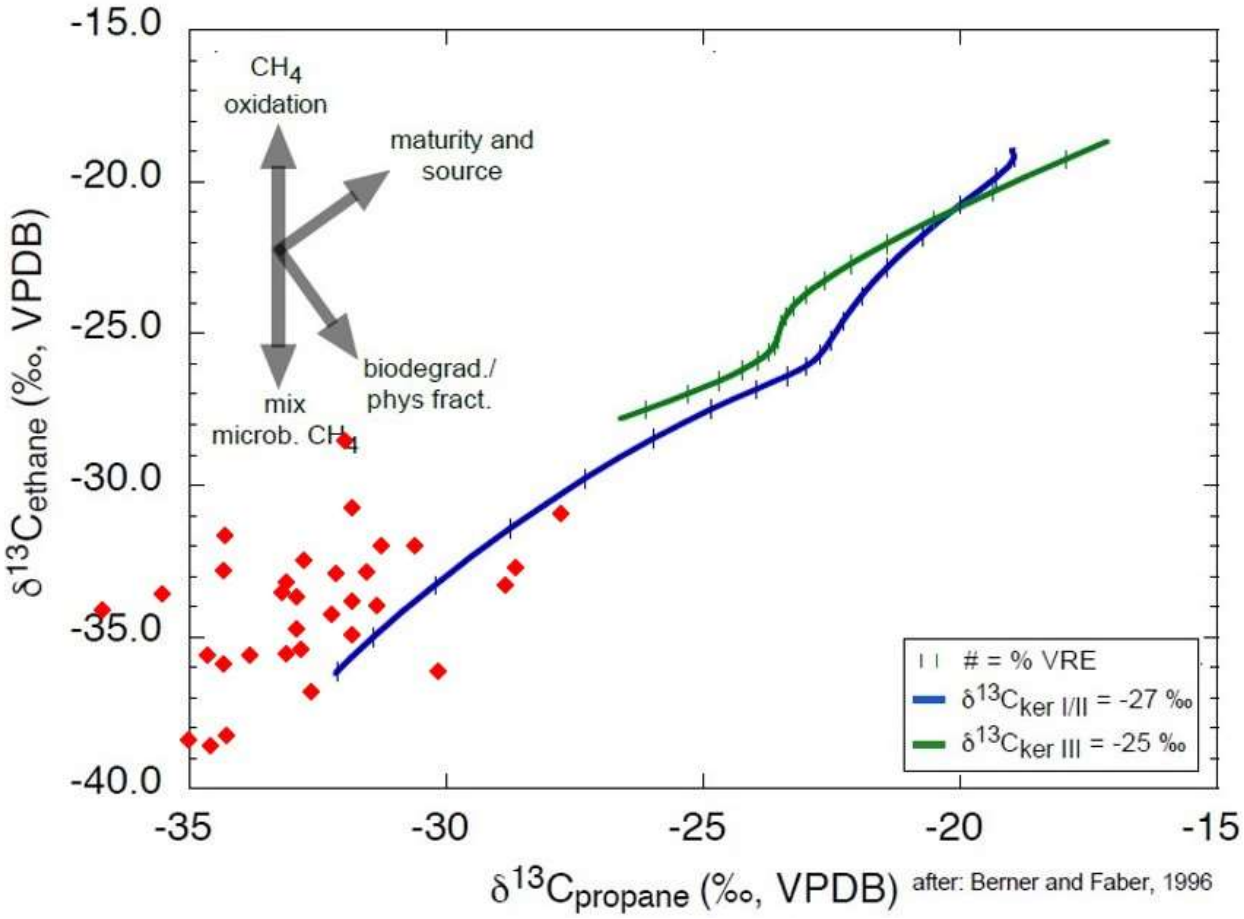

Figure A 44. ISO profile data – Interpretive ISO $\delta^{13}C_2$ versus $\delta^{13}C_3$ plot for WA#32990 (Upper Cretaceous to Triassic VT well. These plots express the depth related confusion clearly with intervals jumping from one set of four levels of conditions to another, but methane appears inconsistent with ethane and propane, Whiticar, 2018 pers. comm., after Berner and Faber 1996, no trendlines).

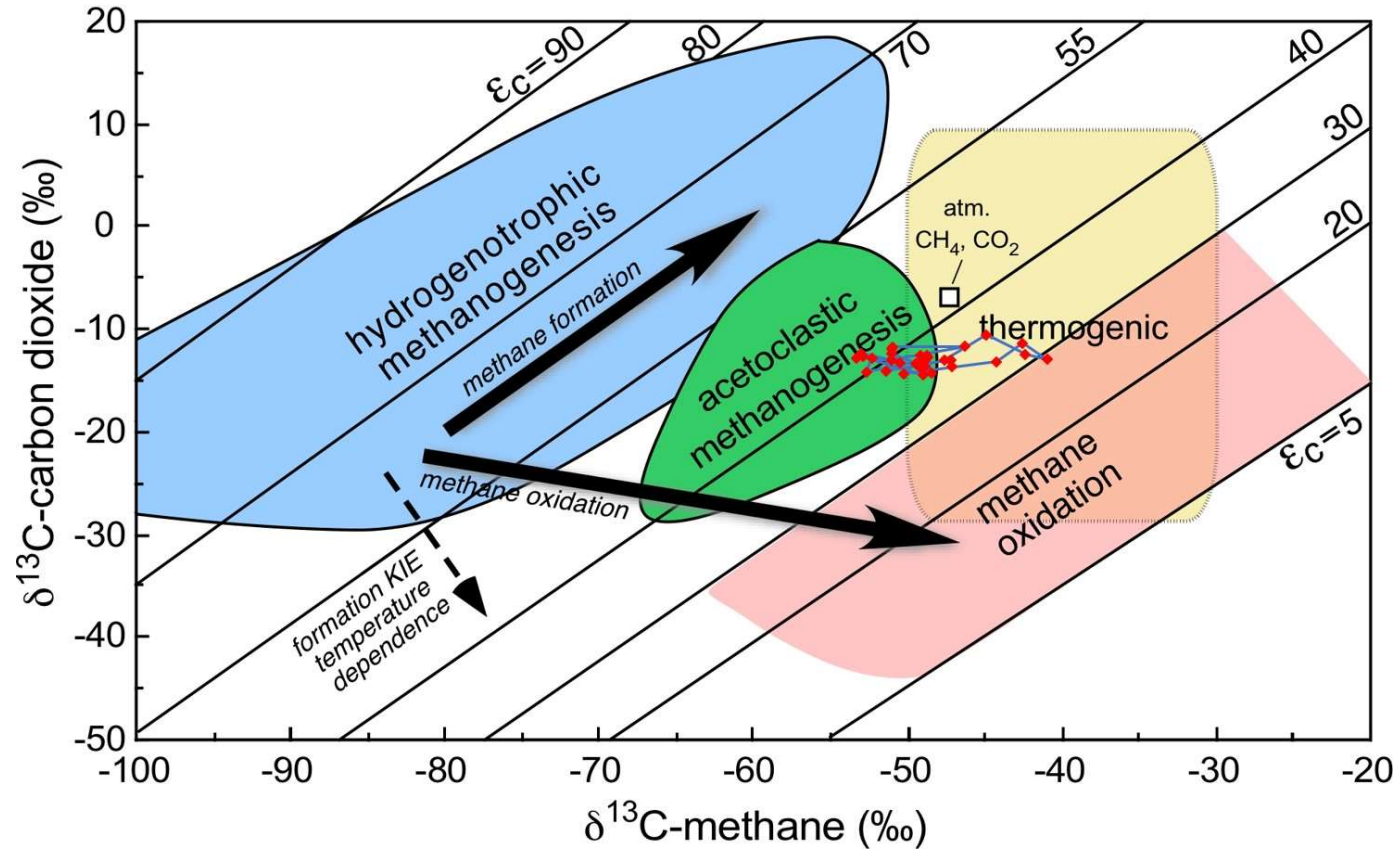

Figure A 45. ISO profile data – Interpretive ISO $\delta^{13}CO_2$ versus $\delta^{13}C_1$ plot WA#32990 (Jurassic to Triassic VT well. The only well with carbon dioxide analysis shows a bit more consistency in that assessment for biological activity for methane generation while hydrocarbon only analysis shows alternation between maturity, mixing paths, and inversions even at shallow depth, Whiticar, 2018 pers. comm., after Whiticar 1999, well profile trendlines).

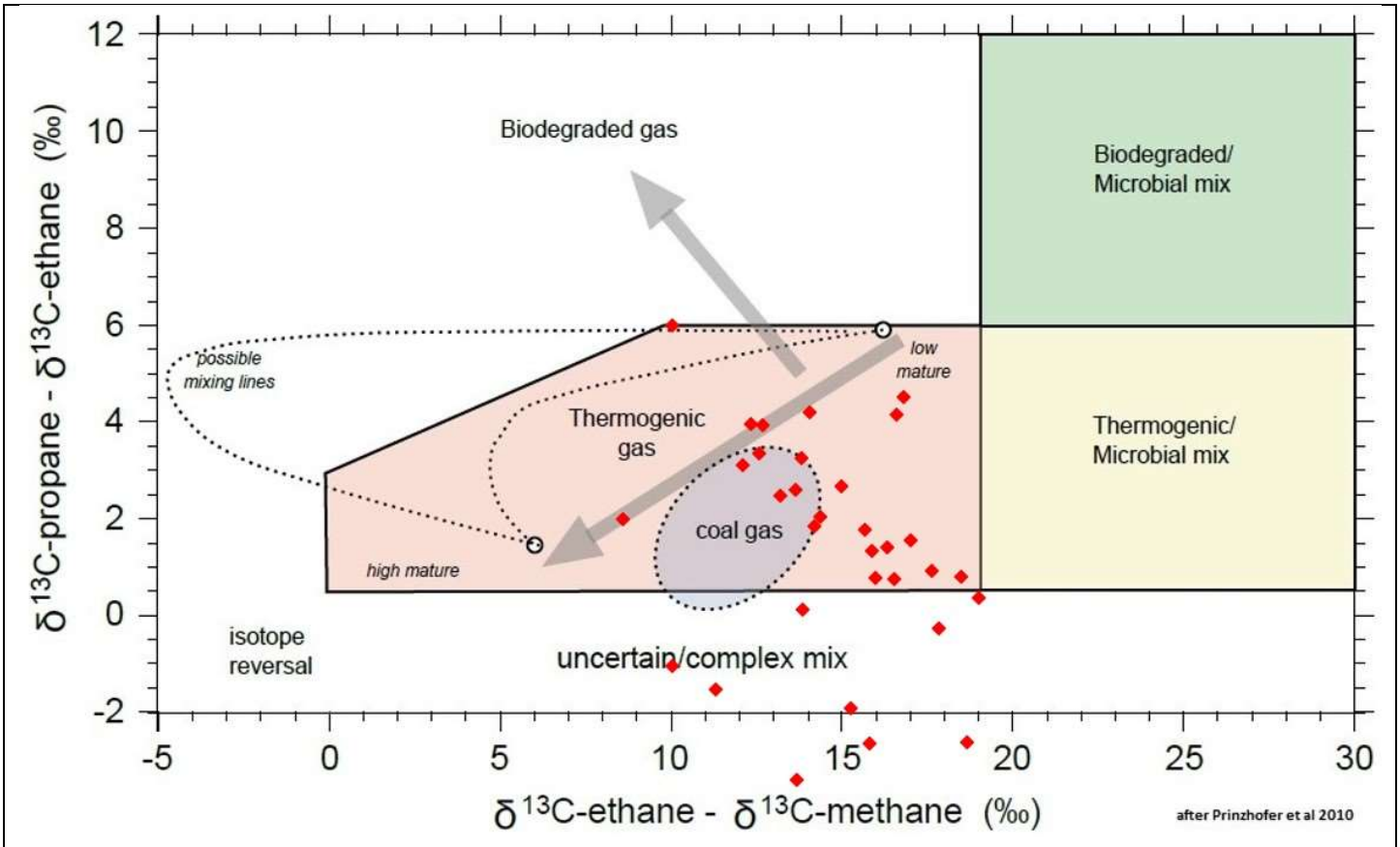

Figure A 46. ISO profile data – Interpretive $\delta^{13}C_2$- $\delta^{13}C_1$ versus $\delta^{13}C_3$- $\delta^{13}C_2$ plot for WA#32990 (Jurassic to Triassic VT well. The carbon dioxide analysis indicates hydrocarbon only analysis confuses maturity, mixing paths, and inversions even at shallow depth, after Whiticar 1999, no trendlines).

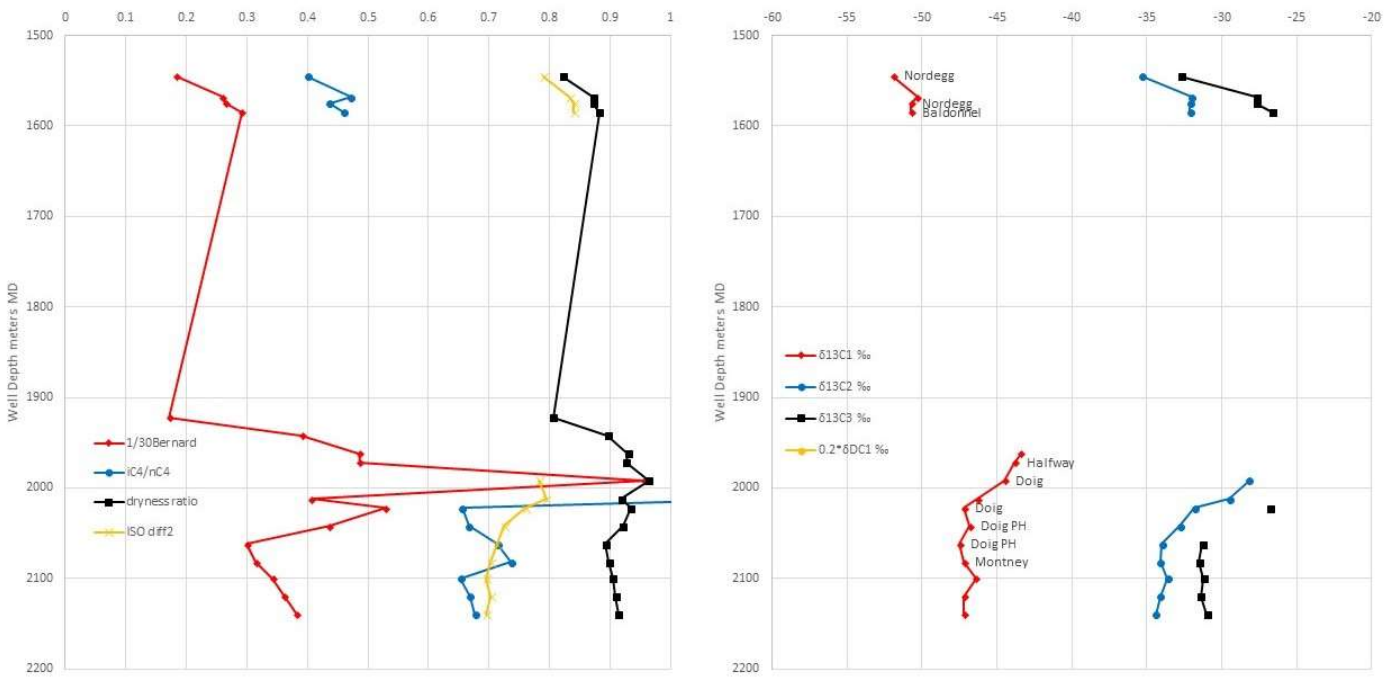

Figure A 47. Well profile, MC ratios and ISO data for WA#28233 (Jurassic to Triassic VT well. A vertical portion of a HZ well where the deviated section is data overlap with the HZ profile figure A39 (which starts in Doig). Thick skipped section of key formations).

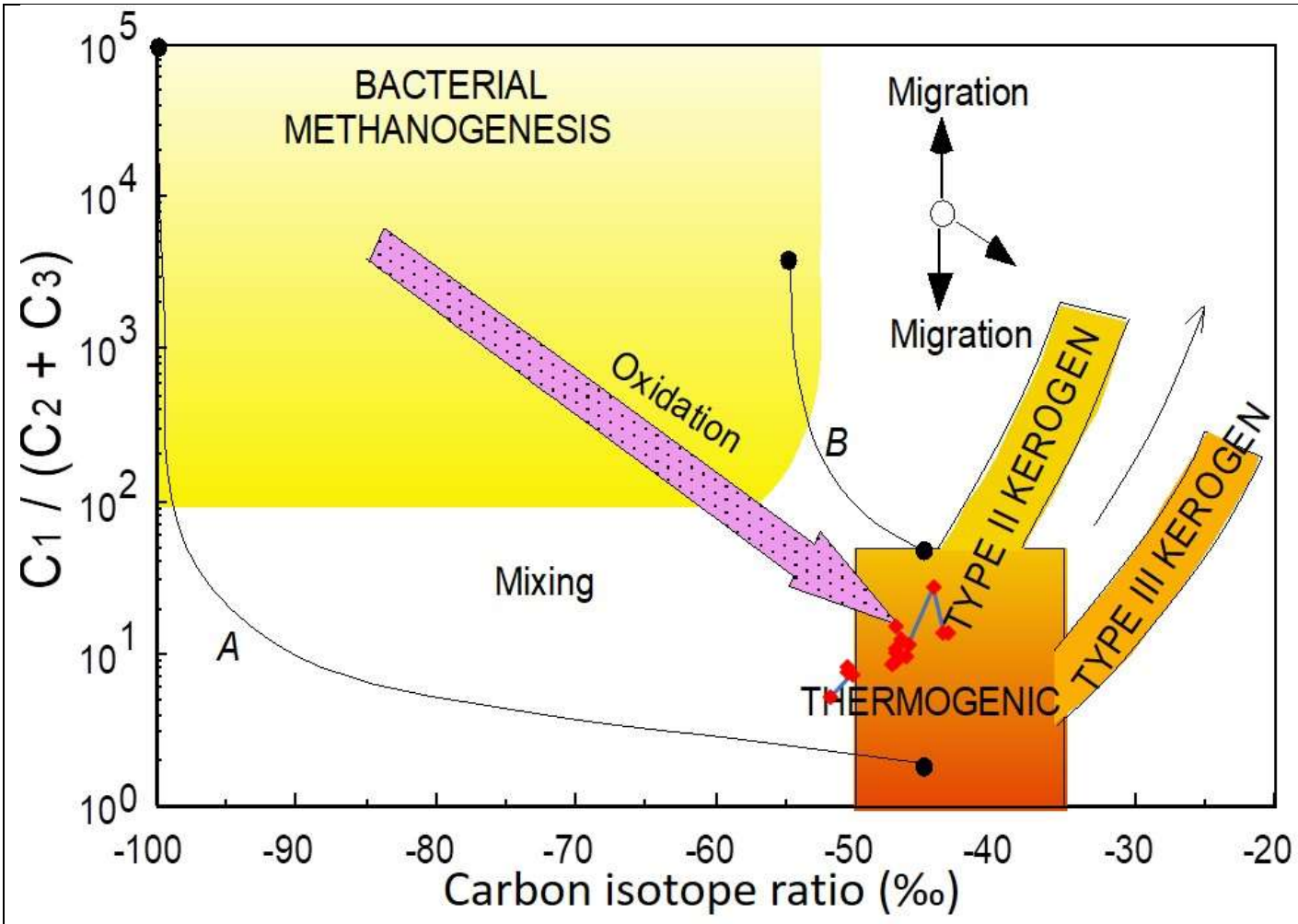

Figure A 48. ISO profile data – Interpretive Bernard Diagram for WA#28233 (Jurassic to Triassic VT well, Whiticar, 2018 pers. comm., after Whiticar 1999).

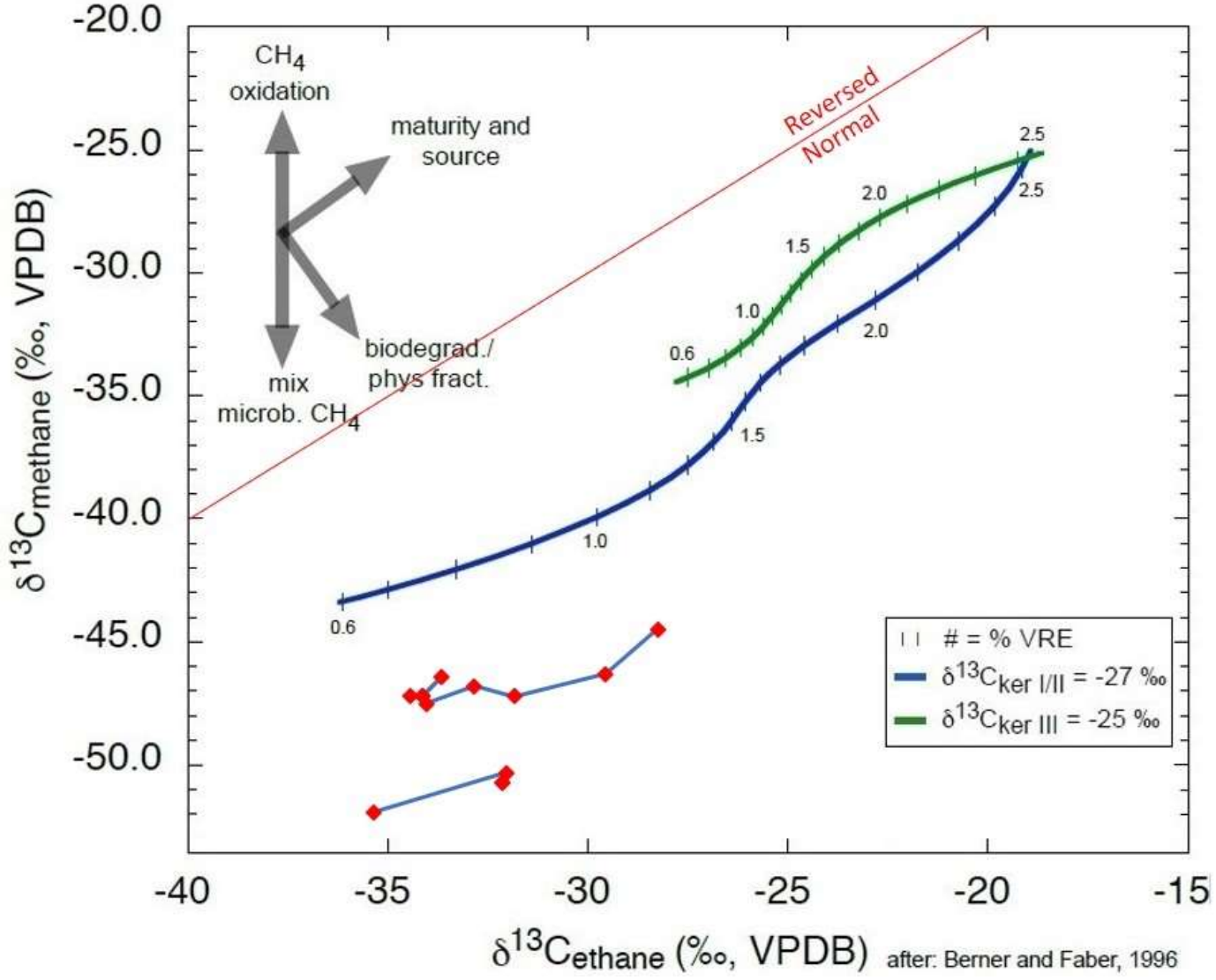

Figure A 49. ISO profile data – Interpretive ISO $\delta^{13}C_1$ versus $\delta^{13}C_2$ plot for WA#28233 (Jurassic to Triassic VT well. Data from shallower strata appears very different from deeper strata with 2 different trends, Whiticar, 2018 pers. comm., after Berner and Faber 1996, well profile trendlines).

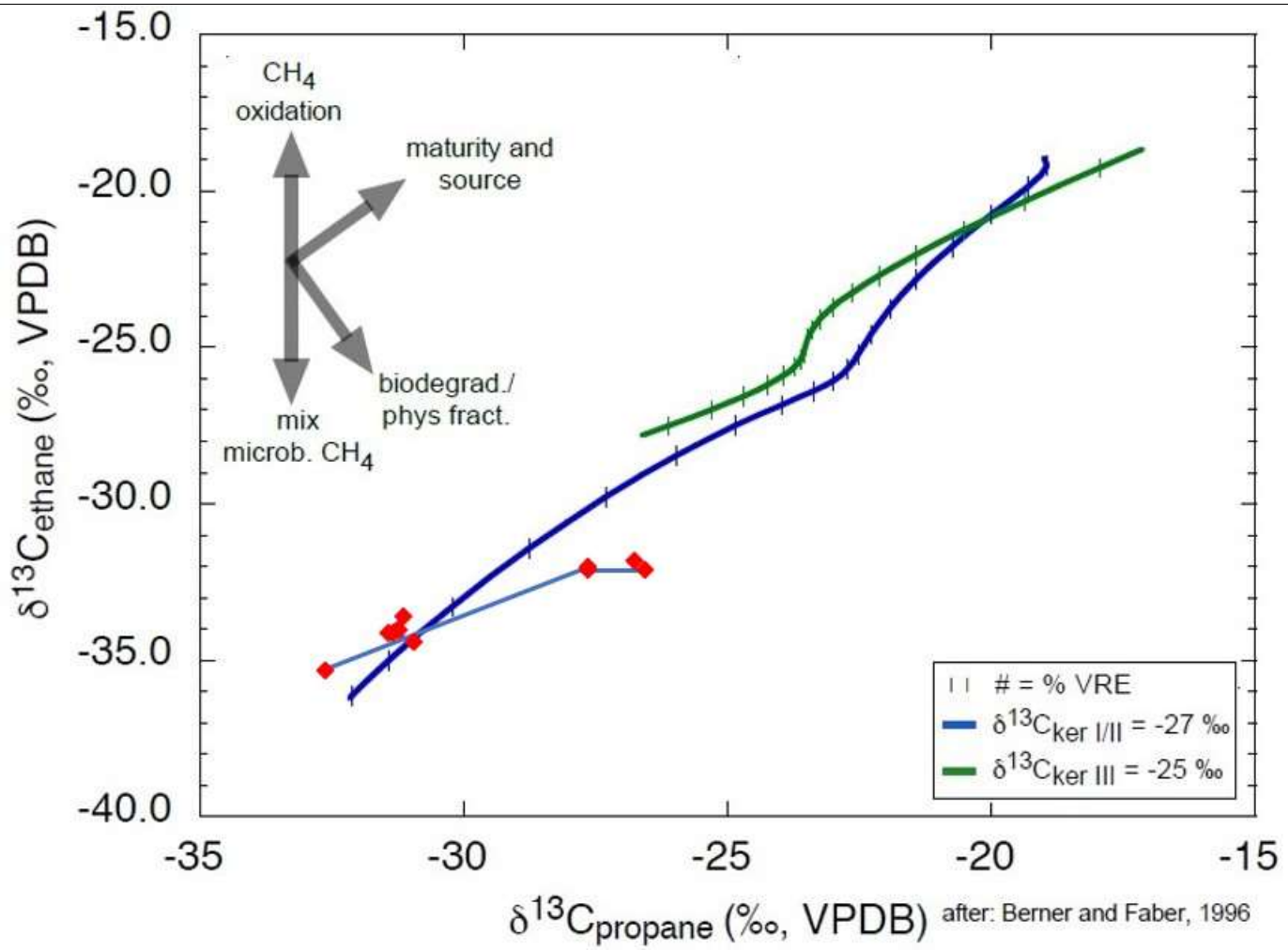

Figure A 50. ISO profile data – Interpretive ISO $\delta^{13}C_2$ versus $\delta^{13}C_3$ plot for WA#28233 (Jurassic to Triassic VT well. Data from shallower strata and deeper strata have methane responding differently from ethane and propane, Whiticar, 2018 pers. comm., after Berner and Faber 1996, well profile trendline).

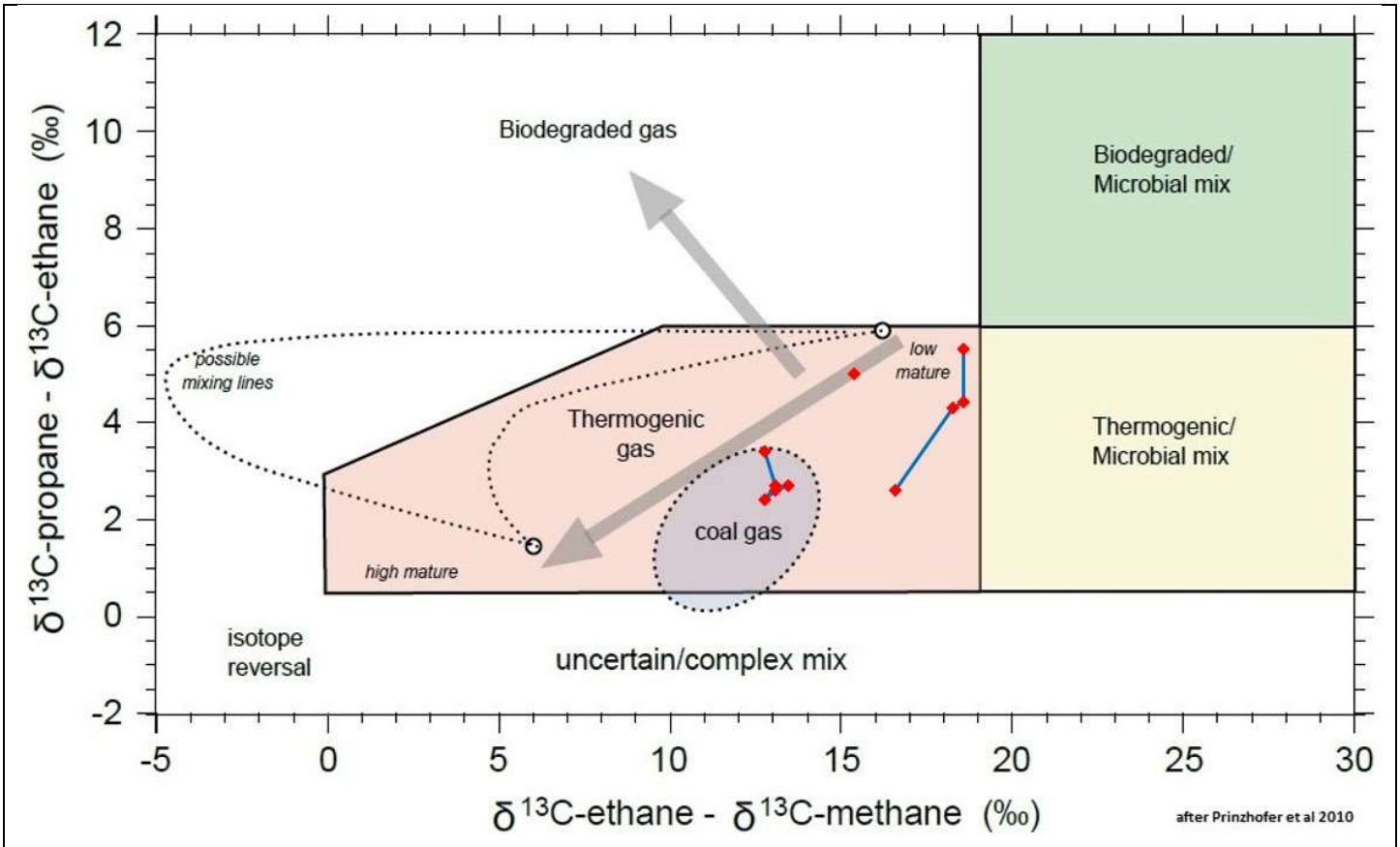

Figure A 51. Interpretive $\delta^{13}C_2$- $\delta^{13}C_1$ versus $\delta^{13}C_3$- $\delta^{13}C_2$ plot for WA#28233 (Jurassic to Triassic VT well. Shallow strata is more mixed low maturity and the start of the Montney in the vertical section is closer to "coal gas" of HZ Montney diagram).

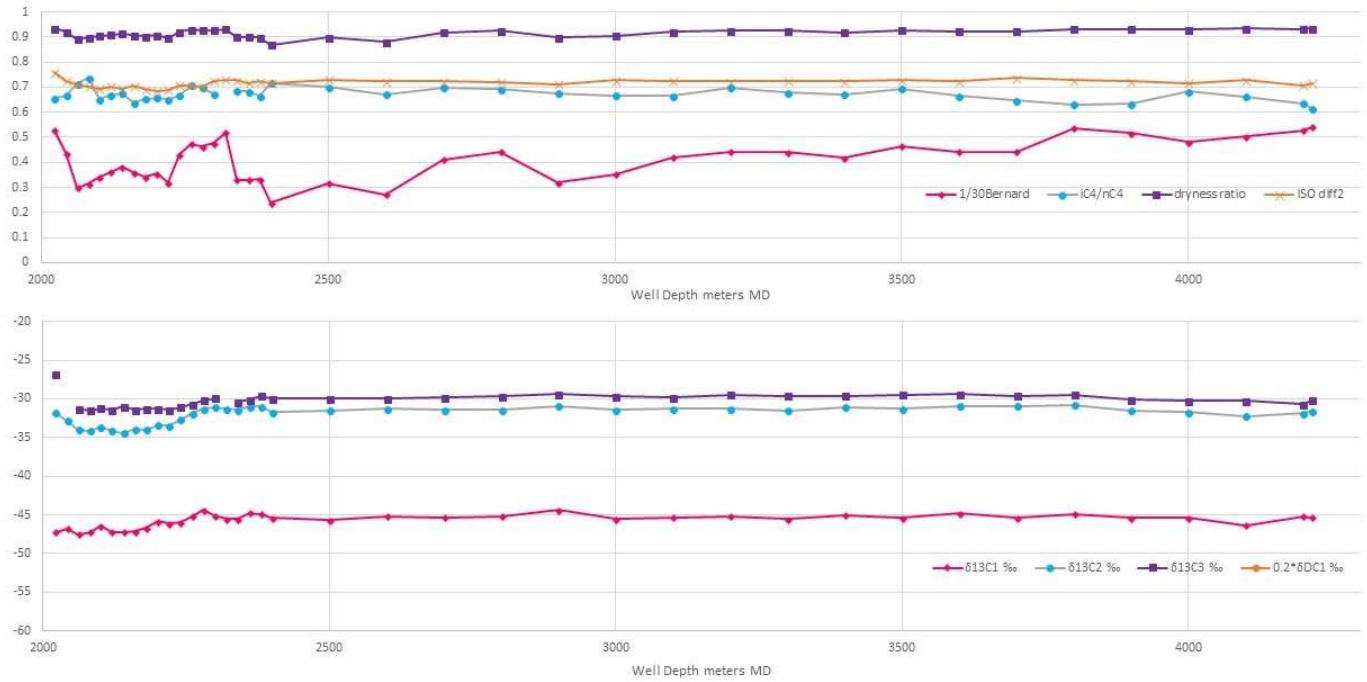

Figure A 52. Well profile, MC ratios and ISO data for WA#28233 (Montney HZ leg with uphole completion included).

Yes DATA, no profile

Figure A 53. Well profile, only 4 data points, all in Montney WA#33348.

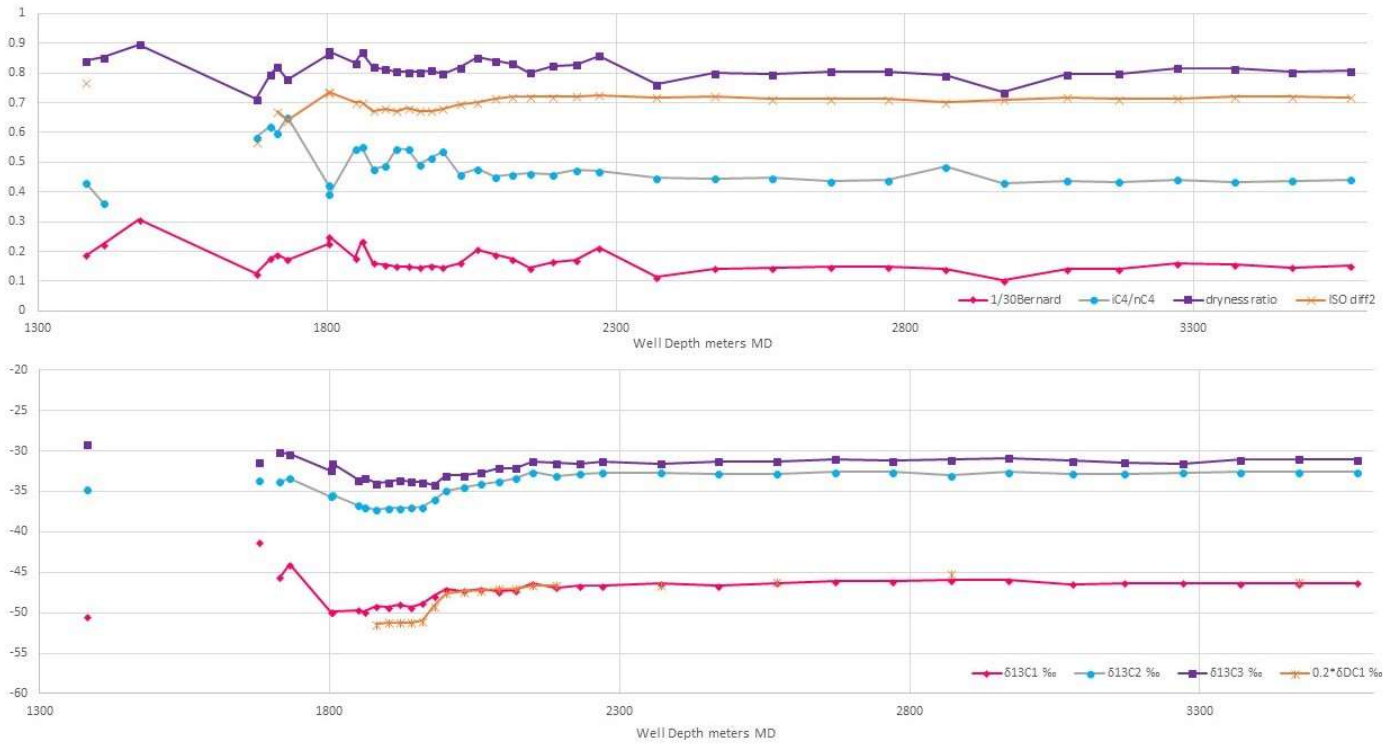

Figure A 54. Well profile, MC ratios and ISO data for WA#30947 (Montney HZ leg with uphole completion included).

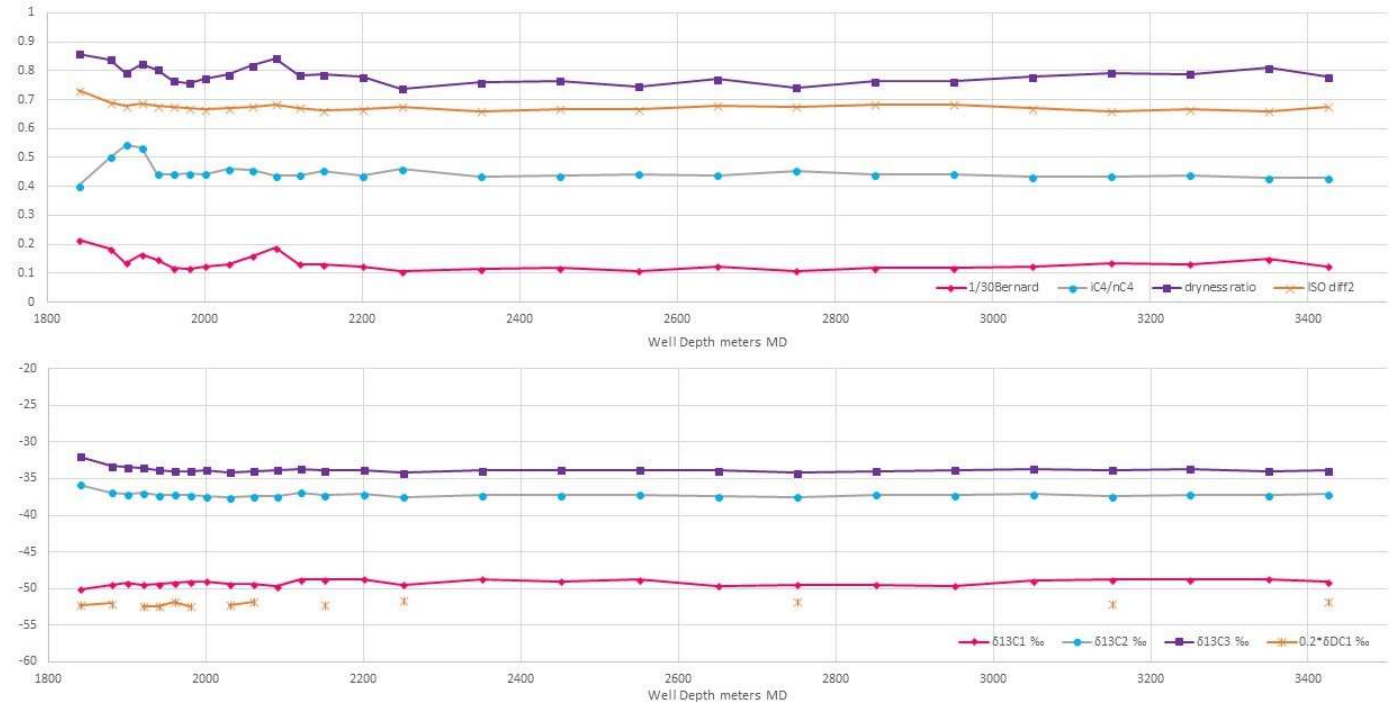

Figure A 55. Well profile, MC ratios and ISO data for WA#30948 (Montney HZ leg with uphole completion included).

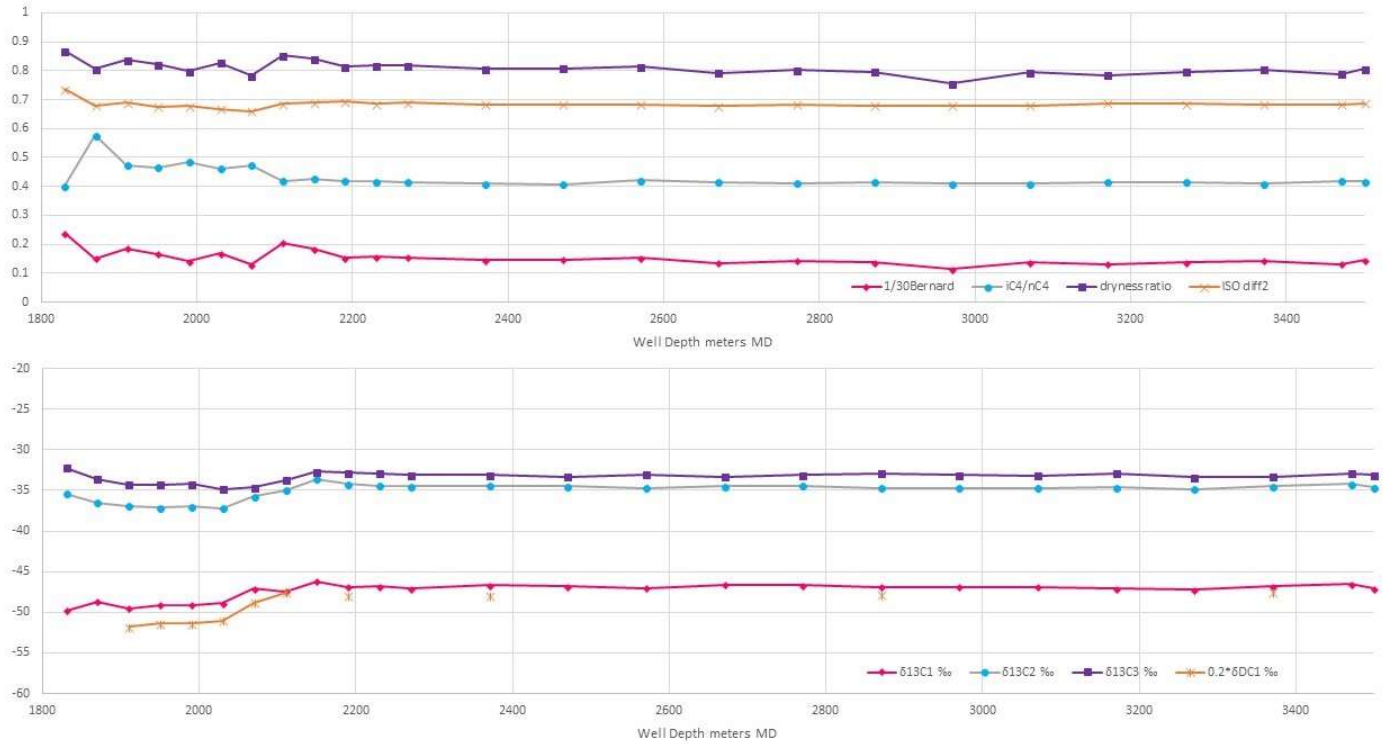

Figure A 56. Well profile, MC ratios and ISO data for WA#30949 (Montney HZ leg with uphole completion included).

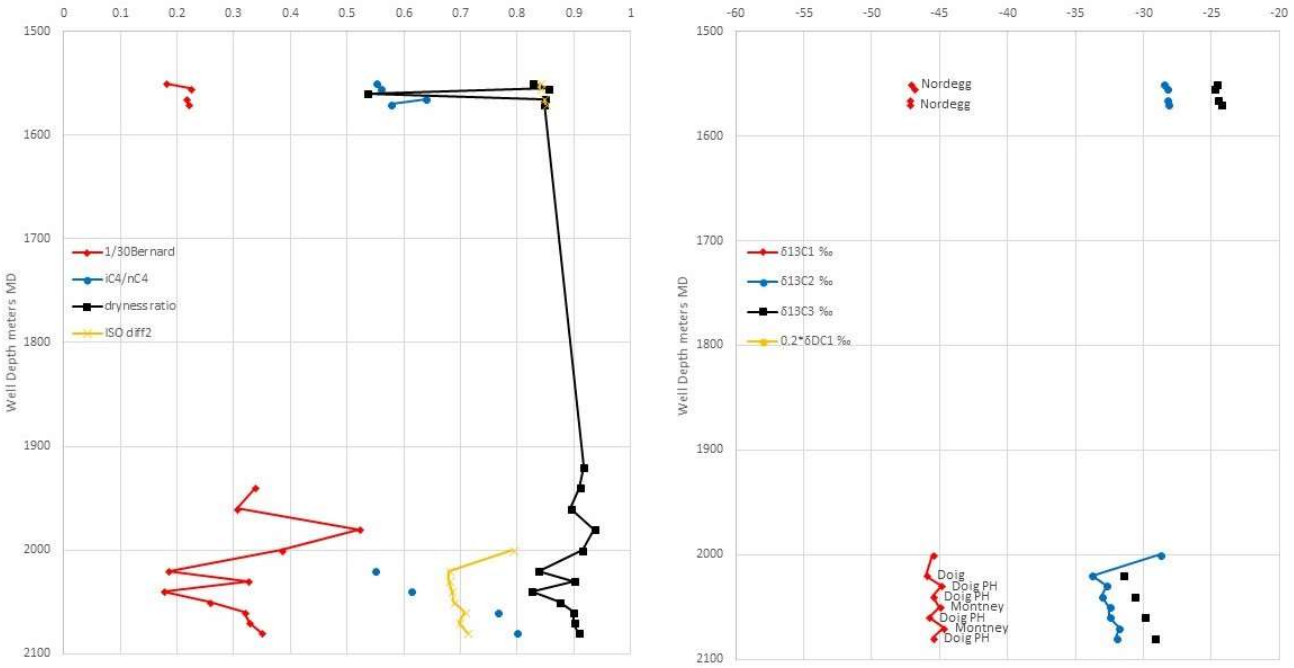

Figure A 57. Well profile, MC ratios and ISO data for WA#28165 (Jurassic to Triassic. A vertical portion of a HZ well where the deviated section is data overlap with the HZ profile figure A62 (which starts in Doig). Thick skipped section of key formations).

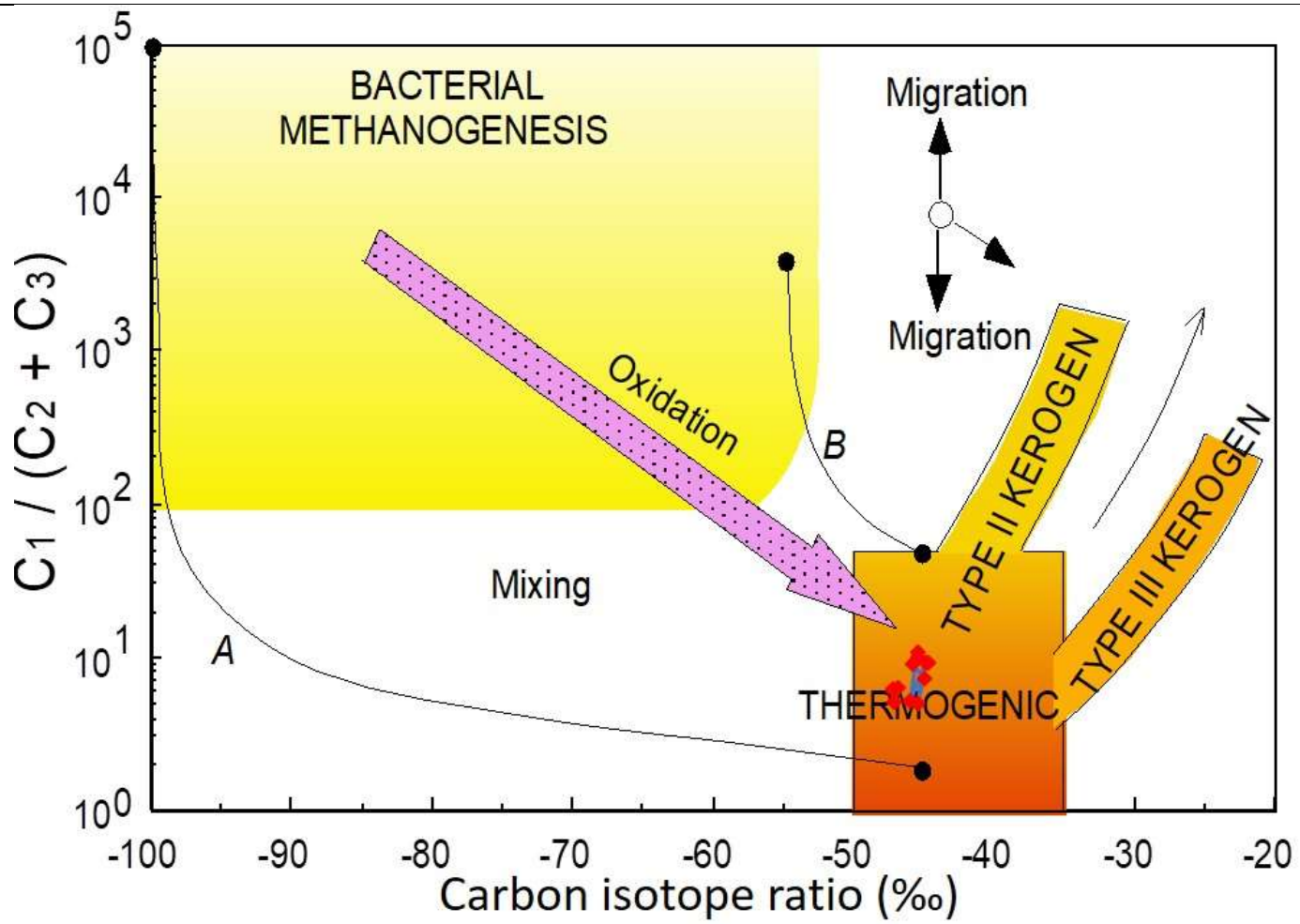

Figure A 58. ISO profile data – Interpretive Bernard Diagram for WA#28165 (Jurassic to Triassic, Whiticar, 2018 pers. comm., after Whiticar 1999).

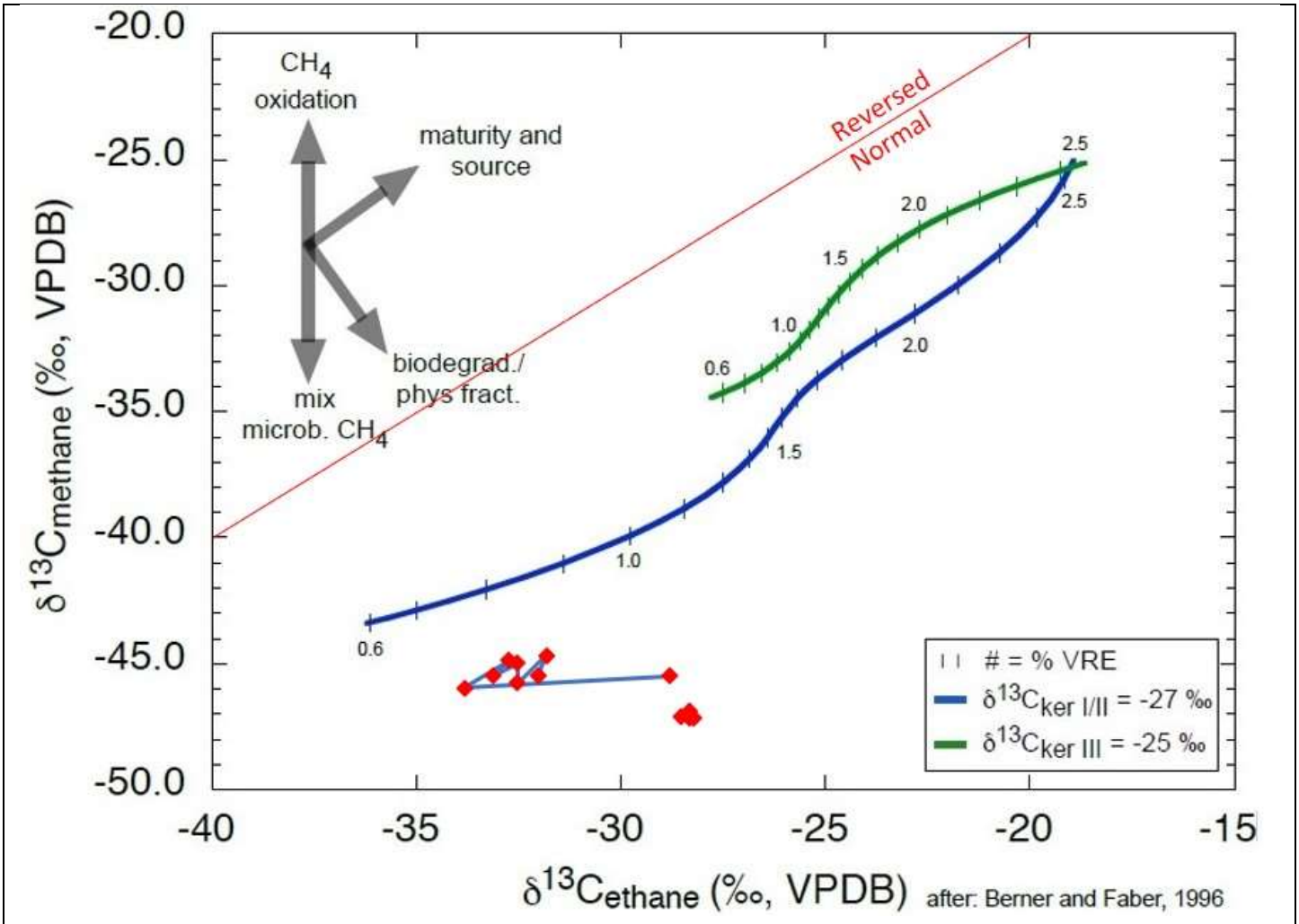

Figure A 59. ISO profile data – Interpretive ISO $\delta^{13}C_1$ versus $\delta^{13}C_2$ plot for WA#28165 (Jurassic to Triassic. Data from shallower strata appears very different from deeper strata with 2 different trends, Whiticar, 2018 pers. comm., after Berner and Faber 1996, well profile trendline).

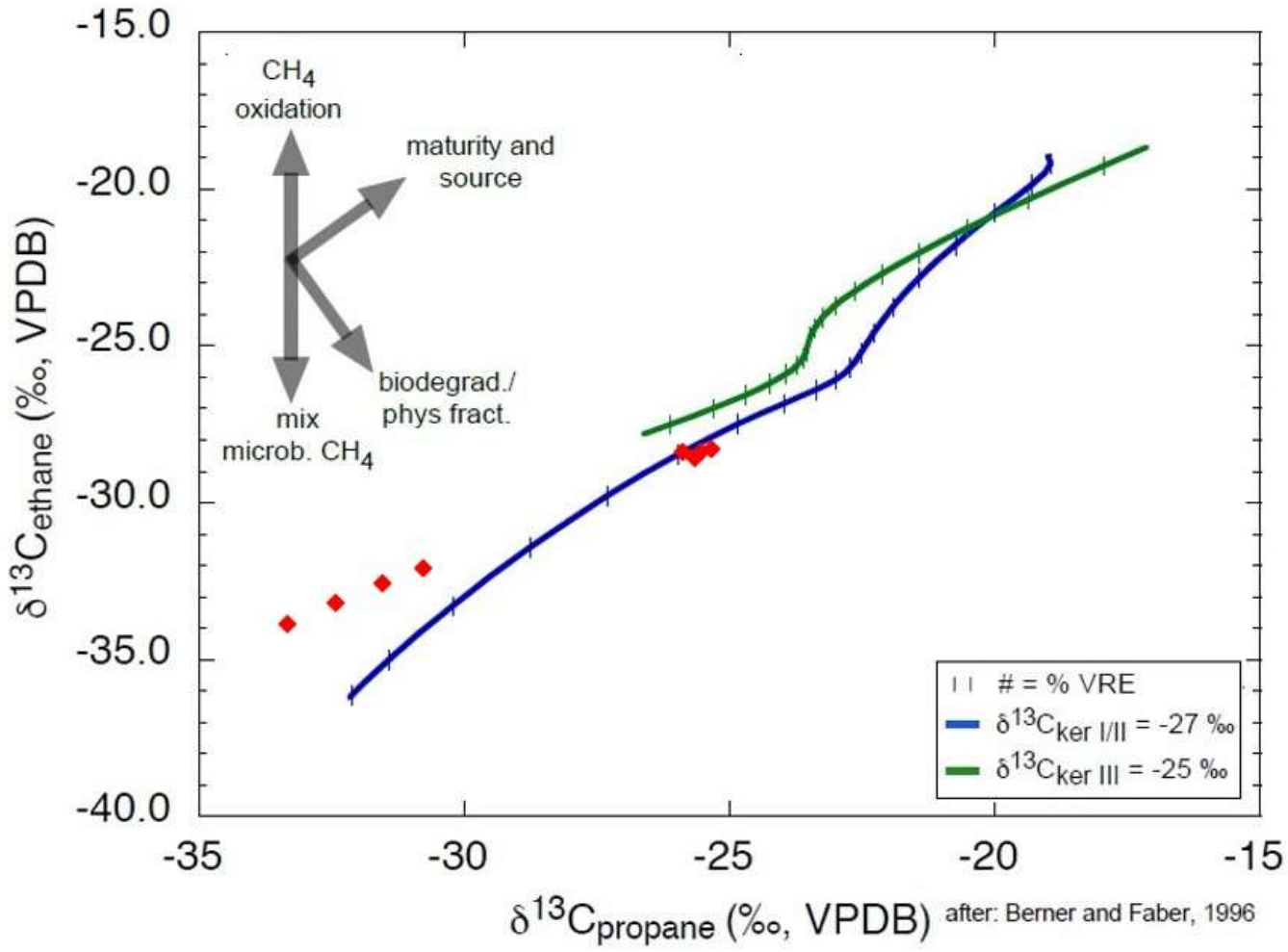

Figure A 60. ISO profile data – Interpretive ISO $\delta^{13}C_2$ versus $\delta^{13}C_3$ plot for WA#28165 (Jurassic to Triassic. Data from shallower strata and deeper strata have methane responding differently from ethane and propane, Whiticar, 2018 pers. comm., after Berner and Faber 1996, no trendlines).

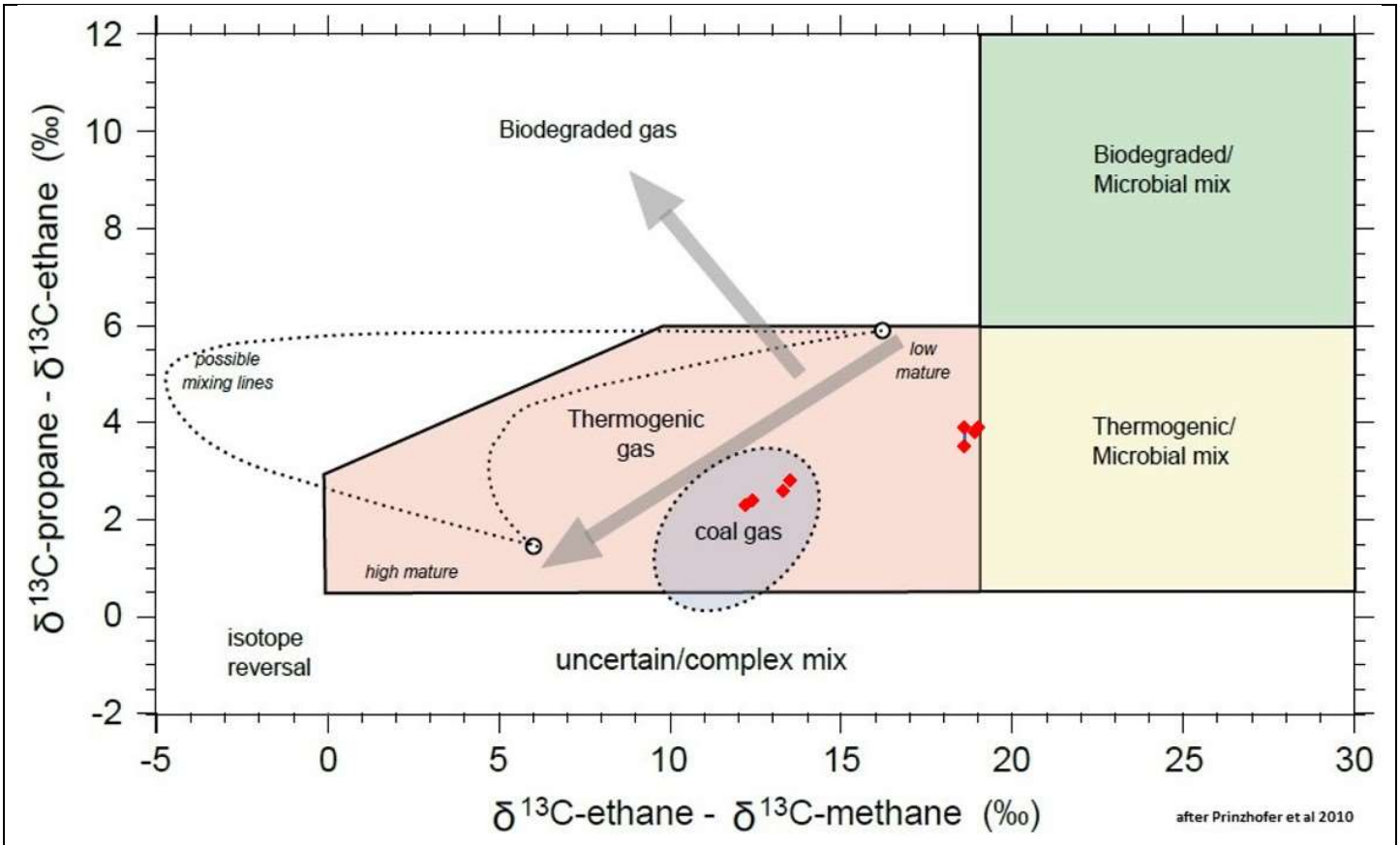

Figure A 61. Interpretive $\delta^{13}C_2$- $\delta^{13}C_1$ versus $\delta^{13}C_3$- $\delta^{13}C_2$ plot for WA#28165 (Jurassic to Triassic. Shallow strata is more mixed low maturity and the start of the Montney in the vertical section is closer to "coal gas" of HZ Montney diagram as figure A05).

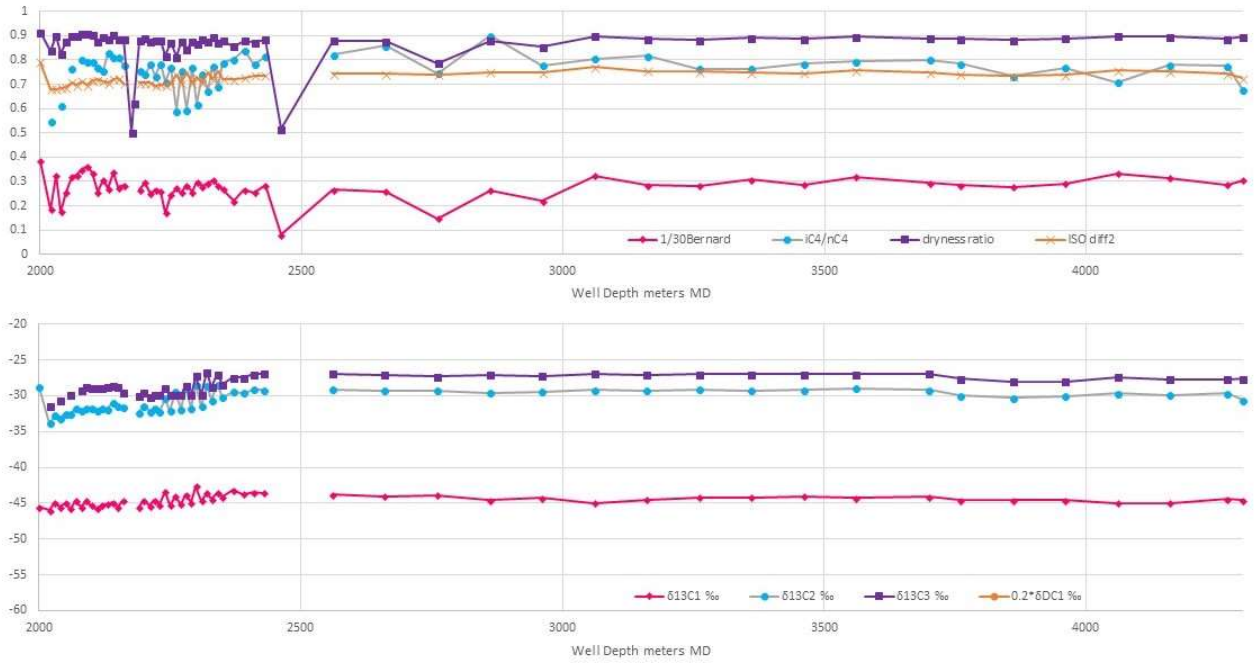

Figure A 62. Well profile, MC ratios and ISO data for WA#28165 (Montney HZ leg with segment of uphole VT from Figures A44, A45, A46 included. For description of "sawtooth" iC4/nC4 and δ^{13}C2/3, see description for WA#28770 horizontal section).

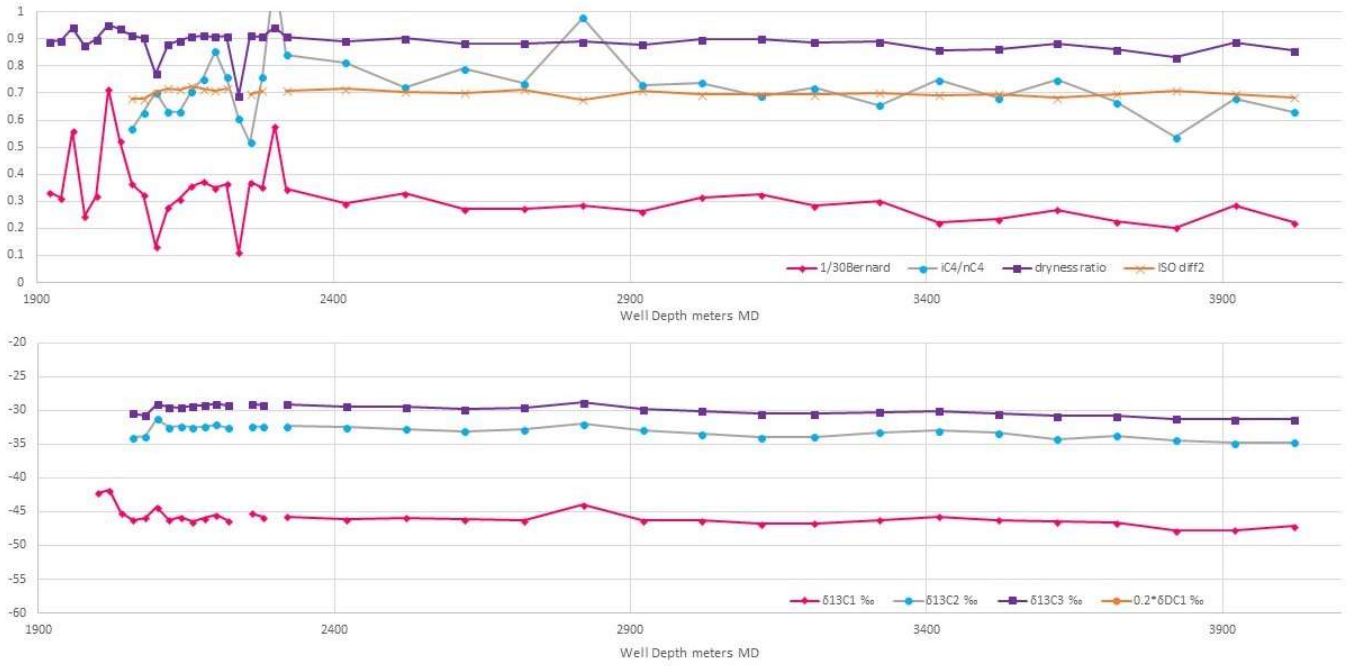

Figure A 63. Well profile, MC ratios and ISO data for WA#28167 (Montney HZ leg with uphole completion included).

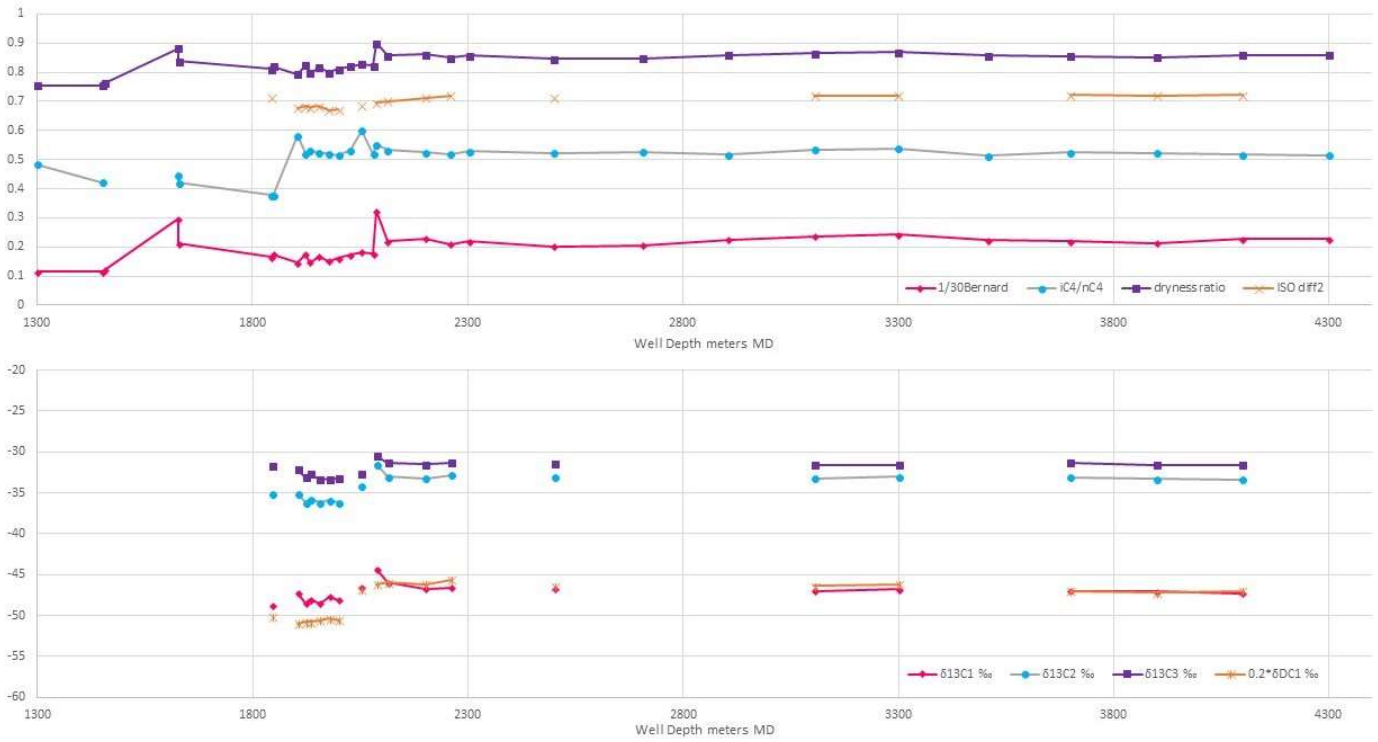

Figure A 64. Well profile, MC ratios and ISO data for WA#31226 (Montney HZ leg with uphole completion included).

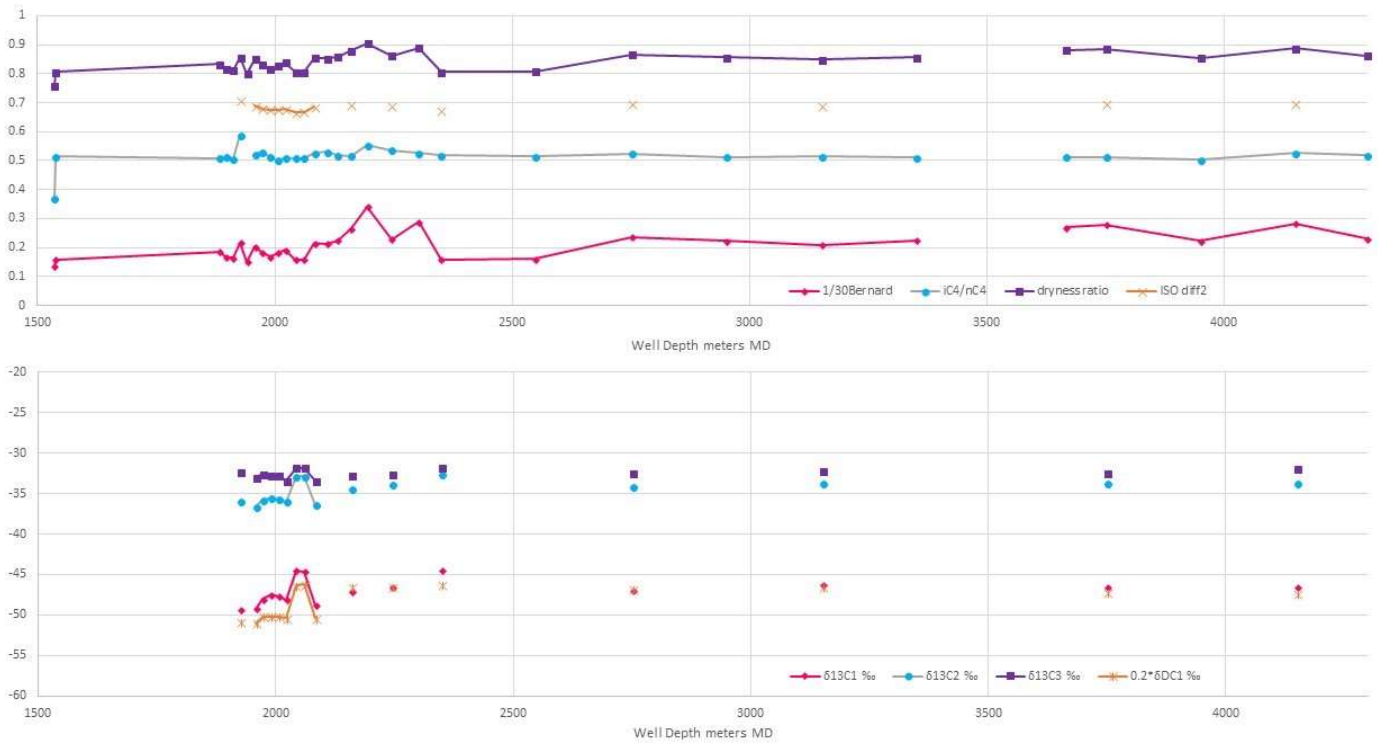

Figure A 65. Well profile, MC ratios and ISO data for WA#31228 (Montney HZ leg with uphole completion included).

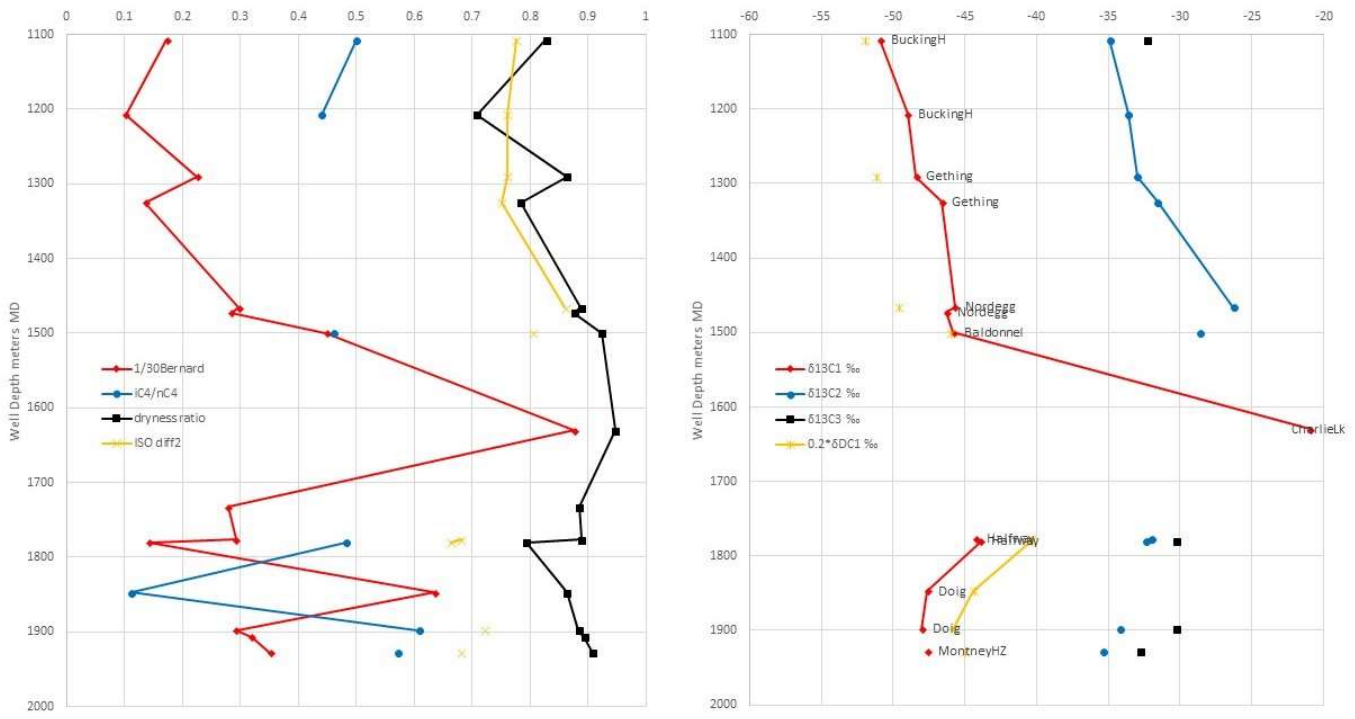

Figure A 66. Well profile, MC ratios and ISO data for WA#31490 (Upper Cretaceous to Triassic VT well. A vertical portion of a HZ well where the deviated section is data overlap with the HZ profile figure A72 (which starts in Doig). Thick skipped section of key formations has one sample present in the Charlie Lake Formation).

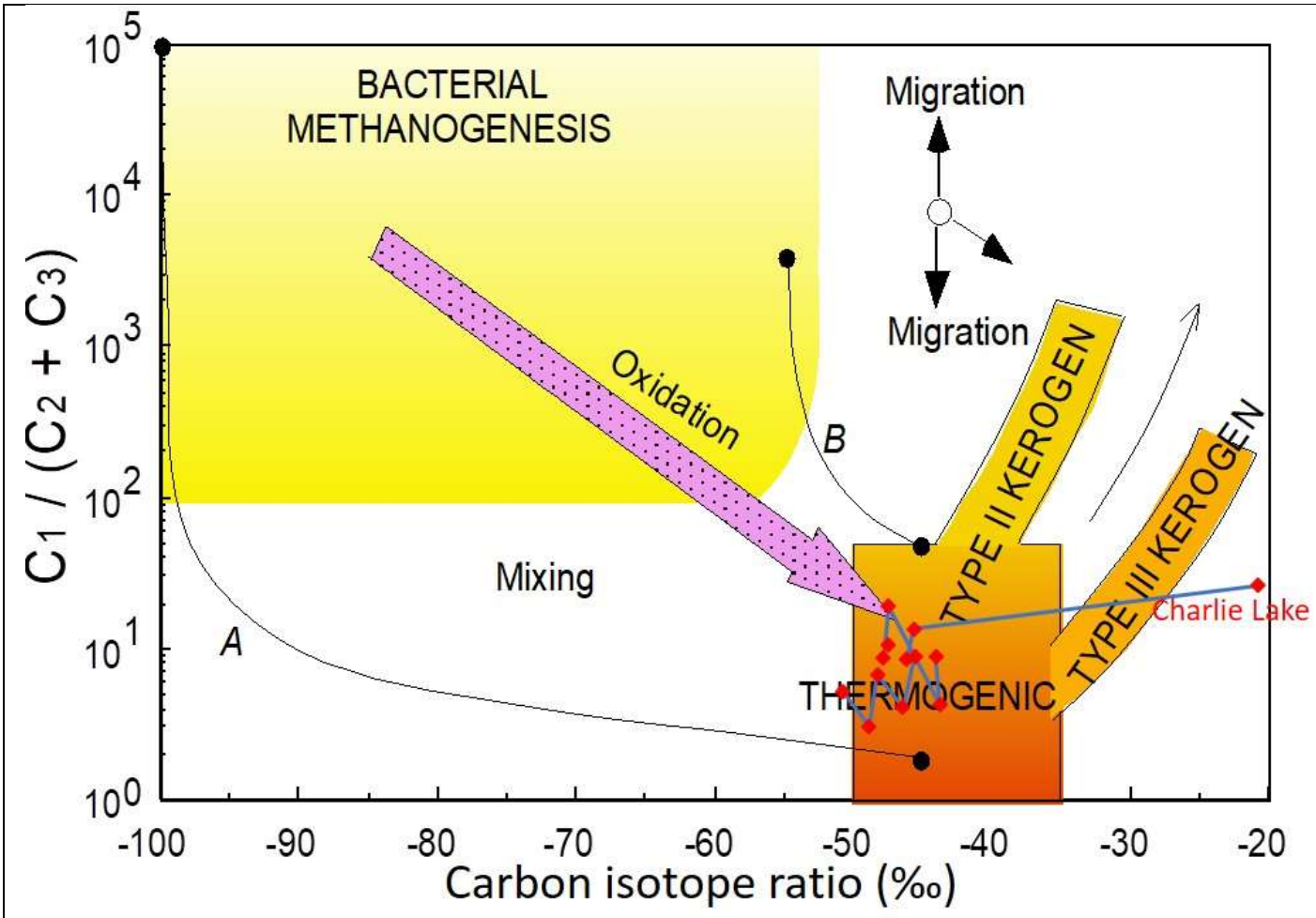

Figure A 67. ISO profile data – Interpretive Bernard Diagram for WA#31490 (Upper Cretaceous to Triassic VT well. Inclusion of rare sample from Charlie Lake Formation shows strata separation between kerogen types, but no corresponding $\delta^{13}C2/C3$ data to form conclusions, Whiticar, 2018 pers. comm., after Whiticar 1999).

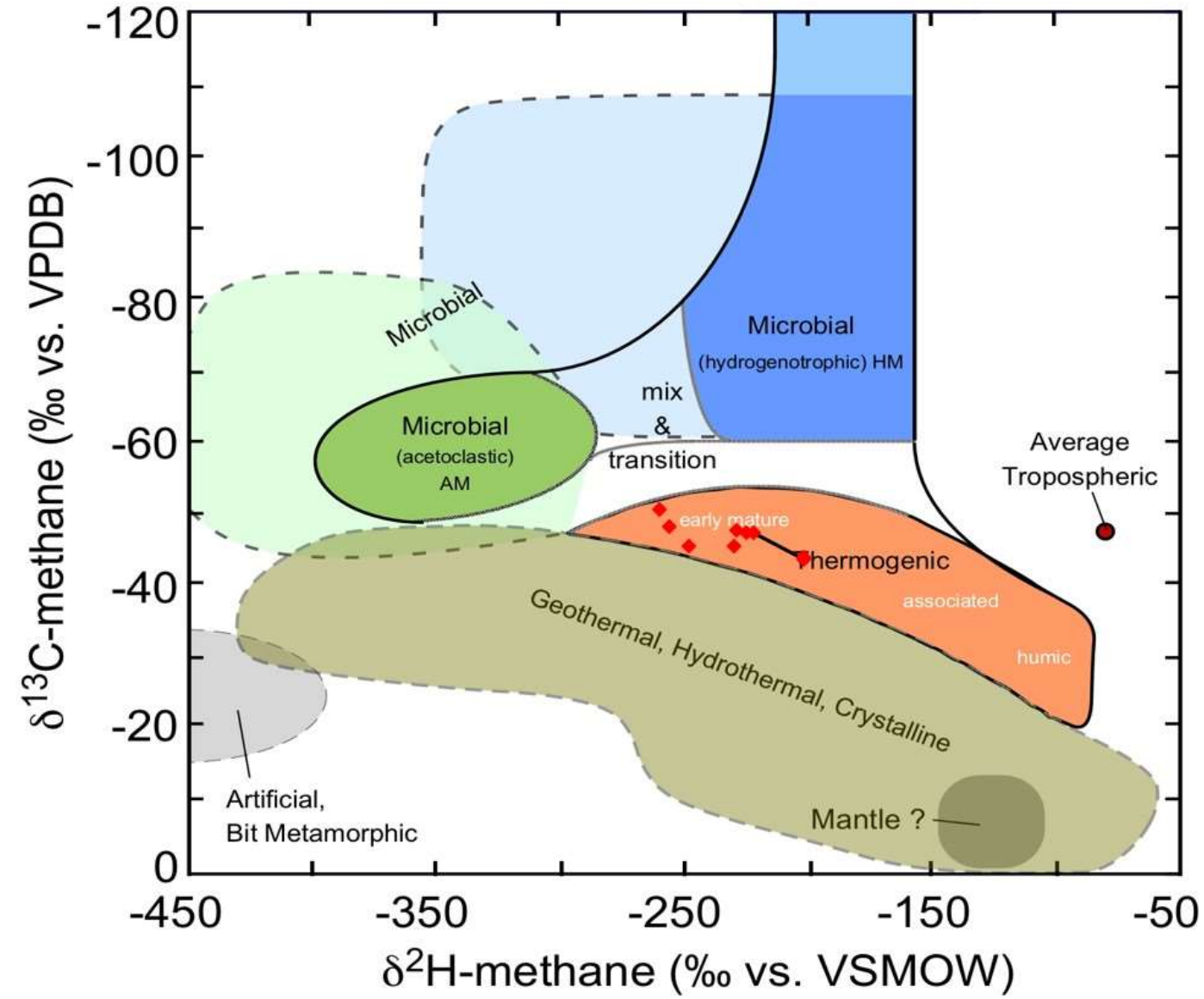

Figure A 68. ISO profile data – Interpretive CD Diagram for WA#31490 (Upper Cretaceous to Triassic VT well, Whiticar, 2018 pers. comm., after Whiticar 1999).

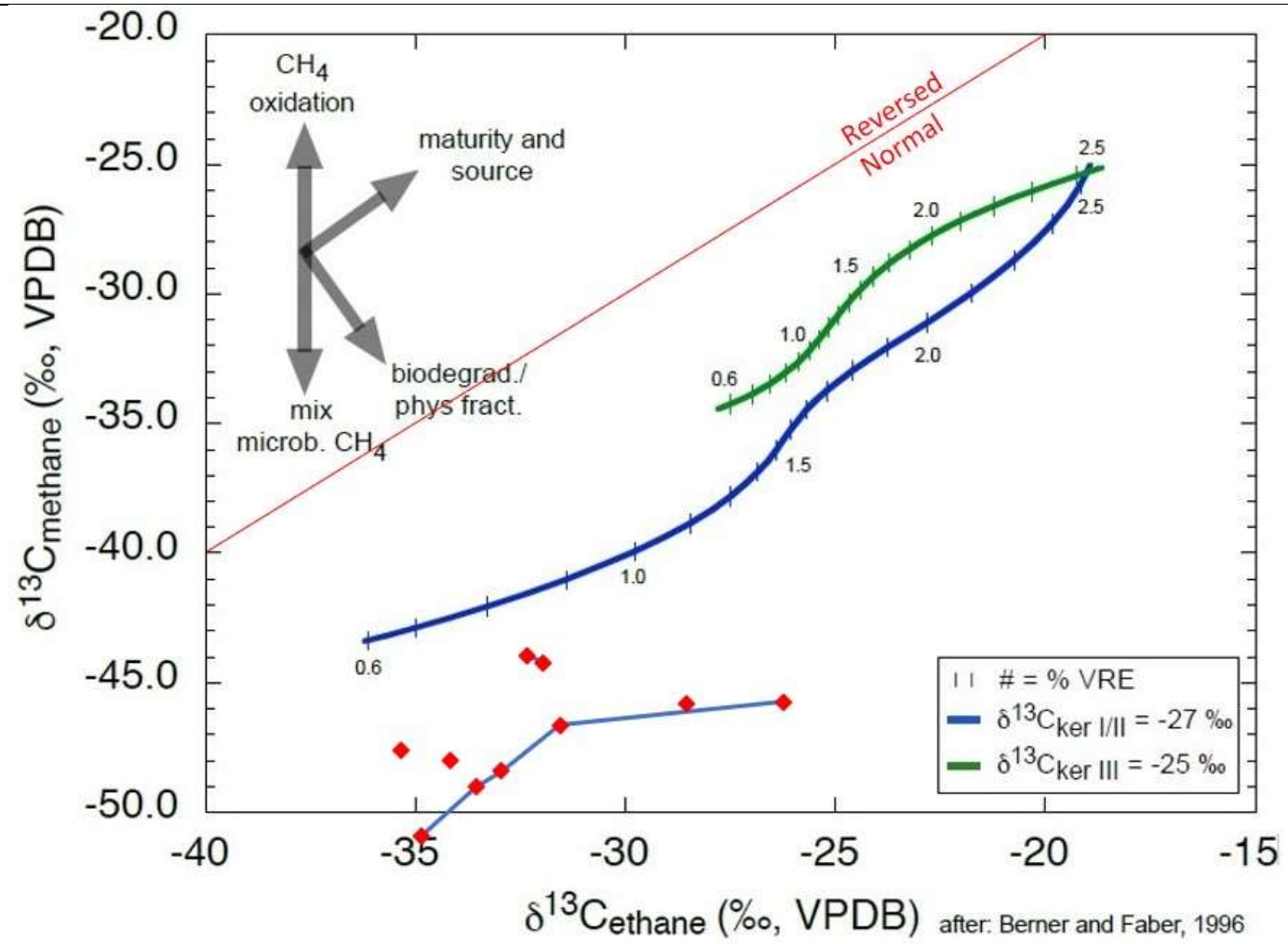

Figure A 69. ISO profile data – Interpretive ISO $\delta^{13}C_1$ versus $\delta^{13}C_2$ plot for WA#31490 (Upper Cretaceous to Triassic VT well. Data from shallower strata appears very different from deeper strata with 2 different trends, Charlie Lake Formation has no data, Whiticar, 2018 pers. comm., after Berner and Faber 1996, well profile trendline).

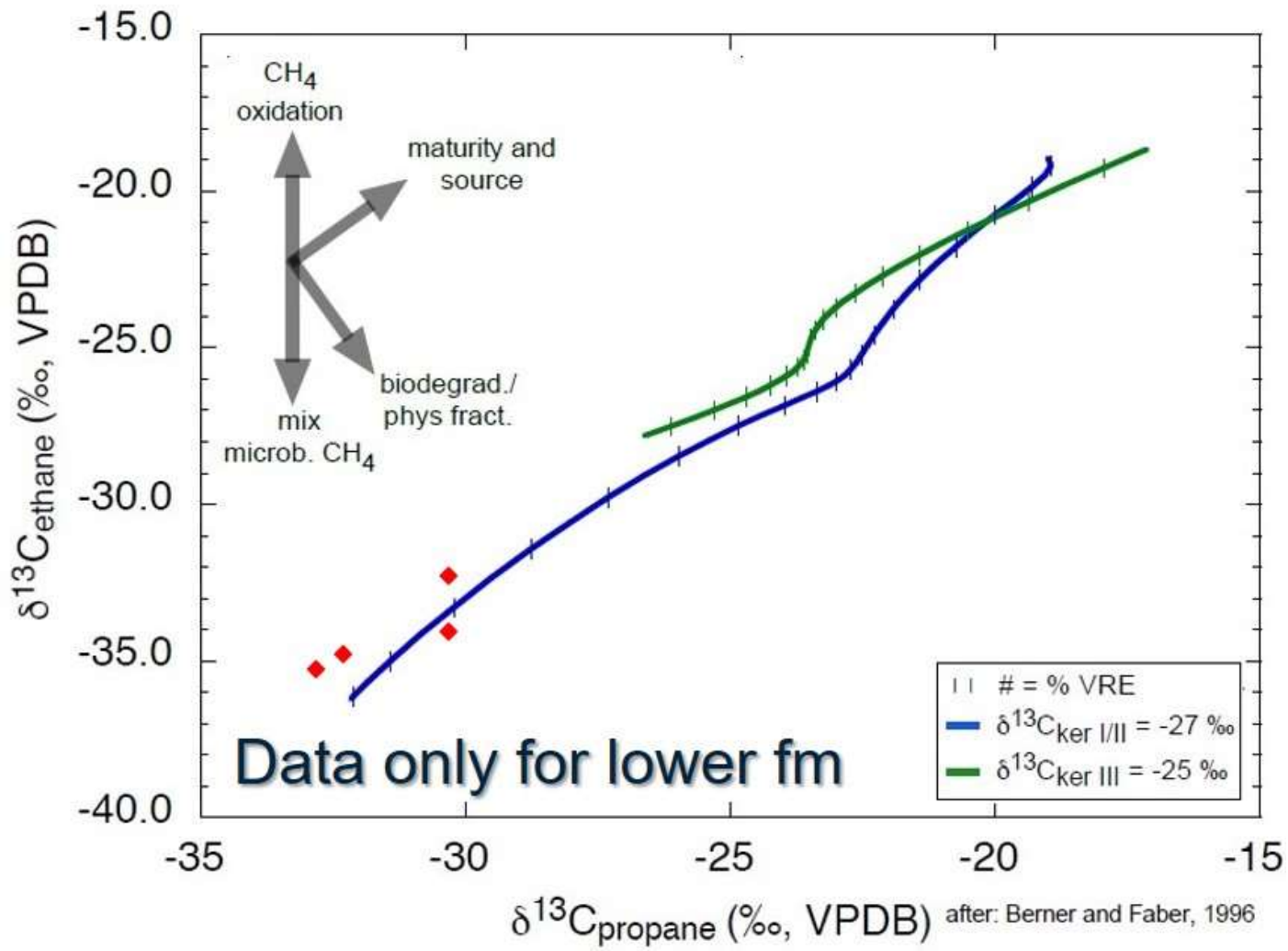

Figure A 70. ISO profile data – Interpretive ISO $\delta^{13}C_2$ versus $\delta^{13}C_3$ plot for WA#31490 (Upper Cretaceous to Triassic VT well. Data from shallower strata and deeper strata have methane responding differently from ethane and propane – Charlie Lake Formation has no data, Whiticar, 2018 pers. comm., after Berner and Faber 1996, no trendlines).

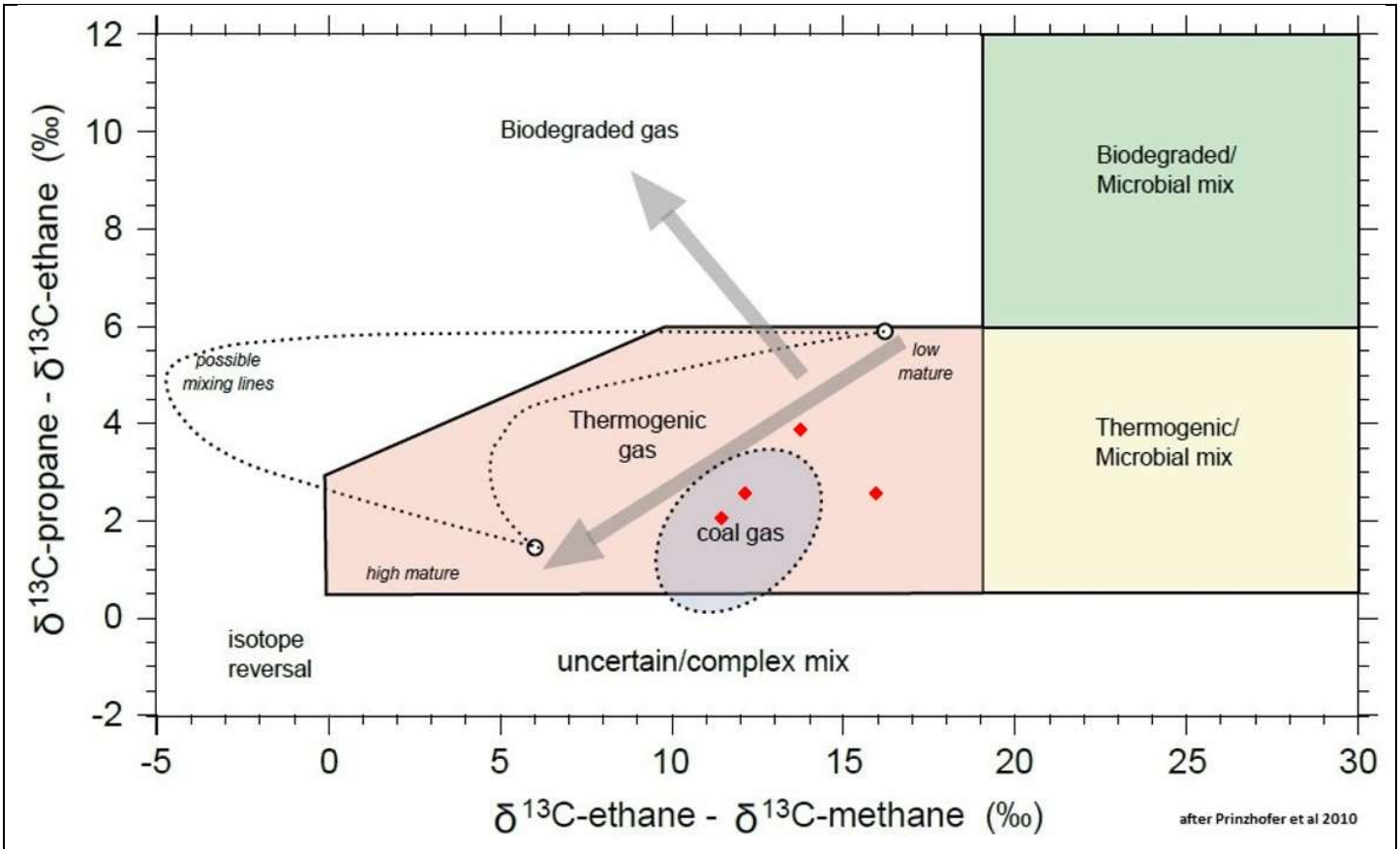

Figure A 71. Interpretive $\delta^{13}C_2$- $\delta^{13}C_1$ versus $\delta^{13}C_3$- $\delta^{13}C_2$ plot for WA#31490 (Upper Cretaceous to Triassic VT well. Start of the Montney in the vertical section is closer to "coal gas" of HZ Montney diagram).

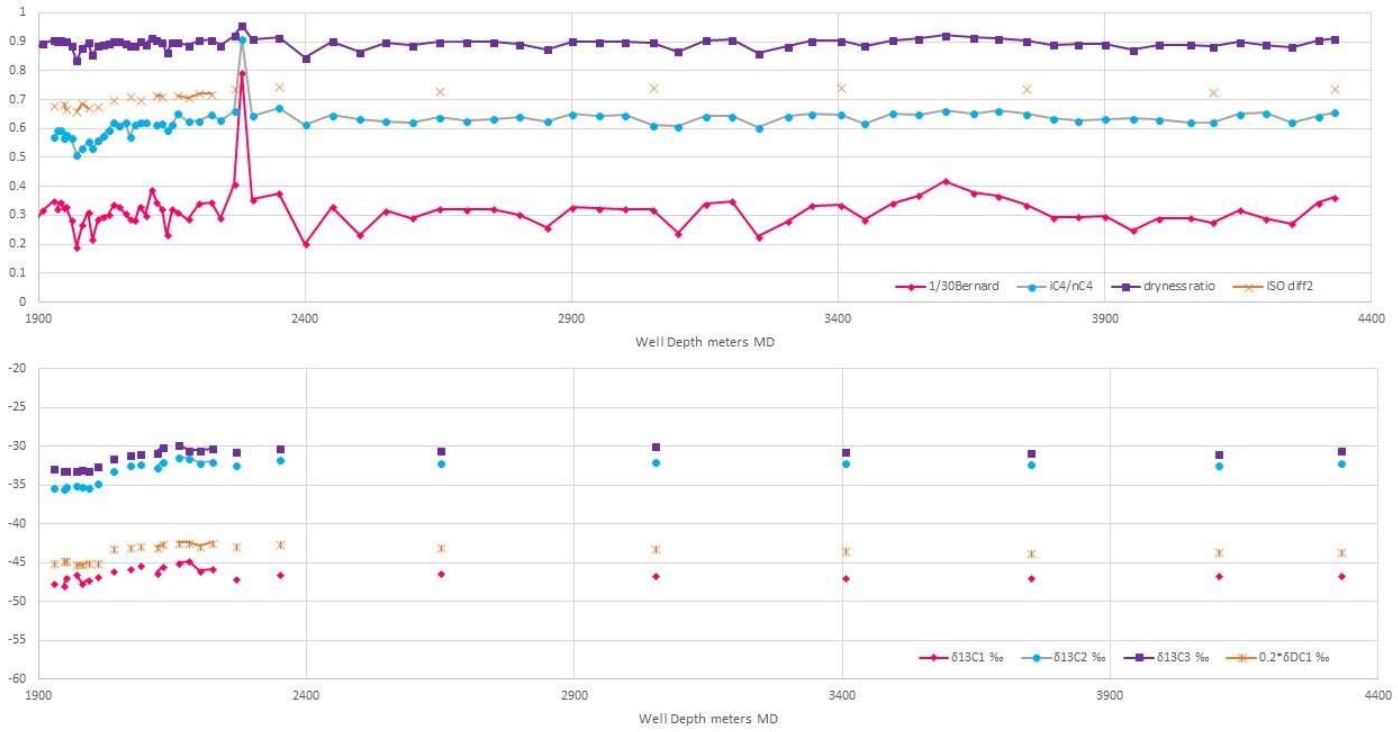

Figure A 72. Well profile, MC ratios and ISO data for WA#31490 (Montney HZ leg with uphole completion included).

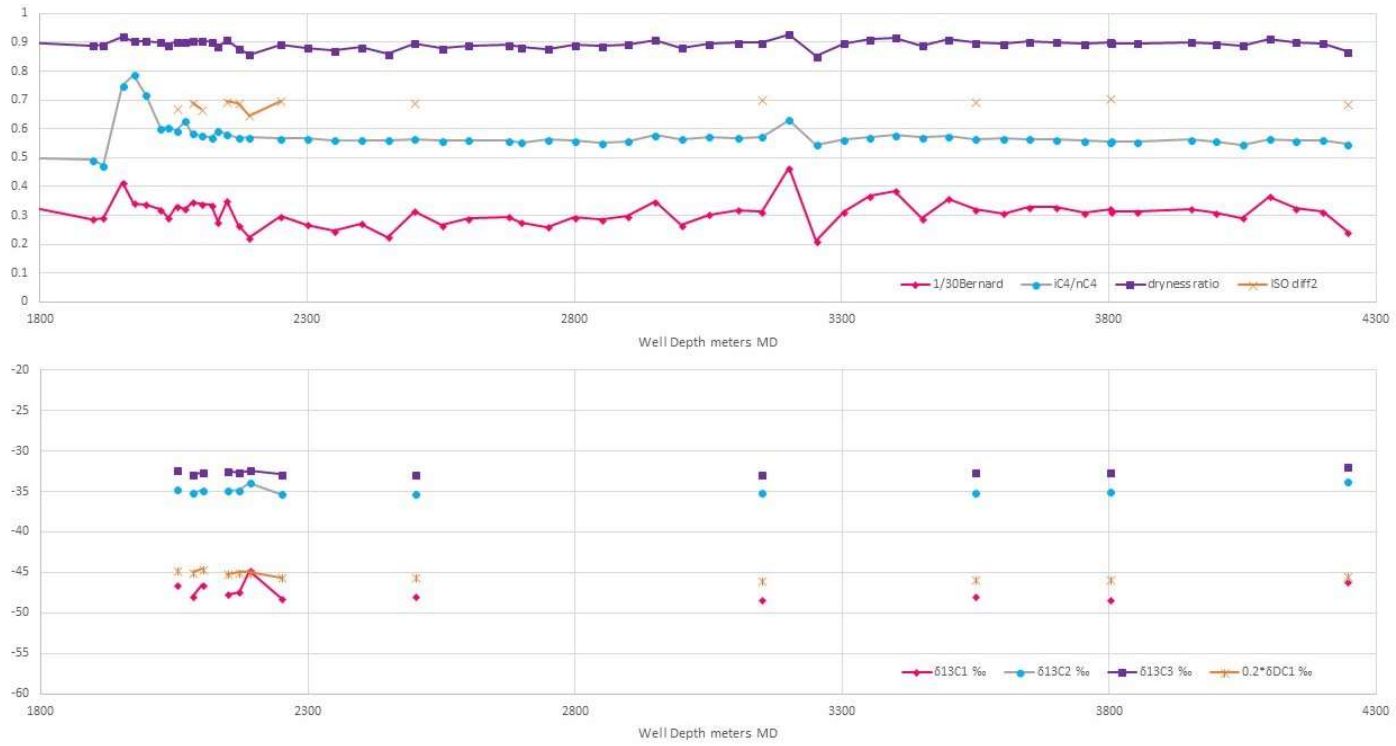

Figure A 73. Well profile, MC ratios and ISO data for WA#31491 (Montney HZ leg with uphole completion included).

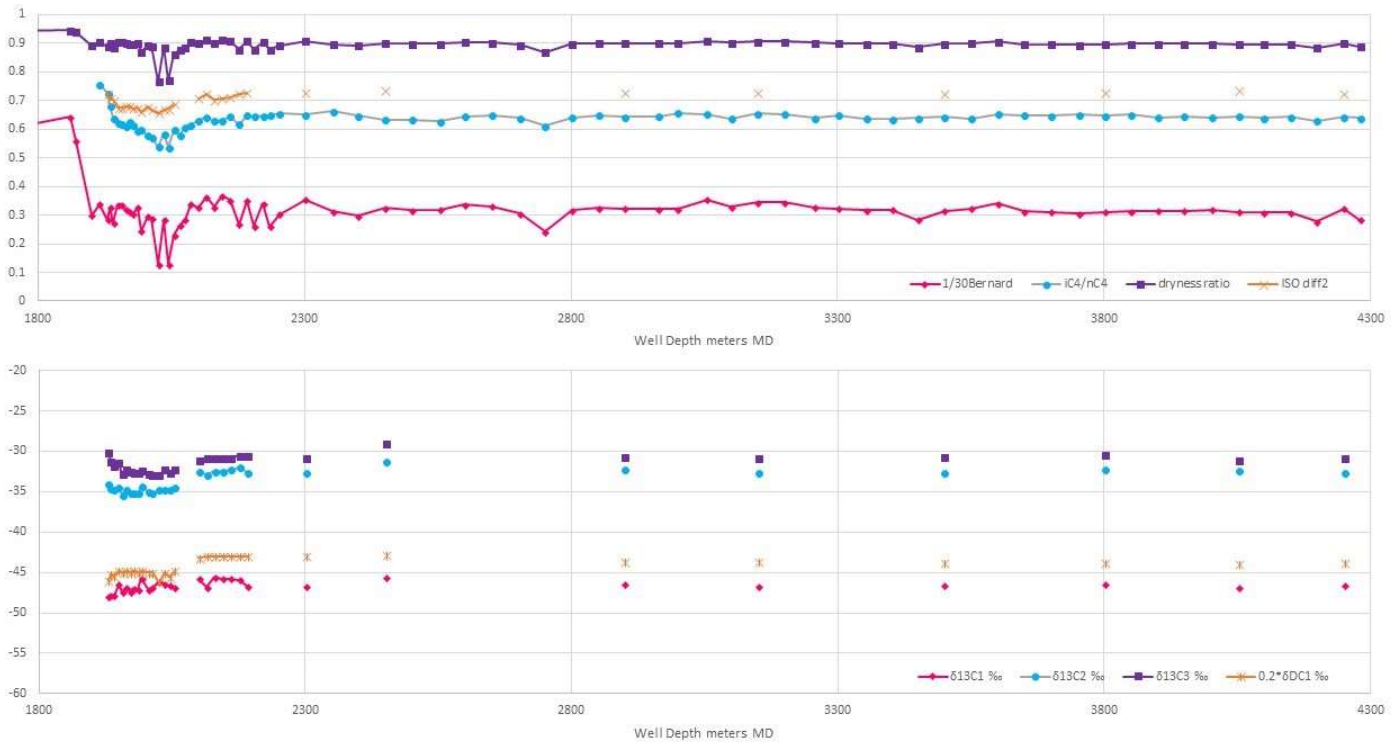

Figure A 74. Well profile, MC ratios and ISO data for WA#31492 (Montney HZ leg with uphole completion included).

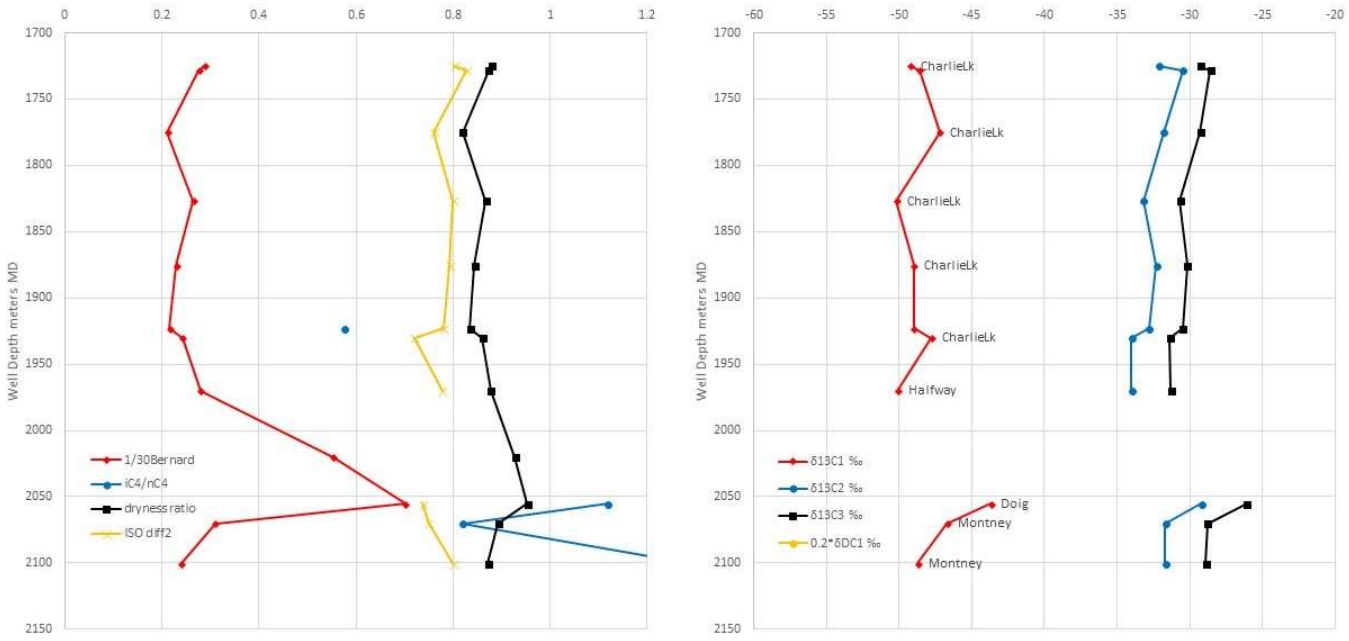

Figure A 75. Well profile, MC ratios and ISO data for WA#30316 (Jurassic to Triassic VT well. A vertical portion of a HZ well where the deviated section is data overlap with the HZ profile figure A80 (which starts in Doig). Key formation sampled with a deviation below which has samples but no analysis for isotopes, but the Doig Formation stands out even without the ISO data in this short profile).

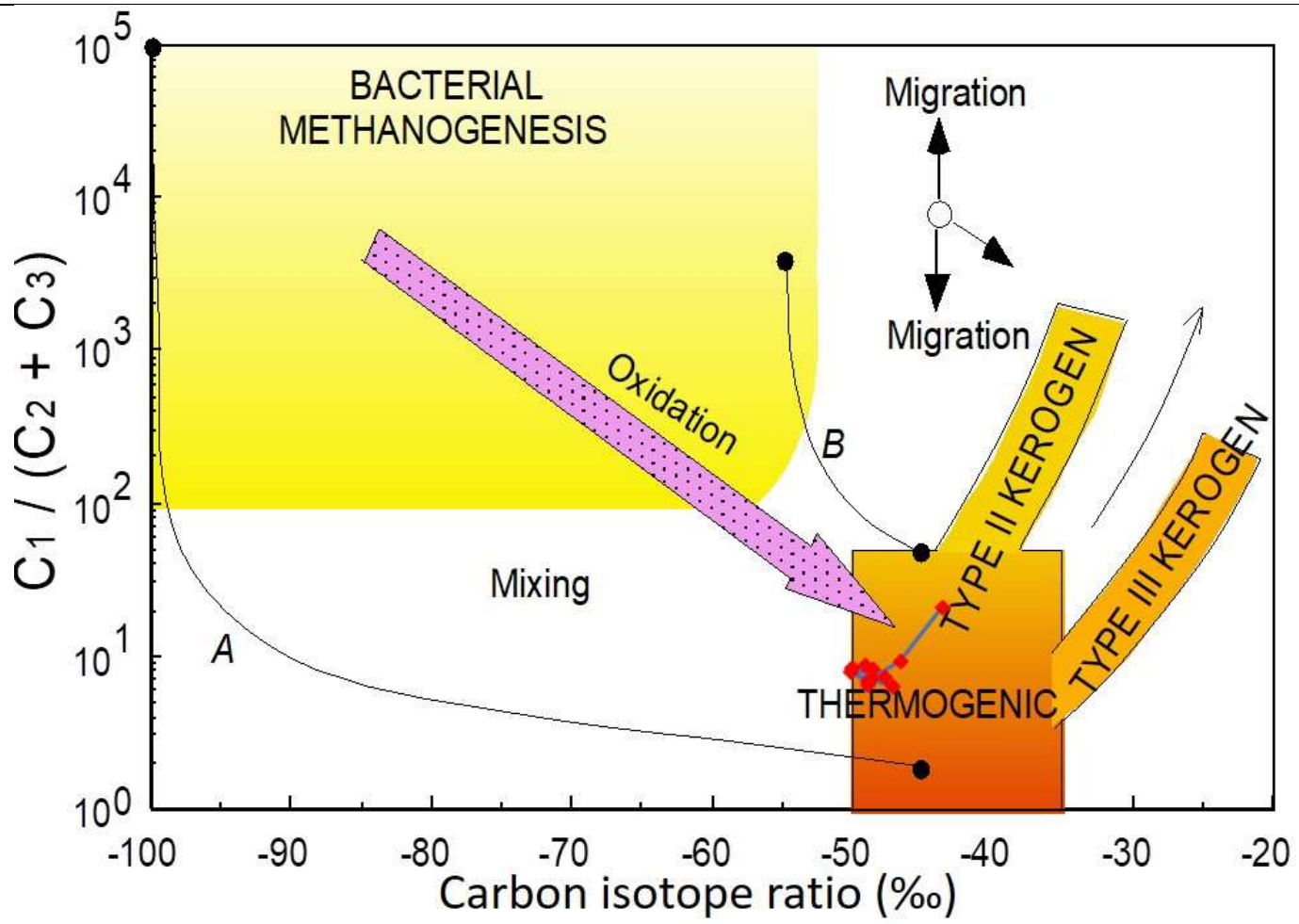

Figure A 76. ISO profile data – Interpretive Bernard Diagram for WA#30316 (Jurassic to Triassic VT well, Doig is apparent highest maturity, Whiticar, 2018 pers. comm., after Whiticar 1999).

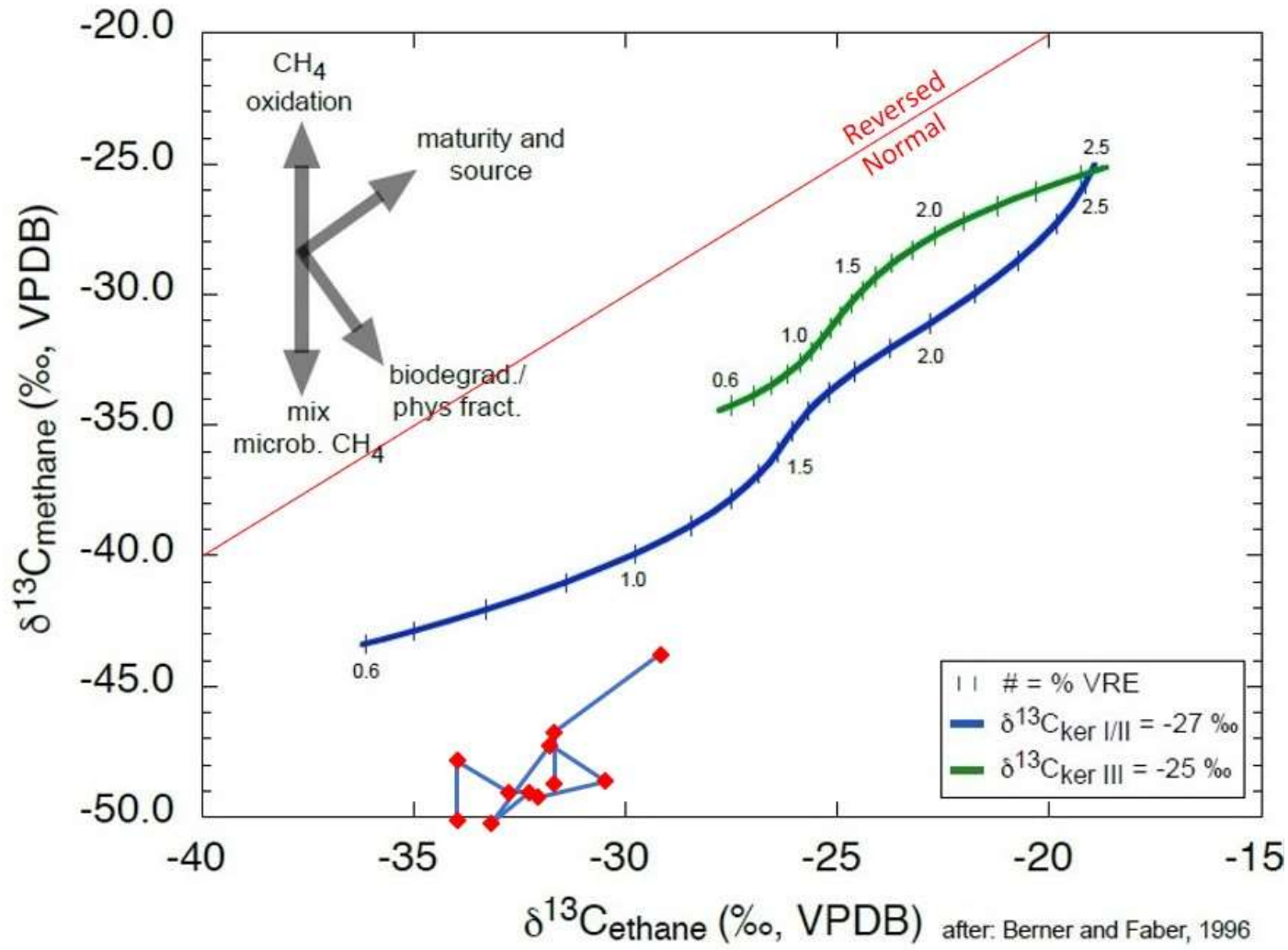

Figure A 77. ISO profile data – Interpretive ISO $\delta^{13}C_1$ versus $\delta^{13}C_2$ plot for WA#30316 (Jurassic to Triassic VT well. Charlie Lake sampling shows no change from kerogen line but Doig sample is the unusual deviation of higher maturity to the upper right with shallower and deeper formations having less apparent maturity, Whiticar, 2018 pers. comm., after Berner and Faber 1996, well profile trendline).

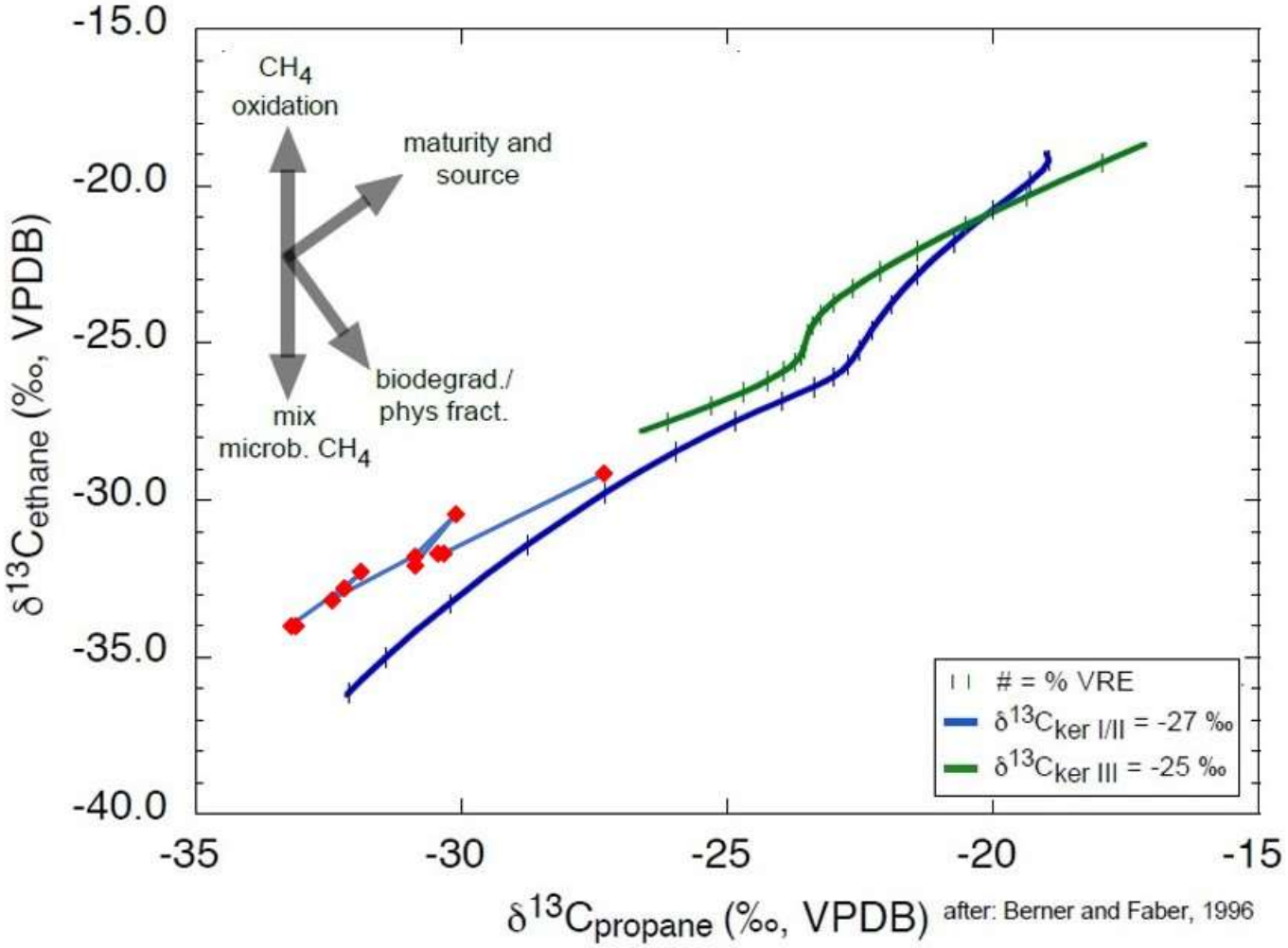

Figure A 78. ISO profile data – Interpretive ISO $\delta^{13}C_2$ versus $\delta^{13}C_3$ plot for WA#30316 (Jurassic to Triassic VT well. Doig sample is the unusual deviation of higher maturity to the upper right with shallower and deeper formations having less apparent maturity. Methane responds differently from ethane and propane, Whiticar, 2018 pers. comm., after Berner and Faber 1996, no trendlines).

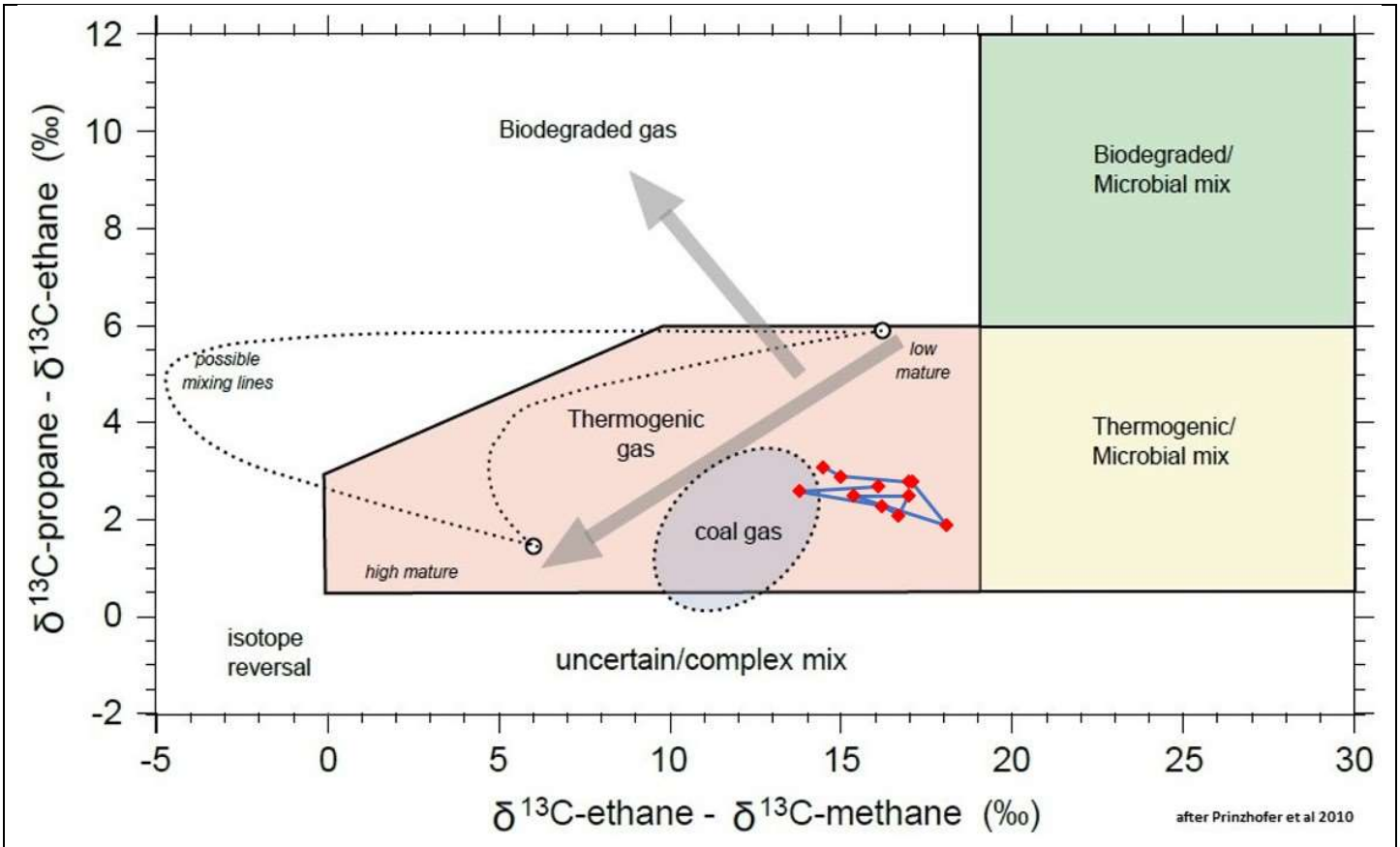

Figure A 79. Interpretive $\delta^{13}C_2$- $\delta^{13}C_1$ versus $\delta^{13}C_3$- $\delta^{13}C_2$ plot for WA#30316 (Jurassic to Triassic VT well. The Montney appears more mixed biogenic [thermal and microbial] than other Montney HZ results).

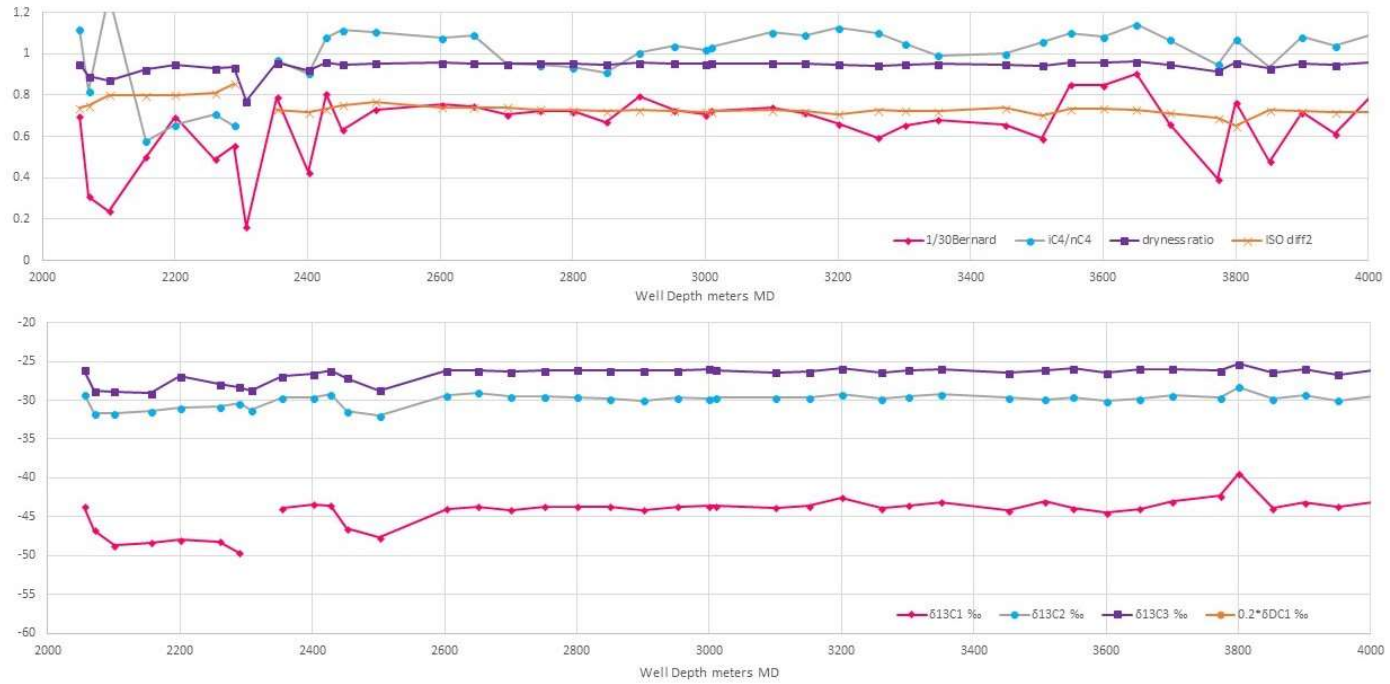

Figure A 80. Well profile, MC ratios and ISO data for WA#30316 (Montney HZ leg with uphole completion included).

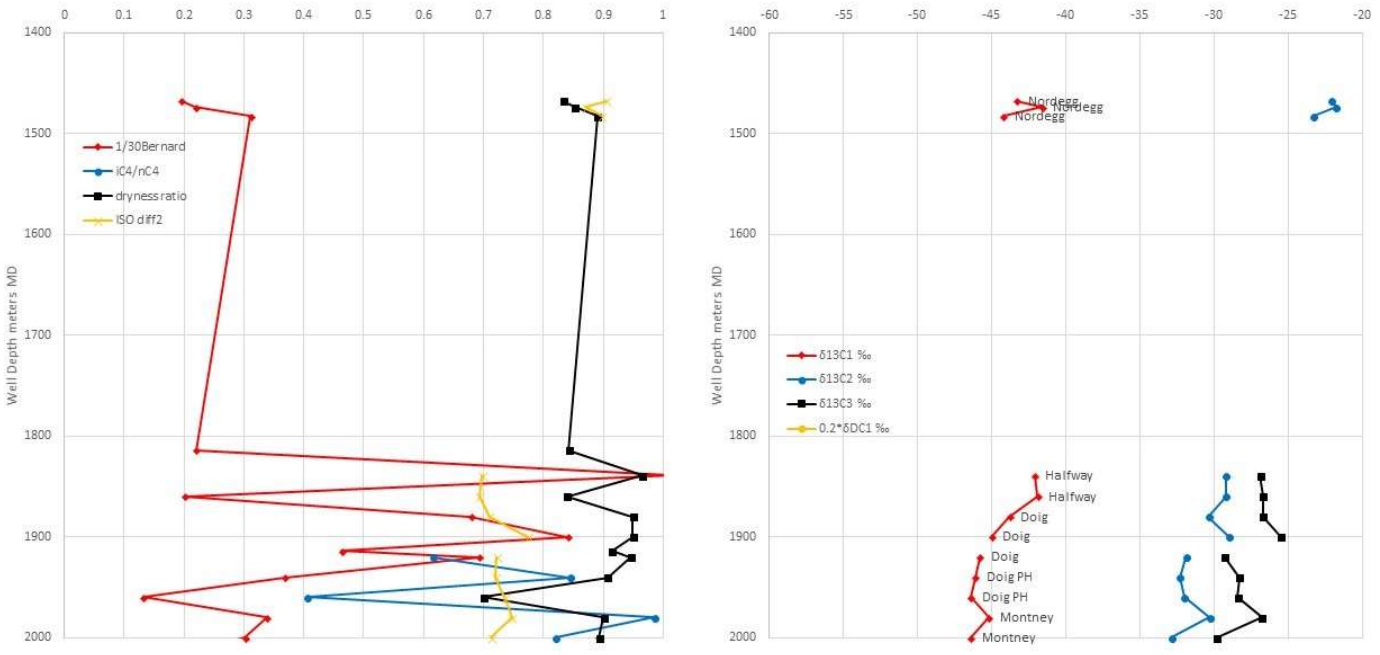

Figure A 81. Well profile, MC ratios and ISO data for WA#28770 (Jurassic to Triassic VT well – A vertical portion of a HZ well where the deviated section is data overlap with the HZ profile figure A86 (which starts in Doig). Key formations are skipped and all Triassic formations are on a similar trend).

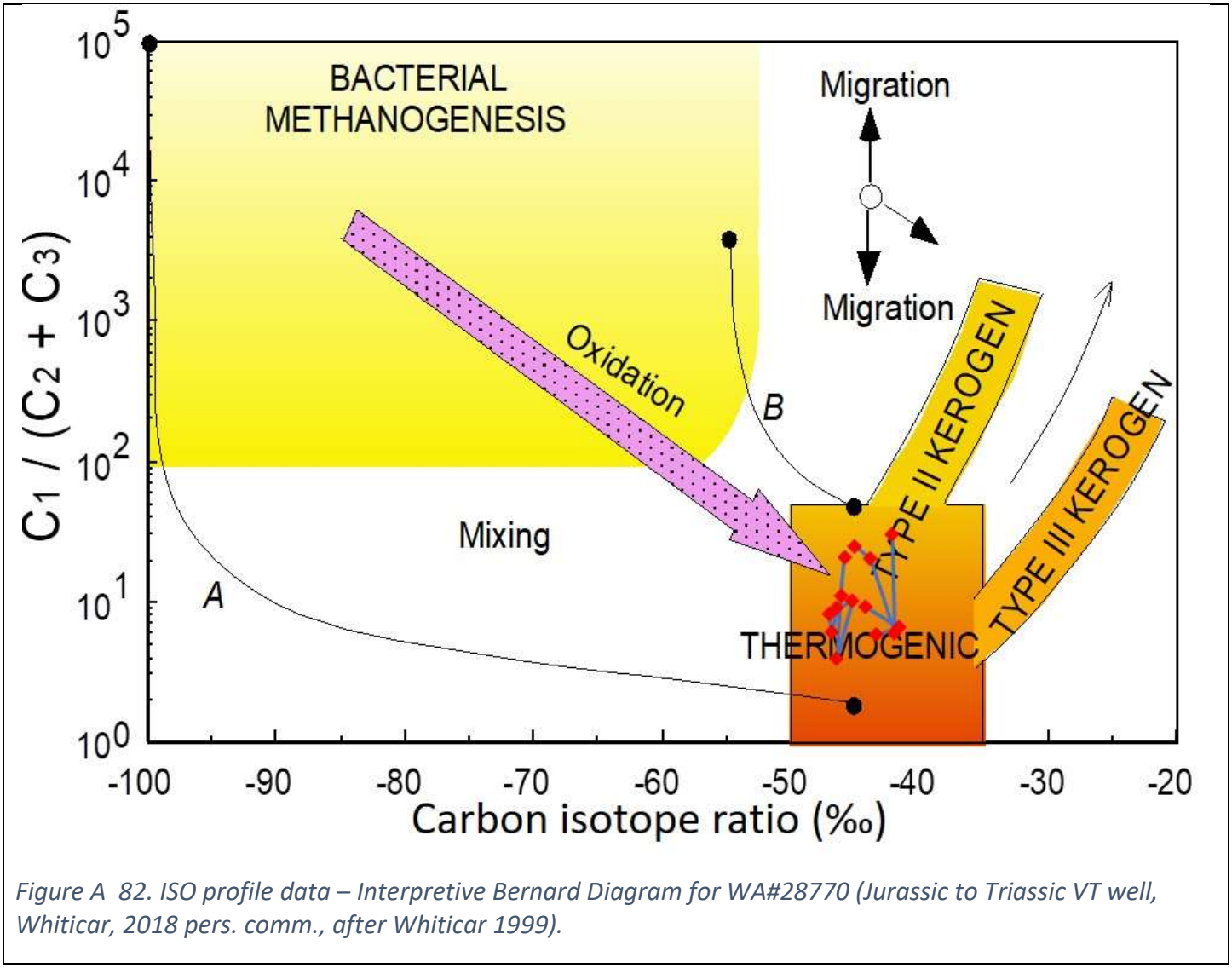

Figure A 82. ISO profile data – Interpretive Bernard Diagram for WA#28770 (Jurassic to Triassic VT well, Whiticar, 2018 pers. comm., after Whiticar 1999).

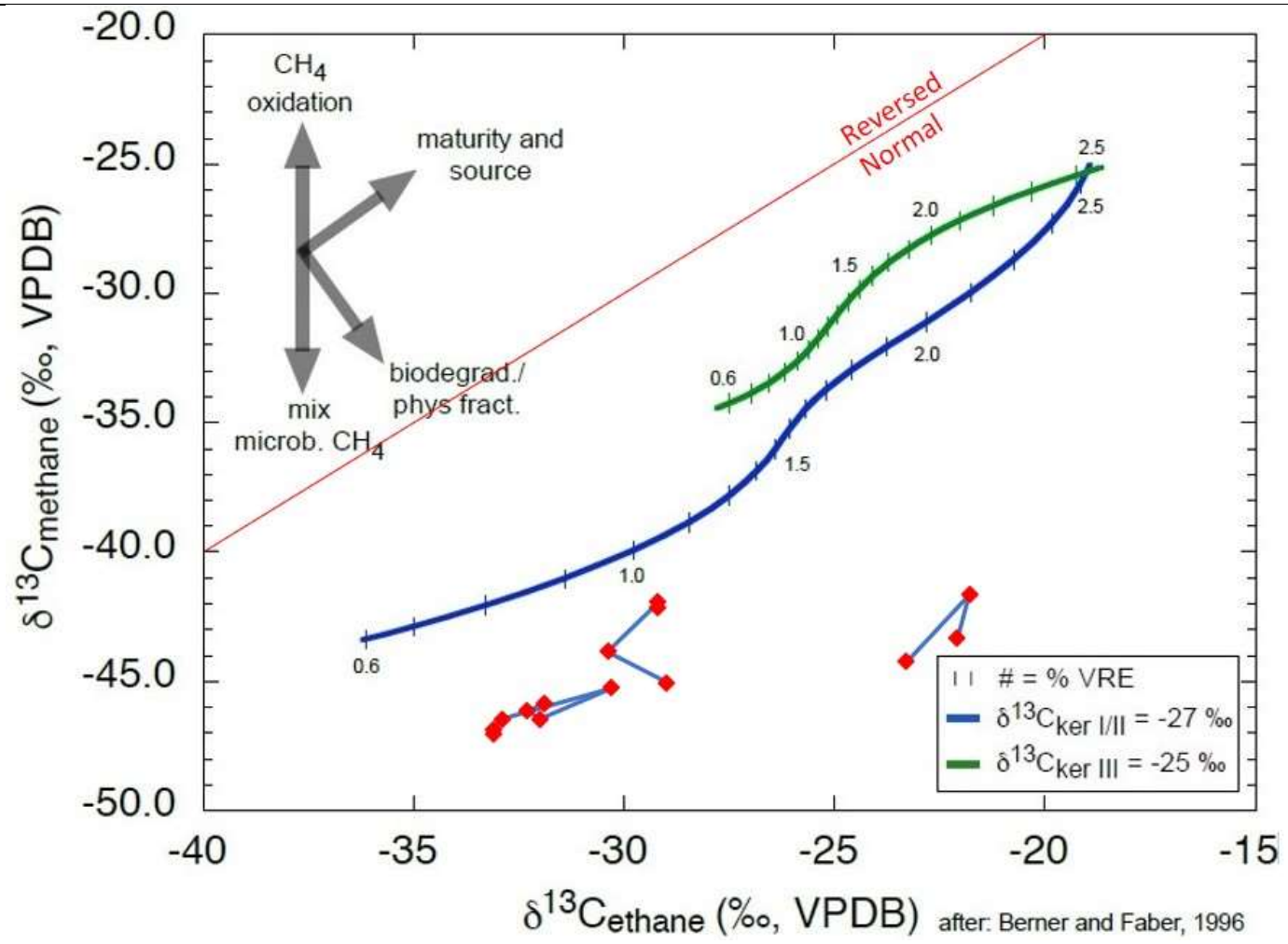

Figure A 83. ISO profile data – Interpretive ISO $\delta^{13}C_1$ versus $\delta^{13}C_2$ plot for WA#28770 (Jurassic to Triassic VT well. Data from shallower strata appears very different and far higher "maturity" from deeper strata with 2 different trends, Whiticar, 2018 pers. comm., after Berner and Faber 1996, well profile trendlines).

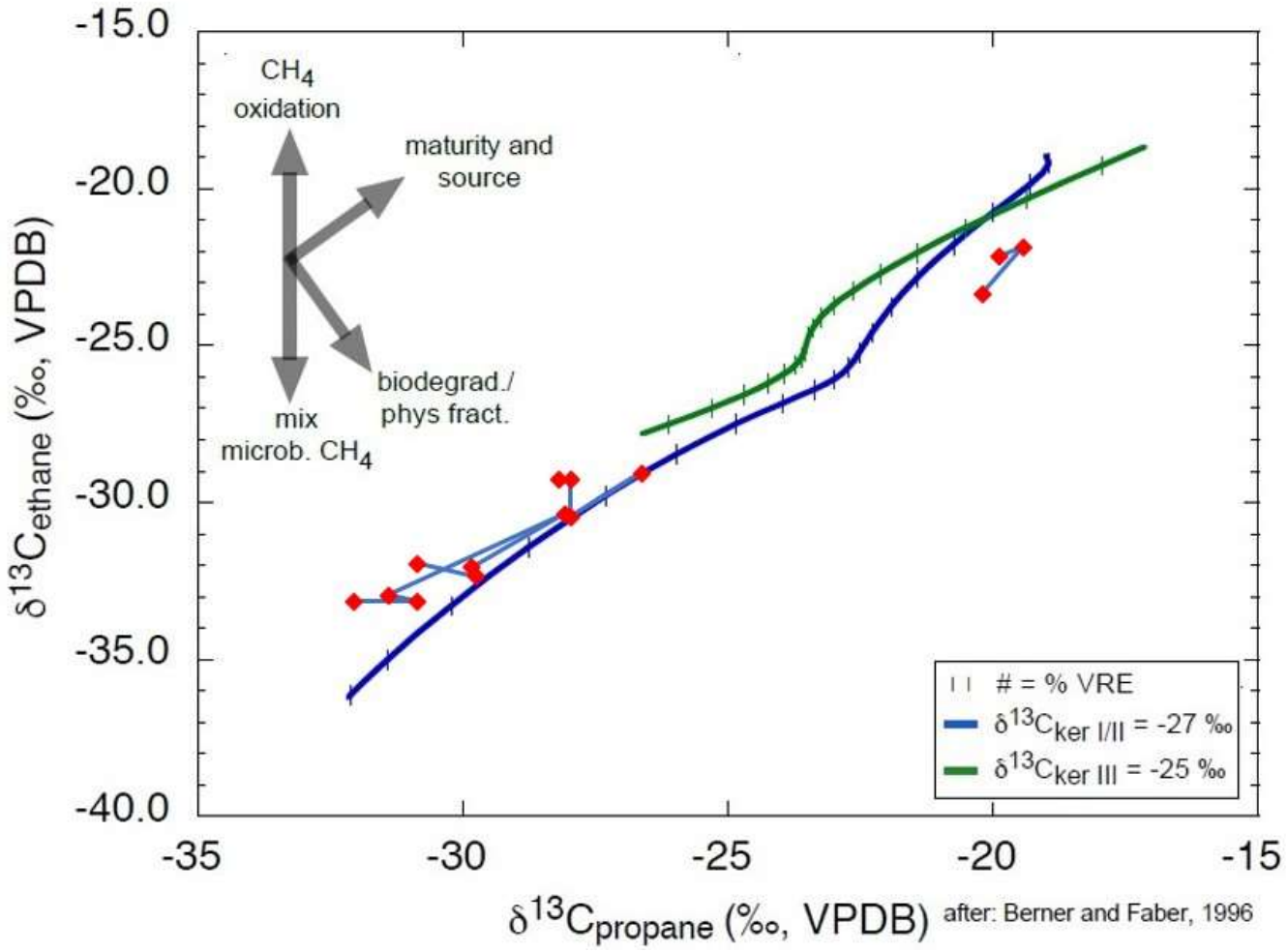

Figure A 84. ISO profile data – Interpretive ISO $\delta^{13}C_2$ versus $\delta^{13}C_3$ plot for WA#28770 (Jurassic to Triassic VT well. Data from shallower strata appears very different and far higher "maturity" from deeper strata, but both have methane responding differently from ethane and propane). (Whiticar, 2018 pers. comm., after Berner and Faber 1996, well profile trendlines).

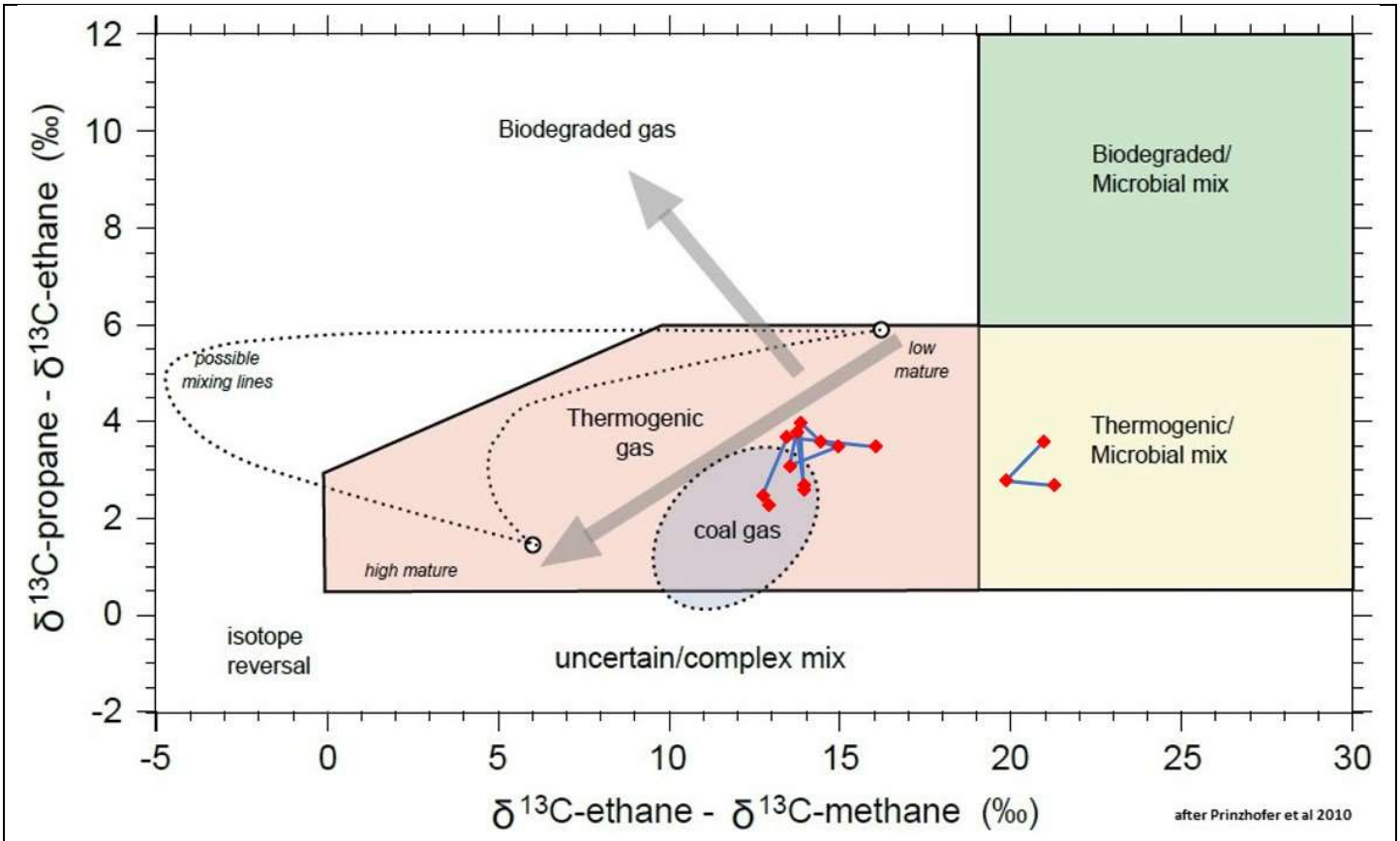

Figure A 85. Interpretive $\delta^{13}C_2$- $\delta^{13}C_1$ versus $\delta^{13}C_3$- $\delta^{13}C_2$ plot for WA#28770 (Jurassic to Triassic VT well. Shallow strata on the right is even more mixed low maturity and the start of the Montney in the vertical section is closer to "coal gas" of HZ Montney diagram).

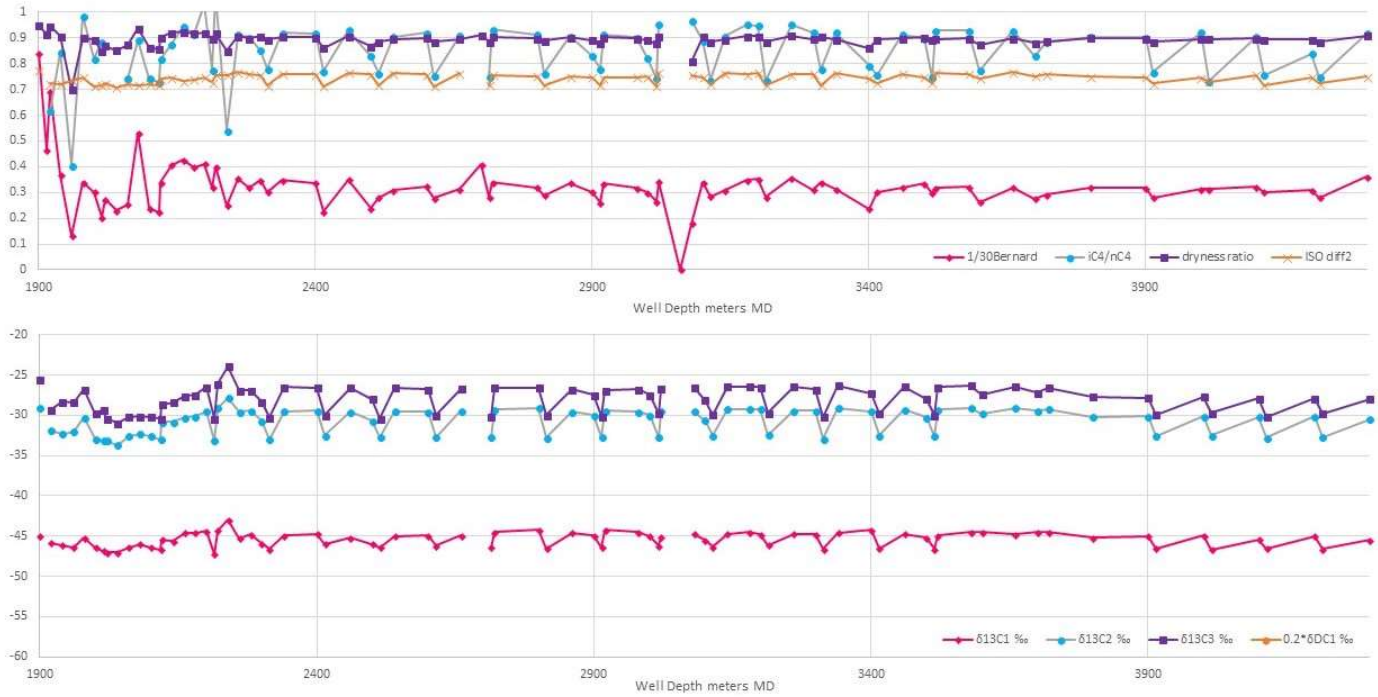

Figure A 86. Well profile, MC ratios and ISO data for WA#28770 (Montney HZ leg with uphole completion included – this is a sample type exception, this profile is multiple sidetracks reported as one well and result as a sawtooth plot).

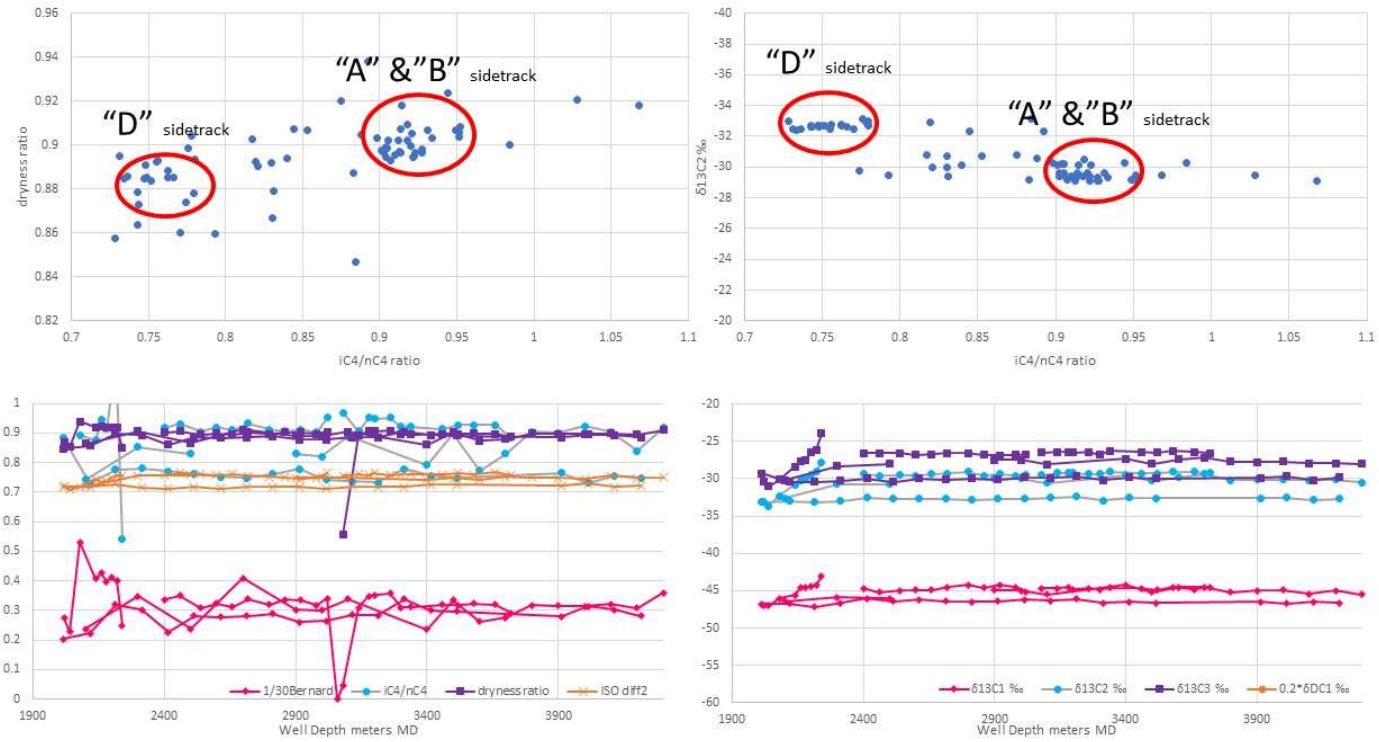

Figure A 87. Special analysis as iC4/nC4 plots for WA#28770 (Montney HZ leg with uphole completion included. The plot of dryness vs iC4/nC4 is not really a strong indication as there is more scatter, but the $\delta^{13}C2$ or $\delta^{13}C3$ vs iC4/nC4 has two fairly tight groupings that correspond very well with the main Montney producing horizon in the three sidetracks. The points outside the circles are in other formations corresponding to the heel of the HZ section that has a strong profile deviation. The profiles are revised to separate the sidetracks. Why is the one sidetrack so different from the others?)

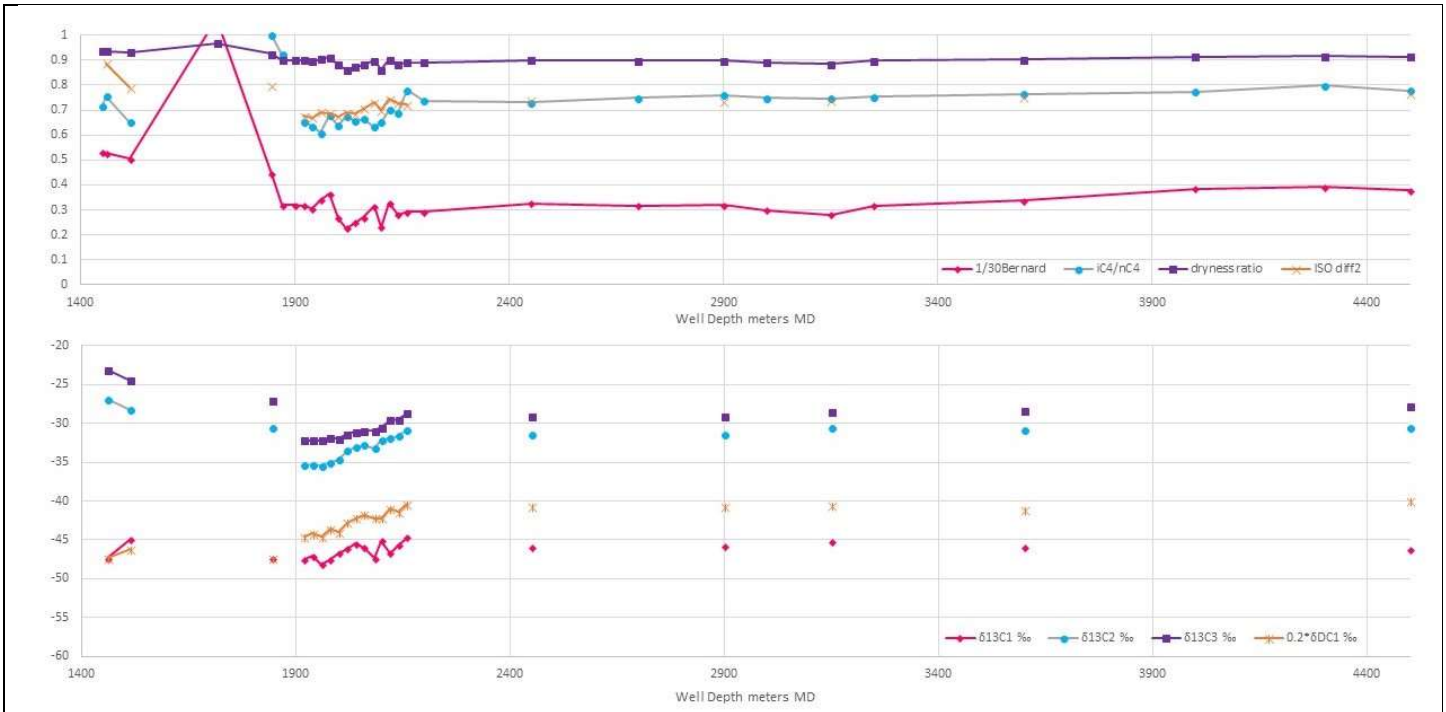

Figure A 88. Well profile, MC ratios and ISO data for WA#30406 (Montney HZ leg with uphole completion included).

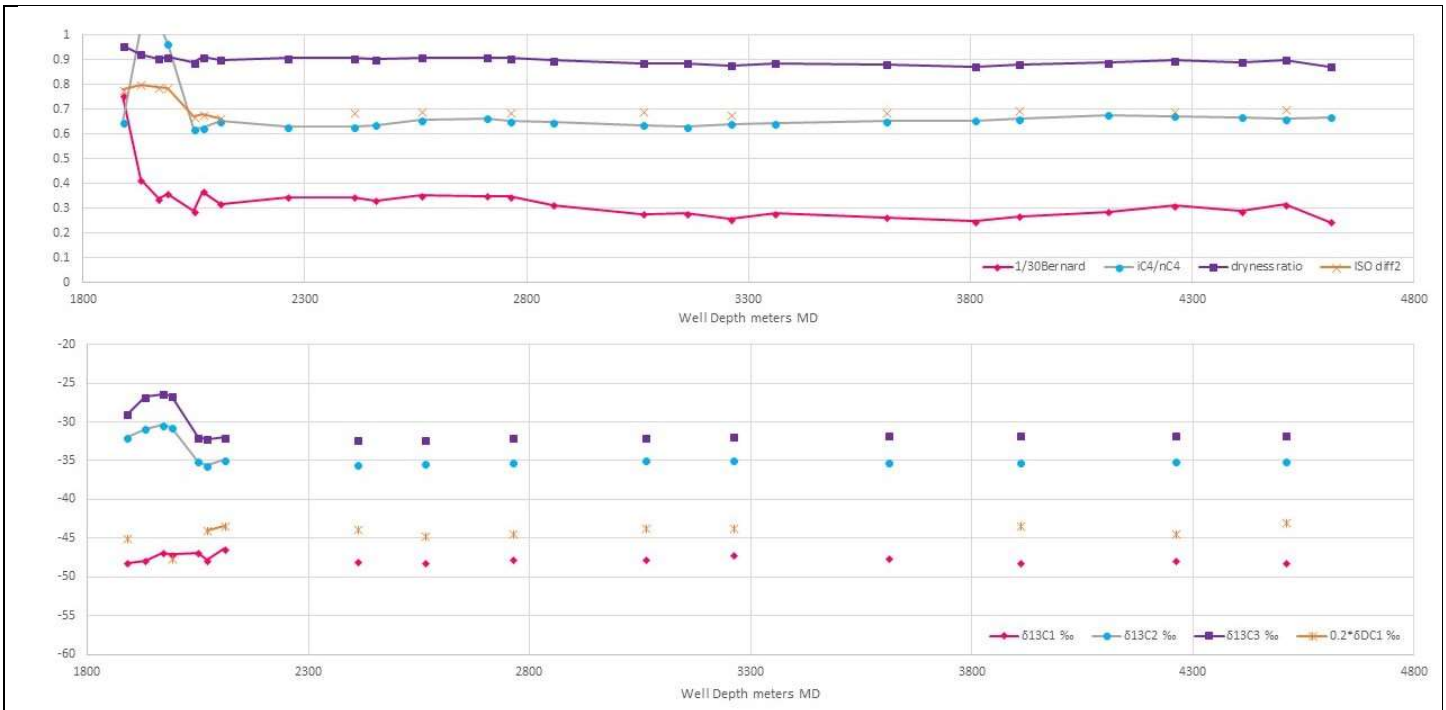

Figure A 89. Well profile, MC ratios and ISO data for WA#30407 (Montney HZ leg with uphole completion included).

No DATA

Figure A 90. Well profile, MC ratios not shown when null ISO data WA#30408.

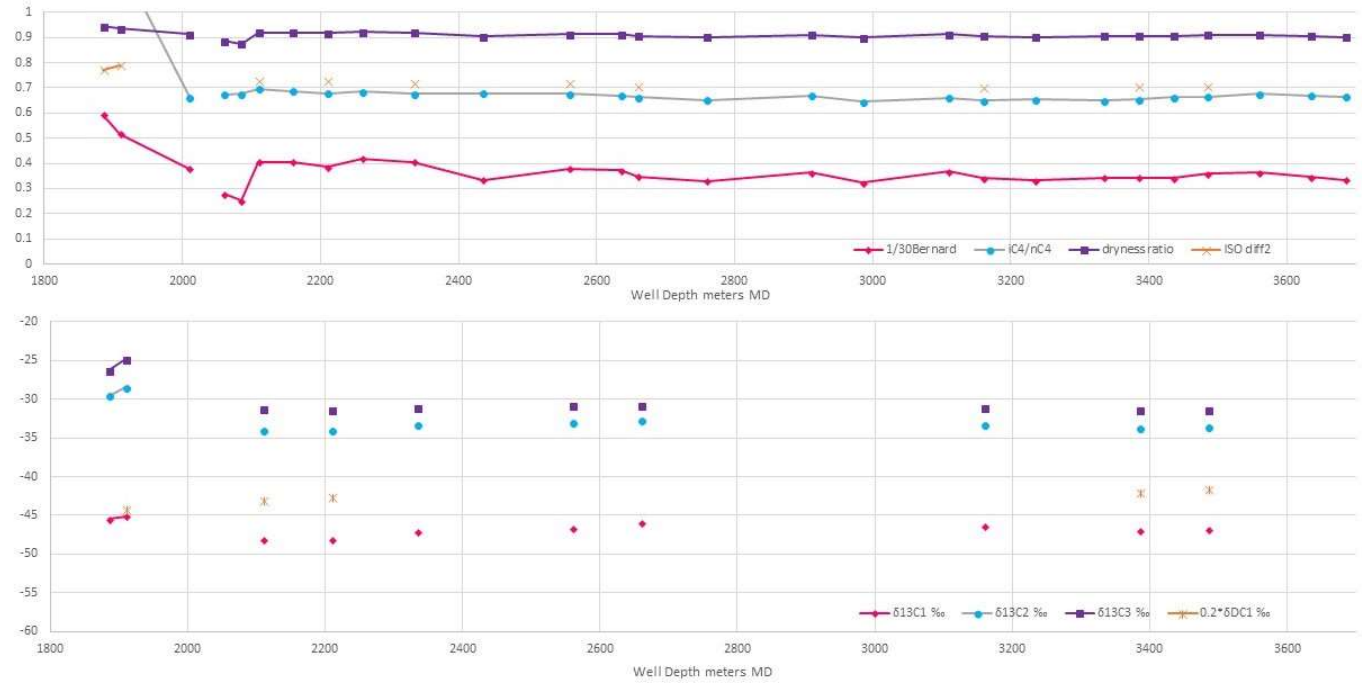

Figure A 91. Well profile, MC ratios and ISO data for WA#28239 (Montney HZ leg with uphole completion included).

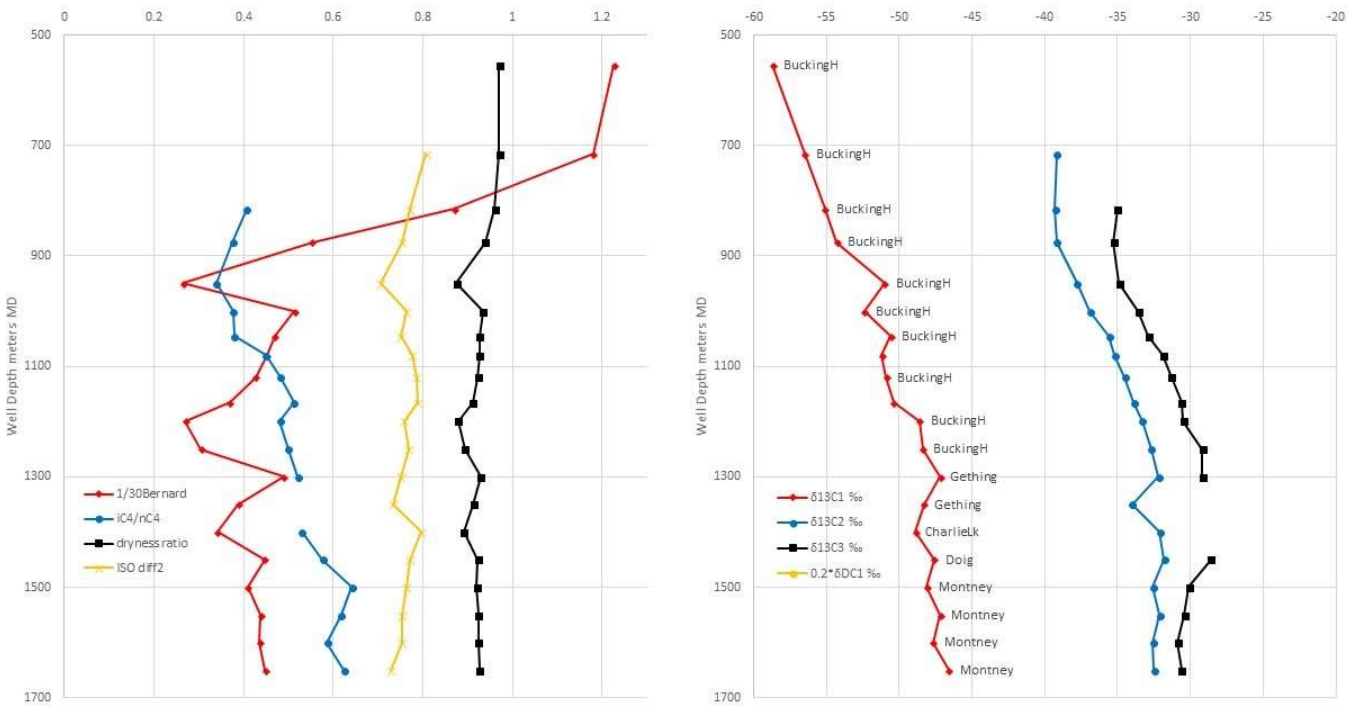

Figure A 92. Well profile, MC ratios and ISO data for WA#29344 (Upper Cretaceous to Triassic VT well. This was an example profile to show a "classic profile" over the complete strata with broad sampling in this case. There is shallow biogenic trending to regular deeper gas with a subtle Gething spike).

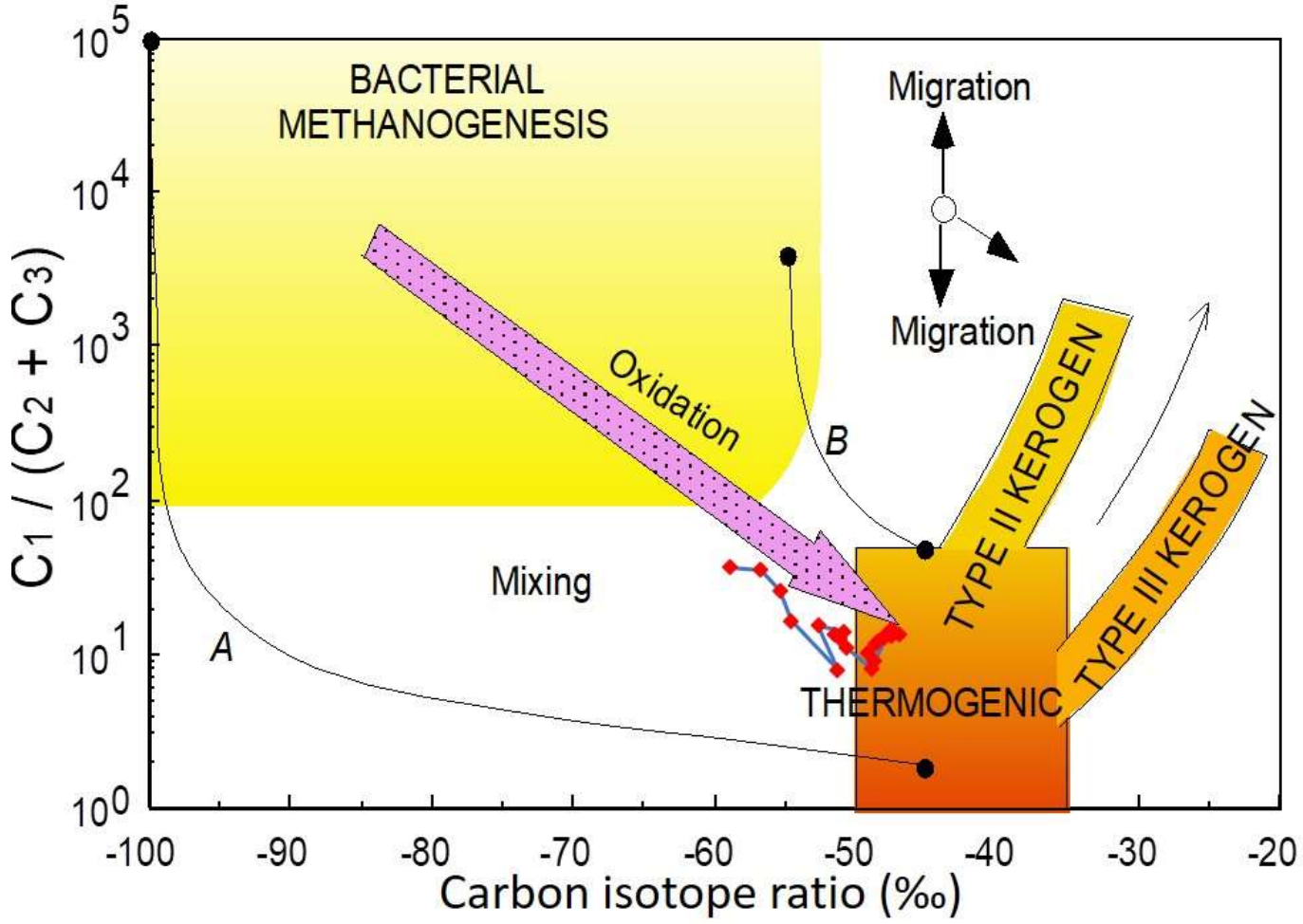

Figure A 93. ISO profile data – Interpretive Bernard Diagram for WA#29344 (Upper Cretaceous to Triassic VT well. The classic profile applies only to a certain stratigraphic limit and then there appears to be stratigraphic sectioning of the geochemistry, Whiticar, 2018 pers. comm., after Whiticar 1999).

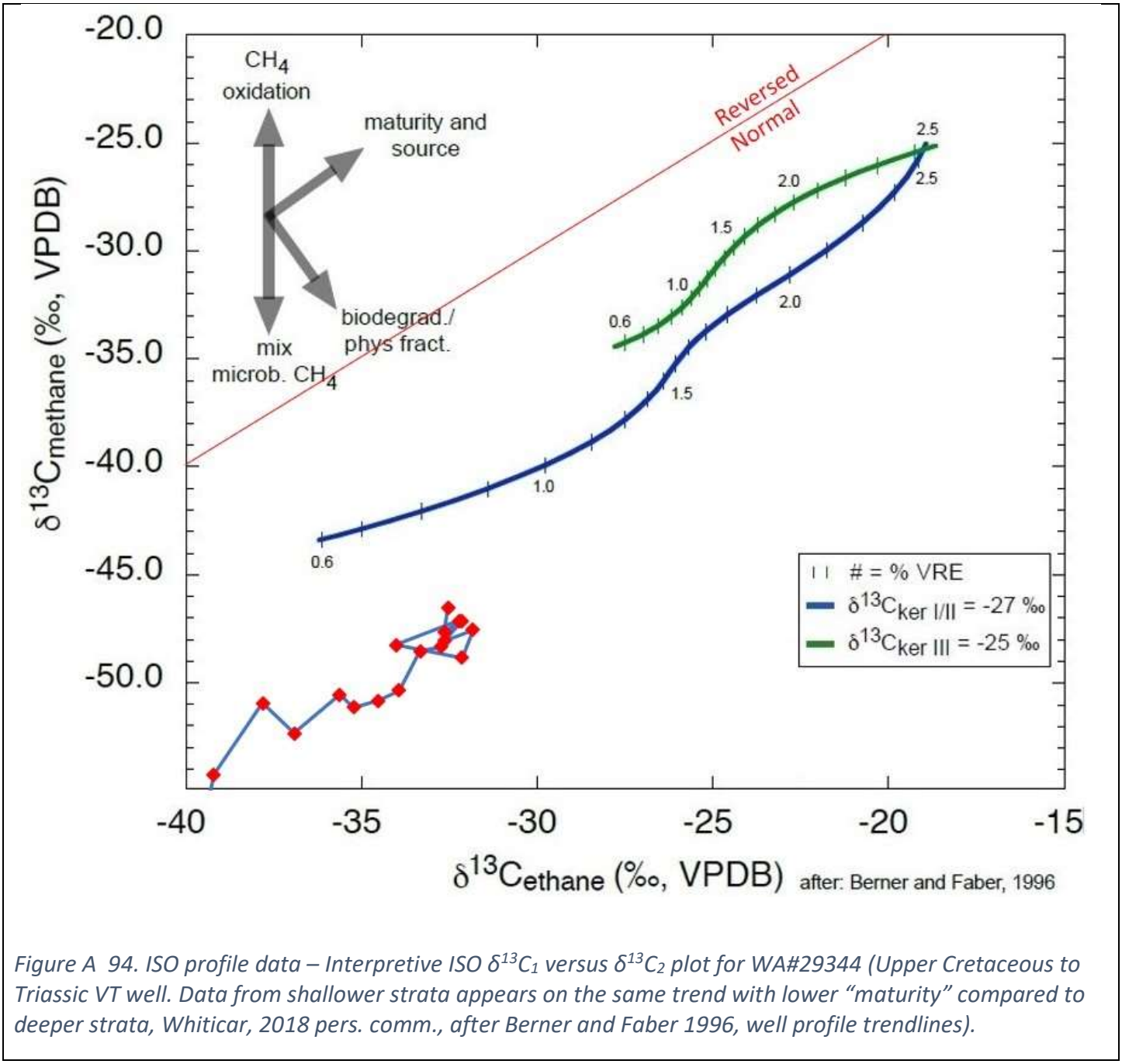

Figure A 94. ISO profile data – Interpretive ISO $\delta^{13}C_1$ versus $\delta^{13}C_2$ plot for WA#29344 (Upper Cretaceous to Triassic VT well. Data from shallower strata appears on the same trend with lower "maturity" compared to deeper strata, Whiticar, 2018 pers. comm., after Berner and Faber 1996, well profile trendlines).

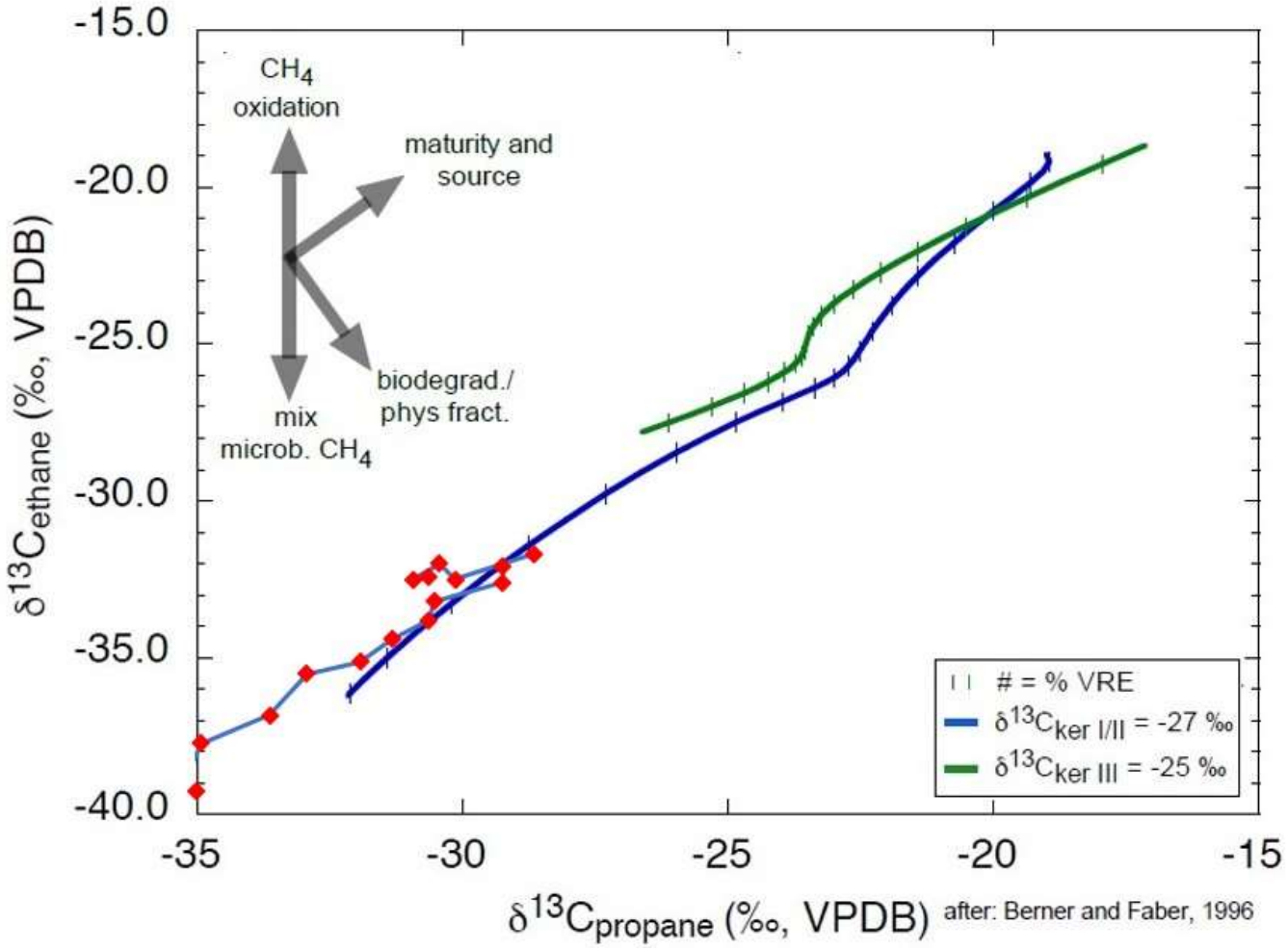

Figure A 95. ISO profile data – Interpretive ISO $\delta^{13}C_2$ versus $\delta^{13}C_3$ plot for WA#29344 (Upper Cretaceous to Triassic VT well. Data from shallower strata appears on the same trend with lower "maturity" compared to deeper strata, but both have methane responding differently from ethane and propane, Whiticar, 2018 pers. comm., after Berner and Faber 1996, no trendlines).

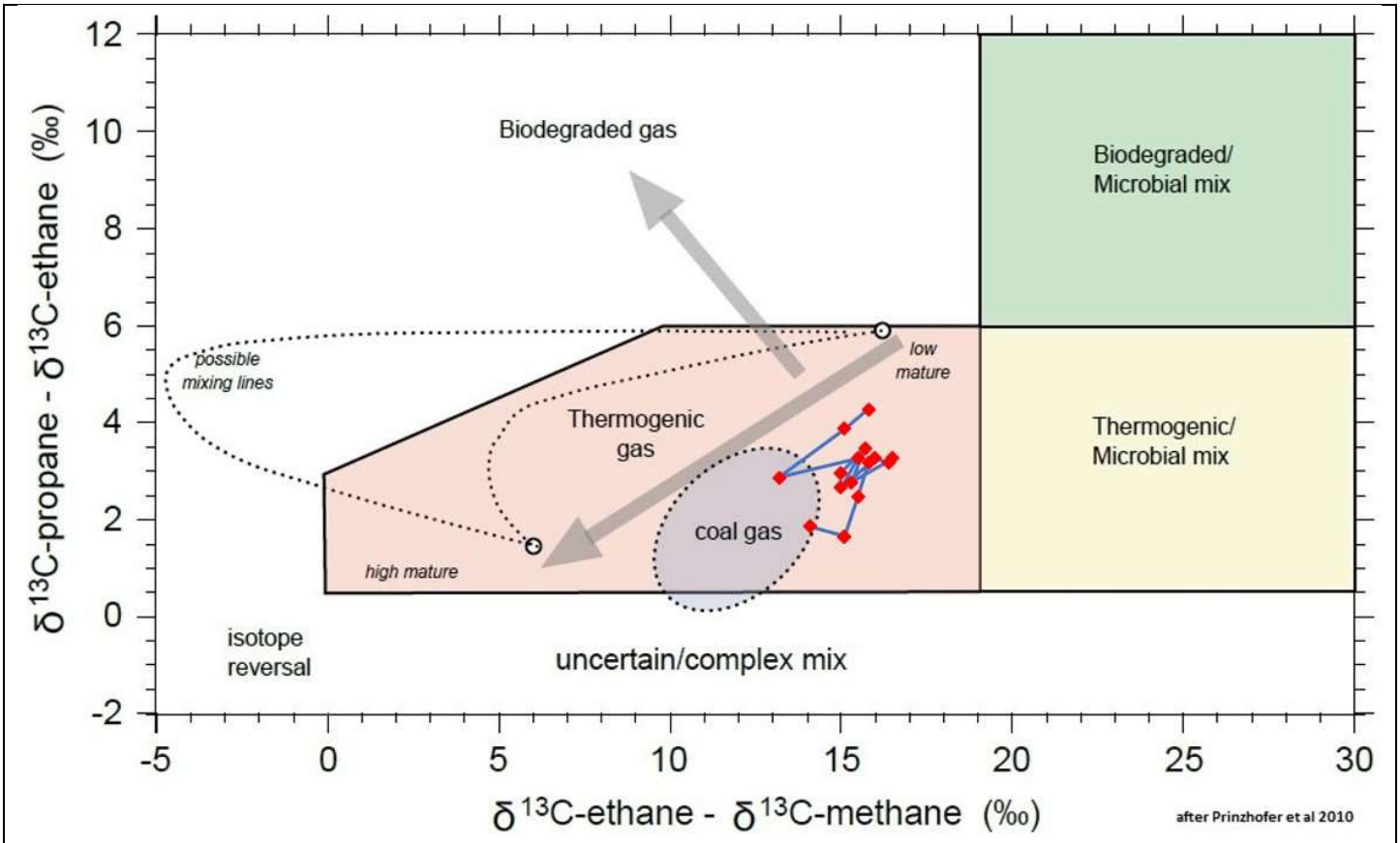

Figure A 96. Interpretive $\delta^{13}C_2$- $\delta^{13}C_1$ versus $\delta^{13}C_3$- $\delta^{13}C_2$ plot for WA#29344 (Upper Cretaceous to Triassic VT well. Shallow strata on the upper right starts trending to the "coal gas" of HZ Montney diagram as figure A05, but then it deviates back to the right as even more mixed low maturity until the middle member of the Montney).

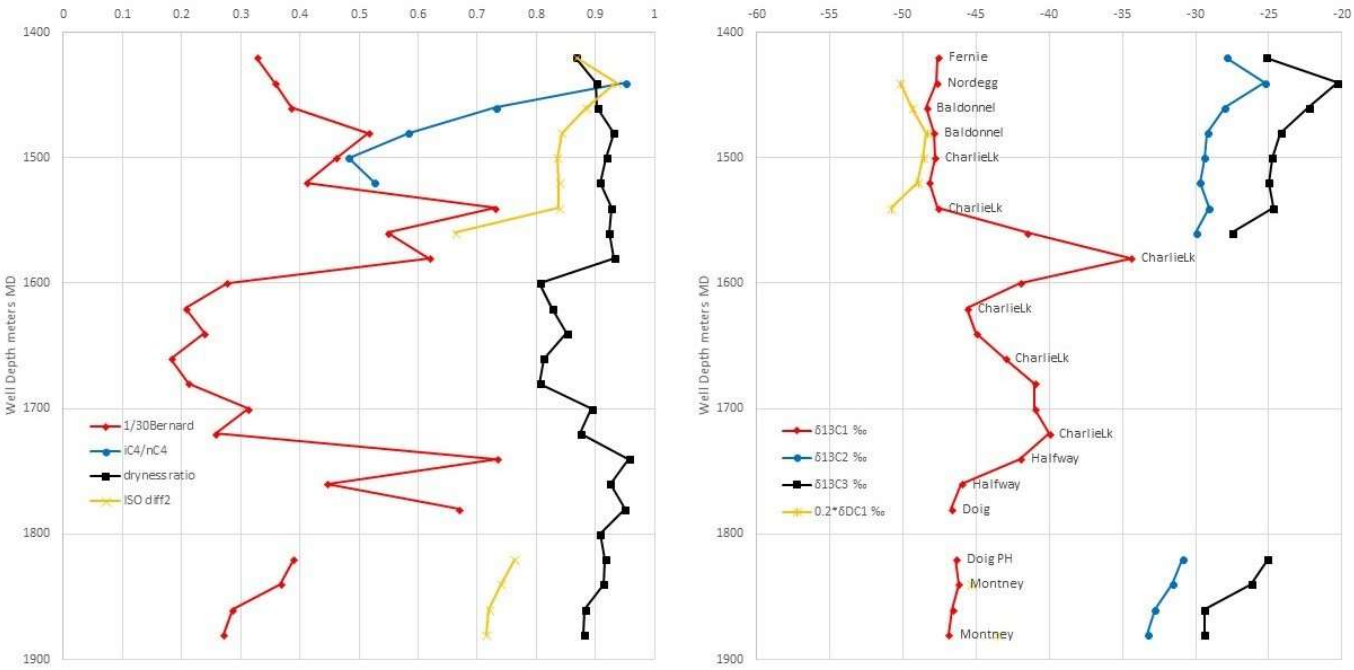

Figure A 97. Well profile, MC ratios and ISO data for WA#28588 (Jurassic to Triassic VT well. This was an example profile to show a "classic profile" over the complete strata with detailed sampling in this case - notice the change in member resolution. Despite sampling, advanced data is not available in the center strata).

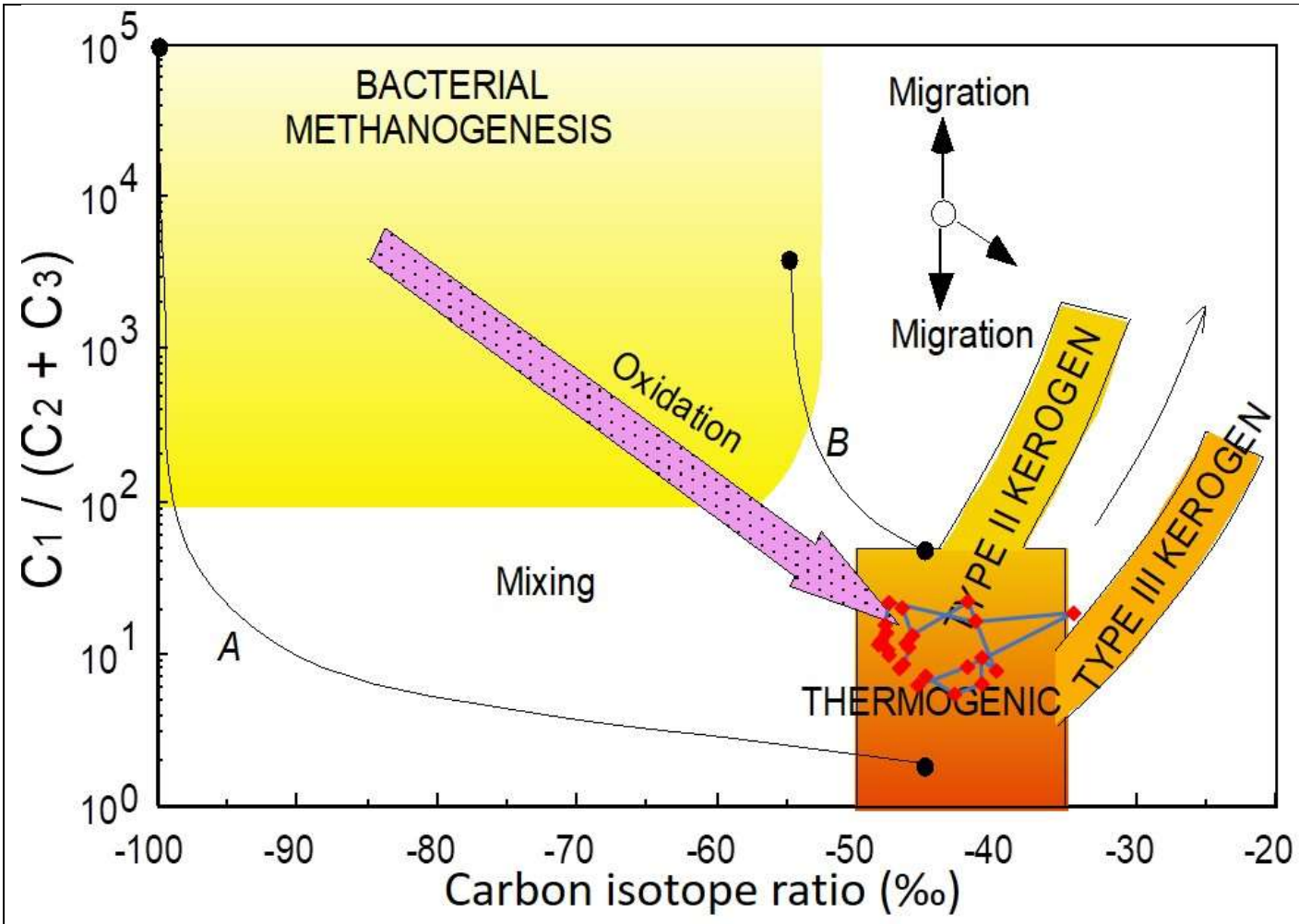

Figure A 98. ISO profile data – Interpretive Bernard Diagram for WA#28588 (Jurassic to Triassic VT well. This level of analysis shows thermogenic gas types for all strata, but Charlie Lake Formation is skewed to Type III kerogen, Whiticar, 2018 pers. comm., after Whiticar 1999).

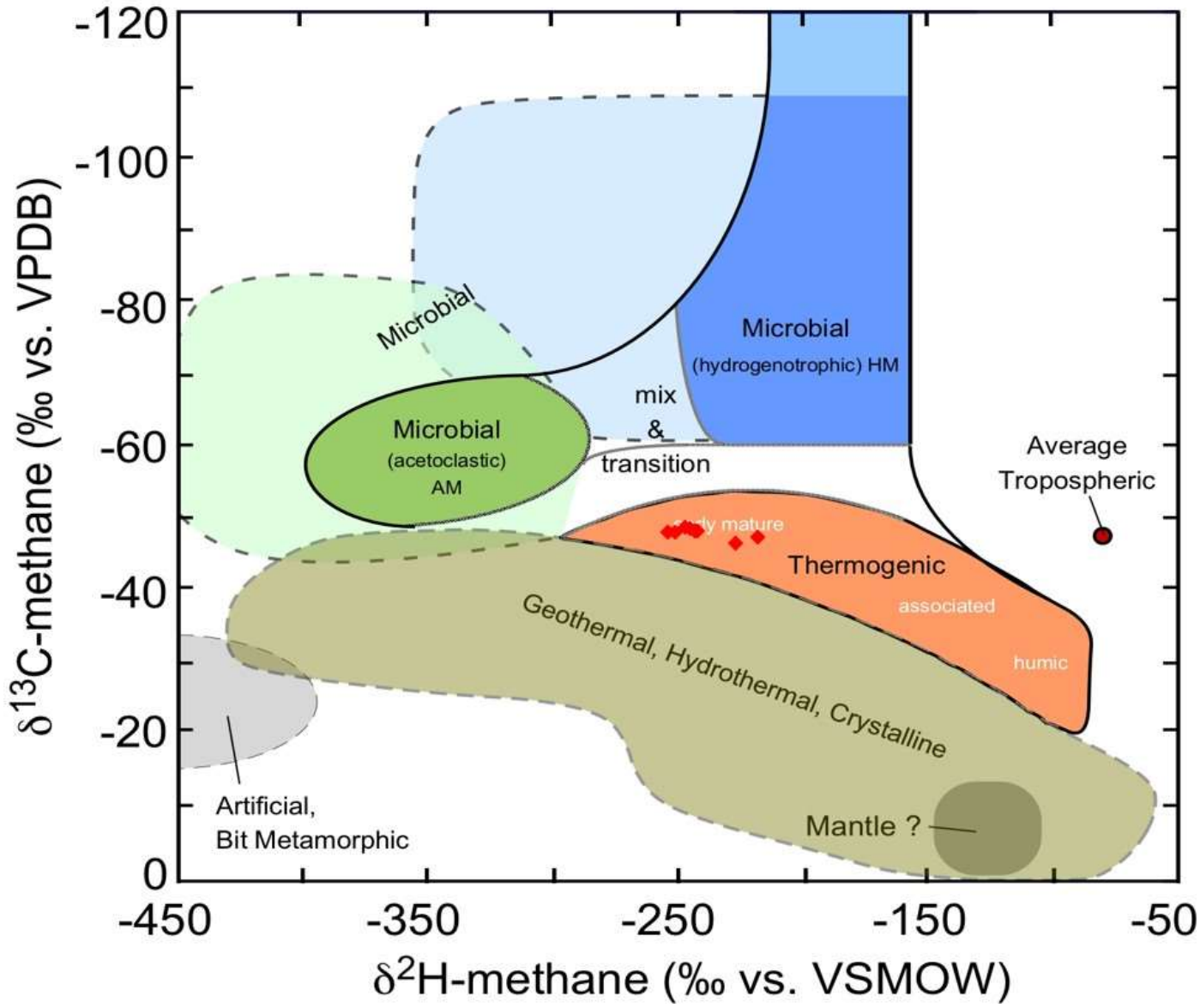

Figure A 99. ISO profile data – Interpretive CD Diagram for WA#28588 (Jurassic to Triassic VT well. This level of analysis shows thermogenic gas types for all strata, Whiticar, 2018 pers. comm., after Whiticar 1999).

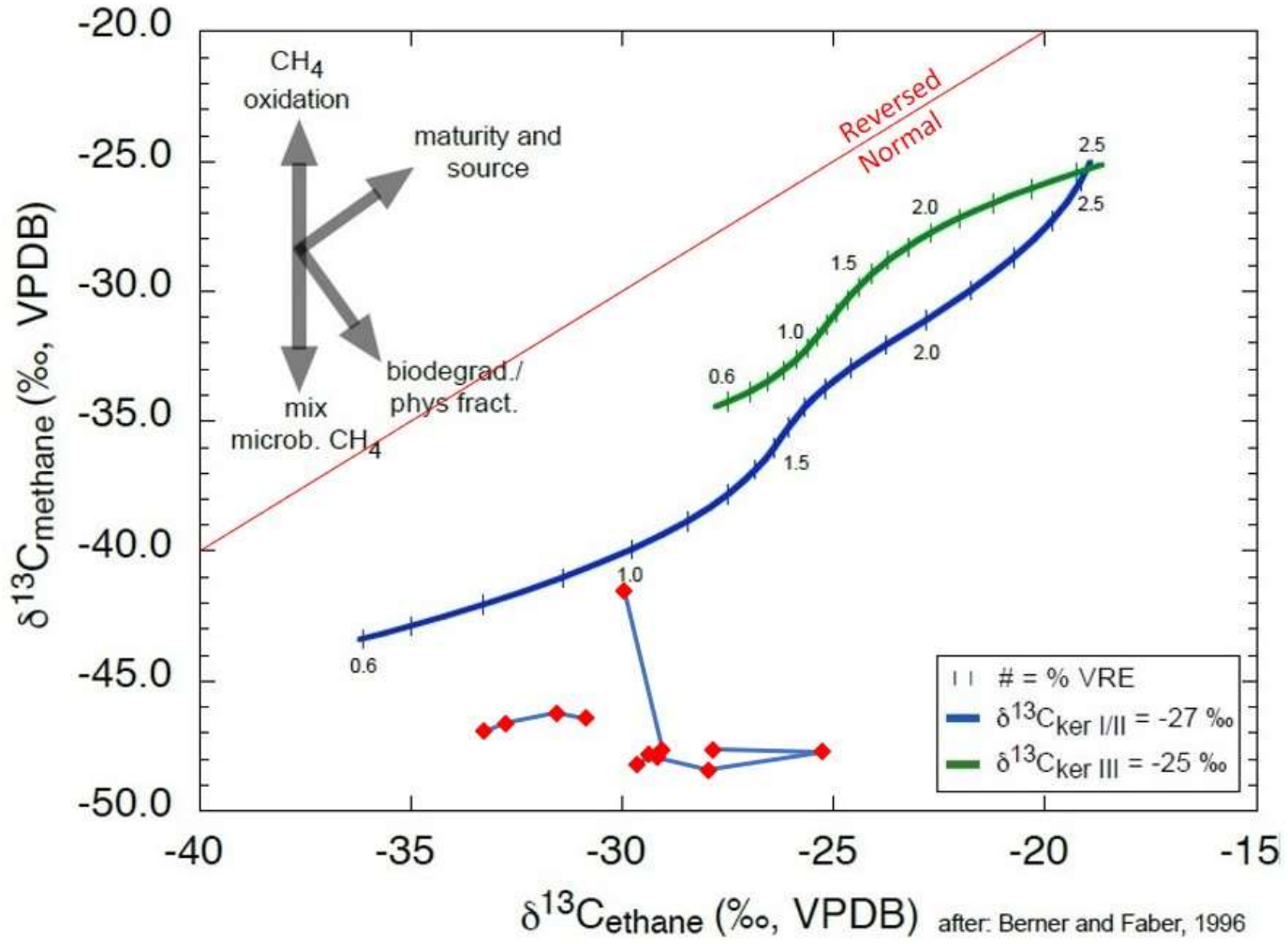

Figure A 100. ISO profile data – Interpretive ISO $\delta^{13}C_1$ versus $\delta^{13}C_2$ plot for WA#28588 (Jurassic to Triassic VT well. Charlie Lake Formation in the middle strata shows a return from $\delta^{13}C1$ depleted to kerogen II that contrasts with kerogen III from Bernard diagram, Whiticar, 2018 pers. comm., after Berner and Faber 1996, well profile trendlines).

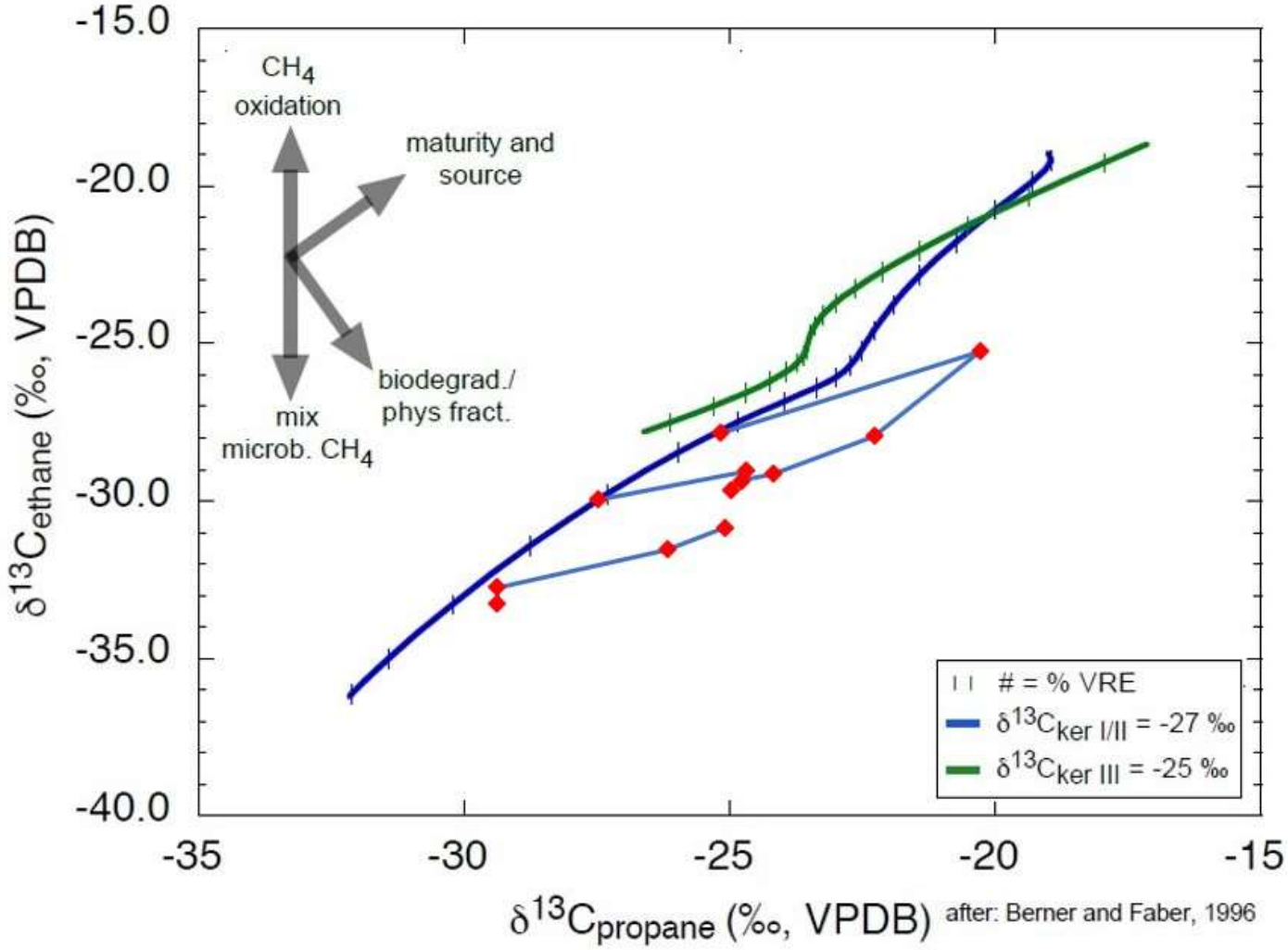

Figure A 101. ISO profile data – Interpretive ISO $\delta^{13}C_2$ versus $\delta^{13}C_3$ plot for WA#28588 (Jurassic to Triassic VT well [same points as previous diagram]. The two separate trends are unique as not seen in $\delta^{13}C2$ versus $\delta^{13}C3$ in other wells, both with methane responding differently from ethane and propane, Whiticar, 2018 pers. comm., after Berner and Faber 1996, well profile trendlines).

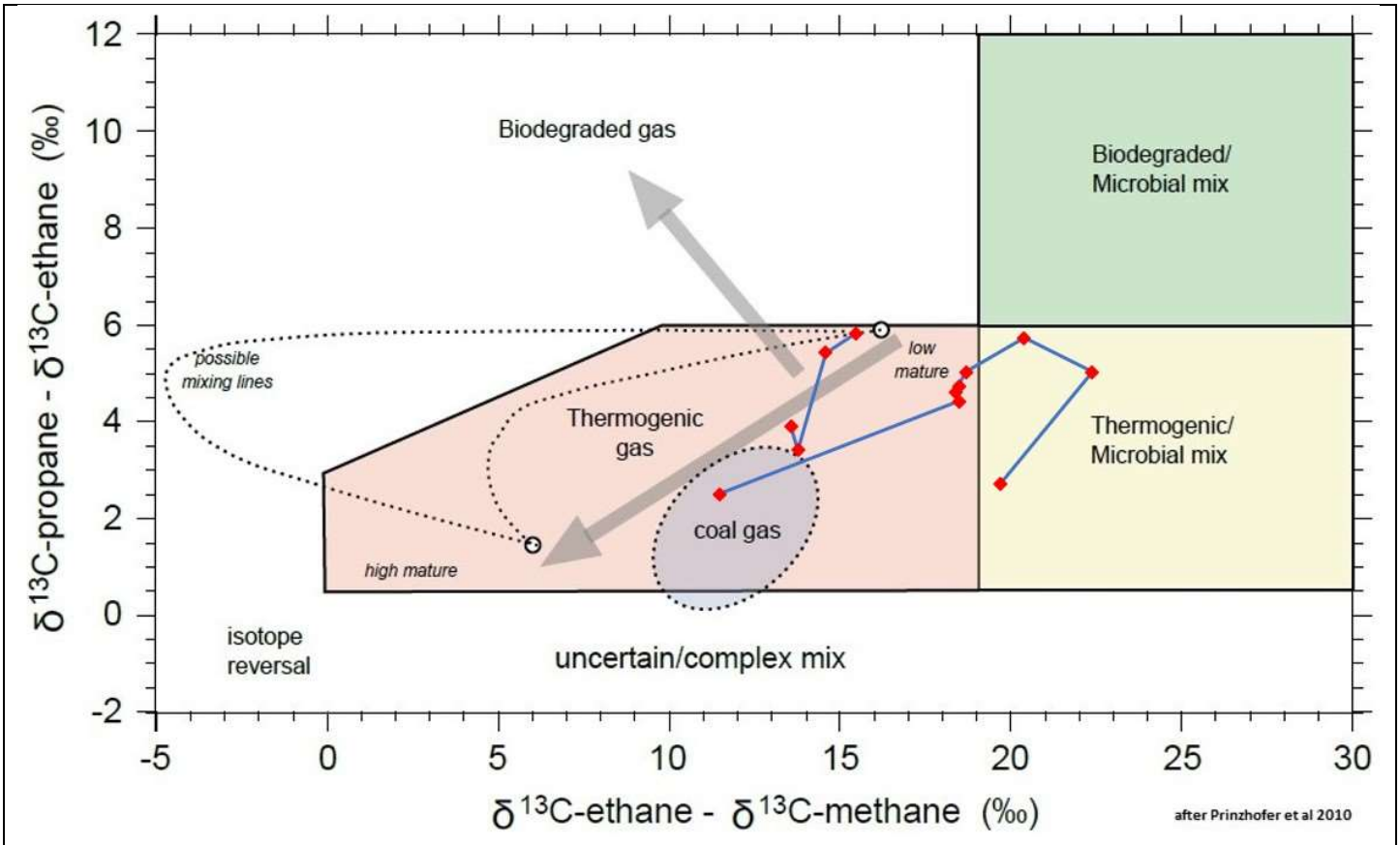

Figure A 102. Interpretive $\delta^{13}C_2$- $\delta^{13}C_1$ versus $\delta^{13}C_3$- $\delta^{13}C_2$ plot for WA#28588 (Jurassic to Triassic VT well. Data from shallower strata appears very different as trending from "low mature" to coal gas, the center strata has no data, but the lower strata resets to lowest maturity on far right with mixing and ends with Montney in the "coal gas" of HZ Montney diagram).

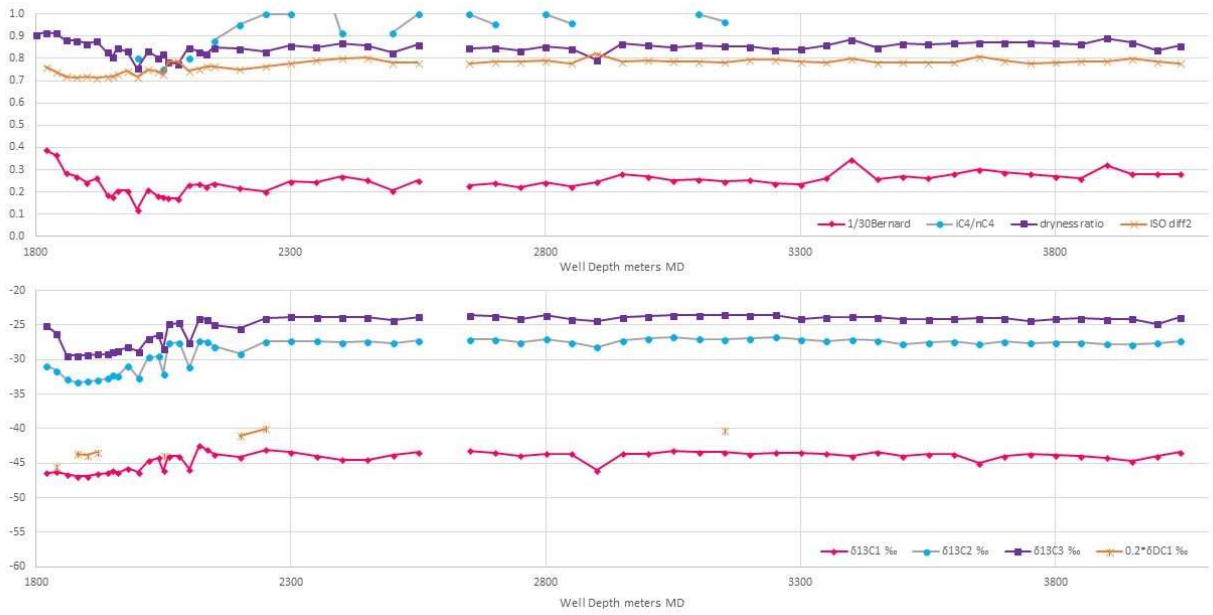

Figure A 103. Well profile, MC ratios and ISO data for WA#28588 (Montney HZ leg with uphole completion included).

Yes DATA, no profile

Figure A 104. Well profile, only 4 data points, all in Montney WA#32739.

No DATA

Figure A 105. Well profile, MC ratios not shown when null ISO data WA#31987.

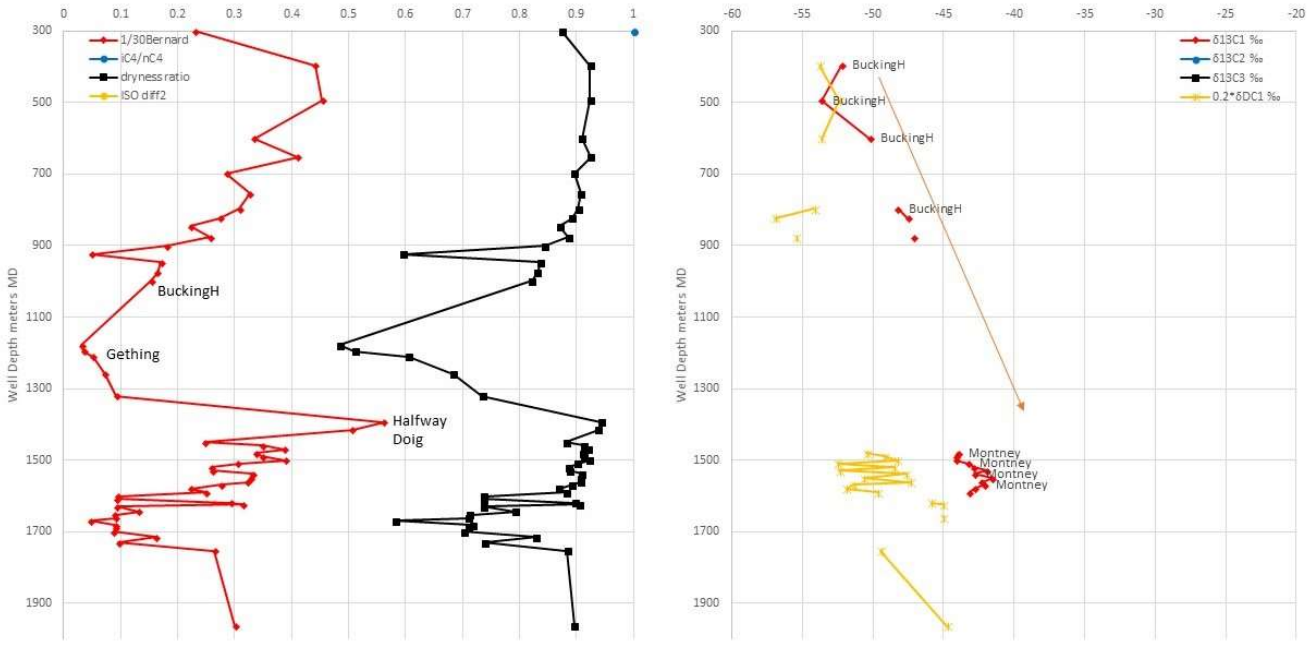

Figure A 106. Well profile, MC ratios and ISO data for WA#30308 (Upper Cretaceous to Triassic VT well. Detailed sampling was completed, but the isotopic analysis is only for 2 formations as the other samples were often less than 1000 ppm. This profile only has iC4/nC4 from MC often at single digit ppm and thus not really reliable as an indicator. There is no clarification on samples having only $\delta^{13}C1$ and δD, but not $\delta^{13}C2$ or $\delta^{13}C3$ measurements, which constrains the interpretive plots).

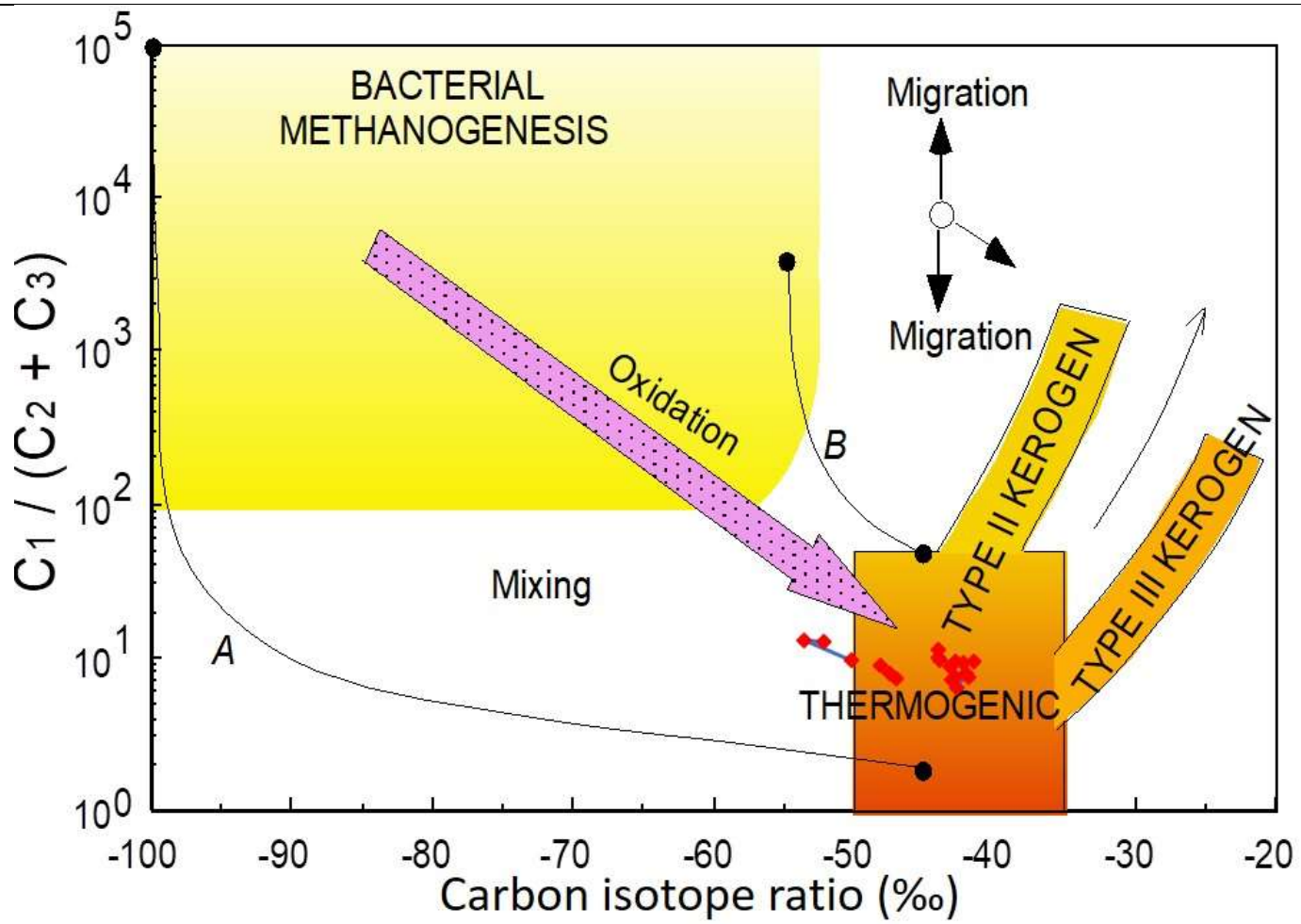

Figure A 107. ISO profile data – Interpretive Bernard Diagram for WA#30308 (Upper Cretaceous to Triassic VT well. There was no analysis of the C2 or C3 fractions, so only 2 plots, Whiticar, 2018 pers. comm., after Whiticar 1999).

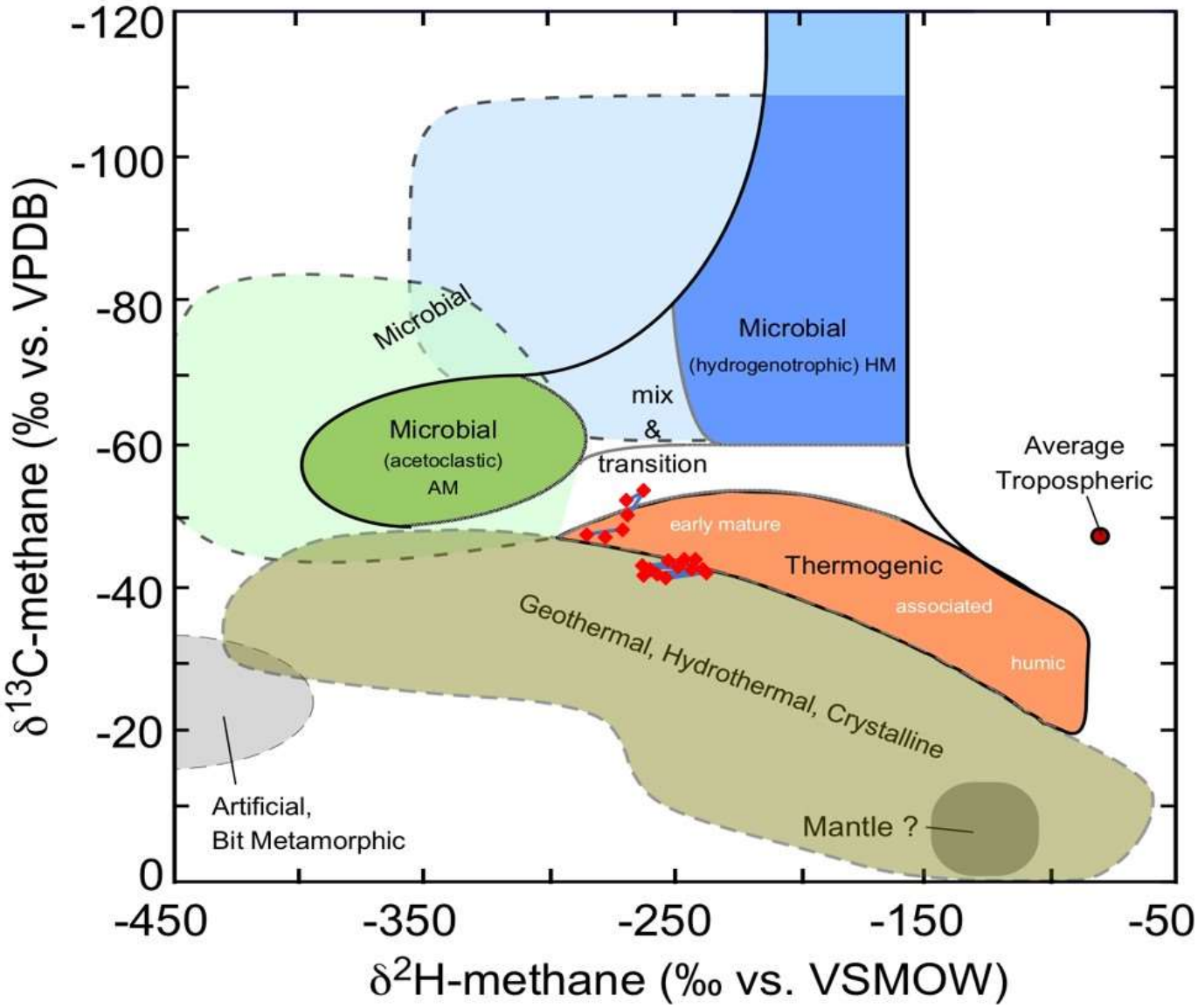

Figure A 108. ISO profile data – Interpretive CD Diagram for WA#30308 (Upper Cretaceous to Triassic VT well. There was no analysis of the C2 or C3 fractions, so only 2 plots are available, Whiticar, 2018 pers. comm., after Whiticar 1999).

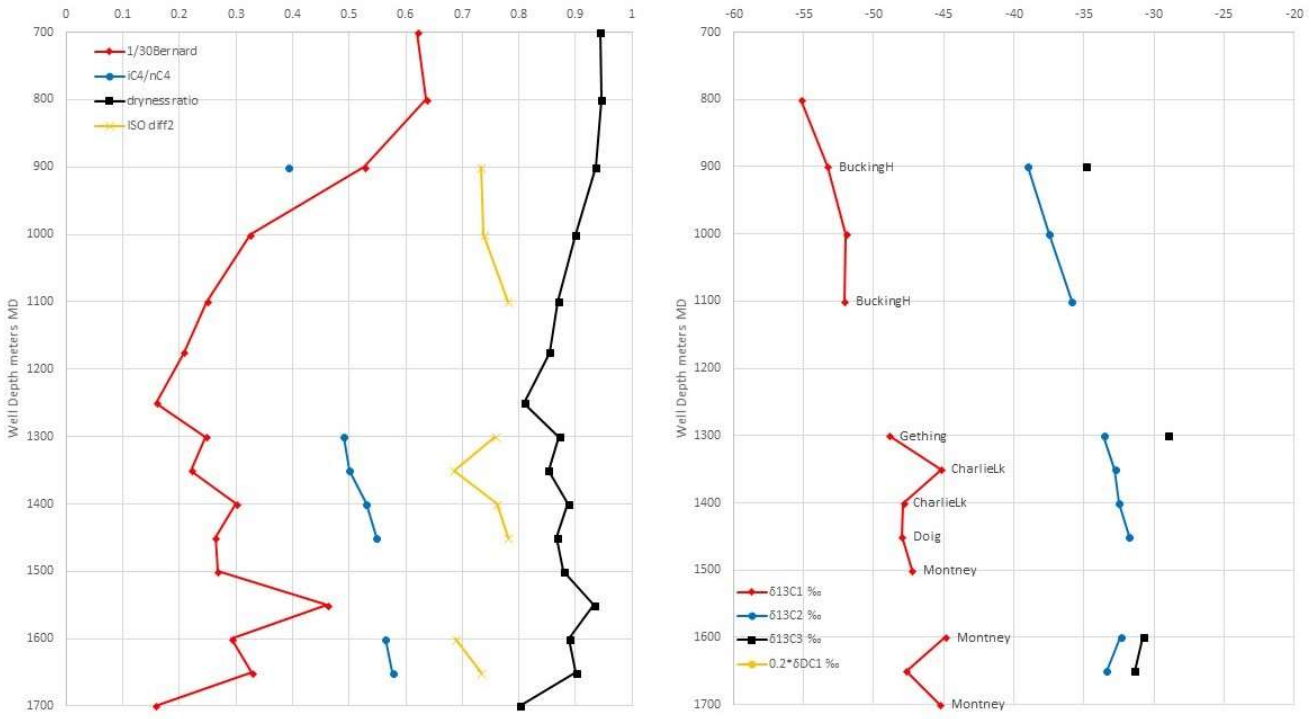

Figure A 109. Well profile, MC ratios and ISO data for WA#32676 (Upper Cretaceous to Triassic VT well. Wider spaced sampling, but more comprehensive isotopic analysis allows for stronger interpretation. This is closer to a "classic profile" with shallow biogenic trending to regular older gas at middle depths, but the Doig is flat and the Montney vertical section shows some complexity).

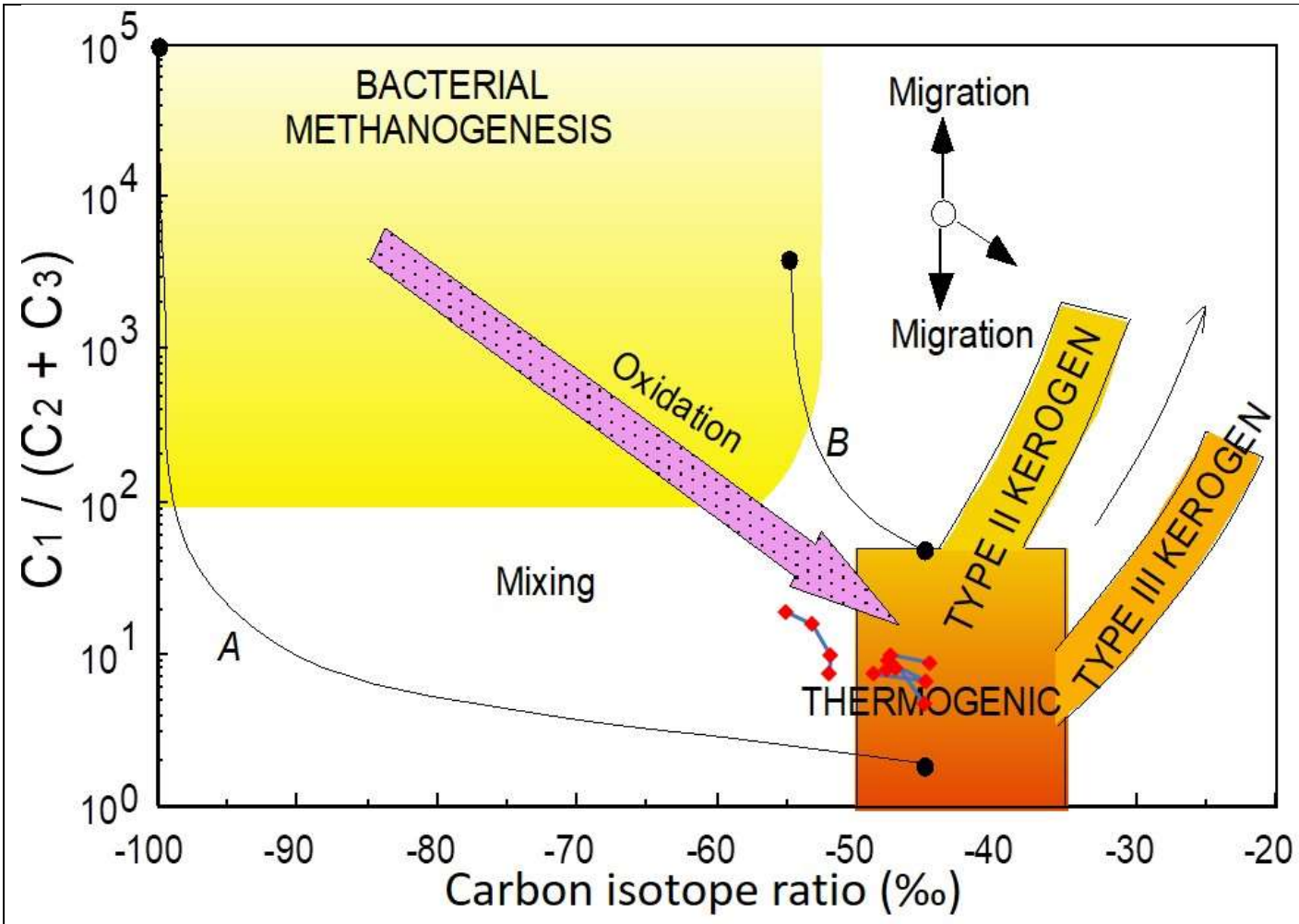

Figure A 110. ISO profile data – Interpretive Bernard Diagram for WA#32676 (Upper Cretaceous to Triassic VT well. Data from shallower strata appears very different from deeper strata, Whiticar, 2018 pers. comm., after Whiticar 1999).

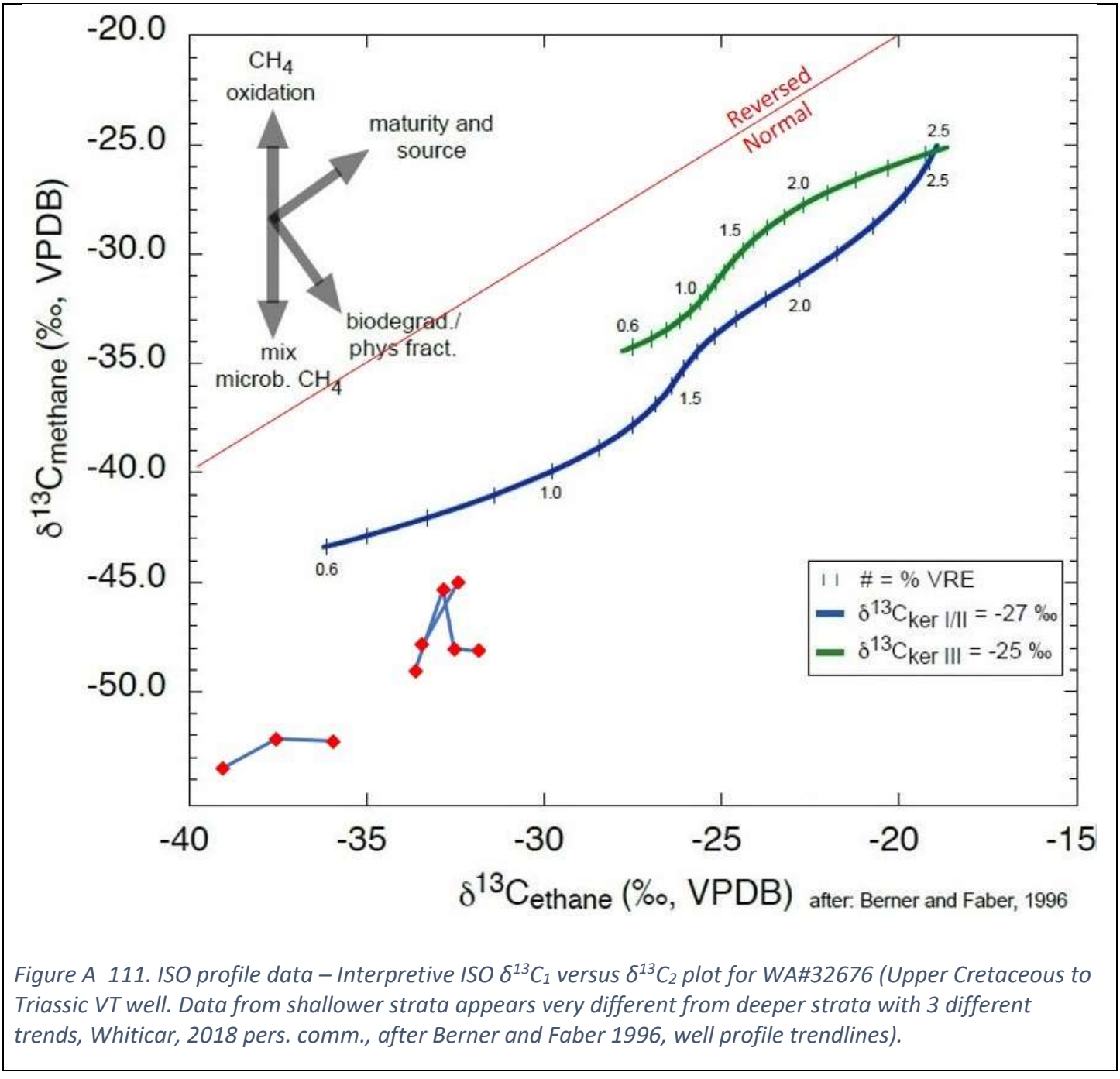

Figure A 111. ISO profile data – Interpretive ISO $\delta^{13}C_1$ versus $\delta^{13}C_2$ plot for WA#32676 (Upper Cretaceous to Triassic VT well. Data from shallower strata appears very different from deeper strata with 3 different trends, Whiticar, 2018 pers. comm., after Berner and Faber 1996, well profile trendlines).

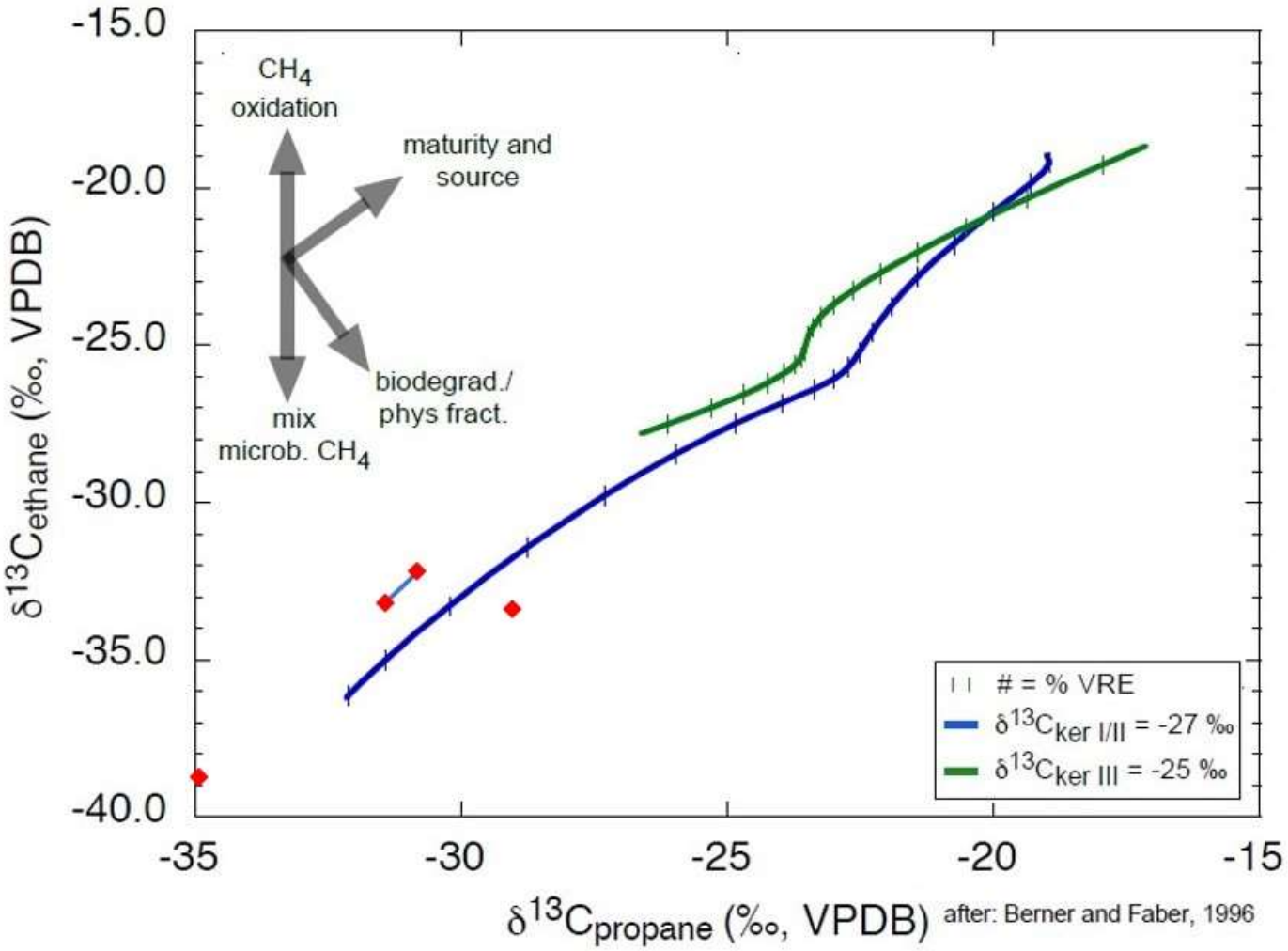

Figure A 112. ISO profile data – Interpretive ISO $\delta^{13}C_2$ versus $\delta^{13}C_3$ plot for WA#32676 (Upper Cretaceous to Triassic VT well. Shallower strata and deeper strata both have methane responding differently from ethane and propane as methane is farther from the kerogen curve and ethane is closer, Whiticar, 2018 pers. comm., after Berner and Faber 1996, well profile trendlines).

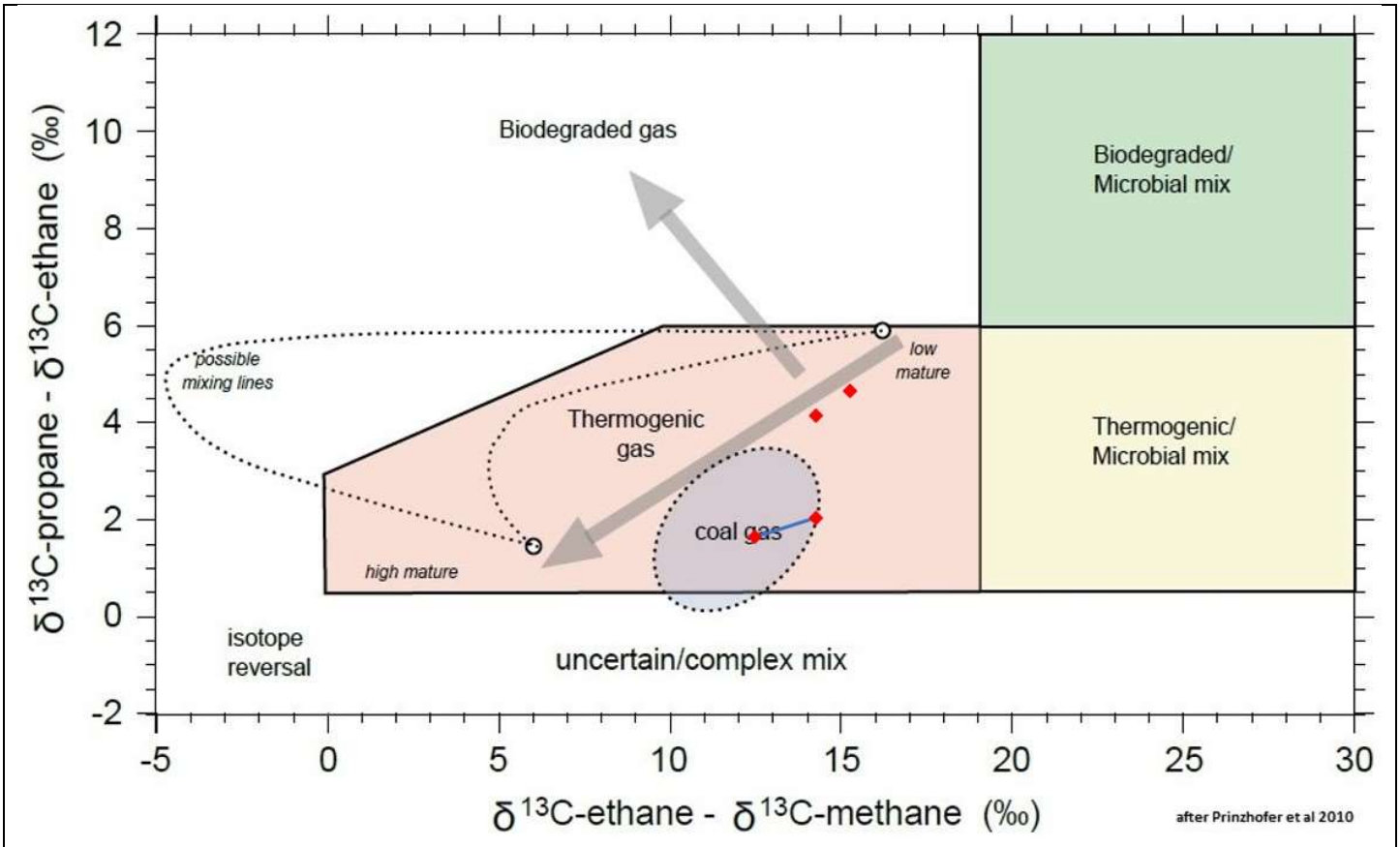

Figure A 113. Interpretive $\delta^{13}C_2$- $\delta^{13}C_1$ versus $\delta^{13}C_3$- $\delta^{13}C_2$ plot for WA#32676 (Upper Cretaceous to Triassic VT well. Start of the Montney Formation is closer to "coal gas" of HZ Montney diagram as figure A05).

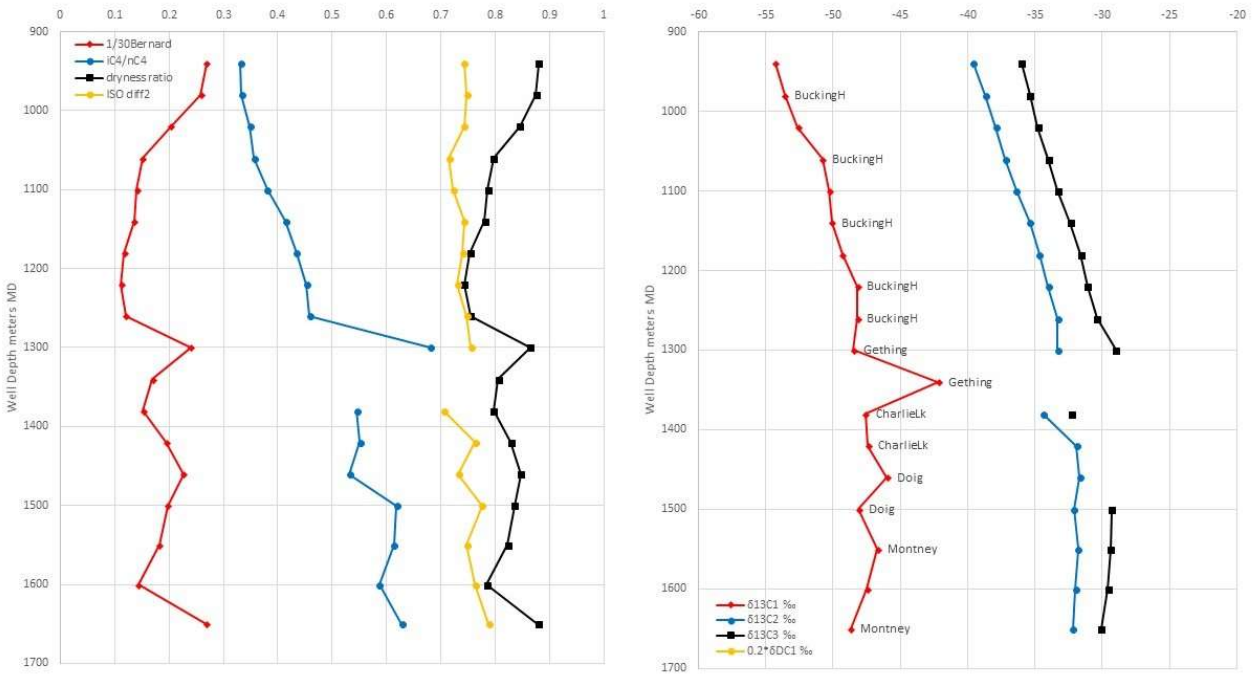

Figure A 114. Well profile, MC ratios and ISO data for WA#31988 (Upper Cretaceous to Triassic VT well. This profile starts too deep for the classic profile that included the biogenic sources and the curves are far straighter than expected - there is a little bump for the Gething, but not for the Doig, and the Halfway is not sampled. More comprehensive isotopic analysis allows for stronger interpretation).

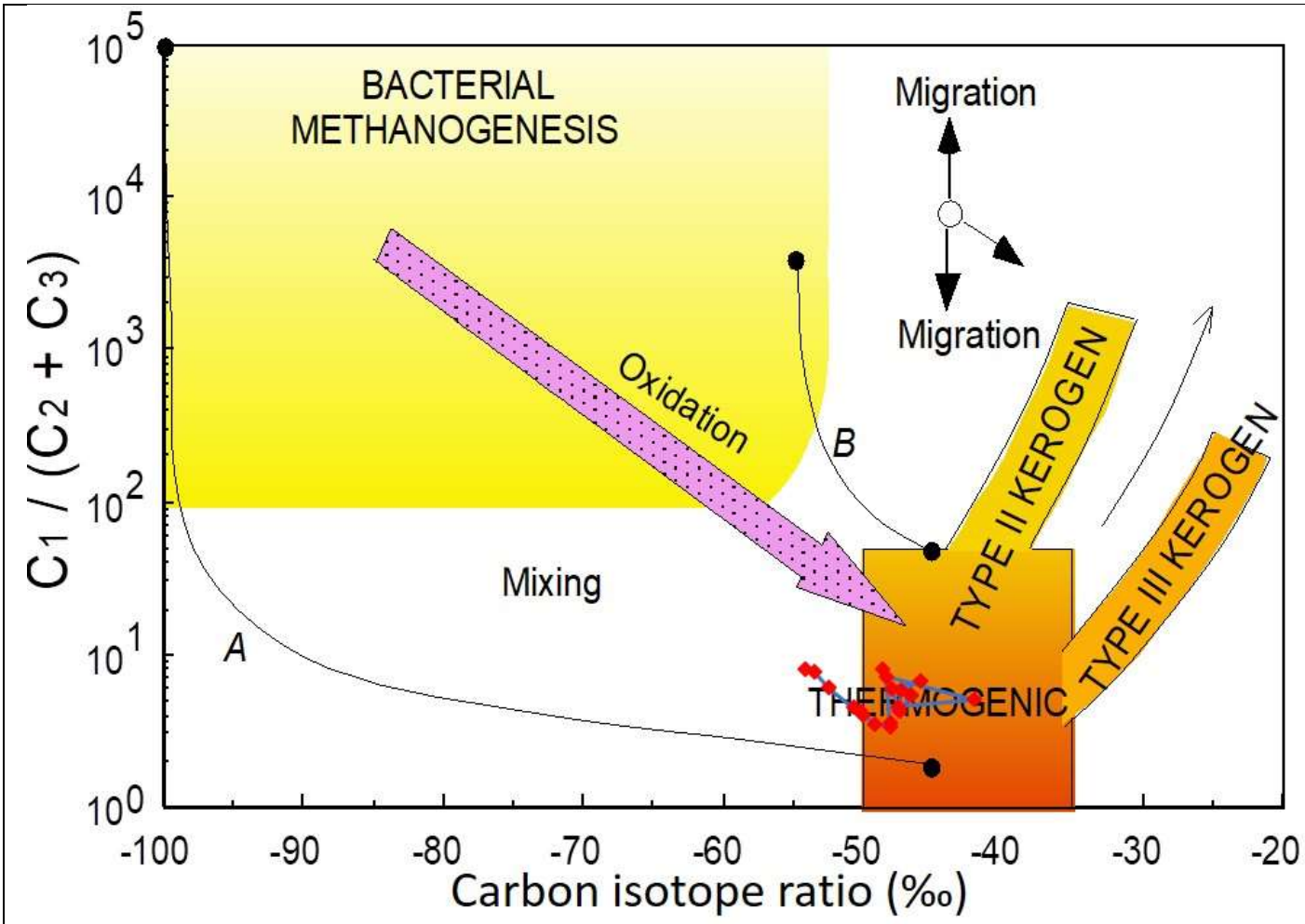

Figure A 115. ISO profile data – Interpretive Bernard Diagram for WA#31988 (Upper Cretaceous to Triassic VT well, Whiticar, 2018 pers. comm., after Whiticar 1999).

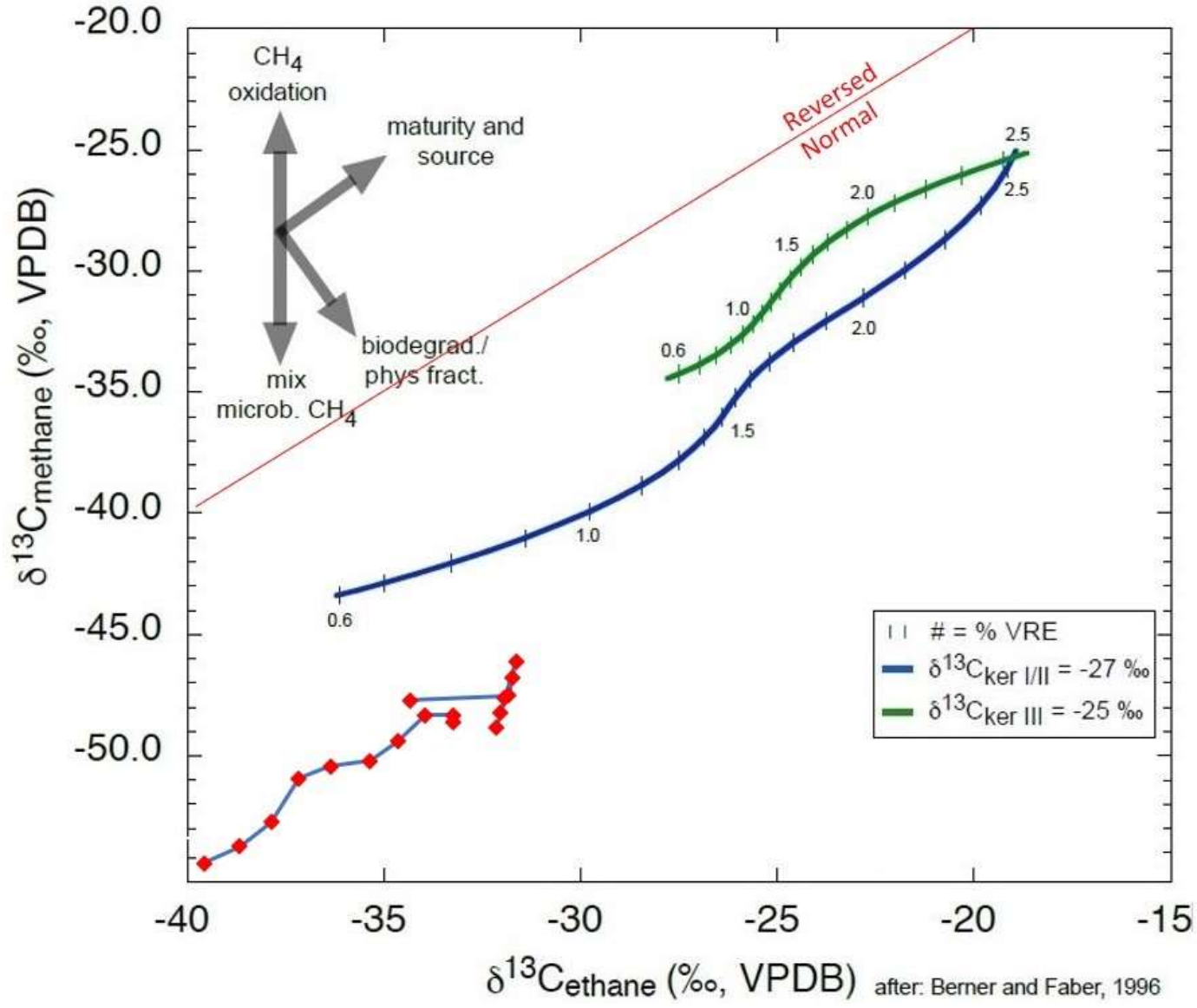

Figure A 116. ISO profile data – Interpretive ISO $\delta^{13}C_1$ versus $\delta^{13}C_2$ plot for WA#31988 (Upper Cretaceous to Triassic VT well. Data from shallower strata appears on trend from deeper strata, but with a different "angle" and both have methane responding differently from ethane and propane, Whiticar, 2018 pers. comm., after Berner and Faber 1996, well profile trendlines).

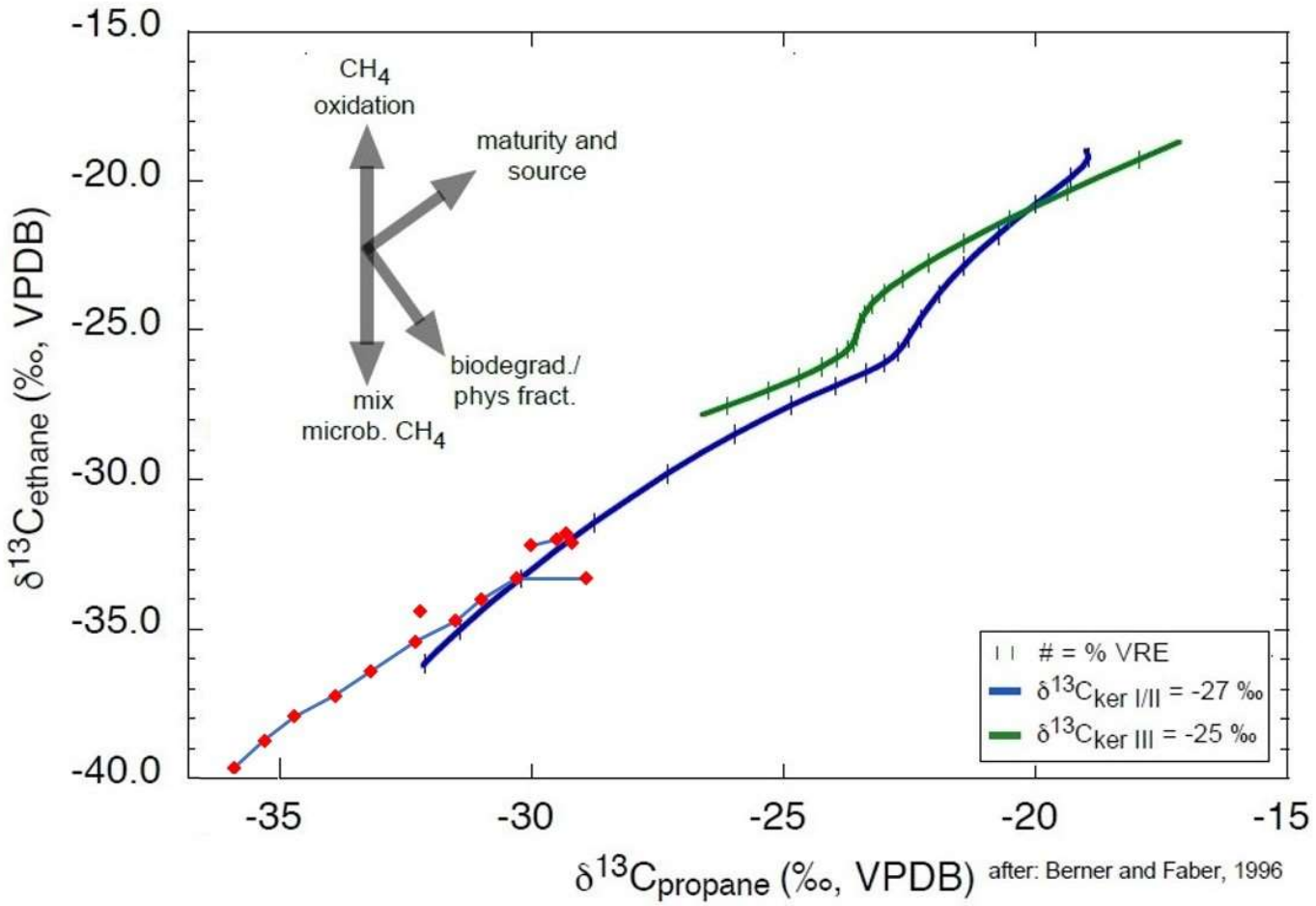

Figure A 117. ISO profile data – Interpretive ISO $\delta^{13}C_2$ versus $\delta^{13}C_3$ plot for WA#31988 (Upper Cretaceous to Triassic VT well. Data from shallower strata appears on trend from deeper strata and both have methane responding differently from ethane and propane, Whiticar, 2018 pers. comm., after Berner and Faber 1996, well profile trendlines).

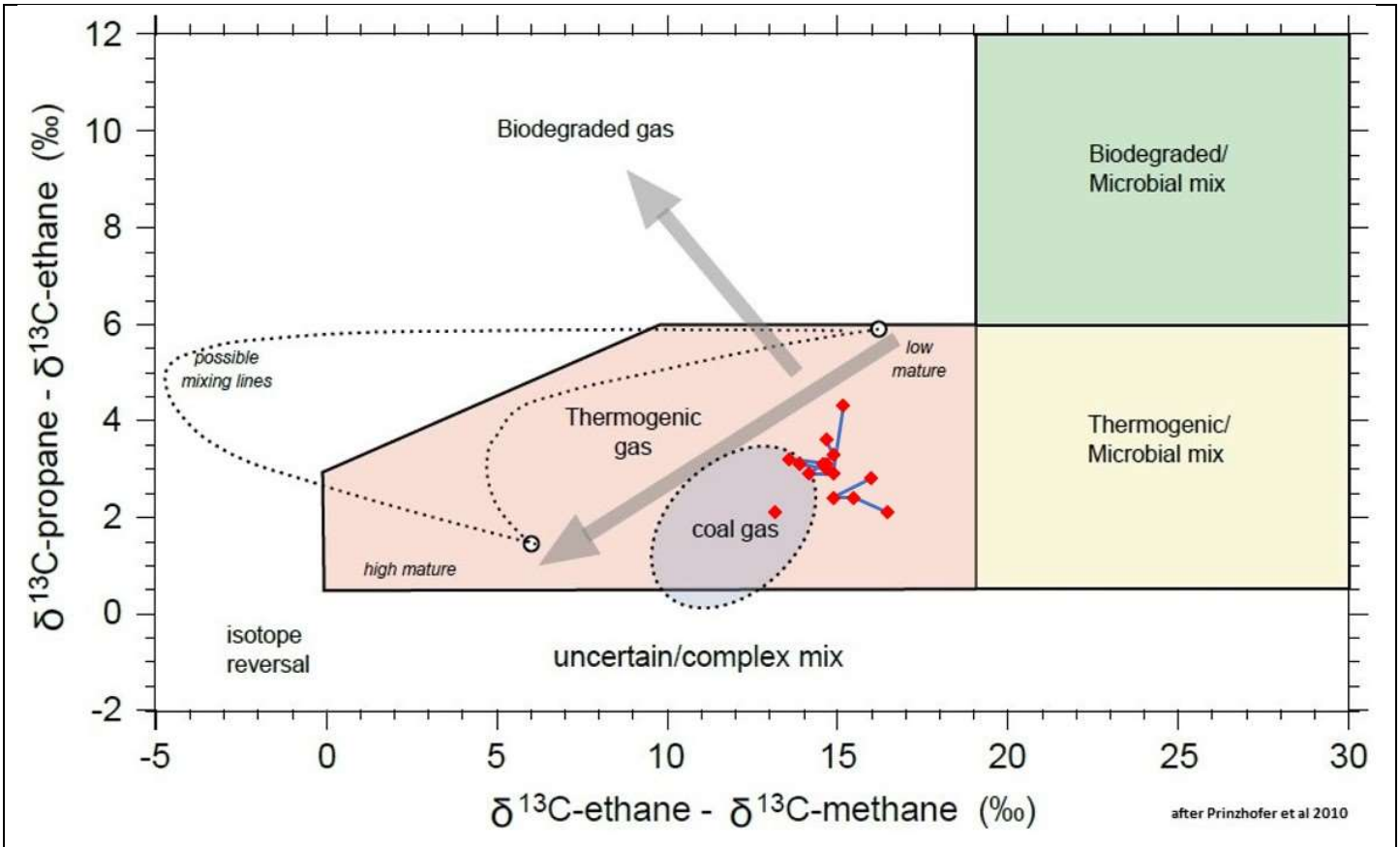

Figure A 118. Interpretive $\delta^{13}C_2$- $\delta^{13}C_1$ versus $\delta^{13}C_3$- $\delta^{13}C_2$ plot for WA#31988 (Upper Cretaceous to Triassic VT well. All shallower strata are less mature than otherwise expected and only the middle Montney approaches the "coal gas" of HZ Montney diagram).

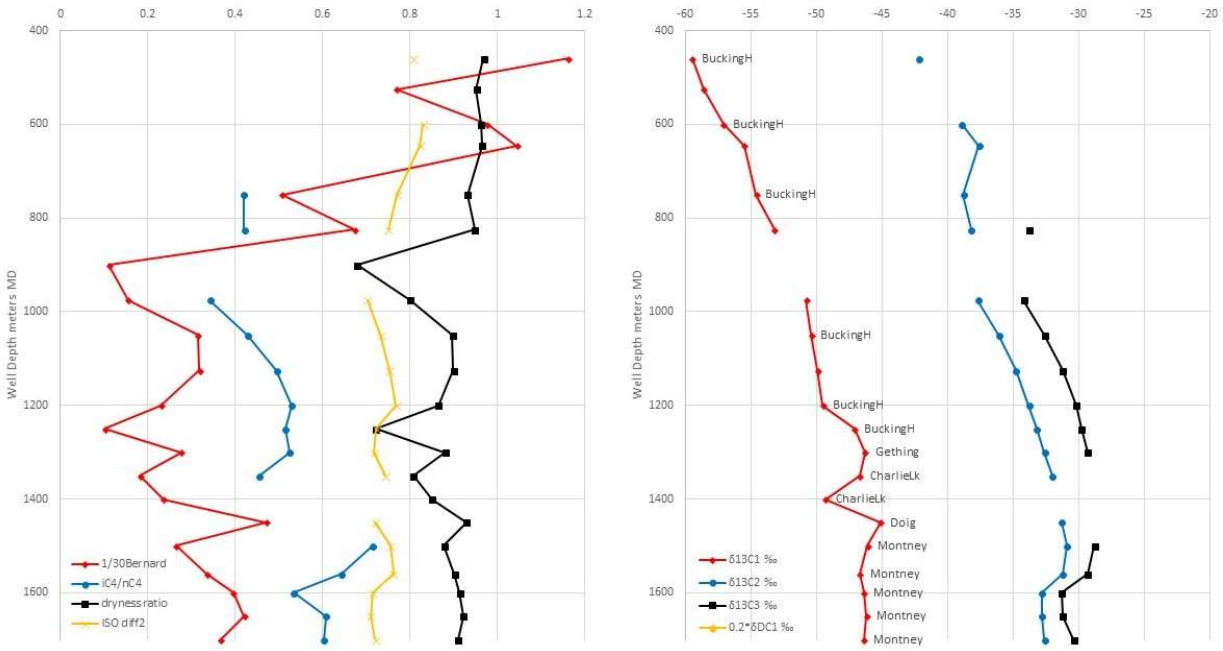

Figure A 119. Well profile, MC ratios and ISO data for WA#32152 (Upper Cretaceous to Triassic VT well. This profile starts shallow and includes the "classic profile" with biogenic sources. There is a little bump for the Gething, but the Charlie Lake Formation is a low, and the Halfway is not sampled. More comprehensive isotopic analysis allows for stronger interpretation).

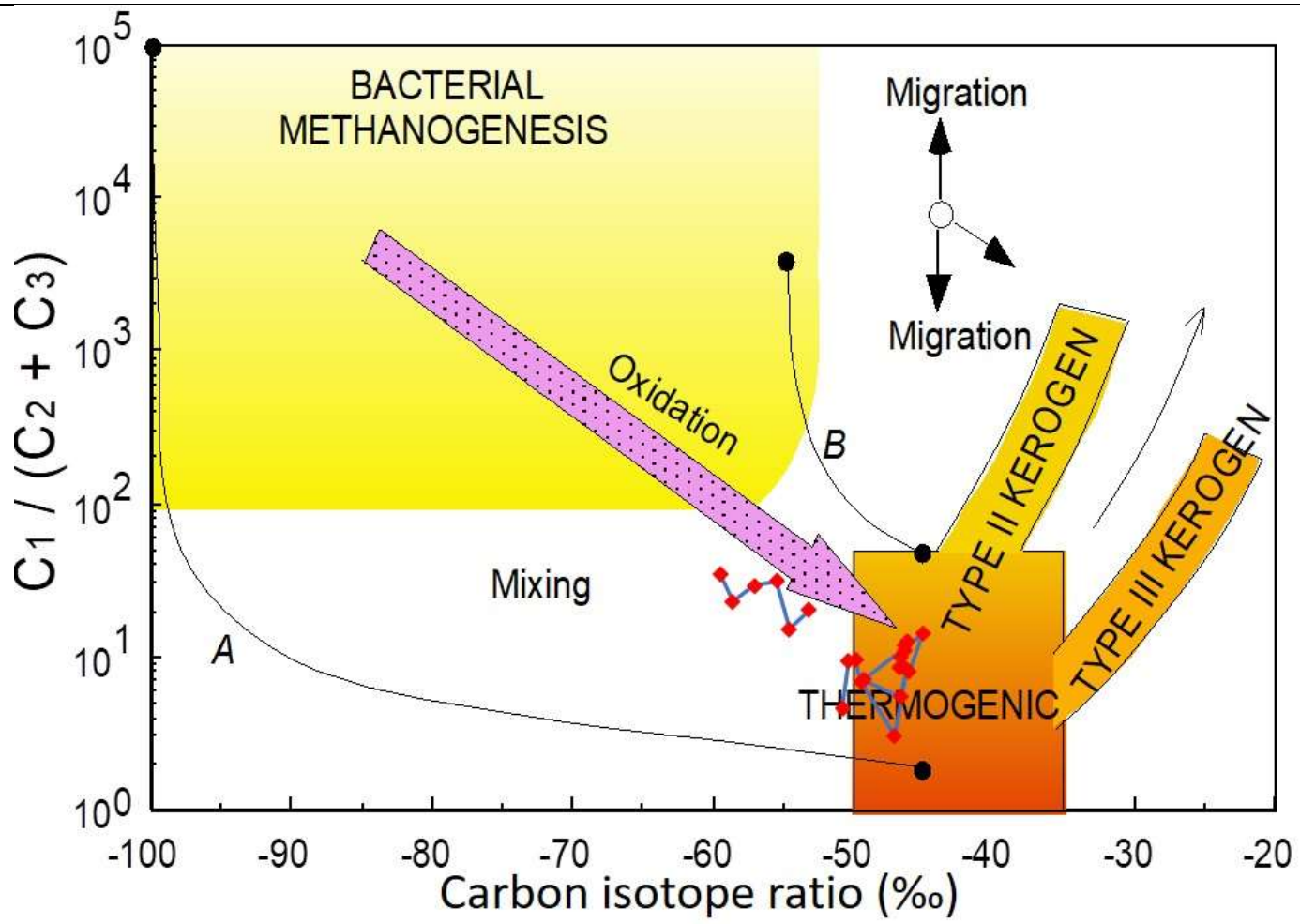

Figure A 120. ISO profile data – Interpretive Bernard Diagram for WA#32152 (Upper Cretaceous to Triassic VT well. Data from shallower strata appears very different and far lower "maturity" than deeper strata. There is no data for δD, Whiticar, 2018 pers. comm., after Whiticar 1999).

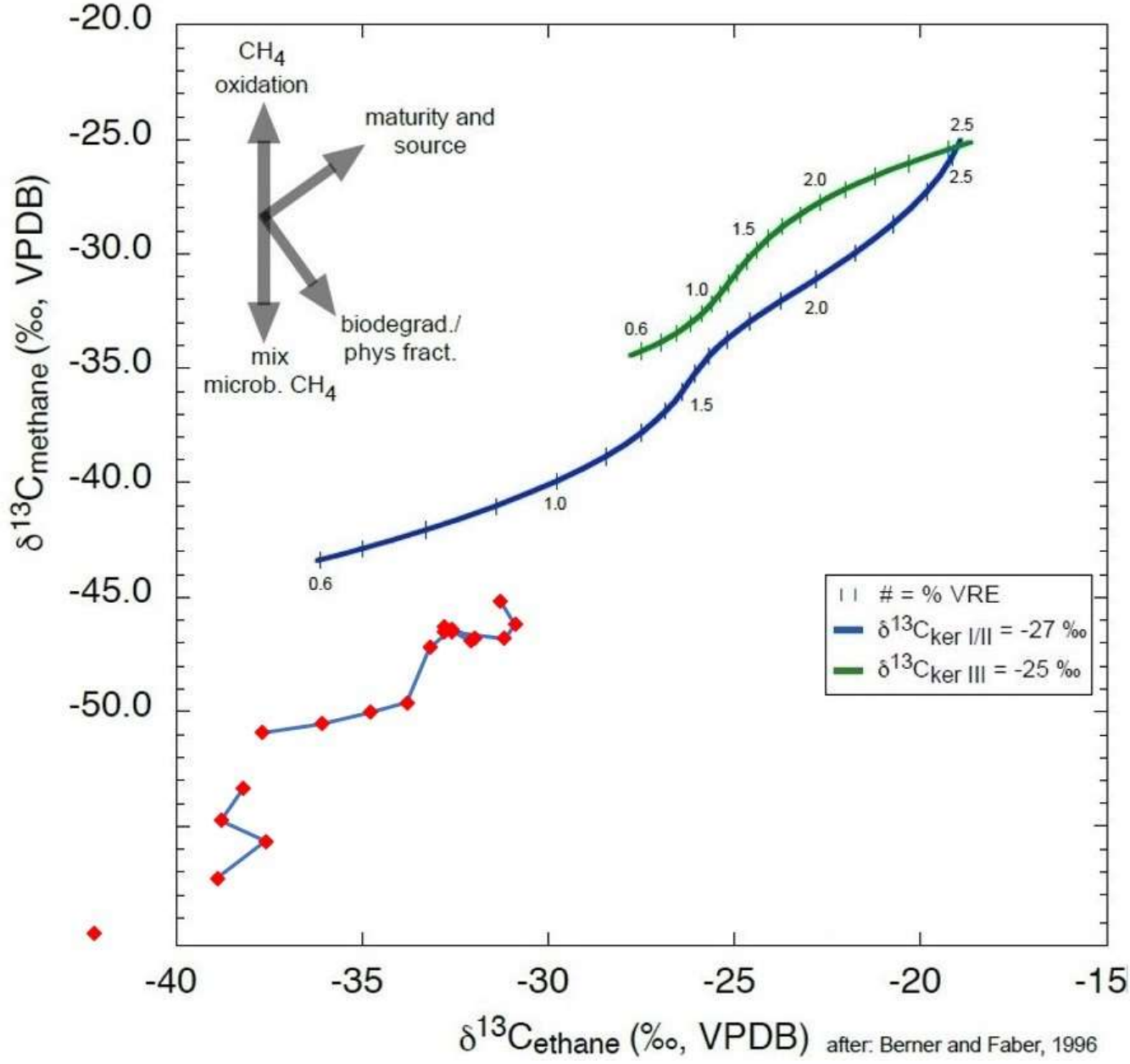

Figure A 121. ISO profile data – Interpretive ISO $\delta^{13}C_1$ versus $\delta^{13}C_2$ plot for WA#32152 (Upper Cretaceous to Triassic VT well. Data from shallower strata appears very different and far lower "maturity" than deeper strata with the shallowest being far lower left off the grid of $\delta^{13}C1$ vs $\delta^{13}C2$. There are 3 different trends for $\delta^{13}C1$, Whiticar, 2018 pers. comm., after Berner and Faber 1996, well profile trendlines).

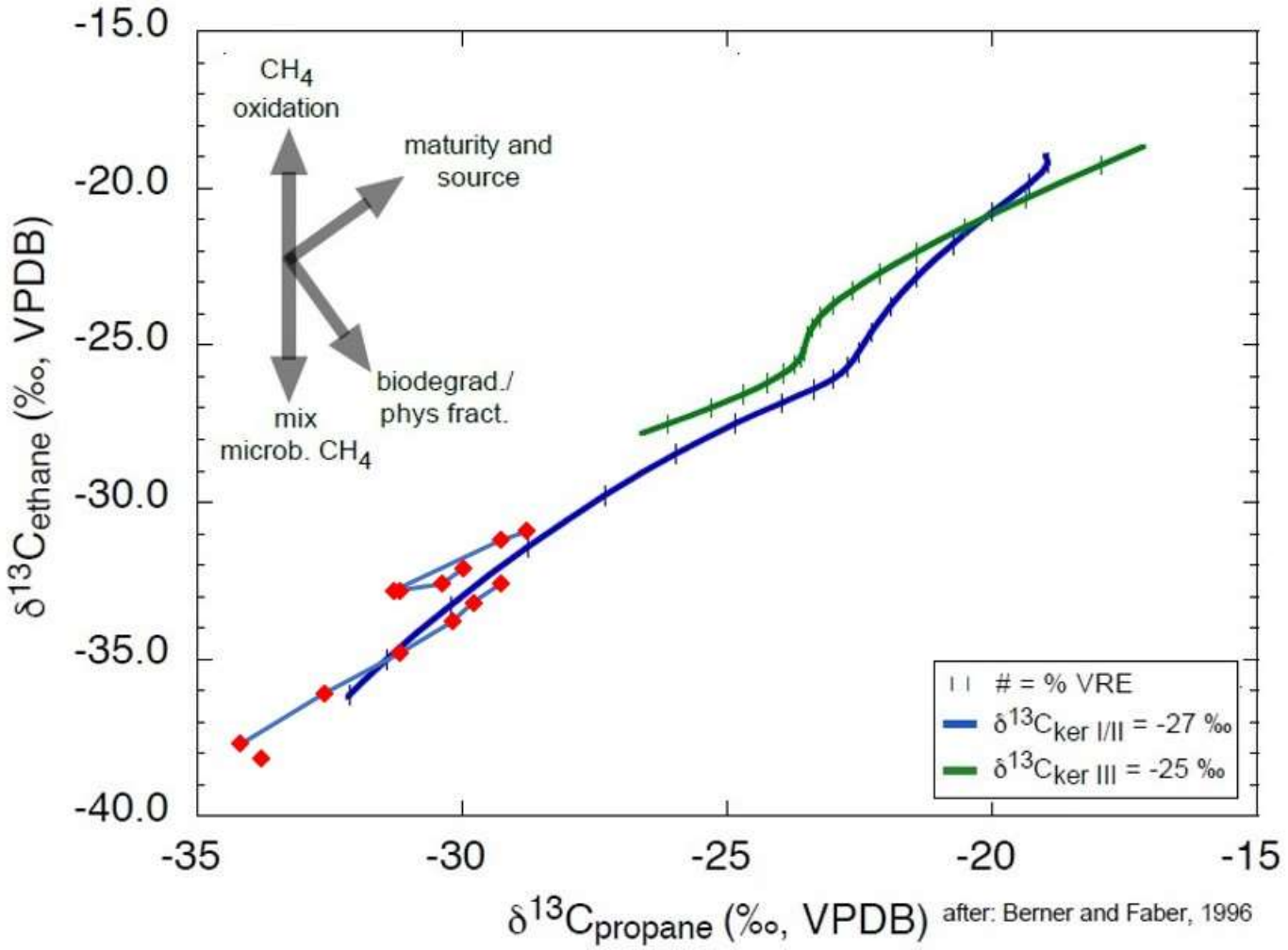

Figure A 122. ISO profile data – Interpretive ISO δ13C_2 versus δ13C_3 plot for WA#32152 (Upper Cretaceous to Triassic VT well. Data from shallower strata appears very different than deeper strata that seem to roll on the curve, methane responds differently from ethane and propane being on or 'above' the type II curve, Whiticar, 2018 pers. comm., after Berner and Faber 1996, well profile trendlines).

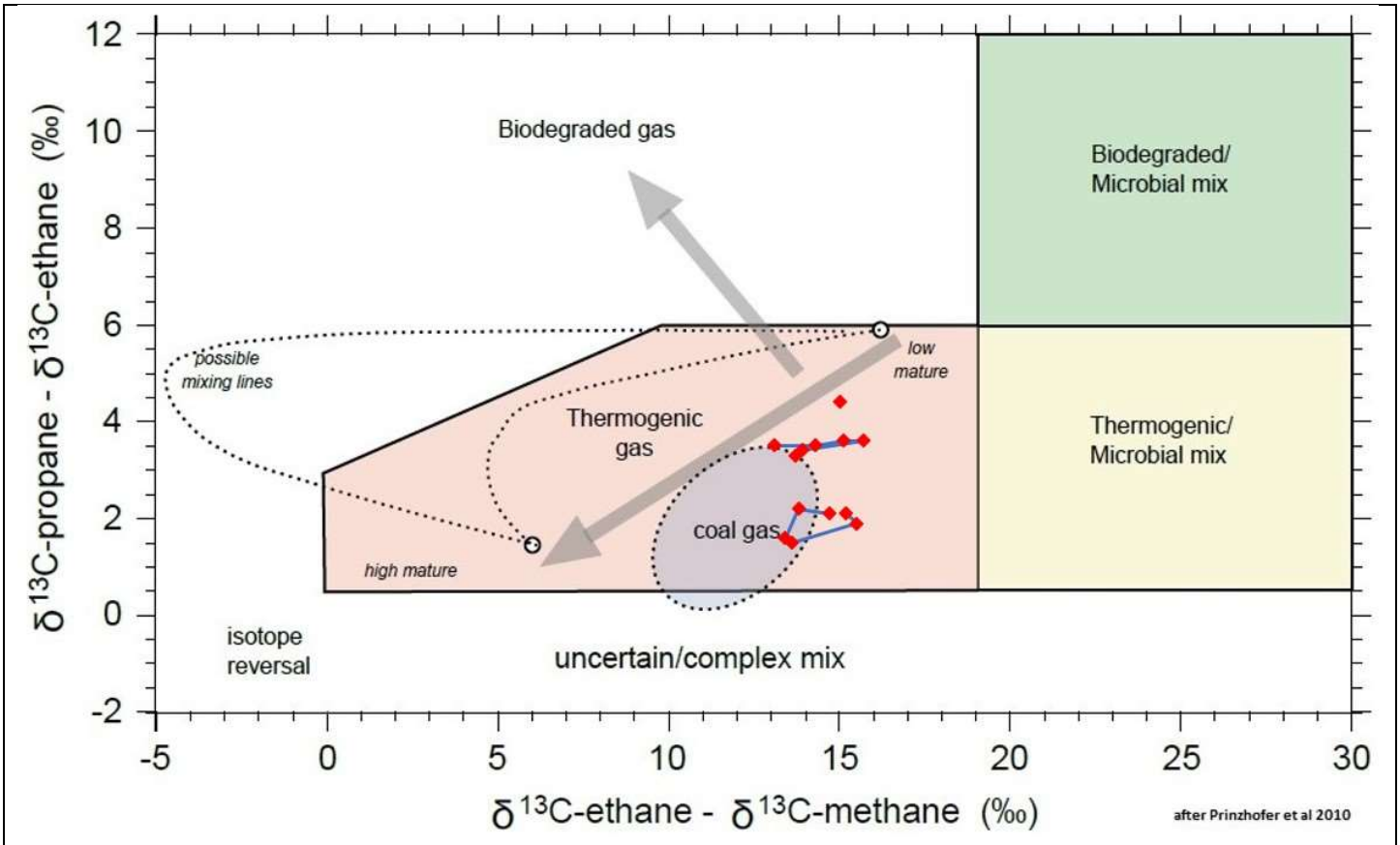

Figure A 123. Interpretive $\delta^{13}C_2$- $\delta^{13}C_1$ versus $\delta^{13}C_3$- $\delta^{13}C_2$ plot for WA#32152 (Upper Cretaceous to Triassic VT well. Shallow strata on the upper portion is even more mixed low maturity and the start of the Montney in the vertical section is closer to "coal gas" of HZ Montney diagram as figure A05).

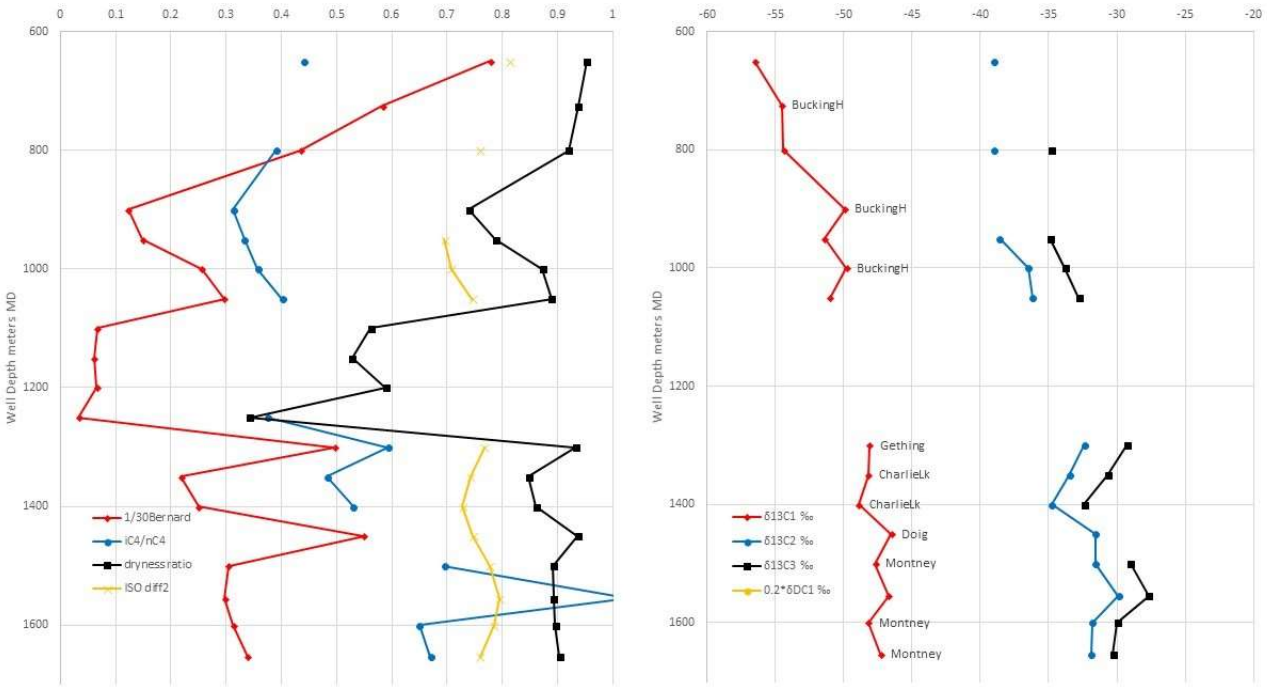

Figure A 124. Well profile, MC ratios and ISO data for WA#32153 (Cretaceous to Triassic VT well. This profile starts shallow and includes the "classic profile" with biogenic sources. There is a bump for the Gething and Doig formations, but the Halfway is not sampled. More comprehensive isotopic analysis allows for stronger interpretation).

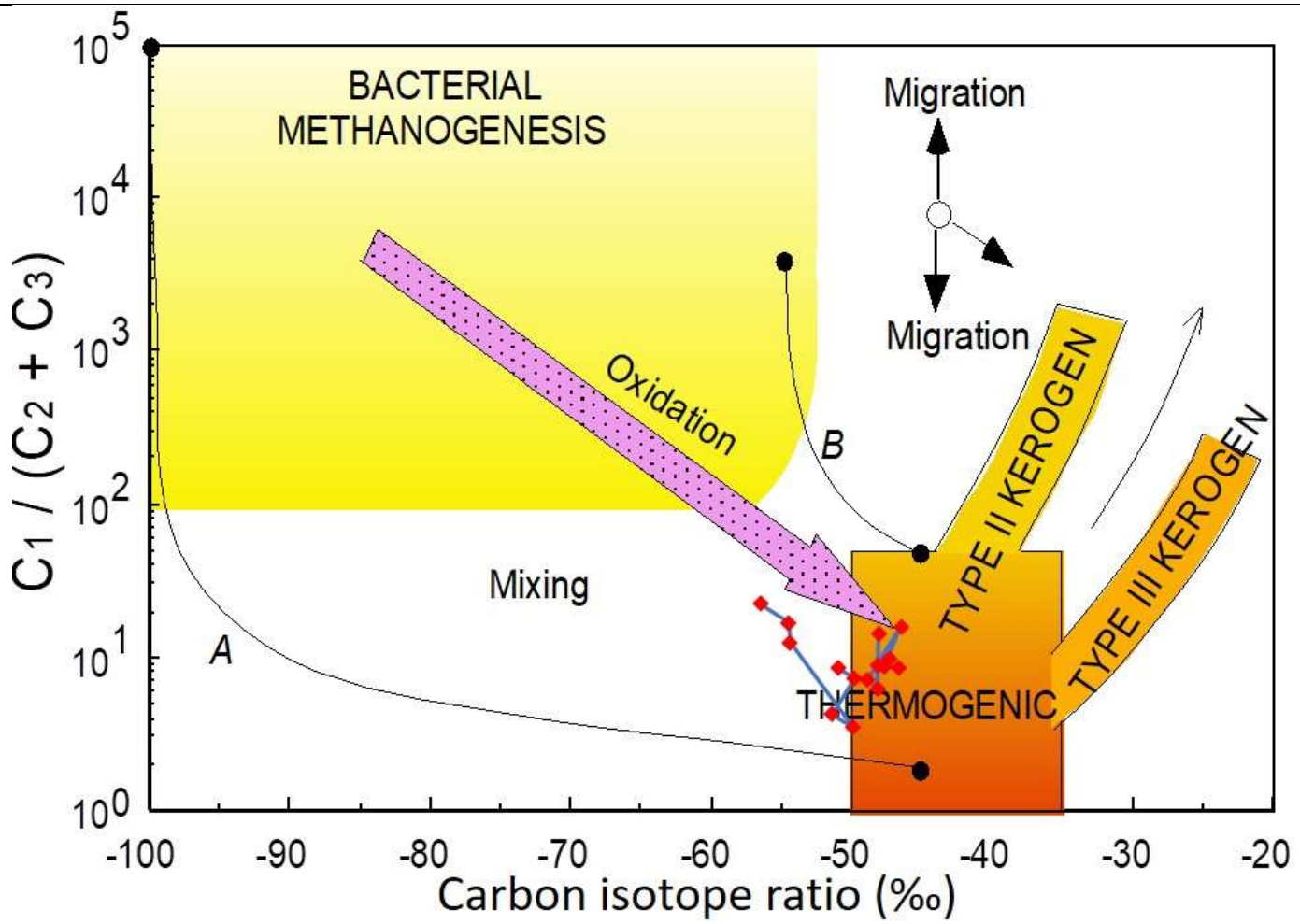

Figure A 125. ISO profile data – Interpretive Bernard Diagram for WA#32153 (Cretaceous to Triassic VT well. Data from shallower strata appears very different and far lower "maturity" than deeper strata, there is no data for δD, Whiticar, 2018 pers. comm., after Whiticar 1999).

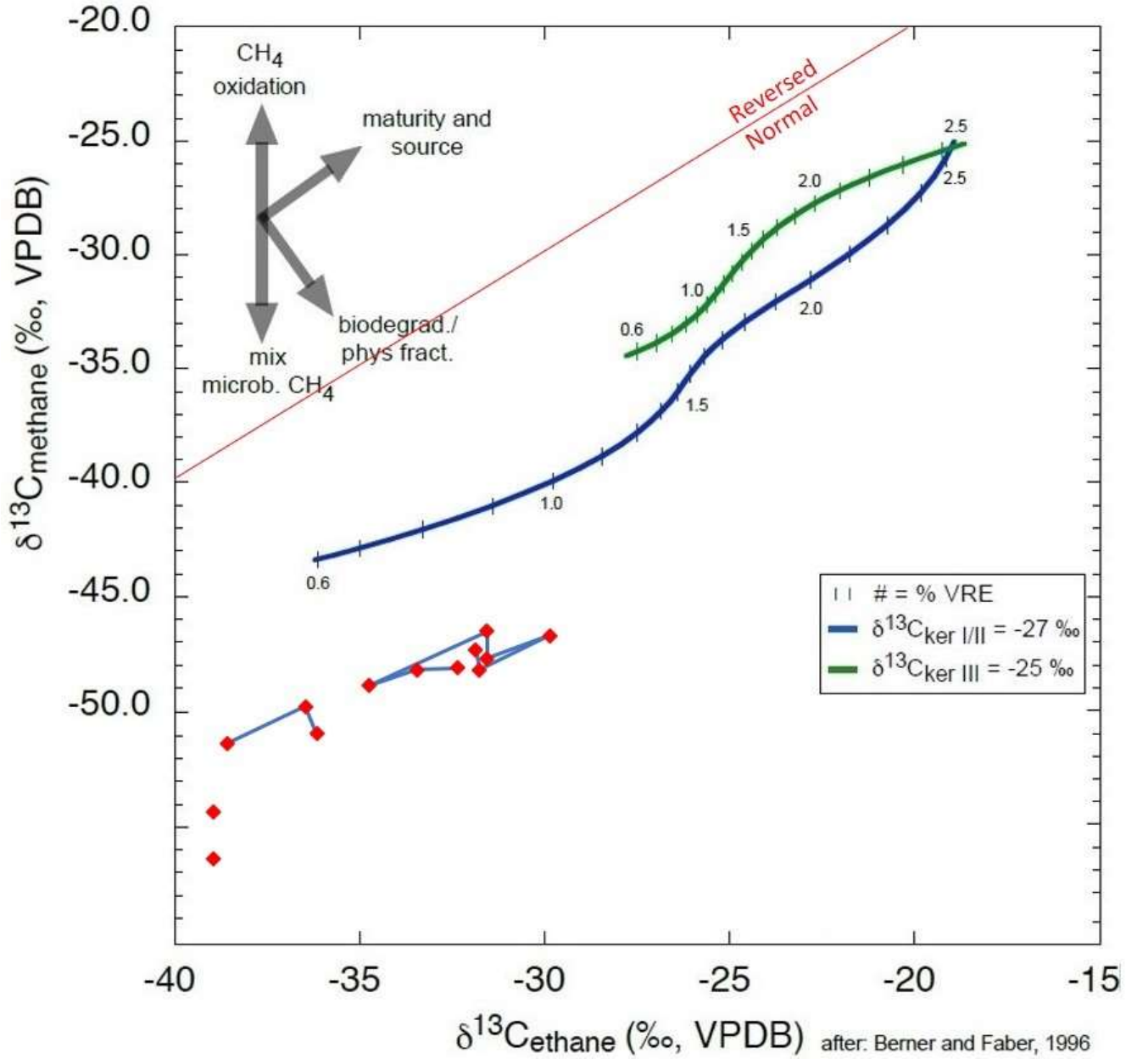

Figure A 126. ISO profile data – Interpretive ISO $\delta^{13}C_1$ versus $\delta^{13}C_2$ plot for WA#32153 (Cretaceous to Triassic VT well. Data from shallower strata appears very different and far lower "maturity" than deeper strata with the shallowest being far lower left on $\delta^{13}C1$ vs $\delta^{13}C2$. There are 2 different trends for $\delta^{13}C1$, Whiticar, 2018 pers. comm., after Berner and Faber 1996, well profile trendlines).

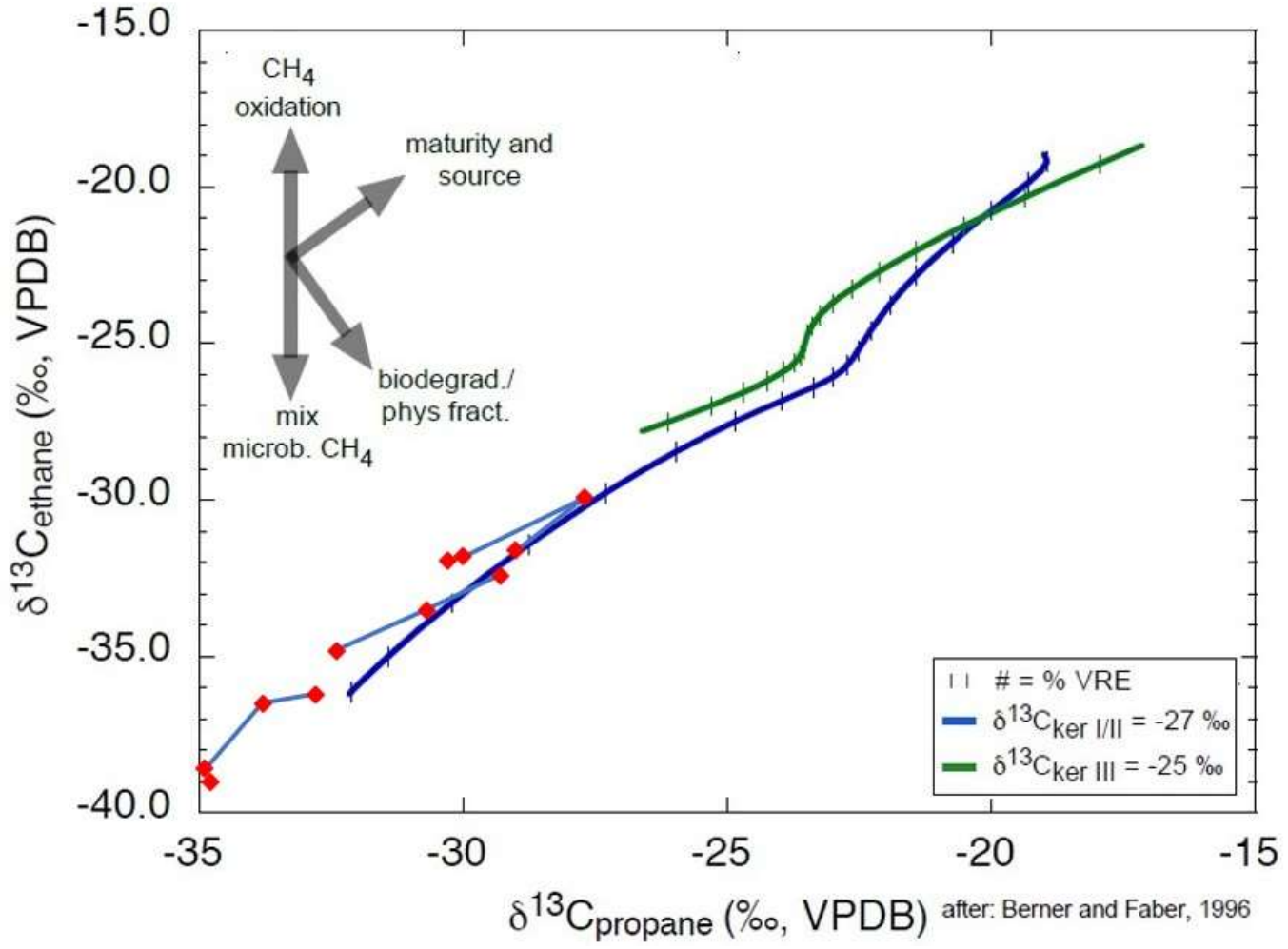

Figure A 127. ISO profile data – Interpretive ISO $\delta^{13}C_2$ versus $\delta^{13}C_3$ plot for WA#32153 (Cretaceous to Triassic VT well. Data from shallower strata appears to be far lower "maturity" than deeper strata, but methane responds differently from ethane and propane being on or above the type II curve, Whiticar, 2018 pers. comm., after Berner and Faber 1996, well profile trendlines).

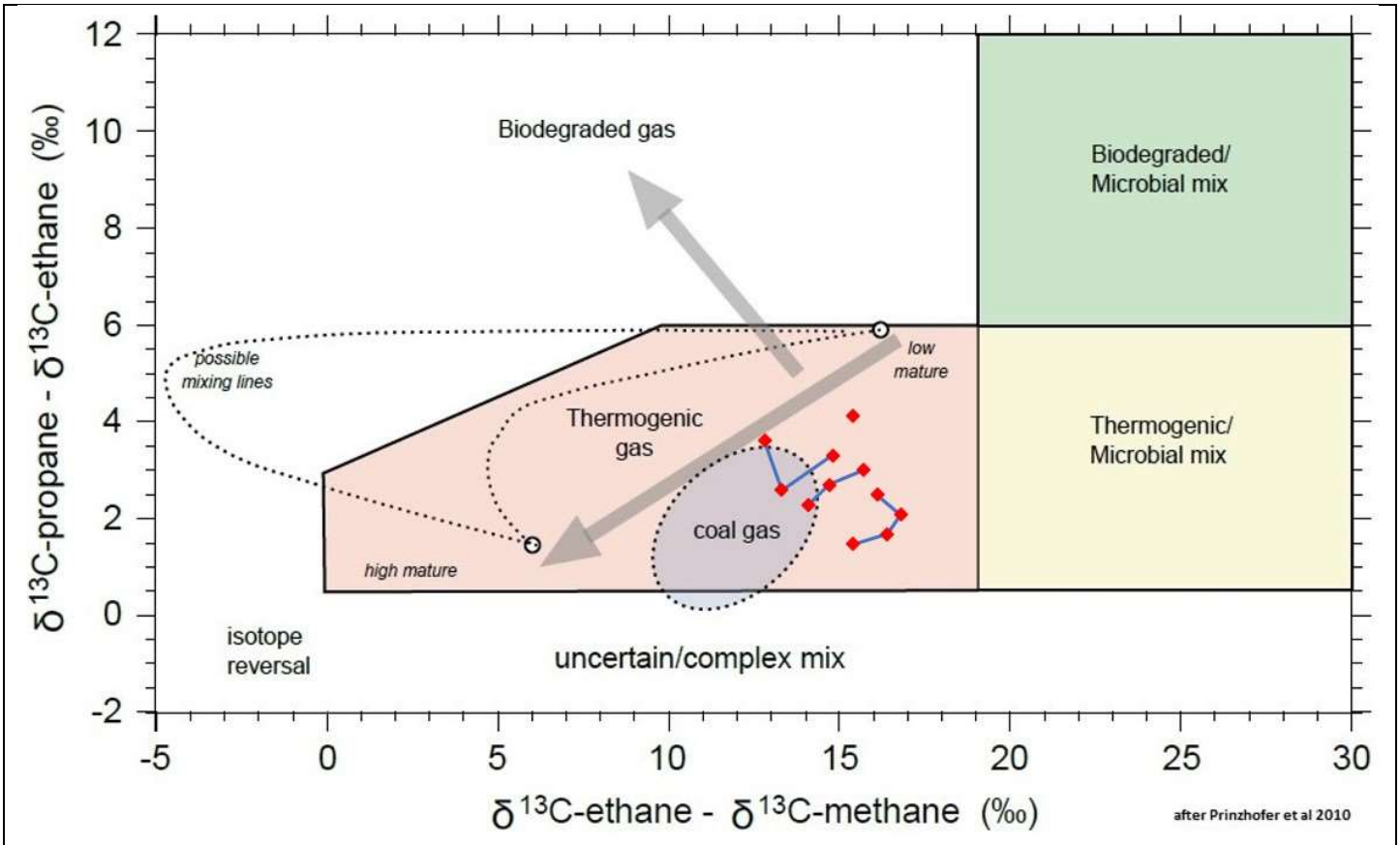

Figure A 128. Interpretive $\delta^{13}C_2$- $\delta^{13}C_1$ versus $\delta^{13}C_3$- $\delta^{13}C_2$ plot for WA#32153 (Cretaceous to Triassic VT well. This analysis shows the complications behind the apparent classic profile).

No DATA

Figure A 129. Well profile, MC ratios not shown when null ISO data WA#30415.

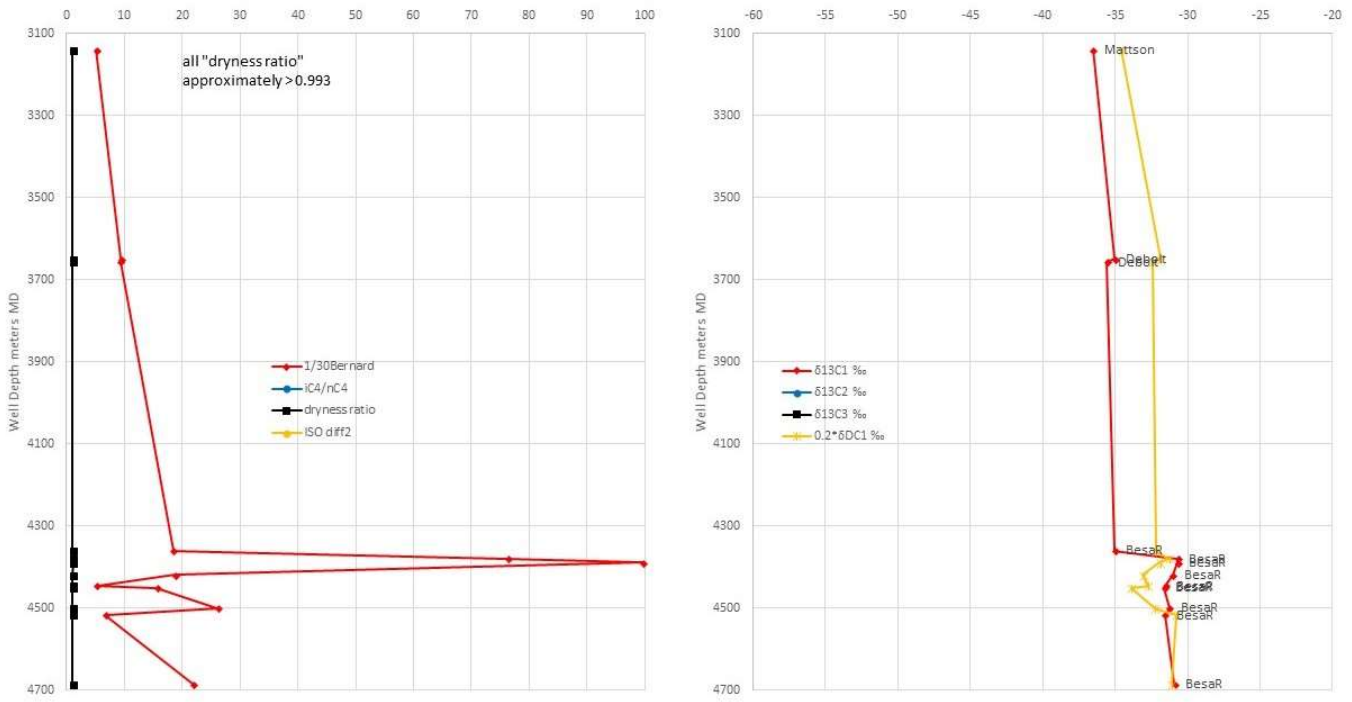

Figure A 130. Well profile, MC ratios and ISO data for WA#29747 (Liard Devonian well with some uphole samples. Far to the north, this profile has a few unusual formations and the ISO data is only for methane as there is very low levels of longer chain hydrocarbons. Note the scale change for the 1/30 Bernard ratio and the dryness ratio really does not do anything as dryness ratios are all between 1.0 and 0.993).

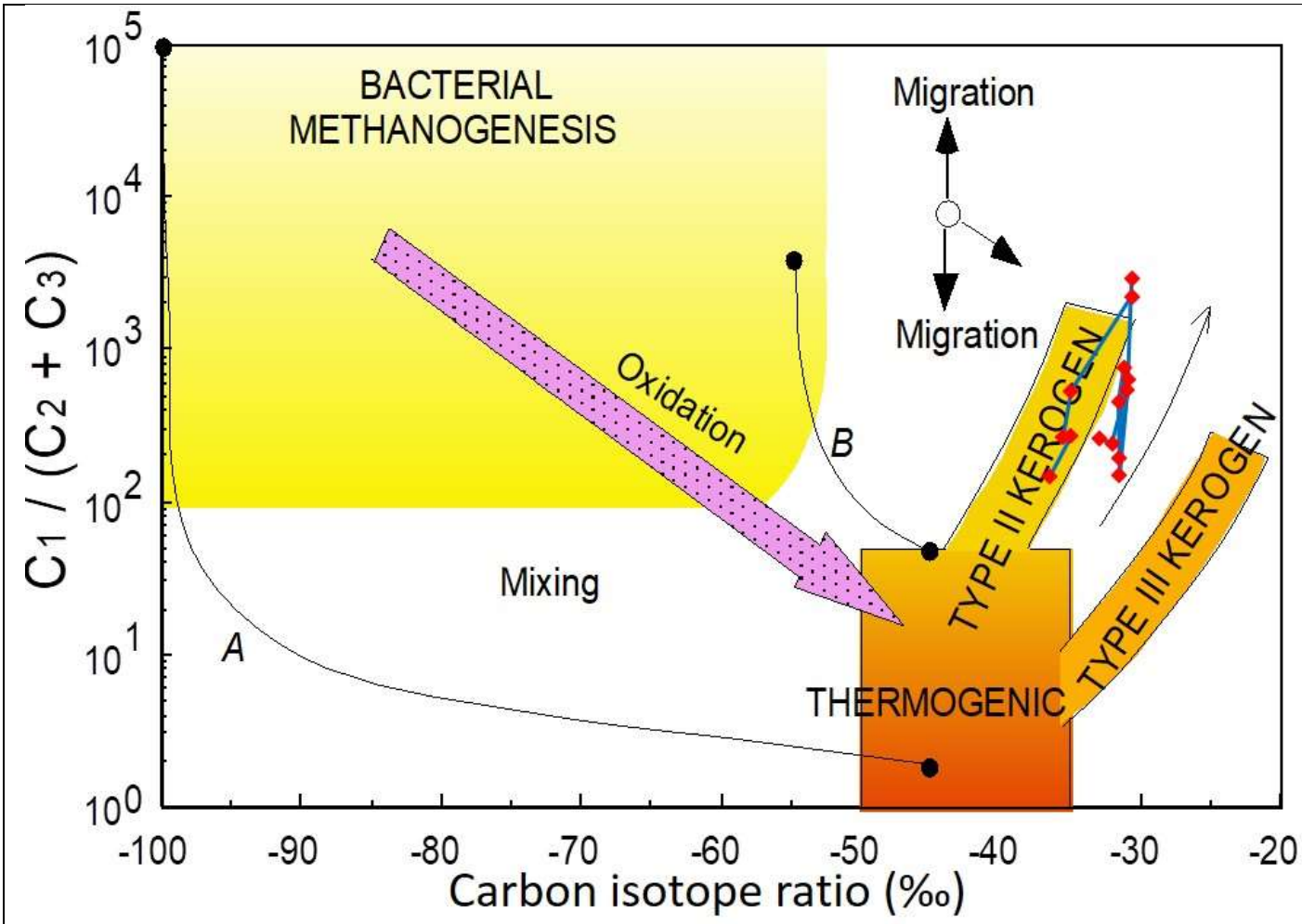

Figure A 131. ISO profile data – Interpretive Bernard Diagram for WA#29747 (Liard Devonian well with some uphole samples. A clear change in gas source for all samples in the target strata of the Besa River formation, but an increase in maturity and then possible rollover is seen, but there is no data for $\delta^{13}C3$ or $\delta^{13}C2$. This is a well that es the line to a higher category of methane source, Whiticar, 2018 pers. comm., after Whiticar 1999).

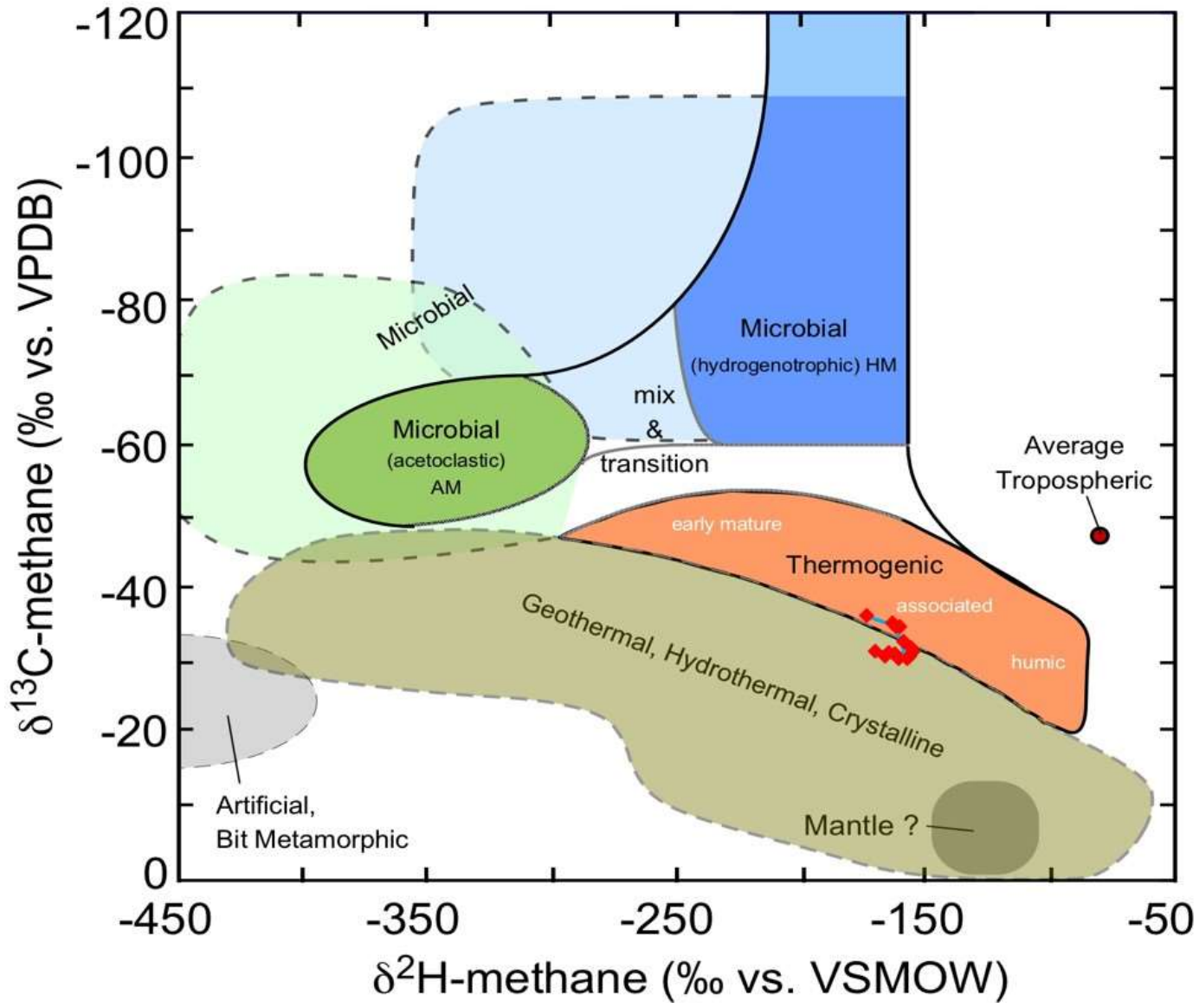

Figure A 132. ISO profile data – Interpretive CD Diagram for WA#29747 (Liard Devonian well with some uphole samples, Whiticar, 2018 pers. comm., after Whiticar 1999).

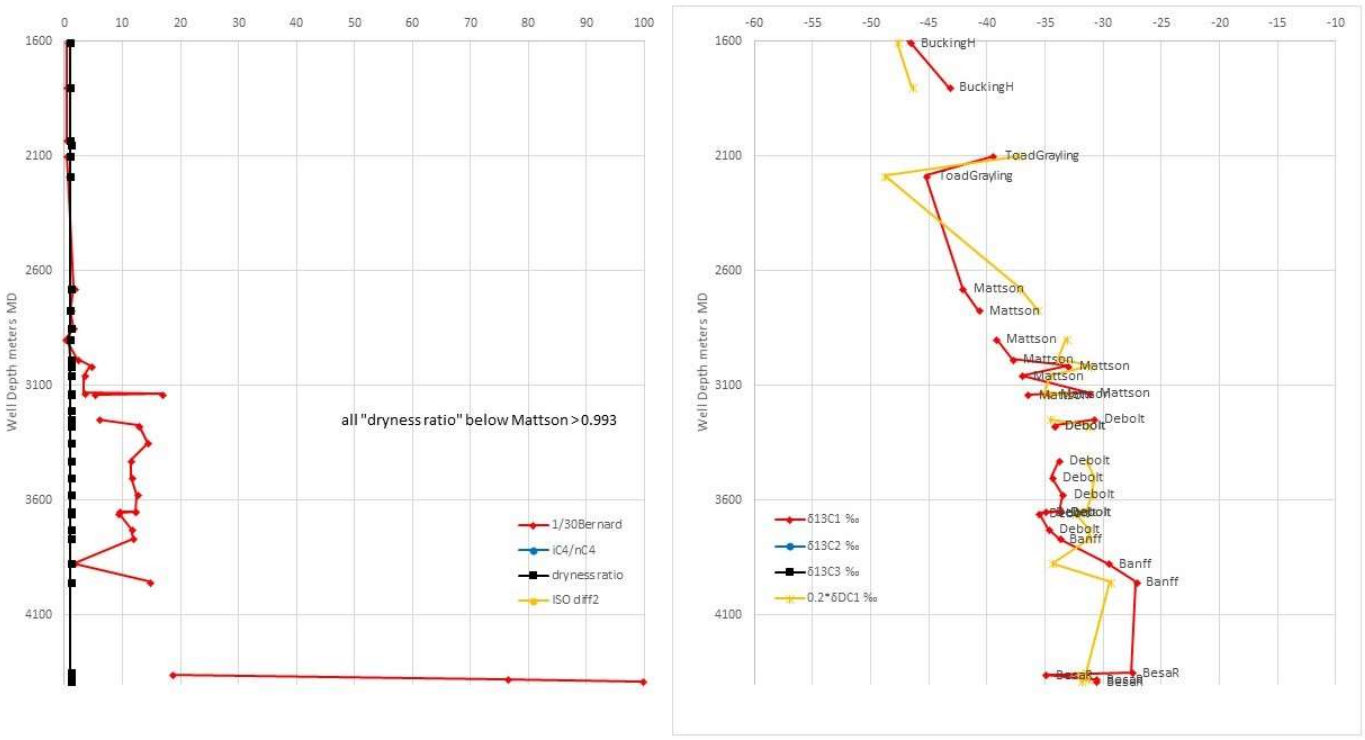

Figure A 133. Well profile, MC ratios and ISO data for WA#29727 (Liard Devonian well with some uphole samples. A vertical portion of a HZ well where the deviated section is data overlap with the HZ profile figure A136. Far to the north, this profile has a few unusual formations and the ISO data is only for methane as there is very low levels of longer chain hydrocarbons. Note the scale change for the 1/30 Bernard ratio and the dryness ratio really does not do anything as they are all between 1.0 and 0.993).

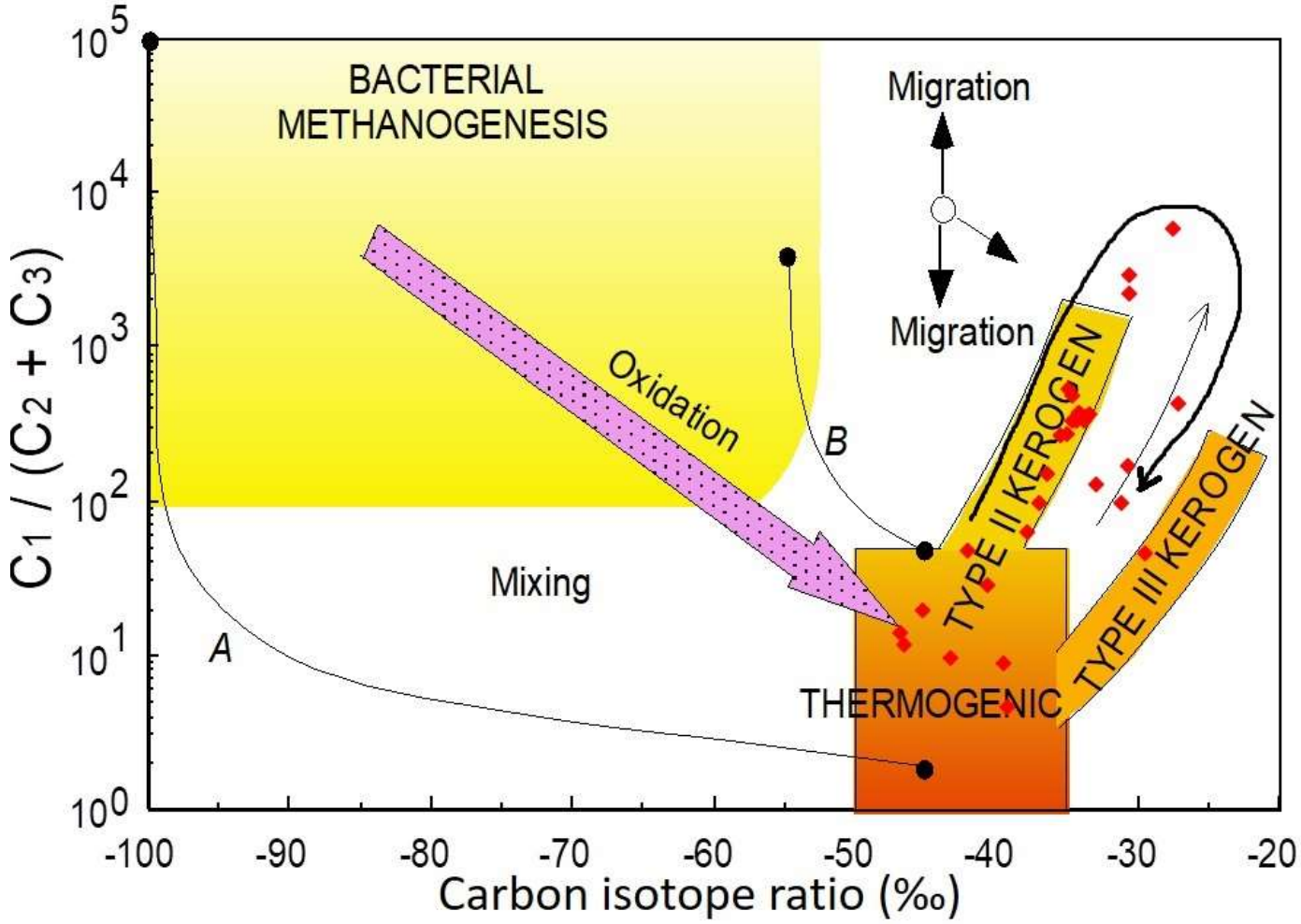

Figure A 134. ISO profile data – Interpretive Bernard Diagram for WA#29727 (Liard Devonian well with some uphole samples. A clear change in gas source for all samples in the target strata of the Besa River formation, but an increase in maturity and then possible rollover is seen, but there is no data for $\delta^{13}C3$ or $\delta^{13}C2$. This is a well that es the line to a higher category of methane source, Whiticar, 2018 pers. comm., after Whiticar 1999).

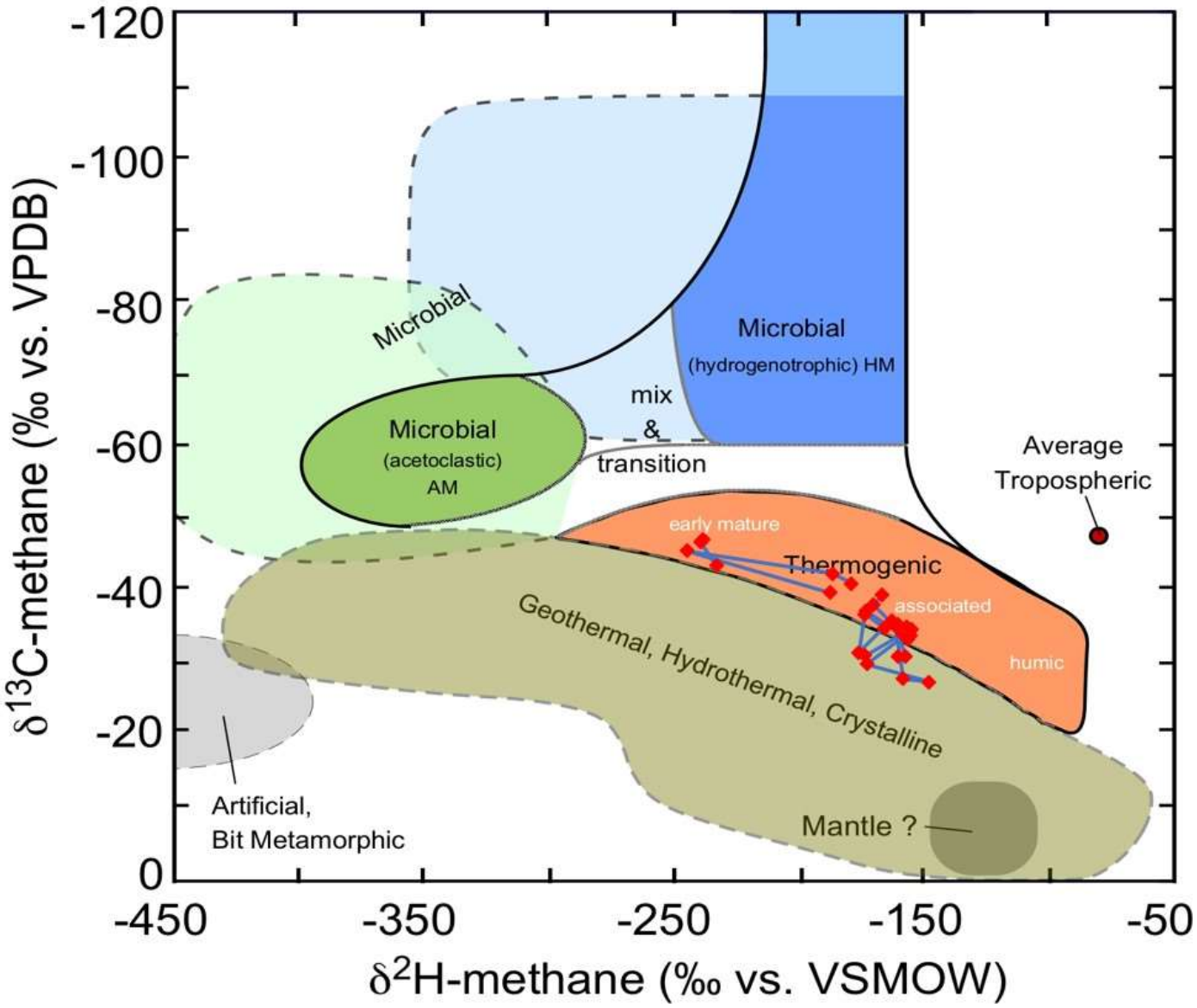

Figure A 135. ISO profile data – Interpretive CD Diagram for WA#29727 (Liard Devonian well with some uphole samples, Whiticar, 2018 pers. comm., after Whiticar 1999).

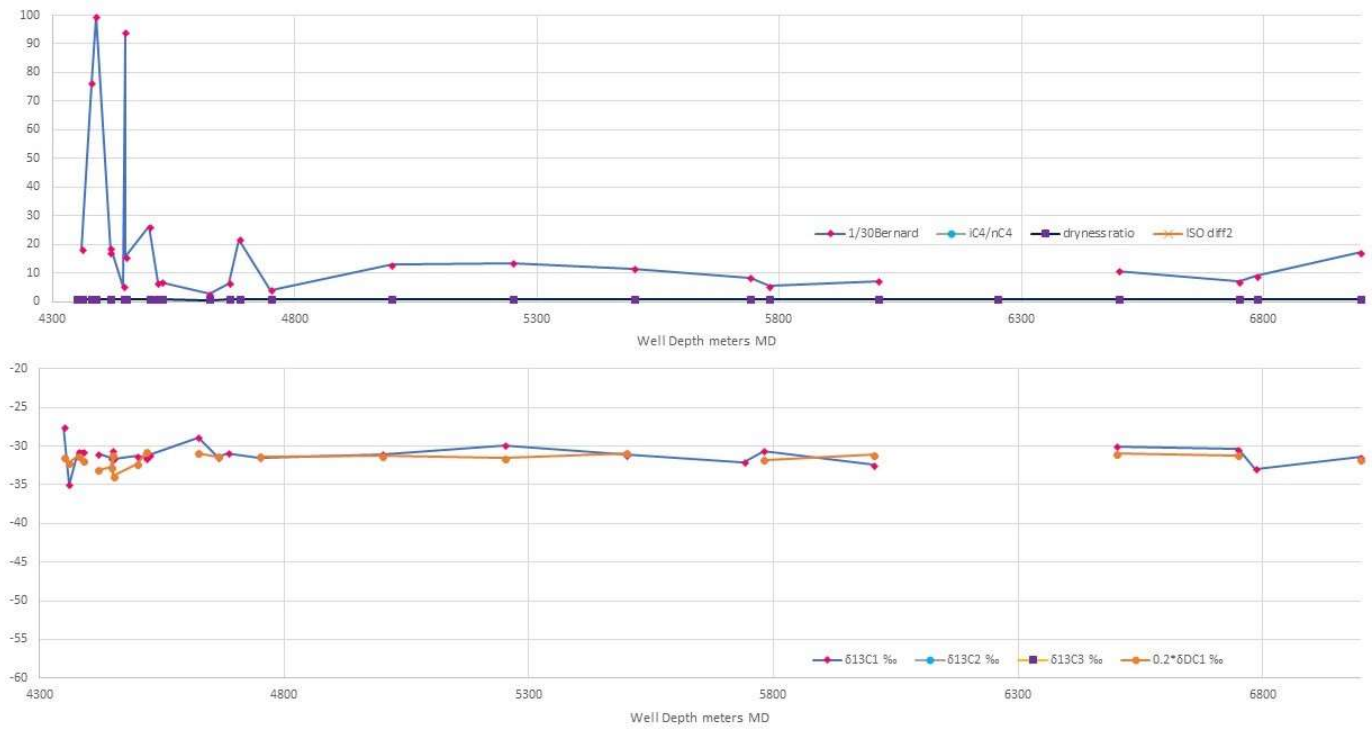

Figure A 136. Well profile, MC ratios and ISO data for WA#29727 (Besa River HZ leg with uphole completion included).

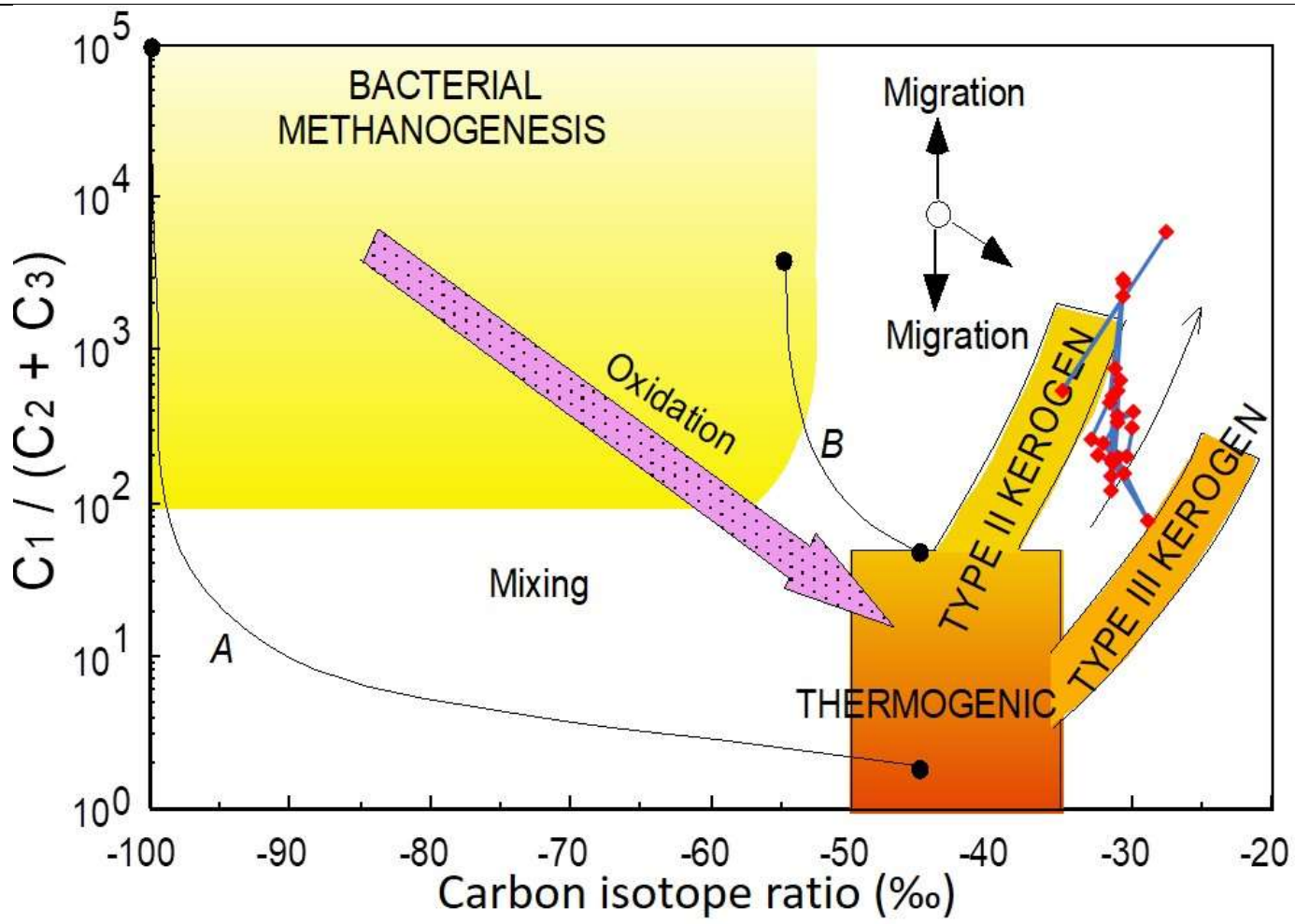

Figure A 137. ISO profile data – Interpretive Bernard Diagram for WA#29727 (Besa River HZ leg post-rollover with some data from uphole completion included. [see previous plot description for this well], (Whiticar, 2018 pers. comm., after Whiticar 1999).

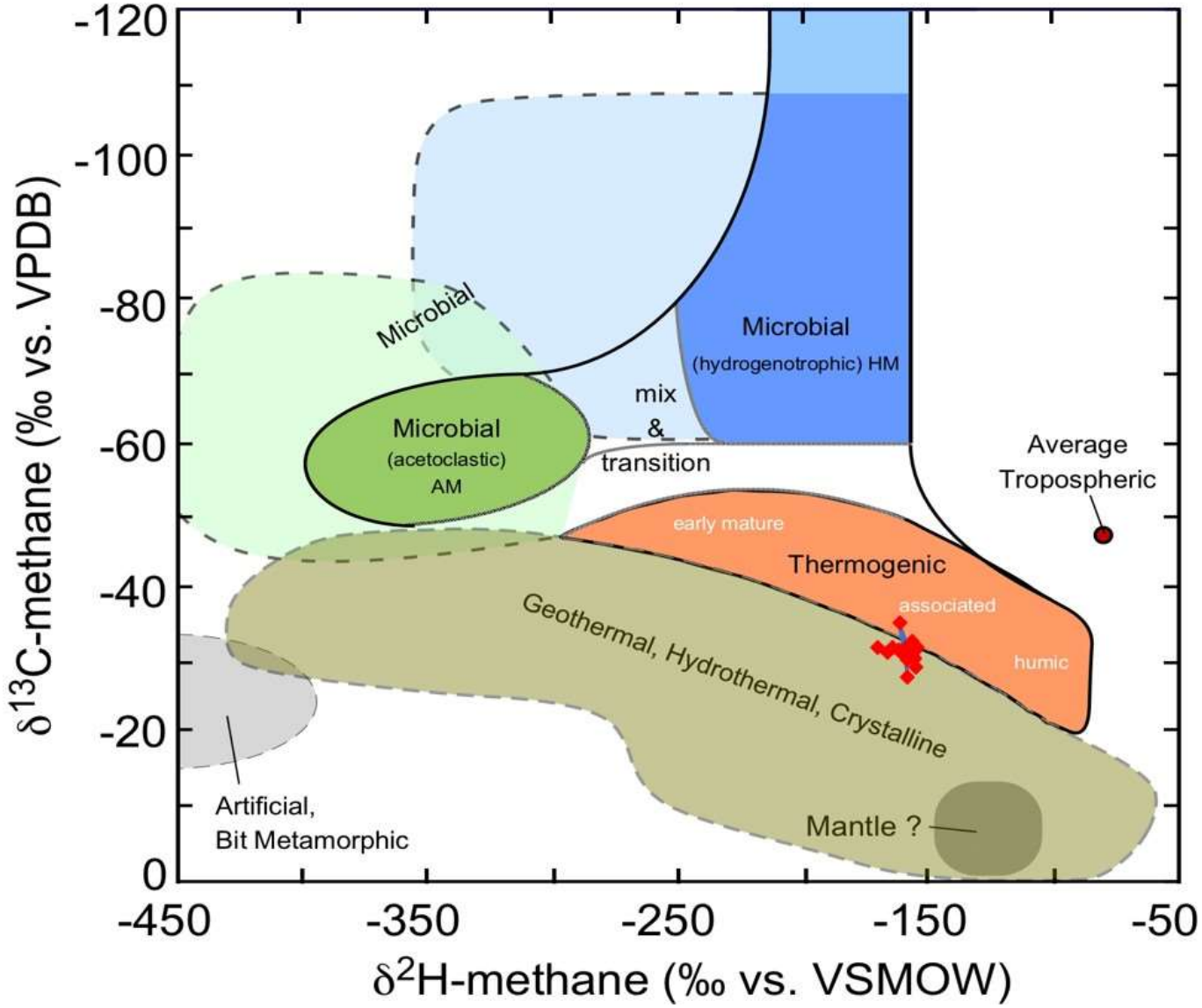

Figure A 138. ISO profile data – Interpretive CD Diagram for WA#29727 (Besa River HZ leg, Whiticar, 2018 pers. comm., after Whiticar 1999).

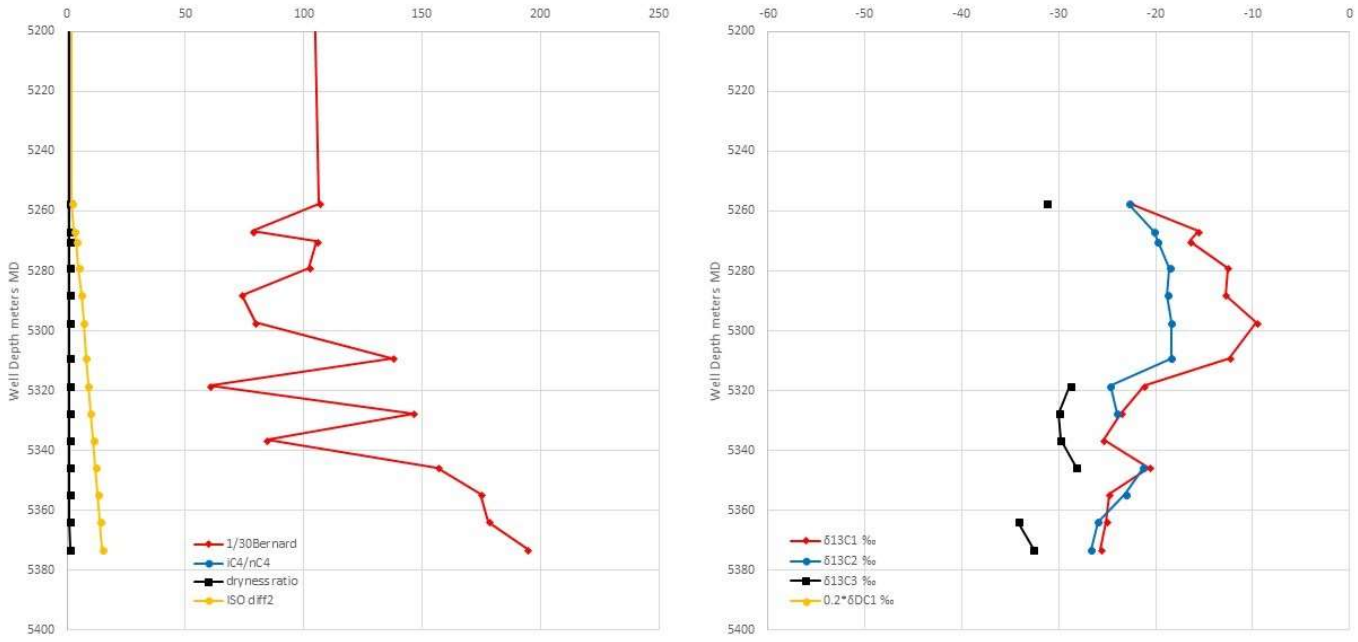

Figure A 139. Well profile, MC ratios and ISO data for WA#29046 (Liard Devonian well with some uphole samples. Far to the north, this profile has only the Besa River Formation sampled, but more comprehensive isotopic analysis allows for stronger interpretation with double isotopic reversal. Note the scale change for the 1/30 Bernard ratio and the dryness ratio really does not do anything as dryness ratios are all between 1.0 and 0.993).

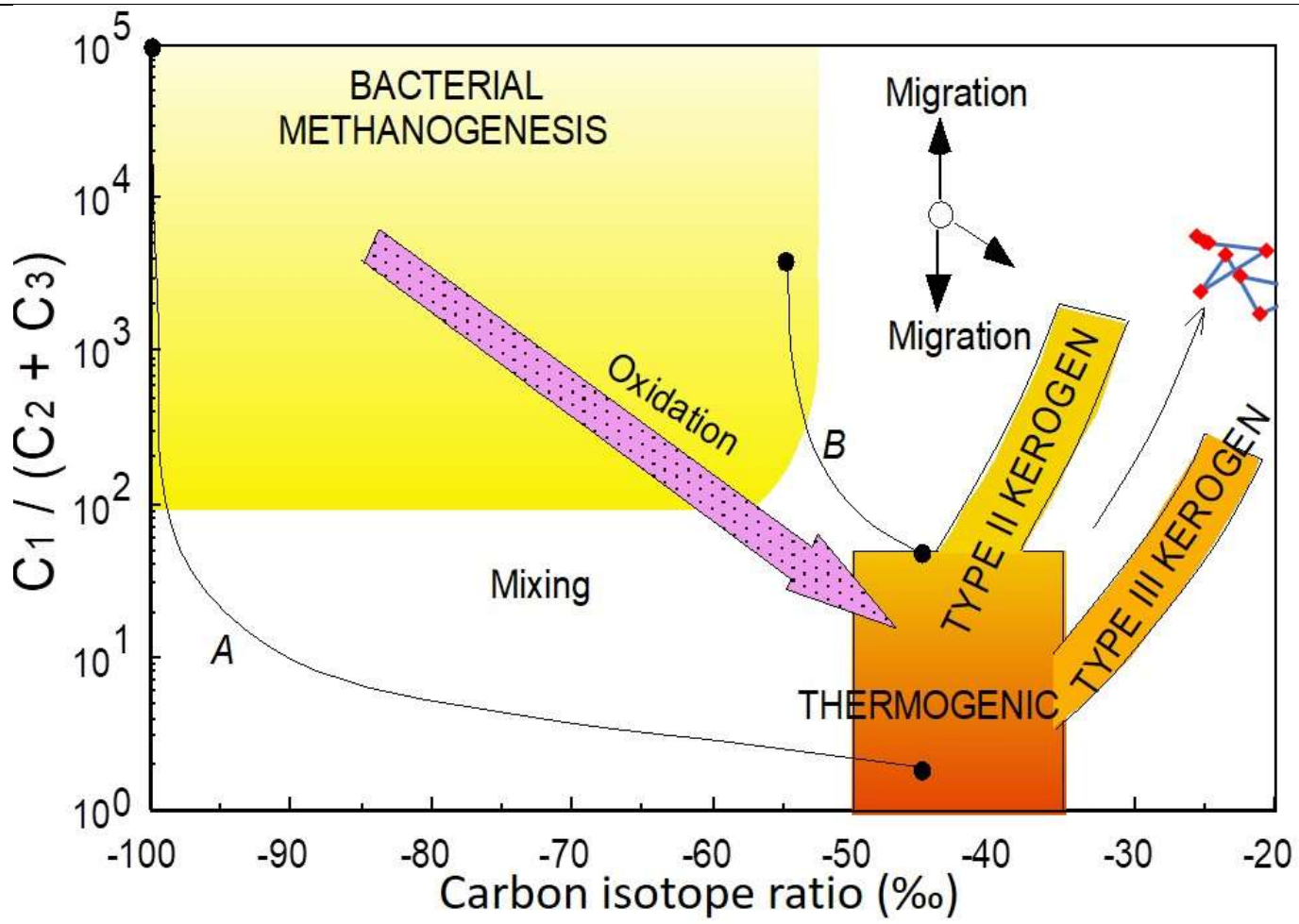

Figure A 140. ISO profile data – Interpretive Bernard Diagram for WA#29046 (Liard Devonian well. high temperature thermogenic gas, Whiticar, 2018 pers. comm., after Whiticar 1999).

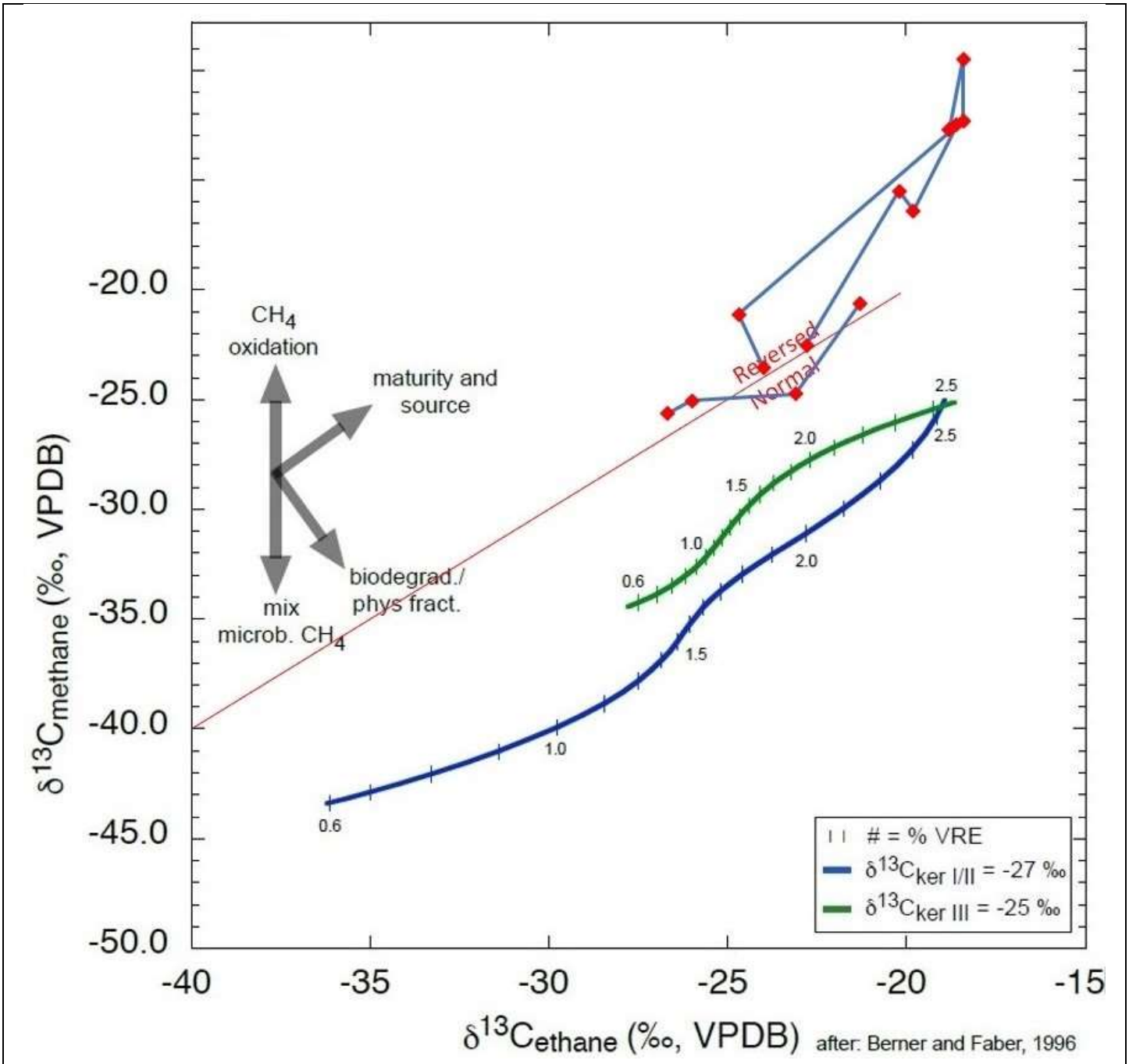

Figure A 141. ISO profile data – Interpretive ISO $\delta^{13}C_1$ versus $\delta^{13}C_2$ plot for WA#29046 (Liard Devonian well. The maturity of this gas is so high that it is plotting above and right of both plots indicating high temperature thermogenic gas with "roll-over" in a fairly comprehensive data package that is rare for this sub-basin, Whiticar, 2018 pers. comm., after Berner and Faber 1996, well profile trendlines).

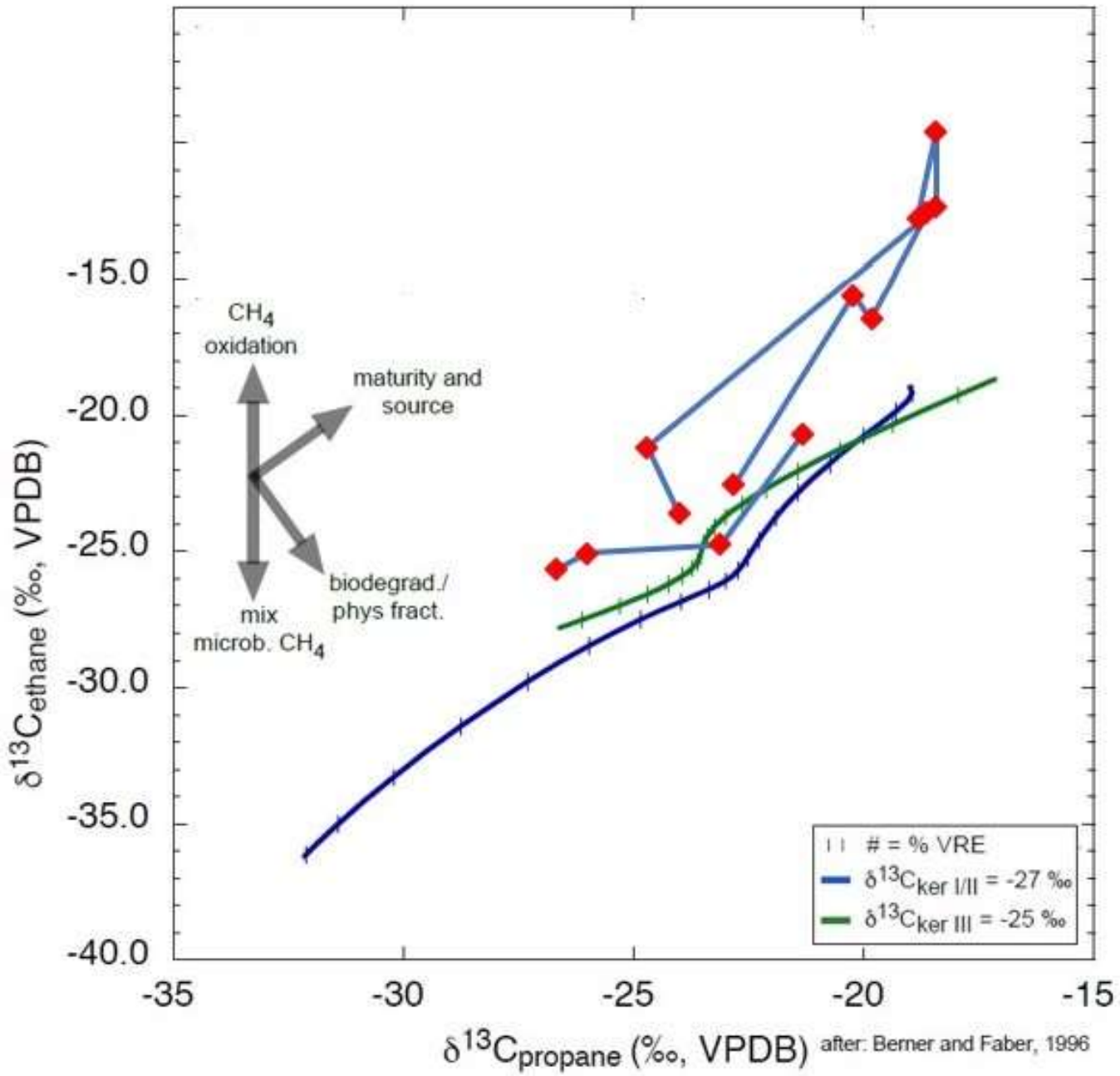

Figure A 142. ISO profile data – Interpretive ISO $\delta^{13}C_2$ versus $\delta^{13}C_3$ plot for WA#29046 (Liard Devonian well. The maturity of this gas is so high that it is plotting above and right of both plots indicating high temperature thermogenic gas with "roll-over" in a fairly comprehensive data package that is rare for this sub-basin, Whiticar, 2018 pers. comm., after Berner and Faber 1996, well profile trendlines).

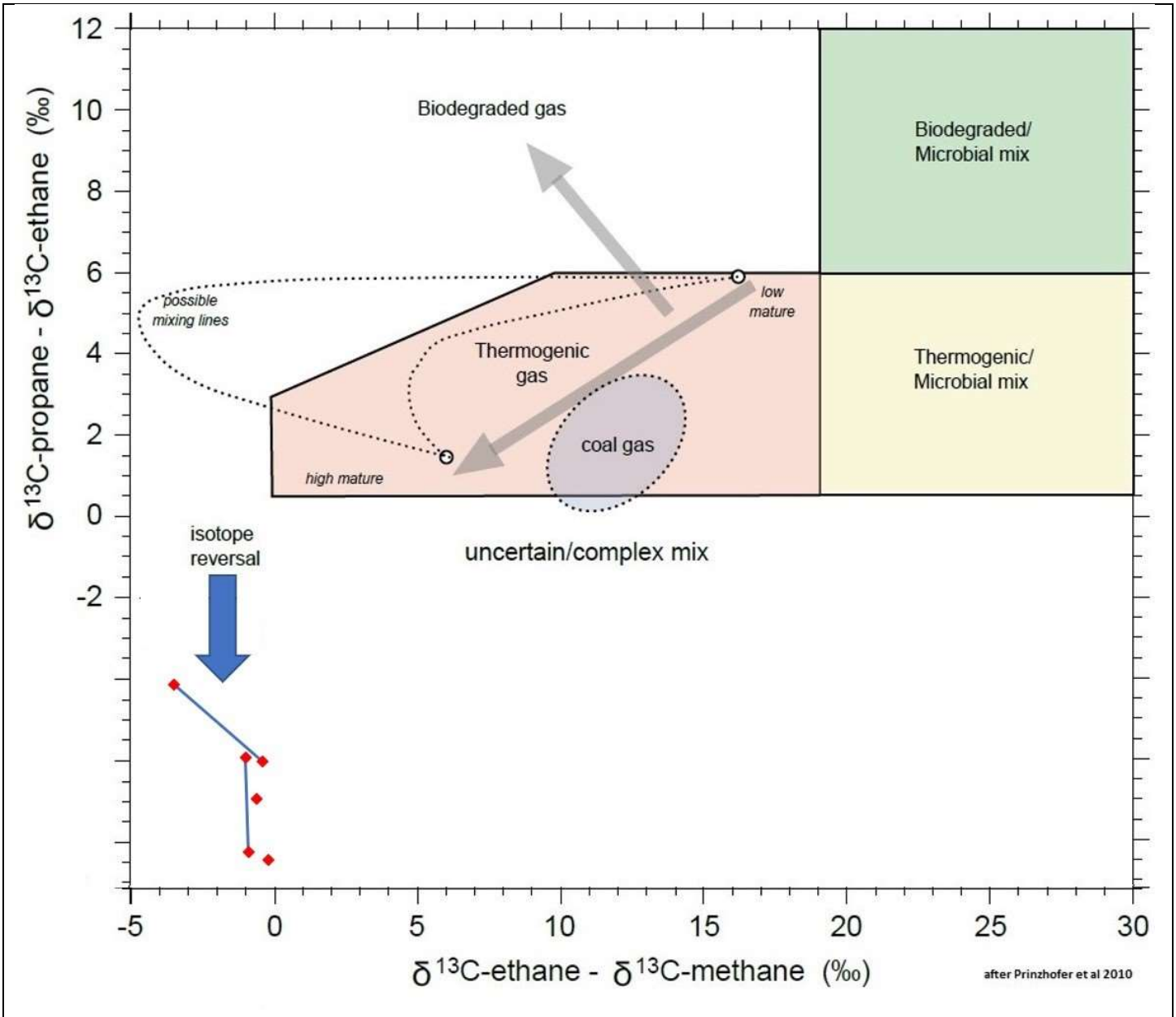

Figure A 143. Interpretive $\delta^{13}C_2$- $\delta^{13}C_1$ versus $\delta^{13}C_3$- $\delta^{13}C_2$ plot for WA#29046 (Liard Devonian well. A strong fit to the isotope reversal needs to expand the plot).

Previously Published profiles: The data in the various Tilley publications (Tilley et al. 2001, Tilley and Muehlenbachs 2006, Tilley and Muehlenbachs 2007, Tilley et al. 2011, Tilley and Muehlenbachs 2012, Tilley and Muehlenbachs 2013) includes a few graphical profiles and one data table.

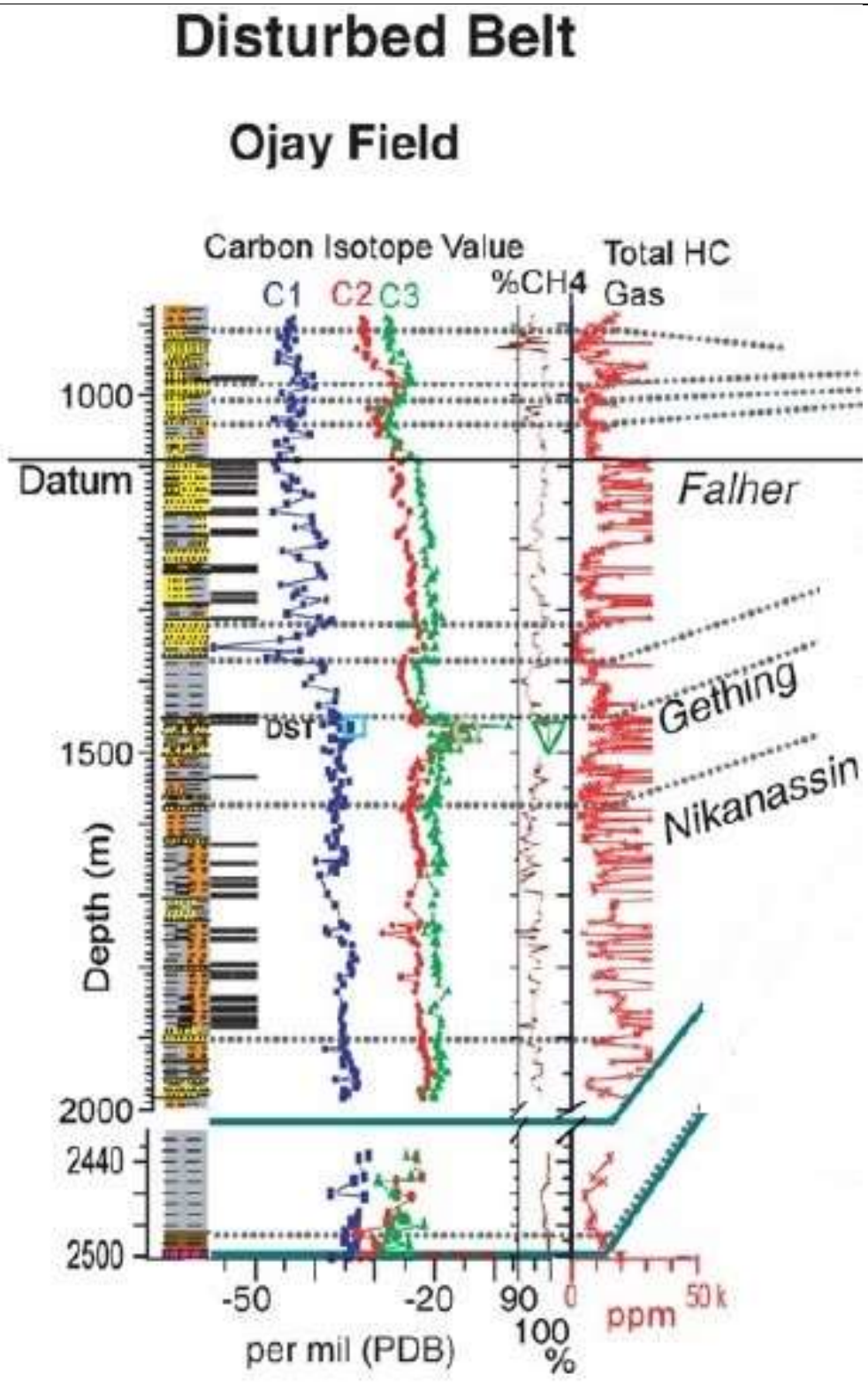

Figure A 144. Vertical profile of Ojay well, part of Tilley and Muehlenbachs 2006 Figure 2 therein

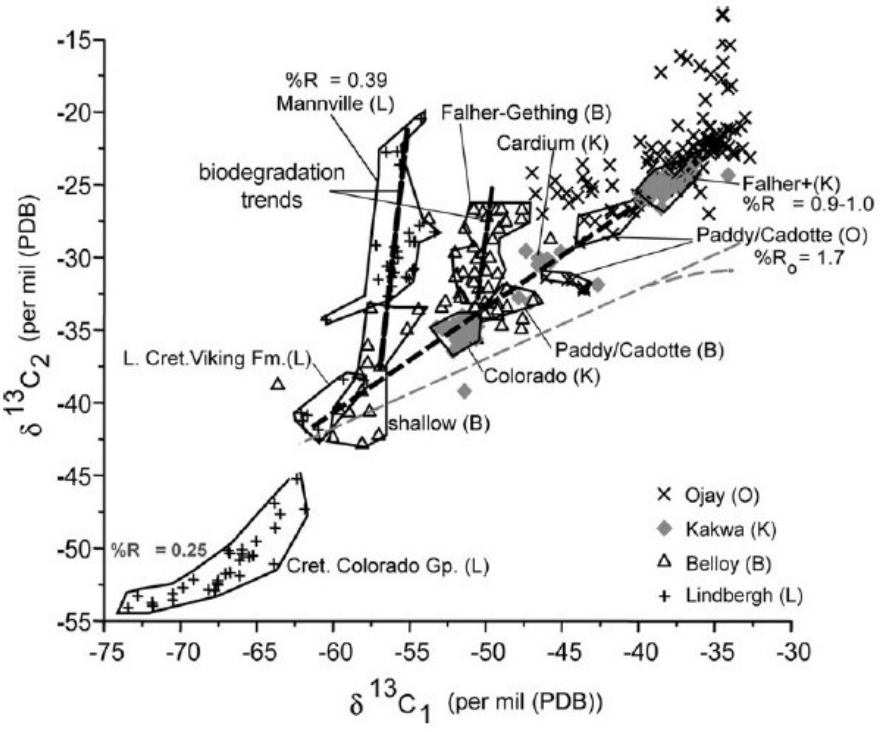

Figure A 145. Interpretive ISO $\delta^{13}C1$ versus $\delta^{13}C2$ plot from Tilley and Muehlenbachs 2006 Figure 6.

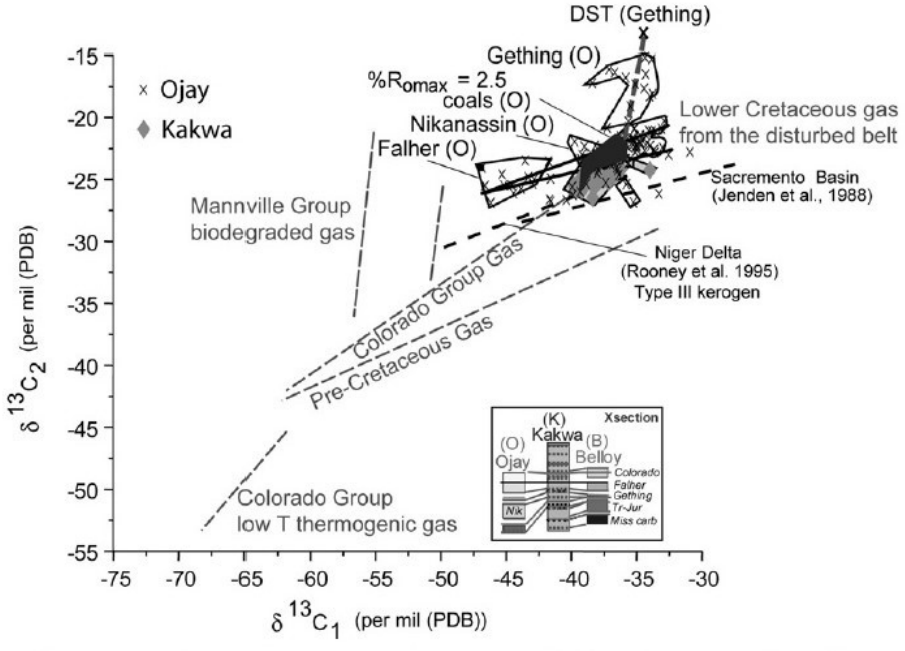

Figure A 146. Interpretive ISO $\delta^{13}C2$ versus $\delta^{13}C1$ plot from Tilley and Muehlenbachs 2006 Figure 7.

Table 006. Data from Tilley and Muehlenbachs 2013. Data is not fully referenced (e.g., to WA#) and geographic locations are ambiguous – the request to authors had no response, thus the data table below is not used further.

Sample	"Rock Unit"	depth(m)	$\delta^{13}C1‰$	$\delta^{13}C2‰$	$\delta^{13}C3‰$
MD1	Montney Fm.	1034	-45.4	-36.5	-35.6
MD2	Doig Fm.	2021	-46.2	-34.6	-33.5
MD3	Montney Fm.	2258	-41.3	-30	-27
MD4	Montney Fm.	2253	-40.4	-29.7	-26.4
MD5	Montney Fm.	2233	-42.2	-30.4	-28.2
MD6	Montney Fm.	2261	-39.6	-29	-25.5
MD7	Montney Fm.	2284	-37.4	-28.5	-26
MD8	Montney Fm.	2386	-39.5	-26.8	-20.5
MD9	Montney Fm.	2411	-41.4	-28.8	-25.9
MD10	Doig Fm.	2302	-36.3	-35.1	-26.8
MD11	Montney Fm.	2300	-36	-27	-23.6
MD12	Doig Fm.	2500	-37.4	-27.2	-21.7
MD13	Doig Fm.	2585	-37.5	-38.8	-33.4
MD14	Montney Fm.	2680	-36.4	-25.7	-19.8
MD15	Montney Fm.	blank	-41.8	-27.9	-22.6
MD16	Doig Fm.	3100	-36.2	-42.2	-41.8
MD17	Doig Fm.	3111	-37.5	-41.4	-43.2
MD18	Montney Fm.	3097	-35.5	-41.5	-40.5
HR1	Horn River Sh.	blank	-27.6	-33.8	blank
HR2	Horn River Sh.	blank	-32.1	-34.9	-38.8
HR3	Horn River Sh.	blank	-31.3	-34.1	-37.3
HR4	Horn River Sh.	blank	-31.2	-32	-35.5
HR5	Horn River Sh.	blank	-30.7	-34.4	-36.9
HR6	Horn River Sh.	blank	-34.5	-34.4	-37.4

The data in Norville (2104) can be distilled down to: a single vertical profile with 80 samples for WA#25702; two horizontal profiles and CD diagram with 79 Muskwa samples for WA#25702 and 14 Otter Park samples for WA#25938; eight HZ wells with post-frac production gas vs elapsed time profiles; six wells with ISO data tabulated (2 wells as mudgas profiles but no depths, and 4 wells as production gas profiles but no dates). The Norville CD Diagram of WA#25702 and WA#25938 HZ leg data is comparable with the trend for WA#29747-29727 that is also in the Liard basin, except the Norville data is completely within the Thermogenic and Humic trends, while WA#29747 shifts down into the Geothermal trend. The Norville $\delta^{13}C2$ vs $\delta^{13}C1$ and $\delta^{13}C3$ vs $\delta^{13}C2$ plots were not calibrated to the source kerogen estimates, but they were in the same range of data as WA#29046. The BF-SEOS data point for the Liard sub-basin, WA#29747-29727, cannot be shown as the gas content in the samples of very dry gas submitted to BC-NGA did not support the determination of $\delta^{13}C2$ or $\delta^{13}C3$.

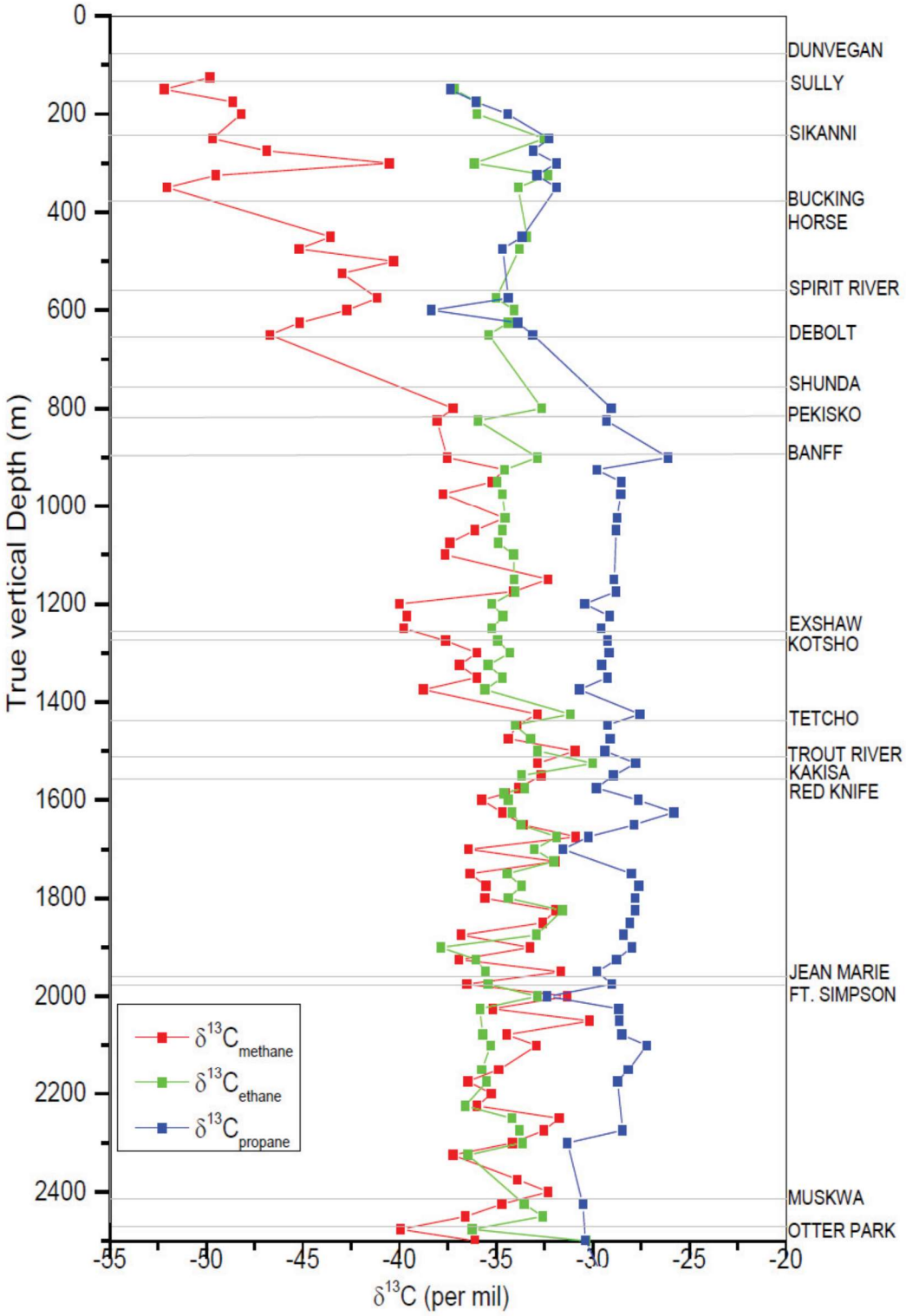

Figure A 147. VT ISO profile for WA#25702 from Norville 2014 figure 2.2

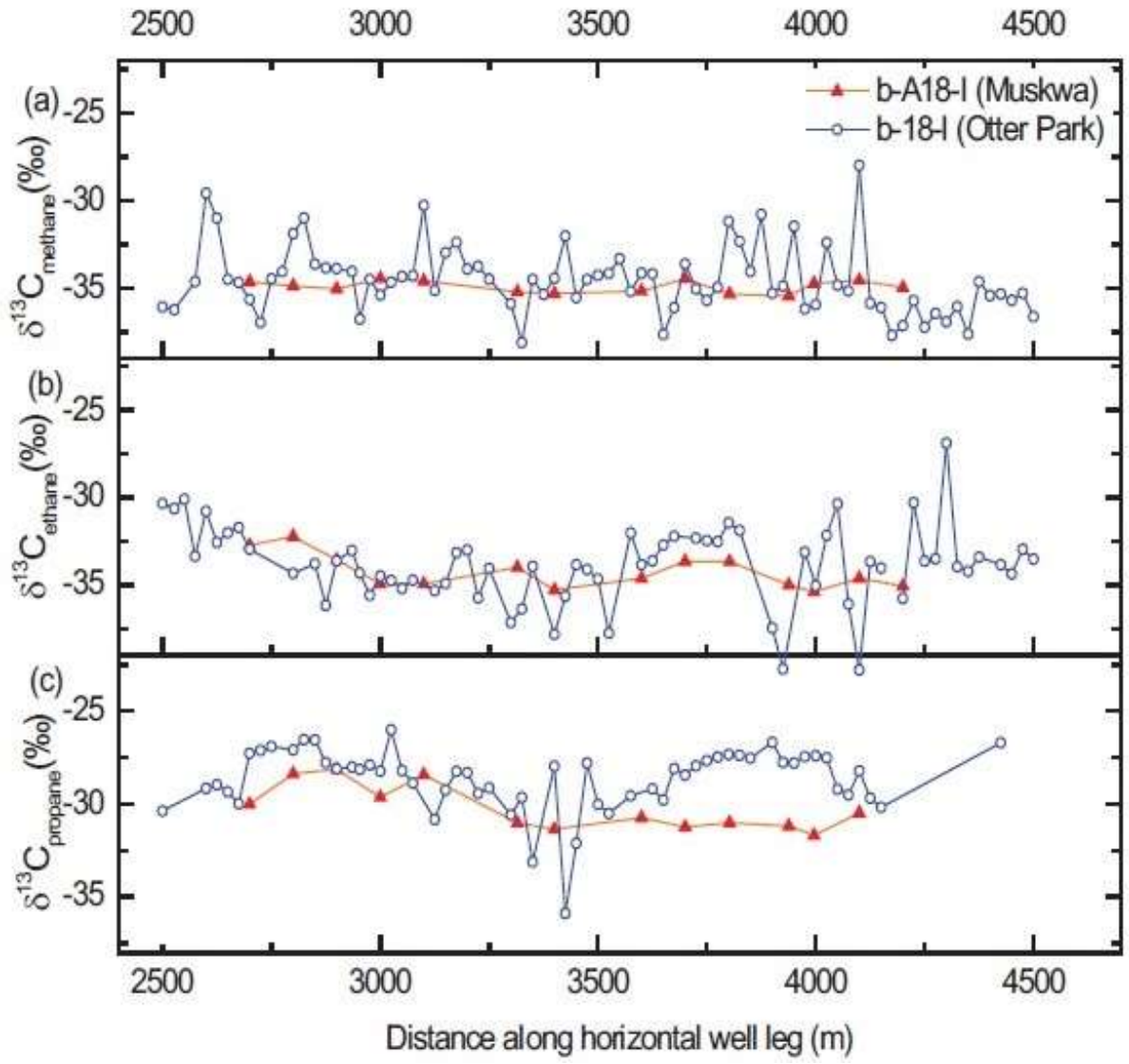

Figure A 148. HZ ISO profiles for WA#25702 and 25938 from Norville 2014 figures 3.8 and 3.9

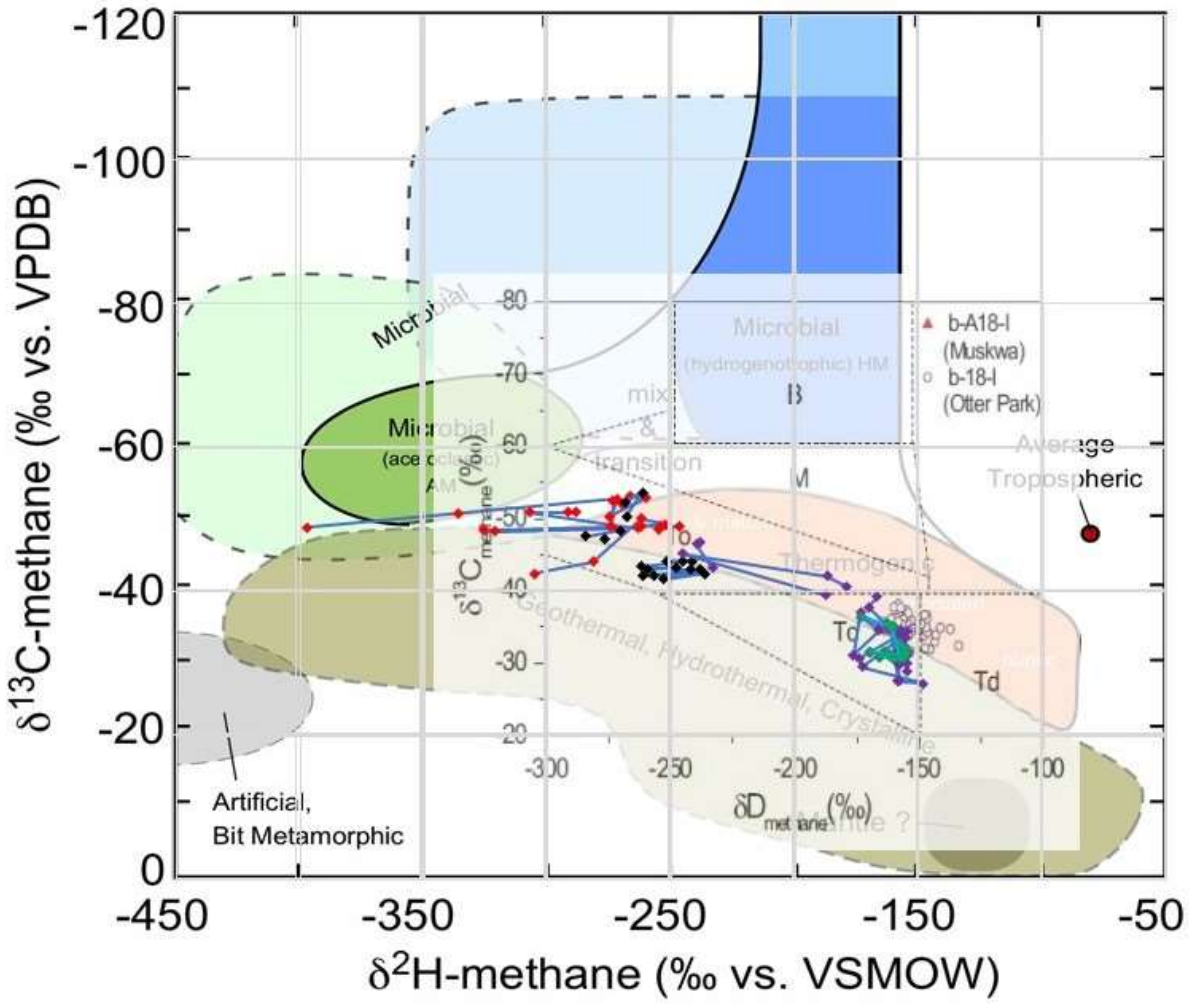

Figure A 149. Partial CD diagram for 2 HZ wells WA#25702 and 25938 from Norville 2014 figure 3.14 superimposed on CD template and BF-SEOS well profiles

Appendix B: BC-NGA Isotopic Map data: maps displayed on http://www.geosciencebc.com server and http://bc-nga.ca/ .

This section of the thesis contains the supporting ISO data presented as interpretive diagrams to support discussion in the main text of the thesis.

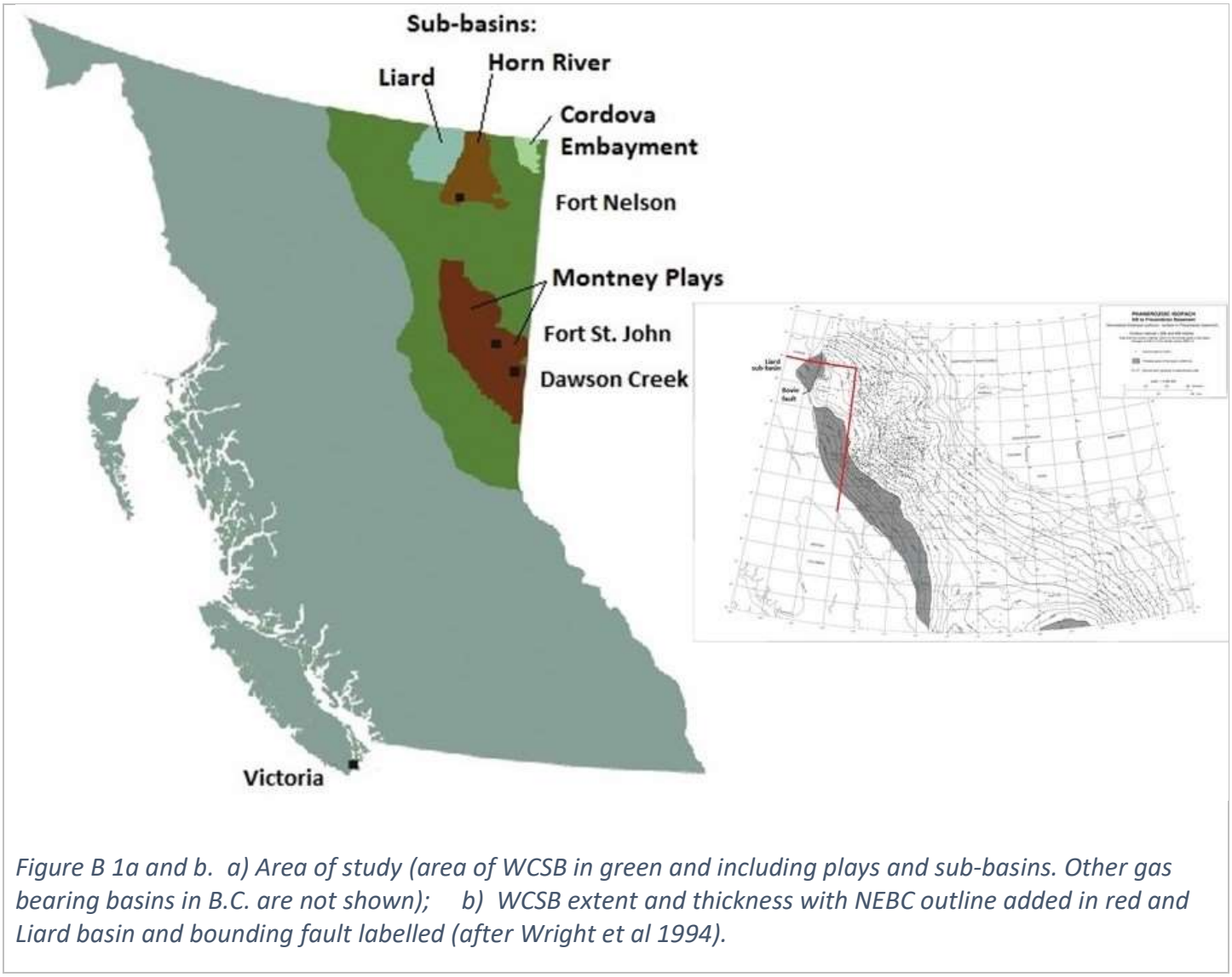

Figure B 1a and b. a) Area of study (area of WCSB in green and including plays and sub-basins. Other gas bearing basins in B.C. are not shown); b) WCSB extent and thickness with NEBC outline added in red and Liard basin and bounding fault labelled (after Wright et al 1994).

The types of plots included here are (see the main text for definitions):

1. Bernard Diagram (each play);
2. CD Diagram (where both $\delta^{13}C_1$ and $\delta^{2}H\text{-}C_1$ have data);
3. Berner-Faber Diagram $\delta^{13}C_1$ vs. $\delta^{13}C_2$ (where both $\delta^{13}C_1$ and $\delta^{13}C_2$ have data);
4. Berner-Faber Diagram $\delta^{13}C_2$ vs. $\delta^{13}C_3$ (where both $\delta^{13}C_2$ and $\delta^{13}C_3$ have data);
5. Plot $\delta^{13}C_1$ vs. $\delta^{13}CO_2$ diagram (where both $\delta^{13}C_1$ and $\delta^{13}CO_2$ have data).
6. Plot of $\delta^{13}C_2\text{-}\delta^{13}C_1$ ‰ versus $\delta^{13}C_3\text{-}\delta^{13}C_2$ ‰

The interpretive diagrams of plays are presented approximately in stratigraphic order from shallowest to deepest.

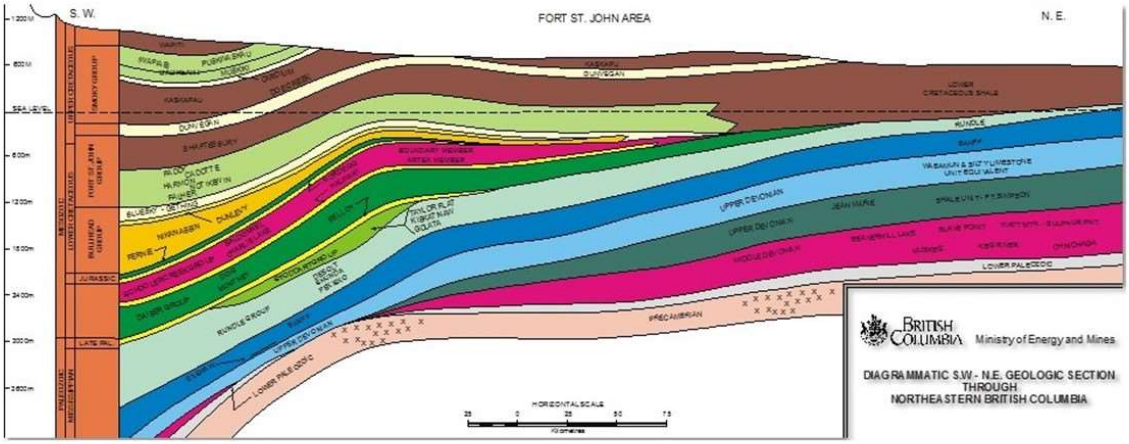
S. W.
FORT ST. JOHN AREA
N. E.
BRITISH COLUMBIA
Ministry of Energy and Mines
DIAGRAMMATIC S.W. - N.E. GEOLOGIC SECTION THROUGH NORTHEASTERN BRITISH COLUMBIA

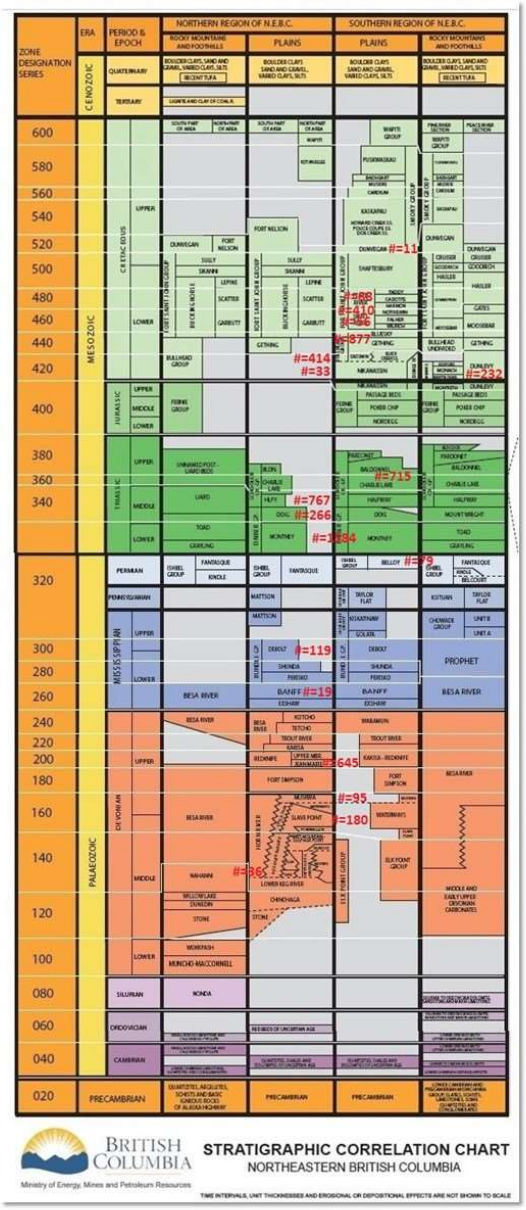
NORTHERN REGION OF N.E.B.C.
SOUTHERN REGION OF N.E.B.C.
ROCKY MOUNTAINS AND FOOTHILLS
PLAINS
CENOZOIC
MESOZOIC
PALAEOZOIC
PRECAMBRIAN
#=119
#=19
#=2645
#=95
#=180
#=365
#=767
#=266
#=414
#=33
#=715
#=79
#=11
#=282
BRITISH COLUMBIA
Ministry of Energy, Mines and Petroleum Resources
STRATIGRAPHIC CORRELATION CHART
NORTHEASTERN BRITISH COLUMBIA

Figure B 2a and b. Stratigraphic chart – All maps: Chart and Schematic -section of the NEBC strata. All plays are listed in Appendix C. The ISO data of plays in Appendix B are presented approximately in stratigraphic order from shallowest to deepest.

Contents of Appendix B

1. “Play 4.00” Surface gas emissions (all types)

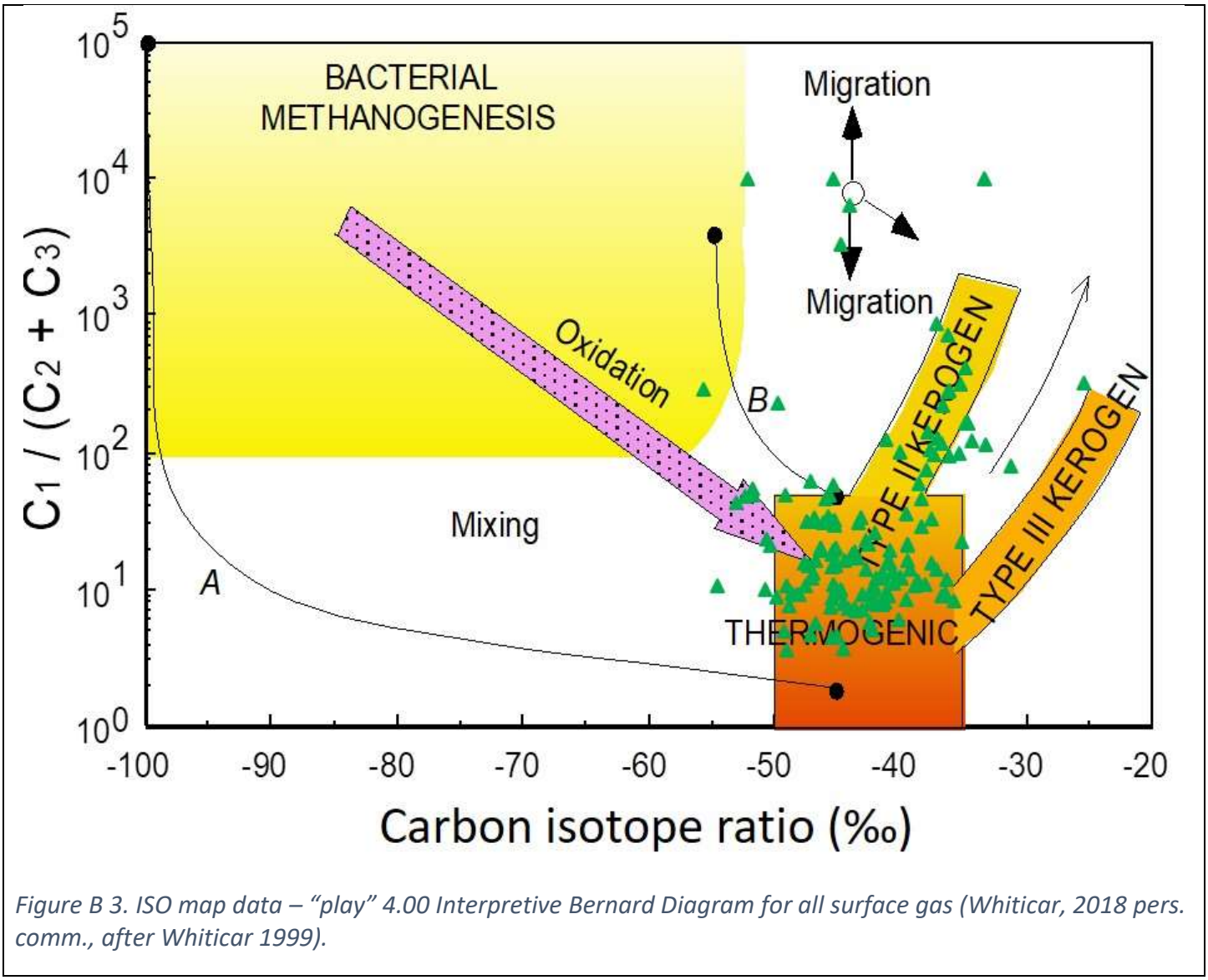

Figure B 3. ISO map data – “play” 4.00 Interpretive Bernard Diagram for all surface gas (Whiticar, 2018 pers. comm., after Whiticar 1999).

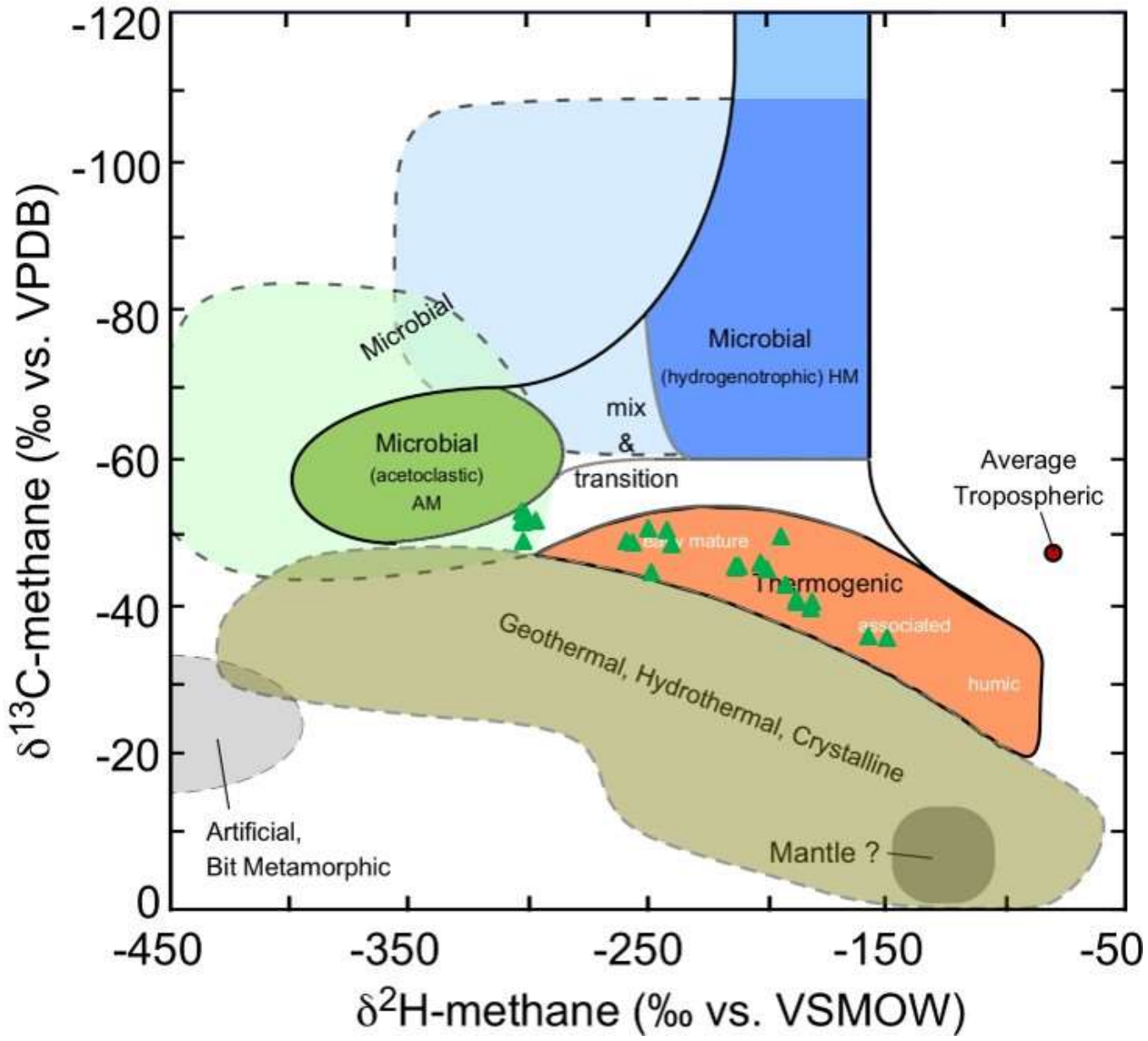

Figure B 4. ISO map data – "play" 4.00 Interpretive CD Diagram for all surface gas (Whiticar, 2018 pers. comm., after Whiticar 1999).

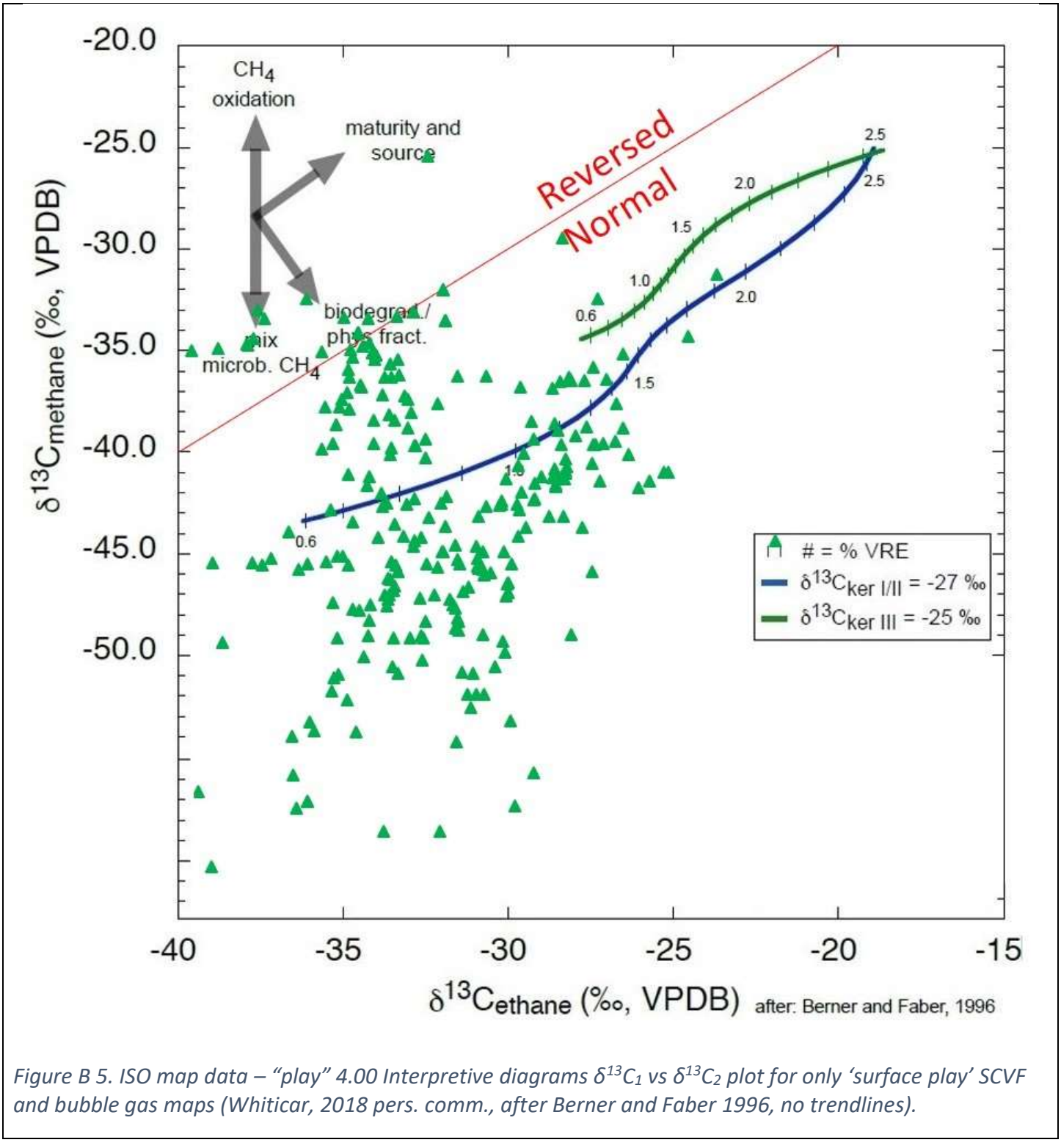

Figure B 5. ISO map data – "play" 4.00 Interpretive diagrams $\delta^{13}C_1$ vs $\delta^{13}C_2$ plot for only 'surface play' SCVF and bubble gas maps (Whiticar, 2018 pers. comm., after Berner and Faber 1996, no trendlines).

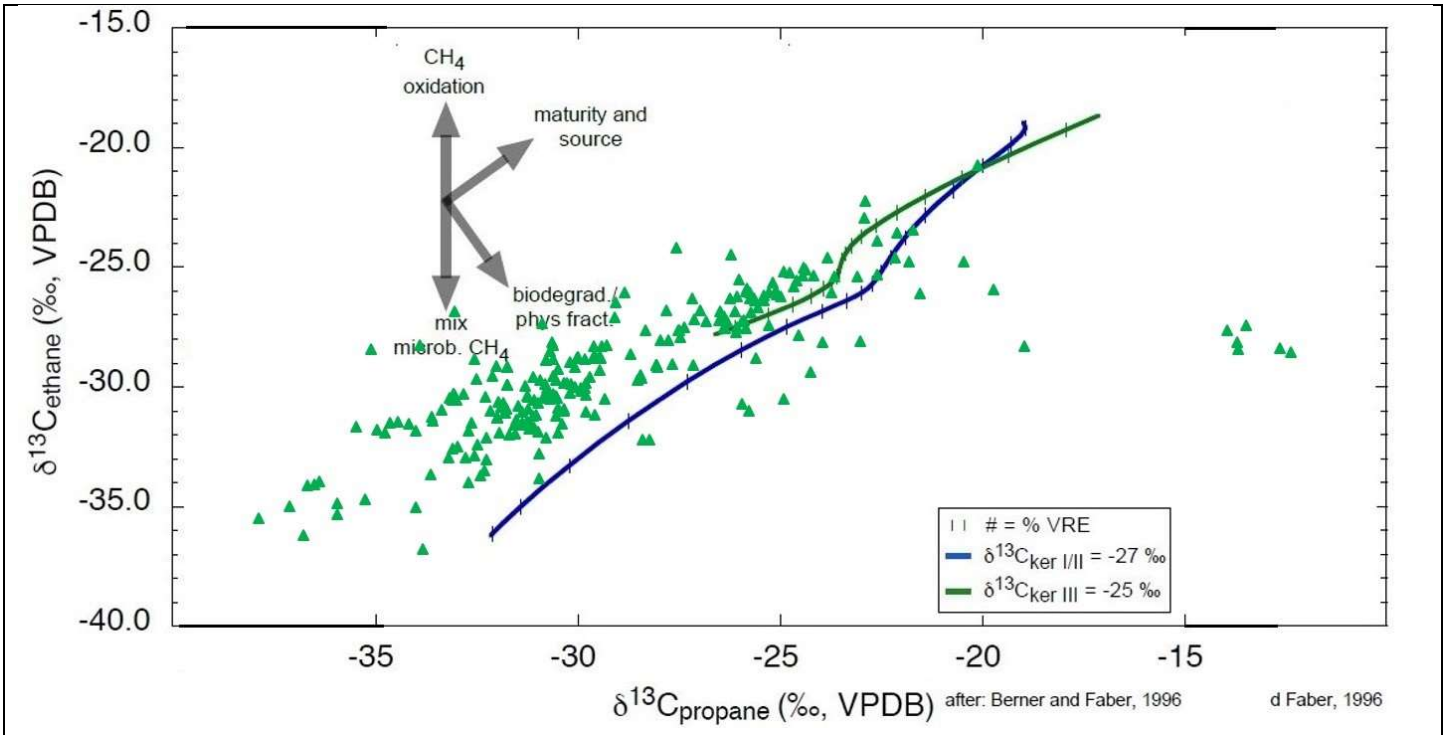

Figure B 6. ISO map data – "play" 4.00 Interpretive diagrams $\delta^{13}C_2$ vs $\delta^{13}C_3$ plot for only 'surface play' SCVF and bubble gas maps (Whiticar, 2018 pers. comm., after Berner and Faber 1996, no trendlines).

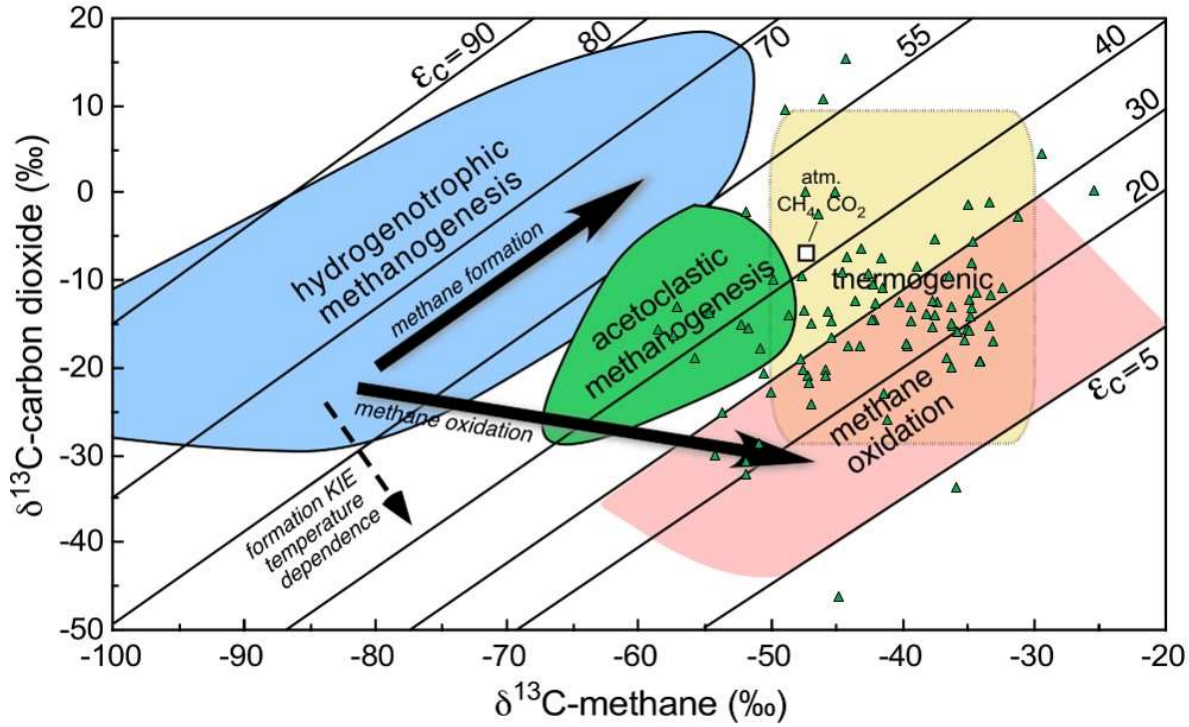

Figure B 7. ISO map data – "play" 4.00 Interpretive diagrams $\delta^{13}CO_2$ additional plot (after Whiticar 1999).

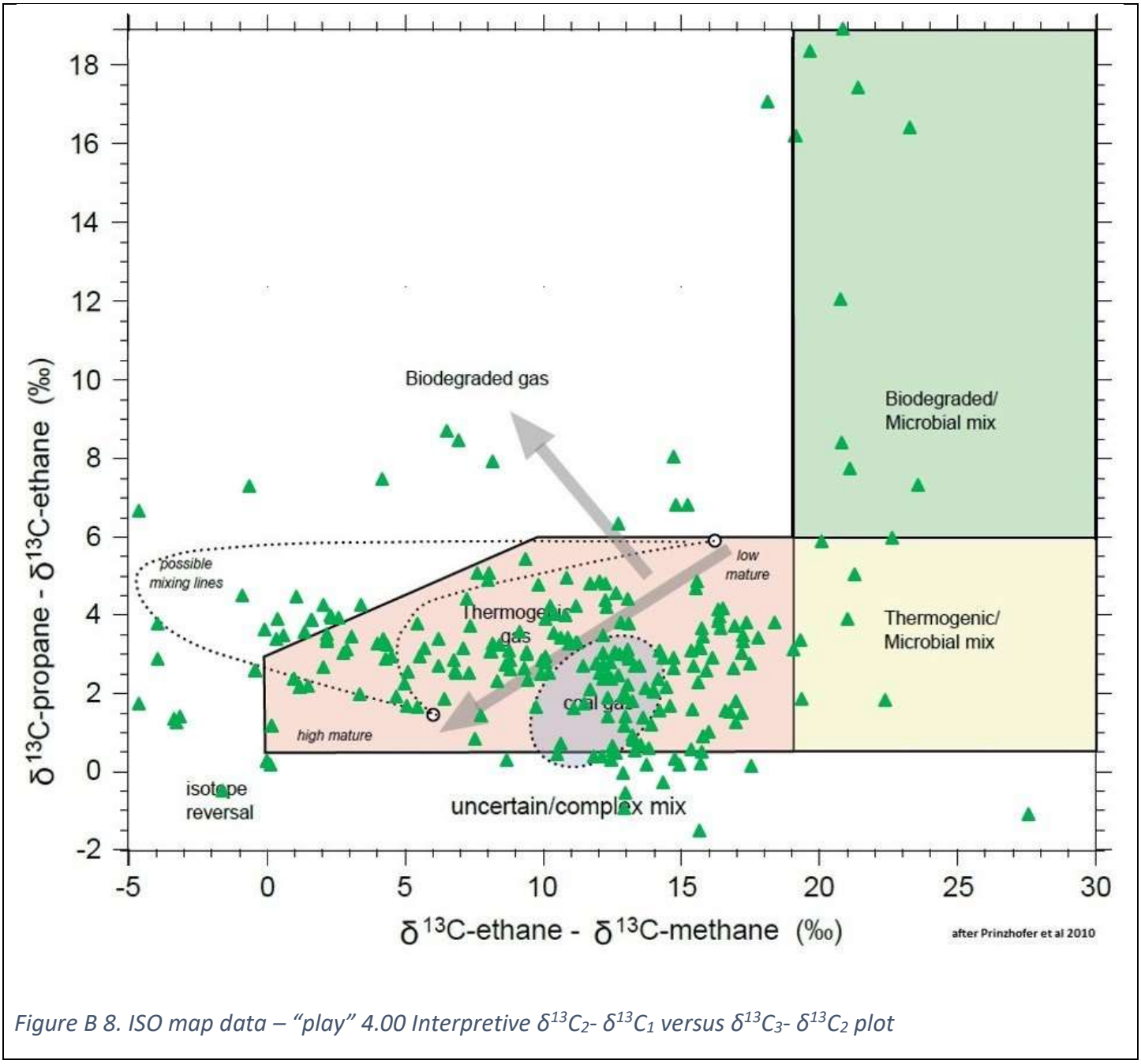

Figure B 8. ISO map data – "play" 4.00 Interpretive $\delta^{13}C_2$- $\delta^{13}C_1$ versus $\delta^{13}C_3$- $\delta^{13}C_2$ plot

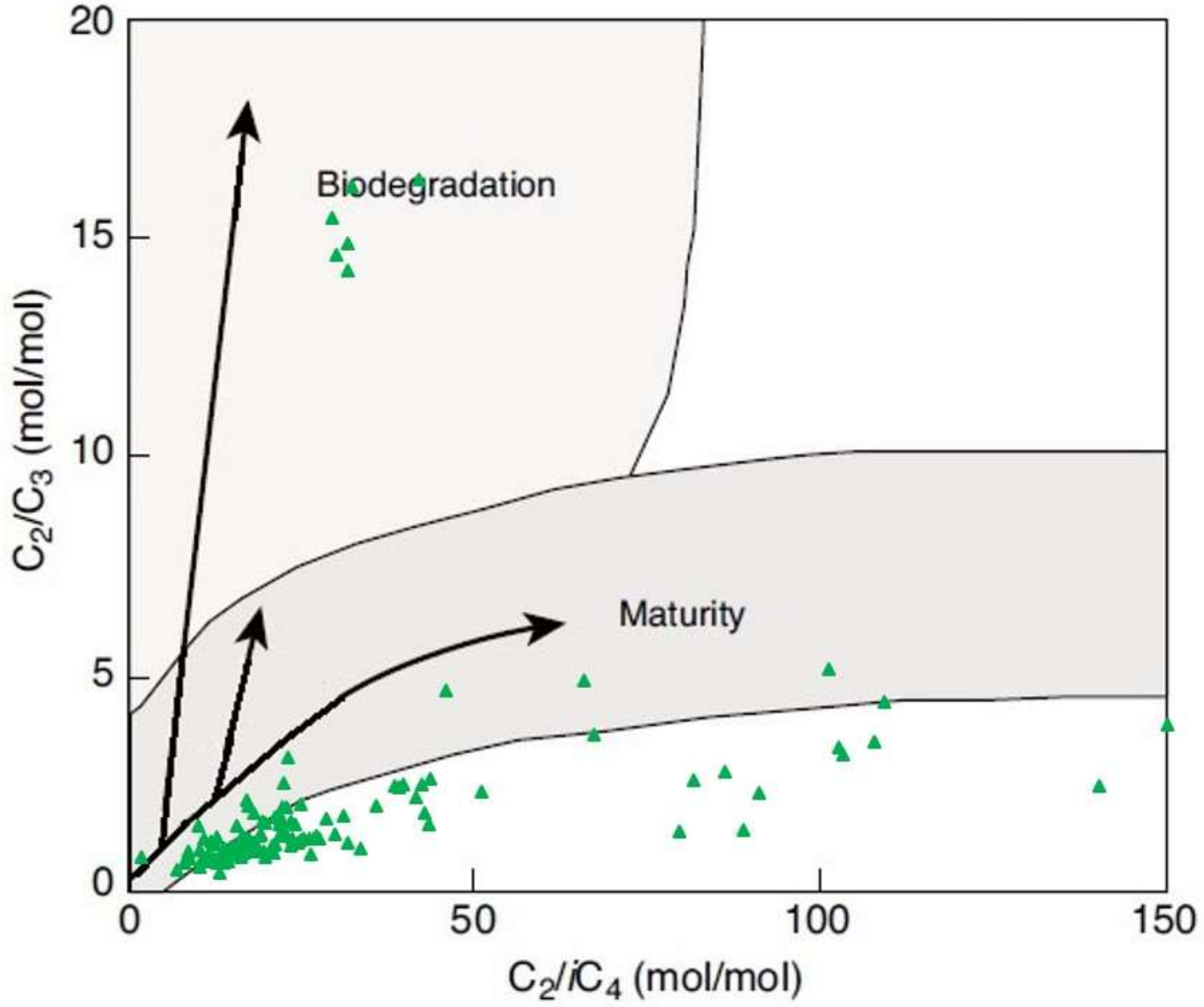

Figure B 9. ISO map data – "play" 4.00 Interpretive diagrams MC (only) Prinzhofer Diagram for 'surface play' SCVF and bubble gas maps (after Prinzhofer and Battani 2003, no trendlines).

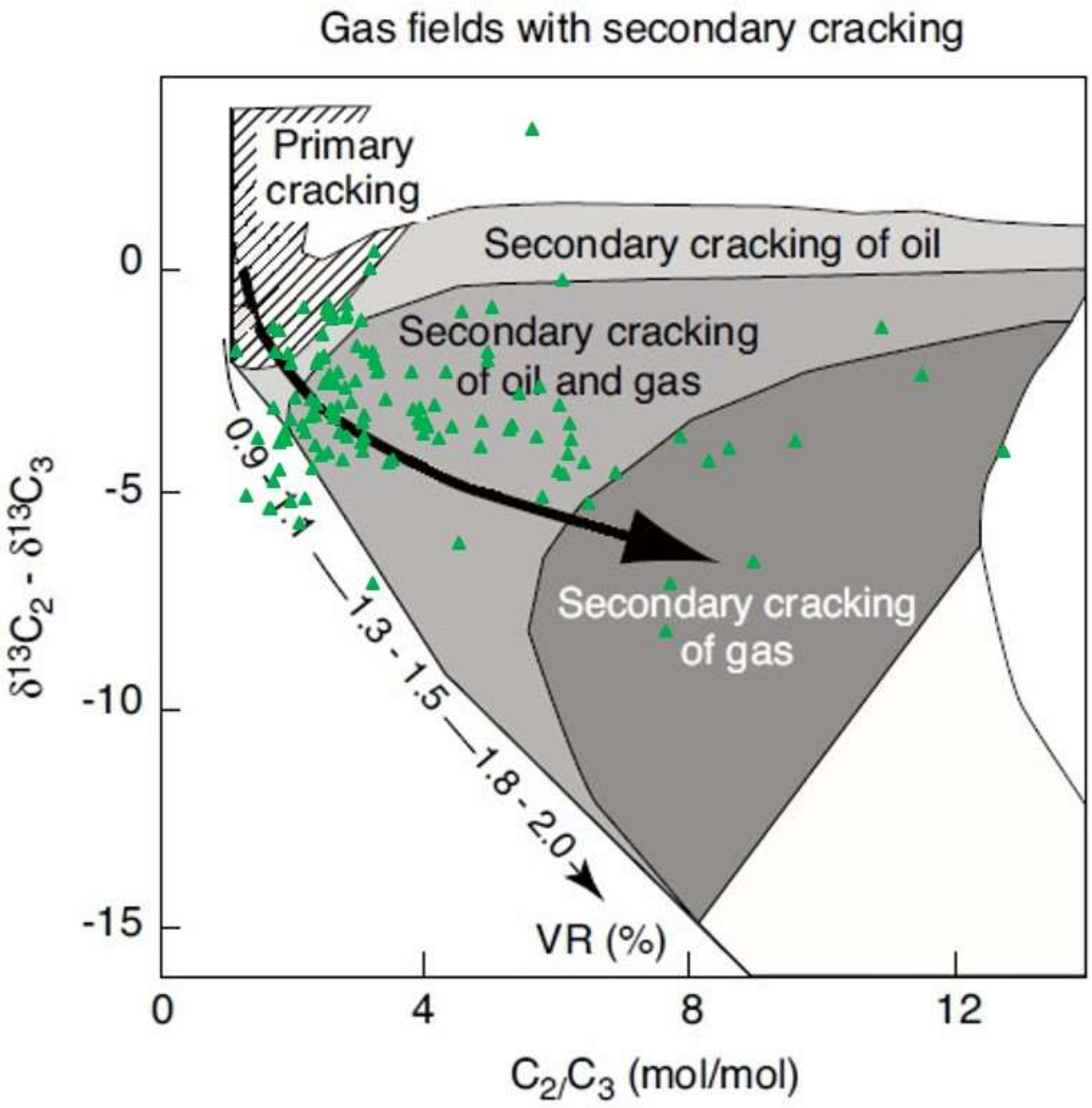

Figure B 10. ISO map data – "play" 4.00 Interpretive diagrams $\delta^{13}C$ Lorant Diagram for 'surface play' SCVF and bubble gas maps (after Prinzhofer and Battani 2003, no trendlines).

2. Play 4.06 Dunvegan (single formation – no ISO data)

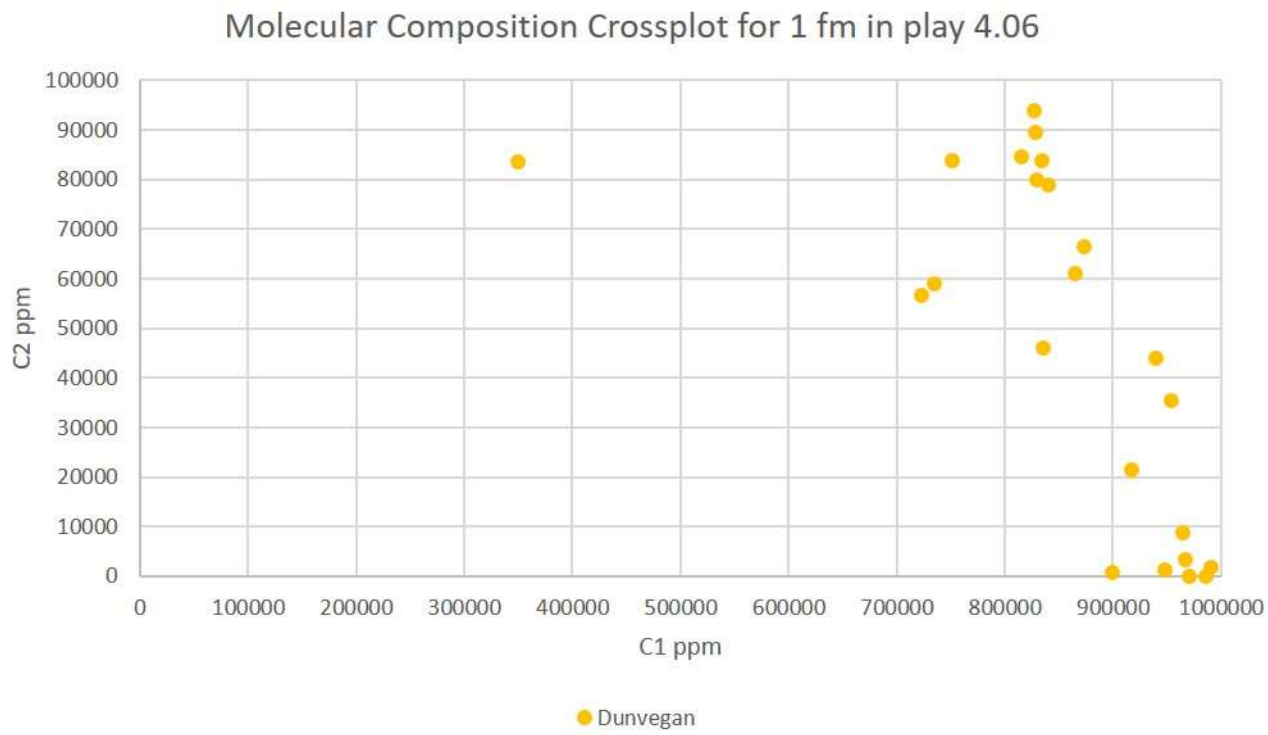

Figure B 11. MC map data – play 4.06 MC (ppm) ethane methane plot for Dunvegan single formation [not to template]

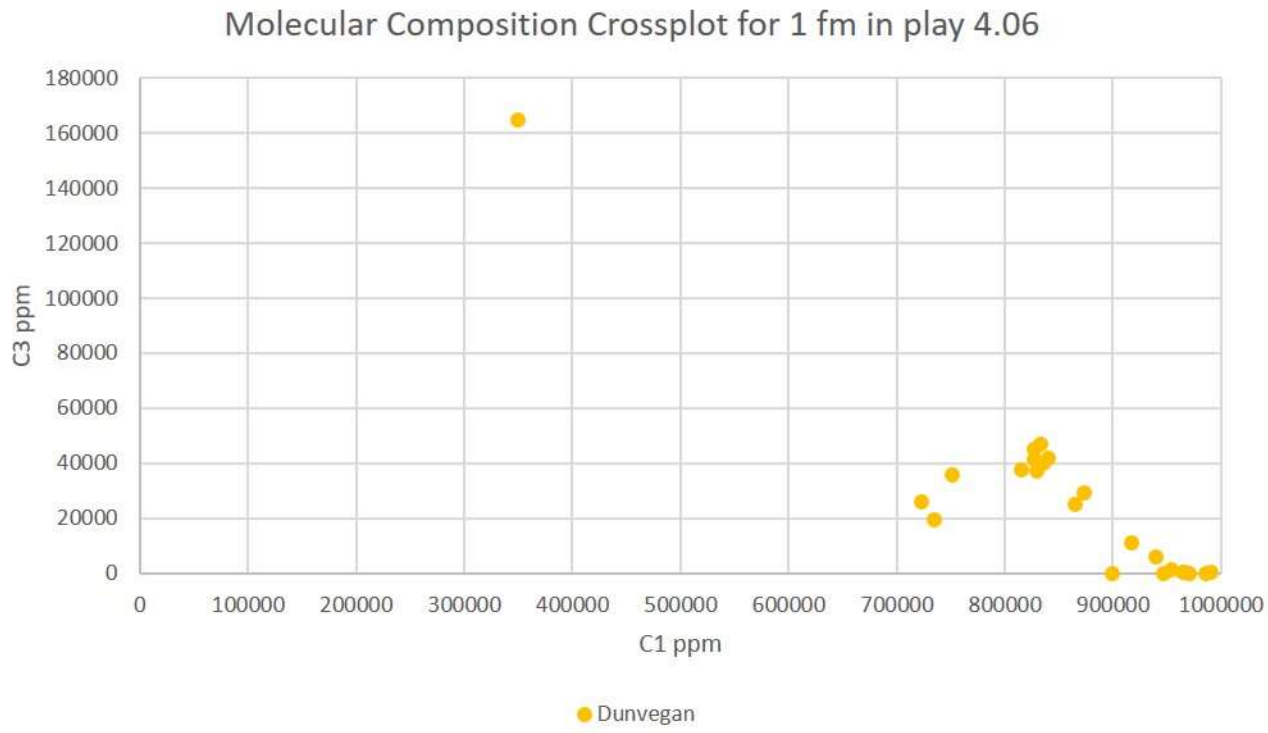

Figure B 12. MC map data – play 4.06 MC (ppm) propane methane plot for Dunvegan single formation [not to template]

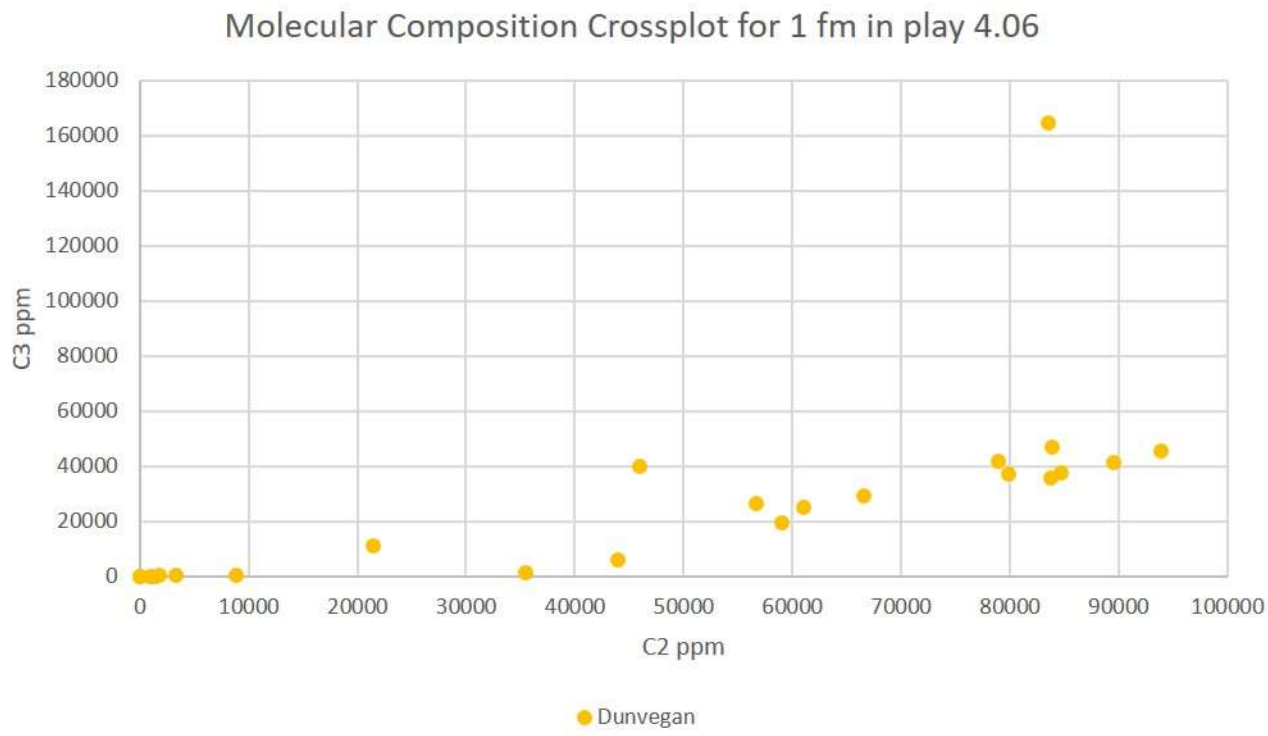

Figure B 13. MC map data – play 4.06 MC (ppm) propane ethane plots for Dunvegan single formation [not to template]

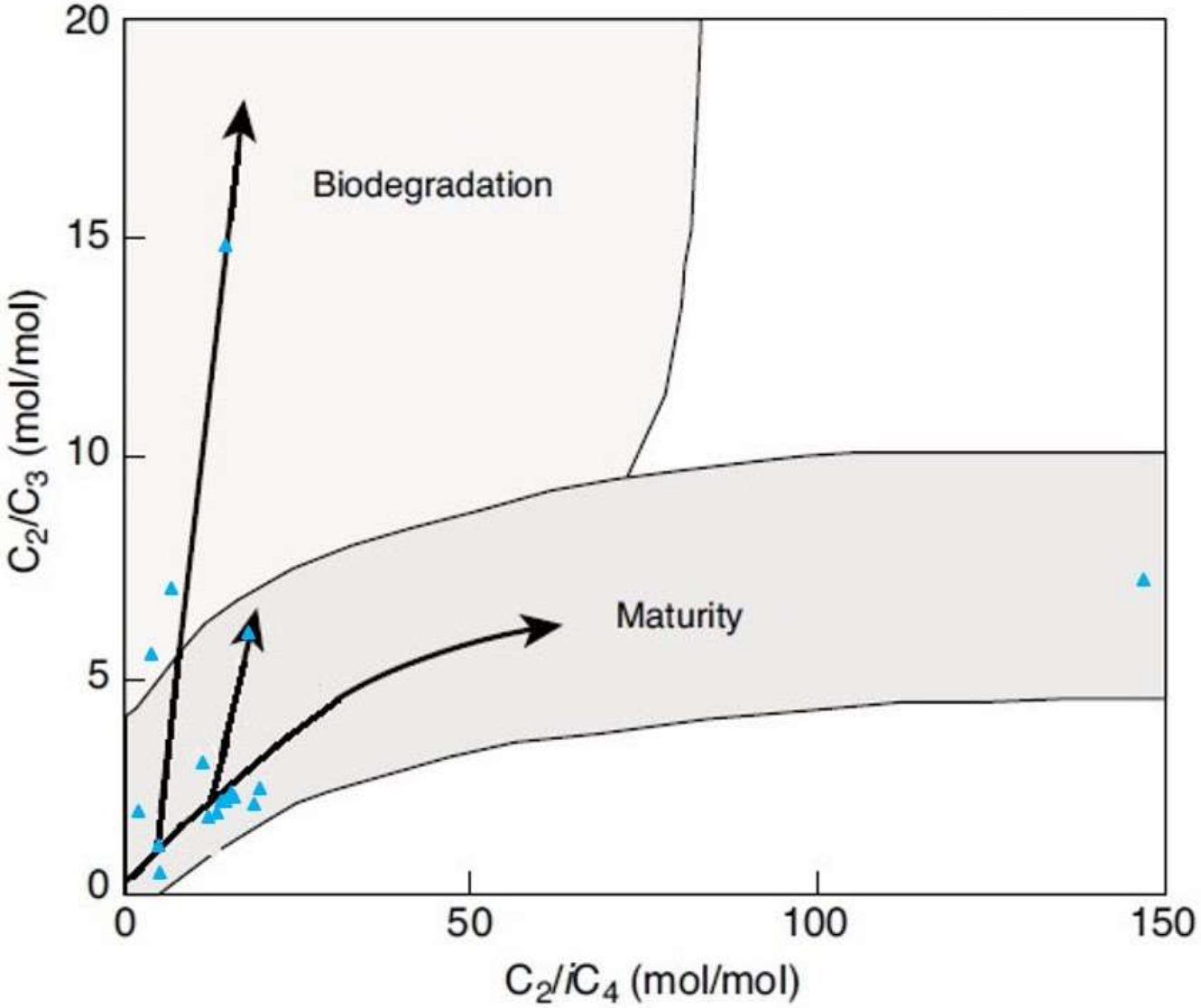

Figure B 14. ISO map data – play 4.06 Interpretive diagrams MC (only) Prinzhofer Diagram for Dunvegan single formation (after Prinzhofer and Battani 2003, no trendlines).

3. Play 4.09 Paddy, Cadotte, Peace River (multiple formations – no ISO data)

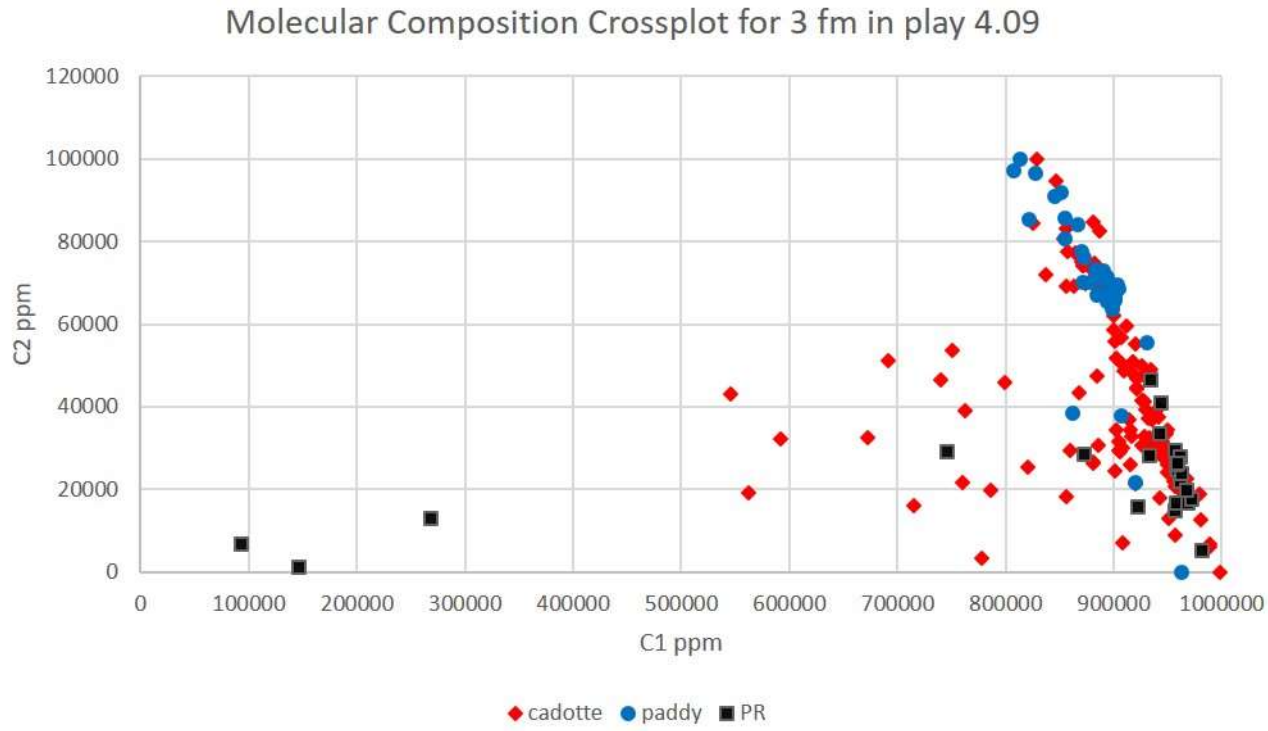

Figure B 15. MC map data – play 4.09 MC (ppm) ethane methane plot for 3 formations [not to template]

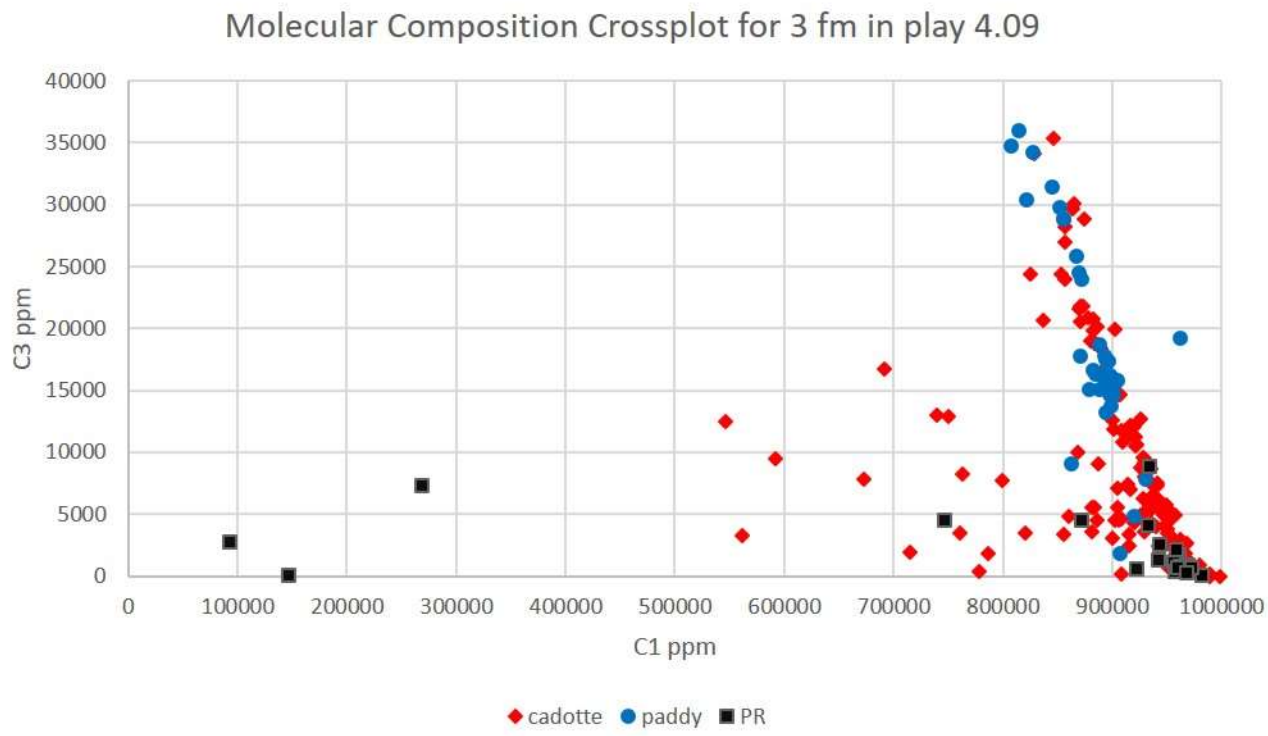

Figure B 16. MC map data – play 4.09 MC (ppm) propane methane plot for 3 formations [not to template]

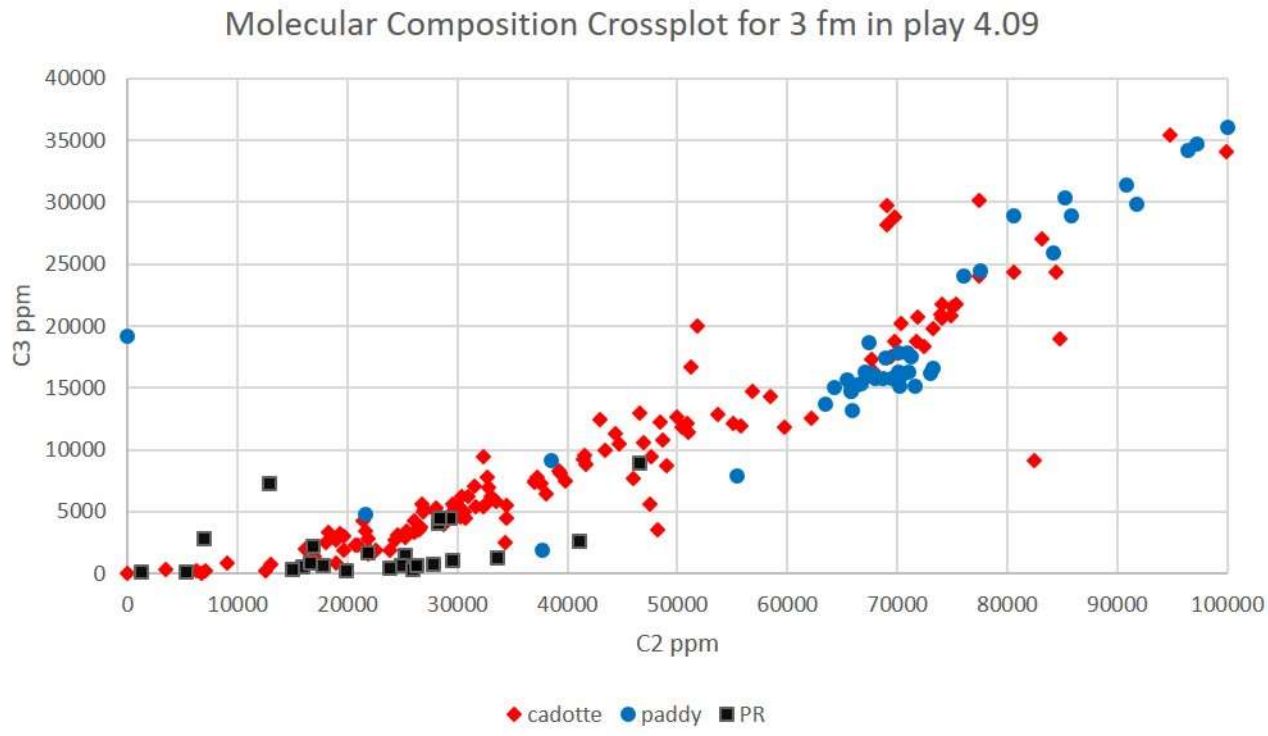

Figure B 17. MC map data – play 4.09 MC (ppm) propane ethane plot for 3 formations [not to template]

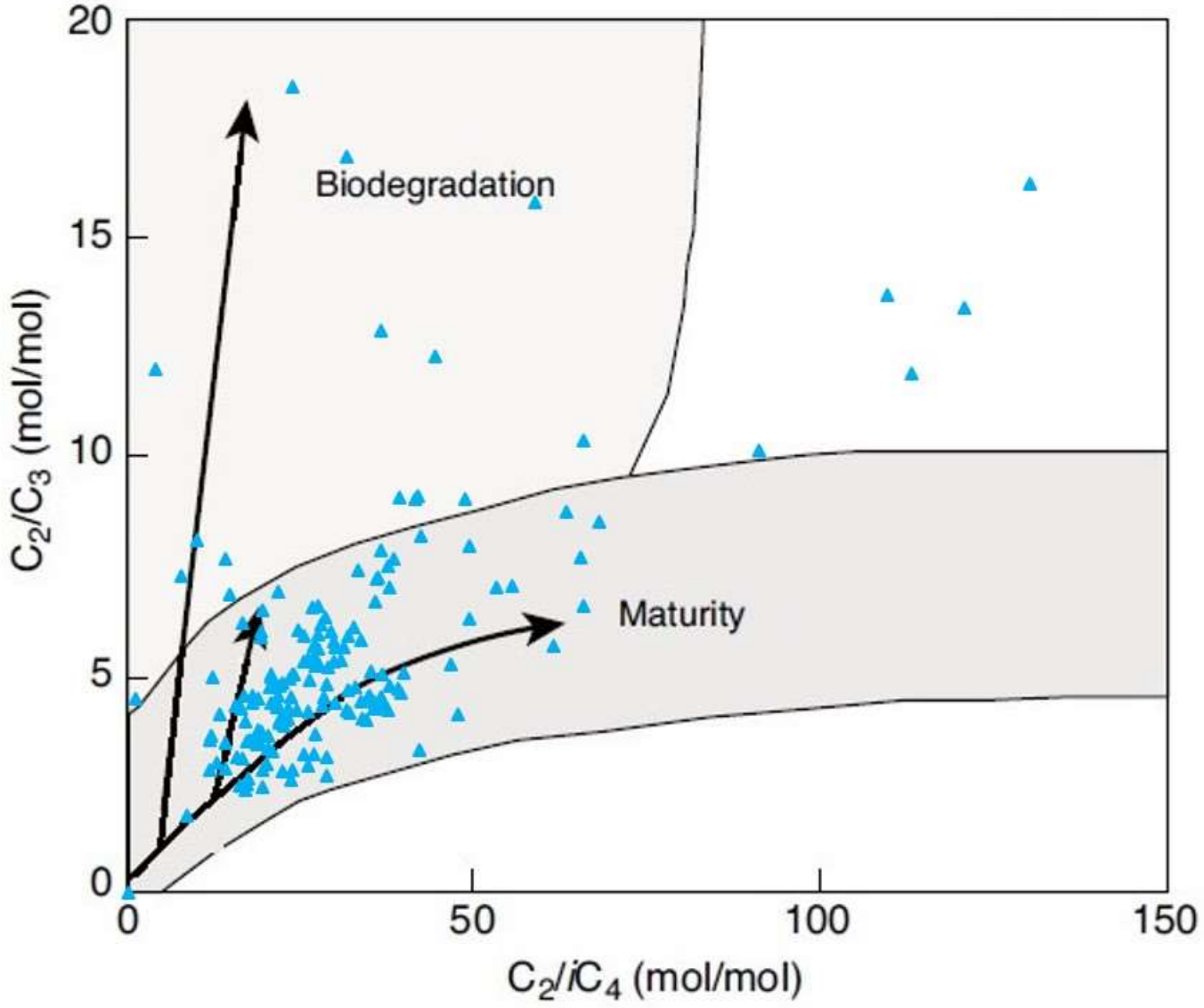

Figure B 18. ISO map data – play 4.09 Interpretive diagrams MC (only) Prinzhofer Diagram for 3 formations (after Prinzhofer and Battani 2003, no trendlines).

4. Play 4.11 Fahler (members), Spirit River (multiple formations – no ISO data)

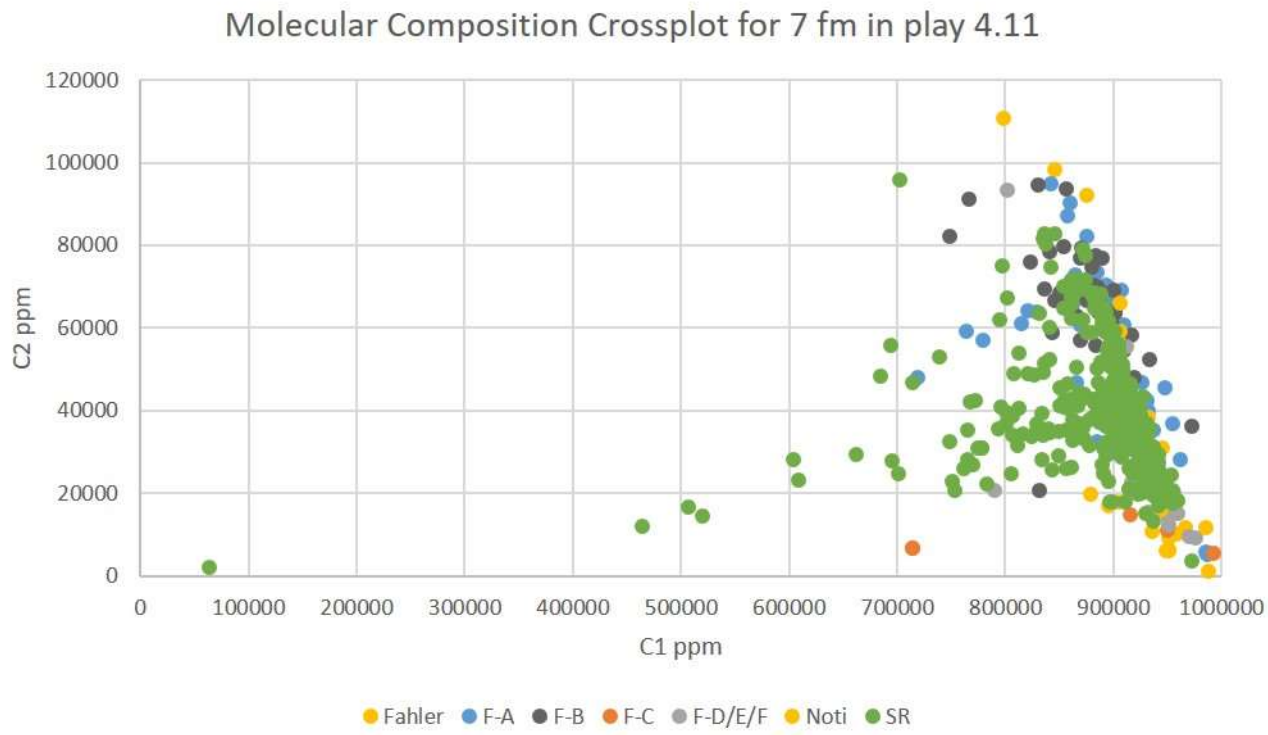

Figure B 19. MC map data – play 4.11 MC (ppm) ethane methane plot for 7 fm/mbr [not to template]

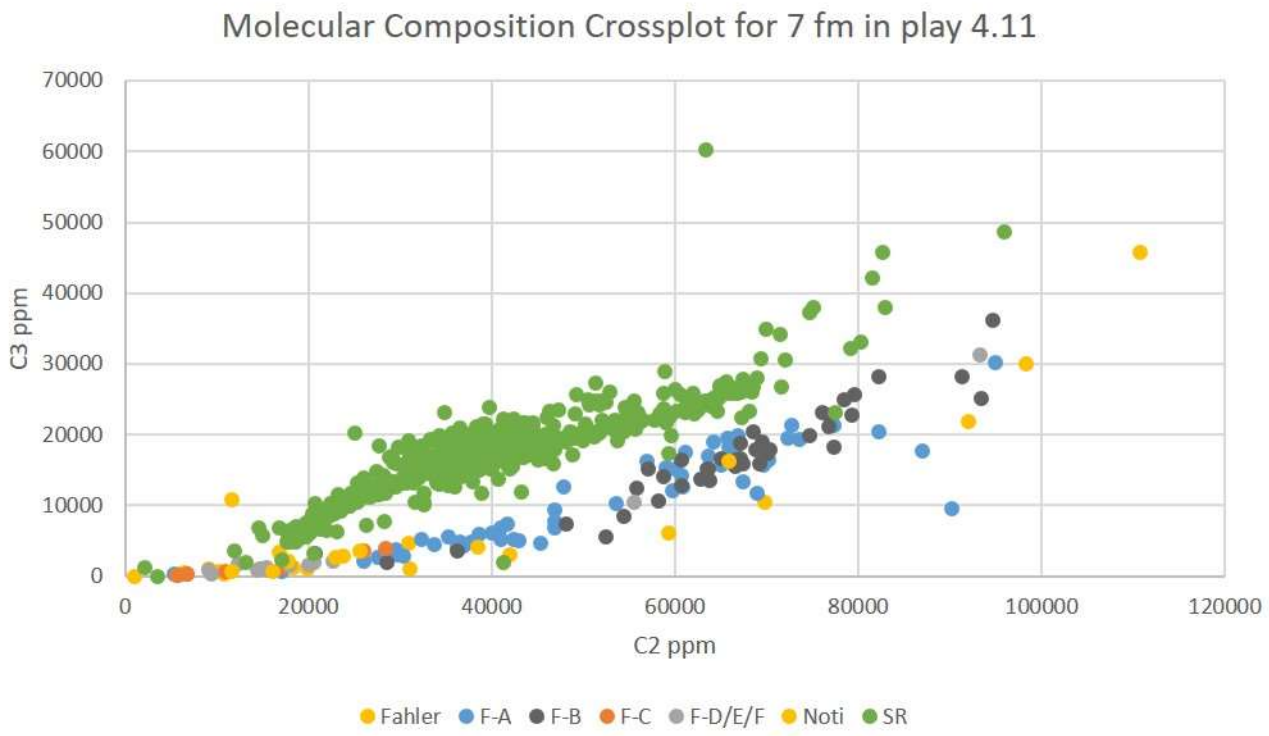

Figure B 20. MC map data – play 4.11 MC (ppm) propane ethane plot for 7 fm/mbr [not to template]

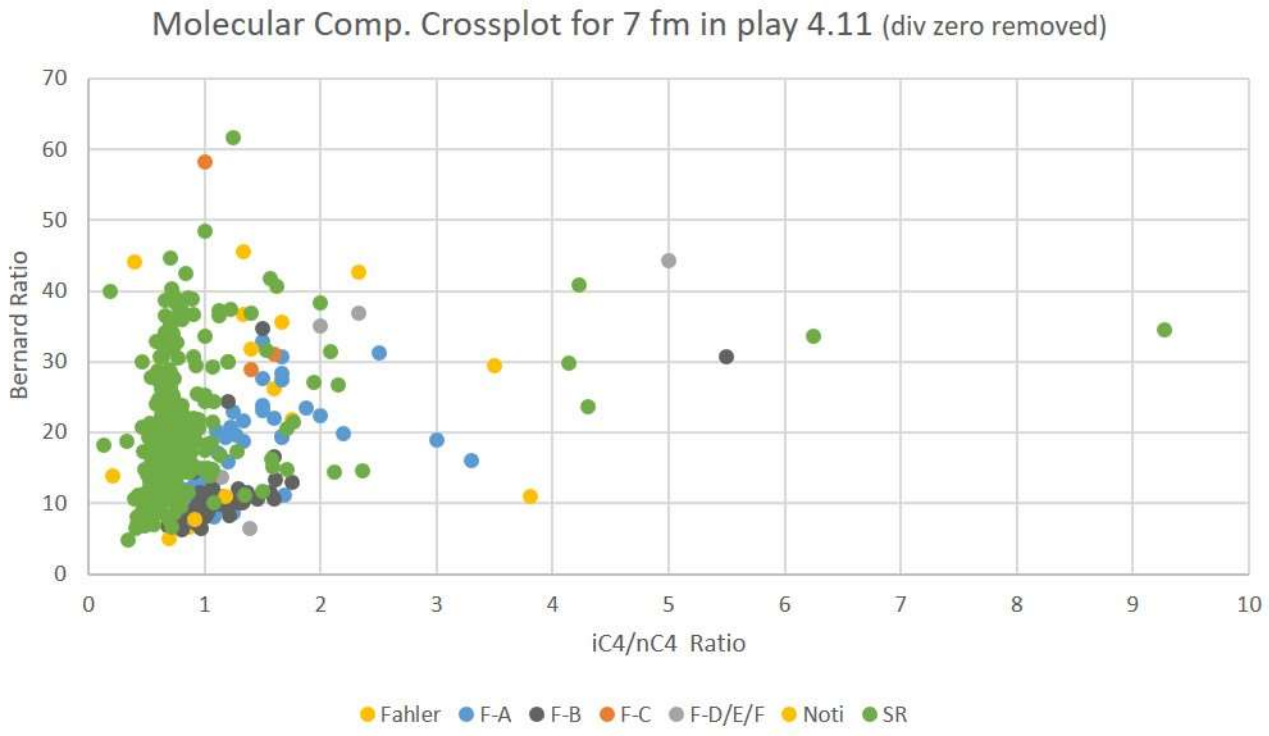

Figure B 21. MC map data – play 4.11 MC (ppm) propane ethane plot for 7 fm/mbr [not to template]

Figure B 22. MC map data – play 4.11 MC (ppm) propane ethane plot for 7 fm/mbr [not to template]

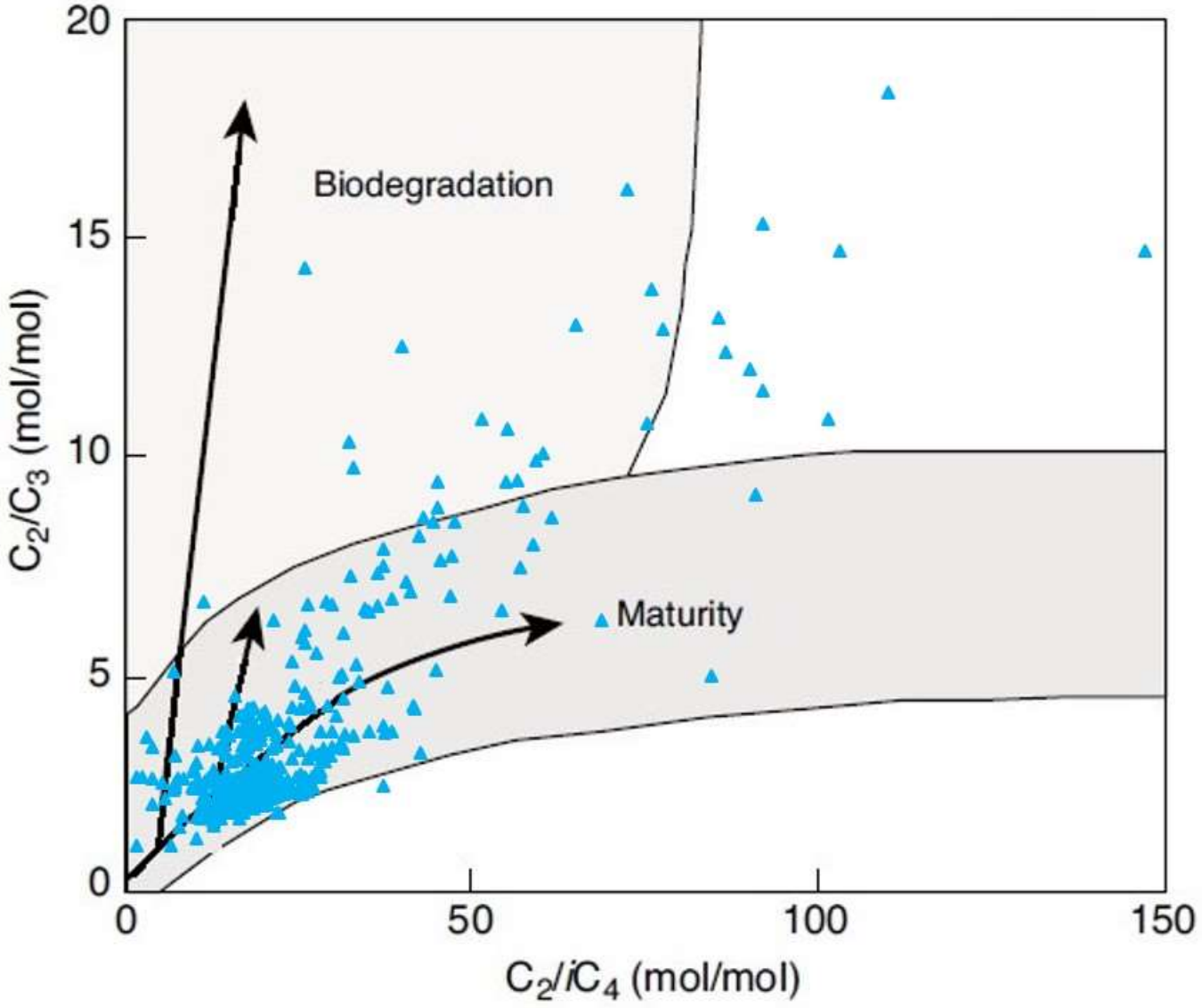

Figure B 23. ISO map data – play 4.11 Interpretive diagrams MC (only) Prinzhofer Diagram for 7 fm/mbr (after Prinzhofer and Battani 2003, no trendlines).

5. Play 4.12 Bluesky, Gething (two formations – both MC & ISO data)

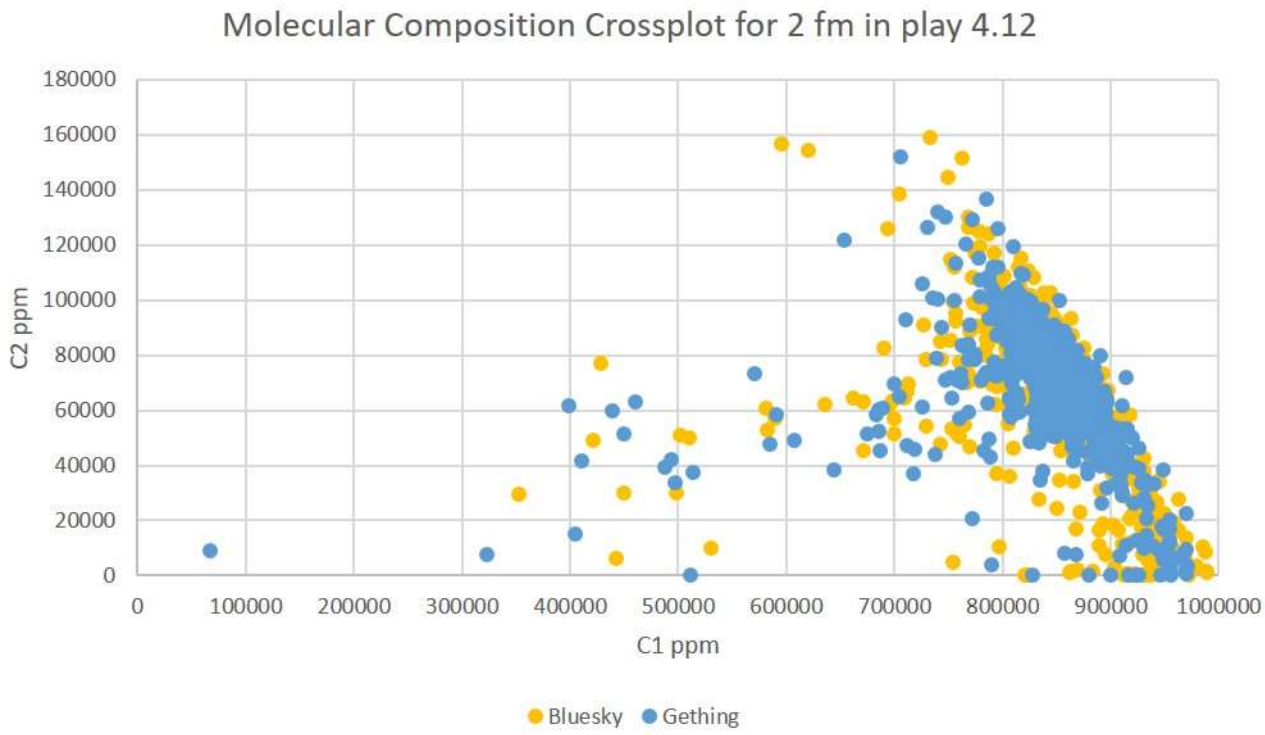

Figure B 24. MC map data – play 4.12 MC (ppm) ethane methane plot for Bluesky, Gething double formation [not to template].

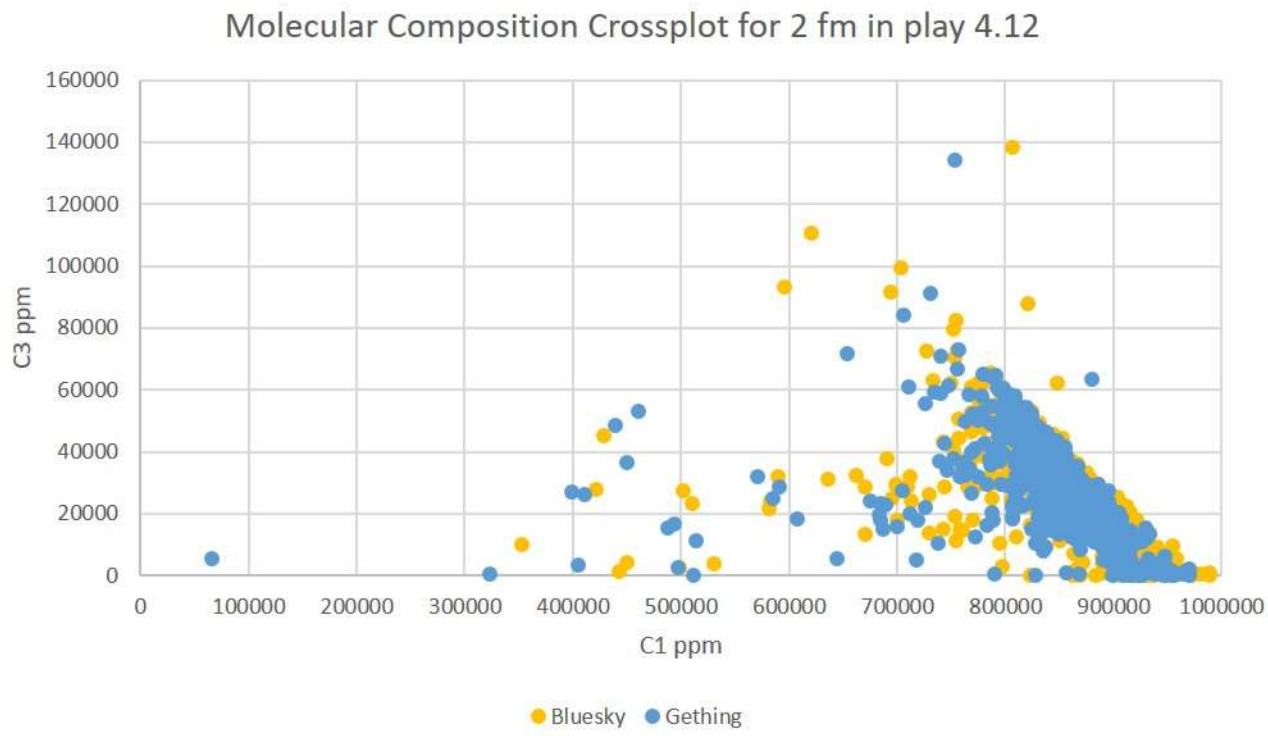

Figure B 25. MC map data – play 4.12 MC (ppm) propane methane plot for Bluesky, Gething double formation [not to template]

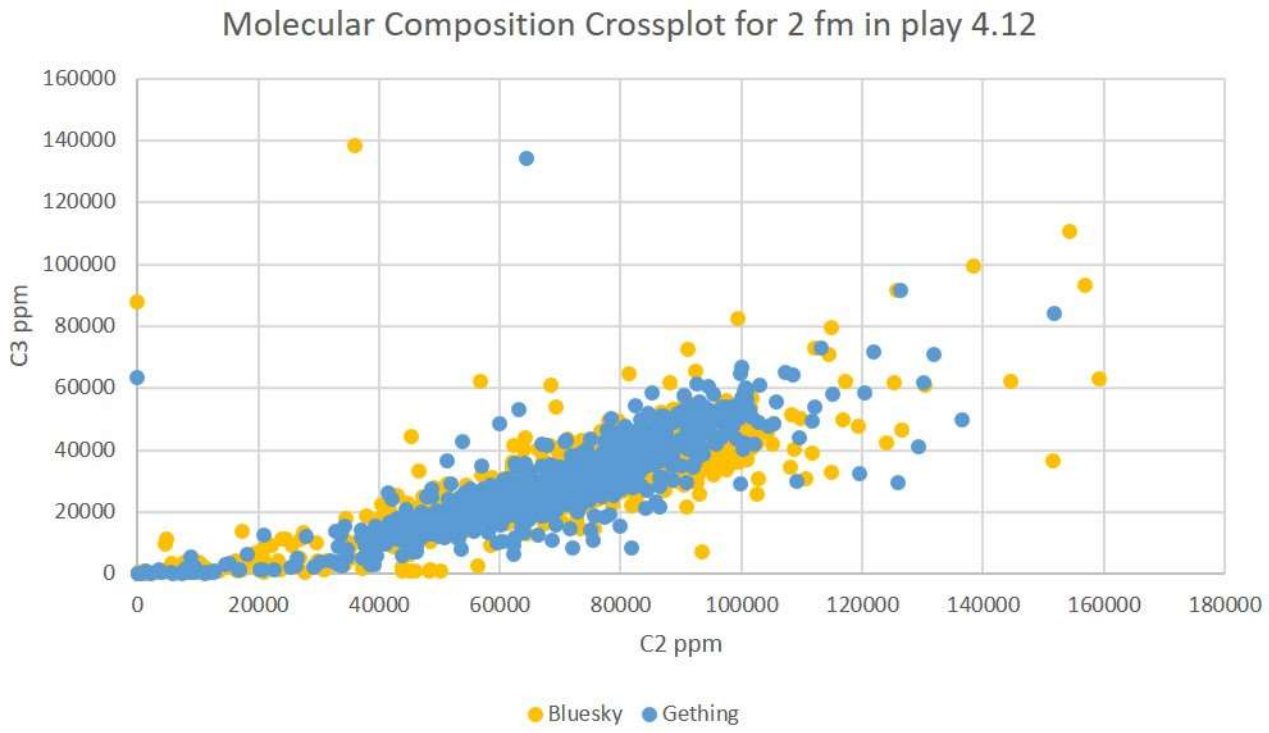

Figure B 26. MC map data – play 4.12 MC (ppm) propane ethane plot for Bluesky, Gething double formation [not to template]

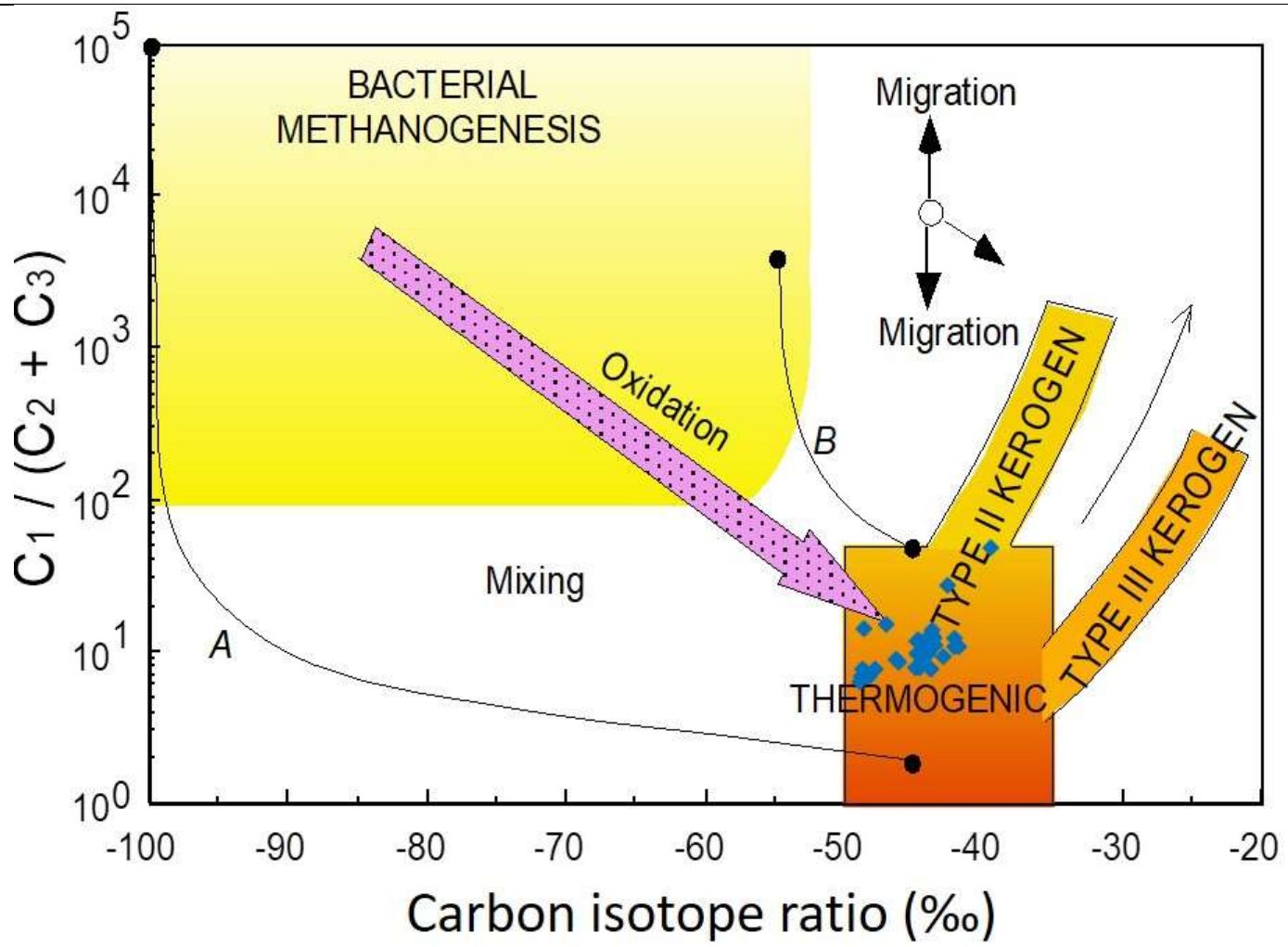

Figure B 27. ISO map data – play 4.12 Interpretive diagrams MC/ISO Bernard Diagram for Bluesky, Gething maps (Whiticar, 2018 pers. comm., after Whiticar 1999, no trendlines).

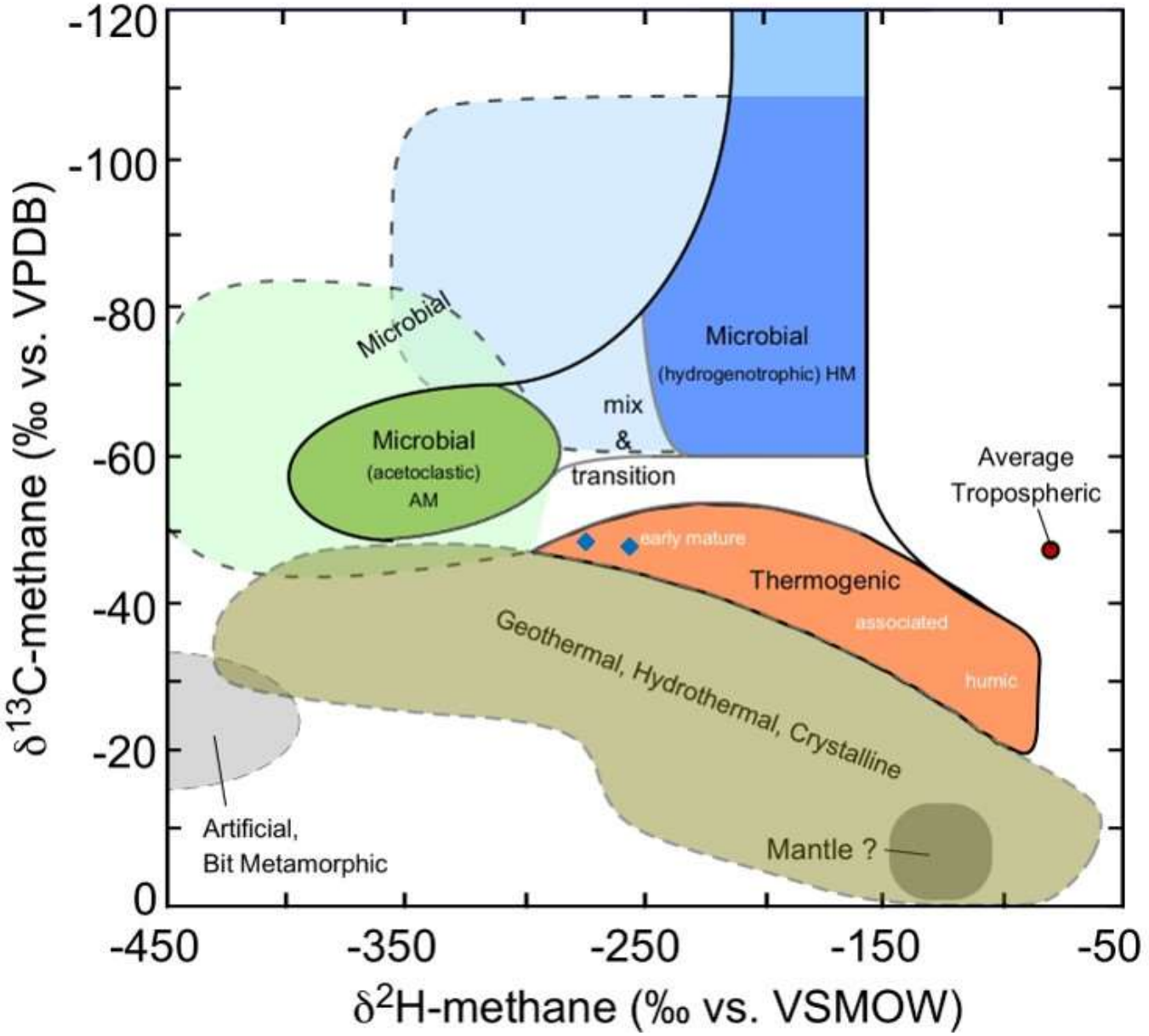

Figure B 28. ISO map data – play 4.12 Interpretive diagrams ISO CD Diagram for Bluesky, Gething maps (Whiticar, 2018 pers. comm., after Whiticar 1999, no trendlines).

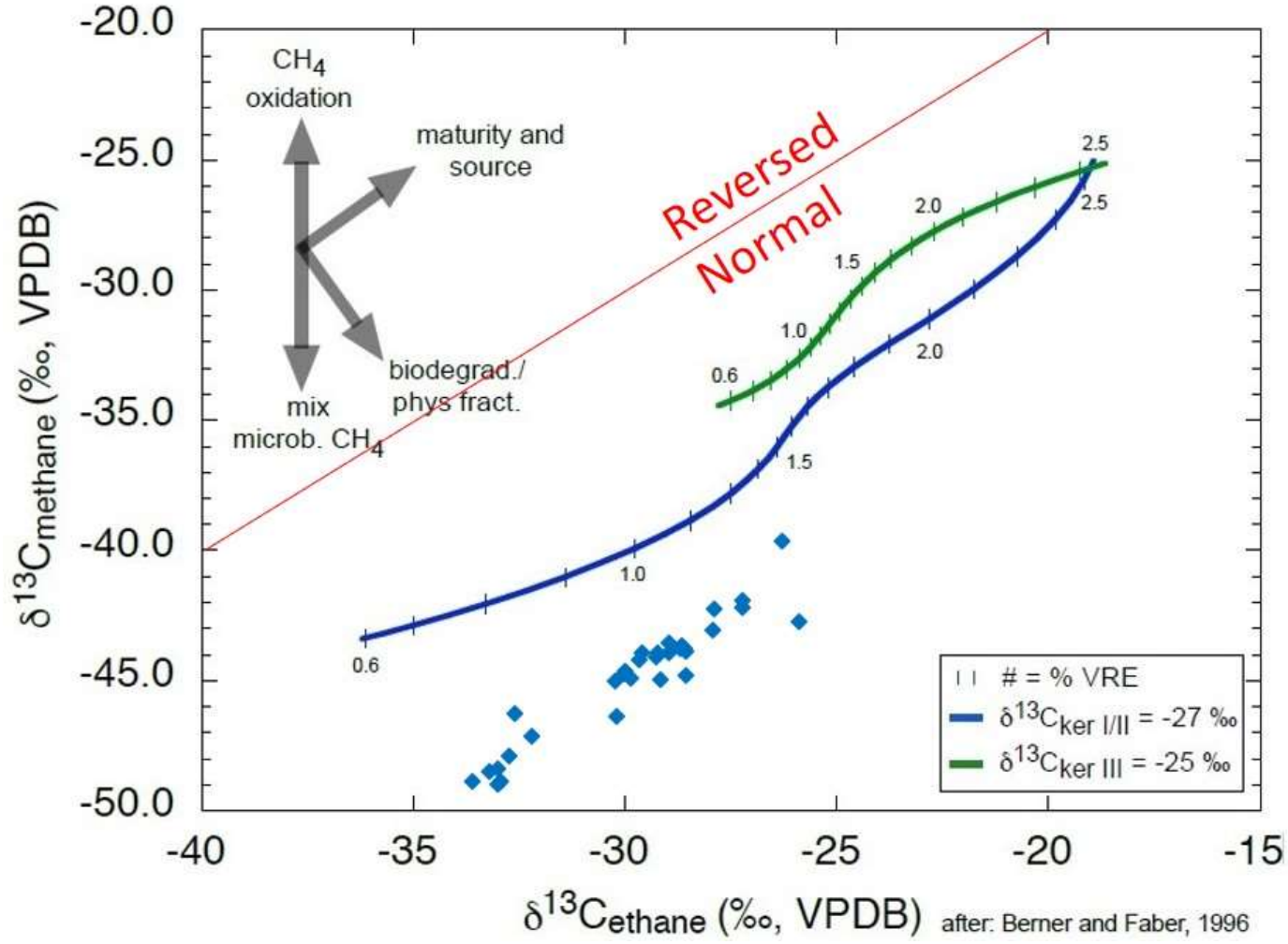

Figure B 29. ISO map data – play 4.12 Interpretive diagrams ISO $\delta^{13}C_1$ vs $\delta^{13}C_2$ plot for Bluesky, Gething maps (Whiticar, 2018 pers. comm., after Berner and Faber 1996, no trendlines).

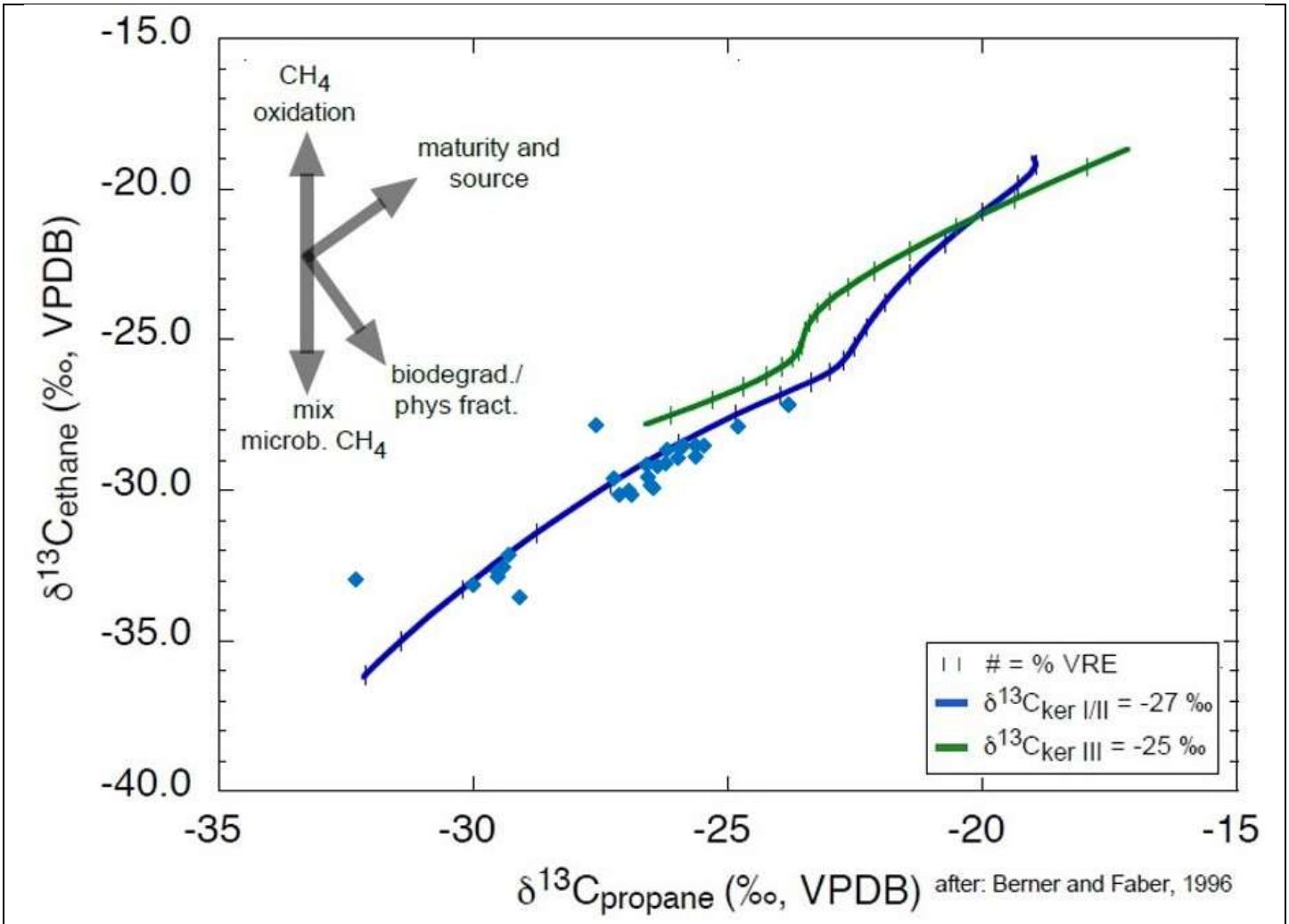

Figure B 30. ISO map data – play 4.12 Interpretive diagrams ISO $\delta^{13}C_2$ vs $\delta^{13}C_3$ plot for Bluesky, Gething maps (Whiticar, 2018 pers. comm., after Berner and Faber 1996, no trendlines).

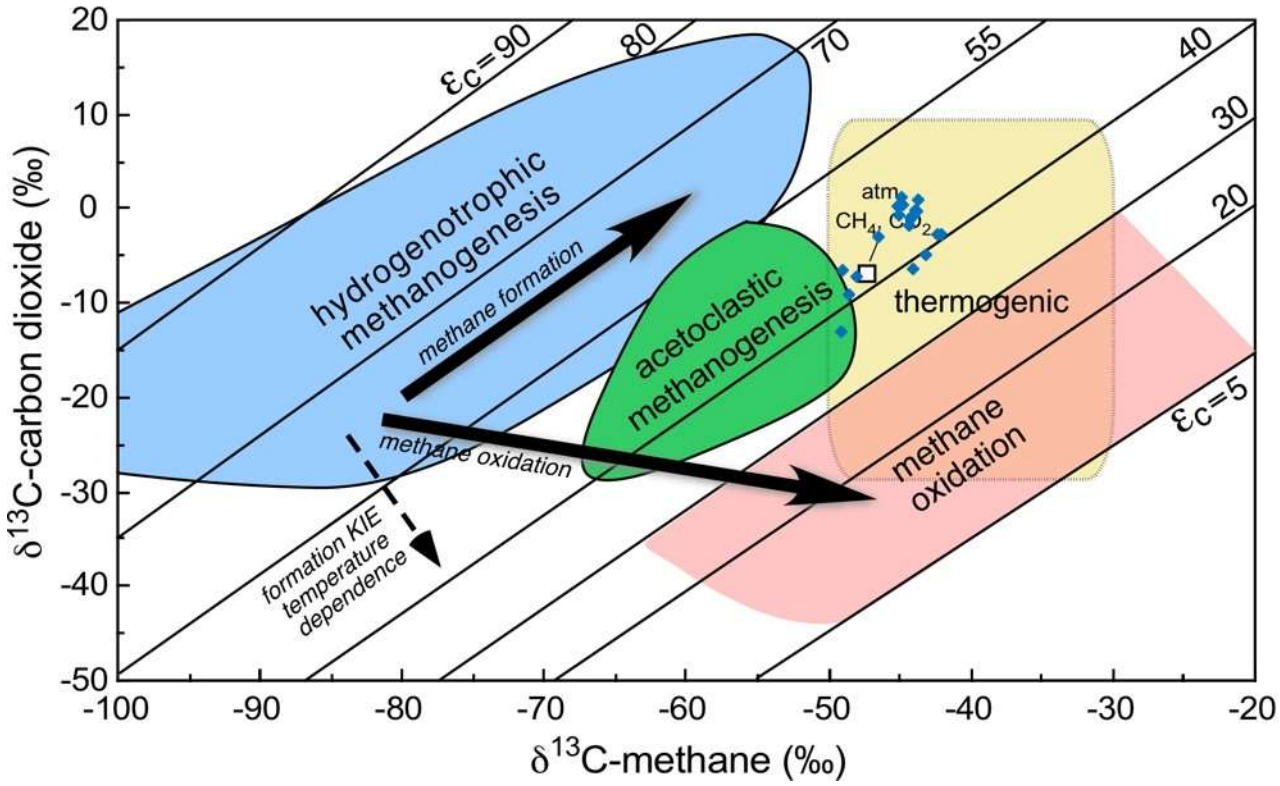

Figure B 31. ISO map data – play 4.12 Interpretive diagrams ISO $\delta^{13}CO_2$ versus $\delta^{13}C1$ plot for Bluesky, Gething maps (after Whiticar 1999, no trendlines).

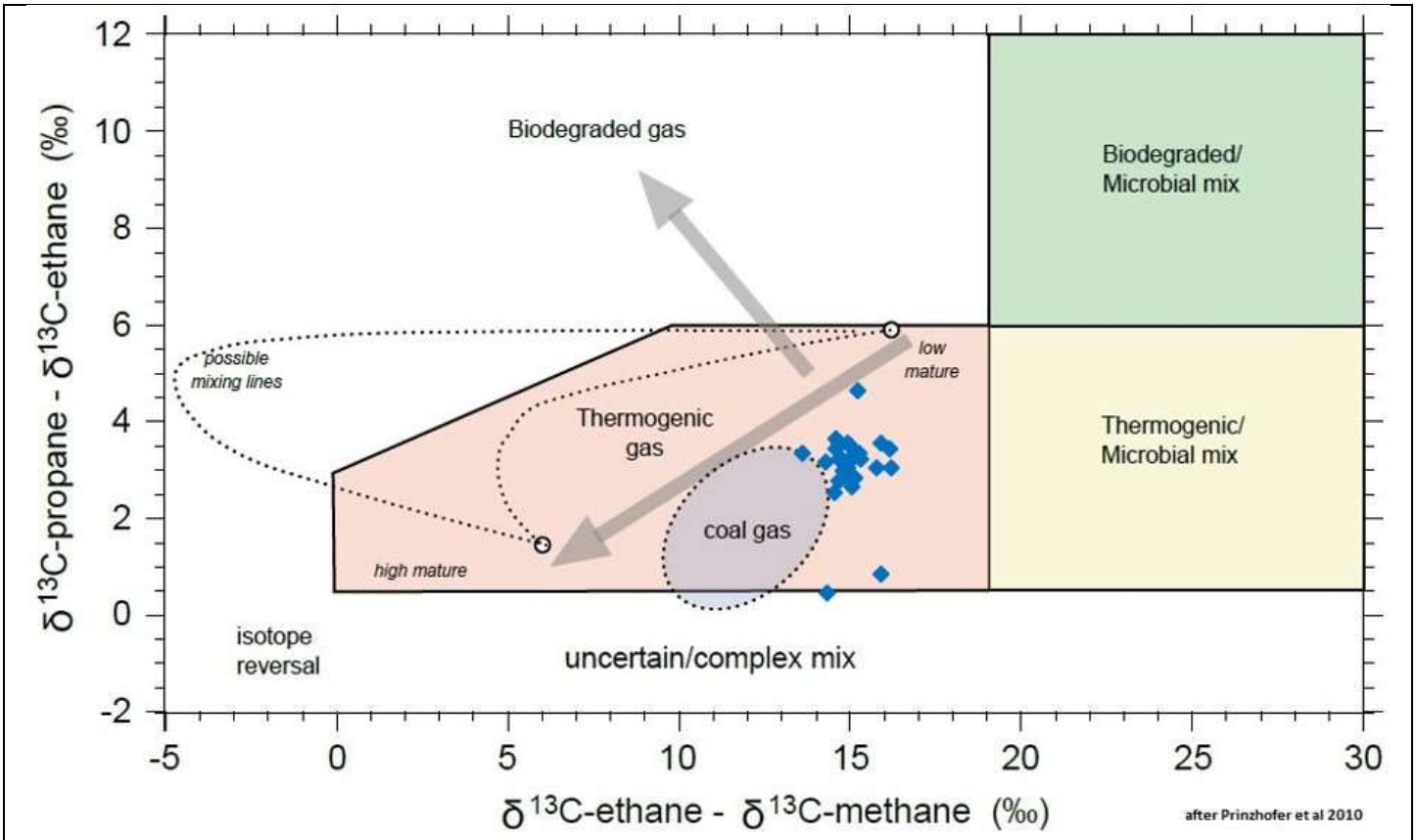

Figure B 32. ISO map data – play 4.12 Interpretive $\delta^{13}C_2$- $\delta^{13}C_1$ versus $\delta^{13}C_3$- $\delta^{13}C_2$ plot for Bluesky, Gething maps (no trendlines).

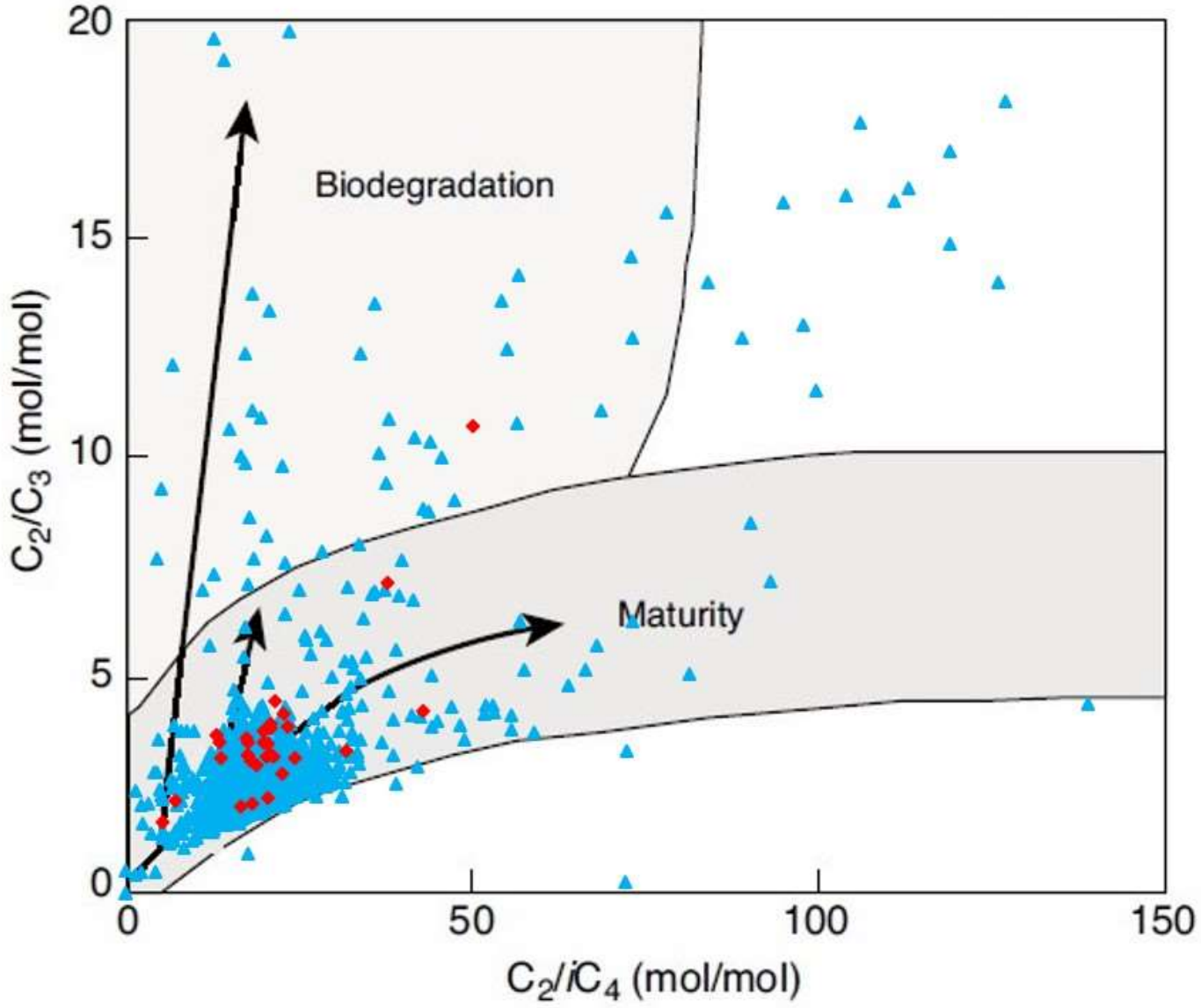

Figure B 33. ISO map data – play 4.12 Interpretive diagrams MC/ISO Prinzhofer Diagram for Bluesky, Gething maps (after Prinzhofer and Battani 2003, no trendlines).

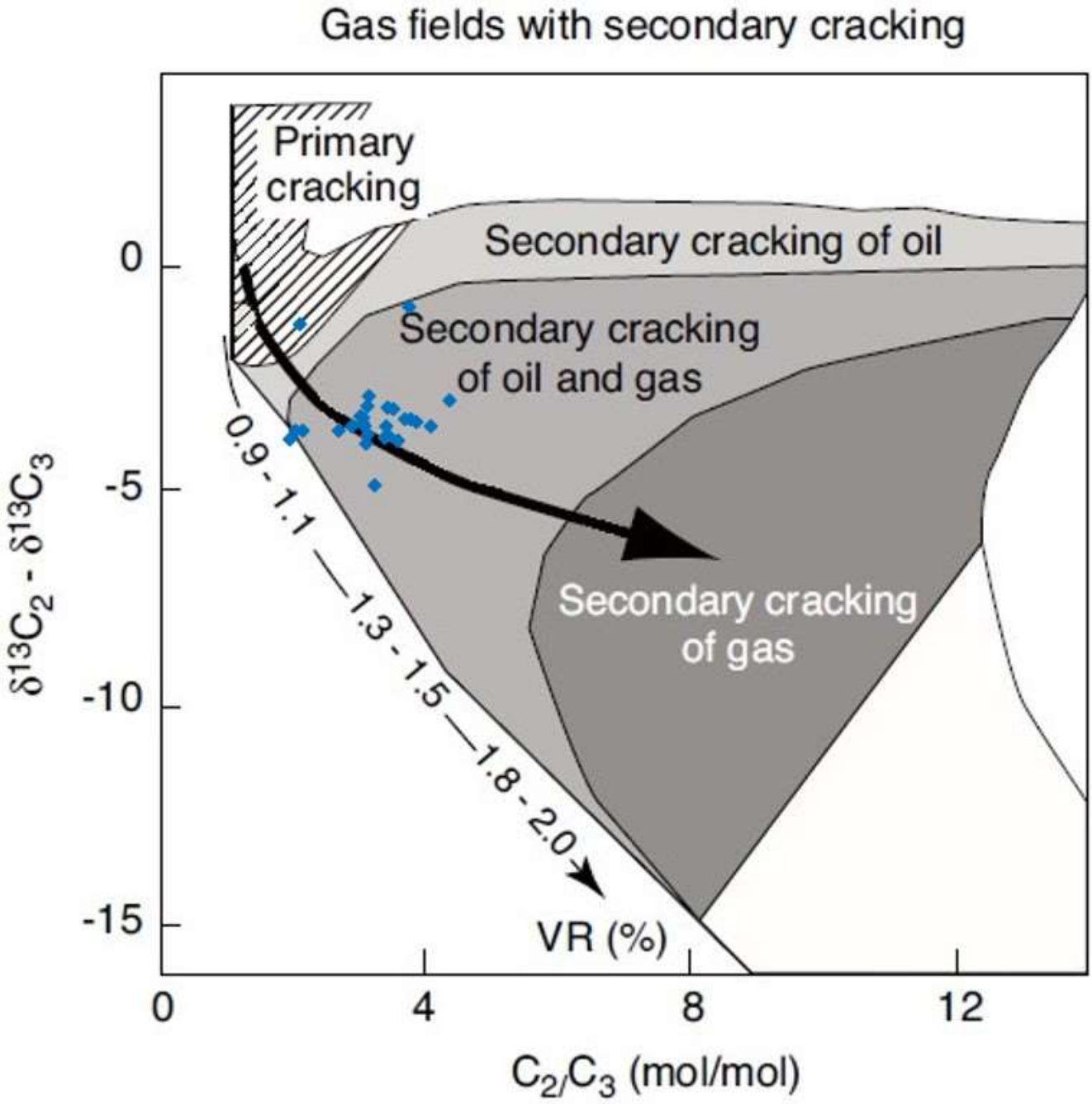

Figure B 34. ISO map data – play 4.12 Interpretive diagrams MC/ISO Lorant Diagram for Bluesky, Gething maps (after Prinzhofer and Battani 2003, no trendlines).

6. Play 4.14 Cadomin, Chinkeh (two formations – both MC & ISO data)

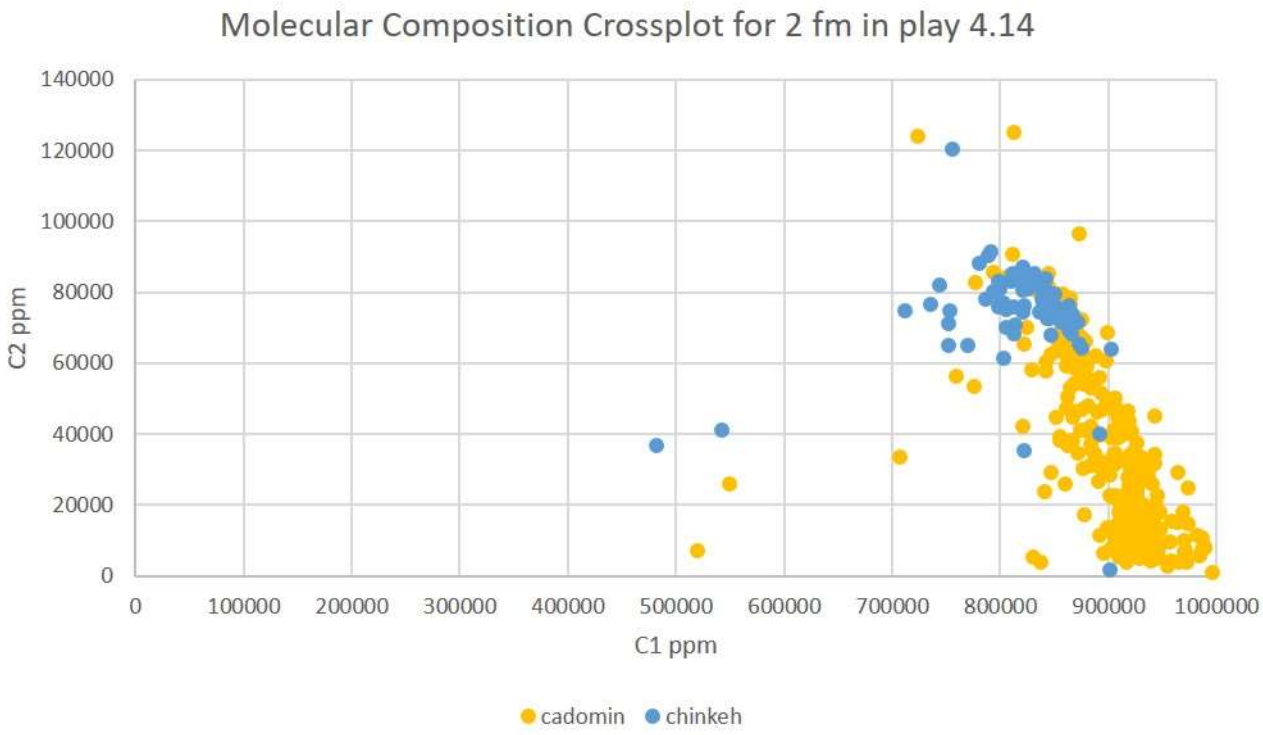

Figure B 35. MC map data – play 4.14 MC (ppm) ethane methane plot for Cadomin, Chinkeh double formation [not to template].

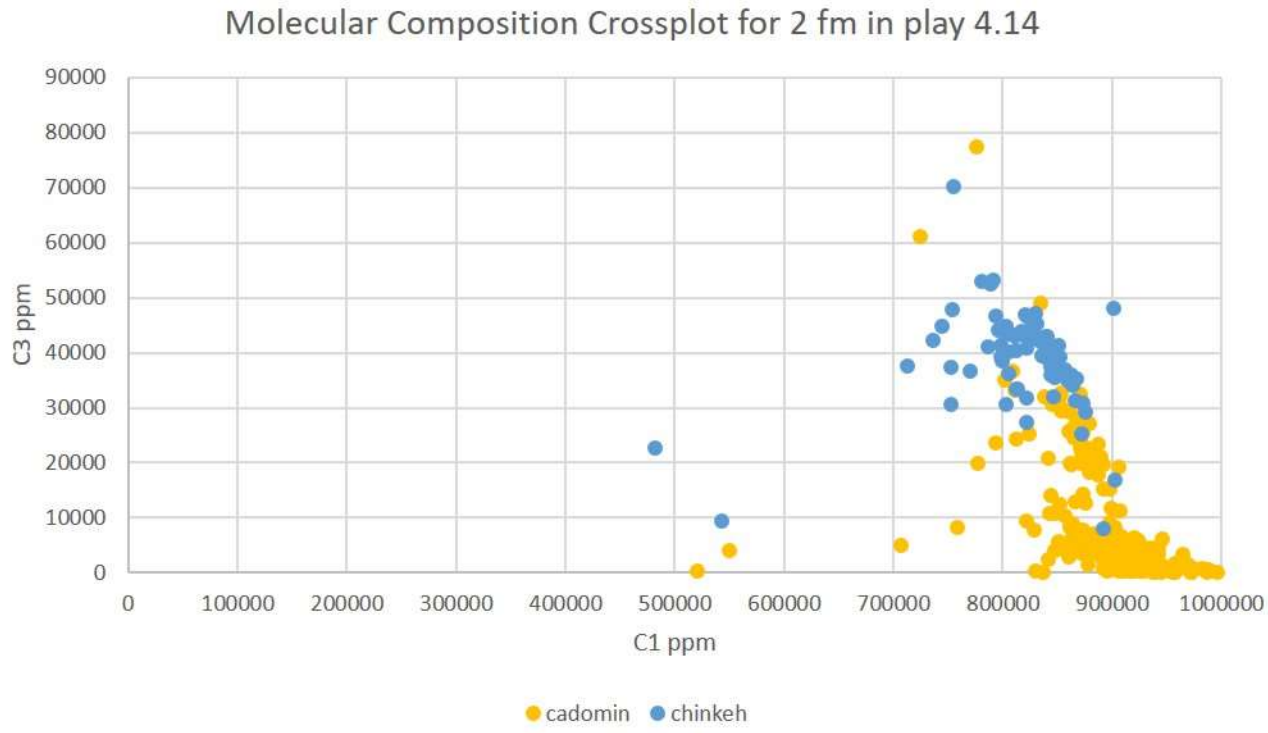

Figure B 36. MC map data – play 4.14 MC (ppm) propane methane plot for Cadomin, Chinkeh double formation [not to template].

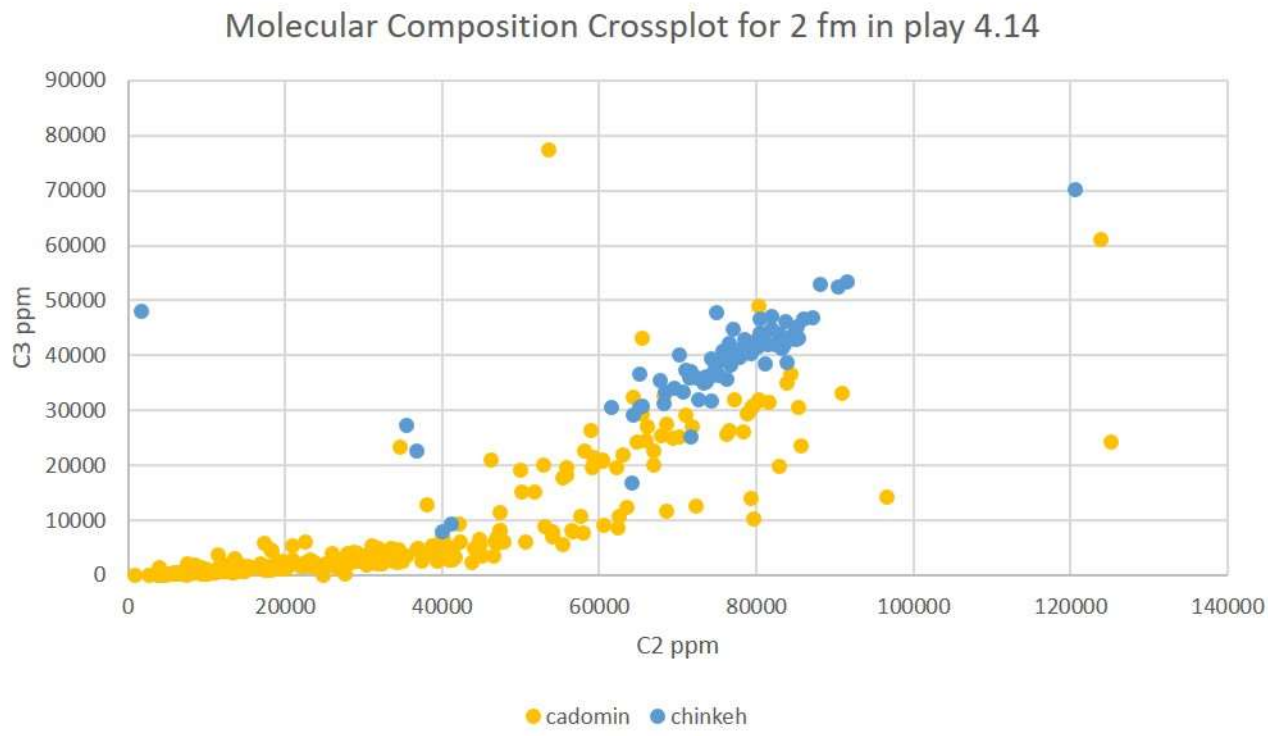

Figure B 37. MC map data – play 4.14 MC (ppm) propane ethane plot for Cadomin, Chinkeh double formation [not to template].

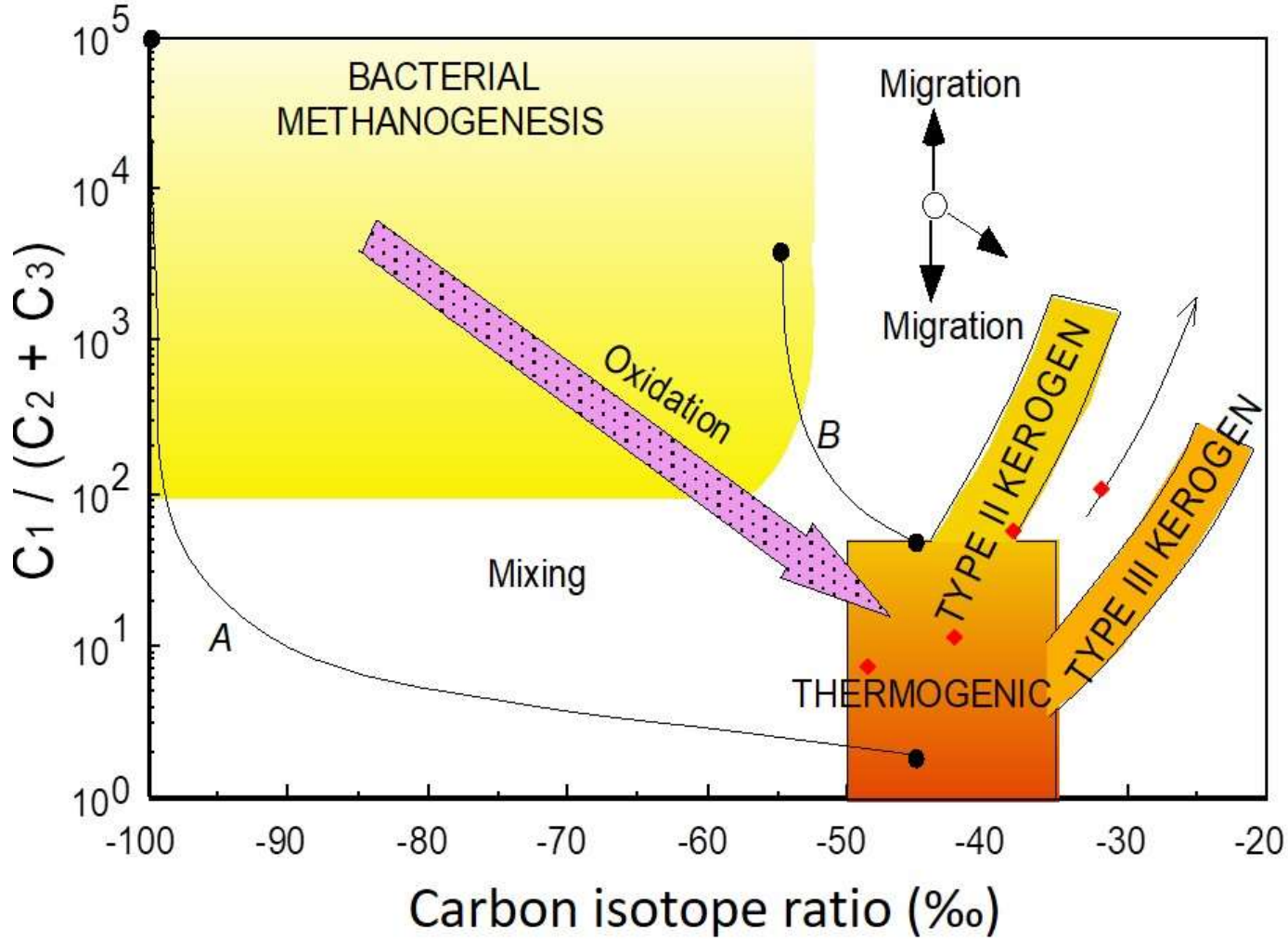

Figure B 38. ISO map data – play 4.14 Interpretive diagrams MC/ISO Bernard Diagram for Cadomin, Chinkeh maps (Whiticar, 2018 pers. comm., after Whiticar 1999, no trendlines).

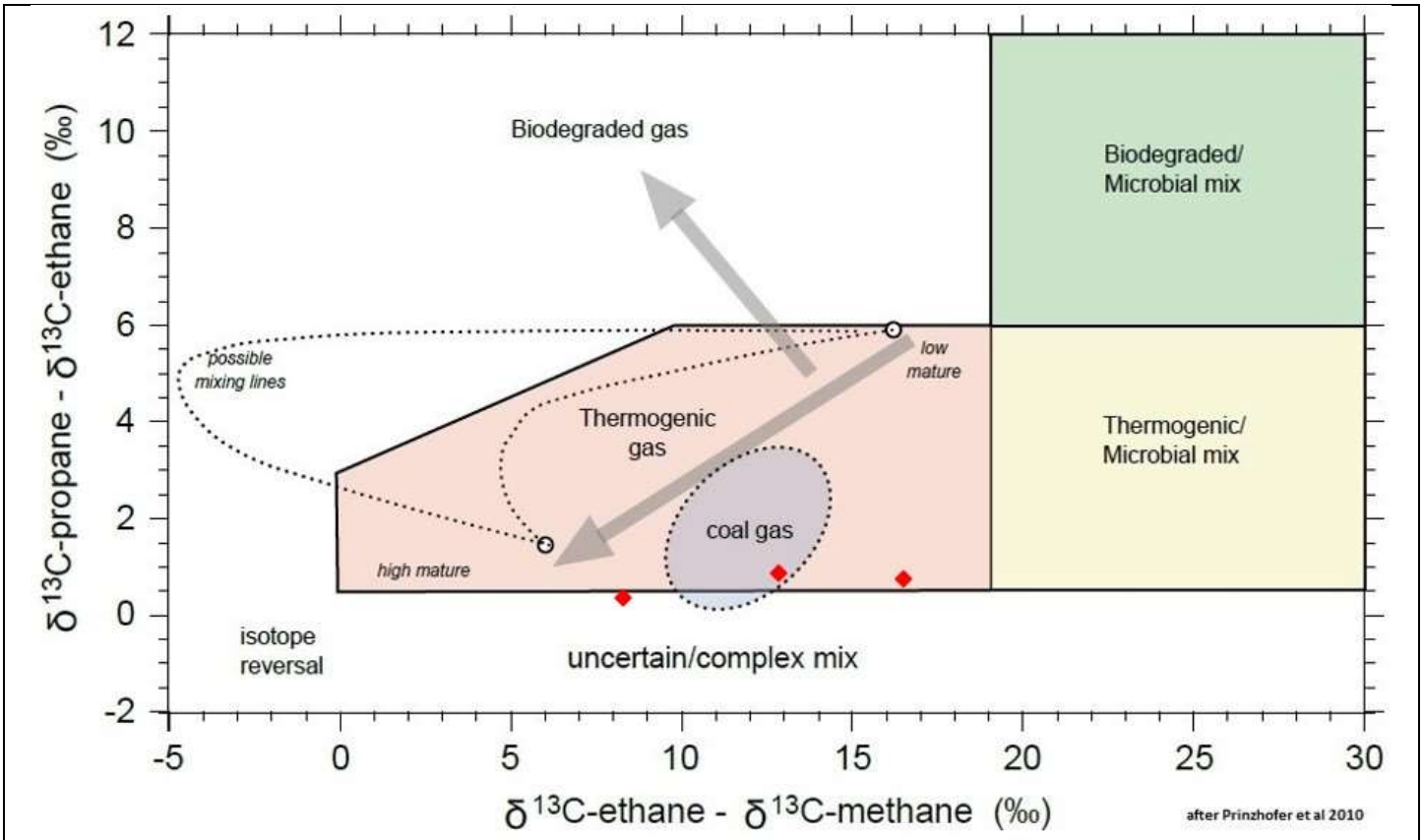

Figure B 39. ISO map data – play 4.14 Interpretive $\delta^{13}C_2$- $\delta^{13}C_1$ versus $\delta^{13}C_3$- $\delta^{13}C_2$ plot for Cadomin, Chinkeh maps (no trendlines, no Deuterium for CD diagram).

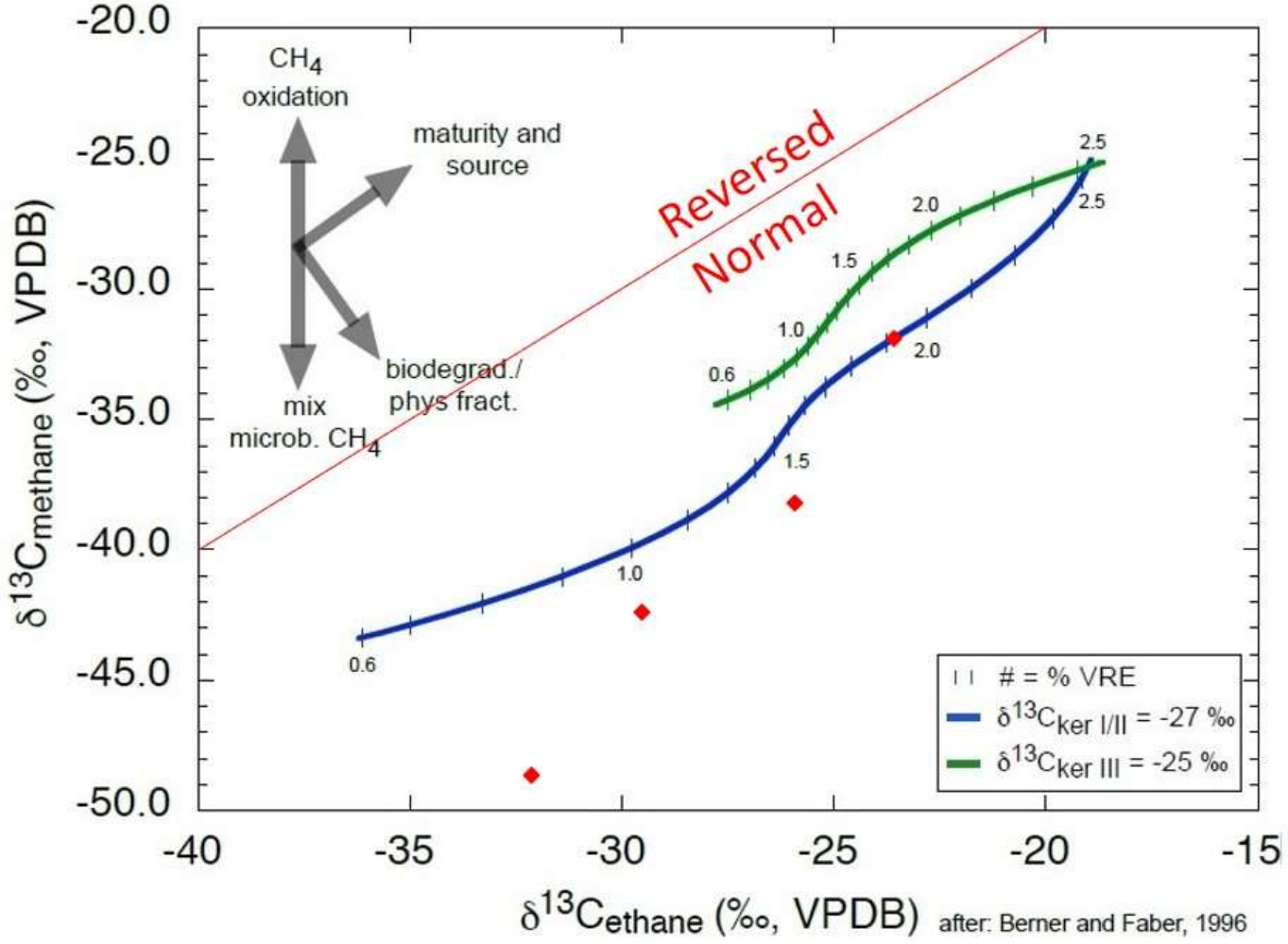

Figure B 40. ISO map data – play 4.14 Interpretive diagrams ISO $\delta^{13}C_1$ vs $\delta^{13}C_2$ plot for Cadomin, Chinkeh maps (after Berner and Faber 1996, no trendlines).

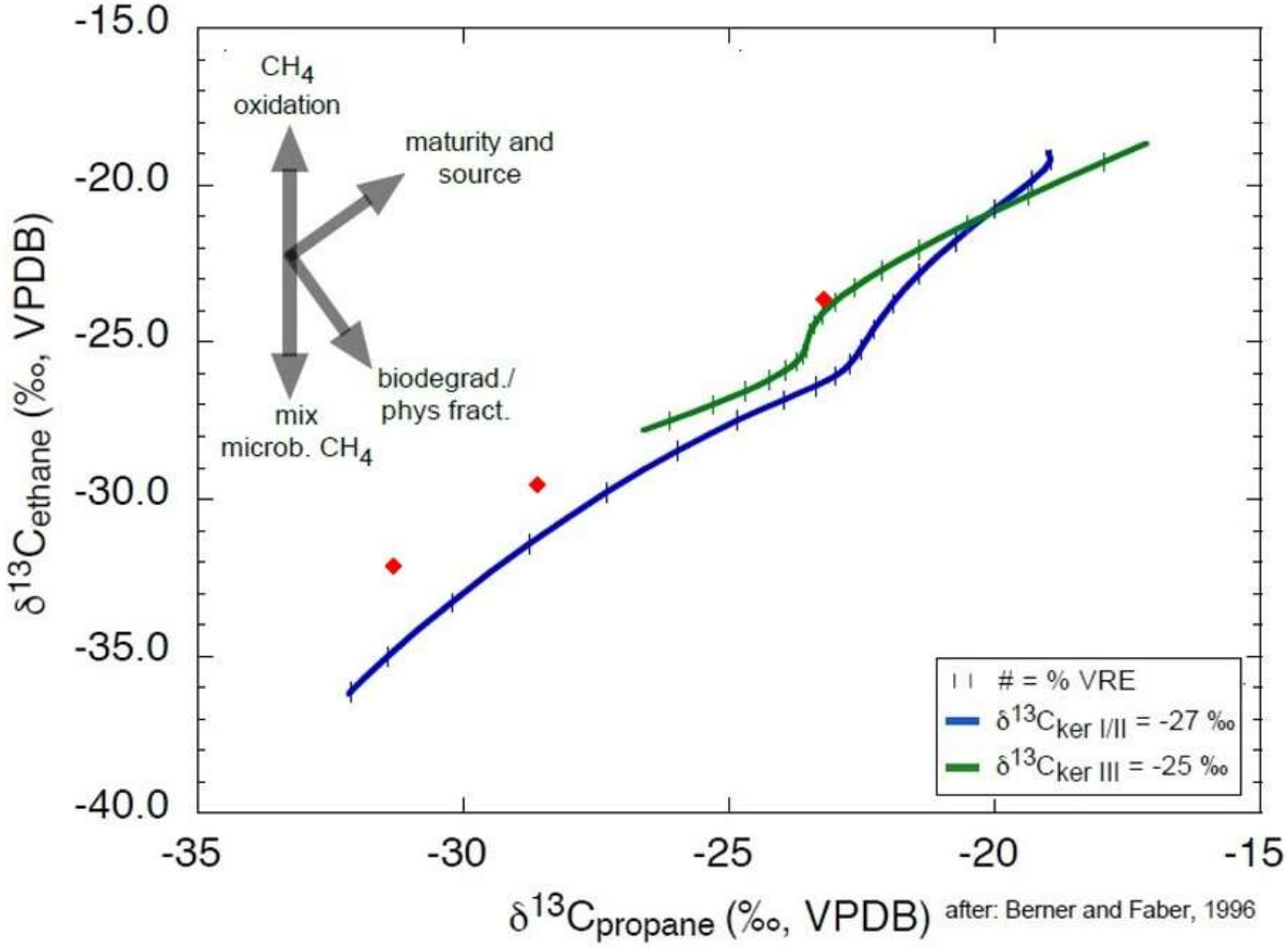

Figure B 41. ISO map data – play 4.14 Interpretive diagrams ISO $\delta^{13}C_2$ vs $\delta^{13}C_3$ plot for Cadomin, Chinkeh maps (Whiticar, 2018 pers. comm., after Berner and Faber 1996, no trendlines).

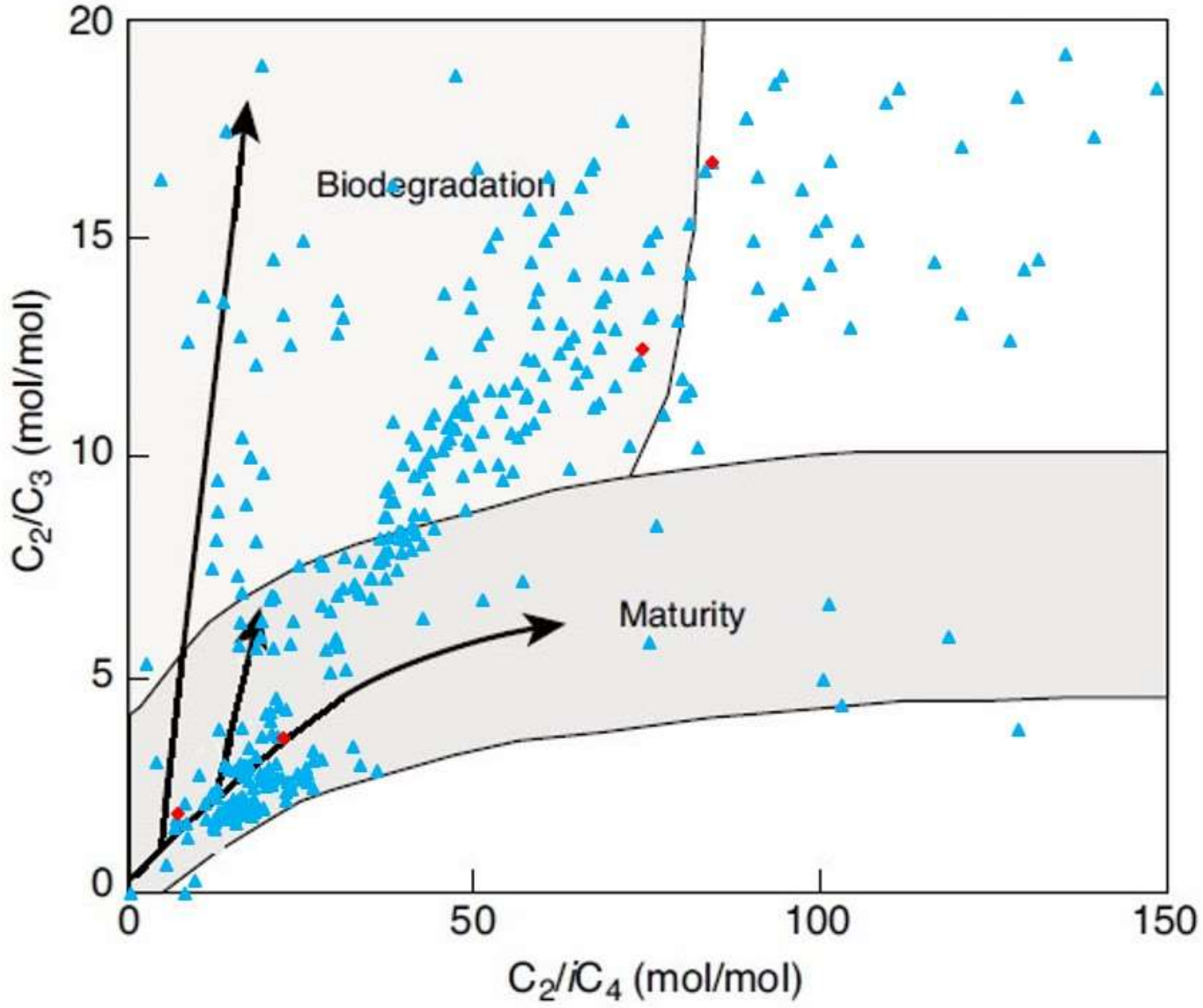

Figure B 42. ISO map data – play 4.14 Interpretive diagrams MC/ISO Prinzhofer Diagram for Cadomin, Chinkeh maps (after Prinzhofer and Battani 2003, no trendlines).

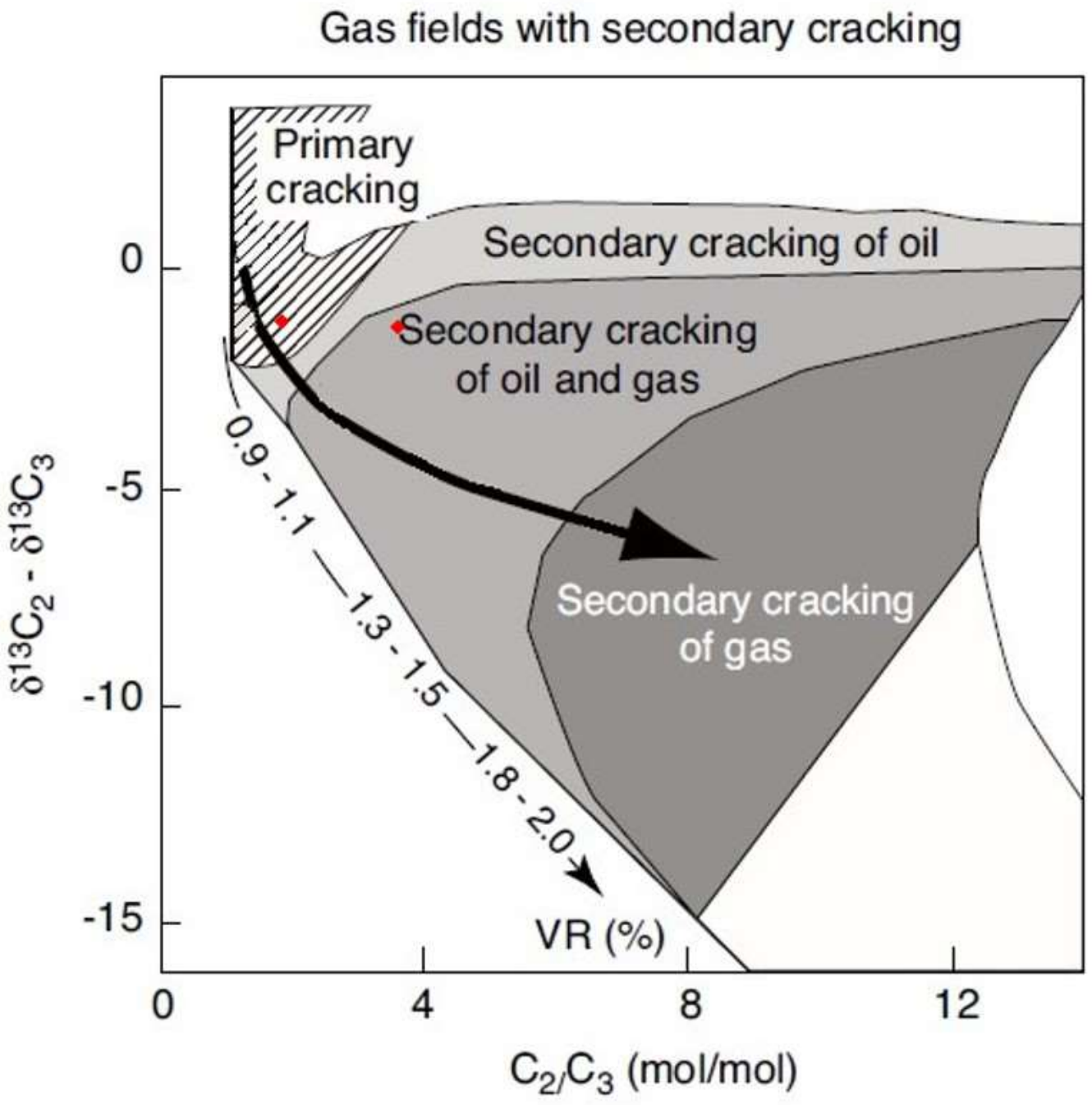

Figure B 43. ISO map data – play 4.14 Interpretive diagrams MC/ISO Prinzhofer Diagram for Cadomin, Chinkeh maps (after Prinzhofer and Battani 2003, no trendlines).

7. Play 4.15 Nikanassin, Buick Creek (two formations – both MC & ISO data)

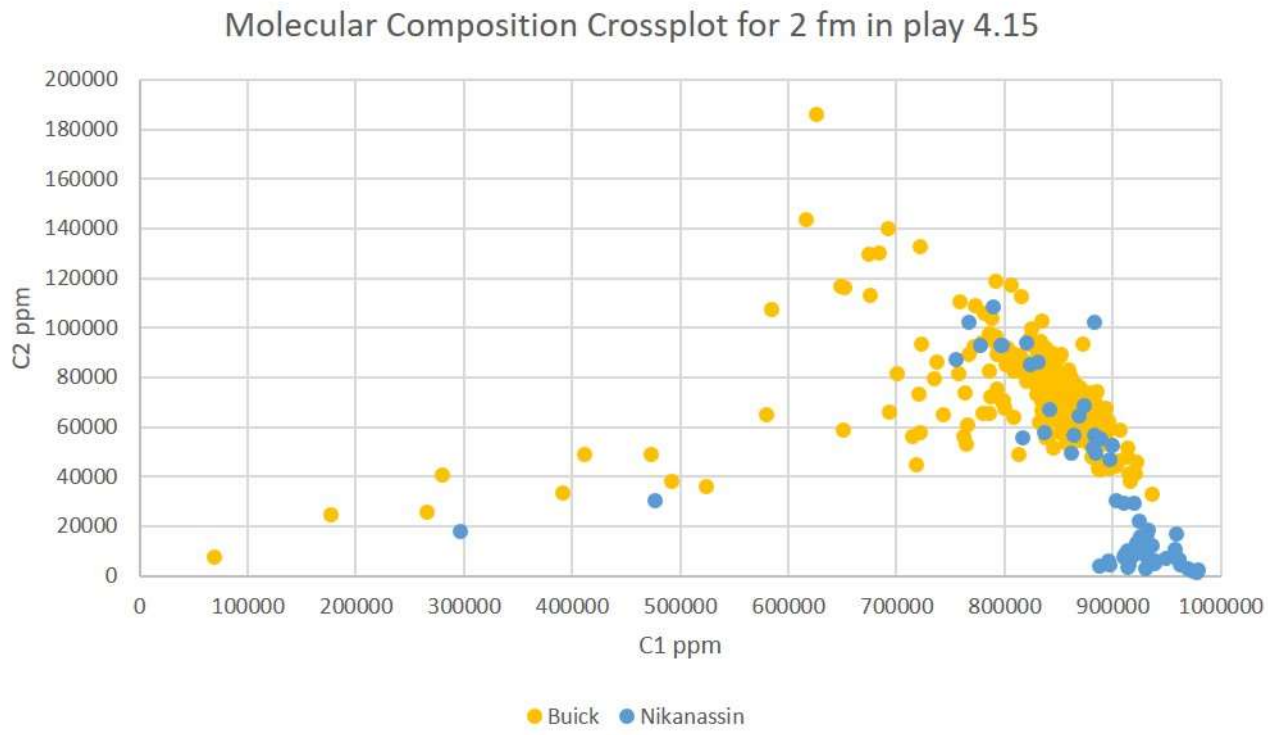

Figure B 44. MC map data – play 4.15 MC (ppm) ethane methane plot for Nikanassin, Buick Creek double formation [not to template].

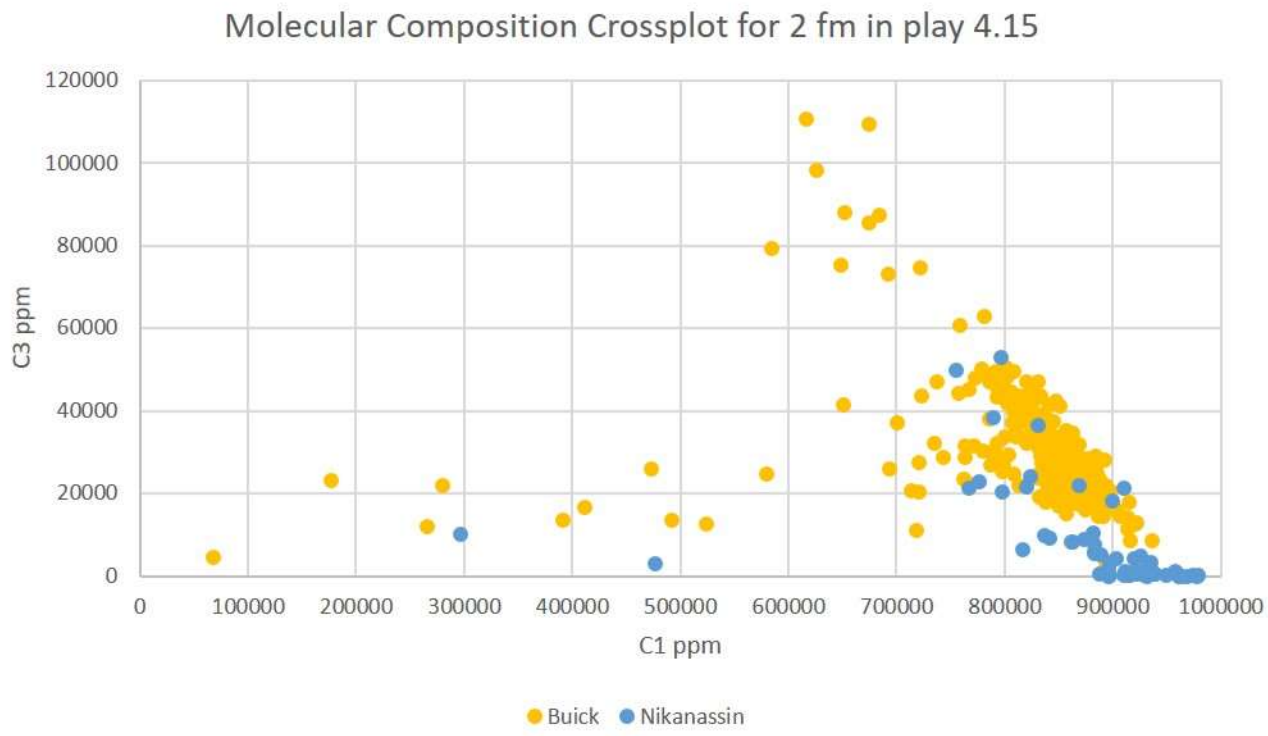

Figure B 45. MC map data – play 4.15 MC (ppm) propane methane plot for Nikanassin, Buick Creek double formation [not to template].

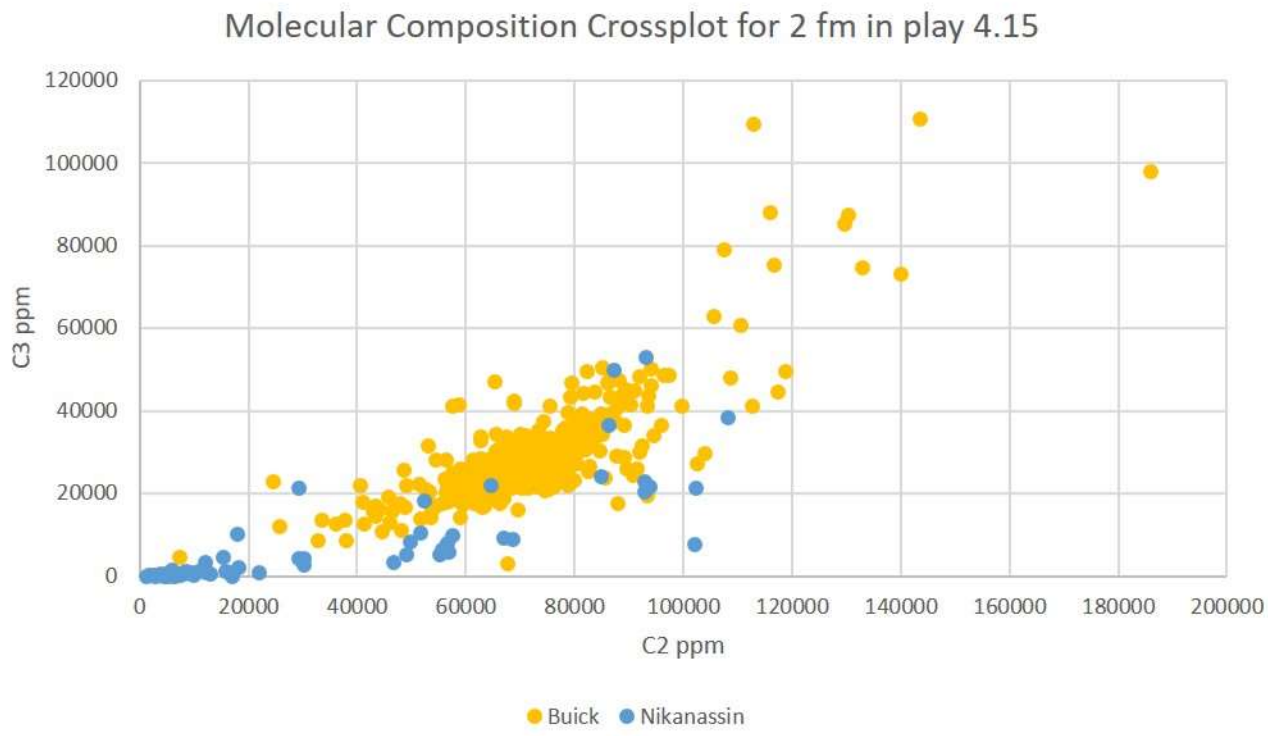

Figure B 46. MC map data – play 4.15 MC (ppm) propane ethane plot for Nikanassin, Buick Creek double formation [not to template].

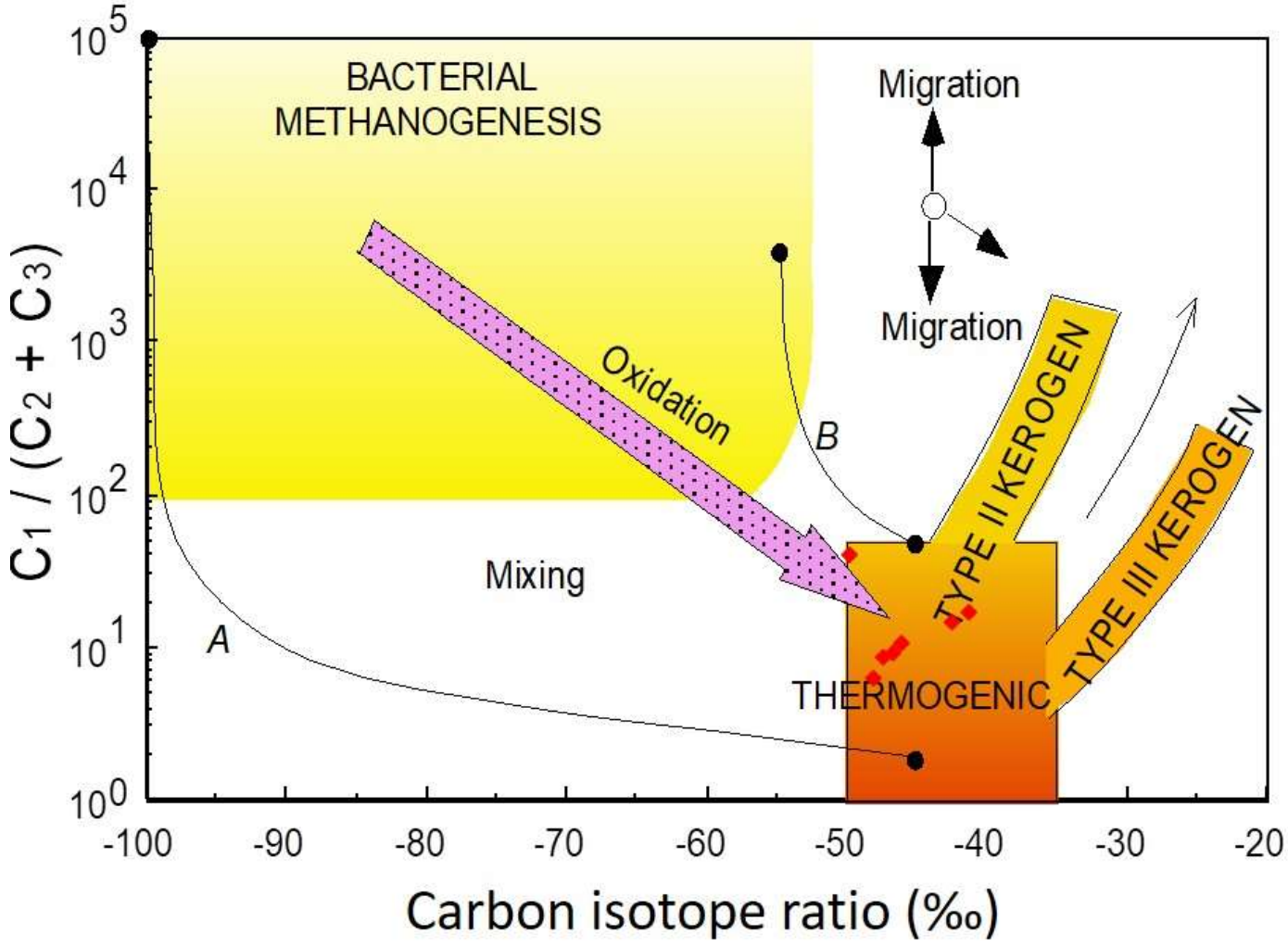

Figure B 47. ISO map data – play 4.15 Interpretive diagrams MC/ISO Bernard Diagram for Nikanassin, Buick Creek maps (Whiticar, 2018 pers. comm., after Whiticar 1999, no trendlines, no Deuterium for CD diagram).

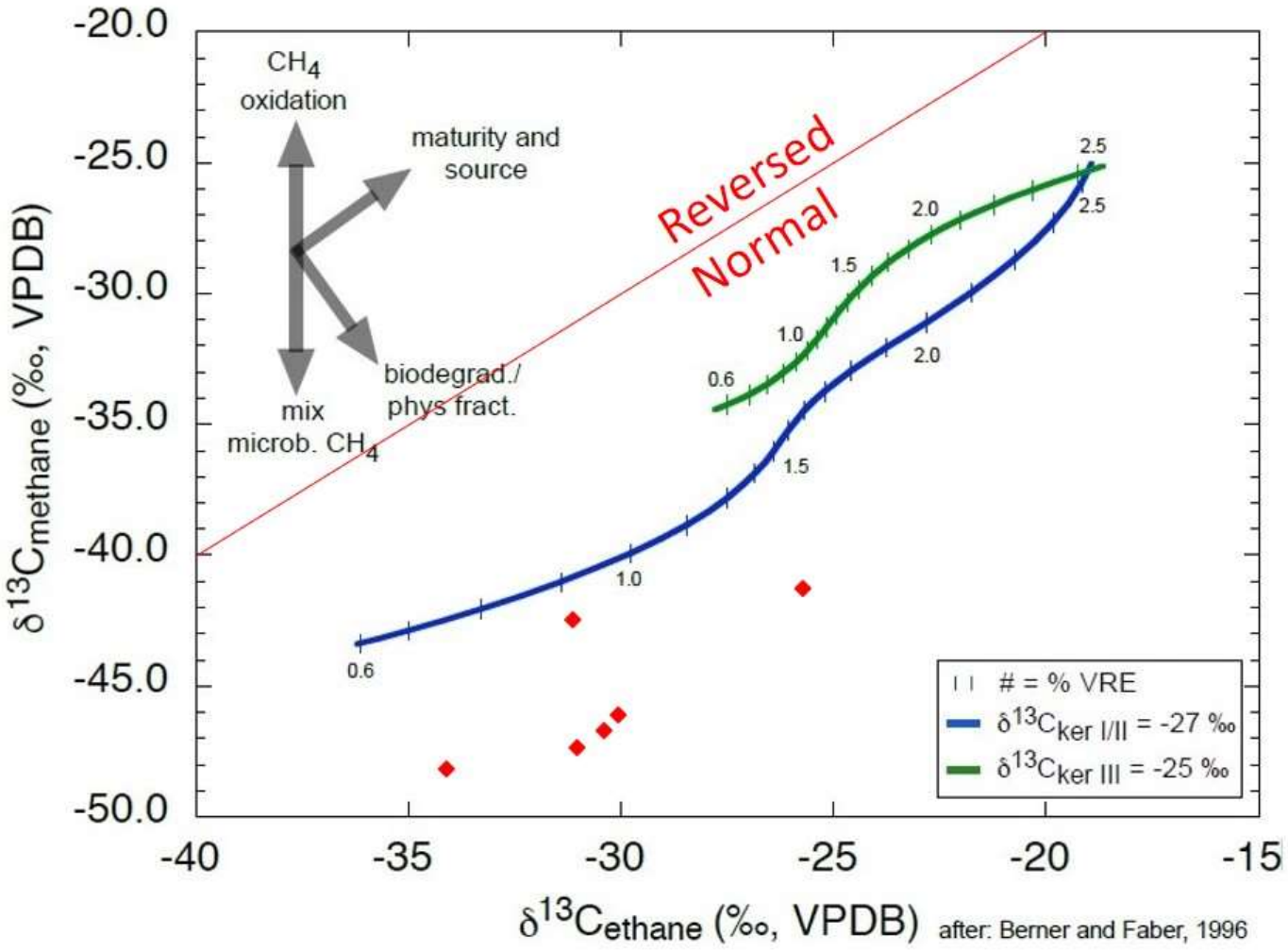

Figure B 48. ISO map data – play 4.15 Interpretive diagrams ISO $\delta^{13}C_1$ vs $\delta^{13}C_2$ plot for Nikanassin, Buick Creek maps (Whiticar, 2018 pers. comm., after Berner and Faber 1996, no trendlines).

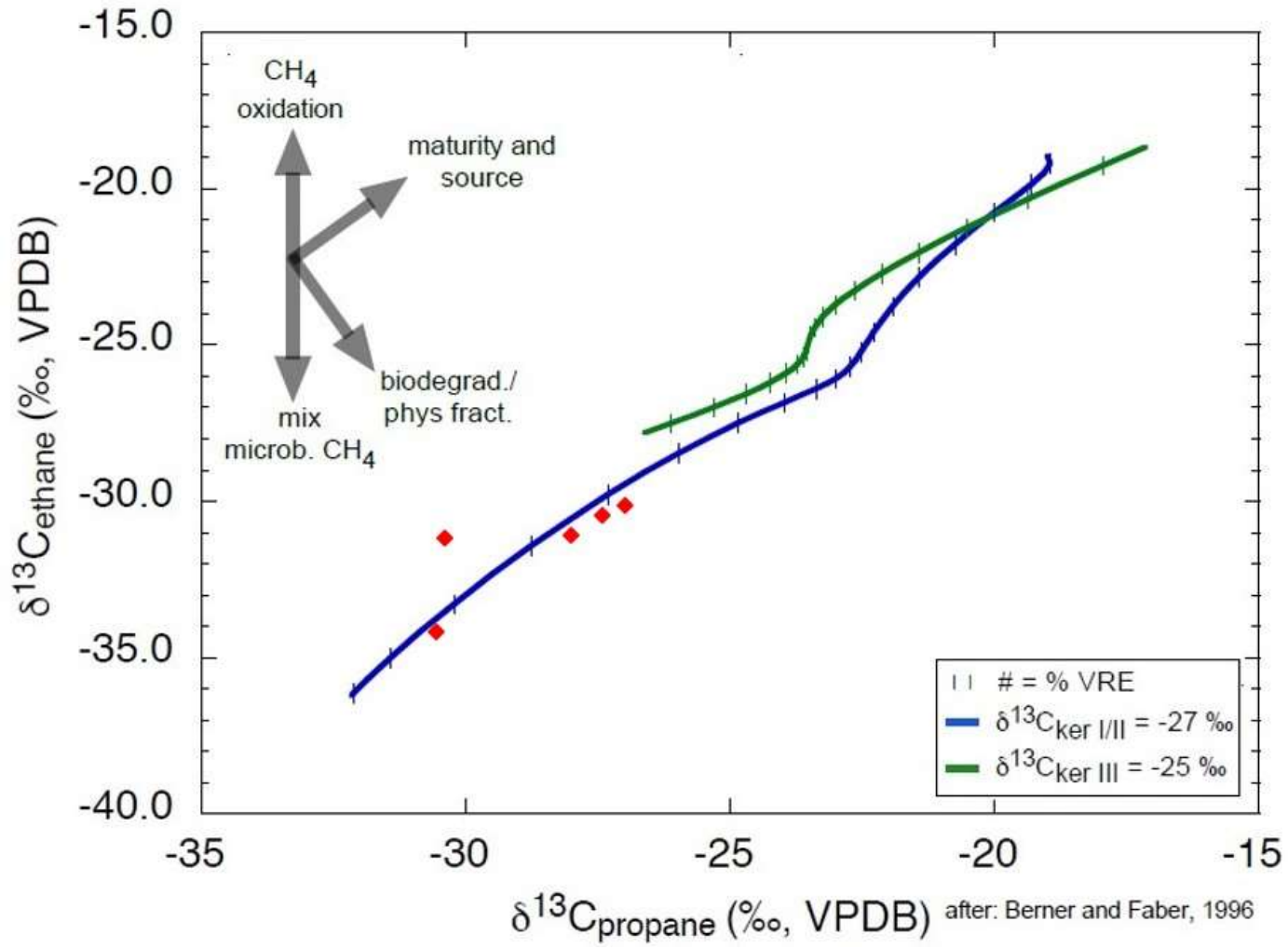

Figure B 49. ISO map data – play 4.15 Interpretive diagrams ISO $\delta^{13}C_2$ vs $\delta^{13}C_3$ plot for Nikanassin, Buick Creek maps (Whiticar, 2018 pers. comm., after Berner and Faber 1996, no trendlines).

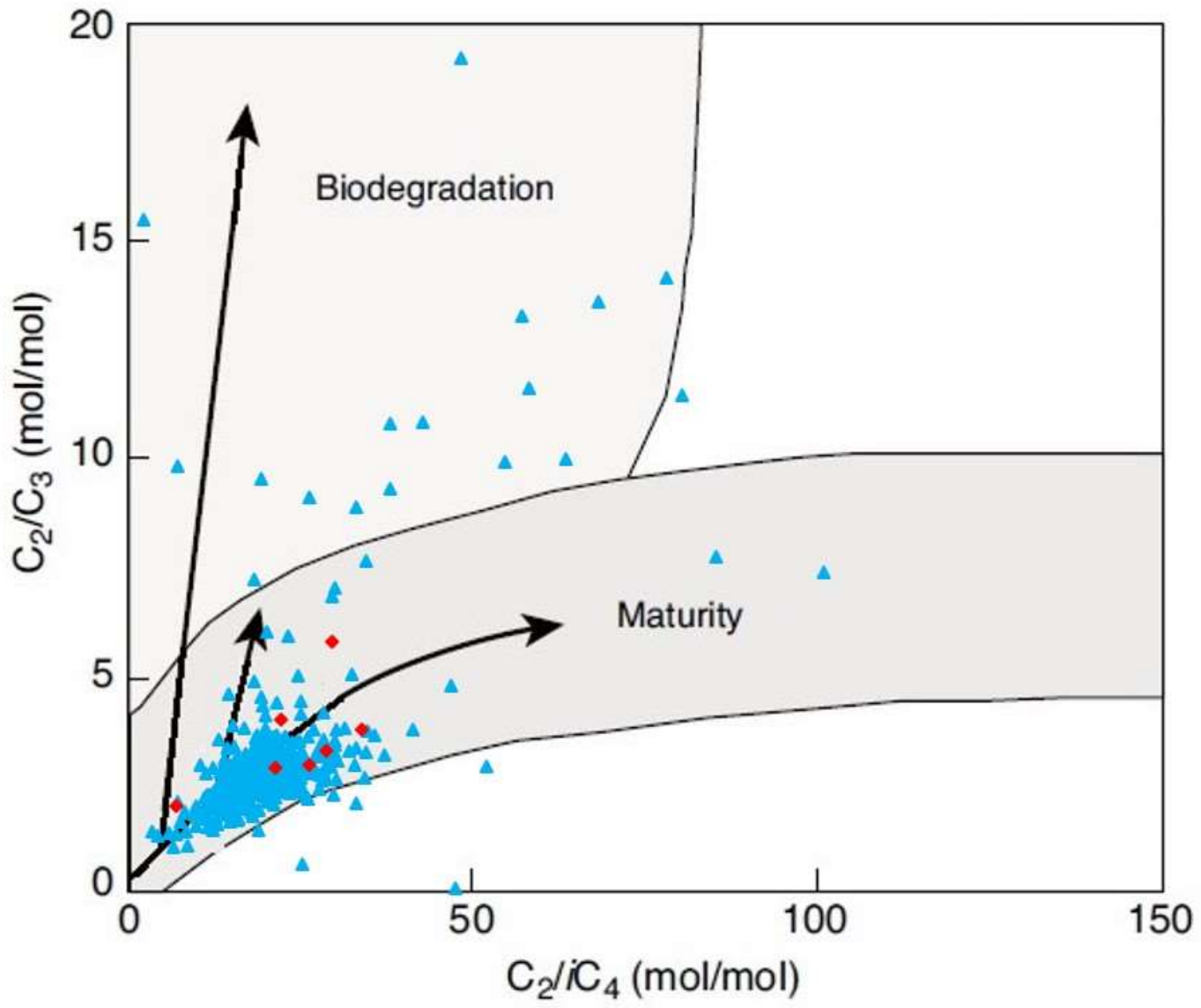

Figure B 50. ISO map data – play 4.15 Interpretive diagrams MC/ISO Prinzhofer Diagram for Nikanassin, Buick Creek maps (after Prinzhofer and Battani 2003, no trendlines).

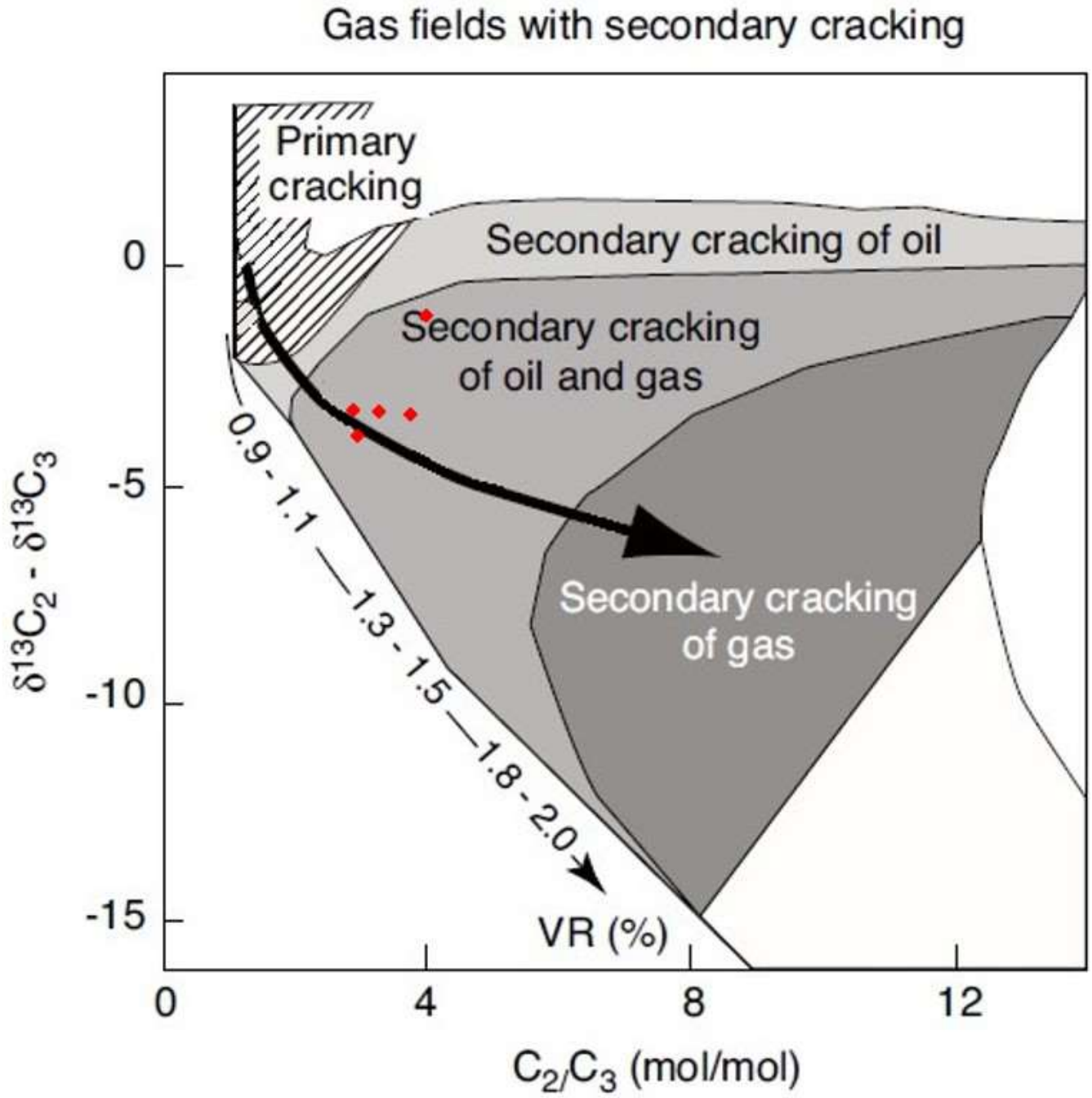

Figure B 51. ISO map data – play 4.15 Interpretive diagrams MC/ISO Lorant Diagram for Nikanassin, Buick Creek maps (after Prinzhofer and Battani 2003, no trendlines).

8. Play 4.15a Fernie (single group, including Nordegg – ISO data only)

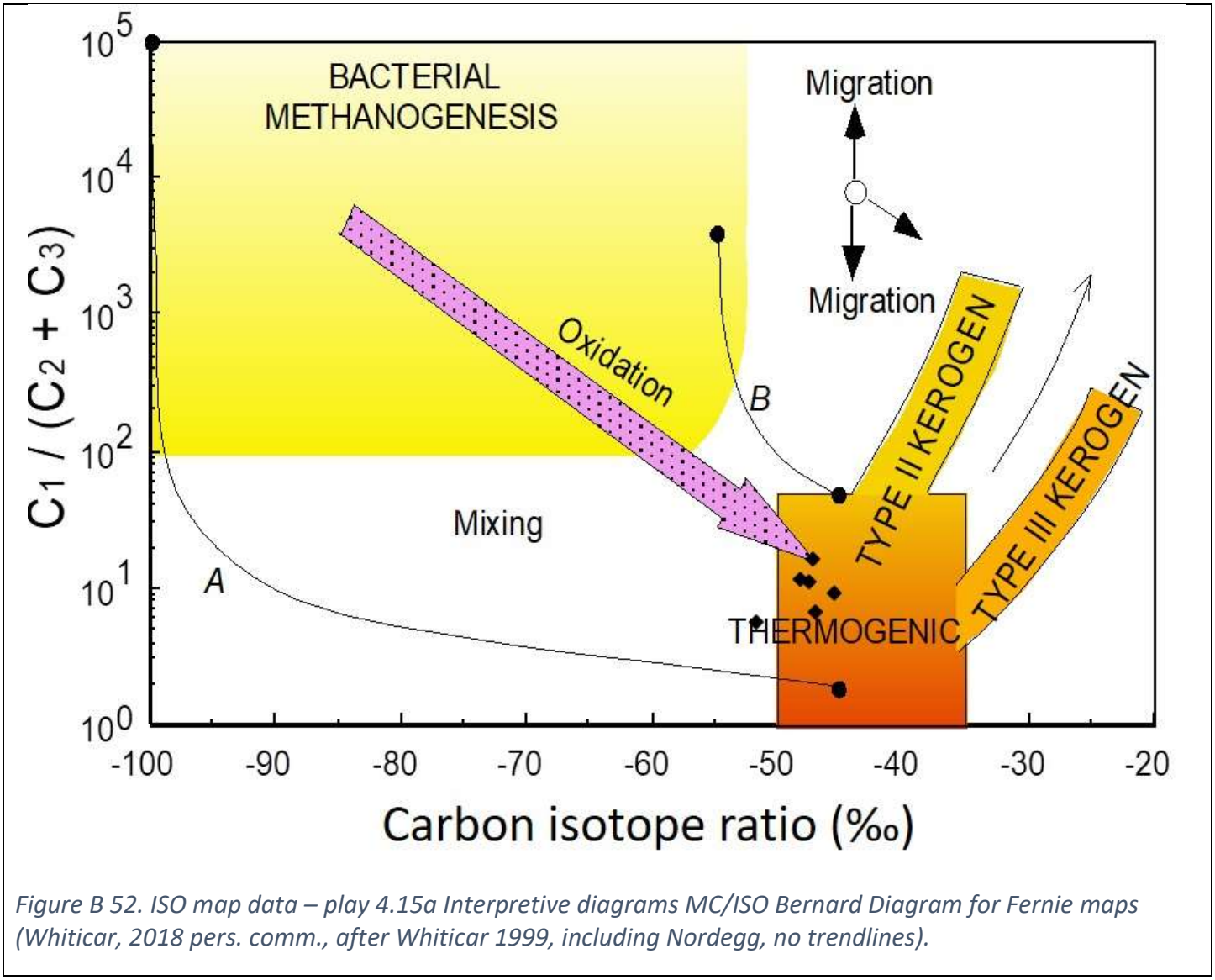

Figure B 52. ISO map data – play 4.15a Interpretive diagrams MC/ISO Bernard Diagram for Fernie maps (Whiticar, 2018 pers. comm., after Whiticar 1999, including Nordegg, no trendlines).

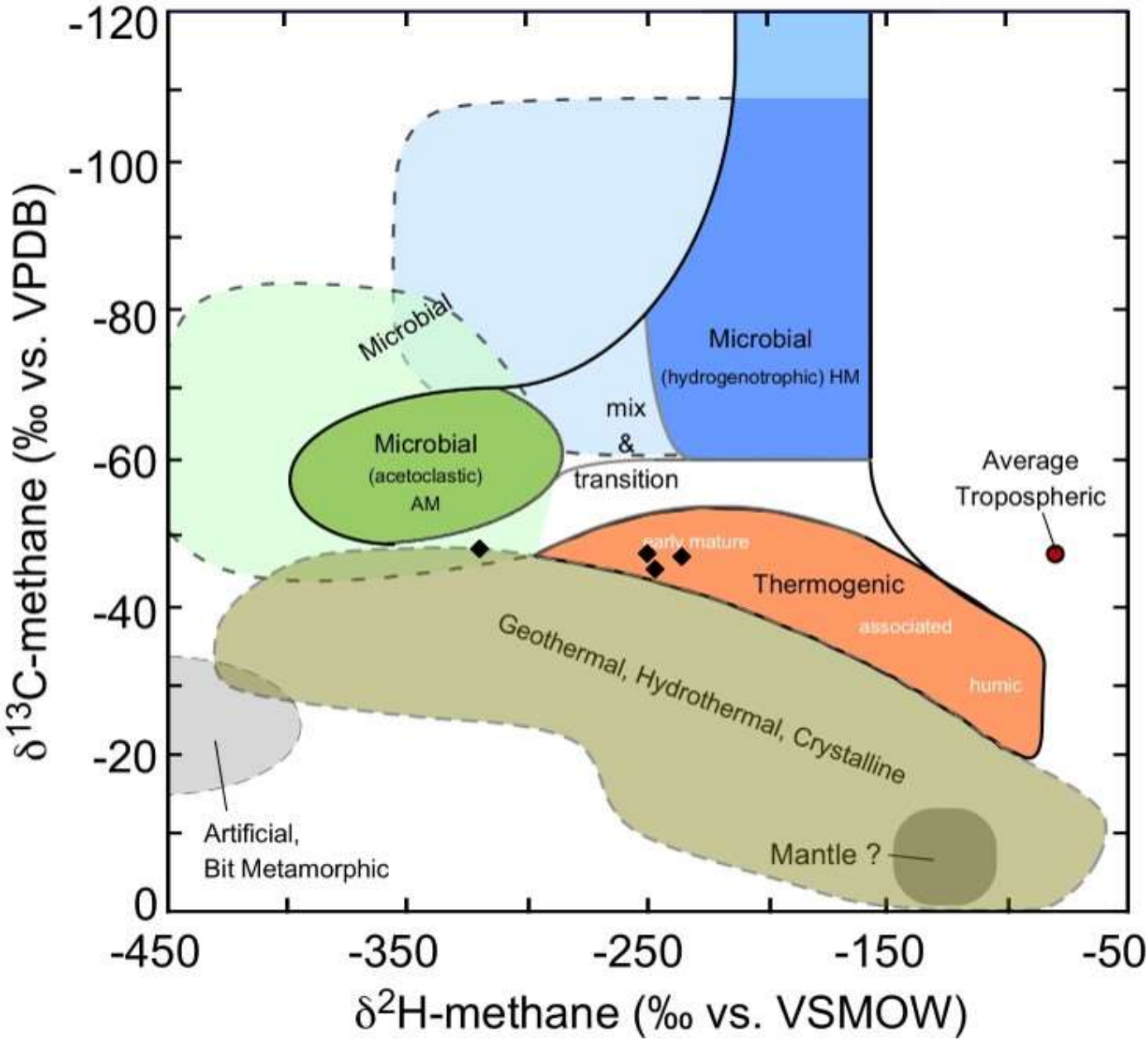

Figure B 53. ISO map data – play 4.15a Interpretive diagrams ISO CD Diagram for Fernie maps (Whiticar, 2018 pers. comm., after Whiticar 1999, including Nordegg, no trendlines).

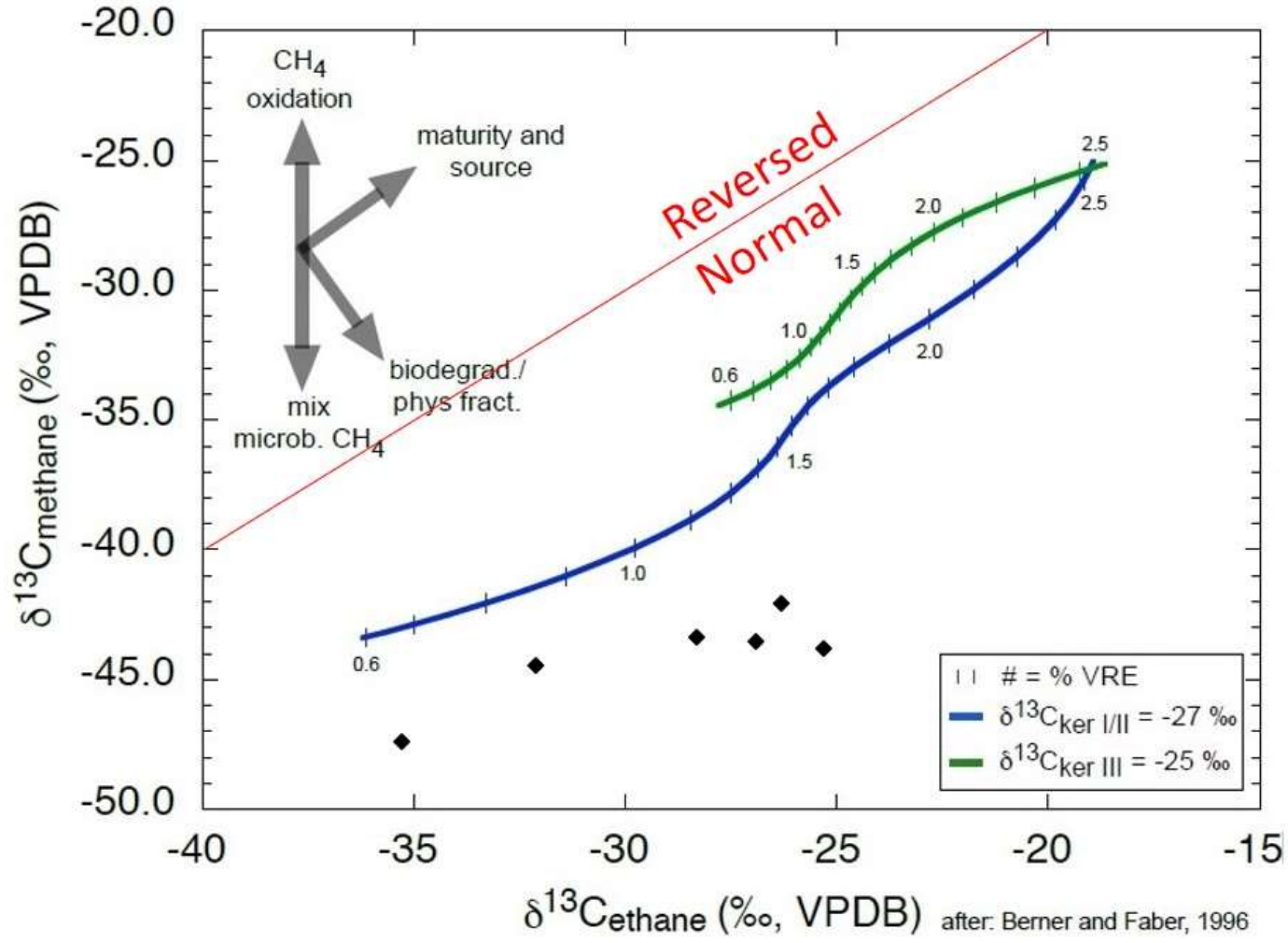

Figure B 54. ISO map data – play 4.15a Interpretive diagrams ISO $\delta^{13}C_1$ vs $\delta^{13}C_2$ plot for Fernie maps (Whiticar, 2018 pers. comm., after Berner and Faber 1996, including Nordegg, no trendlines).

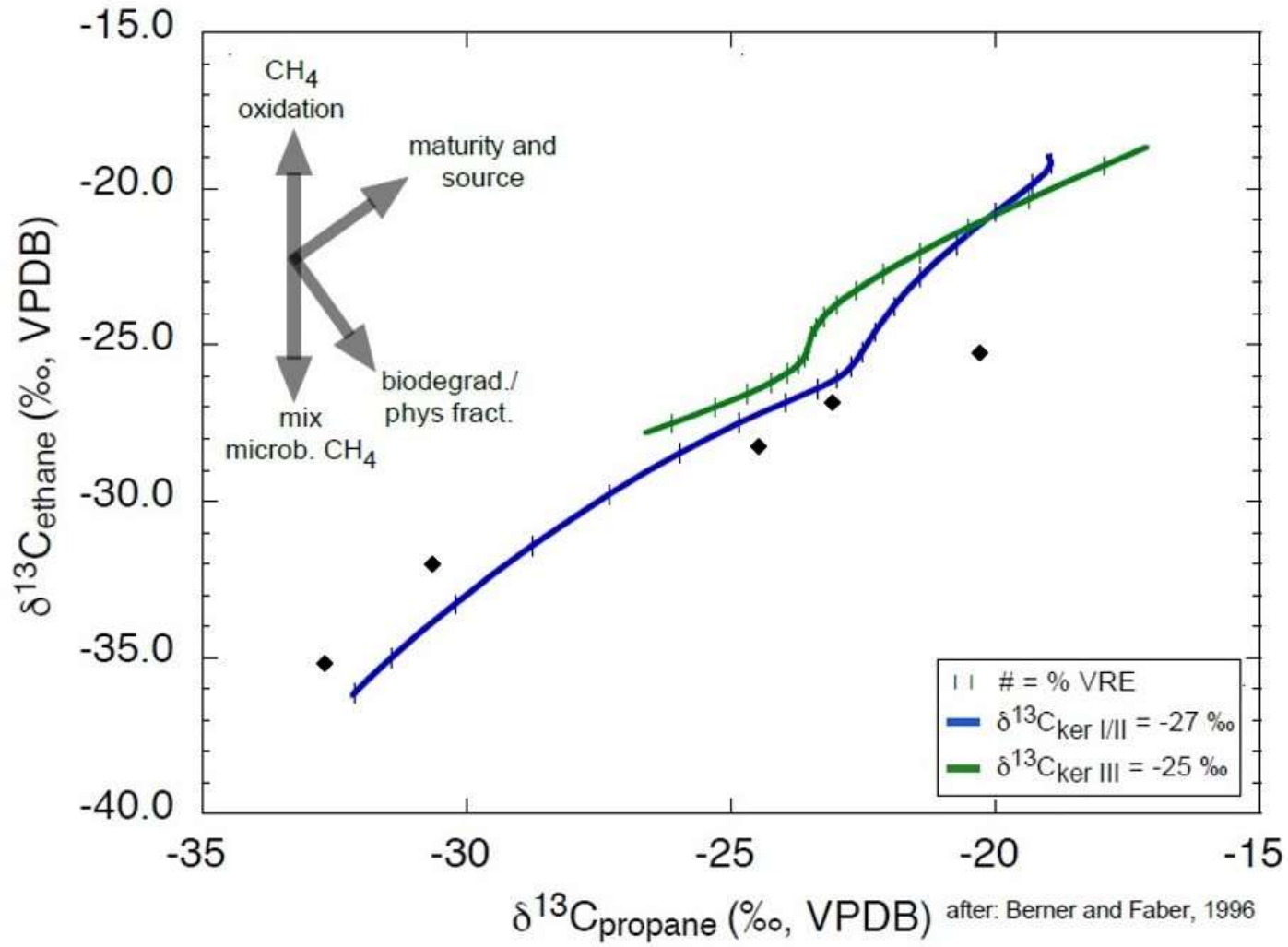

Figure B 55. ISO map data – play 4.15a Interpretive diagrams ISO $\delta^{13}C_2$ vs $\delta^{13}C_3$ plot for Fernie maps (Whiticar, 2018 pers. comm., after Berner and Faber 1996, including Nordegg, no trendlines).

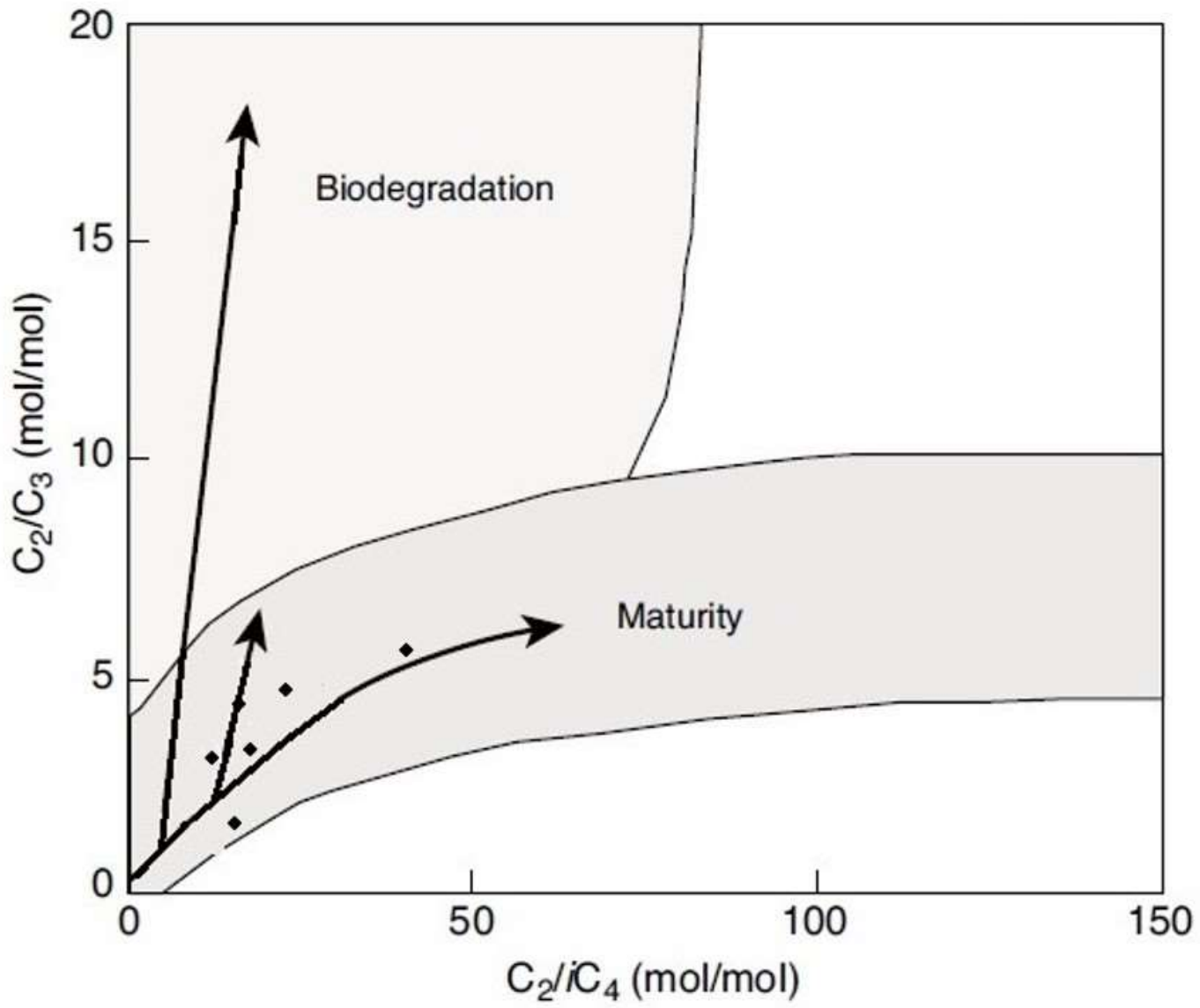

Figure B 56. ISO map data – play 4.15a Interpretive diagrams MC Prinzhofer Diagram for Fernie maps (including Nordegg, after Prinzhofer and Battani 2003, no trendlines).

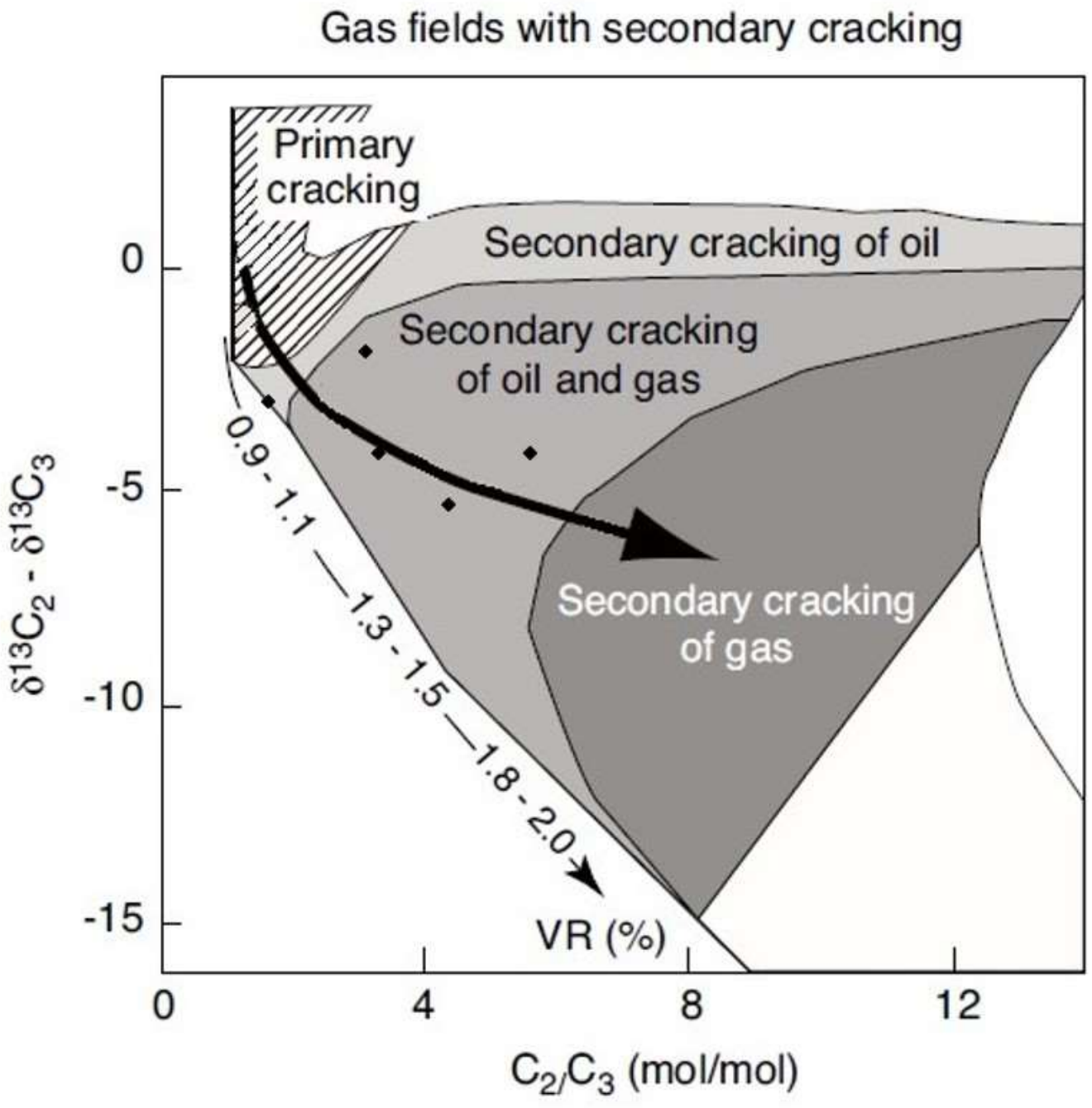

Figure B 57. ISO map data – play 4.15a Interpretive diagrams MC Lorant Diagram for Fernie maps (including Nordegg, after Prinzhofer and Battani 2003, no trendlines).

9. Play 4.16 Charlie Lake, Baldonnel, Pardonet (multiple formations and members – both MC & ISO data)

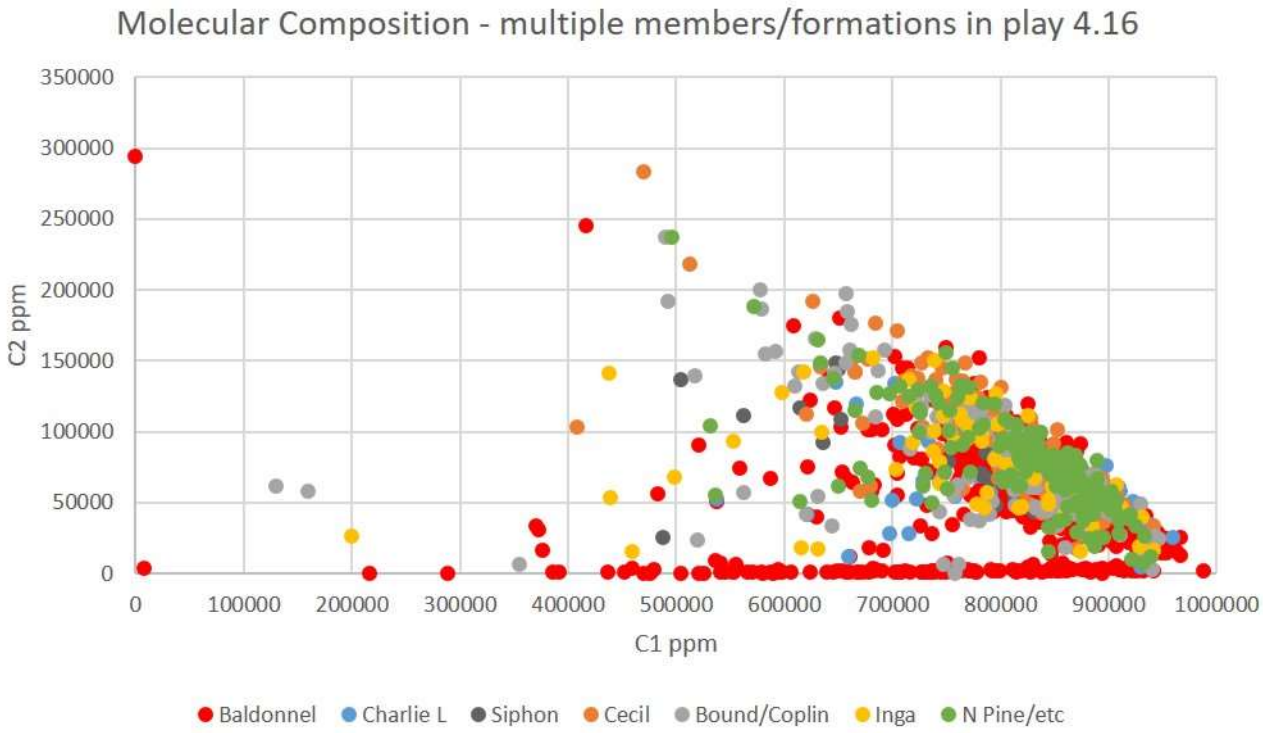

Figure B 58. MC map data – play 4.16 MC (ppm) ethane methane plot for Charlie Lake, Baldonnel, Pardonet multiple formations and some member splits for Charlie Lake [no data for Pardonet, not to template].

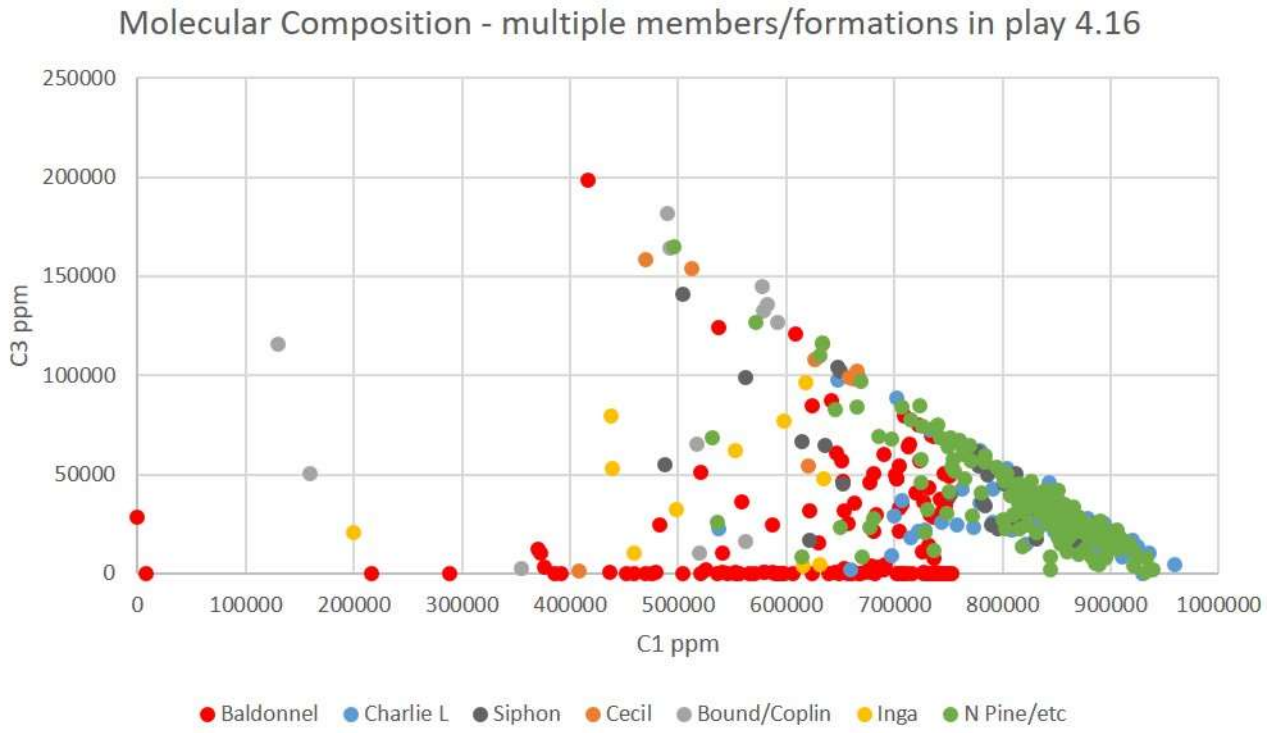

Figure B 59. MC map data – play 4.16 MC (ppm) propane methane plot for Charlie Lake, Baldonnel, Pardonet multiple formations and some member splits for Charlie Lake [no data for Pardonet, not to template].

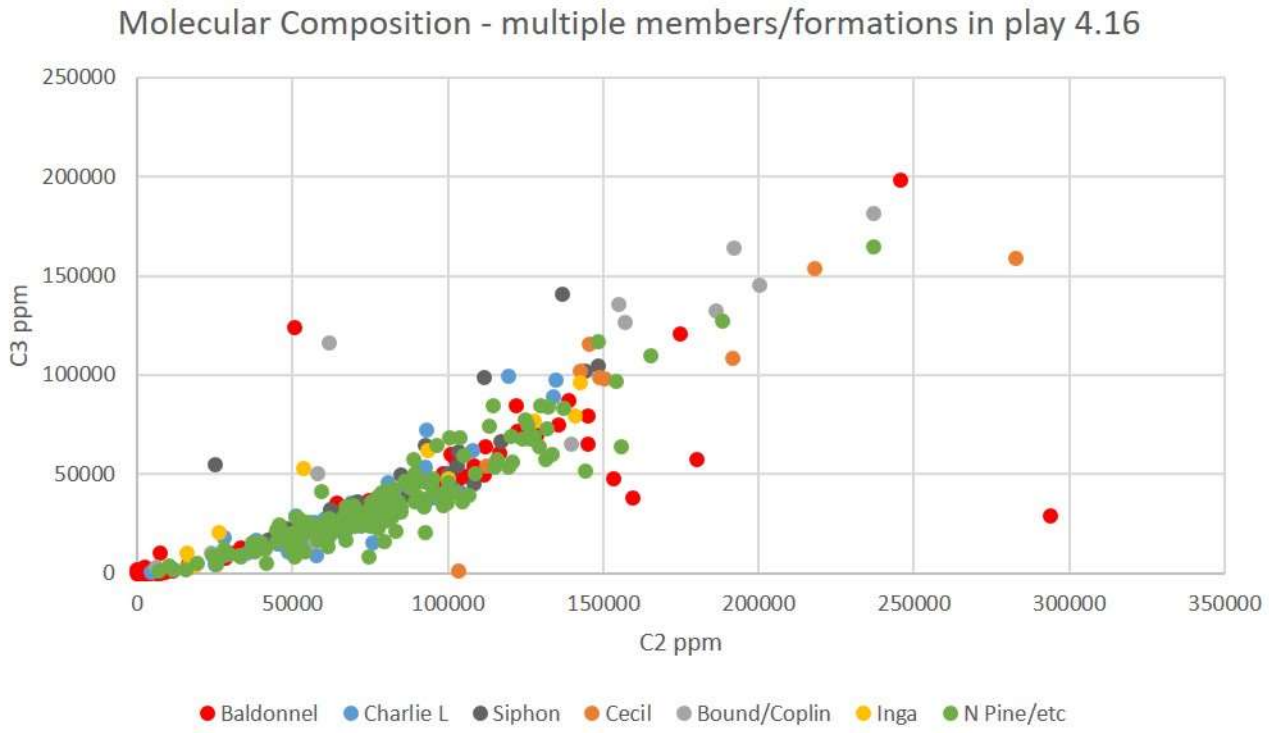

Figure B 60. MC map data – play 4.16 MC (ppm) propane ethane plot for Charlie Lake, Baldonnel, Pardonet multiple formations and some member splits for Charlie Lake [no data for Pardonet, not to template].

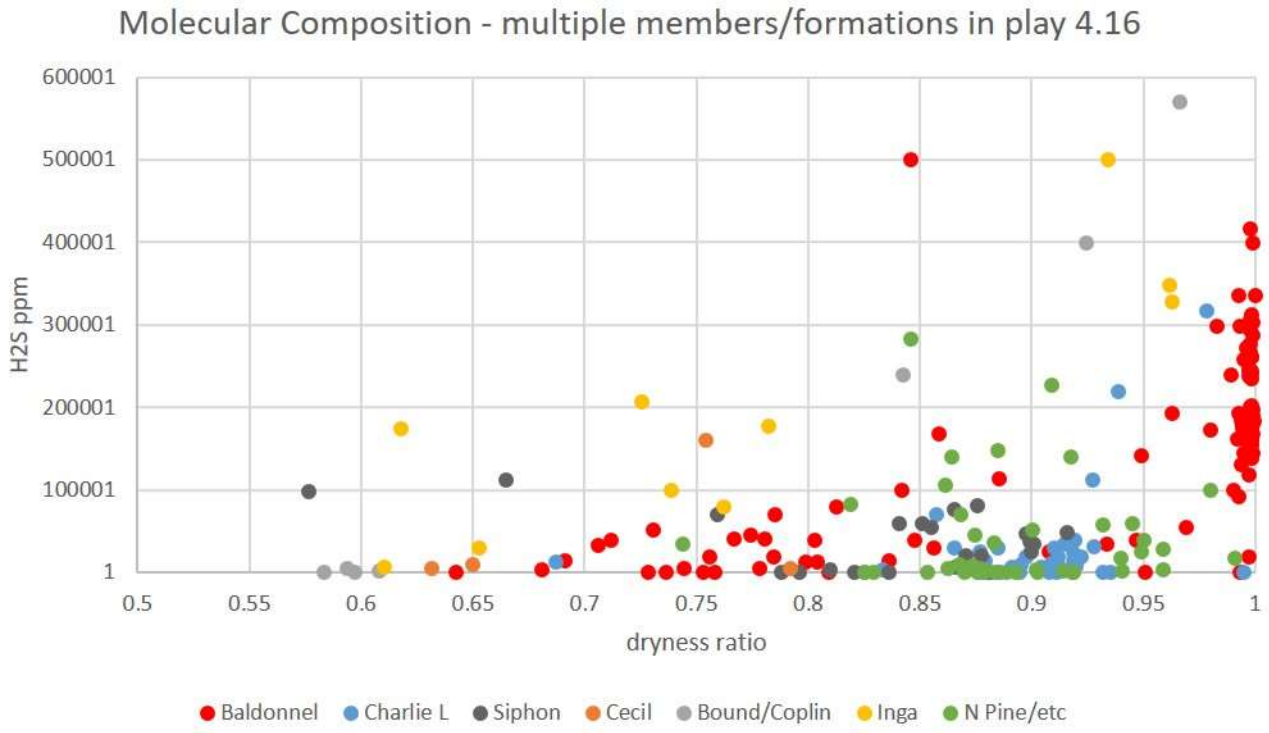

Figure B 61. MC map data – play 4.16 MC (ppm) sour gas versus dryness ratio plot for Charlie Lake, Baldonnel, Pardonet multiple formations and some member splits for Charlie Lake [no data for Pardonet, not to template].

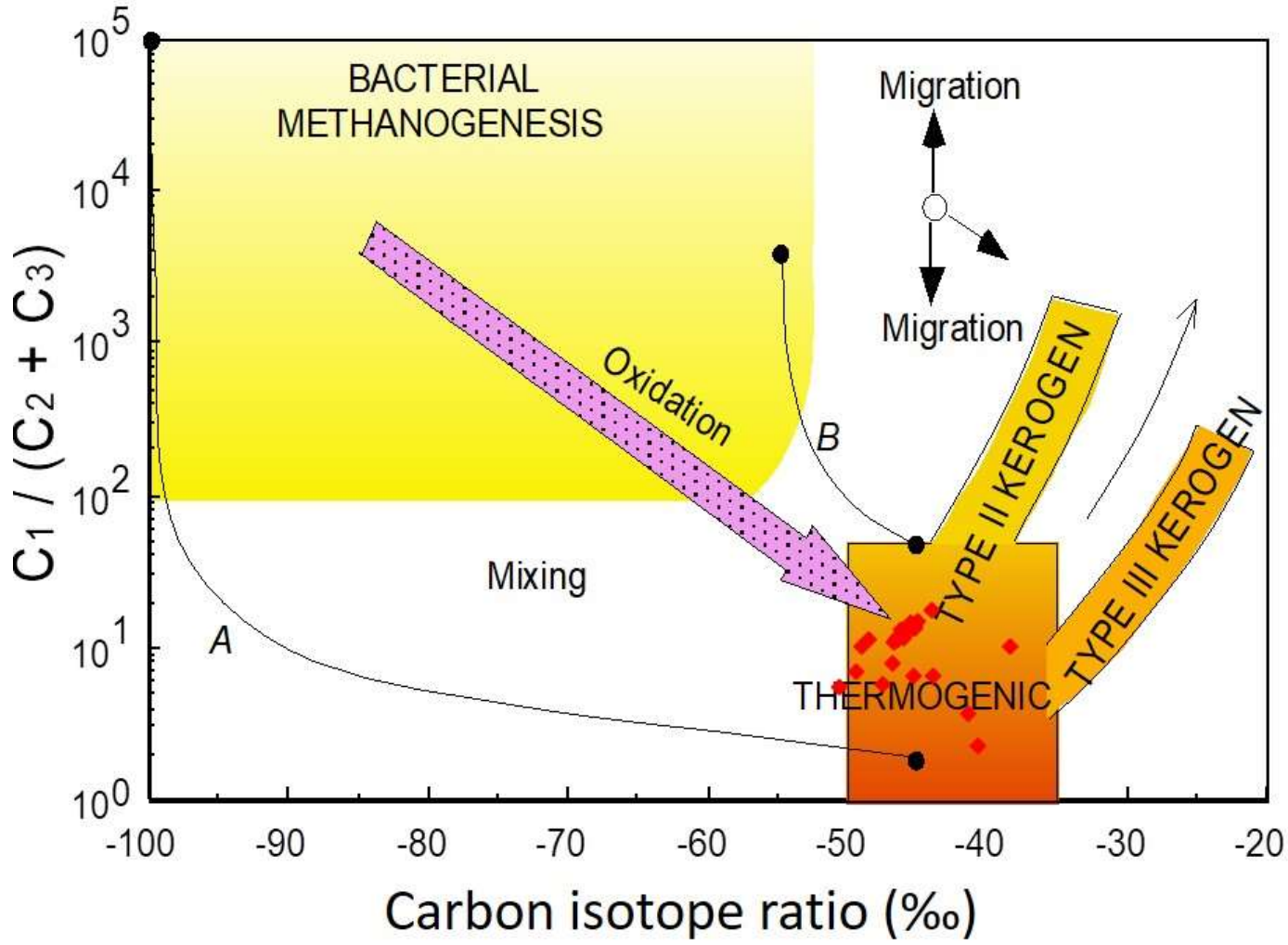

Figure B 62. ISO map data – play 4.16 Interpretive diagrams MC/ISO Bernard Diagram for Charlie Lake, Baldonnel, Pardonet maps (Whiticar, 2018 pers. comm., after Whiticar 1999, no data for Pardonet, no trendlines).

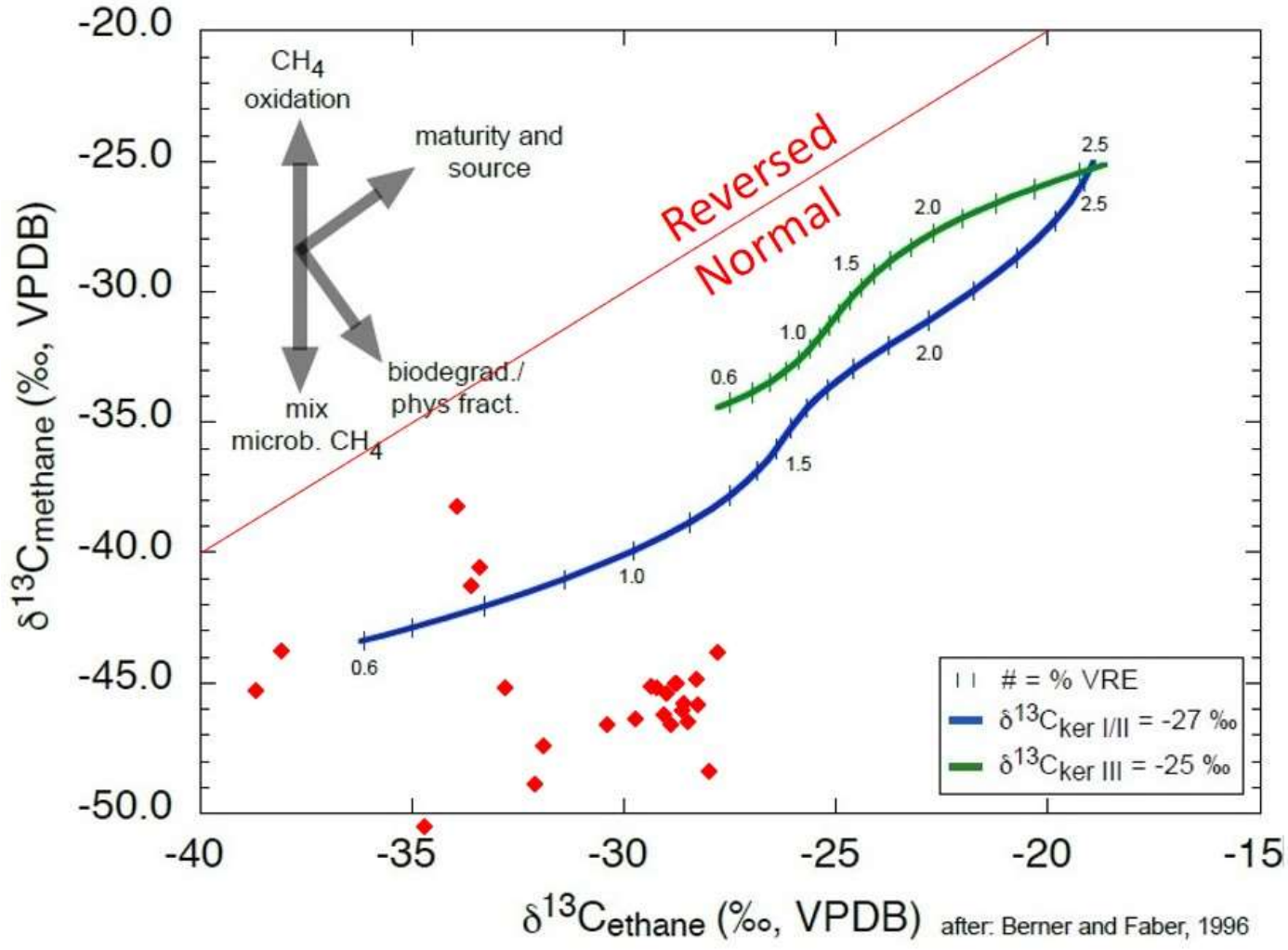

Figure B 63. ISO map data – play 4.16 Interpretive diagrams ISO $\delta^{13}C_1$ vs $\delta^{13}C_2$ plot for Charlie Lake, Baldonnel, Pardonet maps (Whiticar, 2018 pers. comm., after Berner and Faber 1996, no data for Pardonet, no trendlines).

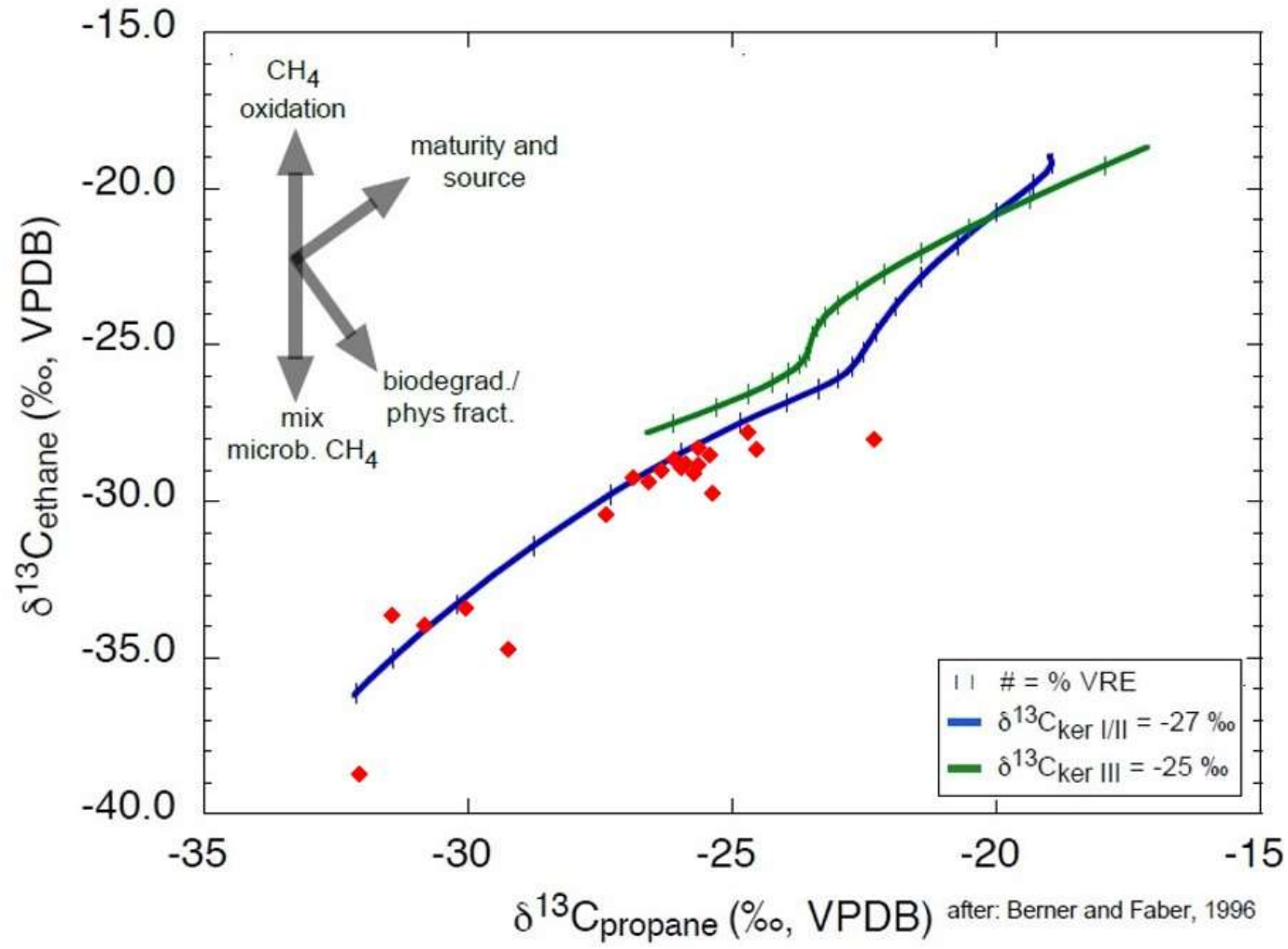

Figure B 64. ISO map data – play 4.16 Interpretive diagrams ISO $\delta^{13}C_2$ vs $\delta^{13}C_3$ plot for Charlie Lake, Baldonnel, Pardonet maps (Whiticar, 2018 pers. comm., after Berner and Faber 1996, no data for Pardonet, no trendlines).

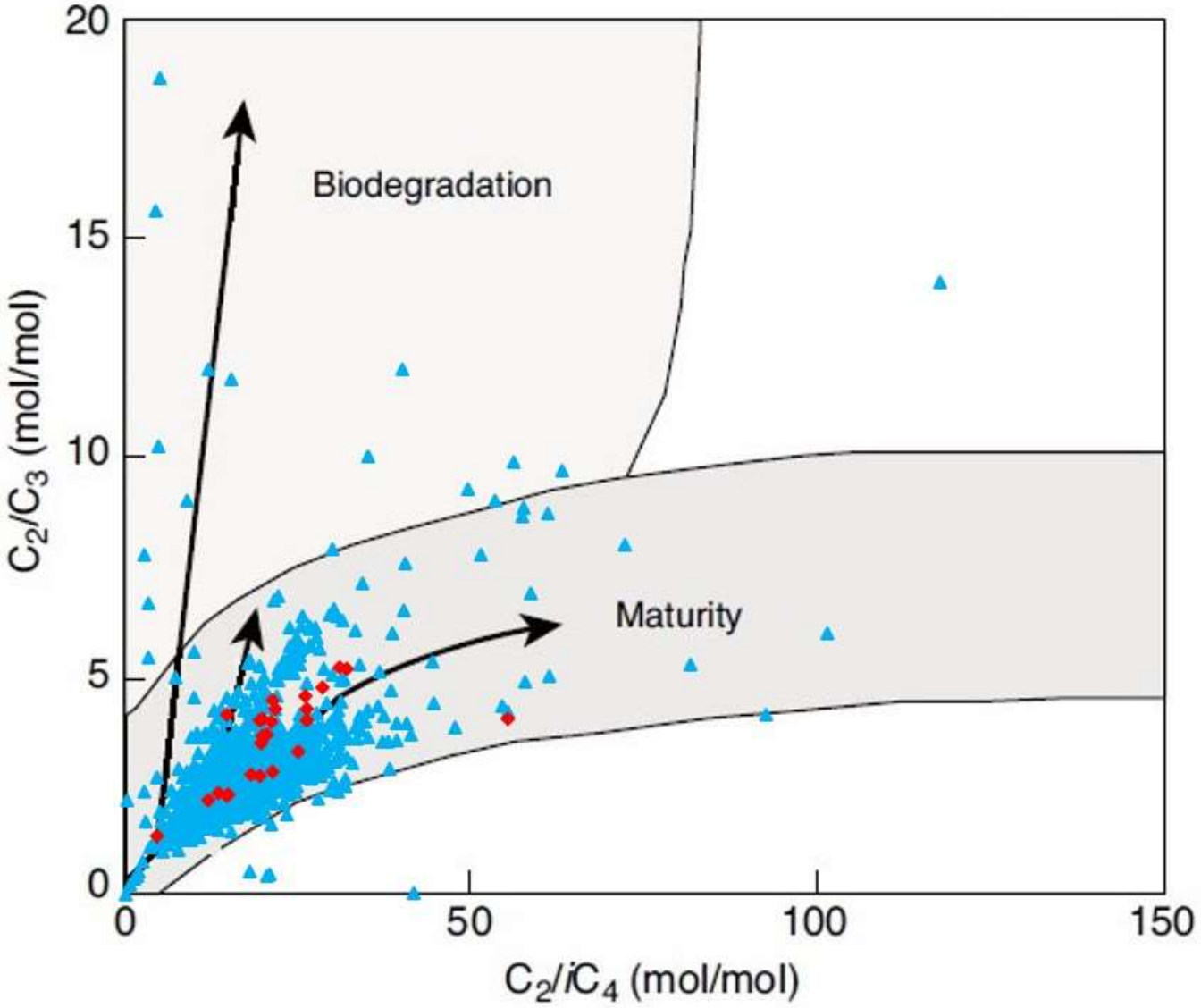

Figure B 65. ISO map data – play 4.16 Interpretive diagrams MC Prinzhofer Diagram for Charlie Lake, Baldonnel, Pardonet maps (after Prinzhofer and Battani 2003, no data for Pardonet, no trendlines).

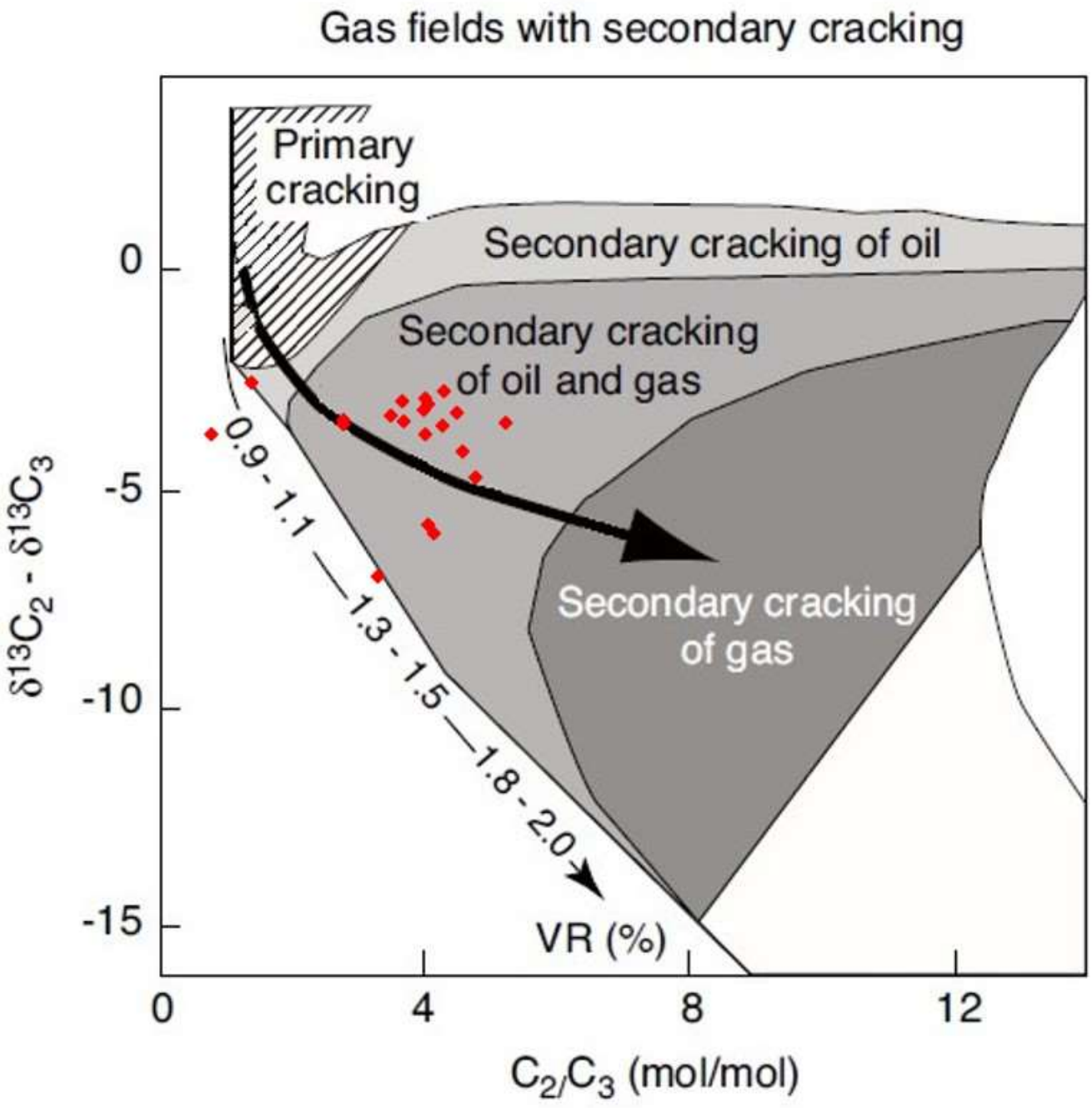

Figure B 66. ISO map data – play 4.16 Interpretive diagrams MC Lorant Diagram for Charlie Lake, Baldonnel, Pardonet maps (after Prinzhofer and Battani 2003, no data for Pardonet, no trendlines).

10. Grouped MC data Play 4.19 Halfway, Play 4.20 Doig + Lower Halfway, Play 4.21 Montney

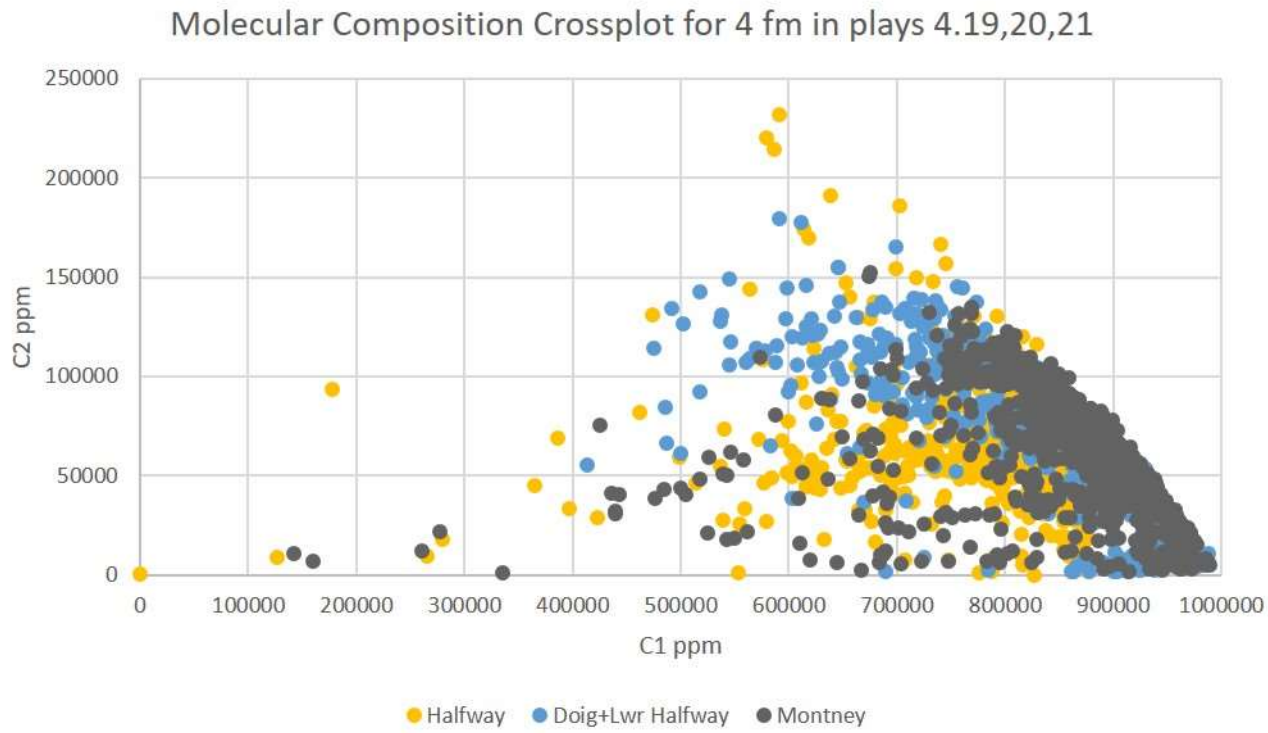

Figure B 67. MC map data – plays 4.19, 4.20, 4.21 MC (ppm) ethane methane plot for Halfway, Doig/Lower Halfway, and Montney formations [not to template].

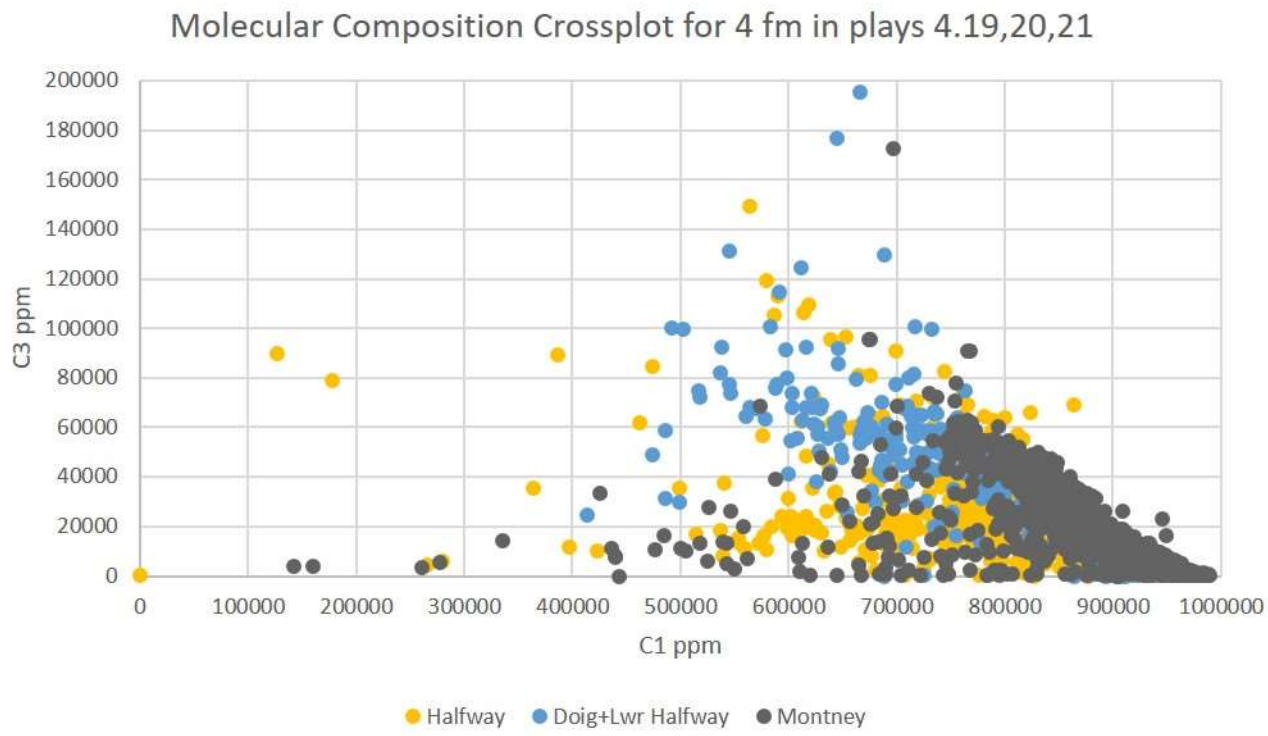

Figure B 68. MC map data – plays 4.19, 4.20, 4.21 MC (ppm) propane methane plot for Halfway, Doig/Lower Halfway, and Montney formations [not to template].

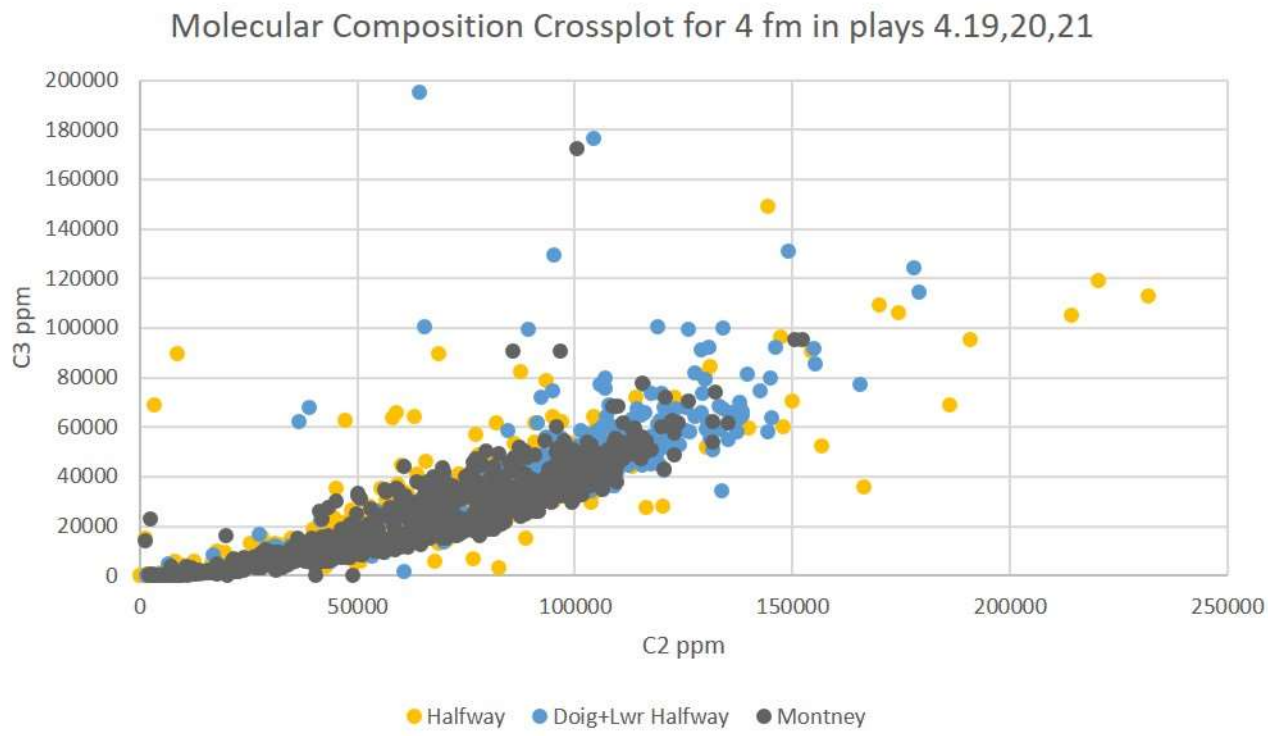

Figure B 69. MC map data – plays 4.19, 4.20, 4.21 MC (ppm) propane ethane plot for Halfway, Doig/Lower Halfway, and Montney formations [not to template].

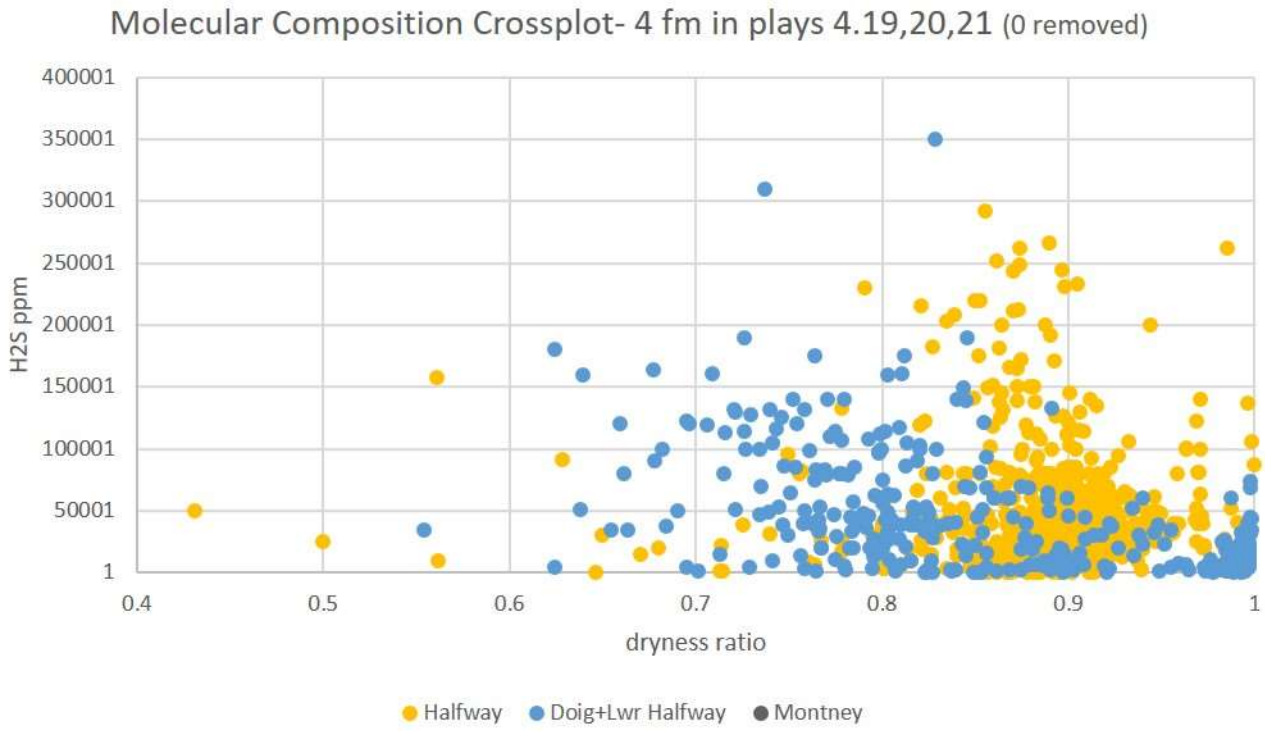

Figure B 70. MC map data – plays 4.19, 4.20, 4.21 MC (ppm) sour gas versus dryness ratio plot for Halfway, Doig/Lower Halfway, and Montney formations [not to template].

11. Play 4.19 Halfway (single formation – both MC & ISO data)

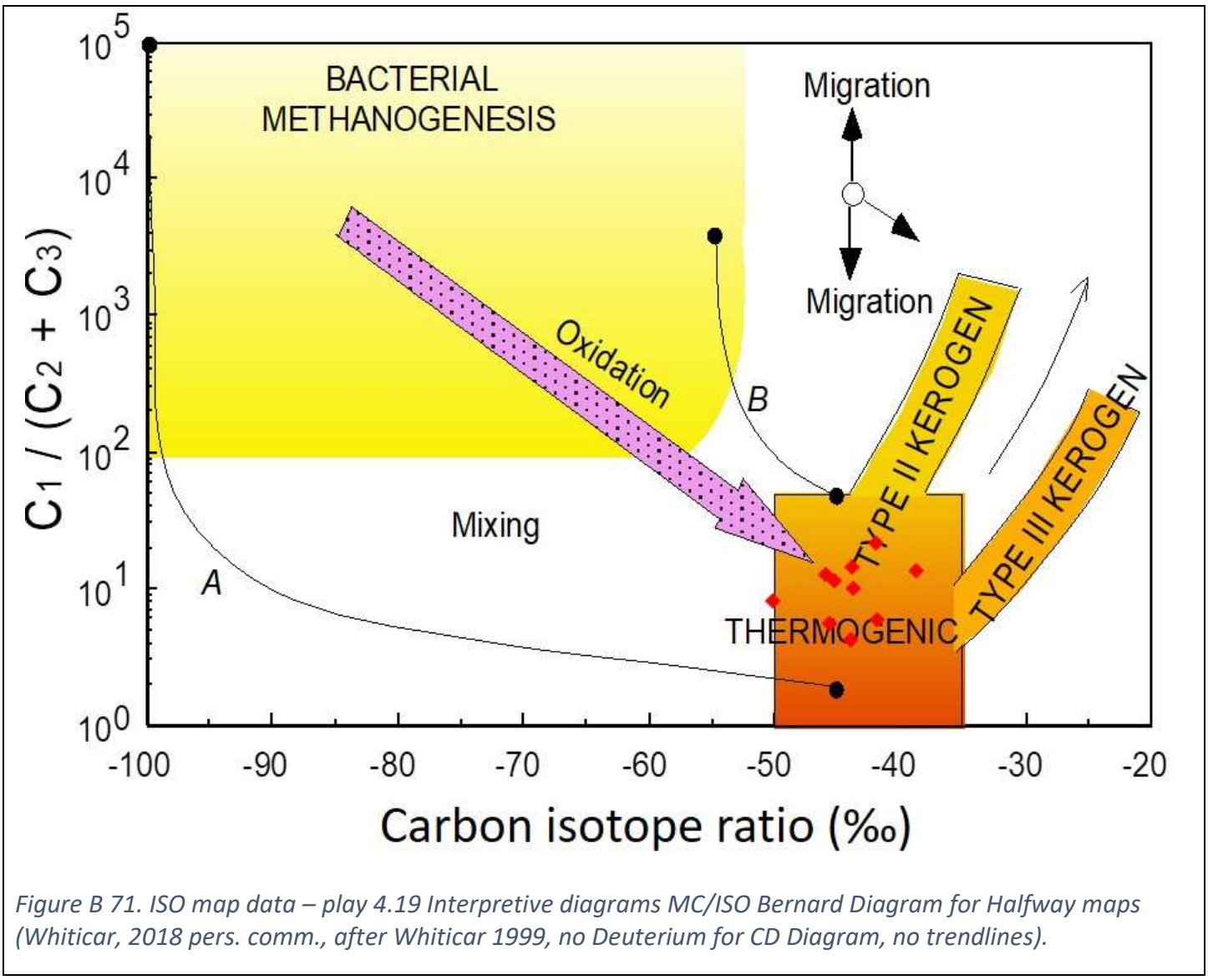

Figure B 71. ISO map data – play 4.19 Interpretive diagrams MC/ISO Bernard Diagram for Halfway maps (Whiticar, 2018 pers. comm., after Whiticar 1999, no Deuterium for CD Diagram, no trendlines).

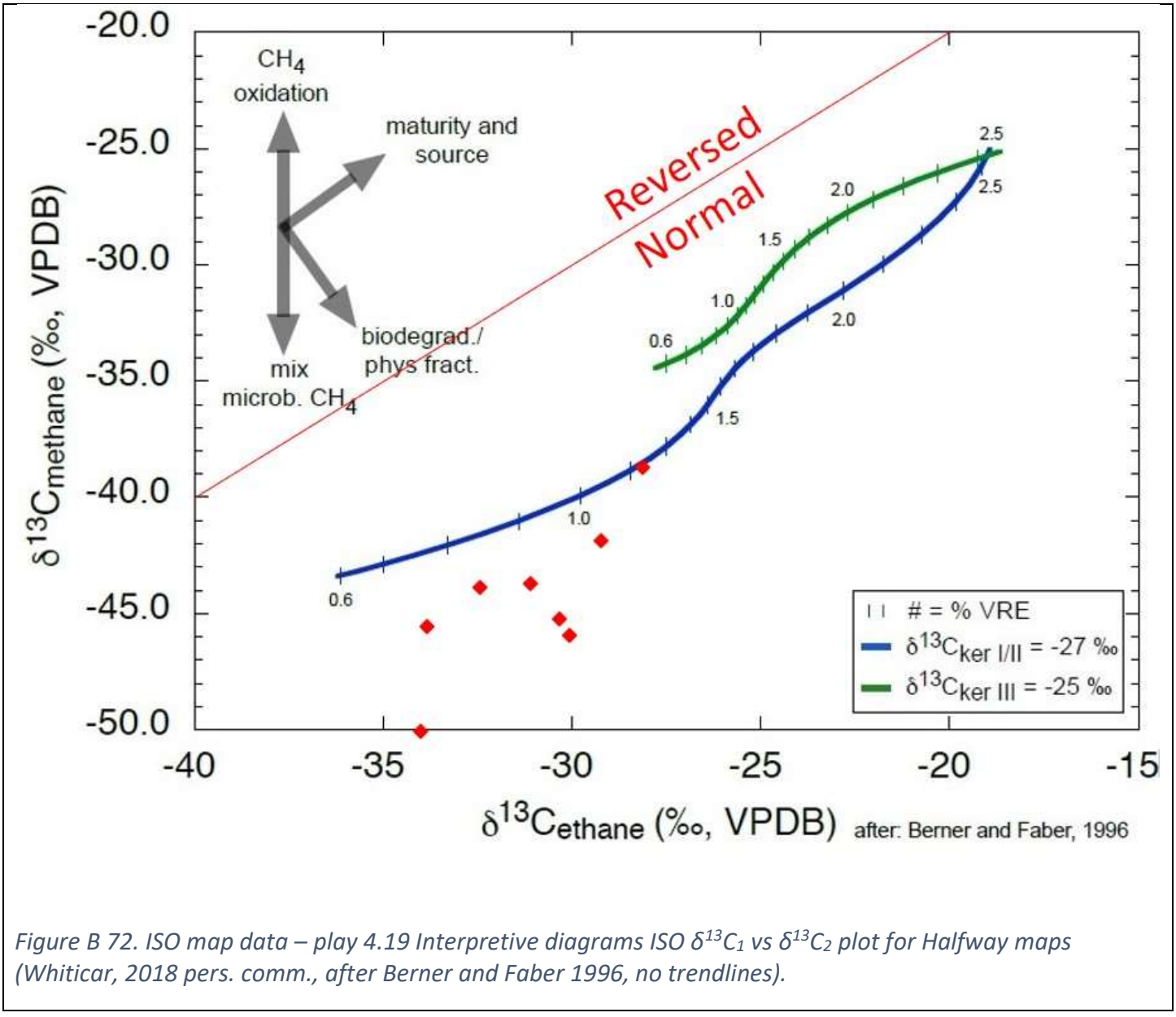

Figure B 72. ISO map data – play 4.19 Interpretive diagrams ISO $\delta^{13}C_1$ vs $\delta^{13}C_2$ plot for Halfway maps (Whiticar, 2018 pers. comm., after Berner and Faber 1996, no trendlines).

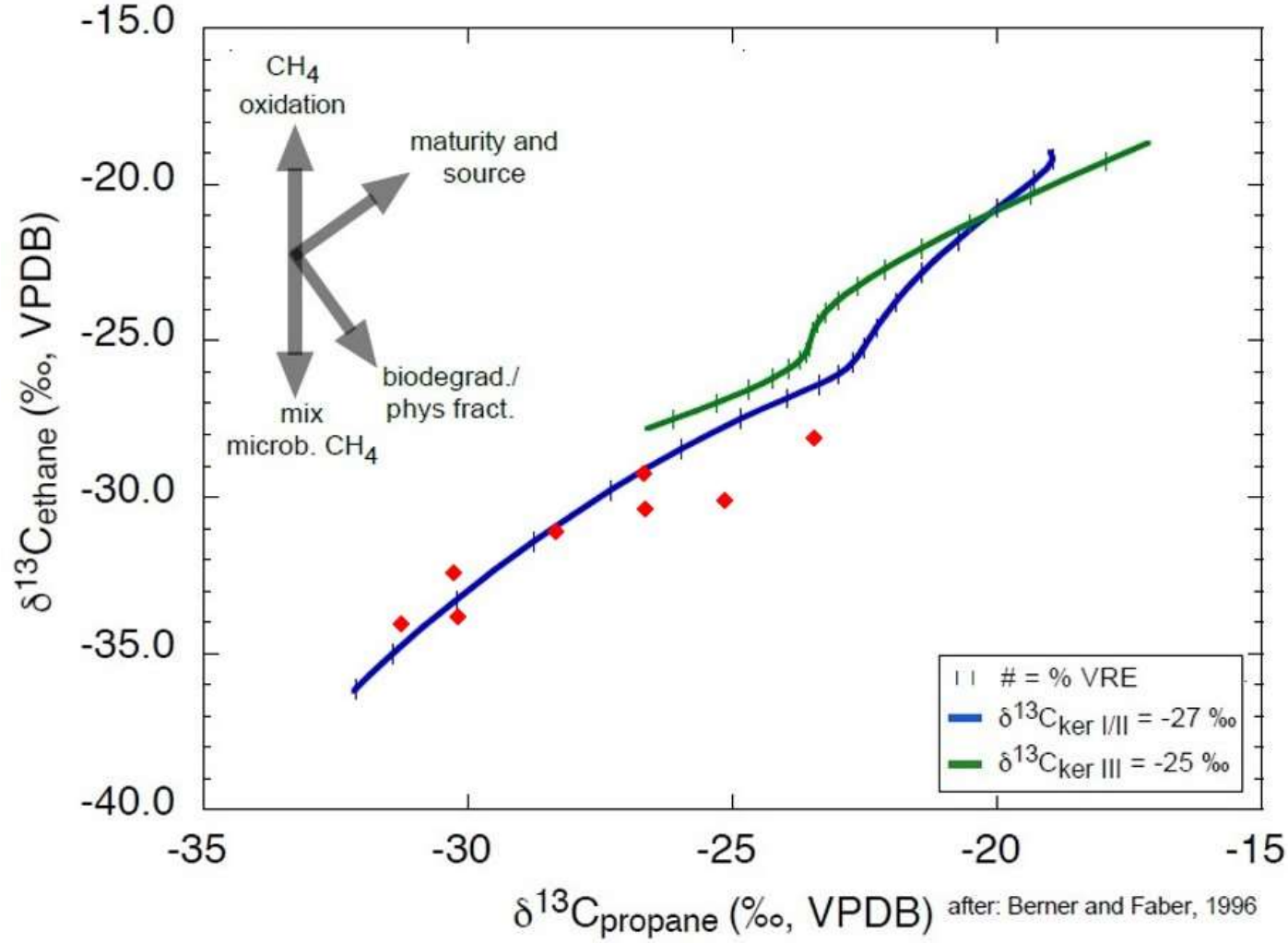

Figure B 73. ISO map data – play 4.19 Interpretive diagrams ISO $\delta^{13}C_2$ vs $\delta^{13}C_3$ plot for Halfway maps (Whiticar, 2018 pers. comm., after Berner and Faber 1996, no trendlines).

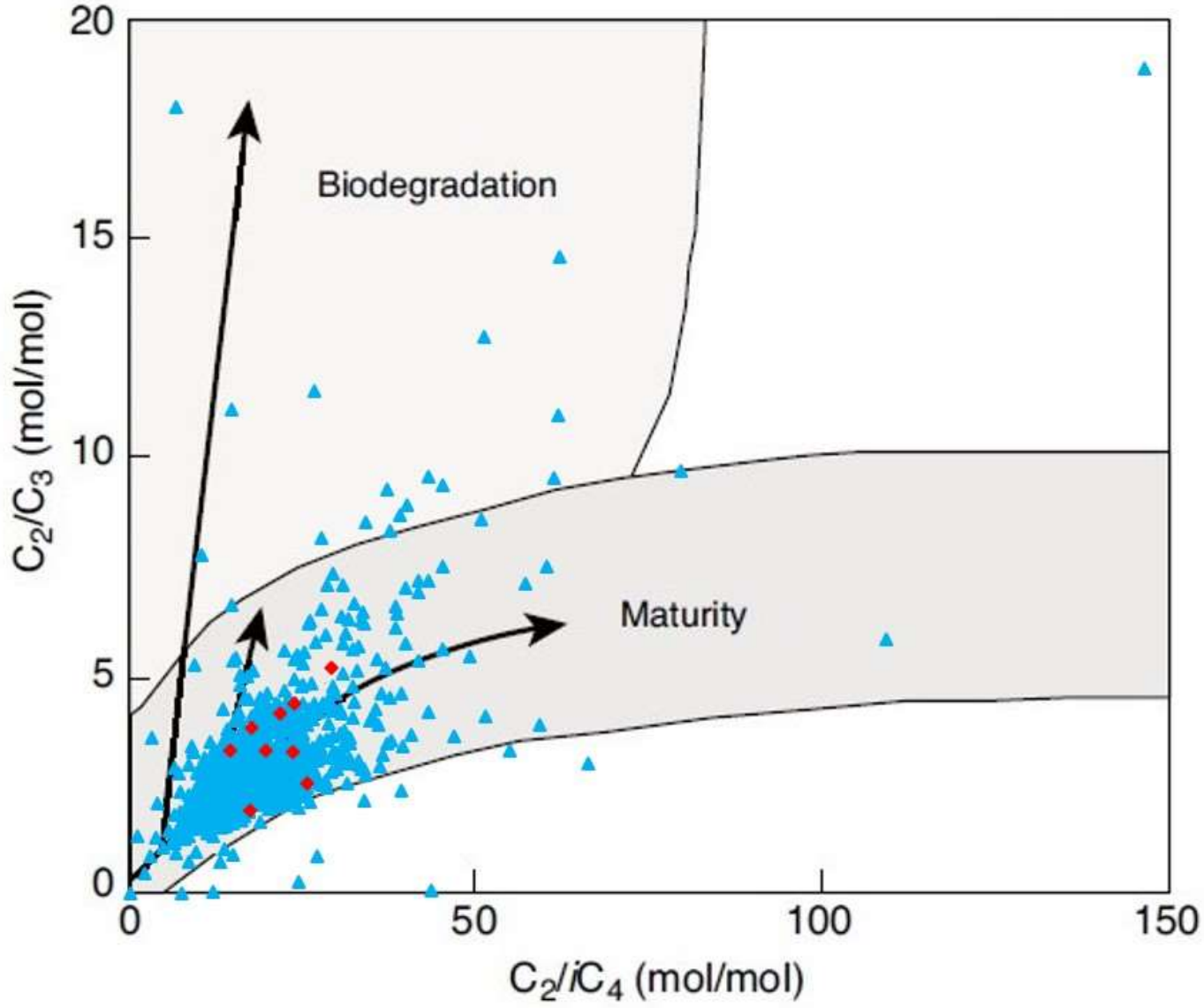

Figure B 74. ISO map data – play 4.19 Interpretive diagrams MC/ISO Prinzhofer Diagram for Halfway maps (after Prinzhofer and Battani 2003, no trendlines).

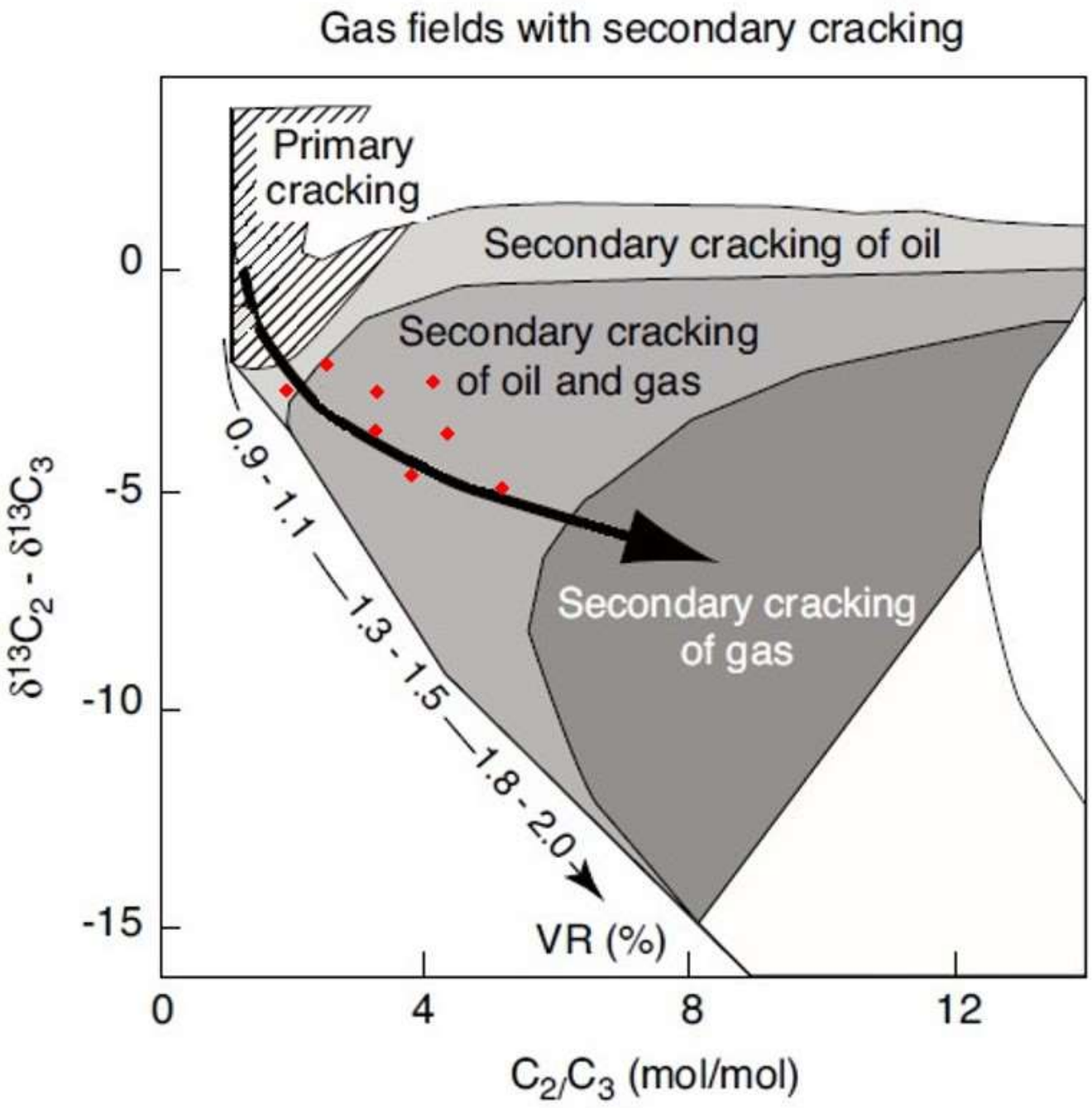

Figure B 75. ISO map data – play 4.19 Interpretive diagrams MC/ISO Lorant Diagram for Halfway maps (after Prinzhofer and Battani 2003, no trendlines).

12. Play 4.20 Doig and Lower Halfway (2 formations – both MC & ISO data)

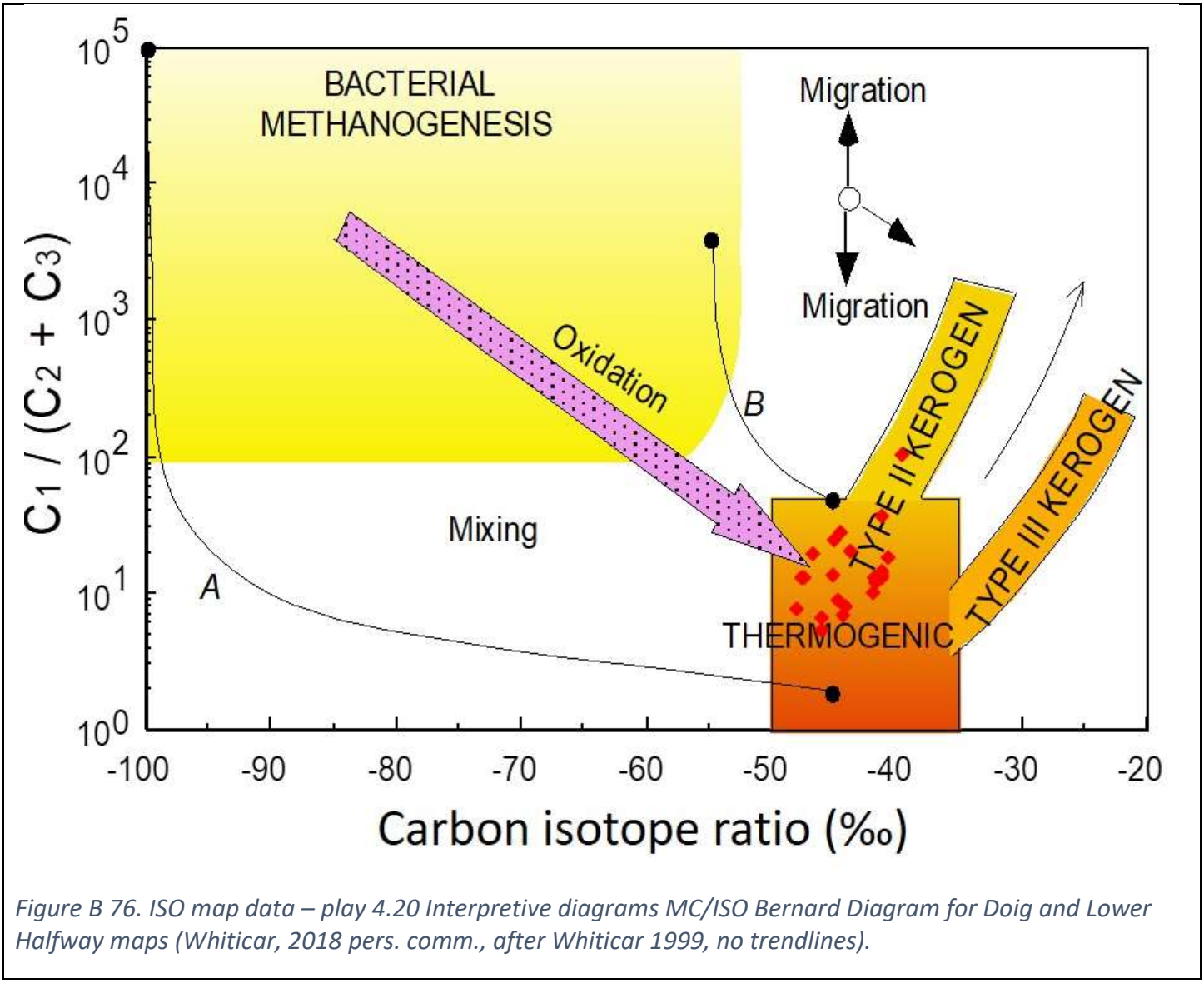

Figure B 76. ISO map data – play 4.20 Interpretive diagrams MC/ISO Bernard Diagram for Doig and Lower Halfway maps (Whiticar, 2018 pers. comm., after Whiticar 1999, no trendlines).

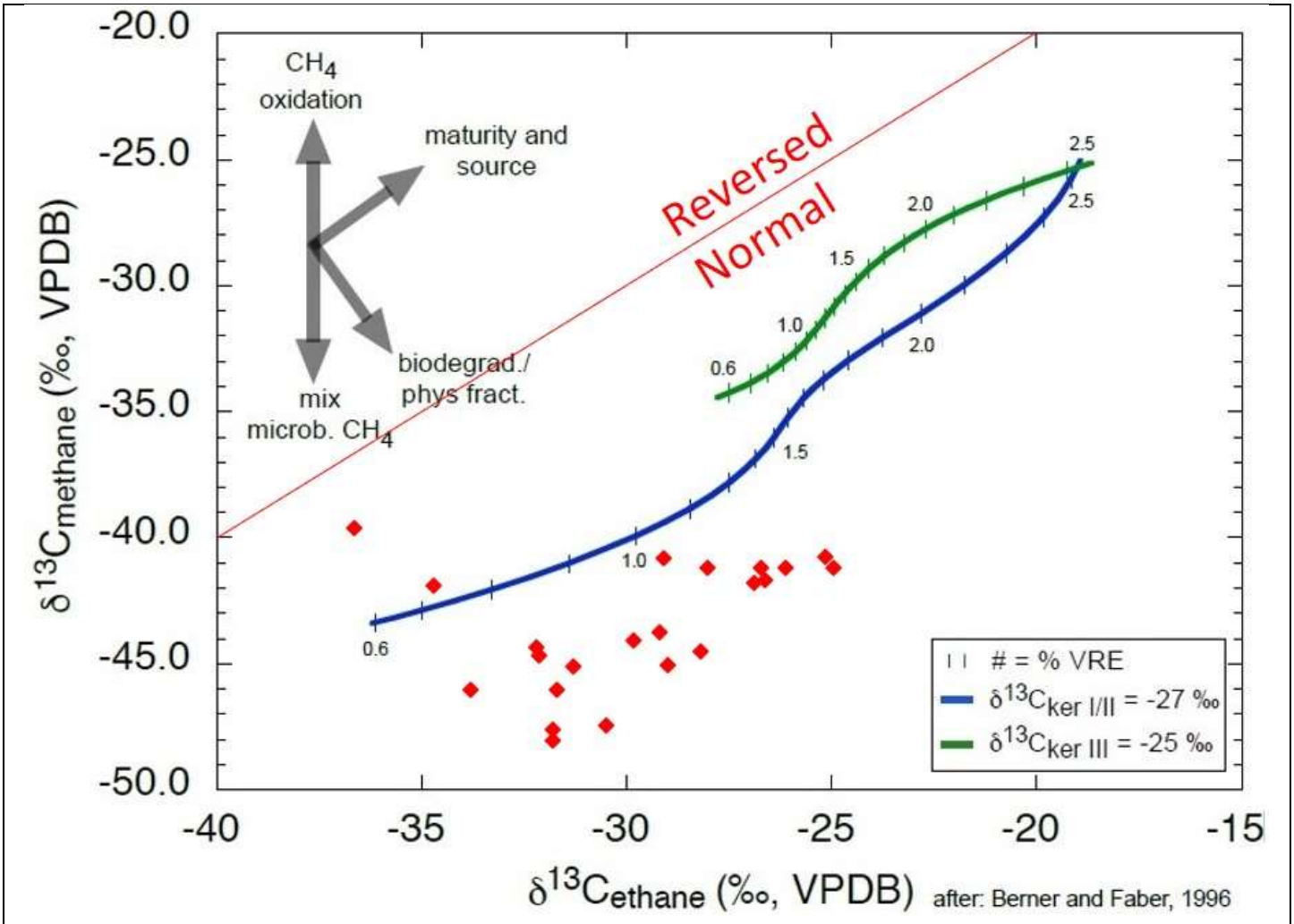

Figure B 77. ISO map data – play 4.20 Interpretive diagrams ISO $\delta^{13}C_1$ vs $\delta^{13}C_2$ plot for Doig and Lower Halfway maps (Whiticar, 2018 pers. comm., after Berner and Faber 1996, no trendlines).

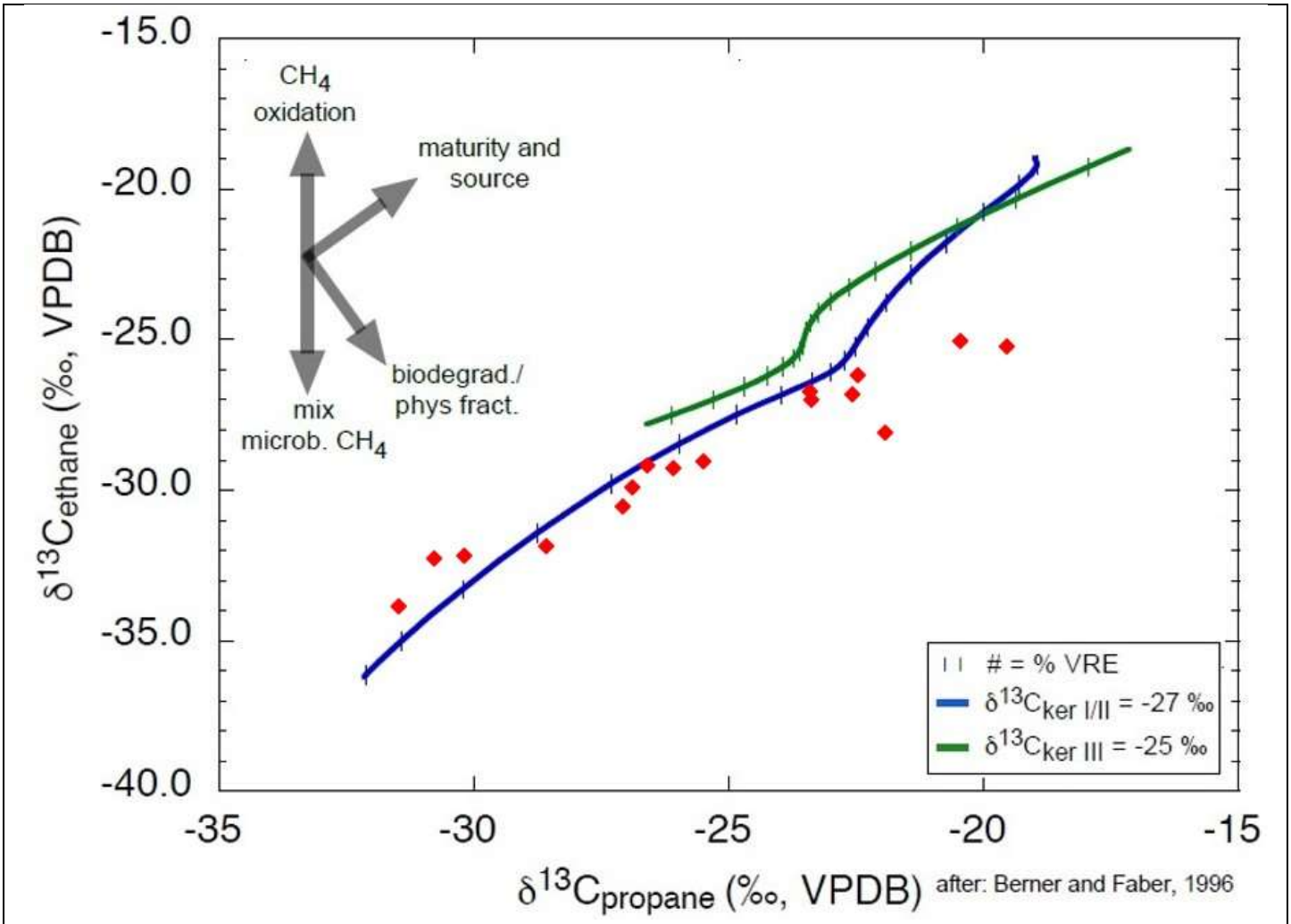

Figure B 78. ISO map data – play 4.20 Interpretive diagrams ISO $\delta^{13}C_2$ vs $\delta^{13}C_3$ plot for Doig and Lower Halfway maps (Whiticar, 2018 pers. comm., after Berner and Faber 1996, no trendlines).

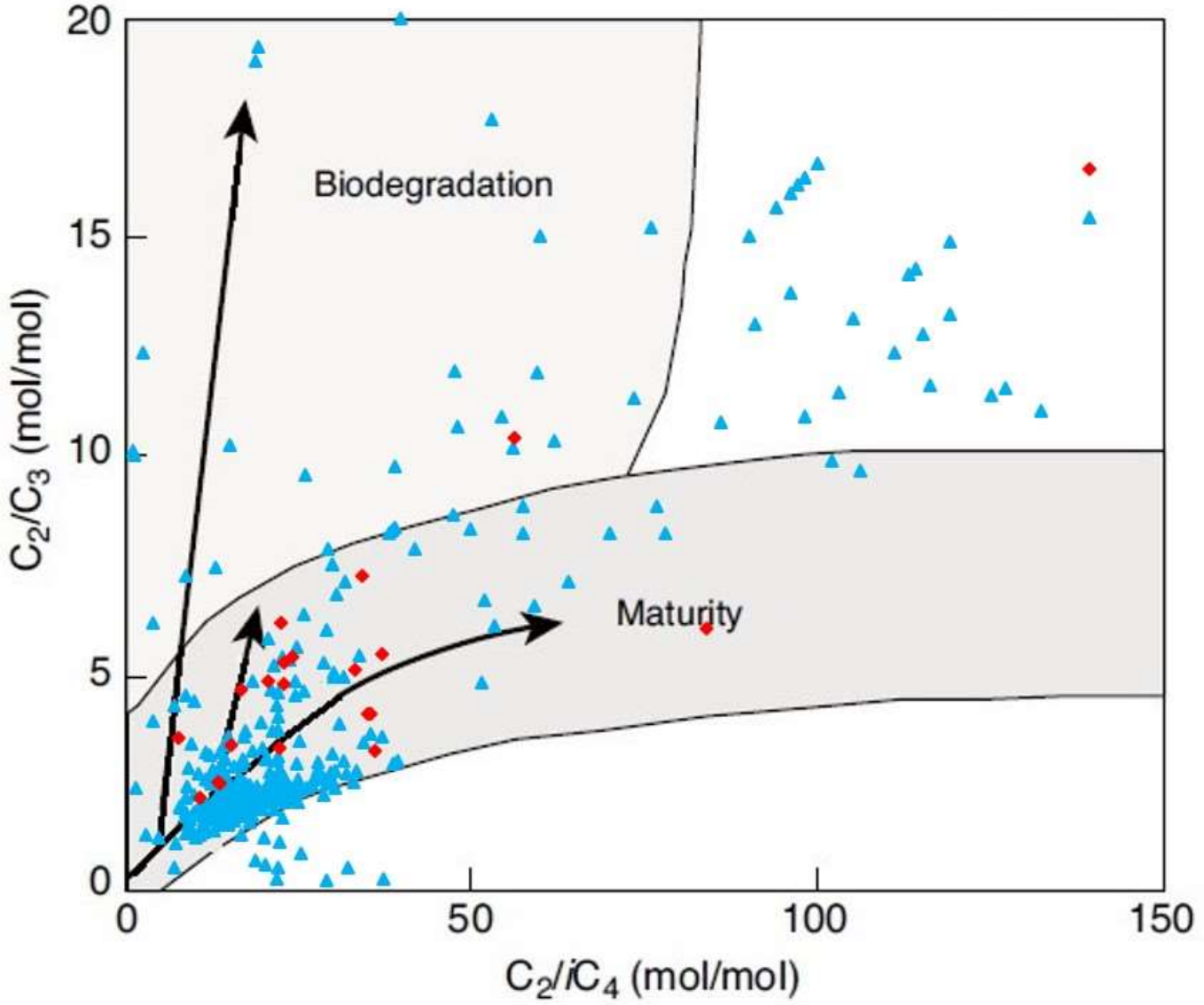

Figure B 79. ISO map data – play 4.20 Interpretive diagrams MC/ISO Prinzhofer Diagram for Doig and Lower Halfway maps (after Prinzhofer and Battani 2003, no trendlines).

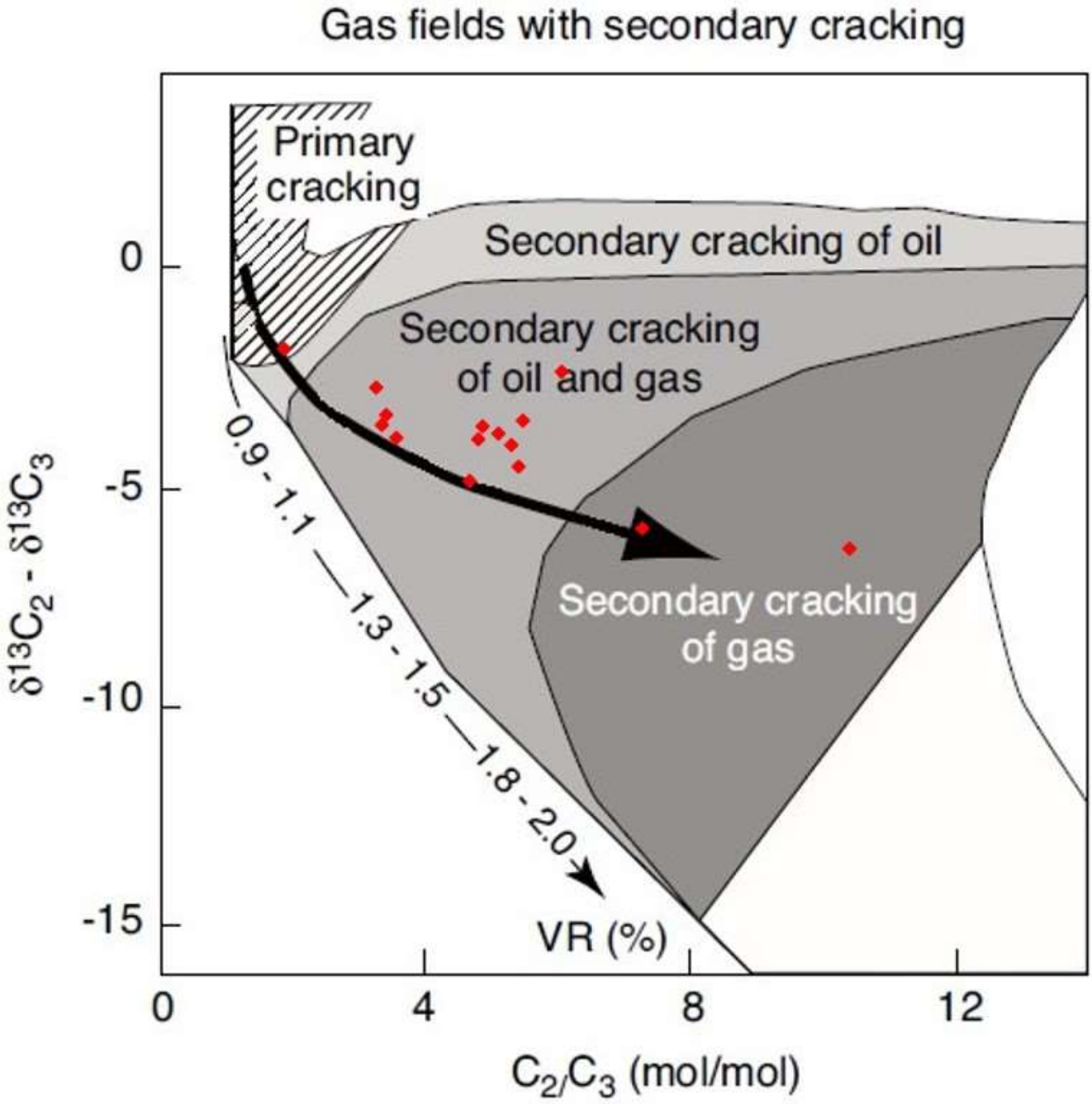

Figure B 80. ISO map data – play 4.20 Interpretive diagrams MC/ISO Lorant Diagram for Doig and Lower Halfway maps (after Prinzhofer and Battani 2003, no trendlines).

13. Play 4.21 Montney (single formation – both MC & ISO data)

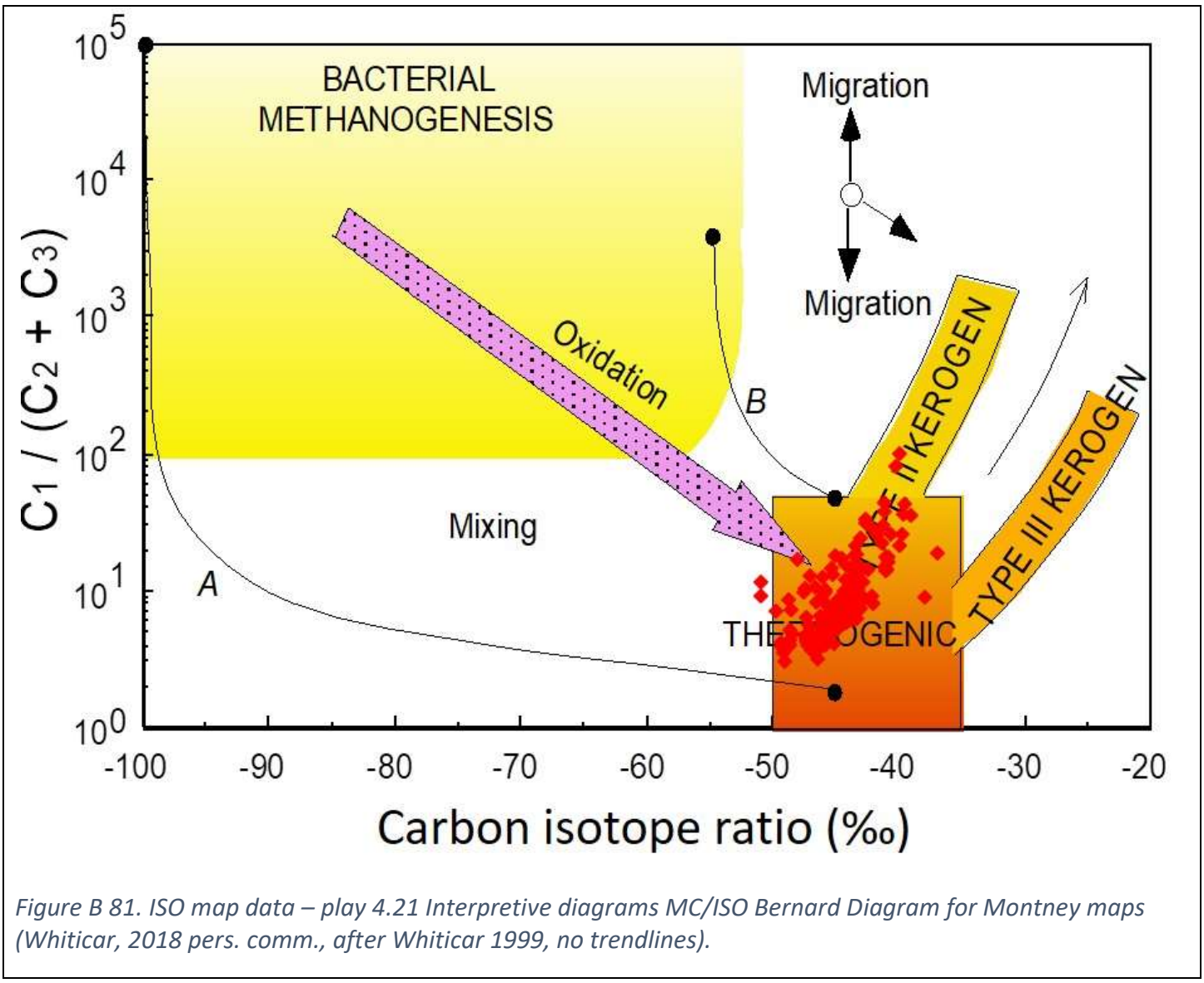

Figure B 81. ISO map data – play 4.21 Interpretive diagrams MC/ISO Bernard Diagram for Montney maps (Whiticar, 2018 pers. comm., after Whiticar 1999, no trendlines).

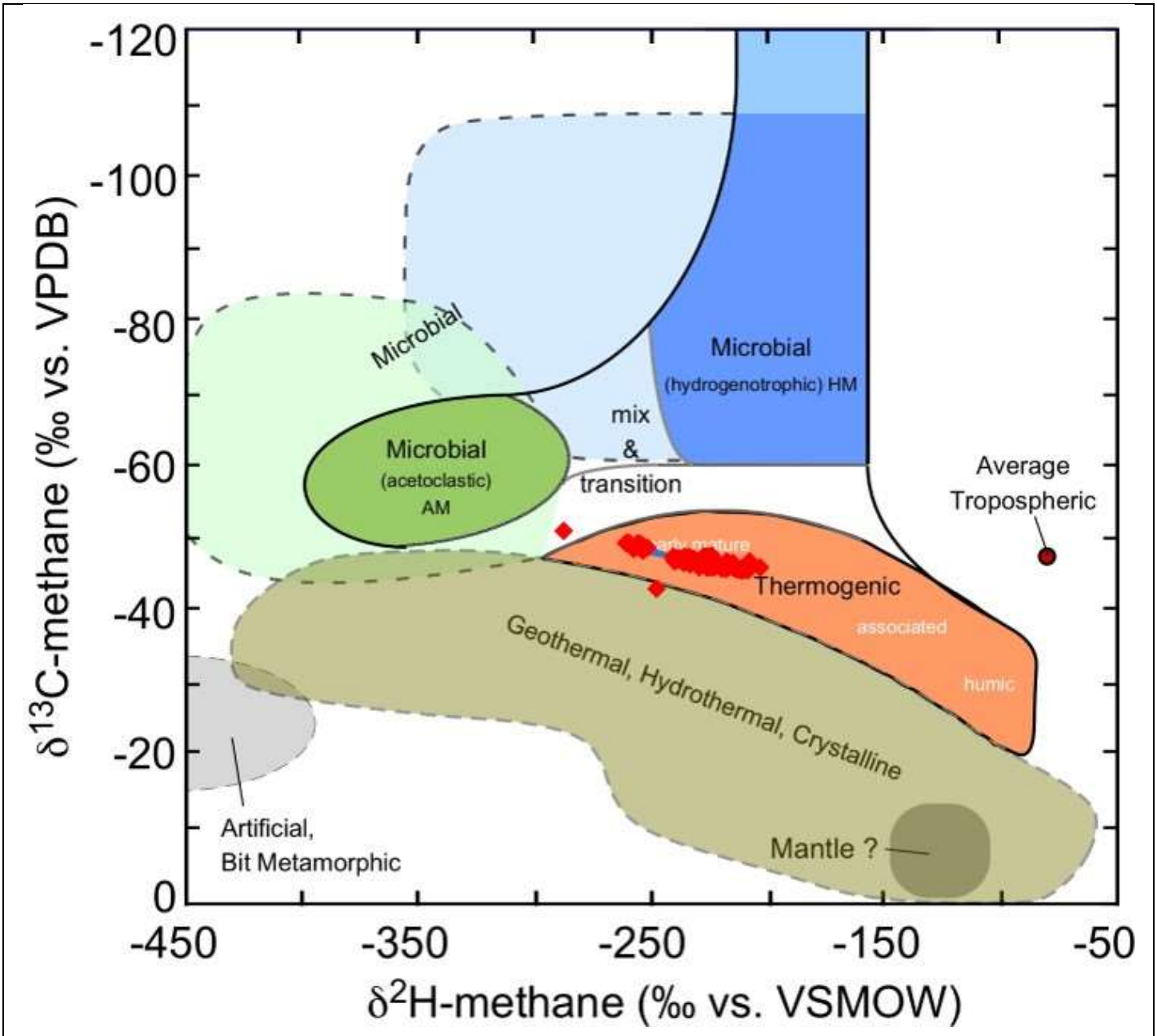

Figure B 82. ISO map data – play 4.21 Interpretive diagrams MC/ISO CD Diagram for Montney maps (Whiticar, 2018 pers. comm., after Whiticar 1999, no trendlines).

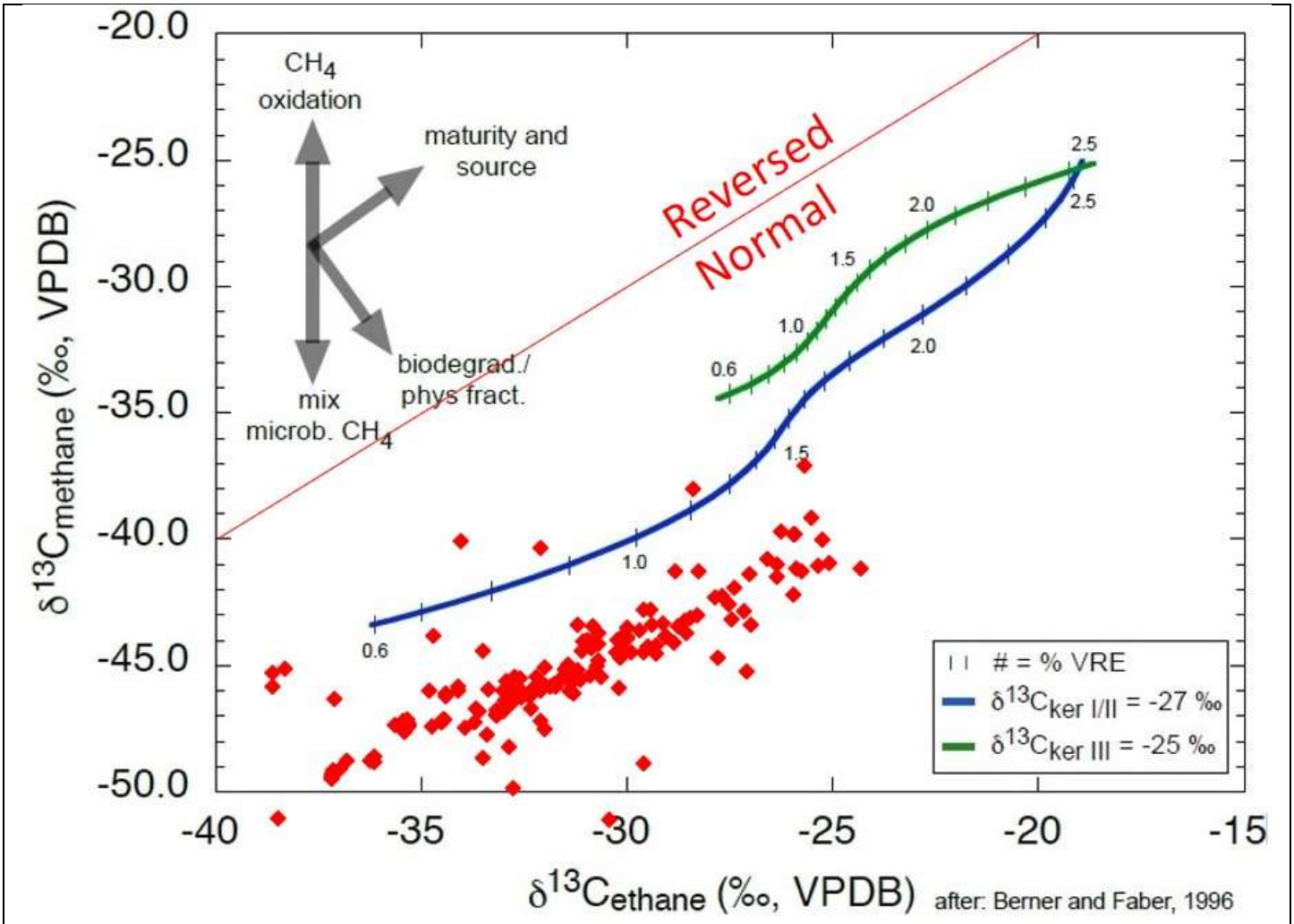

Figure B 83. ISO map data – play 4.21 Interpretive diagrams ISO $\delta^{13}C_1$ vs $\delta^{13}C_2$ plot for Montney maps (Whiticar, 2018 pers. comm., after Berner and Faber 1996, no trendlines).

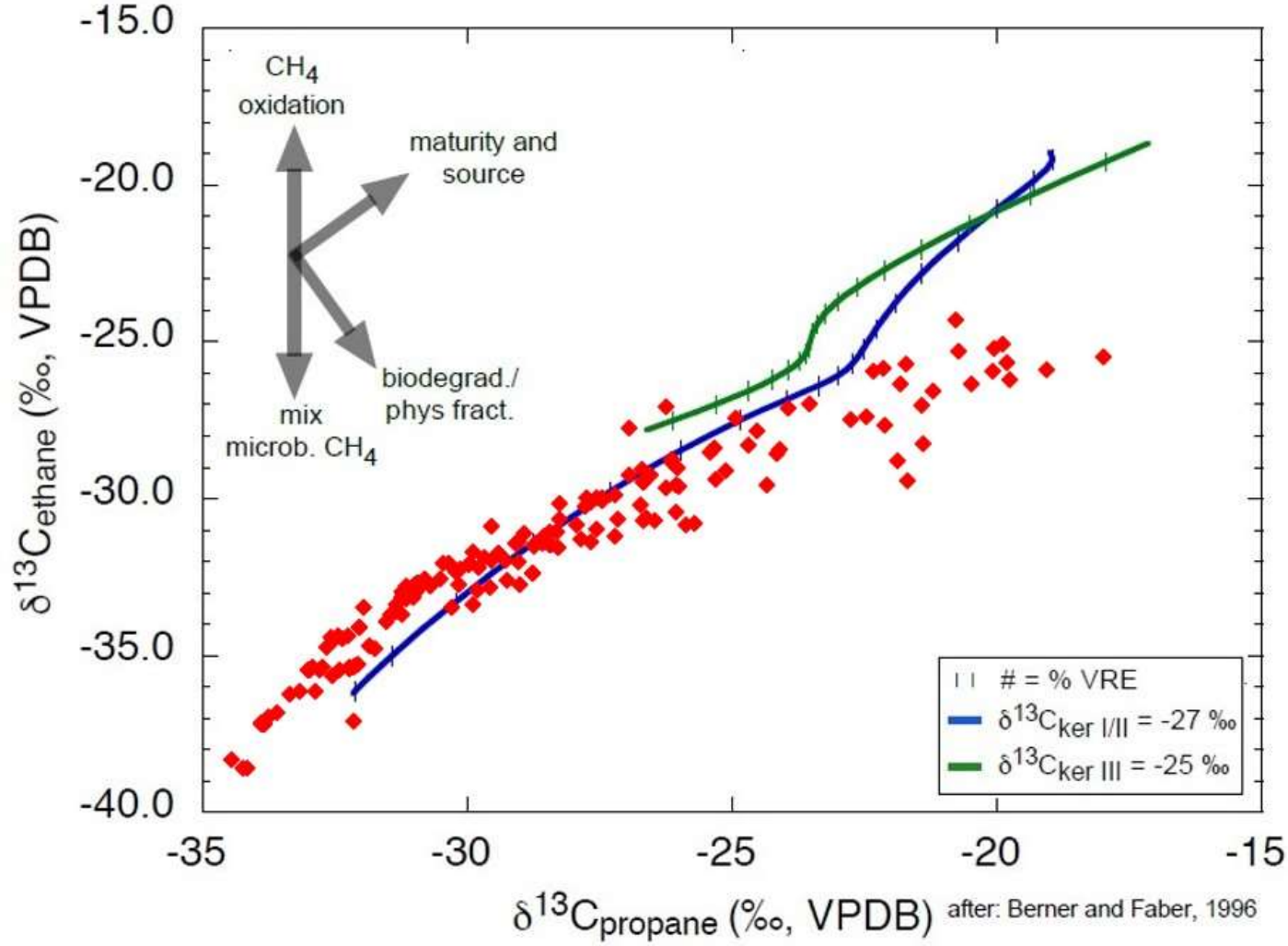

Figure B 84. ISO map data – play 4.21 Interpretive diagrams ISO $\delta^{13}C_2$ vs $\delta^{13}C_3$ plot for Montney maps (Whiticar, 2018 pers. comm., after Berner and Faber 1996, no trendlines).

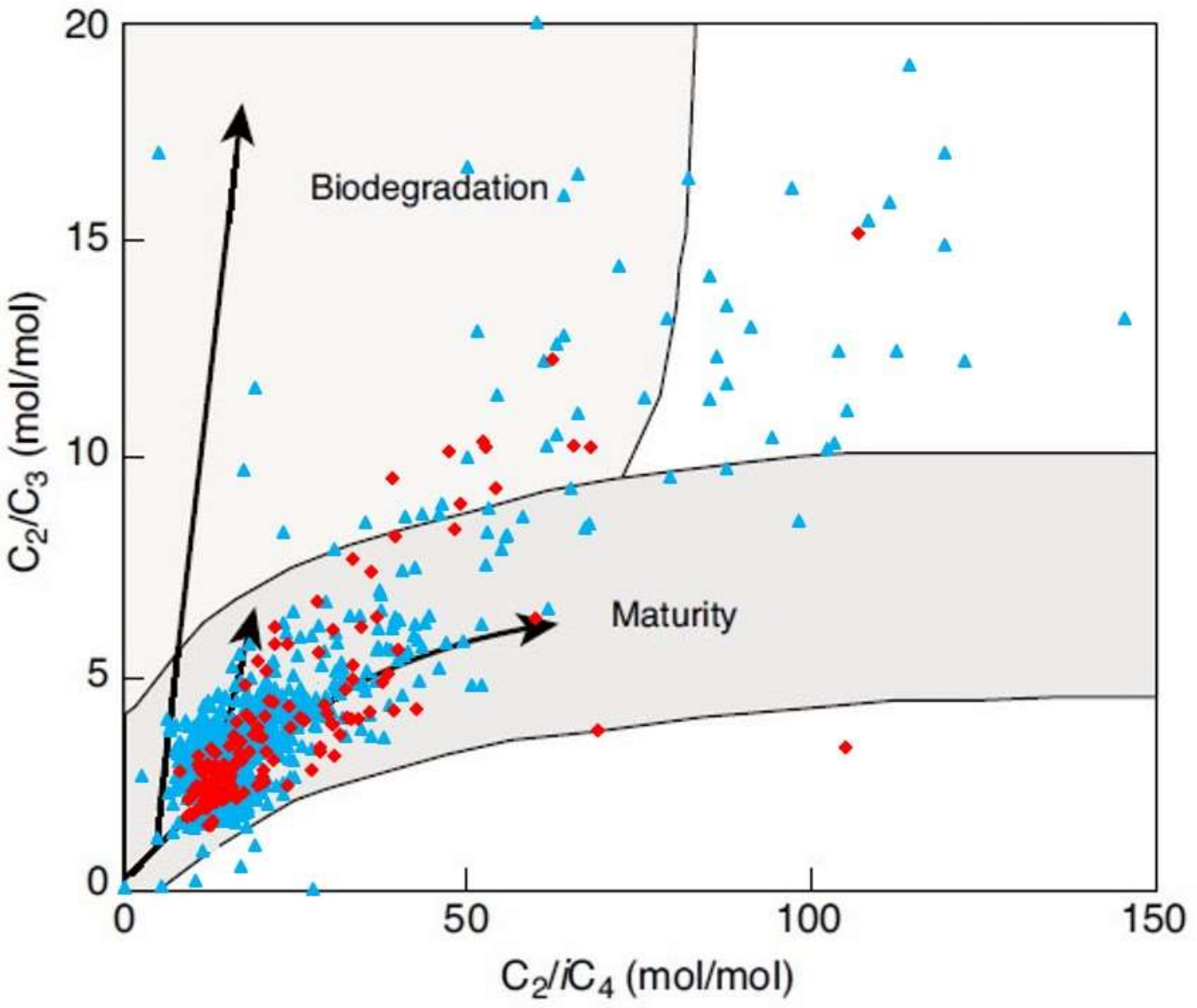

Figure B 85. ISO map data – play 4.21 Interpretive diagrams MC/ISO Prinzhofer Diagram for Montney maps (after Prinzhofer and Battani 2003, no trendlines).

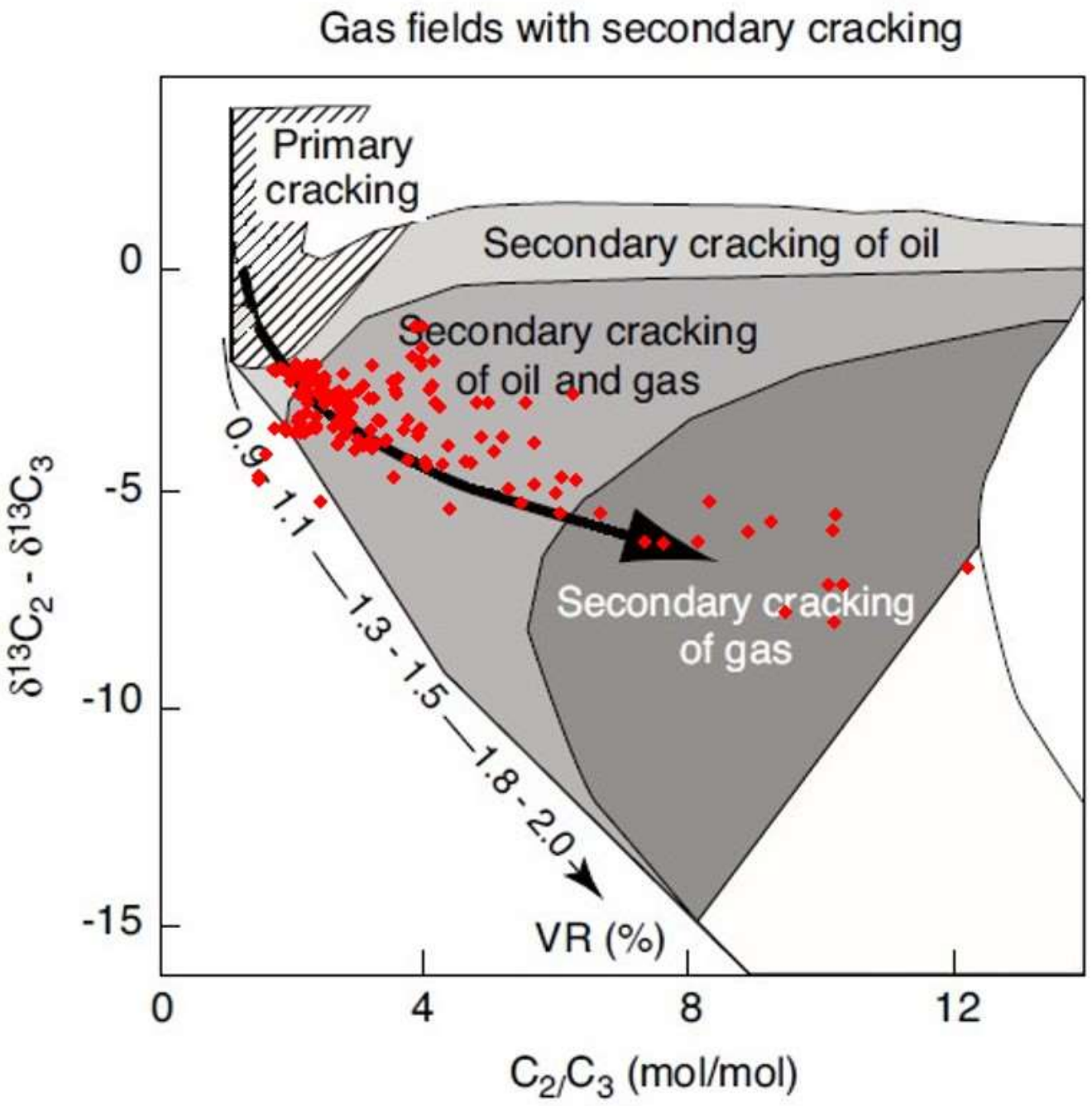

Figure B 86. ISO map data – play 4.21 Interpretive diagrams MC/ISO Lorant Diagram for Montney maps (after Prinzhofer and Battani 2003, no trendlines).

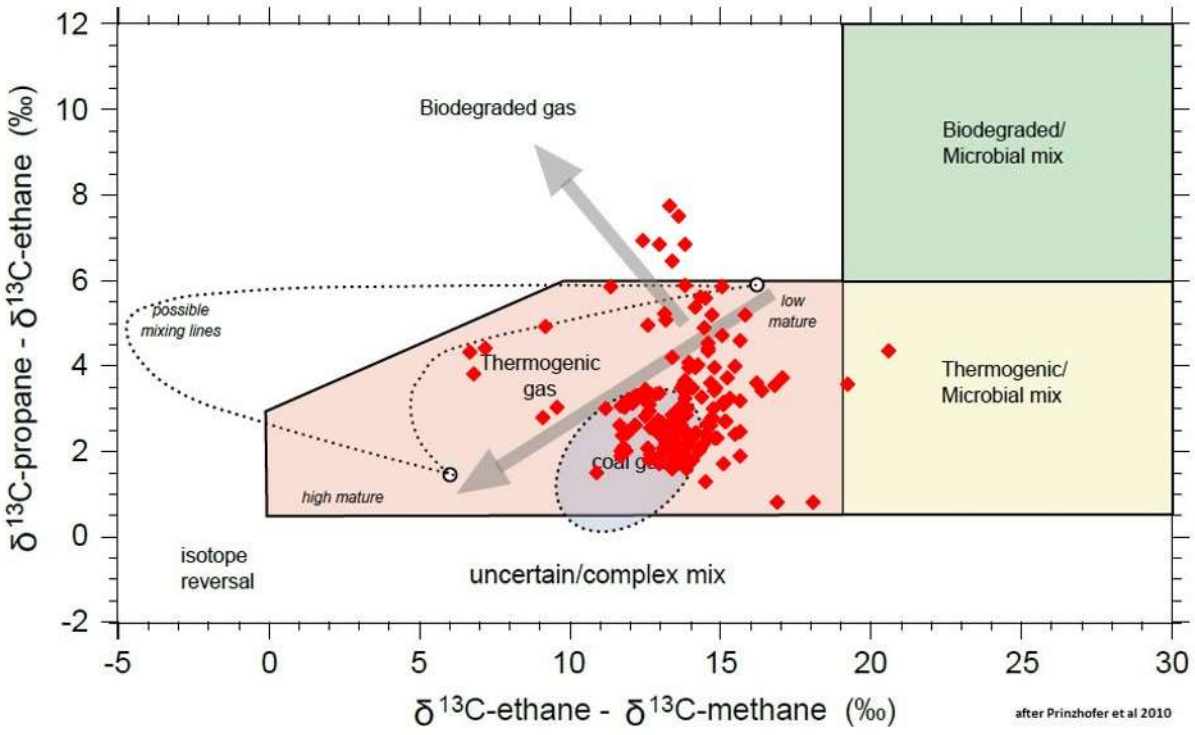

Figure B 87. ISO map data – play 4.21 Interpretive $\delta^{13}C_2$- $\delta^{13}C_1$ versus $\delta^{13}C_3$- $\delta^{13}C_2$ plot for Montney maps (no trendlines).

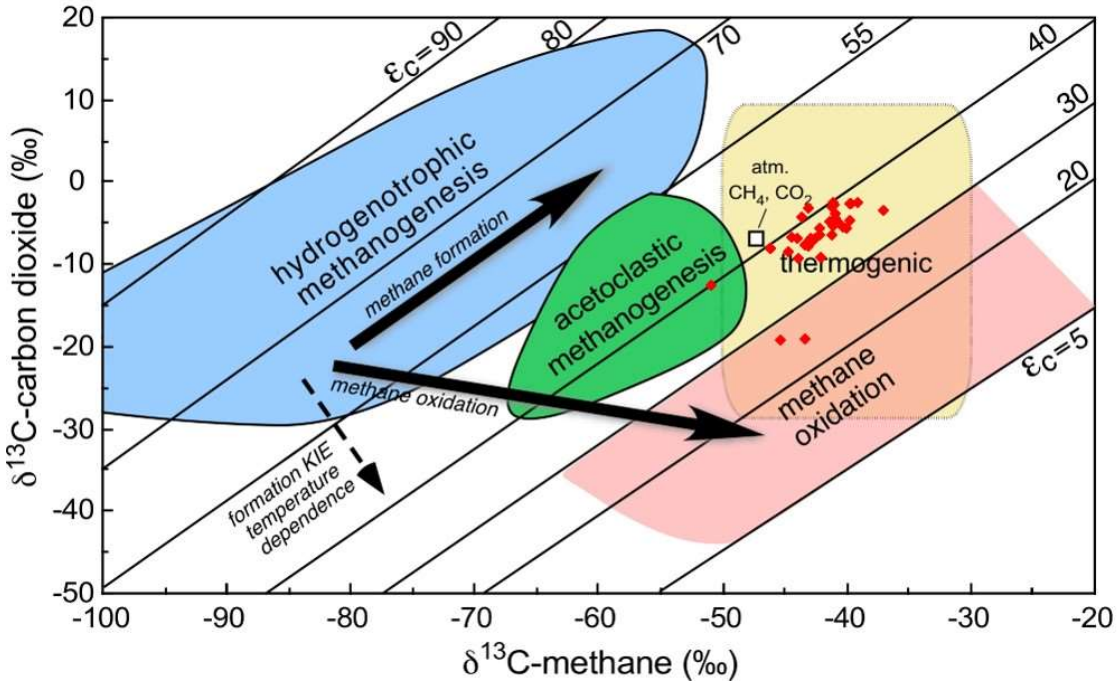

Figure B 88. ISO map data – play 4.21 Interpretive diagrams ISO $\delta^{13}CO_2$ plot for Montney maps (no trendlines).

14. Plays 4.22/23 Debolt, Belloy, Kiskatinaw, Shunda, Mattson, Taylor Flat, Belcourt (multiple formations – only MC data for many)

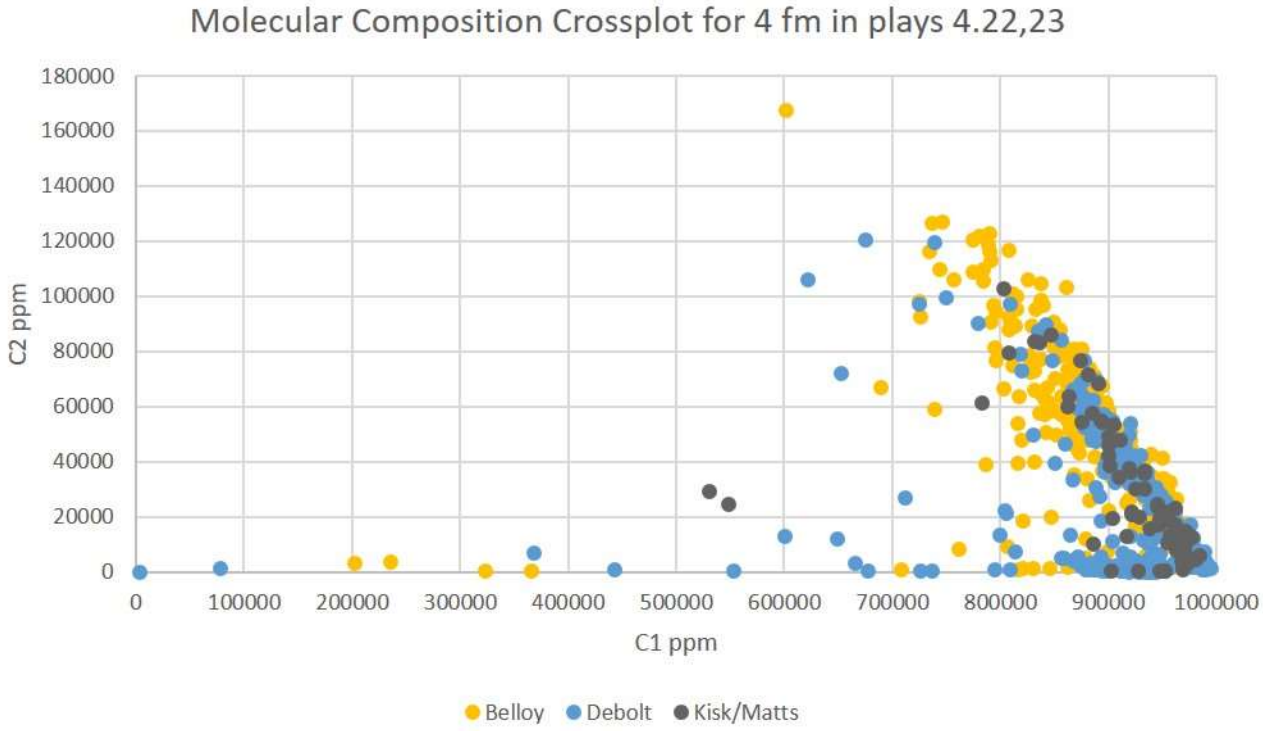

Figure B 89. MC map data – play 4.22/23 MC (ppm) ethane methane plot for Debolt, Belloy, etc. formations [not to template].

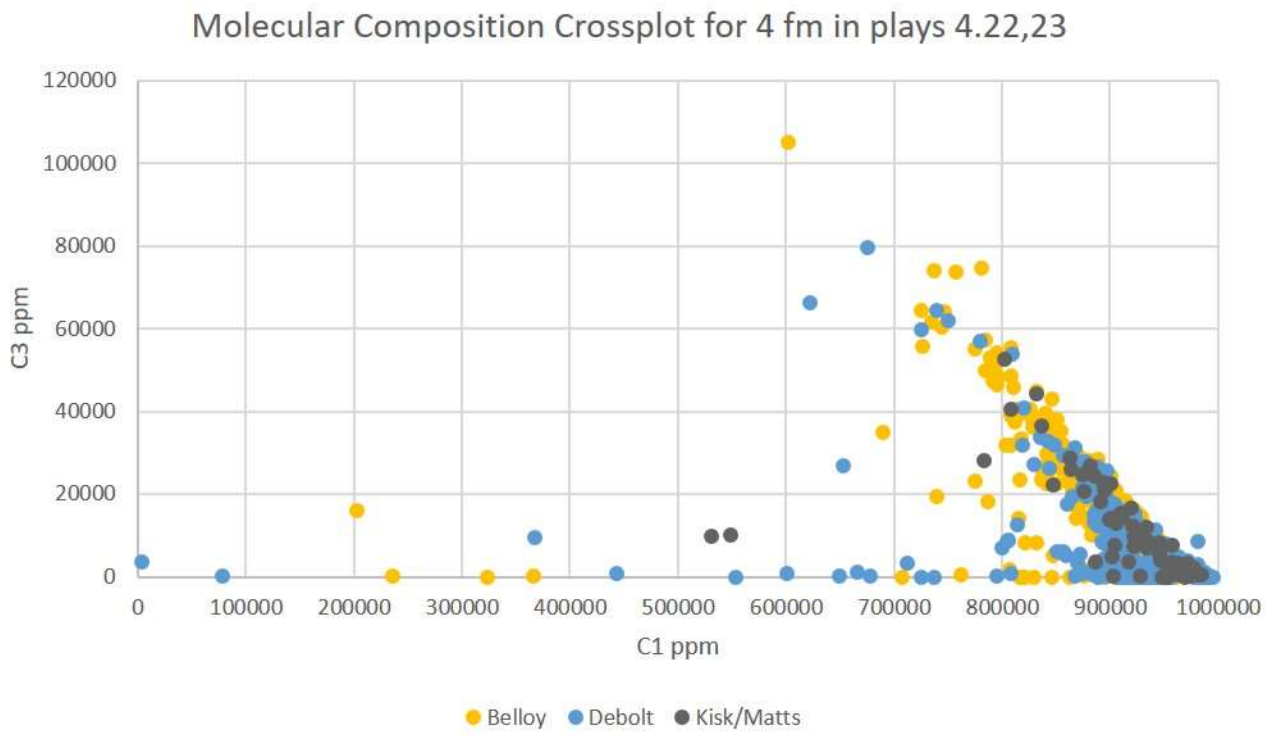

Figure B 90. MC map data – play 4.22/23 MC (ppm) propane methane plot for Debolt, Belloy, etc. formations [not to template].

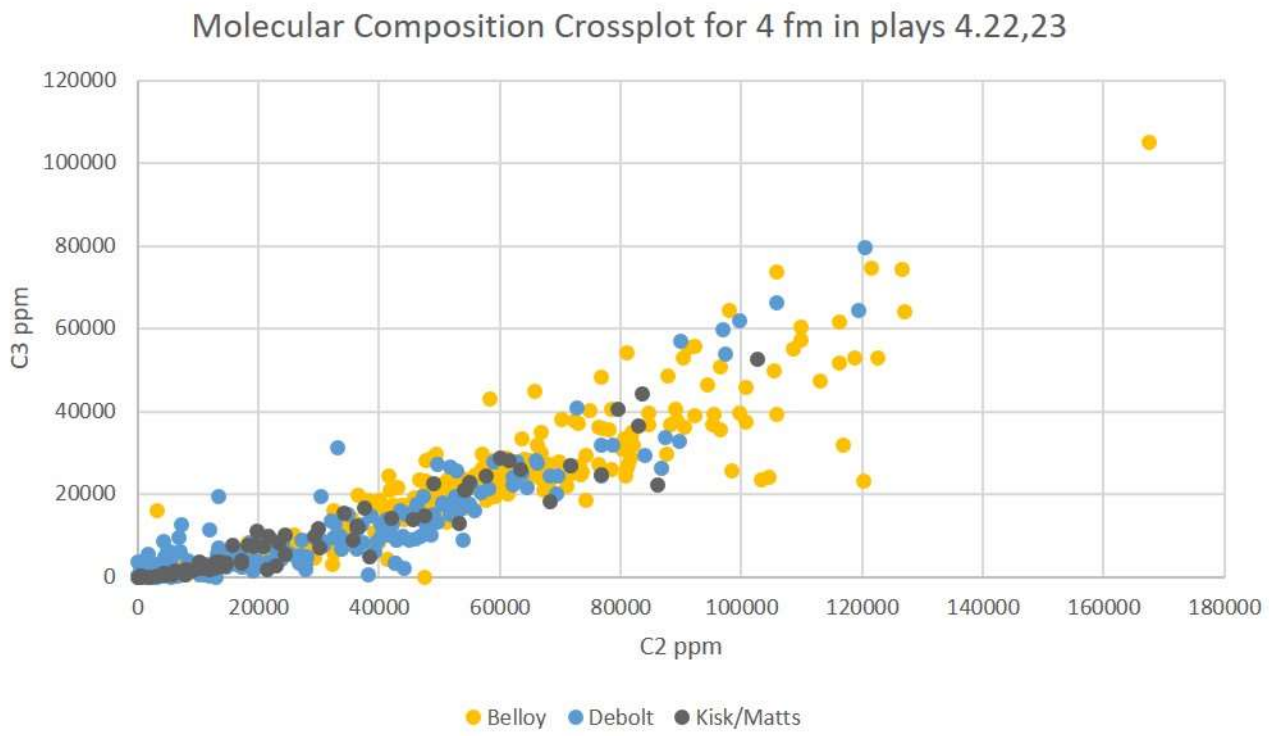

Figure B 91. MC map data – play 4.22/23 MC (ppm) propane ethane plot for Debolt, Belloy, etc. formations [not to template].

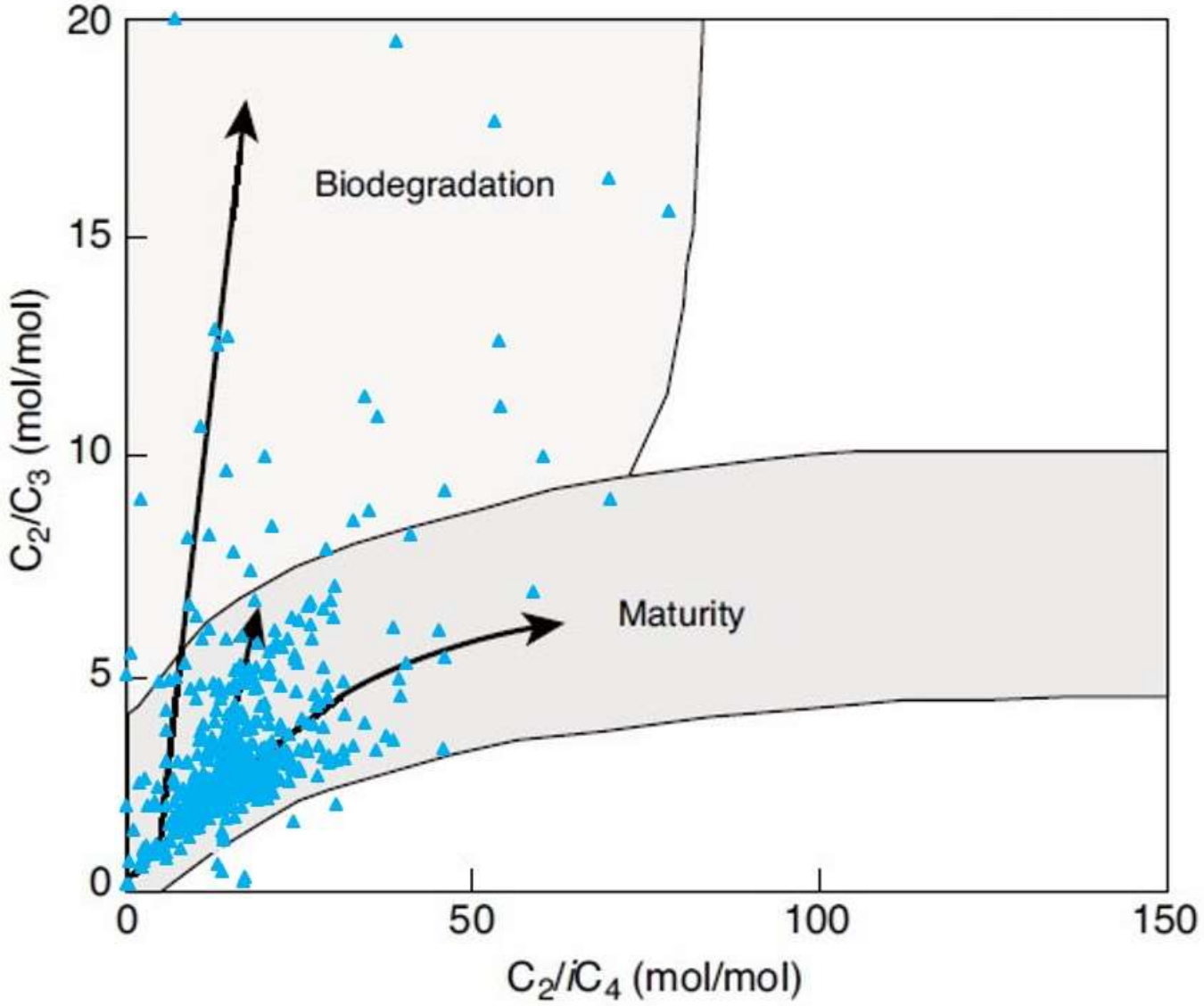

Figure B 92. ISO map data – play 4.22/23 Interpretive diagrams MC/ISO Prinzhofer Diagram for Debolt, Belloy, etc. maps (after Prinzhofer and Battani 2003, no trendlines).

14a. Play 4.24 Debolt (subset of section 14) ISO only data

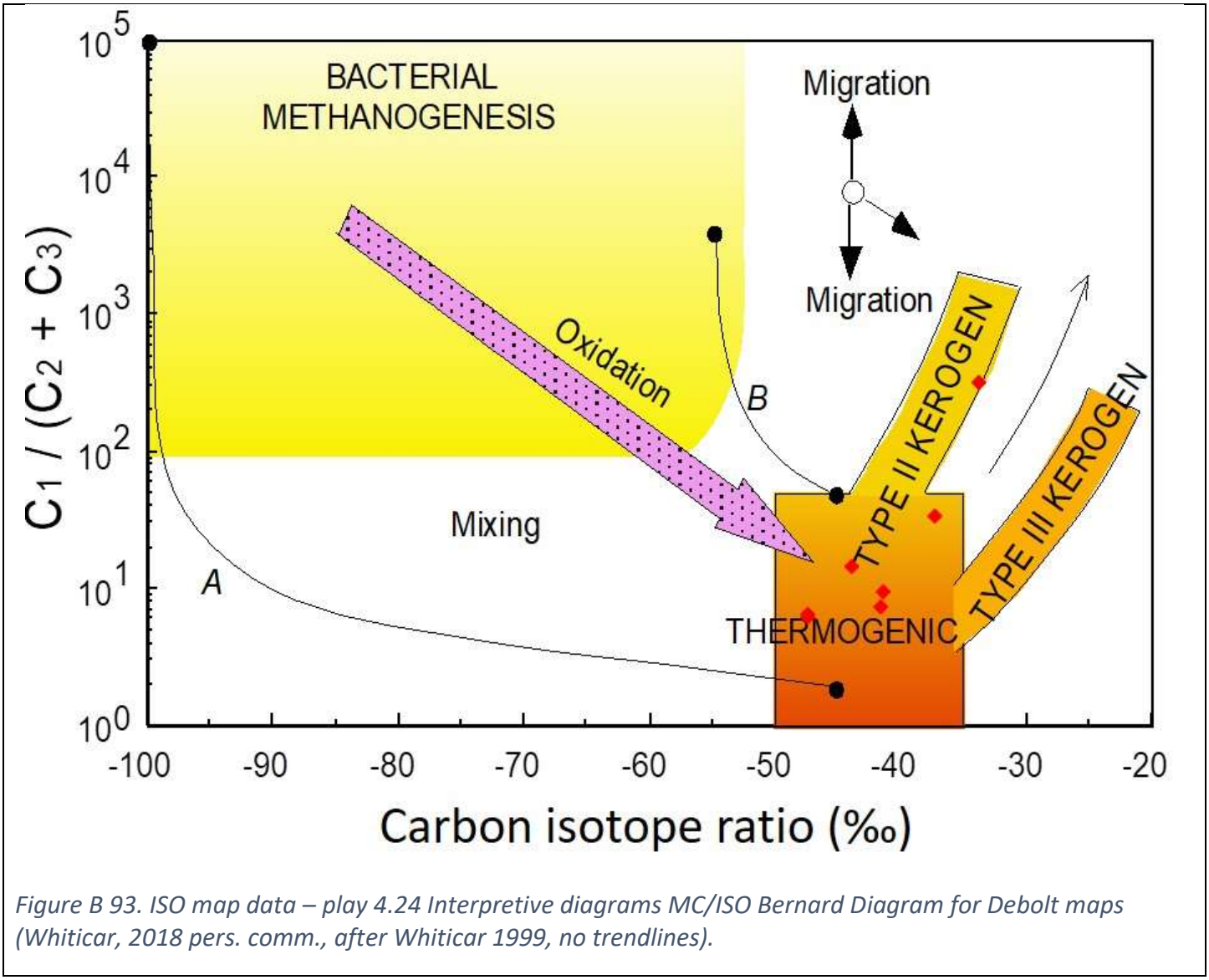

Figure B 93. ISO map data – play 4.24 Interpretive diagrams MC/ISO Bernard Diagram for Debolt maps (Whiticar, 2018 pers. comm., after Whiticar 1999, no trendlines).

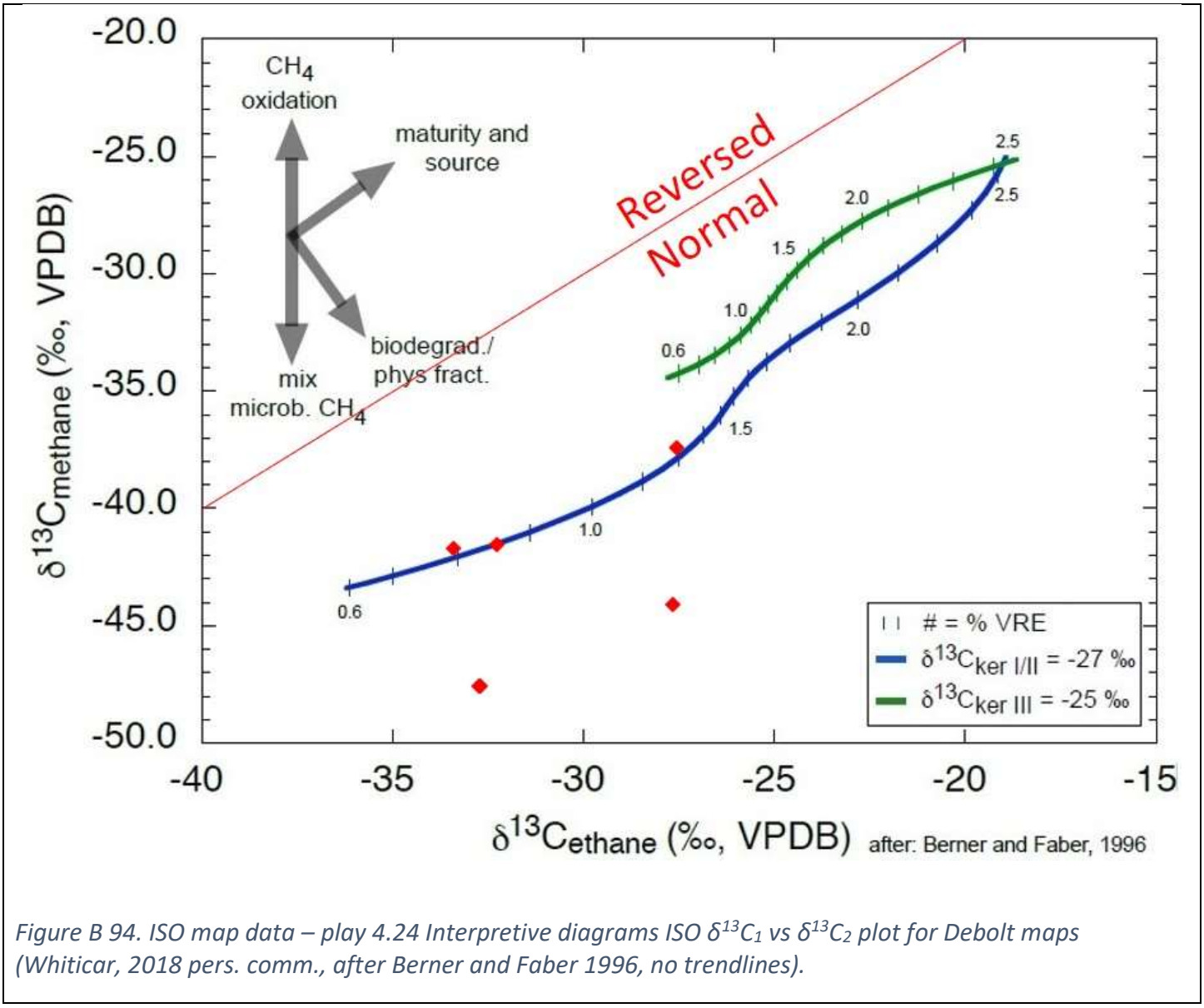

Figure B 94. ISO map data – play 4.24 Interpretive diagrams ISO $\delta^{13}C_1$ vs $\delta^{13}C_2$ plot for Debolt maps (Whiticar, 2018 pers. comm., after Berner and Faber 1996, no trendlines).

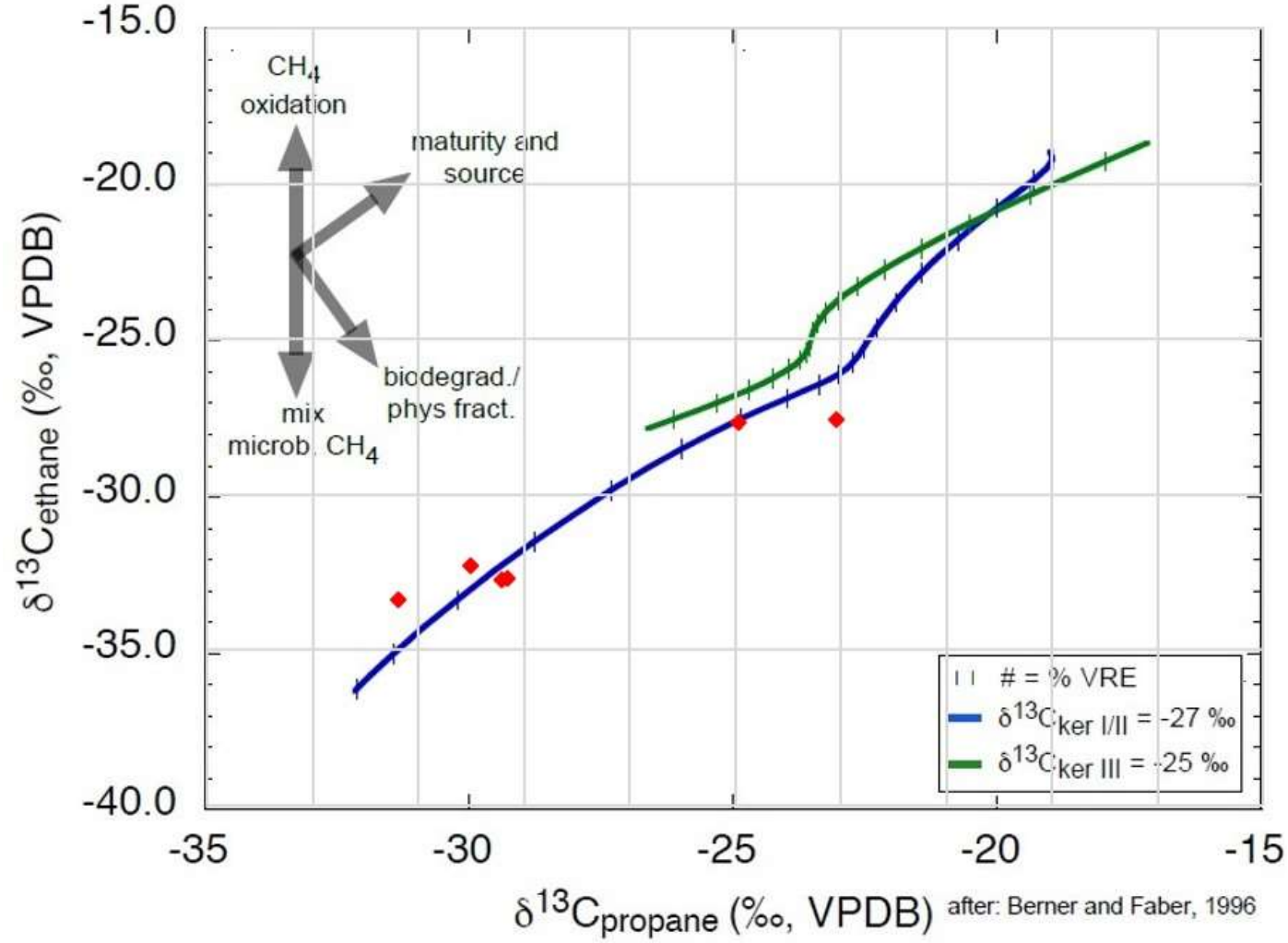

Figure B 95. ISO map data – play 4.24 Interpretive diagrams ISO $\delta^{13}C_2$ vs $\delta^{13}C_3$ plot for Debolt maps (Whiticar, 2018 pers. comm., after Berner and Faber 1996, no trendlines).

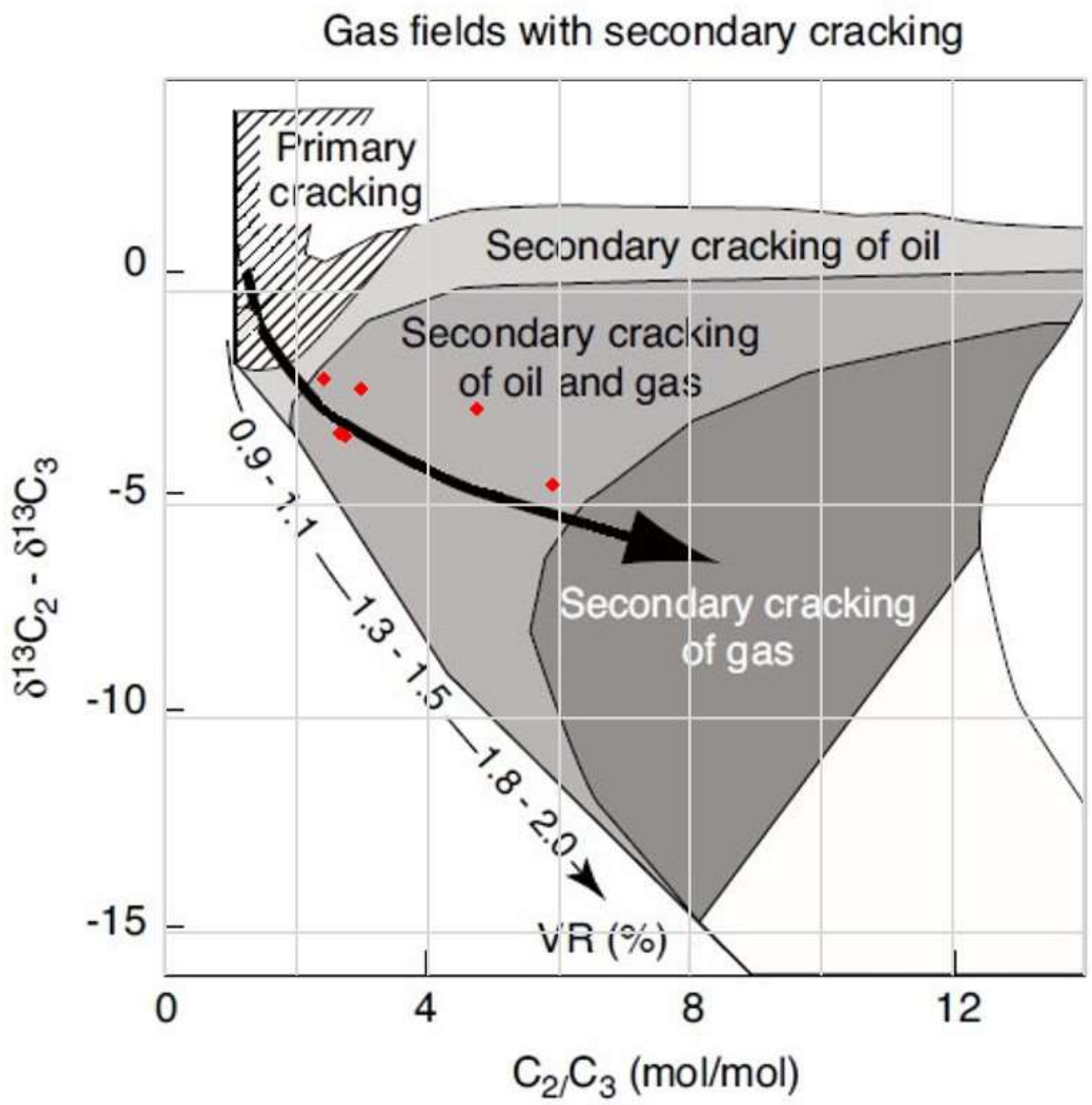

Figure B 96. ISO map data – play 4.24 Interpretive diagrams MC/ISO Prinzhofer Diagram for Debolt maps (after Prinzhofer and Battani 2003, no trendlines).

15. Play 4.25 Banff, Exshaw (2 formations – only MC data)

(There are 2 uncertain ISO data points not used)

Figure B 97. MC map data – play 4.25 MC (ppm) ethane methane plot for Banff, Exshaw formations [not to template].

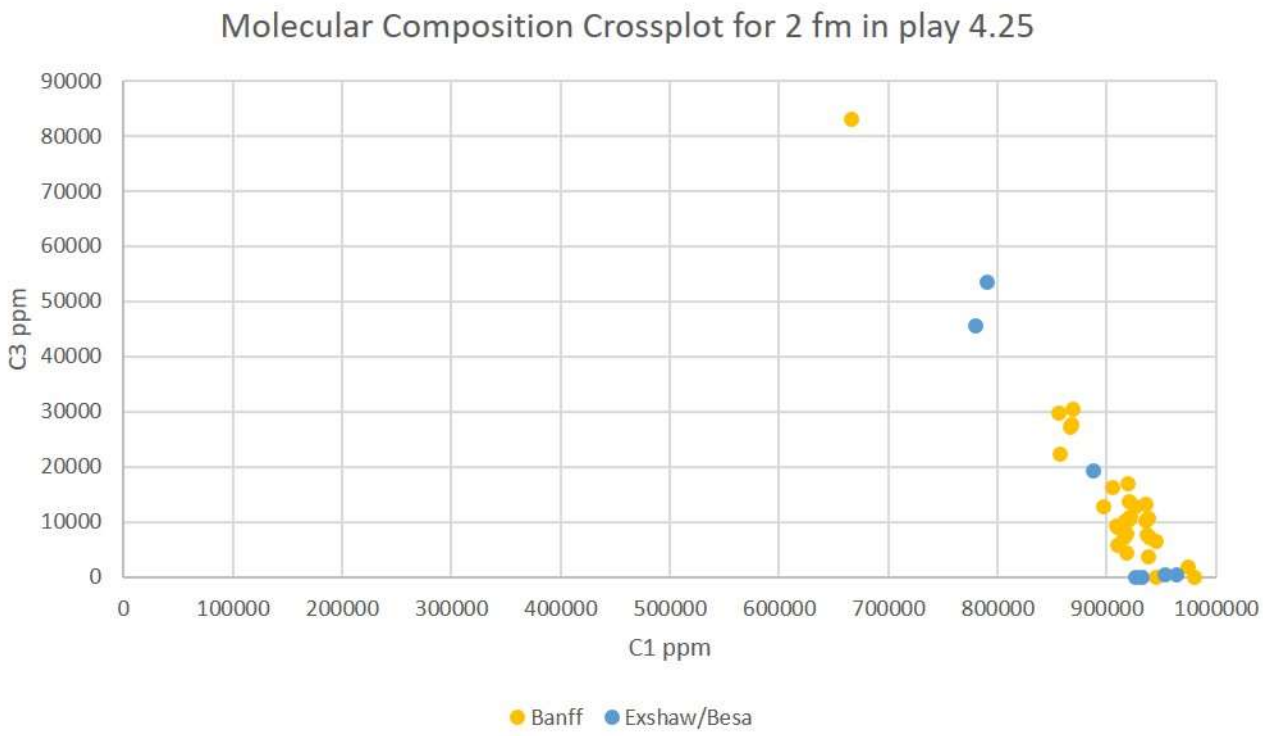

Figure B 98. MC map data – play 4.25 MC (ppm) propane methane plot for Banff, Exshaw formations [not to template].

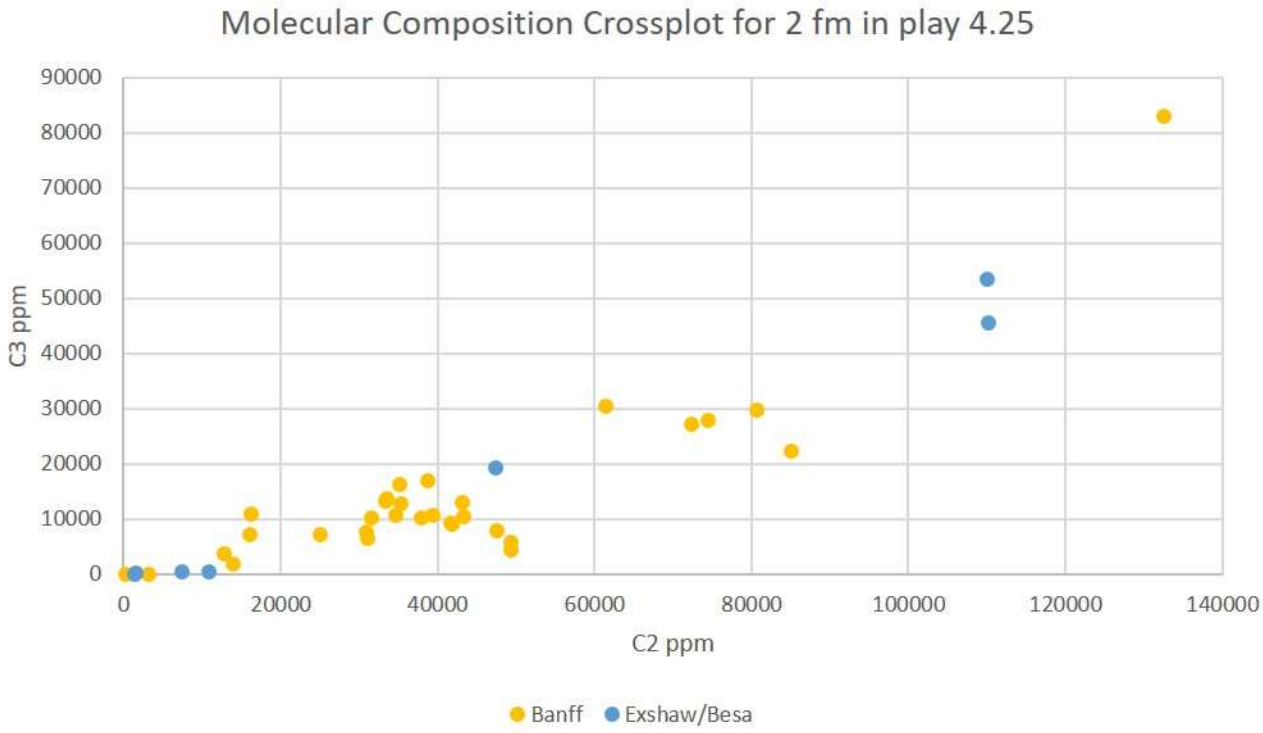

Figure B 99. MC map data – play 4.25 MC (ppm) propane ethane plot for Banff, Exshaw formations [not to template].

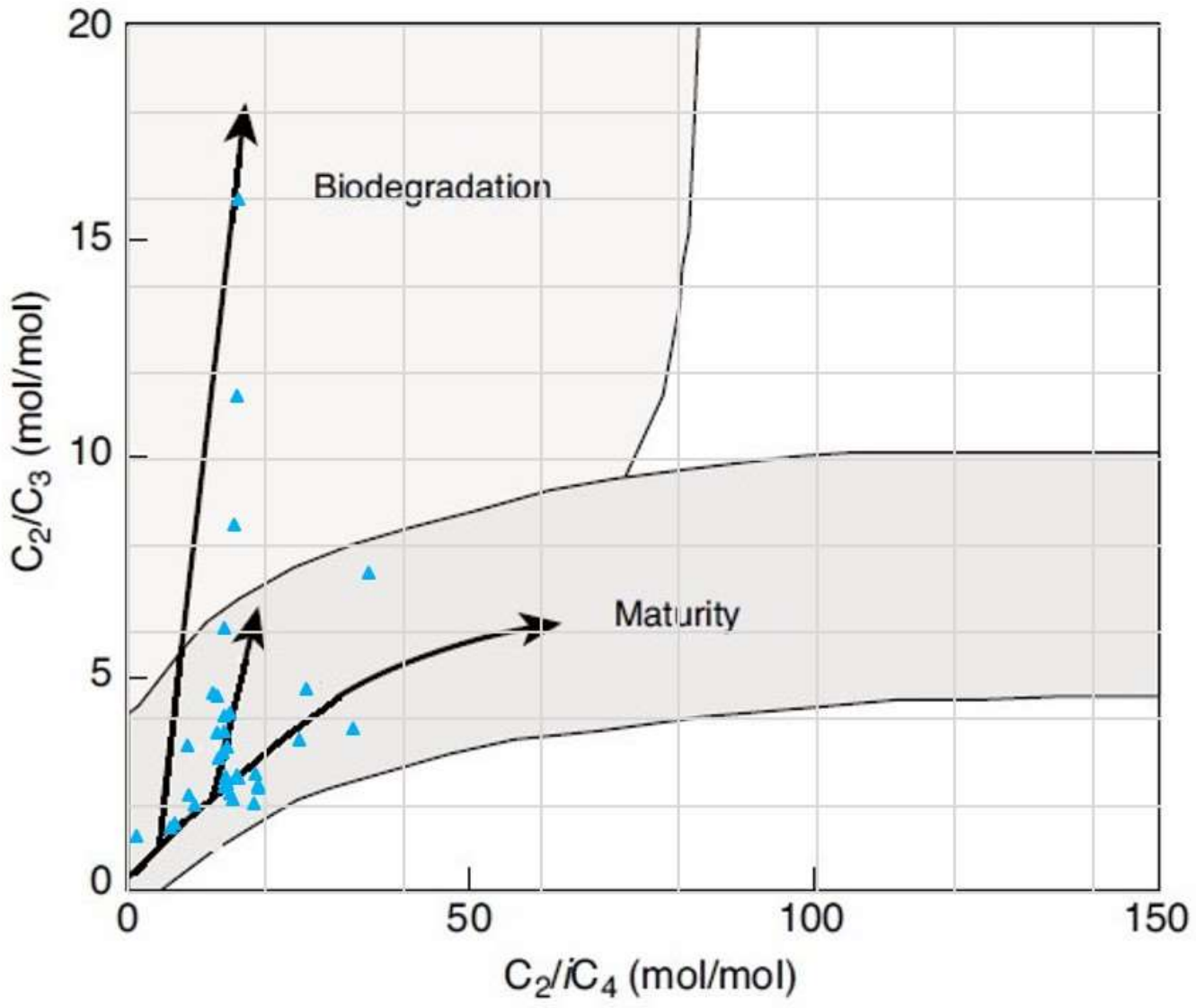

Figure B 100. ISO map data – play 4.25 Interpretive diagrams MC Prinzhofer Diagram for Banff, Exshaw maps (after Prinzhofer and Battani 2003, no trendlines).

16. Plays 4.28/30 Jean Marie, Muskwa, Slave Point, Evie, Pine Point, etc. (multiple formations – both MC/ISO data)

Figure B 101. MC map data – plays 4.28/30 MC (ppm) ethane methane plot for Jean Marie, Muskwa, Slave Point, Evie, Pine Point, formations [Muskwa/Evie mudgas have low ppm C2/C3, not to template].

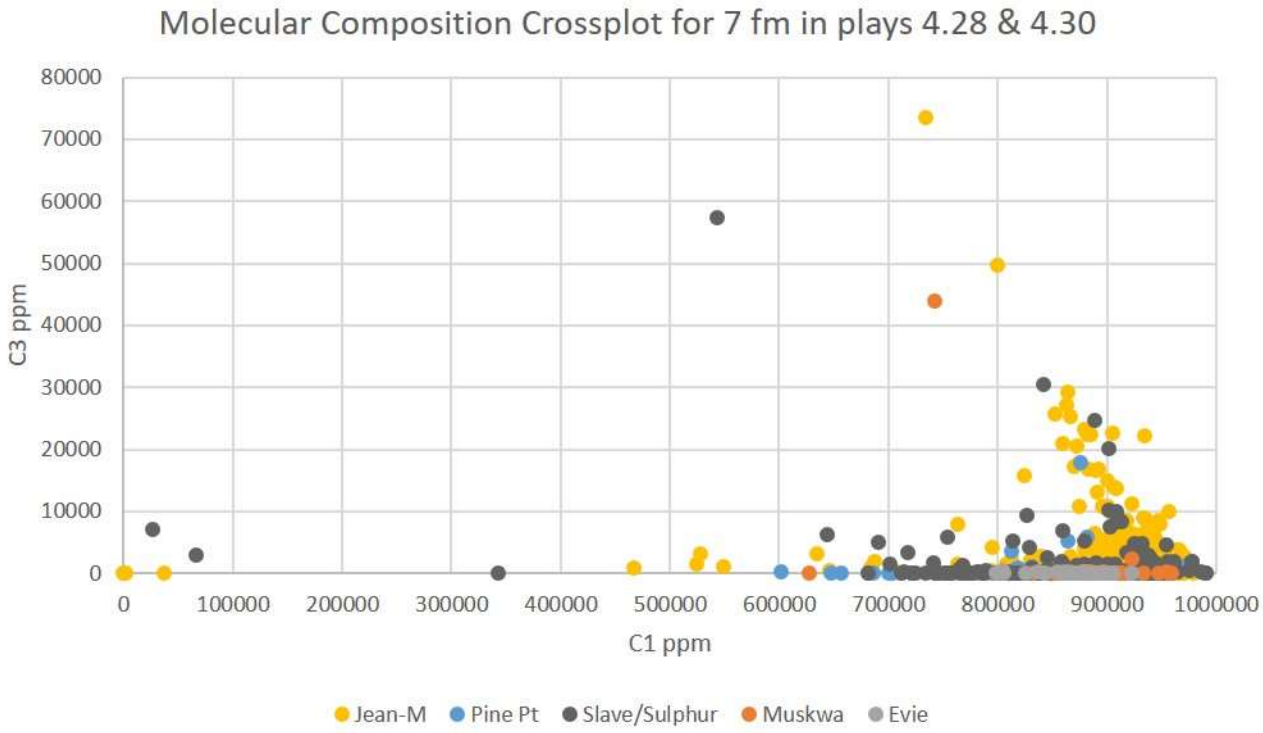

Figure B 102. MC map data – plays 4.28/30 MC (ppm) propane methane plot for Jean Marie, Muskwa, Slave Point, Evie, Pine Point, formations [Muskwa/Evie mudgas have low ppm C2/C3, not to template].

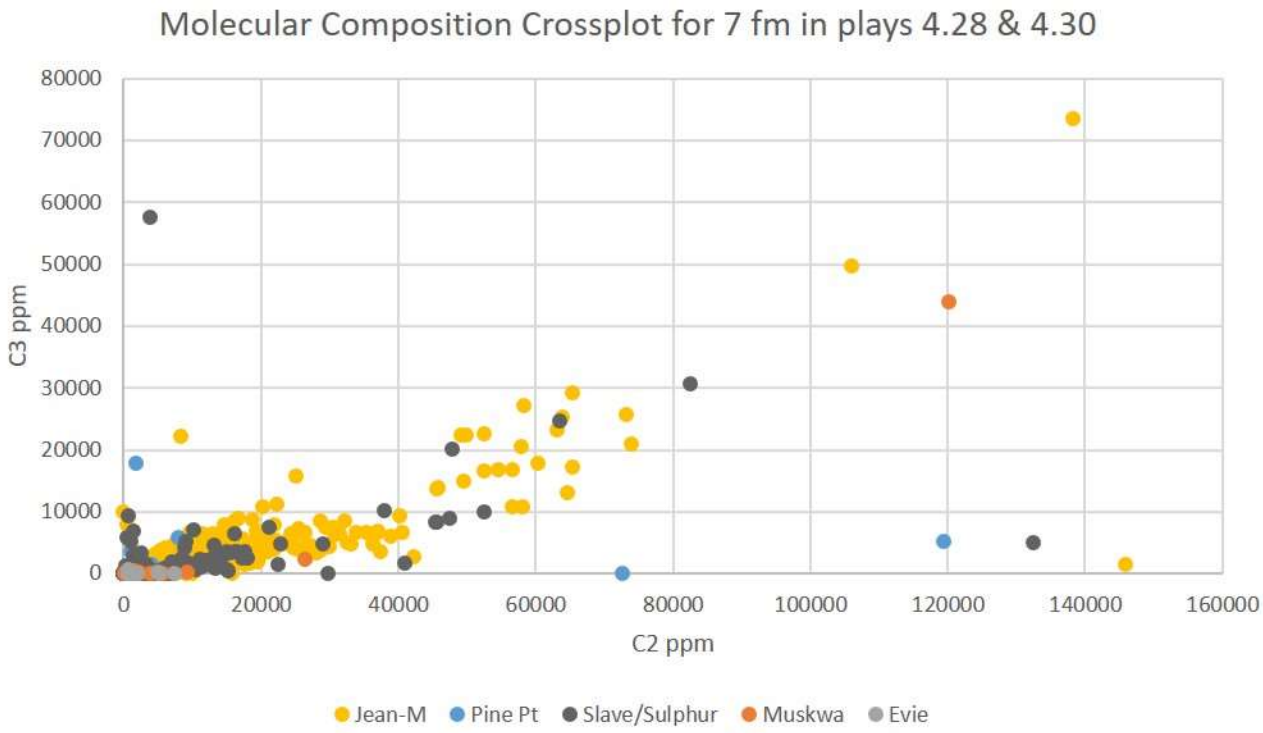

Figure B 103. MC map data – plays 4.28/30 MC (ppm) propane ethane plot for Jean Marie, Muskwa, Slave Point, Evie, Pine Point, formations [Muskwa/Evie mudgas have low ppm C2/C3, not to template].

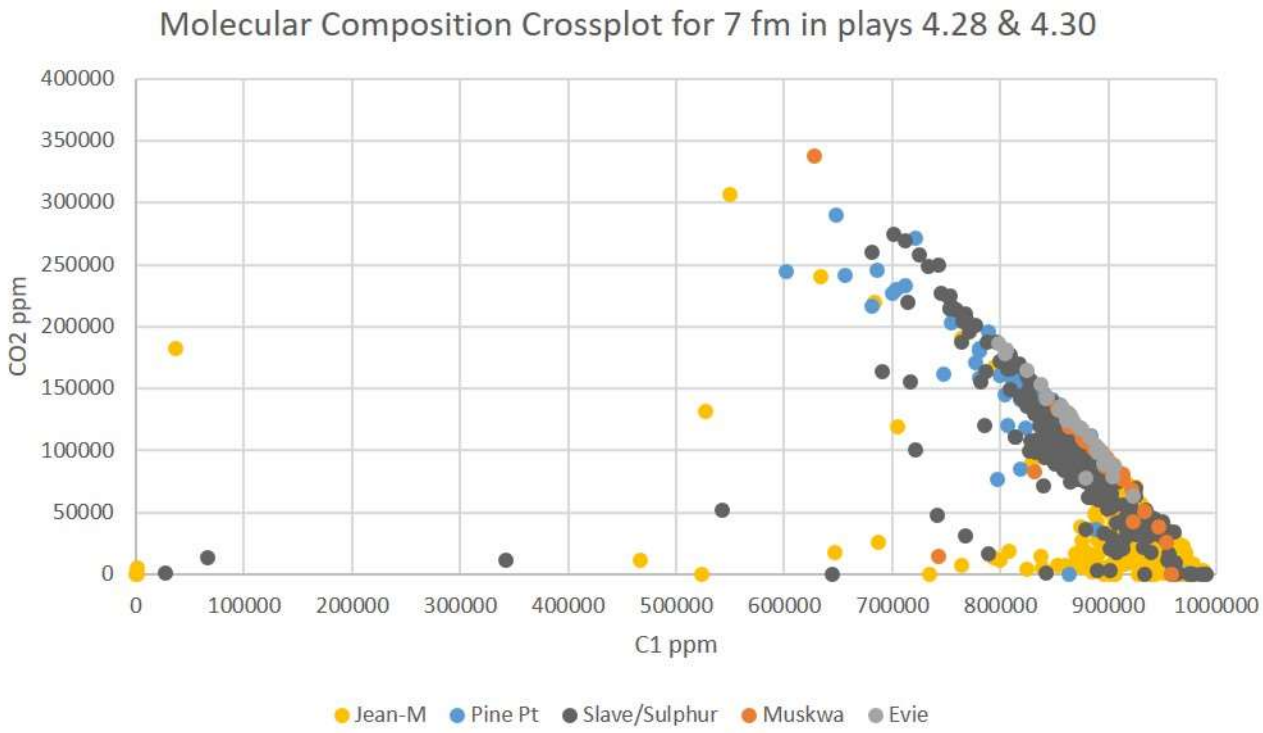

Figure B 104. MC map data – plays 4.28/30 MC (ppm) carbon dioxide methane plot for Jean Marie, Muskwa, Slave Point, Evie, Pine Point, formations [not to template].

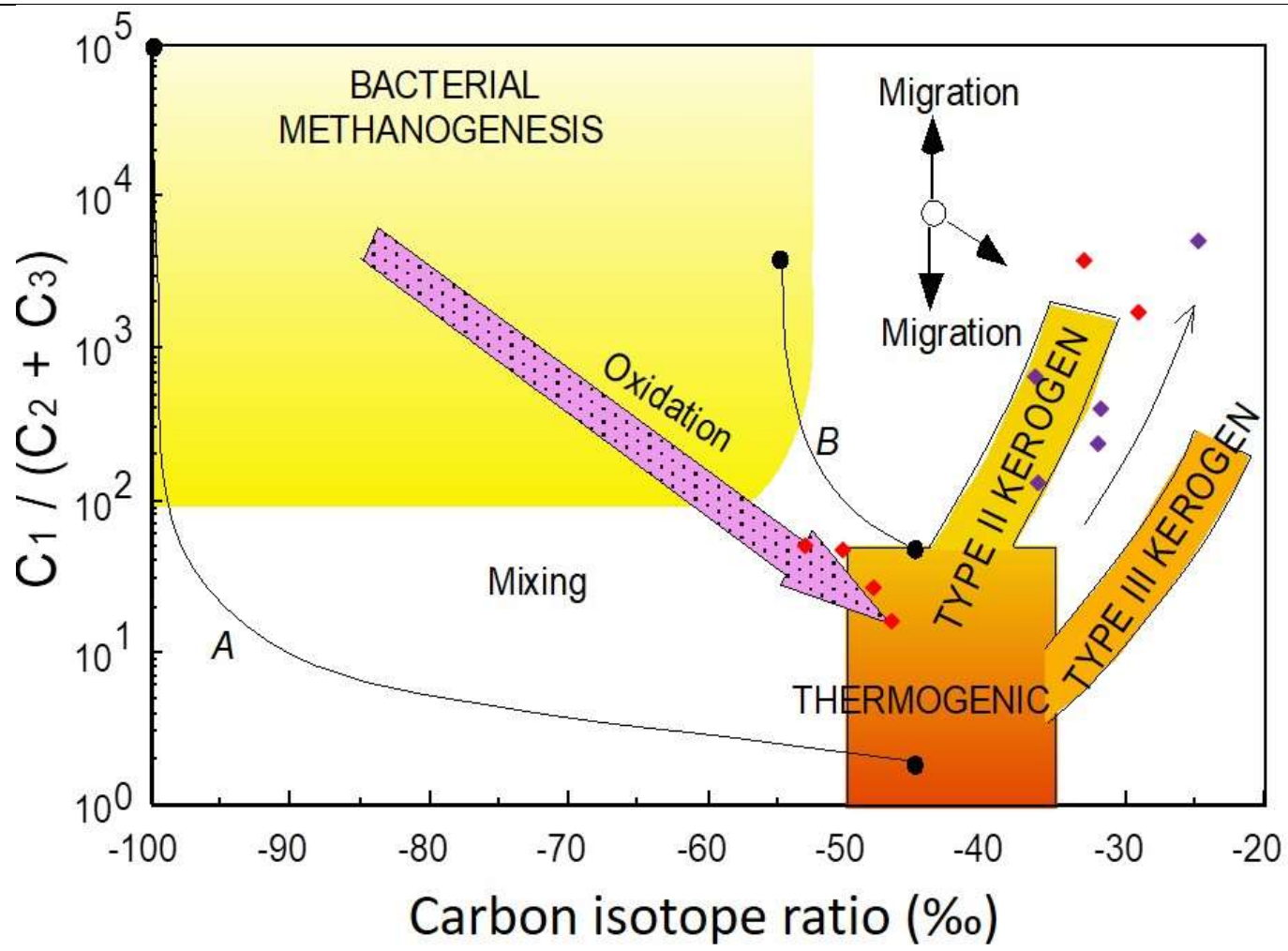

Figure B 105. ISO map data – plays 4.28/30 Interpretive diagrams MC/ISO Bernard Diagram for Jean Marie, Muskwa, Slave Point, Evie, Pine Point, maps (Whiticar, 2018 pers. comm., after Whiticar 1999, Muskwa/Evie mudgas have low ppm C2/C3, JM/Muskwa=purple, Slave/Evie=red, no trendlines).

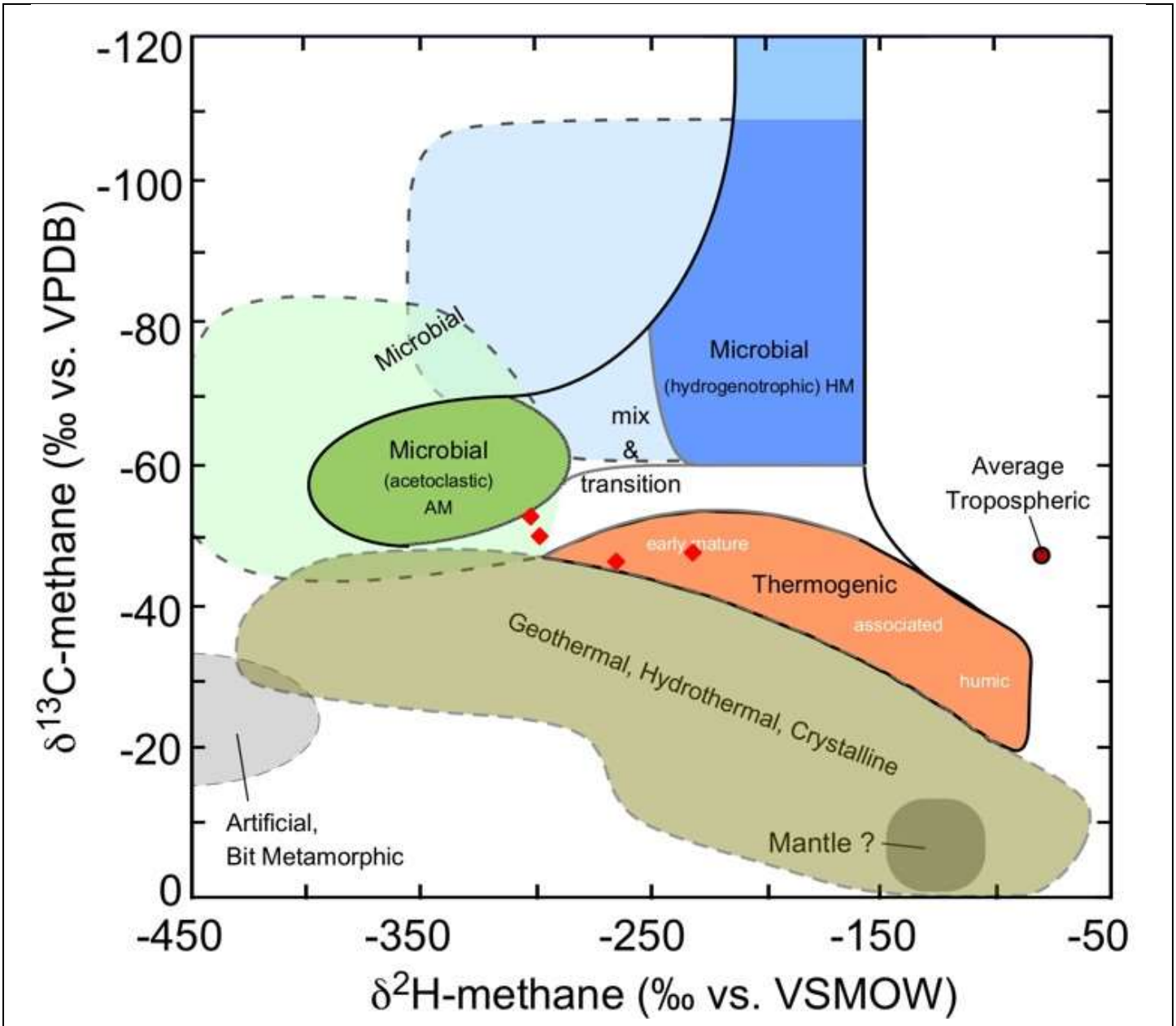

Figure B 106. ISO map data – plays 4.28/30 Interpretive diagrams MC/ISO CD Diagram for Jean Marie, Muskwa, Slave Point, Evie, Pine Point, maps (Whiticar, 2018 pers. comm., after Whiticar 1999, Muskwa/Evie mudgas have low ppm C2/C3, JM/Muskwa=purple, Slave/Evie=red, no trendlines).

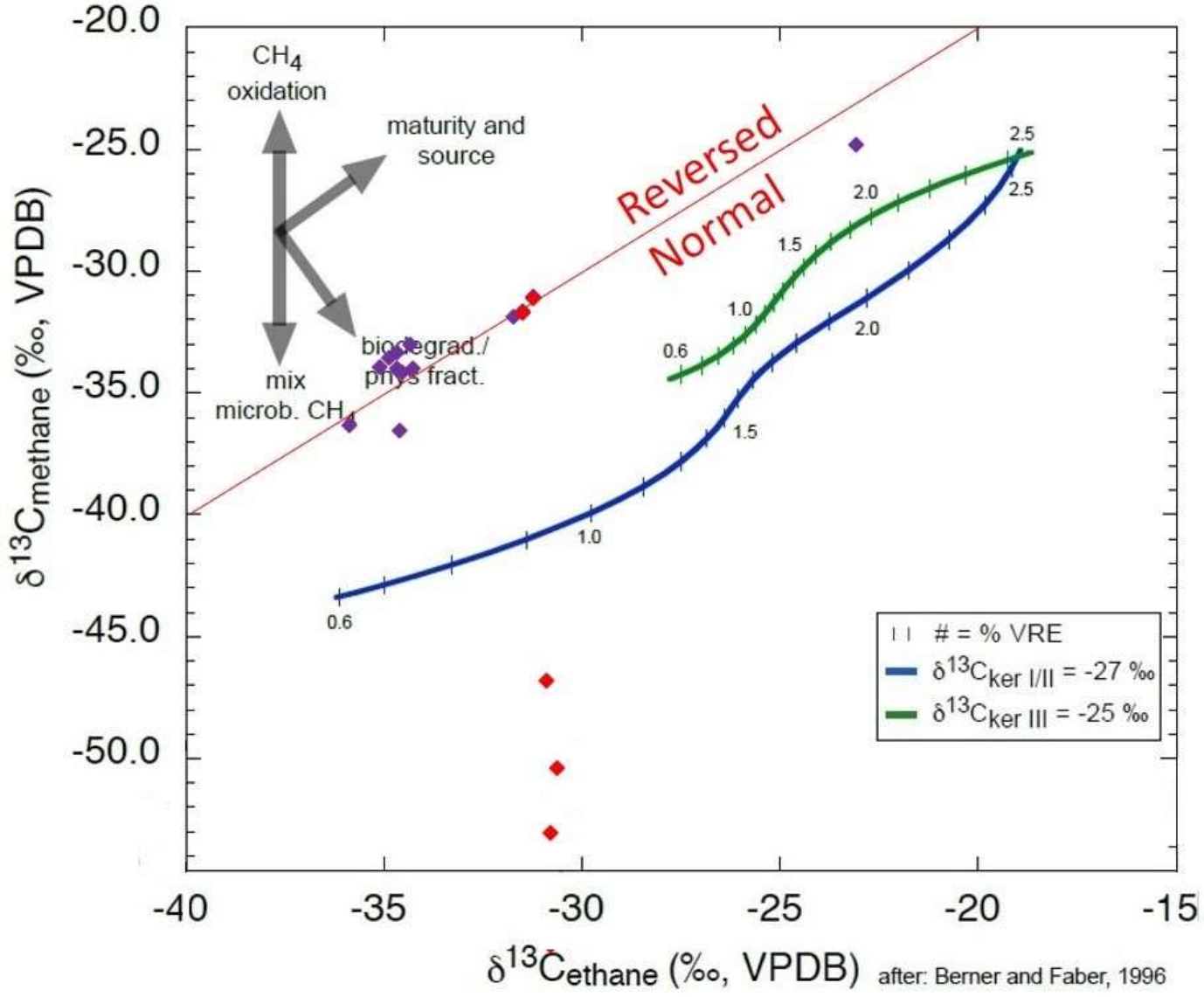

Figure B 107. ISO map data – plays 4.28/30 Interpretive diagrams ISO $\delta^{13}C_1$ vs $\delta^{13}C_2$ plot for Jean Marie, Muskwa, Slave Point, Evie, Pine Point, maps (Whiticar, 2018 pers. comm., after Berner and Faber 1996, Muskwa/Evie mudgas have low ppm C2/C3, JM/Muskwa=purple, Slave/Evie=red, no trendlines).

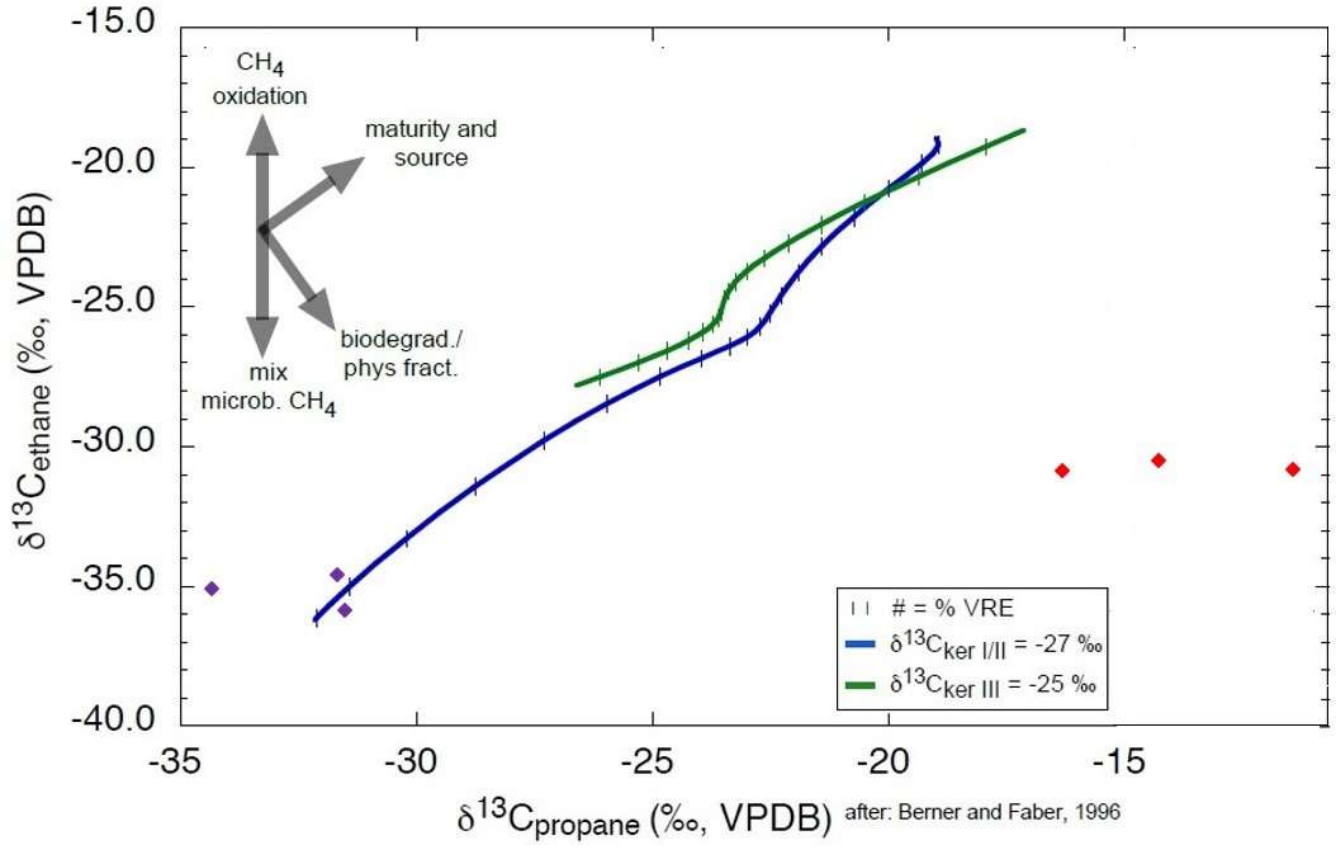

Figure B 108. ISO map data – plays 4.28/30 Interpretive diagrams ISO $\delta^{13}C_2$ vs $\delta^{13}C_3$ plot for Jean Marie, Muskwa, Slave Point, Evie, Pine Point, maps (Whiticar, 2018 pers. comm., after Berner and Faber 1996, Muskwa/Evie mudgas have low ppm C2/C3, JM/Muskwa=purple, Slave/Evie=red, no trendlines).

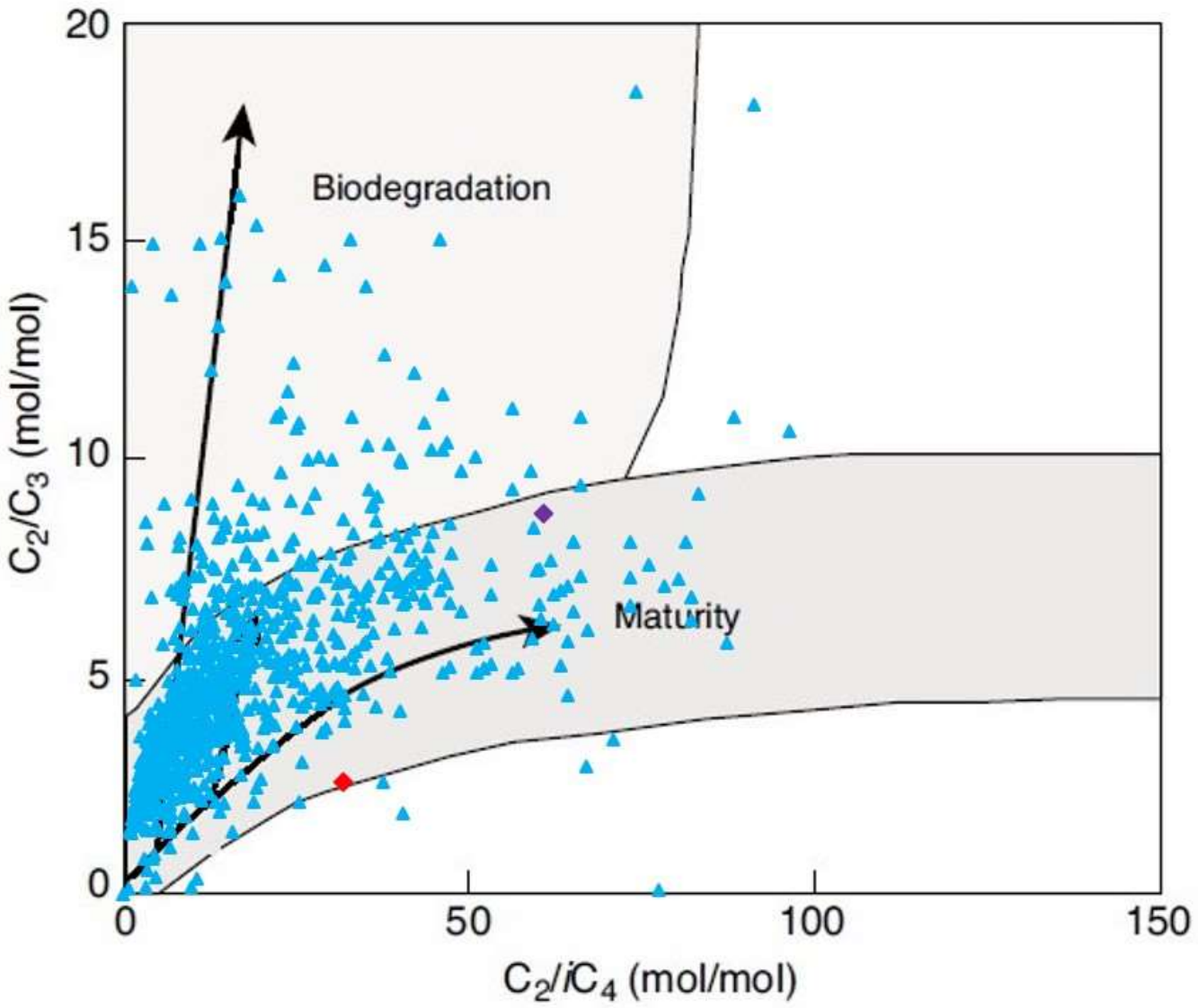

Figure B 109. ISO map data – plays 4.28/30 Interpretive diagrams MC/ISO Prinzhofer Diagram for Jean Marie, Muskwa, Slave Point, Evie, Pine Point, maps (after Prinzhofer and Battani 2003, Muskwa/Evie mudgas have low ppm C2/C3, JM/Muskwa=purple, Slave/Evie=red, no trendlines).

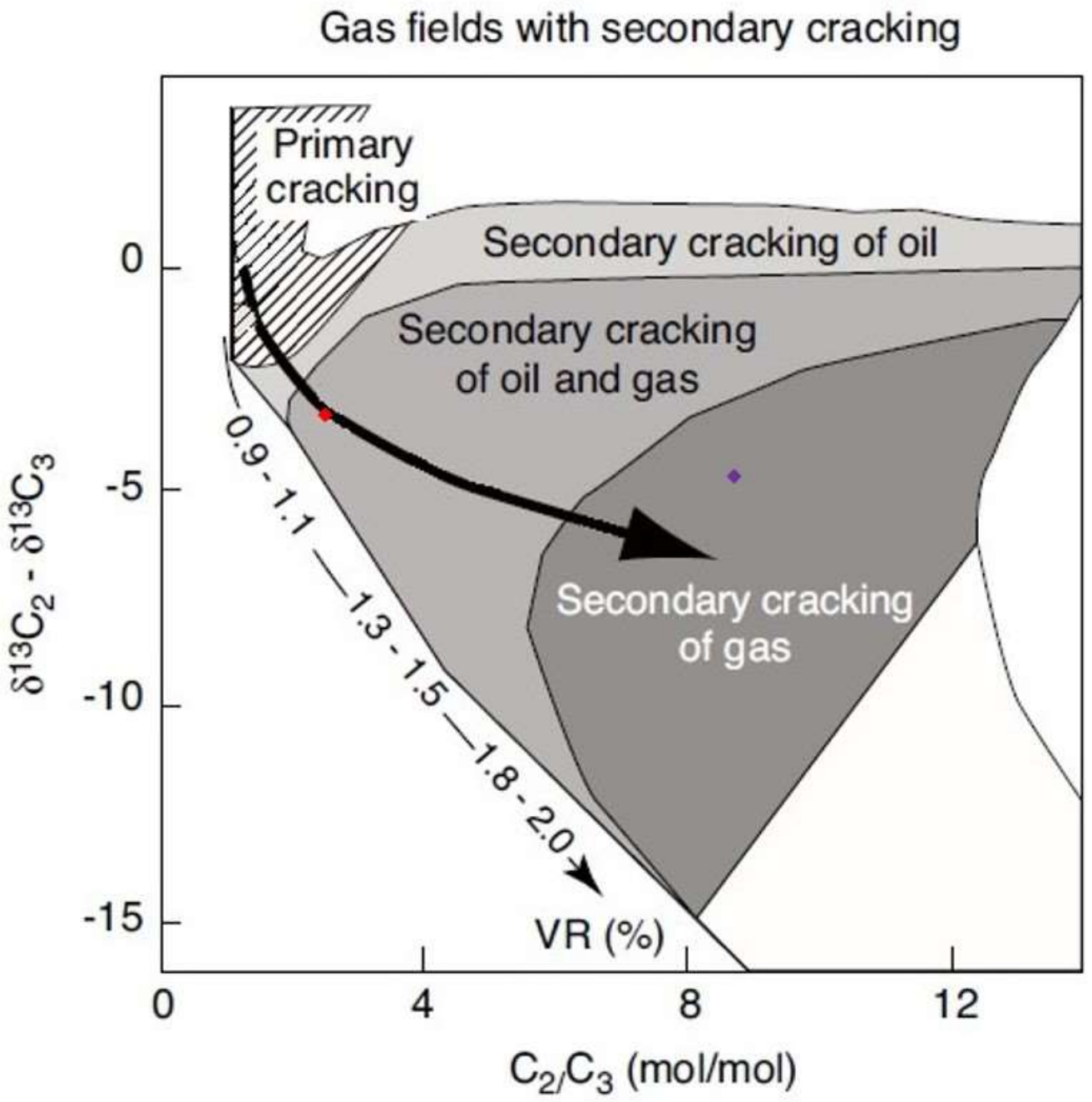

Figure B 110. ISO map data – plays 4.28/30 Interpretive diagrams MC/ISO Lorant Diagram for Jean Marie, Muskwa, Slave Point, Evie, Pine Point, maps (after Prinzhofer and Battani 2003, Muskwa/Evie mudgas have low ppm C2/C3, JM/Muskwa=purple, Slave/Evie=red, no trendlines).

Appendix C: metadata and individual map tabulation

header	previous	format	description	use	profile	4.00	4.01	4.02	4.03	4.04	4.05	4.06	4.07	4.08	4.09	4.10	4.11	4.12	4.13	4.14	4.15	4.15a	4.16	4.17	4.18	4.19	4.20	4.21	4.22	4.23	4.24	4.25	4.26	4.27	4.28	4.29	4.29a	4.30	4.31	4.32	4.32a	4.33
PLAY NAME	comment line	comment lin	comment line	comment line	Mudga	Surface	Tertian	Belly Ri	Chinool	Cardiur	Doe Cre	Dunveg	Sikanni	Scatter	Paddy I	Cadotte	Spirit R	Bluesky	Gething	Cadomi	Nikana	Fernie (	Charlie	Upper (	Lower (	Halfwa	Doig / L	Montne	Belloy /	Mattso	Debolt	Banff /	Wabam	Kakisa I	Jean M	Leduc F	Muskw	Slave P	Watt M	Sulphur	Evie	Nahanr
ISO sample count	comment line	comment lin	comment line	comment line	2002	252	n/a	n/a	n/a	n/a	n/a	0	n/a	n/a	0	blende	0	23	blende	1	4	added	14	blende	blende	4	10	146	0	0	6	0	n/a	n/a	2	n/a	12	6	n/a	blende	2	n/a
ISO well count	comment line	comment lin	comment line	comment line	70	151	n/a	n/a	n/a	n/a	n/a	0	n/a	n/a	0	blende	0	20	blende	1	4	added	14	blende	blende	4	10	93	0	0	5	0	n/a	n/a	2	n/a	10	3	n/a	blende	1	n/a
total map locations	comment line	comment lin	comment line	comment line	n/a	252	n/a	n/a	n/a	n/a	n/a	23	n/a	n/a	204	blende	641	1833	blende	463	513	added	1778	blende	blende	1423	429	1116	272	82	305	39	n/a	n/a	859	n/a	57	499	n/a	blende	38	n/a
map	n/a	numeric1	map vs ISO vs profile	main display t	n/a	n/a	n/a	n/a	n/a	n/a	n/a	n/a	n/a	n/a	n/a	n/a	n/a	n/a	n/a	n/a	n/a	n/a	n/a	n/a	n/a	n/a	n/a	n/a	n/a	n/a	n/a	n/a	n/a	n/a	n/a	n/a	n/a	n/a	n/a	n/a	n/a
UTM_E	UTM E	numeric1	10 degree UTM grid ea	01 temp as st	n/a	n/a	n/a	n/a	n/a	n/a	n/a	n/a	n/a	n/a	n/a	n/a	n/a	n/a	n/a	n/a	n/a	n/a	n/a	n/a	n/a	n/a	n/a	n/a	n/a	n/a	n/a	n/a	n/a	n/a	n/a	n/a	n/a	n/a	n/a	n/a	n/a
UTM_N	UTM N	numeric1	10 degree UTM grid nc	02 temp as st	n/a	n/a	n/a	n/a	n/a	n/a	n/a	n/a	n/a	n/a	n/a	n/a	n/a	n/a	n/a	n/a	n/a	n/a	n/a	n/a	n/a	n/a	n/a	n/a	n/a	n/a	n/a	n/a	n/a	n/a	n/a	n/a	n/a	n/a	n/a	n/a	n/a
test_index	test index (WA	text	concatenated WA# do	03 dbkey	n/a	n/a	n/a	n/a	n/a	n/a	n/a	n/a	n/a	n/a	n/a	n/a	n/a	n/a	n/a	n/a	n/a	n/a	n/a	n/a	n/a	n/a	n/a	n/a	n/a	n/a	n/a	n/a	n/a	n/a	n/a	n/a	n/a	n/a	n/a	n/a	n/a
WA_num	WA#	numeric1	Well Authorization nu	04 join key to	n/a	n/a	n/a	n/a	n/a	n/a	n/a	n/a	n/a	n/a	n/a	n/a	n/a	n/a	n/a	n/a	n/a	n/a	n/a	n/a	n/a	n/a	n/a	n/a	n/a	n/a	n/a	n/a	n/a	n/a	n/a	n/a	n/a	n/a	n/a	n/a	n/a
ISO_diff	not for GBC	not for GBC	not for GBC	not for GBC	n/a	n/a	n/a	n/a	n/a	n/a	n/a	n/a	n/a	n/a	n/a	n/a	n/a	n/a	n/a	n/a	n/a	n/a	n/a	n/a	n/a	n/a	n/a	n/a	n/a	n/a	n/a	n/a	n/a	n/a	n/a	n/a	n/a	n/a	n/a	n/a	n/a
Depth 2 M	Depth 2 M	text	comment field or seco	not for GBC	n/a	n/a	n/a	n/a	n/a	n/a	n/a	n/a	n/a	n/a	n/a	n/a	n/a	n/a	n/a	n/a	n/a	n/a	n/a	n/a	n/a	n/a	n/a	n/a	n/a	n/a	n/a	n/a	n/a	n/a	n/a	n/a	n/a	n/a	n/a	n/a	n/a
Depth_m	Depth 1 M	numeric1	primary depth value ir	13 location in	n/a	n/a	n/a	n/a	n/a	n/a	n/a	n/a	n/a	n/a	n/a	n/a	n/a	n/a	n/a	n/a	n/a	n/a	n/a	n/a	n/a	n/a	n/a	n/a	n/a	n/a	n/a	n/a	n/a	n/a	n/a	n/a	n/a	n/a	n/a	n/a	n/a
Sample_Date	Sample Date	date	date that the sample v	14 date indica	n/a	n/a	n/a	n/a	n/a	n/a	n/a	n/a	n/a	n/a	n/a	n/a	n/a	n/a	n/a	n/a	n/a	n/a	n/a	n/a	n/a	n/a	n/a	n/a	n/a	n/a	n/a	n/a	n/a	n/a	n/a	n/a	n/a	n/a	n/a	n/a	n/a
Sample_type	Sample type	text	description code for sa	15 sample ind	n/a	n/a	n/a	n/a	n/a	n/a	n/a	n/a	n/a	n/a	n/a	n/a	n/a	n/a	n/a	n/a	n/a	n/a	n/a	n/a	n/a	n/a	n/a	n/a	n/a	n/a	n/a	n/a	n/a	n/a	n/a	n/a	n/a	n/a	n/a	n/a	n/a
fm_OGC_code	fm OGC code	text	correlation code for te	16 source cod	n/a	n/a	n/a	n/a	n/a	n/a	n/a	n/a	n/a	n/a	n/a	n/a	n/a	n/a	n/a	n/a	n/a	n/a	n/a	n/a	n/a	n/a	n/a	n/a	n/a	n/a	n/a	n/a	n/a	n/a	n/a	n/a	n/a	n/a	n/a	n/a	n/a
fm_PRCL	fm PRCL Hayes	text	correlation name for t	17 recorrelati	1993	n/a	n/a	n/a	n/a	n/a	n/a	23	n/a	n/a	4	blende	33	306	blende	46	504	714	blende	blende	24	116	182	29	38	49	39	n/a	n/a	1	n/a	0	125	n/a	blende	0	n/a
fm_category	fm category	text	key field for mapping t	18 final forma	n/a	n/a	n/a	n/a	n/a	n/a	n/a	n/a	n/a	n/a	n/a	n/a	n/a	n/a	n/a	n/a	n/a	n/a	n/a	n/a	n/a	n/a	n/a	n/a	n/a	n/a	n/a	n/a	n/a	n/a	n/a	n/a	n/a	n/a	n/a	n/a	n/a
iC4/nC4	iC4/nC4	numeric1	internal comparison o	mapped for th	n/a	yes	n/a	n/a	n/a	n/a	n/a	yes	n/a	n/a	yes	n/a	yes	yes	n/a	yes	yes	yes	yes	n/a	n/a	yes	yes	yes	yes	yes	yes	yes	n/a	n/a	yes	n/a	yes	yes	n/a	n/a	n/a	n/a
dryness ratio	dryness ratio	numeric1	internal comparison o	mapped for th	n/a	yes	n/a	n/a	n/a	n/a	n/a	yes	n/a	n/a	yes	n/a	yes	yes	n/a	yes	yes	yes	yes	n/a	n/a	yes	yes	yes	yes	yes	yes	yes	n/a	n/a	yes	n/a	yes	yes	n/a	n/a	yes	n/a
iso ratio descr	iso ratio descr	numeric1	internal comparison o	mapped for th	n/a	yes	n/a	n/a	n/a	n/a	n/a	n/a	n/a	n/a	n/a	n/a	n/a	yes	n/a	n/a	yes	n/a	yes	n/a	n/a	yes	yes	yes	n/a	n/a	yes	n/a	n/a	n/a	n/a	n/a	yes	n/a	n/a	n/a	n/a	n/a
MC_normalized_Ber	norm C1/C2+C	numeric1	active calculation for p	11 attr as key	n/a	yes	n/a	n/a	n/a	n/a	n/a	yes	n/a	n/a	yes	n/a	yes	yes	n/a	yes	yes	yes	yes	n/a	n/a	yes	yes	yes	yes	yes	yes	yes	n/a	n/a	yes	n/a	yes	yes	n/a	n/a	yes	n/a
H2S_sour_ppm	H2S ppm	numeric1	Hydrogen Sulphide mc	19 attr as sup	n/a	ND er	n/a	n/a	n/a	n/a	n/a	yes	n/a	n/a	n/a	n/a	yes	yes	n/a	yes	yes	n/a	yes	n/a	n/a	yes	yes	yes	yes	yes	yes	n/a	n/a	n/a	yes	n/a	n/a	yes	n/a	n/a	n/a	n/a
C1Methane_ppm	C1 ppm	numeric1	Methane molecular cc	20 attr as sup	n/a	n/a	n/a	n/a	n/a	n/a	n/a	yes	n/a	n/a	yes	n/a	yes	yes	n/a	yes	yes	n/a	yes	n/a	n/a	yes	yes	yes	yes	yes	yes	yes	n/a	n/a	yes	n/a	yes	yes	n/a	n/a	chk	n/a
C1_iso13C_permil	δ13C1 ‰	numeric1	Carbon isotopes of Me	21 attr as sup	n/a	yes	n/a	n/a	n/a	n/a	n/a	n/a	n/a	n/a	n/a	n/a	n/a	yes	n/a	yes	yes	yes	yes	n/a	n/a	yes	yes	yes	n/a	n/a	yes	n/a	n/a	n/a	n/a	n/a	yes	n/a	n/a	n/a	n/a	n/a
C1_isoD_permil	δDC1 ‰	numeric1	Hydrogen isotopes of I	22 attr as sup	n/a	yes	n/a	n/a	n/a	n/a	n/a	n/a	n/a	n/a	n/a	n/a	n/a	n/a	n/a	n/a	n/a	yes	yes	n/a	n/a	n/a	n/a	yes	n/a	n/a	n/a	n/a	n/a	n/a	n/a	n/a	n/a	n/a	n/a	n/a	n/a	n/a
C2Ethane_ppm	C2 ppm	numeric1	Ethane molecular com	23 attr as sup	n/a	n/a	n/a	n/a	n/a	n/a	n/a	yes	n/a	n/a	yes	n/a	yes	yes	n/a	yes	yes	n/a	yes	n/a	n/a	yes	yes	yes	yes	yes	yes	yes	n/a	n/a	yes	n/a	yes	yes	n/a	n/a	yes	n/a
C2_iso13C_permil	δ13C2 ‰	numeric1	Carbon isotopes of Eth	24 attr as sup	n/a	yes	n/a	n/a	n/a	n/a	n/a	n/a	n/a	n/a	n/a	n/a	n/a	yes	n/a	yes	yes	yes	yes	n/a	n/a	yes	yes	yes	n/a	n/a	yes	n/a	n/a	n/a	n/a	n/a	yes	n/a	n/a	n/a	n/a	n/a
C2_isoD_permil	δDC2 ‰	numeric1	Hydrogen isotopes of I	25 attr as sup	n/a	n/a	n/a	n/a	n/a	n/a	n/a	n/a	n/a	n/a	n/a	n/a	n/a	n/a	n/a	n/a	n/a	n/a	n/a	n/a	n/a	n/a	n/a	n/a	n/a	n/a	n/a	n/a	n/a	n/a	n/a	n/a	n/a	n/a	n/a	n/a	n/a
C3Propane_ppm	C3 ppm	numeric1	Propane molecular co	26 attr as sup	n/a	n/a	n/a	n/a	n/a	n/a	n/a	yes	n/a	n/a	yes	n/a	yes	yes	n/a	yes	yes	n/a	yes	n/a	n/a	yes	yes	yes	yes	yes	yes	yes	n/a	n/a	yes	n/a	yes	yes	n/a	n/a	n/a	n/a
C3_iso13C_permil	δ13C3 ‰	numeric1	Carbon isotopes of Pr	27 attr as sup	n/a	yes	n/a	n/a	n/a	n/a	n/a	n/a	n/a	n/a	n/a	n/a	n/a	yes	n/a	yes	yes	yes	yes	n/a	n/a	yes	yes	yes	n/a	n/a	n/a	n/a	n/a	n/a	n/a	n/a	yes	n/a	n/a	n/a	n/a	n/a
C3_isoD_permil	δDC3 ‰	numeric1	Hydrogen isotopes of I	28 attr as sup	n/a	n/a	n/a	n/a	n/a	n/a	n/a	n/a	n/a	n/a	n/a	n/a	n/a	n/a	n/a	n/a	n/a	n/a	n/a	n/a	n/a	n/a	n/a	n/a	n/a	n/a	n/a	n/a	n/a	n/a	n/a	n/a	n/a	n/a	n/a	n/a	n/a
C4iButane_ppm	iC4 ppm	numeric1	iso-Butane molecular (	29 attr as sup	n/a	n/a	n/a	n/a	n/a	n/a	n/a	yes	n/a	n/a	yes	n/a	yes	yes	n/a	yes	yes	n/a	yes	n/a	n/a	yes	yes	yes	yes	yes	yes	yes	n/a	n/a	yes	n/a	yes	yes	n/a	n/a	n/a	n/a
C4i_iso13C_permil	δ13iC4 ‰	numeric1	Carbon isotopes of iso	30 attr as sup	n/a	n/a	n/a	n/a	n/a	n/a	n/a	n/a	n/a	n/a	n/a	n/a	n/a	yes	n/a	n/a	n/a	n/a	n/a	n/a	n/a	n/a	yes	yes	n/a	n/a	n/a	n/a	n/a	n/a	n/a	n/a	n/a	n/a	n/a	n/a	n/a	n/a
C4nButane_ppm	nC4 ppm	numeric1	n-Butane molecular cc	31 attr as sup	n/a	n/a	n/a	n/a	n/a	n/a	n/a	yes	n/a	n/a	yes	n/a	yes	yes	n/a	yes	yes	n/a	yes	n/a	n/a	yes	yes	yes	yes	yes	yes	yes	n/a	n/a	yes	n/a	yes	yes	n/a	n/a	n/a	n/a
C4n_iso13C_permil	δ13nC4 ‰	numeric1	Carbon isotopes of n-E	32 attr as sup	n/a	yes	n/a	n/a	n/a	n/a	n/a	n/a	n/a	n/a	n/a	n/a	n/a	yes	n/a	n/a	n/a	n/a	n/a	n/a	n/a	n/a	yes	yes	n/a	n/a	n/a	n/a	n/a	n/a	n/a	n/a	n/a	n/a	n/a	n/a	n/a	n/a
iC5 ppm	iC5 ppm	numeric1	iso-Pentane molecular	not for GBC	n/a	n/a	n/a	n/a	n/a	n/a	n/a	yes	n/a	n/a	yes	n/a	yes	yes	n/a	yes	yes	n/a	yes	n/a	n/a	yes	yes	yes	yes	yes	yes	yes	n/a	n/a	yes	n/a	yes	yes	n/a	n/a	n/a	n/a
C5nPentane_ppm	nC5 ppm	numeric1	n-Pentane molecular c	33 attr as sup	n/a	n/a	n/a	n/a	n/a	n/a	n/a	yes	n/a	n/a	yes	n/a	yes	yes	n/a	yes	yes	n/a	yes	n/a	n/a	yes	yes	yes	yes	yes	yes	yes	n/a	n/a	yes	n/a	n/a	n/a	n/a	n/a	n/a	n/a
C5n_iso13C_permil	δ13nC5 ‰	numeric1	Carbon isotopes of n-F	34 attr as sup	n/a	n/a	n/a	n/a	n/a	n/a	n/a	n/a	n/a	n/a	n/a	n/a	n/a	yes	n/a	n/a	n/a	n/a	n/a	n/a	n/a	n/a	n/a	yes	n/a	n/a	n/a	n/a	n/a	n/a	n/a	n/a	n/a	n/a	n/a	n/a	n/a	n/a
C6HexanesPlus_ppm	my C6+ ppm	numeric1	Hexanes and higher m	35 attr as sup	n/a	n/a	n/a	n/a	n/a	n/a	n/a	n/a	n/a	n/a	n/a	n/a	n/a	yes	n/a	yes	yes	n/a	yes	n/a	n/a	yes	yes	yes	yes	yes	yes	yes	n/a	n/a	yes	n/a	n/a	n/a	n/a	n/a	n/a	n/a
CO2_ppm	CO2 ppm	numeric1	Carbon Dioxide molec	36 attr as sup	n/a	n/a	n/a	n/a	n/a	n/a	n/a	n/a	n/a	n/a	n/a	n/a	yes	yes	n/a	yes	yes	n/a	yes	n/a	n/a	yes	yes	yes	yes	yes	yes	yes	n/a	n/a	yes	n/a	yes	yes	n/a	n/a	yes	n/a
CO2_iso13C_permil	δ13CO2 ‰	numeric1	Carbon isotopes of Ca	37 attr as sup	n/a	n/a	n/a	n/a	n/a	n/a	n/a	n/a	n/a	n/a	n/a	n/a	n/a	yes	n/a	n/a	n/a	n/a	n/a	n/a	n/a	n/a	n/a	yes	n/a	n/a	n/a	n/a	n/a	n/a	n/a	n/a	n/a	n/a	n/a	n/a	n/a	n/a
timegrad_H2S	ΔT H2S change	numeric1	change of H2S in ppm,	05 attr as key	n/a	n/a	n/a	n/a	n/a	n/a	n/a	n/a	n/a	n/a	n/a	n/a	n/a	yes	n/a	yes	yes	n/a	yes	n/a	n/a	yes	yes	yes	yes	yes	yes	yes	n/a	n/a	n/a	n/a	n/a	yes	n/a	n/a	n/a	n/a
timegrad_Bernard	ΔT C1/C2+C3 c	numeric1	change of MC as Bern	06 attr as key	n/a	n/a	n/a	n/a	n/a	n/a	n/a	n/a	n/a	n/a	yes	n/a	yes	yes	n/a	yes	yes	n/a	yes	n/a	n/a	yes	yes	yes	yes	yes	yes	yes	n/a	n/a	n/a	n/a	n/a	yes	n/a	n/a	n/a	n/a
timegrad_CO2	ΔT CO2 change	numeric1	change of CO2 in ppm	07 attr as key	n/a	n/a	n/a	n/a	n/a	n/a	n/a	n/a	n/a	n/a	yes	n/a	yes	yes	n/a	yes	yes	n/a	yes	n/a	n/a	yes	yes	yes	yes	yes	yes	yes	n/a	n/a	n/a	n/a	n/a	yes	n/a	n/a	n/a	n/a
start_H2S	Yint H2S	numeric1	initial H2S ppm in time	08 attr as key	n/a	n/a	n/a	n/a	n/a	n/a	n/a	n/a	n/a	n/a	n/a	n/a	n/a	yes	n/a	yes	yes	n/a	yes	n/a	n/a	yes	yes	yes	yes	yes	yes	yes	n/a	n/a	n/a	n/a	n/a	yes	n/a	n/a	n/a	n/a
start_Bernard	Yint C1/C2+C3	numeric1	initial Bernard as a rat	09 attr as key	n/a	n/a	n/a	n/a	n/a	n/a	n/a	n/a	n/a	n/a	yes	n/a	yes	yes	n/a	yes	yes	n/a	yes	n/a	n/a	yes	yes	yes	yes	yes	yes	yes	n/a	n/a	n/a	n/a	n/a	yes	n/a	n/a	n/a	n/a
start_CO2	Yint CO2	numeric1	initial CO2 ppm in time	10 attr as key	n/a	n/a	n/a	n/a	n/a	n/a	n/a	n/a	n/a	n/a	yes	n/a	yes	yes	n/a	yes	yes	n/a	yes	n/a	n/a	yes	yes	yes	yes	yes	yes	yes	n/a	n/a	n/a	n/a	n/a	yes	n/a	n/a	n/a	n/a
N2_ppm	N2 ppm	numeric1	Nitrogen molecular co	38 attr as sup	n/a	n/a	n/a	n/a	n/a	n/a	n/a	n/a	n/a	n/a	n/a	n/a	n/a	n/a	n/a	n/a	n/a	n/a	n/a	n/a	n/a	n/a	n/a	n/a	n/a	n/a	n/a	n/a	n/a	n/a	n/a	n/a	n/a	n/a	n/a	n/a	n/a
O2plusAr_ppm	O2+Ar ppm	numeric1	Oxygen Argon molecu	39 attr as sup	n/a	n/a	n/a	n/a	n/a	n/a	n/a	n/a	n/a	n/a	n/a	n/a	n/a	n/a	n/a	n/a	n/a	n/a	n/a	n/a	n/a	n/a	n/a	n/a	n/a	n/a	n/a	n/a	n/a	n/a	n/a	n/a	n/a	n/a	n/a	n/a	n/a
CO ppm	CO ppm	numeric1	minor MC field - Carbc	not for GBC	n/a	n/a	n/a	n/a	n/a	n/a	n/a	n/a	n/a	n/a	n/a	n/a	n/a	n/a	n/a	n/a	n/a	n/a	n/a	n/a	n/a	n/a	n/a	n/a	n/a	n/a	n/a	n/a	n/a	n/a	n/a	n/a	n/a	n/a	n/a	n/a	n/a
He ppm	He ppm	numeric1	minor MC field - Heliu	not for GBC	n/a	n/a	n/a	n/a	n/a	n/a	n/a	n/a	n/a	n/a	n/a	n/a	n/a	n/a	n/a	n/a	n/a	n/a	n/a	n/a	n/a	n/a	n/a	n/a	n/a	n/a	n/a	n/a	n/a	n/a	n/a	n/a	n/a	n/a	n/a	n/a	n/a
H2 ppm	H2 ppm	numeric1	minor MC field - Hydr	not for GBC	n/a	n/a	n/a	n/a	n/a	n/a	n/a	n/a	n/a	n/a	n/a	n/a	n/a	n/a	n/a	n/a	n/a	n/a	n/a	n/a	n/a	n/a	n/a	n/a	n/a	n/a	n/a	n/a	n/a	n/a	n/a	n/a	n/a	n/a	n/a	n/a	n/a
Lab_name	Lab name	text	key field on formating	40 link to anal	n/a	n/a	n/a	n/a	n/a	n/a	n/a	n/a	n/a	n/a	n/a	n/a	n/a	n/a	n/a	n/a	n/a	n/a	n/a	n/a	n/a	n/a	n/a	n/a	n/a	n/a	n/a	n/a	n/a	n/a	n/a	n/a	n/a	n/a	n/a	n/a	n/a
Job#	Job#	text	variable use file numb	not for GBC	n/a	n/a	n/a	n/a	n/a	n/a	n/a	n/a	n/a	n/a	n/a	n/a	n/a	n/a	n/a	n/a	n/a	n/a	n/a	n/a	n/a	n/a	n/a	n/a	n/a	n/a	n/a	n/a	n/a	n/a	n/a	n/a	n/a	n/a	n/a	n/a	n/a
CanOrCoreTrac	Can# or CoreTi	text	secondary field for qu	41 link to anal	n/a	n/a	n/a	n/a	n/a	n/a	n/a	n/a	n/a	n/a	n/a	n/a	n/a	n/a	n/a	n/a	n/a	n/a	n/a	n/a	n/a	n/a	n/a	n/a	n/a	n/a	n/a	n/a	n/a	n/a	n/a	n/a	n/a	n/a	n/a	n/a	n/a
OP Lab No.	OP Lab No.	text	variable use file numb	not for GBC	n/a	n/a	n/a	n/a	n/a	n/a	n/a	n/a	n/a	n/a	n/a	n/a	n/a	n/a	n/a	n/a	n/a	n/a	n/a	n/a	n/a	n/a	n/a	n/a	n/a	n/a	n/a	n/a	n/a	n/a	n/a	n/a	n/a	n/a	n/a	n/a	n/a
Lab Lab No.	Lab Lab No.	text	variable use file numb	not for GBC	n/a	n/a	n/a	n/a	n/a	n/a	n/a	n/a	n/a	n/a	n/a	n/a	n/a	n/a	n/a	n/a	n/a	n/a	n/a	n/a	n/a	n/a	n/a	n/a	n/a	n/a	n/a	n/a	n/a	n/a	n/a	n/a	n/a	n/a	n/a	n/a	n/a
OP Job#	OP Job#	text	variable use file numb	not for GBC	n/a	n/a	n/a	n/a	n/a	n/a	n/a	n/a	n/a	n/a	n/a	n/a	n/a	n/a	n/a	n/a	n/a	n/a	n/a	n/a	n/a	n/a	n/a	n/a	n/a	n/a	n/a	n/a	n/a	n/a	n/a	n/a	n/a	n/a	n/a	n/a	n/a
Lab_Sample_ID	Lab Sample ID	text	key field for queries to	42 link to anal	n/a	n/a	n/a	n/a	n/a	n/a	n/a	n/a	n/a	n/a	n/a	n/a	n/a	n/a	n/a	n/a	n/a	n/a	n/a	n/a	n/a	n/a	n/a	n/a	n/a	n/a	n/a	n/a	n/a	n/a	n/a	n/a	n/a	n/a	n/a	n/a	n/a
comment line	comment line	comment lin	text to data conversions																																						
comment line	comment line	comment lin	TSTM=-9999																																						
comment line	comment line	comment lin	nd=-9998																																						
comment line	comment line	comment lin	n/a=-9997																																						
comment line	comment line	comment lin	error=-9996																																						
comment line	comment line	comment lin	blank=-9995																																						
comment line	comment line	comment lin	TRACE=-9994																																						